frontiers | Research Topics

Epigenomic and epitranscriptomic basis of development and human disease

Edited by
Yujing Li, Xuekun Li, Zhao-Qian Teng and Shunliang Xu

Published in
Frontiers in Cell and Developmental Biology
Frontiers in Genetics

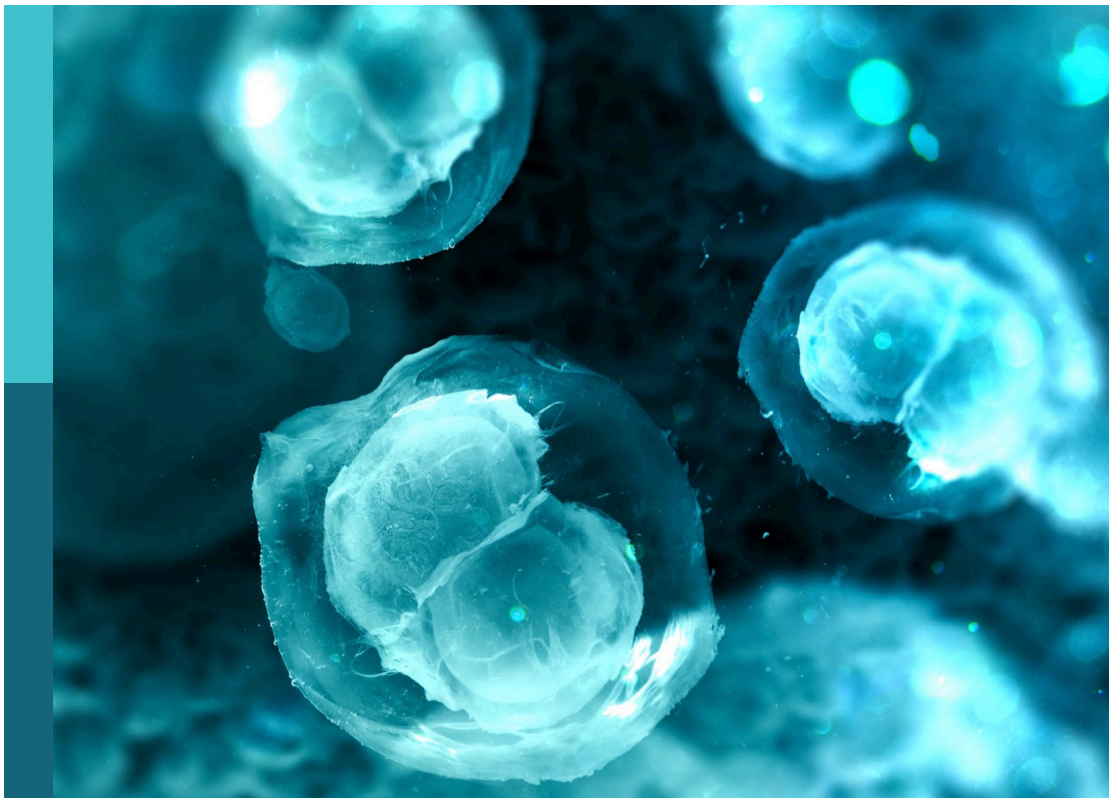

ISSN 1664-8714
ISBN 978-2-83251-817-5
DOI 10.3389/978-2-83251-817-5

About Frontiers

Frontiers is more than just an open access publisher of scholarly articles: it is a pioneering approach to the world of academia, radically improving the way scholarly research is managed. The grand vision of Frontiers is a world where all people have an equal opportunity to seek, share and generate knowledge. Frontiers provides immediate and permanent online open access to all its publications, but this alone is not enough to realize our grand goals.

Frontiers journal series

The Frontiers journal series is a multi-tier and interdisciplinary set of open-access, online journals, promising a paradigm shift from the current review, selection and dissemination processes in academic publishing. All Frontiers journals are driven by researchers for researchers; therefore, they constitute a service to the scholarly community. At the same time, the *Frontiers journal series* operates on a revolutionary invention, the tiered publishing system, initially addressing specific communities of scholars, and gradually climbing up to broader public understanding, thus serving the interests of the lay society, too.

Dedication to quality

Each Frontiers article is a landmark of the highest quality, thanks to genuinely collaborative interactions between authors and review editors, who include some of the world's best academicians. Research must be certified by peers before entering a stream of knowledge that may eventually reach the public - and shape society; therefore, Frontiers only applies the most rigorous and unbiased reviews. Frontiers revolutionizes research publishing by freely delivering the most outstanding research, evaluated with no bias from both the academic and social point of view. By applying the most advanced information technologies, Frontiers is catapulting scholarly publishing into a new generation.

What are Frontiers Research Topics?

Frontiers Research Topics are very popular trademarks of the *Frontiers journals series*: they are collections of at least ten articles, all centered on a particular subject. With their unique mix of varied contributions from Original Research to Review Articles, Frontiers Research Topics unify the most influential researchers, the latest key findings and historical advances in a hot research area.

Find out more on how to host your own Frontiers Research Topic or contribute to one as an author by contacting the Frontiers editorial office: frontiersin.org/about/contact

Epigenomic and epitranscriptomic basis of development and human disease

Topic editors

Yujing Li — Emory University, United States
Xuekun Li — Zhejiang University, China
Zhao-Qian Teng — Institute of Zoology, Chinese Academy of Sciences (CAS), China
Shunliang Xu — The Second Hospital of Shandong University, China

Citation

Li, Y., Li, X., Teng, Z.-Q., Xu, S., eds. (2023). *Epigenomic and epitranscriptomic basis of development and human disease*. Lausanne: Frontiers Media SA.
doi: 10.3389/978-2-83251-817-5

The authors declare that the research was conducted in the absence of any commercial or financial relationships that could be construed as a potential conflict of interest.

Table of contents

frontiers | Frontiers in Cell and Developmental Biology

TYPE Editorial
PUBLISHED 20 February 2023
DOI 10.3389/fcell.2023.1128745

OPEN ACCESS

EDITED AND REVIEWED BY
Michael E. Symonds,
University of Nottingham,
United Kingdom

*CORRESPONDENCE
Shunliang Xu,
slxu@live.com
Zhao-Qian Teng,
tengzq@ioz.ac.cn
Xuekun Li,
xuekun_li@zju.edu.cn
Yujing Li,
yli29@emory.edu

SPECIALTY SECTION
This article was submitted to Epigenomics and Epigenetics, a section of the journal Frontiers in Cell and Developmental Biology

RECEIVED 21 December 2022
ACCEPTED 30 January 2023
PUBLISHED 20 February 2023

CITATION
Xu S, Teng Z-Q, Li X and Li Y (2023), Editorial: Epigenomic and epitranscriptomic basis of development and human disease.
Front. Cell Dev. Biol. 11:1128745.
doi: 10.3389/fcell.2023.1128745

Editorial: Epigenomic and epitranscriptomic basis of development and human disease

Shunliang Xu[1]*, Zhao-Qian Teng[2]*, Xuekun Li[3]* and Yujing Li[4]*

[1]Department of Neurology, The Second Hospital, Cheeloo College of Medicine, Shandong University, Jinan, China, [2]Institute of Zoology, Chinese Academy of Sciences (CAS), Beijing, China, [3]Institute of Translational Medicine, School of Medicine, Zhejiang University, Hangzhou, China, [4]Department of Human genetics, Emory University School of Medicine, Atlanta, GA, United States

KEYWORDS

epigenomics, epitranscriptomics, development, human disease, base modifications, histone modifications

Editorial on the Research Topic
Epigenomic and epitranscriptomic basis of development and human disease

Dynamic and precise regulation of gene expression is orchestrated genetically and epigenetically in accordance with developmental stages and in response to environment stimuli. Aberrant genetic or epigenetic events could devastate gene expression, contributing to pathogenesis of disease. Epigenetic markers of base modifications such as 5-cytosine (5-mC), 5-hydroxycytosine (5-hmC) and adenosine methylation m^{6}A have been appreciated as of the well-characterized and the most important epigenetic/epitranscriptomic markers essentially functional in almost all the biological process of mammals. The main components in the machine complexes responsible for generation and functions of these epi-markers have been characterized in recent years. These components display tissue-specific and delicate spatiotemporal patterns, and their fine-tuned orchestration contributes to the precise and dynamic regulation of the epigenomic and the epitranscriptomic landscapes, ensuring the normal growth, development, and reproduction. More importantly, the emerging evidence links the aberrant regulation of these epi-markers to pathogenesis of multiple diseases, potentially translatable to clinical applications for therapy.

This Research Topic mainly focuses on the epigenomic and epitranscriptomic basis of human diseases. The aim of the topic is to provide a broad overview of current research on epigenetic aspect of development and pathogenesis of human diseases.

Total 13 of articles published in this Research Topic focus on epigenetic regulation of learning and memory, immunological functions, and tumorigenesis. Two of them are related to base modification and human disease. Xu et al., found that deficiency in TET1, one of the erasers for base demethylation impairs learning and memory. In addition to neurological disorder, methylation status is also linked to cancers. One research article addresses the critical role of histone methyltransferase KMT5B on initiation of glioblastoma (GBM) *via* epigenetically regulating a subset of GBM-related genes associated with hypermethylation and 5-hmC loss of genomic DNA Lopez et al.

Histone modifications are associated with lipogenesis and obesity by repression or activation of gene expression. Two research articles are related to the link of histone modifications with metabolic disorders and autophagy involved in pulpitis. Wang et al. found that dynamic histone modifications could activate a subset of genes involved in lipogenesis, energy metabolism and inflammation under the high-fat diet (HFD) conditions, addressing the contribution of the eating habits to the related pathology *via* histone modification.

Autophagy is regulated epigenetically as well during development. Yin et al., screened several groups of writers and erasers for histone methylations under TNFα treatment, providing important information on the epigenetic regulation of autophagy genes during pulpitis, and more importantly this study could be translated to a novel clinical therapy.

As a summary, the research and review articles published in this Research Topic provide important scientific information in a convenient manner that is targeted toward readers with interest in the *epigenomic and epitranscriptomic basis of development and human diseases*.

Author contributions

SX and YL drafted the editorial. Z-QT and XL revised the manuscript and approved the final version.

Conflict of interest

The authors declare that the research was conducted in the absence of any commercial or financial relationships that could be construed as a potential conflict of interest.

Publisher's note

frontiers in Cell and Developmental Biology

DATA REPORT
published: 30 March 2021
doi: 10.3389/fcell.2021.651145

An ATAC-seq Dataset Uncovers the Regulatory Landscape During Axolotl Limb Regeneration

Xiaoyu Wei[1,2†], Hanbo Li[2,3†], Yang Guo[3†], Xiaoying Zhao[3†], Yang Liu[1,2], Xuanxuan Zou[1,2], Li Zhou[2,3], Yue Yuan[1,2], Yating Qin[2,3], Chunyan Mao[2,3], Guodong Huang[2], Yeya Yu[2,4], Qiuting Deng[1,2], Weimin Feng[1,2], Jiangshan Xu[1,2], Mingyue Wang[2], Shanshan Liu[2,3], Huanming Yang[1,2,5], Longqi Liu[1,2,6], Chuanyu Liu[2,6] and Ying Gu[1,2,7*]*

[1] BGI Education Center, University of Chinese Academy of Sciences, Shenzhen, China, [2] BGI-Shenzhen, Shenzhen, China, [3] BGI-Qingdao, BGI-Shenzhen, Qingdao, China, [4] BGI College, Zhengzhou University, Zhengzhou, China, [5] James D. Watson Institute of Genome Sciences, Hangzhou, China, [6] Shenzhen Bay Laboratory, Shenzhen, China, [7] Guangdong Provincial Key Laboratory of Genome Read and Write, BGI-Shenzhen, Shenzhen, China

OPEN ACCESS

Edited by:
Zhao-Qian Teng,
Chinese Academy of Sciences (CAS), China

Reviewed by:
Gufa Lin,
Tongji University, China
Zong Wei,
Mayo Clinic Arizona, United States

***Correspondence:**
Ying Gu
guying@genomics.cn
Chuanyu Liu
liuchuanyu@genomics.cn

†These authors have contributed equally to this work

Specialty section:
This article was submitted to Epigenomics and Epigenetics, a section of the journal Frontiers in Cell and Developmental Biology

Received: 08 January 2021
Accepted: 26 February 2021
Published: 30 March 2021

Citation:
Wei X, Li H, Guo Y, Zhao X, Liu Y, Zou X, Zhou L, Yuan Y, Qin Y, Mao C, Huang G, Yu Y, Deng Q, Feng W, Xu J, Wang M, Liu S, Yang H, Liu L, Liu C and Gu Y (2021) An ATAC-seq Dataset Uncovers the Regulatory Landscape During Axolotl Limb Regeneration. Front. Cell Dev. Biol. 9:651145. doi: 10.3389/fcell.2021.651145

Keywords: limb, regenertion, axolotl, ATAC-seq, regulatory element

INTRODUCTION

Tissue regenerative potential varies significantly across species, tissues, and ages (Yun, 2015; Iismaa et al., 2018). For example, planarian can reconstruct its whole body from small fragments of the original organism (Pellettieri et al., 2010; Zeng et al., 2018); in contrast, many vertebrate organs, such as the heart, can only regenerate primarily through preexisting proliferating cardiomyocytes, like in adult zebrafish and neonatal mice (Vivien et al., 2016). Since Spallanzani first reported the salamander regeneration in 1760s, scientists have been devoted to decipher the codes of such powerful regenerative capability (Dinsmore, 1991). Using different methods to analyze the cellular and molecular phenomena during salamander limb or tail regeneration, researchers revealed complex processes including clotting, immune activation, apoptosis, and reprogramming (Tanaka, 2016). Within such process, a mass of cells called blastema proliferates from the wounded site and fully regenerates the lost body part (McCusker et al., 2015; Haas and Whited, 2017).

Axolotl (*Ambystoma mexicanum*) is a species of salamander, which has been used as the model animal to investigate key biological processes such as embryo development, limb regeneration, and central nervous system regeneration for nearly 150 years (Pietsch, 1961; Schreckenberg and Jacobson, 1975; Seyedhassantehrani et al., 2017). Although several studies have focused on bulk transcriptome studies (Monaghan et al., 2009; Campbell et al., 2011; Knapp et al., 2013; Stewart et al., 2013; Wu et al., 2013; Bryant et al., 2017), the axolotl genome was not assembled until 2018 with features of large sizes (32 Gb) and abundant repetitive sequences (Nowoshilow et al., 2018). Interestingly, in axolotl, intron size expands 13- to 25-fold in non–developmentally related orthologous genes and 6- to 11-fold in developmentally related orthologous genes as compared to human, mouse, and frog, thus indicating that a more complex regulatory network in non-coding regions may play an important role in both development and regeneration (Nowoshilow et al., 2018). Since the first axolotl genome assembly, multiple studies have been carried out to investigate the transcriptomic patterns of axolotl limb regeneration at single-cell resolution (Gerber et al., 2018; Leigh et al., 2018; Qin et al., 2020). These studies used single-cell gene expression variations to reflect dynamic cell population changes and cell fate transitions, as well as unique immune responses during regeneration (Tsai et al., 2019; Li et al., 2020; Rodgers et al., 2020). Standing on the shoulder of these studies and looking forward, analysis of the epigenetic regulations, which are responsible for the dynamic gene expression changes, will help scientists to better understand the underlying mechanisms of the regenerative process.

To identify crucial regulatory elements and transcription factors (TFs) that drive or support the regenerative response, the assay for transposase-accessible chromatin using sequencing (ATAC-seq) has been used to profile the chromatin accessibility dynamics in multiple species (Buenrostro et al., 2015). For instance, a genome-wide scan for TF binding motifs in thousands of chromatin regions revealed by ATAC-seq highlighted the role of EGR (early growth response) as a pioneer factor to directly activate regeneration-related genes in *Hofstenia* (Gehrke et al., 2019). In addition to TFs, enhancers also have great significance in regeneration. The conserved teleost regeneration response enhancers in zebrafish and African killifish (*Nothobranchius furzeri*) were uncovered by histone H3K27ac chromatin immunoprecipitation sequencing (ChIP-seq, a marker for active enhancers), bulk RNA sequencing (RNA-seq), and single-cell RNA sequencing (scRNA-seq) (Wang et al., 2020). These studies suggested that epigenetic regulatory elements play fundamental roles in regeneration. However, how the non-coding axolotl genome responds to wounding to regulate gene expression and consequently drive the process of limb regeneration remains to be elucidated.

Here, we present a comprehensive dataset of chromatin accessibility for eight stages of the axolotl limb regeneration process, including homeostatic [uninjured control, 0 h after amputation (0 hpa)], trauma (3 hpa), wounding healing (1 day after amputation, 1 dpa), early-bud blastema (3 dpa), midbud blastema (7 dpa), late-bud blastema (14 dpa), palette stage (22 dpa), and redifferentiated stages (33 dpa) (**Figure 1A**). These time points represent the main events during axolotl limb regeneration, making this dataset a valuable platform to understand the complex regulatory network from an overall perspective. We generated 24 samples from the eight stages of limb tissues (three biological replicates per group). Systematic analysis of our dataset identified a total of 342,341 peaks, of which 33,604 showed transient dynamic patterns. We further investigated the occupancy of TFs in clusters with different peaks, which may help to explain the activation and manipulation of these regulatory elements during injury response and regeneration process (**Figure 1B**).

MATERIALS AND METHODS

Sample Collection

The institutional review board approved all experiments in this study on the ethics committee of BGI (permit BGI-IRB 19059). Axolotl breeding, housing, and tissue isolation were performed as previously described (Li et al., 2020). Briefly, we anesthetized the axolotls with 0.2% Tricaine (ethyl 3-aminobenzoate methane sulfonate) before the amputation surgery. The lower forearm tissues were isolated at eight time points including the homeostatic stage (uninjured control, 0 hpa), trauma (3 hpa), wound healing stage (1 dpa), early-bud blastema (3 dpa), midbud blastema (7 dpa), late-bud blastema (14 dpa), palette (22 dpa), and redifferentiation stage (33 dpa), with three replicates for each stage. These eight time points represent the main phases of axolotl limb regeneration. All tissues were washed with amphibian phosphate-buffered saline for three times before further operation. Tissues were enzymatically digested to cell suspension using 0.2% collagenase type I (BBI, cat. #A004194-0001) and 0.2% collagenase type II (BBI, cat. #A004174-0001) at room temperature for 1 h.

ATAC-seq Library Preparation and Sequencing

Tissues were transferred to the bottom of the Dounce Homogenizer and dounced within 1 mL 1× Homogenization Buffer Stable Master Mix until resistance goes away (∼30 strokes). The cells were then passed through a 100-μm strainer into a clean Dounce Homogenizer and dounced again for 20 strokes. Nuclei were collected through a 40-μm strainer and counted. Around 50,000 nuclei were transferred into a tube containing 1 mL wash buffer (ATAC-RSB+0.1% Tween-20), and then the samples were centrifuged at 500 rcf at 4°C for 5 min. Transposition reaction was performed as the Omni-ATAC-seq method (Corces et al., 2017). Nuclei were then transferred into 50 μL transposition reaction mixture containing 10 μL of 5× TAG buffer (BGI, cat. #BGE005B01), 2.5 μL of transposase (100 nM final, BGI, cat. #BGE005), 31.5 μL of PBS, 0.5 μL of 1% digitonin, 0.5 μL of 10% Tween-20, and 5 μL of H_2O for 30 min at 37°C in a thermomixer by 1,000 rpm.

The transposed DNA was purified with a DNA MinElute kit (Qiagen, Germany) and eluted with 20 μL nuclease-free H_2O. The purified DNA was amplified for eight cycles using a reaction mixture containing 2.5 μL of Tn5 Ad153 N5 primer (20 μM), 2.5 μL of Tn5 Ad153 N7 primer (20 μM), 25 μL of NEB Next High-Fidelity 2× polymerase chain reaction (PCR) Master Mix, with a PCR protocol of 72°C for 5 min, 98°C for 30 s, and then eight cycles of 98°C for 10 s, 63°C for 30 s,72°C for 1 min, finally by 72°C for 10 min and hold at 4°C. The 300- to 500-bp size PCR product was selected using AMPure XP beads (Agencourt, cat. #A63882) according to the manual. All libraries were further prepared based on BGISEQ-500 sequencing platform with pair-end 50-bp read length (Huang et al., 2017).

Preprocessing of the ATAC-seq Datasets

The data of ATAC-seq were trimmed with SOAPnuke (Chen et al., 2018), and reads were aligned to axolotl genome (Nowoshilow et al., 2018) (https://www.axolotl-omics.org/assemblies) by using Sentieon bwa mem (parameter: -K 100,000,000 -M -t 40) (Li, 2013). Subsequently, we filtered out reads with mapping quality of <30. PCR duplicate reads were discarded by applying Picard's MarkDuplicates (http://broadinstitute.github.io/picard/) (Picard Toolkit, 2019). We next performed model-based analysis of ChIP-seq (MACS2) to identify the peak regions with options -B, -q 0.01 –nomodel, -f BAM (Zhang et al., 2008). The irreproducible discovery rate (IDR) method was employed to identify reproducible high-quality peaks between each two biological replicates (Li et al., 2011). Peak signal can be visualized in IGV by the Broad Institute (http://software.broadinstitute.org/software/igv/). A standard peak list was established by merging reproducible peaks of each two replicates for each time point. The standard peak count matrix was calculated using the intersect function of BedTools (Quinlan and Hall, 2010).

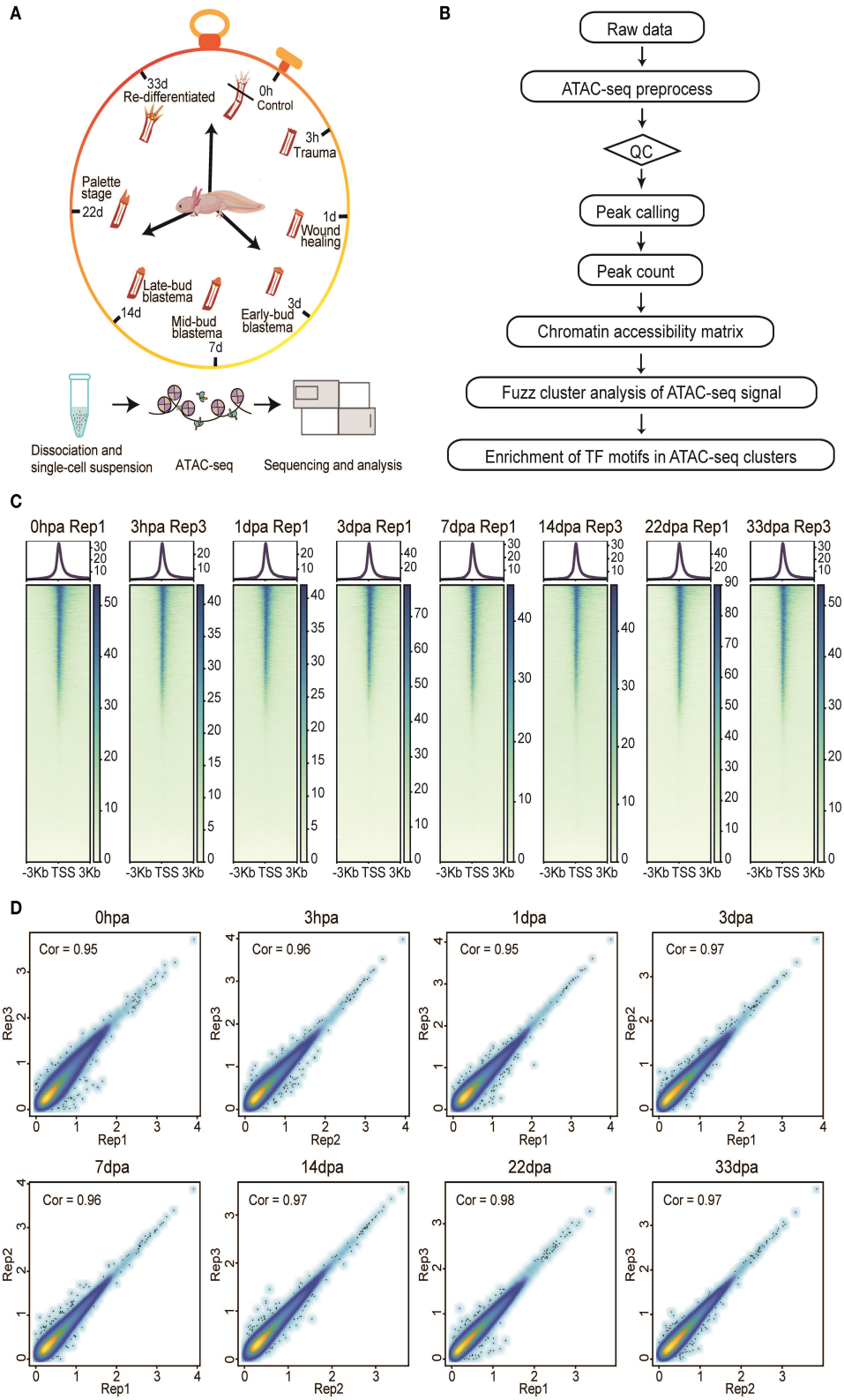

FIGURE 1 | Overview of the experimental, data analysis workflow, and ATAC-seq data quality metrics. **(A)** Three biological replicates ($n > 3$) from eight stages of the axolotl limb regeneration process were collected for ATAC-seq profiling. **(B)** The analysis workflow for ATAC-seq profiles. **(C)** The ATAC-seq signal enrichment around the transcription start sites (TSSs) for eight representative samples. **(D)** Scatter plots showing the Pearson correlations between biological replicates.

Identification of Dynamic Chromatin Accessible Regions

Reads per million mapped reads (RPM) algorithm was used to normalize the raw count matrix (Wei, 2020). Pearson correlations based on the Log10 RPM matrix were used to calculate the coefficients between different biological replicates across every stage. The RPM matrix for biological replicates was aggregated, and peaks with an average of RPM <1 at all time points were removed. Peaks across time with <50 coefficient of variation were filtered out to form a pseudocluster prior to clustering, which reflects the regions with stable accessibility throughout the regeneration. The remaining peaks were then transformed into normalized data using *Z* score method, followed by performing time course c-means fuzzy clustering with a cluster membership cutoff of 0.8 (Kumar and Futschik, 2007).

Relative genomic region was determined by overlapping each peak with features defined in the custom's annotated genes. The distance to transcription start sites (TSSs) was calculated according to the distance between the peak center and the nearest TSSs using the *distanceToNearest* function in GenomicRanges packages (Lawrence et al., 2013).

Functional enrichment of peaks in each cluster with distance to TSSs <10,000 bp was performed by using the clusterProfiler R package (Yu et al., 2012), with a *q*-value threshold of 0.1 for statistical significance.

The findMotifsGenome.pl script of the HOMER software was employed to perform transcript factor enrichment analysis in regeneration dynamic peaks with default settings (Heinz et al., 2010).

Pseudobulk RNA-seq Analysis

To investigate the correlation between chromatin dynamics and gene expression changes, we took advantage of single-cell RNA-seq data of these eight stages we published previously and calculated the average expression of each gene to construct a pseudobulk gene expression matrix (Li et al., 2020). Correlation analysis was done between the chromatin accessibility of promoters (TSS ± 2 kb) and closest genes' expression.

RESULTS

ATAC-seq Quality Control and Reproducibility of Biological Samples

We inspected our ATAC-seq dataset by regularly used statistics, such as the number of total reads, number of mapped reads, percentage of mapped reads, the number of usable reads, the percentage of final usable reads, and the number of peaks (**Supplementary Table 1**). We generated more than 1,000 million ATAC-seq reads for each replicate on average. Among these reads, we detected strong enrichment around TSSs (Wei, 2020) (**Figure 1C**). Moreover, size periodicity of the chromatin accessibility fragments corresponding to integer multiples of nucleosomes (Wei, 2020) demonstrated the reliability of our dataset, this being consistent with previously published ATAC-seq profiles (Buenrostro et al., 2013) (**Supplementary Figure 1**).

To assess the reproducibility of chromatin accessibility regions between biological replicates, we used the IDR method to filter peaks that overlapped between replicates in each regeneration stage. Pearson correlations based on the Log_{10} RPM matrix were used to calculate the coefficients, showing that a correlation coefficient is higher than 0.9 between each two replicates in each stage, with the exception of replicate 1 from 3 hpa, which was removed for downstream analysis (**Figure 1D**).

Temporal Dynamics of Chromatin Accessibility During Regeneration

To explore the chromatin accessibility with temporal dynamic features during regeneration, we used normalized ATAC-seq read counts in peaks to perform time-course fuzzy clustering. This approach yielded six separated clusters, which indicate six distinct categories defined by regions: (1) those that become accessible transiently at 22- and 33-dpa stages, cluster 1 (C1, $n = 5{,}930$); (2) regions that are close in the intermediate period of regeneration but accessible after 14 dpa, cluster 2 (C2, $n = 3{,}838$); (3) regions in which accessibility is established only at 22-dpa stage, cluster 3 (C3, $n = 6{,}797$); (4) regions accessible in the control but that exhibit loss of accessibility shortly at 3 hpa and later stages, cluster 4 (C4, $n = 2{,}454$); (5) regions that are accessible in specifically at 3 hpa and 14 dpa, cluster 5 (C5, $n = 7{,}727$); (6) regions that are stably accessible at the intermediate stages of regeneration, cluster 6 (C6, $n = 6{,}858$). This clustering highlighted several characteristics of chromatin reconfiguration during regeneration (**Figure 2A**). These data collectively demonstrated that the chromatin state is remodeling rapidly in the first few hours following amputation, to prepare for the subsequent regeneration process. The dynamics of chromatin accessibility provides a new perspective to understand the cell fate decision in axolotl limb regeneration process.

Peaks in C1 are highly enriched in Gene Ontology (GO) terms related to axonogenesis. Examples of C1 include a promoter in the *Ndnf* locus, which is a novel neurotrophic factor derived from neurons that may be useful in the treatment of neuronal degeneration diseases and nerve injuries (Kuang et al., 2010). C2 consists of elements that are highly accessible in the extracellular matrix organization and connective tissue development. For example, *Col11a2*, a fibril-forming collagen found mainly in the cartilage extracellular matrix, is important for the integrity and development of the skeleton (Lui et al., 1996). We also found some genes associated to limb morphogenesis in C3 such as the Hoxbox gene, *Evx2*, and *Hoxd10* (Herault et al., 1996; Tarchini and Duboule, 2006). GO terms enriched in C4 were related to muscle cell development, whereas those in C5 were related to epidermis development. Interestingly, we observed some immune response–related GO terms in C6, such as T-cell activation and myeloid cell differentiation (**Figures 2B,C**), which is consistent with the inflammatory process following injury (**Supplementary Figure 2**).

TF Enrichment of Dynamic *cis*-Regulatory Elements

Our analysis also indicated that the binding site for TF that bound to C1 is enriched for NeuroG2 (**Figure 2D**). NeuroG2 is a TF that can specify a neuronal fate and expressed in neural

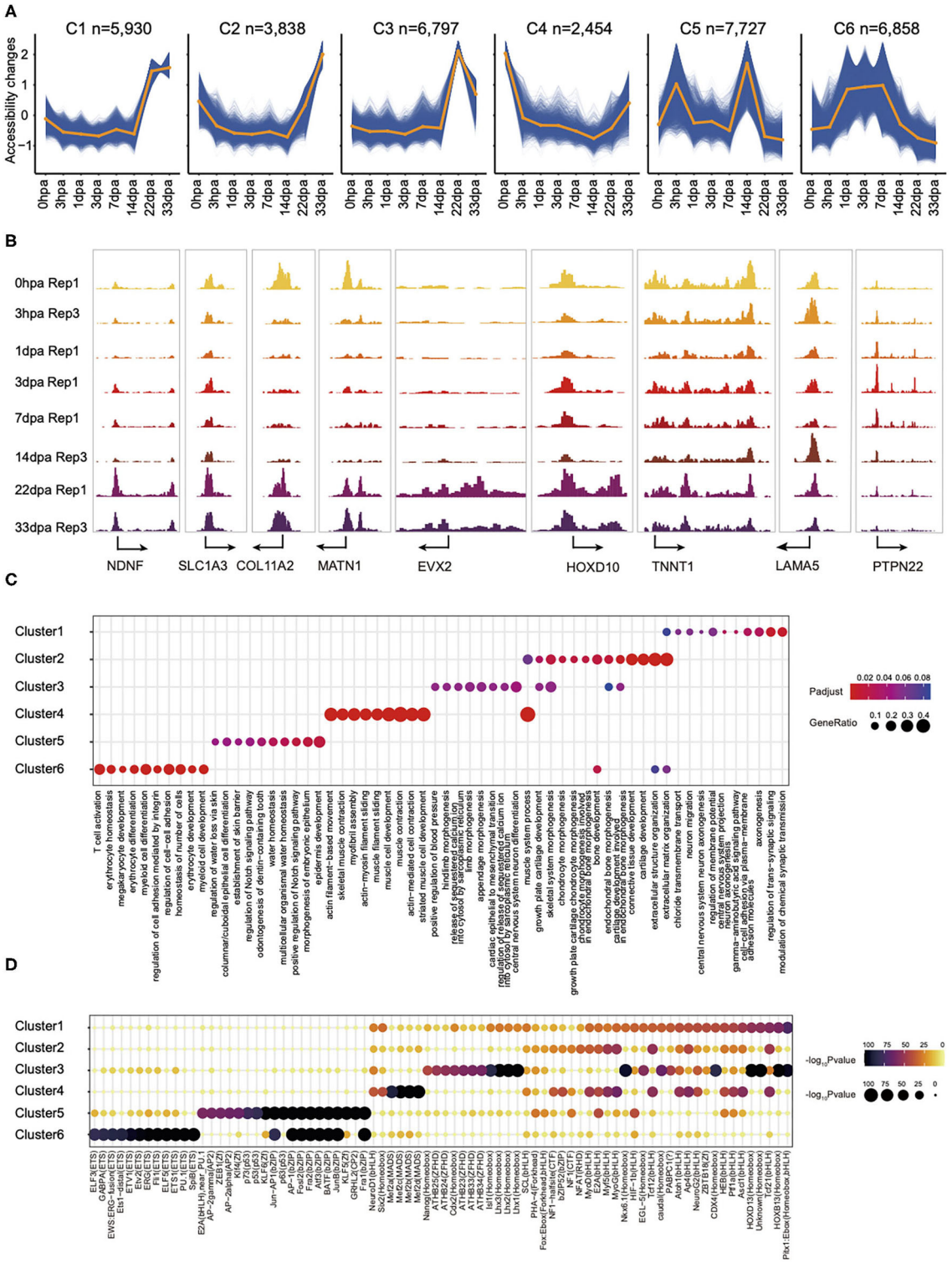

FIGURE 2 | The landscape of chromatin accessibility dynamic changes in axolotl limb regeneration and potential function of dynamic elements identification. **(A)** Fuzzy cluster analysis of ATAC-seq signal. Line plots show standardized ATAC-seq signal, with individual blue lines representing individual loci and the orange line representing the cluster center's values. **(B)** Genome browser views of ATAC-seq signal for the dynamic peaks. **(C)** Enrichment of GO terms in ATAC-seq clusters. Where a point is present, a significant enrichment for the go term of biological process (*x* axis) was found in the ATAC-seq clusters (*y* axis). Point size represents the gene ratio in the go term, and color represents the adjusted *P*-value. **(D)** Enrichment of the indicated TF motifs in each ATAC-seq cluster. The size and color of each point represent the motif enrichment *P*-value (–log10 *P*-value).

progenitor cells within the developing central and peripheral nervous systems (Dennis et al., 2019). Notably, we also observed major binding events for the pioneer factor PU.1 in C6, this being a master transcriptional regulator in activating many target genes during both myeloid and B-lymphoid development (Turkistany and DeKoter, 2011). In addition, transcript factors from the MyoG, MyoD, and Mef families, which are essential for the development of functional skeletal muscle, were found in C4 (Al-Khalili et al., 2004; Ganassi et al., 2020). Taken together, we provide a high-quality comprehensive dataset to study the regenerative epigenomic dynamics of axolotl limb regeneration.

CONCLUSIONS

To summarize, by applying the state-of-the-art technique ATAC-seq, we provide the first chromatin accessibility landscape in axolotl regenerative limb tissues from the immediate response stage to the complete recovery stage. These data will be of great importance to the studies of various scientific disciplines such as development, cell reprogramming, and mechanisms underlying regeneration. Further analysis of these datasets by focusing on the differentially regulated regions may help deduce key regulatory elements that are critical for regeneration initiation in the axolotl limb in the future.

DATA AVAILABILITY STATEMENT

All raw data have been submitted to the CNGB (Nucleotide Sequence Archive) (https://db.cngb.org/search/project/CNP0001445/), and also the NCBI (SRA) (https://www.ncbi.nlm.nih.gov/search/all/?term=PRJNA682840).

ETHICS STATEMENT

The animal study was reviewed and approved by the Ethics Committee of BGI.

AUTHOR CONTRIBUTIONS

XW, YGu, HL, CL, YGuo, and XZh conceived the idea. YGuo and XZh collected samples. XZh and YGuo generated the data. HL, YYua, YQ, CM, JX, MW, YYu, and QD assisted with the experiments. XW analyzed the data with the assistance from YL, XZo, LZ, GH, and WF. XW wrote the manuscript with the input of HL, YGuo, and XZh. YGu and CL supervised the study and revised the manuscript. LL, HY, and SL provided helpful comments on this study. All authors reviewed and approved the final manuscript.

FUNDING

This work was supported by the Strategic Priority Research Program of the Chinese Academy of Sciences (Grant No. XDA16010000) and Guangdong Provincial Key Laboratory of Genome Read and Write (2017B030301011).

ACKNOWLEDGMENTS

We thank the Center for Digitizing Cells, Institute of SuperCells, BGI-Shenzhen for helpful comments. This work is supported by China National GeneBank for providing sequencing service. We also thank Liang Chen from Hubei Key Laboratory of Cell Homeostasis, College of Life Sciences, Wuhan University and Giacoma Volpe from GIBH for valuable advice.

SUPPLEMENTARY MATERIAL

The Supplementary Material for this article can be found online at: https://www.frontiersin.org/articles/10.3389/fcell.2021.651145/full#supplementary-material

Supplementary Table 1 | ATAC-seq metadata and mapping statistics. *Mapped reads: total number of reads minus number of unaligned reads. *Usable reads: number of mapped reads minus number of low mapping quality and duplicate reads.

Supplementary Figure 1 | The insert size distribution of ATAC-seq profiles for the same samples shown in **Figure 2A**.

Supplementary Figure 2 | Decomposition of chromatin accessibility and gene expression dynamics during axolotl limb regeneration. **(A)** Chromatin accessibility dynamics of promoters (TSS ± 2 kb) in six clusters. **(B)** Pseudobulk gene expression in **(A)**. **(C)** Heatmap shows the correlation between bulk ATAC-seq and pseudobulk RNA for each gene in C6. **(D)** Chromatin accessibility and gene expression for genes in C6.

REFERENCES

Al-Khalili, L., Chibalin, A. V., Yu, M., Sjodin, B., Nylén, C., Zierath, J. R., et al. (2004). MEF2 activation in differentiated primary human skeletal muscle cultures requires coordinated involvement of parallel pathways. *Am. J. Physiol. Cell Physiol.* 286, C1410–C1416. doi: 10.1152/ajpcell.00444.2003

Bryant, D. M., Johnson, K., DiTommaso, T., Tickle, T., Couger, M. B., Payzin-Dogru, D., et al. (2017). A tissue-mapped axolotl de novo transcriptome enables identification of limb regeneration factors. *Cell Rep*. 18, 762–776. doi: 10.1016/j.celrep.2016.12.063

Buenrostro, J. D., Giresi, P. G., Zaba, L. C., Chang, H. Y., and Greenleaf, W. J. (2013). Transposition of native chromatin for fast and sensitive epigenomic profiling of open chromatin, DNA-binding proteins and nucleosome position. *Nat. Methods* 10:1213. doi: 10.1038/nmeth.2688

Buenrostro, J. D., Wu, B., Chang, H. Y., and Greenleaf, W. J. (2015). ATAC-seq: a method for assaying chromatin accessibility genome-wide. *Curr. Protoc. Mol. Biol*. 109, 21–29. doi: 10.1002/0471142727.mb2129s109

Campbell, L. J., Suárez-Castillo, E. C., Ortiz-Zuazaga, H., Knapp, D., Tanaka, E. M., and Crews, C. M. J. D.D. (2011). Gene expression profile of the regeneration epithelium during axolotl limb regeneration. *Dev. Dyn*. 240, 1826–1840. doi: 10.1002/dvdy.22669

Chen, Y., Chen, Y., Shi, C., Huang, Z., Zhang, Y., Li, S., et al. (2018). SOAPnuke: a MapReduce acceleration-supported software for integrated quality control and preprocessing of high-throughput sequencing data. *Gigascience* 7:gix120. doi: 10.1093/gigascience/gix120

Corces, M. R., Trevino, A. E., Hamilton, E. G., Greenside, P. G., Sinnott-Armstrong, N. A., Vesuna, S., et al. (2017). An improved ATAC-seq protocol reduces background and enables interrogation of frozen tissues. *Nat. Methods* 14, 959–962. doi: 10.1038/nmeth.4396

Dennis, D. J., Han, S., and Schuurmans, C. (2019). bHLH transcription factors in neural development, disease, and reprogramming. *Brain Res*. 1705, 48–65. doi: 10.1016/j.brainres.2018.03.013

Dinsmore, C. E. (1991). A *H*istory of *R*egeneration *Research: Milestones in the Evolution of a Science*. Cambridge: Cambridge University Press.

Ganassi, M., Badodi, S., Wanders, K., Zammit, P. S., and Hughes, S. M. (2020). Myogenin is an essential regulator of adult myofibre growth and muscle stem cell homeostasis. *Elife* 9:e60445. doi: 10.7554/eLife.60445.sa2

Gehrke, A. R., Neverett, E., Luo, Y.-J., Brandt, A., Ricci, L., Hulett, R. E., et al. (2019). Acoel genome reveals the regulatory landscape of whole-body regeneration. *Science* 363:6173. doi: 10.1126/science.aau6173

Gerber, T., Murawala, P., Knapp, D., Masselink, W., Schuez, M., Hermann, S., et al. (2018). Single-cell analysis uncovers convergence of cell identities during axolotl limb regeneration. *Science* 362:681. doi: 10.1126/science.aaq0681

Haas, B. J., and Whited, J. L. (2017). Advances in decoding axolotl limb regeneration. *Trends Genet*. 33, 553–565. doi: 10.1016/j.tig.2017.05.006

Heinz, S., Benner, C., Spann, N., Bertolino, E., Lin, Y. C., Laslo, P., et al. (2010). Simple combinations of lineage-determining transcription factors prime cis-regulatory elements required for macrophage and B cell identities. *Mol. Cell* 38, 576–589. doi: 10.1016/j.molcel.2010.05.004

Herault, Y., Hraba-Renevey, S., Van der Hoeven, F., and Duboule, D. (1996). Function of the Evx-2 gene in the morphogenesis of vertebrate limbs. *EMBO J.* 15, 6727–6738. doi: 10.1002/j.1460-2075.1996.tb01062.x

Huang, J., Liang, X., Xuan, Y., Geng, C., Li, Y., Lu, H., et al. (2017). A reference human genome dataset of the BGISEQ-500 sequencer. *Gigascience* 6:gix024. doi: 10.1093/gigascience/gix024

Iismaa, S. E., Kaidonis, X., Nicks, A. M., Bogush, N., Kikuchi, K., Naqvi, N., et al. (2018). Comparative regenerative mechanisms across different mammalian tissues. *NPJ Regen. Med.* 3, 1–20. doi: 10.1038/s41536-018-0044-5

Knapp, D., Schulz, H., Rascon, C. A., Volkmer, M., Scholz, J., Nacu, E., et al. (2013). Comparative transcriptional profiling of the axolotl limb identifies a tripartite regeneration-specific gene program. *PLoS ONE* 8:e61352. doi: 10.1371/journal.pone.0061352

Kuang, X.-L., Zhao, X.-M., Xu, H.-F., Shi, Y.-Y., Deng, J.-B., and Sun, G.-T. (2010). Spatio-temporal expression of a novel neuron-derived neurotrophic factor (NDNF) in mouse brains during development. *BMC Neurosci.* 11, 1–11. doi: 10.1186/1471-2202-11-137

Kumar, L., and Futschik, M. E. (2007). Mfuzz: a software package for soft clustering of microarray data. *Bioinformation* 2:5. doi: 10.6026/97320630002005

Lawrence, M., Huber, W., Pages, H., Aboyoun, P., Carlson, M., Gentleman, R., et al. (2013). Software for computing and annotating genomic ranges. *PLoS Comput. Biol.* 9:e1003118. doi: 10.1371/journal.pcbi.1003118

Leigh, N. D., Dunlap, G. S., Johnson, K., Mariano, R., Oshiro, R., Wong, A. Y., et al. (2018). Transcriptomic landscape of the blastema niche in regenerating adult axolotl limbs at single-cell resolution. *Nat. Commun.* 9, 1–14. doi: 10.1038/s41467-018-07604-0

Li, H. (2013). Aligning sequence reads, clone sequences and assembly contigs with BWA-MEM. *arXiv [Preprint]*. arXiv:1303.3997. doi: 10.6084/M9.FIGSHARE.963153.V1

Li, H., Wei, X., Zhou, L., Zhang, W., Wang, C., Guo, Y., et al. (2020). Dynamic cell transition and immune response landscapes of axolotl limb regeneration revealed by single-cell analysis. *Protein Cell* 12, 57–66. doi: 10.1007/s13238-020-00763-1

Li, Q., Brown, J. B., Huang, H., and Bickel, P. J. (2011). Measuring reproducibility of high-throughput experiments. *Ann. Appl. Stat.* 5, 1752–1779. doi: 10.1214/11-AOAS466

Lui, V. C., Ng, L. J., Sat, E. W., and Cheah, K. S. (1996). The human α2 (XI) collagen gene (COL11A2): completion of coding information, identification of the promoter sequence, and precise localization within the major histocompatibility complex reveal overlap with the KE5 gene. *Genomics* 32, 401–412. doi: 10.1006/geno.1996.0135

McCusker, C., Bryant, S. V., and Gardiner, D. M. (2015). The axolotl limb blastema: cellular and molecular mechanisms driving blastema formation and limb regeneration in tetrapods. *Regeneration* 2, 54–71. doi: 10.1002/reg2.32

Monaghan, J. R., Epp, L. G., Putta, S., Page, R. B., Walker, J. A., Beachy, C. K., et al. (2009). Microarray and cDNA sequence analysis of transcription during nerve-dependent limb regeneration. *BMC Biol.* 7:1. doi: 10.1186/1741-7007-7-1

Nowoshilow, S., Schloissnig, S., Fei, J.-F., Dahl, A., Pang, A. W., Pippel, M., et al. (2018). The axolotl genome and the evolution of key tissue formation regulators. *Nature* 554, 50–55. doi: 10.1038/nature25458

Pellettieri, J., Fitzgerald, P., Watanabe, S., Mancuso, J., Green, D. R., and Alvarado, A. S. (2010). Cell death and tissue remodeling in planarian regeneration. *Dev. Biol.* 338, 76–85. doi: 10.1016/j.ydbio.2009.09.015

Picard Toolkit (2019). *Broad Institute, GitHub Repository*. Available online at: http://broadinstitute.github.io/picard/

Pietsch, P. (1961). Differentiation in regeneration I. The development of muscle and cartilage following deplantation of regenerating limb blastemata of Amblystoma larvae. *Dev. Biol.* 3, 255–264. doi: 10.1016/0012-1606(61)90046-X

Qin, T., Fan, C.-m., Wang, T.-z., Sun, H., Zhao, Y.-y., Yan, R.-j., et al. (2020). Single-cell RNA-seq reveals novel mitochondria-related musculoskeletal cell populations during adult axolotl limb regeneration process. *Cell Death Diff.* 28, 1110–1125. doi: 10.1038/s41418-020-00640-8

Quinlan, A. R., and Hall, I. M. (2010). BEDTools: a flexible suite of utilities for comparing genomic features. *Bioinformatics* 26, 841–842. doi: 10.1093/bioinformatics/btq033

Rodgers, A. K., Smith, J. J., and Voss, S. R. (2020). Identification of immune and non-immune cells in regenerating axolotl limbs by single-cell sequencing. *Exp. Cell Res.* 394:112149. doi: 10.1016/j.yexcr.2020.112149

Schreckenberg, G., and Jacobson, A. (1975). Normal stages of development of the axolotl, Ambystoma mexicanum. *Dev. Biol.* 42, 391–399. doi: 10.1016/0012-1606(75)90343-7

Seyedhassantehrani, N., Otsuka, T., Singh, S., and Gardiner, D. M. (2017). The axolotl limb regeneration model as a discovery tool for engineering the stem cell niche. *Curr. Stem Cell Rep.* 3, 156–163. doi: 10.1007/s40778-017-0085-5

Stewart, R., Rascón, C. A., Tian, S., Nie, J., Barry, C., Chu, L. F., et al. (2013). Comparative RNA-seq analysis in the unsequenced axolotl: the oncogene burst highlights early gene expression in the blastema *PLoS Comput. Biol.* 9:e1002936. doi: 10.1371/journal.pcbi.1002936

Tanaka, E. M. (2016). The molecular and cellular choreography of appendage regeneration. *Cell* 165, 1598–1608. doi: 10.1016/j.cell.2016.05.038

Tarchini, B., and Duboule, D. (2006). Control of Hoxd genes' collinearity during early limb development. *Dev. Cell* 10, 93–103. doi: 10.1016/j.devcel.2005.11.014

Tsai, S. L., Baselga-Garriga, C., and Melton, D. A. (2019). Blastemal progenitors modulate immune signaling during early limb regeneration. *Development* 146:e169128. doi: 10.1242/dev.169128

Turkistany, S. A., and DeKoter, R. P. (2011). The transcription factor PU. 1 is a critical regulator of cellular communication in the immune system. *Arch. Immunol. Ther. Exp.* 59, 431–440. doi: 10.1007/s00005-011-0147-9

Vivien, C. J., Hudson, J. E., and Porrello, E. R. (2016). Evolution, comparative biology and ontogeny of vertebrate heart regeneration. *NPJ Regen. Med.* 1, 1–14. doi: 10.1038/npjregenmed.2016.12

Wang, W., Hu, C.-K., Zeng, A., Alegre, D., Hu, D., Gotting, K., et al. (2020). Changes in regeneration-responsive enhancers shape regenerative capacities in vertebrates. *Science* 369:3090. doi: 10.1126/science.aaz3090

Wei, X. (2020). *An ATAC-seq Dataset Uncovers the Regulatory Landscape Axolotl Limb Regeneration*. Available online at: https://doi.org/10.6084/m9.figshare.13370468.v1

Wu, C. H., Tsai, M. H., Ho, C. C., Chen, C. Y., and Lee, H. S. J. B.G. (2013). De novo transcriptome sequencing of axolotl blastema for identification of differentially expressed genes during limb regeneration. *BMC Genomics* 14:434. doi: 10.1186/1471-2164-14-434

Yu, G., Wang, L.-G., Han, Y., and He, Q.-Y. (2012). clusterProfiler: an R package for comparing biological themes among gene clusters. *Omics* 16, 284–287. doi: 10.1089/omi.2011.0118

Yun, M. H. (2015). Changes in regenerative capacity through lifespan. *Int. J. Mol. Sci.* 16, 25392–25432. doi: 10.3390/ijms161025392

Zeng, A., Li, H., Guo, L., Gao, X., McKinney, S., Wang, Y., et al. (2018). Prospectively isolated tetraspanin(+) neoblasts are adult pluripotent stem cells underlying planaria regeneration. *Cell* 173, 1593–1608. doi: 10.1016/j.cell.2018.05.006

Zhang, Y., Liu, T., Meyer, C. A., Eeckhoute, J., Johnson, D. S., Bernstein, B. E., et al. (2008). Model-based analysis of ChIP-Seq (MACS). *Genome Biol.* 9, 1–9. doi: 10.1186/gb-2008-9-9-r137

Conflict of Interest: The authors declare that the research was conducted in the absence of any commercial or financial relationships that could be construed as a potential conflict of interest.

frontiers in Cell and Developmental Biology

REVIEW
published: 25 May 2021
doi: 10.3389/fcell.2021.679662

m^{6}A Modification in Mammalian Nervous System Development, Functions, Disorders, and Injuries

Jun Yu[1,2], *Yuanchu She*[1] *and Sheng-Jian Ji*[1]*

[1] *Shenzhen Key Laboratory of Gene Regulation and Systems Biology, Brain Research Center, Department of Biology, School of Life Sciences, Southern University of Science and Technology, Shenzhen, China,* [2] *SUSTech-HKU Joint Ph.D. Program, School of Biomedical Sciences, Li Ka Shing Faculty of Medicine, The University of Hong Kong, Hong Kong, China*

N^6-methyladenosine (m^{6}A) modification, as the most prevalent internal modification on mRNA, has been implicated in many biological processes through regulating mRNA metabolism. Given that m^{6}A modification is highly enriched in the mammalian brain, this dynamic modification provides a crucial new layer of epitranscriptomic regulation of the nervous system. Here, in this review, we summarize the recent progress on studies of m^{6}A modification in the mammalian nervous system ranging from neuronal development to basic and advanced brain functions. We also highlight the detailed underlying mechanisms in each process mediated by m^{6}A writers, erasers, and readers. Besides, the involvement of dysregulated m^{6}A modification in neurological disorders and injuries is discussed as well.

Keywords: m^{6}A modification, nervous system, development, neurological disorders, learning and memory

OPEN ACCESS

Edited by:
Xuekun Li,
Zhejiang University, China

Reviewed by:
Ki-Jun Yoon,
Korea Advanced Institute of Science and Technology, South Korea
Sunita Singh,
Baylor College of Medicine, United States

****Correspondence:***
Sheng-Jian Ji
jisj@sustech.edu.cn

Specialty section:
This article was submitted to Epigenomics and Epigenetics, a section of the journal Frontiers in Cell and Developmental Biology

Received: *12 March 2021*
Accepted: *03 May 2021*
Published: *25 May 2021*

Citation:
Yu J, She Y and Ji S-J (2021) m^{6}A Modification in Mammalian Nervous System Development, Functions, Disorders, and Injuries. Front. Cell Dev. Biol. 9:679662. doi: 10.3389/fcell.2021.679662

INTRODUCTION

Messenger RNAs (mRNAs) play crucial roles in biological processes, which not only serve as messengers that pass genetic information from DNA to protein but also bear various post-transcriptional regulation mechanisms. Modifications on mRNA have been studied for several decades (Boccaletto et al., 2018). Other than 5′ cap and 3′ polyadenylation, numerous modified nucleotides such as *N*^{6}-methyladenosine (m^{6}A), *N*^{1}-methyladenosine (m^{1}A), *N*^{6},2′-O-dimethyladenosine (m^{6}A$_m$), 5-methylcytosine (m^{5}C), and 5-hydroxymethylcytosine (hm^{5}C) have been identified (Roundtree et al., 2017a). Modifications on mRNAs can change the structural properties of modified mRNAs, which affects the accessibility and affinity to specific RNA binding proteins (RBPs). Similar to chemical modifications on DNA and histone proteins, mRNA modifications have profound significance to biological processes.

m^{6}A modification, as the most prevalent internal chemical modification on mRNA, was found more than four decades ago (Desrosiers et al., 1974; Adams and Cory, 1975; Furuichi et al., 1975; Wei et al., 1975). However, due to the lack of detection methods, functional studies on m^{6}A were greatly hindered. The discovery of the first m^{6}A demethylase in 2011 led to a resurgence in exploring m^{6}A modification (Cao et al., 2016). Moreover, with the advances in biochemistry and sequencing technology in recent years, much progress has been achieved on m^{6}A modification.

The abundance of m^{6}A was estimated in a ratio of 0.1–0.4% of adenosine in mammals (about 3∼5 m^{6}A modification per mRNA) (Rottman et al., 1974; Wei et al., 1975; Fu et al., 2014). It occurs on the consensus motif DRACH (D means a non-cytosine base, R refers to G/A, A is the m^{6}A modified site, and H represents a non-guanine base) (Fu et al., 2014; Livneh et al., 2020).

m^{6}A modification is preferentially distributed in long coding exons, 3′ untranslated regions (UTR), and near the stop codon of mRNAs (Dominissini et al., 2012; Meyer et al., 2012). m^{6}A has been found to be dynamically regulated and involved in many biological processes by affecting the fate of modified mRNA. In this review, we will summarize the recent findings of m^{6}A modification in the nervous system from development to higher functions and from neurological disorders to injuries.

m^{6}A WRITERS, ERASERS, AND READERS

m^{6}A Writers

The deposition of m^{6}A modification on mRNA is mediated by a multi-component methyltransferase complex. The methyltransferases are also called m^{6}A writers, including methyltransferase-like 3 (METTL3), methyltransferase-like 14 (METTL14), and Wilms tumor 1-associated protein (WTAP) (Bokar et al., 1997; Liu et al., 2014; Ping et al., 2014; Schwartz et al., 2014). During the methylation process, METTL3 and METTL14 form a stable heterodimer complex and work synergistically to regulate adenosine methylation. METTL3 is the catalytically active enzymatic component, while METTL14 is an allosteric activator (Sledz and Jinek, 2016; Wang P. et al., 2016; Wang X. et al., 2016). This METTL3-METTL14 complex catalyzes the vast majority of m^{6}A modification on mRNA, as ablation of METTL3 or inactivation of METTL14 in mouse embryonic stem cells leads to the loss of more than 99% of total m^{6}A in mRNA (Geula et al., 2015). The remaining modified m^{6}A residues in mRNA could be catalyzed by METTL16 or other potential methyltransferases (Zaccara et al., 2019). WTAP is a critical adaptor that translocates the METTL3-METTL14 complex into nuclear speckles, thus facilitating the methylation efficiency (Ping et al., 2014; Schwartz et al., 2014).

m^{6}A Erasers

The discovery of m^{6}A erasers (demethylases) proves that m^{6}A is a dynamic and reversible modification. The first m^{6}A eraser, fat mass and obesity-associated (FTO), was discovered in 2011 (Jia et al., 2011). FTO belongs to the Fe (II) and α-ketoglutarate-dependent AlkB family (Gerken et al., 2007), which was initially found to be associated with body weight and food intake in mice (Fischer et al., 2009; Church et al., 2010). It can effectively demethylate m^{6}A in both RNA and DNA *in vitro* (Jia et al., 2011). *In vivo*, FTO also demethylates specific mRNAs that affect neuronal signaling in the mouse brain (Hess et al., 2013). However, FTO was further found to preferentially demethylate m^{6}A$_m$ in the 5′ cap of mRNA (Mauer et al., 2017). Thus, more studies from the third parties would be required to solve this scientific dispute.

The second eraser of m^{6}A, alkB homolog 5 (ALKBH5), was related to fertility in mice (Zheng et al., 2013). It also belongs to the Fe (II) and α-ketoglutarate-dependent AlkB family. ALKBH5 can catalyze the demethylation of m^{6}A modification on mRNA both *in vitro* and *in vivo*, which influences the nuclear RNA export and metabolism (Zheng et al., 2013). Unlike FTO, ALKBH5 cannot demethylate m^{6}A$_m$ (Mauer et al., 2017).

m^{6}A Readers

N^6-methyladenosine modification exerts its function by recruiting m^{6}A-binding proteins, which are also called m^{6}A readers. There are two ways of reader proteins to bind to m^{6}A modification: direct binding and indirect binding. Direct binding relies on a specialized domain within the readers, which can directly recognize and bind to m^{6}A. The first direct reader proteins identified were the YTH (YT521-B homology) domain-containing proteins (Dominissini et al., 2012). The YTH domain is a highly conserved RNA binding domain identified in a wide range of eukaryotes (Stoilov et al., 2002). There are three classes of YTH domain-containing proteins in mammals, including the YTH domain-containing family protein (YTHDF) family, YTH domain-containing protein 1 (YTHDC1), and YTH domain-containing protein 2 (YTHDC2) (Patil et al., 2018). The indirect reader proteins include HNRNPC, HNRNPG, HNRNPA2B1, and IGF2bp proteins, which can bind m^{6}A through the mechanism of m^{6}A-dependent mRNA structural change (Zaccara et al., 2019).

Transcriptome-wide binding sequencing studies of endogenous (Patil et al., 2016) or overexpressed YTH proteins (Wang et al., 2014, 2015) using crosslinking and immunoprecipitation (CLIP) experiments showed that most YTH proteins bind to the m^{6}A consensus motif in mRNA. The distribution of the YTHDF family proteins' binding sites is similar to the distribution pattern of m^{6}A on mRNA (Patil et al., 2016). YTHDF proteins and YTHDC1 can recognize and selectively bind m^{6}A through an aromatic cage (hydrophobic pocket) formed by three tryptophans in the YTH domain (Li et al., 2014; Luo and Tong, 2014; Theler et al., 2014; Xu et al., 2014).

YTHDF Family Proteins

YTHDF family proteins contain three members: YTHDF1, YTHDF2, and YTHDF3. YTHDF proteins have the same binding specificity toward m^{6}A-modified mRNA (Xu et al., 2015). These three proteins share high similarity in amino acid sequence over their entire length and are expressed mainly in the cytoplasm (Patil et al., 2018). YTHDF proteins have almost identical YTH domains at C-terminal. Apart from the YTH domain, YTHDF family proteins contain a low-complexity region with no recognizable modular protein domain and include several P/Q/N-rich domains (Patil et al., 2018). The function of this low-complexity region is to lead mRNA-YTHDF complexes to undergo liquid-liquid phase separation to different endogenous compartments, like processing bodies (P-bodies), neuronal RNA granules, or stress granules (Ries et al., 2019).

YTHDF1

The role of YTHDF1 was found to promote the translation efficiency of m^{6}A-modified mRNA (Wang et al., 2015). It was shown that YTHDF1 plays a dual role in this process by delivering m^{6}A-modified mRNA to translation machinery and enhancing translation initiation (Wang et al., 2015). This could

be possibly caused by the loop structure mediated by eIF4G and the interaction between YTHDF1 and eIF3 (Wang et al., 2015).

YTHDF2

YTH domain-containing protein 2 was found to be implicated in enhancing the degradation of m^{6}A-modified mRNA (Wang et al., 2014). In this process, YTHDF2 binds to m^{6}A-modified mRNA and translocates those mRNA from the translatable pool into P-bodies, which are mRNA decay sites (Wang et al., 2014). However, other studies did not find the existence of YTHDF2 in P-bodies (Hubstenberger et al., 2017). The possible explanation is that the association between YTHDF2 and P-bodies is transient, which results in the difficulty to detect YTHDF2 in P-bodies. Another study found that YTHDF2 regulates mRNA stability by mediating mRNA deadenylation first and then translocating to P-bodies (Du et al., 2016). The N-terminal region of YTHDF2 is capable of recruiting the CCR4-NOT deadenylase complex, causing the deadenylation of mRNA (Du et al., 2016), which finally degrades mRNA. YTHDF2 also regulate endoribonucleolytic cleavage of m^{6}A-modified mRNA through interaction with RNase P/MRP, which is bridged by HRSP12 (Park et al., 2019).

YTHDF3

The role of YTHDF3 was characterized as working together with YTHDF1 and YTHDF2 to regulate the metabolism of m^{6}A-modified mRNA (Shi et al., 2017). It has a combined effect of YTHDF1 and YTHDF2, promoting both translation and decay of m^{6}A-modified mRNA (Shi et al., 2017). Knockdown of YTHDF3 reduces the RNA-binding specificity of both YTHDF1 and YTHDF2 (Shi et al., 2017). Compared with YTHDF1 and YTHDF2, YTHDF3 exerts its function on the early life cycle of RNA in the cytosol (Shi et al., 2017). When m^{6}A-modified mRNA is transported to the cytoplasm, it might be initially recognized by YTHDF3. The binding of YTHDF3 could then facilitate YTHDF1 binding to the mRNA and together promote translation. Subsequently, the mRNA might be bound and partitioned among YTHDF proteins and eventually recognized by YTHDF2 for degradation.

However, a recent study has argued that all the YTHDF proteins function redundantly to mediate mRNA degradation (Zaccara and Jaffrey, 2020). Thus, more studies are needed to explore their functions in detail.

YTHDC1

YTH domain-containing protein 1 is predominantly expressed in nuclear speckles (Hartmann et al., 1999). It has been shown that YTHDC1 mediates splicing (Xiao et al., 2016), and nuclear export of mRNA (Roundtree et al., 2017b). As active transcription occurs in nuclear speckles, YTHDC1 may bind m^{6}A-modified mRNAs and affect their splicing. By recruiting pre-mRNA splicing factor SRSF3 and inhibiting SRSF10, YTHDC1 facilitates exon inclusion in target m^{6}A-modified mRNA (Xiao et al., 2016). YTHDC1 can also selectively promote the transport of m^{6}A-modified mRNA from nuclear to cytoplasm through interacting with nuclear mRNA receptors NXF1 and SRSF3 (Roundtree et al., 2017b). Besides, transcriptome-wide UV crosslinking immunoprecipitation (CLIP) study showed that YTHDC1 preferentially binds m^{6}A residues in long non-coding RNAs (Patil et al., 2016), whereas the YTHDF family readers prefer to bind m^{6}A sites on mRNA. The proper function of the long non-coding RNA, *X-inactive specific transcript (XIST)*, which regulates X chromosome inactivation and transcriptional silencing of genes on the X chromosome, needs YTHDC1 to bind its m^{6}A sites (Patil et al., 2016). In addition, YTHDC1 can interact with the H3K9me2 demethylase KDM3B to promote H3K9me2 demethylation and gene expression (Li et al., 2020b).

YTHDC2

YTH domain-containing protein 2 is expressed both in the nucleus and cytoplasm. Unlike the other m^{6}A readers that are universally expressed, YTHDC2 is enriched in testes (Bailey et al., 2017; Hsu et al., 2017; Wojtas et al., 2017; Jain et al., 2018). YTHDC2 can promote the translation efficiency of its target mRNAs and also decrease mRNA levels (Hsu et al., 2017; Kretschmer et al., 2018). YTHDC2 promotes germ cell fate transition from mitosis to meiosis (Bailey et al., 2017). *Ythdc2* knockout mice show defects in spermatogenesis (Bailey et al., 2017; Hsu et al., 2017).

THE DISTRIBUTION OF m^{6}A IN THE NERVOUS SYSTEM

N^6-methyladenosine is widely distributed in many mouse tissues, with the highest expression in the brain (Meyer et al., 2012; Chang et al., 2017). Immunostaining with a specific m^{6}A antibody revealed wide-spread and strong m^{6}A signals in the developing mouse brain, spinal cord, and dorsal root ganglion (DRG) (**Figure 1**). Transcriptome-wide m^{6}A sequencing showed that distinct m^{6}A methylation patterns occur in different brain regions or at different stages in the same region, suggesting the critical dynamic involvement of m^{6}A modification in neuronal development (Chang et al., 2017). In the mouse cerebral cortex and cerebellum, neurons have relatively higher m^{6}A levels than glia cells (Chang et al., 2017). The highly methylated mRNAs are associated with processes such as synapse assembly and axon guidance, suggesting that m^{6}A modification plays an essential role in neuronal development and brain functions (Chang et al., 2017).

THE FUNCTIONS OF m^{6}A IN THE MAMMALIAN NERVOUS SYSTEM

For the past 5 years, tremendous progress has been made, showing that m^{6}A modification can regulate multiple neuronal developmental processes and functions in mammals. We summarize these findings in **Table 1** and discuss the details in the following parts.

Differentiation and Neurogenesis

Cortex

During neuronal development, neurogenesis is a precisely orchestrated process (Kohwi and Doe, 2013). In the cerebral

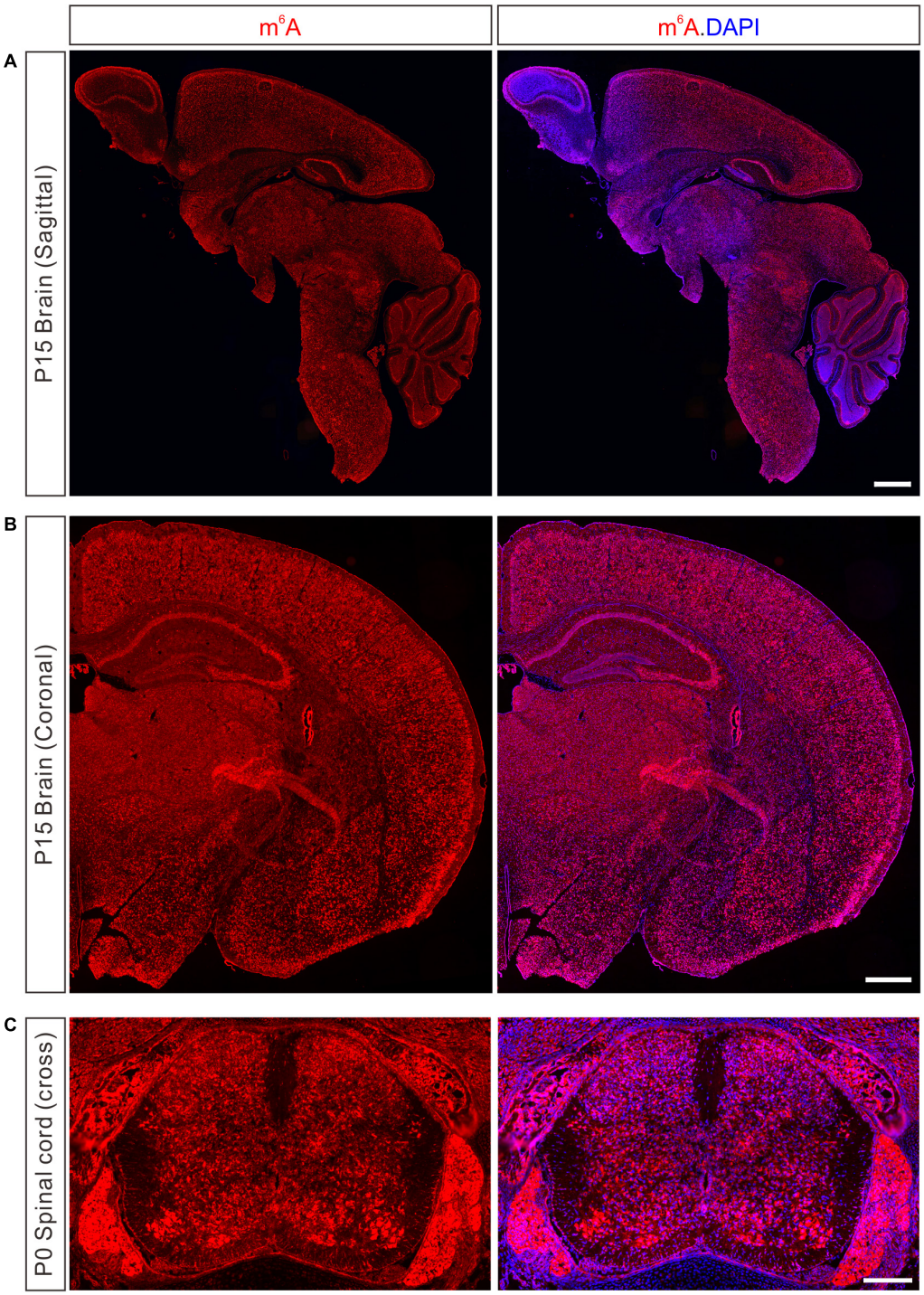

FIGURE 1 | Detection of m^{6}A modification in the developing nervous system of mouse. **(A)** Immunostaining of m^{6}A in sagittal section of P15 mouse brain. Scale bar, 1 mm. **(B)** Immunostaining of m^{6}A in coronal section of P15 mouse brain. Scale bar, 500 μm. **(C)** Immunostaining of m^{6}A in cross-section of P0 mouse spinal cord and DRG. Scale bar, 200 μm.

cortex, radial glia cells (RGCs), also known as neural stem cells (NSCs), are the principal progenitor cells that generate consecutive different types of neurons which further migrate to different layers. m^{6}A modification has been shown to regulate this exquisitely timed process (Yoon et al., 2017; Wang Y. et al., 2018). When m^{6}A modification was ablated in the nervous system using *Nestin-Cre;Mettl14*$^{f/f}$ conditional knockout (cKO) mice, the cell cycle of RGCs was prolonged

and cortical neurogenesis extended into postnatal stages, causing brutal postnatal death (Yoon et al., 2017). These were due to the failure of m^{6}A-dependent decay of mRNAs encoding proteins related to stem cell, cell cycle and neurogenesis in neural stem cells (Yoon et al., 2017). Another study also found cortical neurogenesis defects in *Nestin-Cre;Mettl14*$^{f/f}$ cKO mice which were characterized with decreased cortical thickness and postnatal death (Wang Y. et al., 2018). In this study, m^{6}A modification was found to mediate NSCs self-renewal, as deletion of *Mettl14* in NSCs led to reduced proliferation and premature differentiation, causing NSC pool loss and insufficient late-born neurons (Wang Y. et al., 2018). The underlying mechanism was that m^{6}A modification could regulate histone modification, inhibiting proliferation-related genes and promoting differentiation-related genes (Wang Y. et al., 2018). These studies provided direct proof that m^{6}A modification can regulate mouse embryonic cortical neurogenesis. However, the seemingly opposite mechanisms described in these two studies after using the same *Nestin-cre* to conditionally knock out *Mettl14* ("prolonged cell cycle and maintenance of radial glia cells" vs. "decreased proliferation and premature differentiation") suggest that further exploration and clarification are needed. In addition, as *Nestin-cre* is generally expressed in the nervous system, how m^{6}A modification specifically affects mouse cortical neurogenesis without affecting other areas in the brain needs further elucidation.

In addition, disrupting the recognition and reading of m^{6}A modification can also phenocopy the effect on cortex neurogenesis (Li et al., 2018; Edens et al., 2019). Self-renewal and spatiotemporal neurogenesis of NSCs were severely affected in the cortex of *Ythdf2* knockout mice, causing retarded cortical development and lethality at late embryonic stages (Li et al., 2018). Both proliferation and differentiation abilities were decreased in *Ythdf2*$^{-/-}$ NSCs, which were indeed caused by the impaired clearance of m^{6}A-modified genes (Li et al., 2018). Another reader protein involved in regulating cortical neurogenesis is fragile X mental retardation protein (FMRP) (Edens et al., 2019). The role of FMRP was to preferentially bind m^{6}A-modified mRNAs and facilitate them to export from nuclear (Edens et al., 2019). Deletion of *Fmr1* cause nuclear retention of m^{6}A-modified mRNAs associated with neural differentiation (Edens et al., 2019). Thus, *Fmr1* KO mice exhibited extended maintenance of NSCs into postnatal stages with delayed NSC cell cycle progression and differentiation.

Cerebellum

Unlike cortical neurogenesis that occurs in embryonic stages, the development of the cerebellum mainly begins postnatally. The cerebellum has generally higher m^{6}A levels than the cerebral cortex (Ma et al., 2018). The expression of m^{6}A modifiers (writers, erasers, and readers) is developmentally regulated and differentially expressed in different cell types and regions in the cerebellum (Ma et al., 2018). Similarly, the mRNAs in the cerebellum show dynamic methylation levels throughout the developmental stages (Chang et al., 2017; Ma et al., 2018). These findings demonstrate that m^{6}A might be required for the development and function of the cerebellum.

Specific deletion of *Mettl3* in the mouse nervous system leads to cerebellar hypoplasia caused by increased apoptosis of newly generated cerebellar granule cells (CGCs) in the external granular layer (Wang C.X. et al., 2018). Due to the loss of m^{6}A, the half-lives of mRNA associated with cerebellar development and apoptosis are extended. In addition, synapse-associated mRNAs show abnormal splicing after *Mettl3* depletion. Those events finally contribute to incorrect cell differentiation and cell death (Wang C.X. et al., 2018). Knockdown of METTL3 results in disorganized structures of Purkinje cells and glial cells in cerebellum (Ma et al., 2018). In addition, deletion of *Alkbh5* in mice exposed to hypobaric hypoxia leads to aberrant proliferation and differentiation due to the dysregulated mRNA nuclear export (Ma et al., 2018). Those findings together prove that m^{6}A acts as a crucial regulator during cerebellar development.

Axon Growth

Fat mass and obesity-associated was unexpectedly found expressed in the axons of mouse DRG neurons, which can dynamically regulate m^{6}A modification on axonal mRNA (Yu et al., 2018). Despite the previous finding that demethylation occurs in nuclear speckles, m^{6}A modification can be dynamically regulated in the highly compartmentalized subcellular structures such as axons. Axonally derived FTO regulates the level of m^{6}A modification on *GAP-43* mRNA and further affects the local translation of *GAP-43* mRNA in axons, eventually controlling axon growth (Yu et al., 2018). This study is the first example of mRNA modification regulating local translation in axons.

Axonal Guidance

Axon guidance cues provided by the floor plate enable the right pathfinding of commissural axons in the developing spinal cord (Colamarino and Tessier-Lavigne, 1995). Robo3.1 is one of the axon guidance receptors from Roundabout (Robo) family that facilitate midline crossing of commissural axons (Chen et al., 2008). The precise spatiotemporal expression of Robo3.1 has been found to be regulated by m^{6}A modification (Zhuang et al., 2019). YTHDF1 can bind to *Robo3.1* mRNA in an m^{6}A dependent manner and promote its translation (Zhuang et al., 2019). Specific deletion of YTHDF1 in commissural neurons using *Atoh1-cre;Ythdf1*$^{f/f}$ *cKO* mice led to axon guidance defects (Zhuang et al., 2019).

Axon Regeneration

Axon regeneration of mouse DRG neurons in the peripheral nervous system (PNS) requires *de novo* gene transcription and translation of regeneration-associated genes (RAGs) (Costigan et al., 2002; Mahar and Cavalli, 2018). Similar to other epigenetic mechanisms, such as DNA methylation (Weng et al., 2017) and histone modification (Gaub et al., 2011; Puttagunta et al., 2014), m^{6}A modification has also been shown to participate in the activation of RAGs (Weng et al., 2018). Sciatic nerve lesion (SNL) substantially increases levels of m^{6}A-modified transcripts *in vivo*. Those transcripts can be divided into three categories:

TABLE 1 | Roles of m^{6}A modification in neuronal development and functions.

Developmental processes and functions	m^{6}A writers, erasers, or readers	Mouse models (KO, cKO) or *in vitro* (KD)	If cKO, which cre line?	Phenotype	Key target mRNAs identified	References
Differentiation, and neurogenesis	METTL14	cKO	*Nestin-cre*	Prolonged cell cycle of radial glia cells; cortical neurogenesis extended into postnatal stages	*Pax6, Sox2, Emx2, Tbr2, Cdk9, Ccnh/Cyclin H,* and *Cdkn1C/p57*	Yoon et al., 2017
	METTL14	cKO	*Nestin-cre*	Reduced proliferation and premature differentiation of NSCs in cortex	*CBP* and *P300*	Wang Y. et al., 2018
	YTHDF2	KO	NA	Decreased proliferation and differentiation of NSPCs in cortex	*Ddr2, Mob3b, Rnf135, Speg, Flrt2, Hlf, Nrp2, Nrxn3, Ptprd,* and *Soat1*	Li et al., 2018
	FMRP	KO	NA	Delayed cell cycle and extended pool of proliferating progenitors to postnatal stages in cortex	*Ptch1, Dll1, Dlg5, Fat4, Gpr161,* and *Spop*	Edens et al., 2019
	METTL3	cKO	*Nestin-cre*	Increased apoptosis of newly generated cerebellar granule cells	*Atoh1, Cxcr4, Gli3, Jag1, Notch2, Sox2, Yap1, Dapk1, Fadd, Ngfr, Grin1, Atp2b3, Grm1,* and *Lrp8*	Wang C.X. et al., 2018
	ALKBH5	KO	NA	Aberrant proliferation and differentiation in cerebellum under hypobaric hypoxia conditions	*Letm1, Opa1,* and *Mphosph9*	Ma et al., 2018
Axon growth	FTO	KD	NA	Knockdown of FTO repressed local mRNA translation and axon growth	*GAP-43*	Yu et al., 2018
Axon guidance	YTHDF1	cKO	*Atoh1-cre*	Misprojection of pre-crossing commissural axons into motor columns of spinal cord	*Robo3.1*	Zhuang et al., 2019
Axon regeneration	METTL14	cKO	*Syn1-cre*	Reduced functional axon regeneration	*Atf3*	Weng et al., 2018
	YTHDF1	KO	NA		NR	
Synapse	YTHDF1, YTHDF3	KD	NA	KD of YTHDF1 or YTHDF3 caused abnormal dendrite spine morphology, reduced PSD95 and GluA1 expression, compromised synaptic transmission of cultured hippocampal neuron	*Apc*	Merkurjev et al., 2018
Adult neurogenesis	FTO	KO	NA	Reduced proliferation and neuronal differentiation of adult neural stem cells (aNSCs); impaired learning and memory	*Bdnf, Akt1, Akt2, Akt3,* and *S6k1*	Li et al., 2017
	FTO	cKO	*Nestin-cre*	Inhibited adult neurogenesis and neuronal development	*Pdgfra and Socs5*	Cao et al., 2020
	METTL3	KD	NA	Inhibited proliferation of aNSCs; skewed differentiation of aNSCs toward glial lineage	*Ezh2*	Chen J. et al., 2019
Gliogenesis	METTL14	cKO	*Olig2-Cre; CNP-Cre*	Loss of mature oligodendrocytes and hypomyelination	*Ptprz1* and *NF155*	Xu H. et al., 2020
	PRRC2A	cKO	*Nestin-cre; Gfap-Cre; Olig2-Cre*	Hypomyelination; locomotive and cognitive defects	*Olig2*	Wu et al., 2019
	METTL14	cKO	*Nestin-cre*	Reduced number of astrocytes in the cortex	NR	Yoon et al., 2017
	METTL3	cKO	*Nestin-cre*	Abolished scaffold organization pattern provided by Bergmann glia in cerebellum	NR	Wang C.X. et al., 2018

(Continued)

TABLE 1 | Continued

Developmental processes and functions	m^{6}A writers, erasers, or readers	Mouse models (KO, cKO) or *in vitro* (KD)	If cKO, which cre line?	Phenotype	Key target mRNAs identified	References
	YTHDF2	KO	NA	Dramatic reduction of GFAP$^+$ astrocytes	NR	Li et al., 2018
Learning and memory	FTO	KD	NA	KD of FTO in hippocampus facilitated contextual fear memory	NR	Walters et al., 2017
	FTO	KD	NA	KD of FTO in medial prefrontal cortex results in increased fear memory consolidation	*Rab33b, Arhgap39, Arhgef17, Crtc1, Gria1,* and *Crtc1*	Widagdo et al., 2016
	METTL3	cKO	*CaMKIIa-cre*	Decreased formation of hippocampus-dependent long-term memory	*Arc, Egr1, c-Fos, Npas4,* and *Nr4a1*	Zhang et al., 2018
	YTHDF1	KO	NA	Defects in learning and memory; impaired synaptic transmission and long-term potentiation	*Bsn* and *Camk2a*	Shi et al., 2018
	FTO	KO	NA	Impaired cocaine-induced behavioral activity and synaptic dopamine release	*Kcnj6, Grin1,* and *Drd3*	Hess et al., 2013
	METTL14	cKO	*Drd1-cre; Adora2a-cre*	Deficiency in striatum-mediated learning and dopamine signaling	*Tac1, Pdyn, Penk, Drd2, Homer1,* and *Cdk5r1*	Koranda et al., 2018

KO, knockout; cKO, conditional knockout; KD, knockdown; NA, not applied; NR, not reported.

transcripts encoding RAGs, injury-induced retrograde signaling molecules, and translation machinery components (Weng et al., 2018). Either loss of METTL14 or YTHDF1 can delay the injury-induced protein translation of RAGs, such as *Atf3*, and cause defective axon regeneration and function recovery (Weng et al., 2018). These findings indicate that m^{6}A modification may affect response to pathological stimulus in the adult nervous system.

Synapse

Low input m^{6}A sequencing of mouse forebrain synaptosomes has revealed a synaptic m^{6}A epitranscriptome (SME) in which 2921 synaptosomal transcripts are m^{6}A-modified (Merkurjev et al., 2018). Transcripts in SME are most significantly enriched in central nervous system development. More than half of the genes in the SME overlapped with the synaptic transcriptome. Surprisingly, those genes are functionally annotated to synapse-associated functions, such as "synapse assembly," "postsynaptic membrane," "long-term synaptic potentiation." In contrast, those hypomethylated transcripts in the synaptic transcriptome were mainly related to metabolic pathways. These findings suggest that m^{6}A modification possibly regulates synapse formation and synaptic function. Dendrite localization of m^{6}A writers, erasers, and readers was detected in mouse cortical pyramidal neurons in brain slices, which further indicates that m^{6}A modification could be dynamically and locally regulated in synapses (Merkurjev et al., 2018). Either knockdown of YTHDF1 or YTHDF3 in cultured hippocampal neurons leads to abnormal dendrite spine morphology, reduced PSD95 clustering, decreased expression of GluA1, thus compromising synaptic transmission (Merkurjev et al., 2018).

Adult Neurogenesis

Adult neurogenesis occurs (yet still in debate) limitedly, and has been shown to be related to neurological and psychiatric disorders (Apple et al., 2017; Kempermann et al., 2018). m^{6}A has also been reported to function in adult neurogenesis. FTO is expressed in adult neural stem cells (aNSCs), and deletion of *Fto* reduces the proliferation and neuronal differentiation of aNSCs (Li et al., 2017; Cao et al., 2020). This is due to the altered expression of several key components that are modified by m^{6}A in the brain-derived neurotrophic factor (BDNF) pathway (Li et al., 2017) and the Pdgfra/Socs5-Stat3 pathway (Cao et al., 2020). On the other hand, depletion of METTL3 also inhibits the proliferation of aNSCs (Chen J. et al., 2019). The mRNA of histone methyltransferase *Ezh2* is modified by m^{6}A (Chen J. et al., 2019). Upon deletion of *Mettl3*, the protein level of Ezh2 deceased, further causing reduced H3K27me3 levels (Chen J. et al., 2019). These studies showed that m^{6}A modification is involved in adult neurogenesis. However, how writers and erasers work together under normal conditions to regulate adult neurogenesis still needs more investigation.

Gliogenesis

Glia cells account for more than 50% of cells in the human brain (Nave, 2010; Rowitch and Kriegstein, 2010). Oligodendrocytes and astrocytes are the two major macroglial cells derived from the neuroepithelium (Rowitch and Kriegstein, 2010). Oligodendrocytes are responsible for the myelination of axons. m^{6}A modification has been shown to control the oligodendrocyte lineage progression. Specific deletion of *Mettl14* in developing oligodendrocyte lineage cells or in postmitotic oligodendrocytes leads to loss of mature oligodendrocytes and hypomyelination

(Xu H. et al., 2020). This is because the loss of METTL14 results in abnormal splicing of many mRNAs which encode proteins associated with the myelinating process, such as protein tyrosine phosphate receptor type Z1 (Ptprz1) and neurofascin 155 (NF155) (Xu H. et al., 2020). Another study discovered a novel m^{6}A reader, Proline-rich coiled-coil 2A (PRRC2A), which regulates oligodendrocyte specification and myelination (Wu et al., 2019). Deletion of *Prrc2a* in oligodendrocyte progenitor cells (OPCs) leads to hypomyelination, locomotive and cognitive defects in mice. Interestingly, PRRC2A directly stabilizes the *Olig2* mRNA in an m^{6}A-dependent manner. Olig2 is known to regulate OPC specification, differentiation and myelination (Lu et al., 2002; Zhou and Anderson, 2002). However, the mechanism of how PRRC2A stabilizes m^{6}A-modified mRNA remains unclear.

In addition to oligodendrocytes, m^{6}A modification also functions in the gliogenesis of astrocytes, which provide structural support, modulate synaptic transmission, and maintain the blood-brain barrier (Rowitch and Kriegstein, 2010). Global deletion of *Mettl14* in the mouse nervous system significantly reduces astrocytes in the cortex (Yoon et al., 2017). The scaffold organization pattern provided by Bergmann glia (a highly diversified type of astrocytes) in the mouse cerebellum is abolished after deleting *Mettl3* in the nervous system (Wang C.X. et al., 2018). As for the m^{6}A readers, *in vitro* differentiation assay of neurospheres showed that deletion of *Ythdf2* in neural stem/progenitor cell (NSPC) caused dramatic reduction of GFAP$^+$ astrocytes (Li et al., 2018). These studies indicate that m^{6}A modification also controls the production of astrocytes. However, the underlying mechanism needs further investigation.

Learning and Memory

Learning and memory require coordinated regulation of gene expression and protein translation. The substantial increase of m^{6}A level from the embryonic brain to the adult brain (Meyer et al., 2012) suggests that the dynamic m^{6}A epitranscriptome could be involved in the regulation of the advanced brain functions.

Fat mass and obesity-associated is highly expressed in the dendrites and synapses of mouse CA1 hippocampal neurons (Walters et al., 2017). Interestingly, the expression of FTO protein decreased in the synaptic fraction, not the nuclear fraction of hippocampus 0.5 h after contextual fear conditioning, indicating that behavioral training-induced memory preferentially decreases FTO levels near synapses (Walters et al., 2017). As expected, with the decrease of FTO, the m^{6}A level on mRNA is significantly increased. Knockdown of FTO in hippocampus facilitated contextual fear memory, suggesting that synaptic FTO could normally restrict memory formation and experience-induced increase of m^{6}A modification could enhance memory formation (Walters et al., 2017). Another study also shows that cue fear conditioning increases m^{6}A level in mouse medial prefrontal cortex (mPFC) (Widagdo et al., 2016). Knockdown of FTO in mPFC results in increased fear memory consolidation (Widagdo et al., 2016). These studies demonstrate that experience or behavior-induced upregulation of m^{6}A modification might participate in the regulation of memory. However, as FTO was also reported to preferentially demethylate m^{6}A$_m$ (Mauer et al., 2017) and m^{6}A$_m$ participates in fear memory (Engel et al., 2018), the possibility that m^{6}A$_m$ may contribute to some of the phenotypes cannot be ruled out.

The study of m^{6}A writer METTL3 provides direct evidence that m^{6}A modification regulates memory formation. Using *CaMKIIa-cre;Mettl3$^{f/f}$* cKO mice, specific deletion of METTL3 in the forebrain excitatory neurons decreases the formation of hippocampus-dependent long-term memory without changing short-term memory and learning ability when adequate training is provided (Zhang et al., 2018). The hippocampus-dependent memory consolidation ability exquisitely relies on the function of METTL3, as the expression of METTL3 in wild-type (WT) mice positively associates with the learning efficacy and overexpression of METTL3 facilitates long-term memory consolidation (Zhang et al., 2018). The formation of long-term memory requires *de novo* protein synthesis of immediate early genes (IEGs), such as *Arc*, *Egr1*, *c-Fos*, *Npas4,* and *Nr4a1*. By affecting the m^{6}A levels on those IEGs, METTL3 eventually promotes their translation, thus enhancing memory (Zhang et al., 2018).

Regarding the roles of m^{6}A reader protein, YTHDF1 was reported to be required in the process of m^{6}A enhanced learning and memory in the hippocampus (Shi et al., 2018). *Ythdf1* mRNA is preferentially located in the mouse hippocampus (Lein et al., 2007), suggesting that it might be involved in learning and memory. When YTHDF1 is ablated entirely from the hippocampus, hippocampus histology, neurogenesis, motor ability, and emotional state are not altered in *Ythdf1* KO mice (Shi et al., 2018). However, by compromising basal synaptic transmission and long-term potentiation (LTP), the learning and memory abilities of *Ythdf1* KO mice in Morris water maze (MWM) and contextual fear conditioning tests are impaired (Shi et al., 2018). Restoring the expression of YTHDF1 in the hippocampus of *Ythdf1* KO mice can successfully rescue the synaptic and behavioral defects (Shi et al., 2018). Further analysis of the underlying molecular mechanism showed that YTHDF1 preferentially recognizes m^{6}A modified mRNAs and facilitates their translation in a neuronal-stimulus-dependent manner. More interestingly, YTHDF1 could translocate into the postsynaptic density (PSD) fraction to facilitate protein synthesis locally in synapses of the hippocampus in response to fear conditioning, thus promote synaptic plasticity and memory formation (Shi et al., 2018).

Learning and memory-related synaptic plasticity requires local translation at synapses (Wang et al., 2009). Due to the dynamic SME (Merkurjev et al., 2018) and the localization of m^{6}A writers, erasers, and readers in synapses, it's highly likely that m^{6}A-dependent local translation of synaptic mRNAs is the central event that occurs in synapses in response to stimuli.

Besides the forebrain, m^{6}A modification also affects synaptic transmission in the midbrain and striatum. It has been shown that FTO can regulate the activity of the dopaminergic (DA) signaling in the mouse midbrain, which controls complex behaviors (Hess et al., 2013). Deletion of *Fto* attenuates neuronal activity controlled by dopamine D2-like receptor and behavioral responses (Hess et al., 2013). Compared with WT mice, *Fto*-deficient mice showed impaired cocaine-induced behavioral

activity and synaptic dopamine release (Hess et al., 2013). Transcriptome-wide m^{6}A sequencing showed that the m^{6}A level of many genes involved in the DA signal pathway is increased in *Fto*-deficient mice. In the adult mouse striatum, specific deletion of *Mettl14* in two distinct but related types of neurons, striatonigral and striatopallidal neurons, leads to deficiency in striatum-mediated learning and dopamine signaling without affecting cell numbers and morphology (Koranda et al., 2018). Interestingly, neuronal and synaptic mRNAs are downregulated in either type of neurons after deletion of *Mettl14*, while upregulated mRNAs are mainly associated with translational regulation and metabolism (Koranda et al., 2018). These m^{6}A-dependent gene regulation increases neuronal excitability and decreases spike frequency adaptation, which finally attenuates striatum-mediated learning and behavioral performance (Koranda et al., 2018). Considering activity-dependent synaptic protein synthesis is vital to synaptic plasticity and learning, it is important to decipher how m^{6}A readers are involved in this process to spatial temporally regulate protein synthesis in response to neuronal activities.

m^{6}A IN NEUROLOGICAL DISORDERS AND INJURIES

Alzheimer's Disease

Transcriptome-wide sequencing of human and mouse brains showed that m^{6}A modification is spatiotemporally regulated during neurodevelopment and aging (Shafik et al., 2021). Increased m^{6}A sites are observed as age increases. The dynamically regulated m^{6}A sites are enriched in alternatively untranslated regions of genes involved in aging-related pathways (Shafik et al., 2021). Alzheimer's disease (AD) is the most common form of dementia among elderly people (Bateman et al., 2012). The m^{6}A levels of many transcripts involved in AD-associated pathways are decreased in the brain of a familial AD mouse model (5XFAD) (Shafik et al., 2021). In contrast, m^{6}A levels are elevated in the cortex and hippocampus of APP/PS1 transgenic mice, another AD mouse model, compared with WT mice (Han et al., 2020). Interestingly, the expression of METTL3 increased, and FTO is decreased in the APP/PS1 mice (Han et al., 2020). These studies show that m^{6}A modification is involved in AD. However, the mechanism by which m^{6}A regulates the progression of AD remains almost unknown.

Parkinson's Disease

Parkinson's disease (PD) is a common neurodegenerative disorder characterized by the early prominent death of dopaminergic neurons (Lees, 2017). The global m^{6}A levels of mRNAs are decreased in the striatum of the PD rat brain and a cellular PD model (6-OHDA-induced PC12 cells), which is mainly due to the increase of FTO protein (Chen X. et al., 2019). The decrease of m^{6}A level could induce the expression of *N*-methyl-*D*-aspartate (NMDA) receptor 1, and increase oxidative stress and Ca^{2+} influx, which finally leads to dopaminergic neuron apoptosis (Chen X. et al., 2019). Conversely, knockdown of FTO in PC12 cells decreases NMDAR1 expression and exhibits anti-apoptosis effect (Chen X. et al., 2019). This study suggests that m^{6}A modification via FTO may play a crucial role in the pathogenesis of PD.

Ischemia/Reperfusion Injury

Ischemic stroke is a severe neurological disease, which is a leading cause of disability in humans (Wang et al., 2017). Cerebral ischemia/reperfusion (I/R) injury rapidly triggers different types of programmed cell death in neurons. Several studies have shown that m^{6}A modification was involved in I/R injury (Si et al., 2020). The expression of METTL3 is significantly decreased at the reperfusion injury period. Decreased m^{6}A level leads to the reduction of miR-335 and stress granule formation (Si et al., 2020). Therefore, by upregulating the expression of miR-335, METTL3-mediated m^{6}A modification can normally promote stress granule formation and improve cell survival of neurons. Contradictorily, another study reported increased m^{6}A levels after I/R injury (Xu K. et al., 2020). The expression of m^{6}A erasers, ALKBH5 and FTO, are decreased but not writers. Overexpression of m^{6}A erasers can alleviate neuronal damage induced by I/R injury (Xu S. et al., 2020). A third study found that oxygen-glucose deprivation/re-oxygenation (OGD/R) increased METTL3-dependent m^{6}A modification of long non-coding RNA D63785 (lnc-D63785), thus causing reduced expression of lnc-D63785 (Xu S. et al., 2020). Downregulation of lnc-D63785 further induces accumulation of miR-422a, which results in neuronal cell apoptosis (Xu S. et al., 2020).

Hypothermia is an effective therapeutic method to alleviate I/R injury (Callaway et al., 2015; Donnino et al., 2015). Hypoxia/reoxygenation (H/R) caused m^{6}A-dependent increase of *PTEN* mRNA stability and consequently upregulation of its protein level, which could be reversed by hypothermia (Diao et al., 2020). Thus hypothermia could activate PI3K/Akt signaling to protect neurons from I/R-induced pyroptosis (Diao et al., 2020). Another study reported that the m^{6}A reader YTHDC1 protects ischemic stroke through mediating *PTEN* mRNA degradation, which further promotes Akt phosphorylation and facilitates neuronal survival (Zhang Z. et al., 2020). These two studies demonstrate that m^{6}A modification could modulate PTEN expression to regulate PI3K/Akt signaling in I/R injury.

Taken together, all these studies demonstrated that m^{6}A modification is involved in the process of I/R injury, which could provide potential therapeutic targets for I/R injury.

Traumatic Brain Injury

Traumatic brain injury (TBI), one of the most severe types of injury, is a major public health threat (Majdan et al., 2017). After TBI, the mRNA and protein levels of METTL3 were significantly decreased in the hippocampus of mice, but not other writers and erasers (Wang et al., 2019). Correspondingly, the m^{6}A level of RNA was downregulated in the hippocampus after TBI. Genome-wide m^{6}A profiling identified that altered peaks of m^{6}A-modified transcripts after TBI were mainly related to the regulation of the metabolic process (Wang et al., 2019). Metabolism alteration induced by brain injury could lead to long-term cognitive and neurological disabilities (McKenna et al., 2015). Therefore,

this study indicates that m^{6}A modification-induced metabolic alteration might be the underlying mechanism of TBI. Thus rectifying altered m^{6}A level might be a potential therapeutic strategy for TBI.

Pathological Pains

N^6-methyladenosine modification has been shown to participate in both inflammatory and neuropathic pain (Li et al., 2020a; Zhang C. et al., 2020). The m^{6}A levels of spinal mRNAs are significantly increased in Complete Freund's Adjuvant (CFA)-induced chronic inflammatory pain mouse model, which shows strong thermal and mechanical hyperalgesia (Zhang C. et al., 2020). The upregulated m^{6}A level is due to the increase of METTL3 in CFA-injected mice, which can modulate the pain sensitization by regulating m^{6}A-dependent pri-miRNA processing. Meanwhile, another study reported that FTO contributes to nerve injury-induced neuropathic pain in the primary sensory neurons in DRG (Li et al., 2020a). Nerve injury activates the transcription factor Runx1, which can bind to *Fto* gene promoter and activate its expression but not m^{6}A readers. Upregulated FTO then demethylates m^{6}A modification on the *Ehmt2* mRNA encoding euchromatic histone lysine methyltransferase 2 and elevates its protein level, thus resulting in neuropathic pain symptoms. Conversely, knockdown of FTO could alleviate nerve injury-associated pain hypersensitivities (Li et al., 2020a). These two studies indicate that m^{6}A modification regulates different pain responses through different mechanisms.

Brain Tumor

N^6-methyladenosine modification has been implicated in various types of cancer including brain tumor (Deng et al., 2018). Glioblastoma is the most common and severe brain tumor. The proliferation and tumorigenesis of glioblastoma stem cells (GSCs) require high expression of the m^{6}A eraser ALKBH5 (Zhang et al., 2017). ALKBH5 demethylates *FOXM1* nascent transcript, maintaining expression of FOXM1 that preserves GSC properties (Zhang et al., 2017). Knockdown of ALKBH5 reduces proliferation of patient-derived GSCs (Zhang et al., 2017). In addition, knockdown of the m^{6}A writers METTL3 and METTL14 significantly increases GSC-initiated tumor progression *in vivo* (Cui et al., 2017). Interestingly, treatment with MA2, an FTO inhibitor, inhibits GSC-initiated tumorigenesis and extends the lifespan of GSC-engrafted mice (Cui et al., 2017). Controversially, another two studies found that clinical aggressiveness of glioblastoma is related to increased expression of METTL3 (Visvanathan et al., 2018; Li et al., 2019). METTL3 promotes GSC stemness by enhancing SOX2 stability in glioblastoma, and METTL3 silencing inhibits tumor growth (Visvanathan et al., 2018). Knockdown of METTL3 suppresses aggressive and tumorigenic properties of GSCs by causing YTHDC1-dependent nonsense-mediated mRNA decay of *SRSF*, and subsequent decrease of SRSF protein level (Li et al., 2019). m^{6}A modification also regulates neuroblastoma, another common malignant brain tumor (Cheng et al., 2020). MYCN is a genetic biomarker of high risk and poor outcome in neuroblastoma. m^{6}A modification in the 3′UTR of *MYCN* promotes its interaction with miR-98, decreasing MYCN expression and inhibiting neuroblastoma progression (Cheng et al., 2020). These studies indicate that m^{6}A modification could be a promising target for anti-brain tumor therapy.

CONCLUSION AND PERSPECTIVES

The nervous system is the most complex and diverse system, with exceptional capabilities that control higher cognitive and emotional functions. The development of the nervous system is a highly coordinated process in which epigenetic mechanisms exert significant effects by spatiotemporally regulating gene expression. Apart from DNA methylation and histone modifications, dynamic mRNA m^{6}A modification provides an additional regulatory layer to regulate gene expression. As described above, m^{6}A modification regulates the development and functions of the nervous system.

The higher function of the nervous system relies on synaptic plasticity. In response to stimuli, the nervous system undergoes extremely swift reactions to adapt its proteome. Neurons are highly compartmentalized cells, and local translation plays a central role in rapidly changing subcellular proteomes in response to extrinsic cues and stimuli. Accumulating evidence has suggested that m^{6}A modification modulates the local translation of mRNAs in axons and synapses. This m^{6}A-dependent local translation could be the principal mechanism that regulates the plasticity of the nervous system. This highlights the requirement of comprehensive studies of m^{6}A modification and local translation of the nervous system. How m^{6}A writers, erasers, and readers function together to spatiotemporally regulate local proteome needs more investigation.

Up to now, there are controversial findings regarding the functions of m^{6}A reader proteins. As YTH proteins share very high similarity in the YTH domains, the mechanism of how these reader proteins select their target mRNA remains unknown. Therefore, it is crucial to deeply decipher the roles and mechanisms of reader proteins on how they divide jobs and coordinate to mediate m^{6}A signaling.

Dysregulation of m^{6}A modification causes neurological diseases. The involvement of m^{6}A in neurological diseases and injuries provides new potential therapeutic targets for treatment. However, the roles of m^{6}A in injury-induced neuronal diseases, psychiatric disorders, and aging-related neurodegenerative disorders are still far beyond understanding. In-depth studies of how m^{6}A signaling modulates neuronal physiology and pathology in the adult brain are in great demand.

AUTHOR CONTRIBUTIONS

JY and S-JJ drafted and revised the manuscript. S-JJ conceived and designed the review. YS helped to edit and revise the manuscript. All authors read and approved the final manuscript.

FUNDING

This work was supported by the National Natural Science Foundation of China (31871038 to S-JJ), Shenzhen-Hong Kong Institute of Brain Science-Shenzhen Fundamental Research Institutions (2019SHIBS0002 and 2021SHIBS0002), High-Level University Construction Fund for Department of Biology (Internal grant no. G02226301), and Science and Technology Innovation Commission of Shenzhen Municipal Government (ZDSYS20200811144002008).

ACKNOWLEDGMENTS

We thank Prof. Chi Wai Lee at The University of Hong Kong (HKU) for co-mentoring the Ph.D. student in the SUSTech-HKU Joint Ph.D. Program.

REFERENCES

Adams, J. M., and Cory, S. (1975). Modified nucleosides and bizarre 5'-termini in mouse myeloma mRNA. *Nature* 255, 28–33. doi: 10.1038/255028a0

Apple, D. M., Fonseca, R. S., and Kokovay, E. (2017). The role of adult neurogenesis in psychiatric and cognitive disorders. *Brain Res.* 1655, 270–276. doi: 10.1016/j.brainres.2016.01.023

Bailey, A. S., Batista, P. J., Gold, R. S., Chen, Y. G., De Rooij, D. G., Chang, H. Y., et al. (2017). The conserved RNA helicase YTHDC2 regulates the transition from proliferation to differentiation in the germline. *Elife* 6:e26116.

Bateman, R. J., Xiong, C., Benzinger, T. L., Fagan, A. M., Goate, A., Fox, N. C., et al. (2012). Clinical and biomarker changes in dominantly inherited Alzheimer's disease. *N. Engl. J. Med.* 367, 795–804.

Boccaletto, P., Machnicka, M. A., Purta, E., Piatkowski, P., Baginski, B., Wirecki, T. K., et al. (2018). MODOMICS: a database of RNA modification pathways. 2017 update. *Nucleic Acids Res.* 46, D303–D307.

Bokar, J. A., Shambaugh, M. E., Polayes, D., Matera, A. G., and Rottman, F. M. (1997). Purification and cDNA cloning of the AdoMet-binding subunit of the human mRNA (N6-adenosine)-methyltransferase. *RNA* 3, 1233–1247.

Callaway, C. W., Donnino, M. W., Fink, E. L., Geocadin, R. G., Golan, E., Kern, K. B., et al. (2015). Part 8: post-cardiac arrest care: 2015 American heart association guidelines update for cardiopulmonary resuscitation and emergency cardiovascular care. *Circulation* 132, S465–S482.

Cao, G., Li, H. B., Yin, Z., and Flavell, R. A. (2016). Recent advances in dynamic m6A RNA modification. *Open Biol.* 6:160003. doi: 10.1098/rsob.160003

Cao, Y., Zhuang, Y., Chen, J., Xu, W., Shou, Y., Huang, X., et al. (2020). Dynamic effects of Fto in regulating the proliferation and differentiation of adult neural stem cells of mice. *Hum. Mol. Genet.* 29, 727–735. doi: 10.1093/hmg/ddz274

Chang, M., Lv, H., Zhang, W., Ma, C., He, X., Zhao, S., et al. (2017). Region-specific RNA m(6)A methylation represents a new layer of control in the gene regulatory network in the mouse brain. *Open Biol.* 7:170166. doi: 10.1098/rsob.170166

Chen, J., Zhang, Y. C., Huang, C., Shen, H., Sun, B., Cheng, X., et al. (2019). m(6)A regulates neurogenesis and neuronal development by modulating histone methyltransferase Ezh2. *Genomics Proteomics Bioinformatics* 17, 154–168. doi: 10.1016/j.gpb.2018.12.007

Chen, X., Yu, C., Guo, M., Zheng, X., Ali, S., Huang, H., et al. (2019). Down-regulation of m6A mRNA methylation is involved in dopaminergic neuronal death. *ACS Chem. Neurosci.* 10, 2355–2363. doi: 10.1021/acschemneuro.8b00657

Chen, Z., Gore, B. B., Long, H., Ma, L., and Tessier-Lavigne, M. (2008). Alternative splicing of the Robo3 axon guidance receptor governs the midline switch from attraction to repulsion. *Neuron* 58, 325–332. doi: 10.1016/j.neuron.2008.02.016

Cheng, J., Xu, L., Deng, L., Xue, L., Meng, Q., Wei, F., et al. (2020). RNA N(6)-methyladenosine modification is required for miR-98/MYCN axis-mediated inhibition of neuroblastoma progression. *Sci. Rep.* 10:13624.

Church, C., Moir, L., Mcmurray, F., Girard, C., Banks, G. T., Teboul, L., et al. (2010). Overexpression of Fto leads to increased food intake and results in obesity. *Nat. Genet.* 42, 1086–1092. doi: 10.1038/ng.713

Colamarino, S. A., and Tessier-Lavigne, M. (1995). The role of the floor plate in axon guidance. *Annu. Rev. Neurosci.* 18, 497–529. doi: 10.1146/annurev.ne.18.030195.002433

Costigan, M., Befort, K., Karchewski, L., Griffin, R. S., D'urso, D., Allchorne, A., et al. (2002). Replicate high-density rat genome oligonucleotide microarrays reveal hundreds of regulated genes in the dorsal root ganglion after peripheral nerve injury. *BMC Neurosci.* 3:16. doi: 10.1186/1471-2202-3-16

Cui, Q., Shi, H., Ye, P., Li, L., Qu, Q., Sun, G., et al. (2017). m(6)A RNA methylation regulates the self-renewal and tumorigenesis of glioblastoma stem cells. *Cell Rep.* 18, 2622–2634. doi: 10.1016/j.celrep.2017.02.059

Deng, X., Su, R., Feng, X., Wei, M., and Chen, J. (2018). Role of N(6)-methyladenosine modification in cancer. *Curr. Opin. Genet. Dev.* 48, 1–7. doi: 10.1016/j.gde.2017.10.005

Desrosiers, R., Friderici, K., and Rottman, F. (1974). Identification of methylated nucleosides in messenger RNA from Novikoff hepatoma cells. *Proc. Natl. Acad. Sci. U.S.A.* 71, 3971–3975. doi: 10.1073/pnas.71.10.3971

Diao, M. Y., Zhu, Y., Yang, J., Xi, S. S., Wen, X., Gu, Q., et al. (2020). Hypothermia protects neurons against ischemia/reperfusion-induced pyroptosis via m6A-mediated activation of PTEN and the PI3K/Akt/GSK-3beta signaling pathway. *Brain Res. Bull.* 159, 25–31. doi: 10.1016/j.brainresbull.2020.03.011

Dominissini, D., Moshitch-Moshkovitz, S., Schwartz, S., Salmon-Divon, M., Ungar, L., Osenberg, S., et al. (2012). Topology of the human and mouse m6A RNA methylomes revealed by m6A-seq. *Nature* 485, 201–206. doi: 10.1038/nature11112

Donnino, M. W., Andersen, L. W., Berg, K. M., Reynolds, J. C., Nolan, J. P., Morley, P. T., et al. (2015). Temperature management after cardiac arrest: an advisory statement by the advanced life support task force of the International Liaison Committee on resuscitation and the American heart association emergency cardiovascular care committee and the council on cardiopulmonary, critical care, perioperative and resuscitation. *Circulation* 132, 2448–2456. doi: 10.1161/cir.0000000000000313

Du, H., Zhao, Y., He, J., Zhang, Y., Xi, H., Liu, M., et al. (2016). YTHDF2 destabilizes m(6)A-containing RNA through direct recruitment of the CCR4-NOT deadenylase complex. *Nat. Commun.* 7:12626.

Edens, B. M., Vissers, C., Su, J., Arumugam, S., Xu, Z., Shi, H., et al. (2019). FMRP modulates neural differentiation through m(6)A-dependent mRNA nuclear export. *Cell Rep.* 28, 845–854.e5.

Engel, M., Eggert, C., Kaplick, P. M., Eder, M., Roh, S., Tietze, L., et al. (2018). The role of m(6)A/m-RNA methylation in stress response regulation. *Neuron* 99, 389–403.e9.

Fischer, J., Koch, L., Emmerling, C., Vierkotten, J., Peters, T., Bruning, J. C., et al. (2009). Inactivation of the Fto gene protects from obesity. *Nature* 458, 894–898.

Fu, Y., Dominissini, D., Rechavi, G., and He, C. (2014). Gene expression regulation mediated through reversible m(6)A RNA methylation. *Nat. Rev. Genet.* 15, 293–306. doi: 10.1038/nrg3724

Furuichi, Y., Morgan, M., Shatkin, A. J., Jelinek, W., Salditt-Georgieff, M., and Darnell, J. E. (1975). Methylated, blocked 5 termini in HeLa cell mRNA. *Proc. Natl. Acad. Sci. U.S.A.* 72, 1904–1908. doi: 10.1073/pnas.72.5.1904

Gaub, P., Joshi, Y., Wuttke, A., Naumann, U., Schnichels, S., Heiduschka, P., et al. (2011). The histone acetyltransferase p300 promotes intrinsic axonal regeneration. *Brain* 134, 2134–2148. doi: 10.1093/brain/awr142

Gerken, T., Girard, C. A., Tung, Y. C., Webby, C. J., Saudek, V., Hewitson, K. S., et al. (2007). The obesity-associated FTO gene encodes a 2-oxoglutarate-dependent nucleic acid demethylase. *Science* 318, 1469–1472. doi: 10.1126/science.1151710

Geula, S., Moshitch-Moshkovitz, S., Dominissini, D., Mansour, A. A., Kol, N., Salmon-Divon, M., et al. (2015). Stem cells. m6A mRNA methylation facilitates resolution of naive pluripotency toward differentiation. *Science* 347, 1002–1006. doi: 10.1126/science.1261417

Han, M., Liu, Z., Xu, Y., Liu, X., Wang, D., Li, F., et al. (2020). Abnormality of m6A mRNA methylation is involved in Alzheimer's disease. *Front. Neurosci.* 14:98. doi: 10.3389/fnins.2020.00098

Hartmann, A. M., Nayler, O., Schwaiger, F. W., Obermeier, A., and Stamm, S. (1999). The interaction and colocalization of Sam68 with the splicing-associated factor YT521-B in nuclear dots is regulated by the Src family kinase p59(fyn). *Mol. Biol. Cell* 10, 3909–3926. doi: 10.1091/mbc.10.11.3909

Hess, M. E., Hess, S., Meyer, K. D., Verhagen, L. A., Koch, L., Bronneke, H. S., et al. (2013). The fat mass and obesity associated gene (Fto) regulates activity of the dopaminergic midbrain circuitry. *Nat. Neurosci.* 16, 1042–1048. doi: 10.1038/nn.3449

Hsu, P. J., Zhu, Y., Ma, H., Guo, Y., Shi, X., Liu, Y., et al. (2017). Ythdc2 is an N(6)-methyladenosine binding protein that regulates mammalian spermatogenesis. *Cell Res.* 27, 1115–1127. doi: 10.1038/cr.2017.99

Hubstenberger, A., Courel, M., Benard, M., Souquere, S., Ernoult-Lange, M., Chouaib, R., et al. (2017). P-body purification reveals the condensation of repressed mRNA regulons. *Mol. Cell* 68, 144–157.e5.

Jain, D., Puno, M. R., Meydan, C., Lailler, N., Mason, C. E., Lima, C. D., et al. (2018). Ketu mutant mice uncover an essential meiotic function for the ancient RNA helicase YTHDC2. *Elife* 7:e30919.

Jia, G., Fu, Y., Zhao, X., Dai, Q., Zheng, G., Yang, Y., et al. (2011). N6-methyladenosine in nuclear RNA is a major substrate of the obesity-associated FTO. *Nat. Chem. Biol.* 7, 885–887. doi: 10.1038/nchembio.687

Kempermann, G., Gage, F. H., Aigner, L., Song, H., Curtis, M. A., Thuret, S., et al. (2018). Human adult neurogenesis: evidence and remaining questions. *Cell Stem Cell* 23, 25–30. doi: 10.1016/j.stem.2018.04.004

Kohwi, M., and Doe, C. Q. (2013). Temporal fate specification and neural progenitor competence during development. *Nat. Rev. Neurosci.* 14, 823–838. doi: 10.1038/nrn3618

Koranda, J. L., Dore, L., Shi, H., Patel, M. J., Vaasjo, L. O., Rao, M. N., et al. (2018). Mettl14 is essential for epitranscriptomic regulation of striatal function and learning. *Neuron* 99, 283–292.e5.

Kretschmer, J., Rao, H., Hackert, P., Sloan, K. E., Hobartner, C., and Bohnsack, M. T. (2018). The m(6)A reader protein YTHDC2 interacts with the small ribosomal subunit and the 5'-3' exoribonuclease XRN1. *RNA* 24, 1339–1350. doi: 10.1261/rna.064238.117

Lees, A. (2017). An essay on the shaking palsy. *Brain* 140, 843–848. doi: 10.1093/brain/awx035

Lein, E. S., Hawrylycz, M. J., Ao, N., Ayres, M., Bensinger, A., Bernard, A., et al. (2007). Genome-wide atlas of gene expression in the adult mouse brain. *Nature* 445, 168–176.

Li, F., Yi, Y., Miao, Y., Long, W., Long, T., Chen, S., et al. (2019). N(6)-methyladenosine modulates nonsense-mediated mRNA decay in human glioblastoma. *Cancer Res.* 79, 5785–5798. doi: 10.1158/0008-5472.can-18-2868

Li, F., Zhao, D., Wu, J., and Shi, Y. (2014). Structure of the YTH domain of human YTHDF2 in complex with an m(6)A mononucleotide reveals an aromatic cage for m(6)A recognition. *Cell Res.* 24, 1490–1492. doi: 10.1038/cr.2014.153

Li, L., Zang, L., Zhang, F., Chen, J., Shen, H., Shu, L., et al. (2017). Fat mass and obesity-associated (FTO) protein regulates adult neurogenesis. *Hum. Mol. Genet.* 26, 2398–2411. doi: 10.1093/hmg/ddx128

Li, M., Zhao, X., Wang, W., Shi, H., Pan, Q., Lu, Z., et al. (2018). Ythdf2-mediated m(6)A mRNA clearance modulates neural development in mice. *Genome Biol.* 19:69.

Li, Y., Guo, X., Sun, L., Xiao, J., Su, S., Du, S., et al. (2020a). N(6)-methyladenosine demethylase FTO contributes to neuropathic pain by stabilizing G9a expression in primary sensory neurons. *Adv. Sci. (Weinh)* 7, 1902402. doi: 10.1002/advs.201902402

Li, Y., Xia, L., Tan, K., Ye, X., Zuo, Z., Li, M., et al. (2020b). N(6)-methyladenosine co-transcriptionally directs the demethylation of histone H3K9me2. *Nat. Genet.* 52, 870–877. doi: 10.1038/s41588-020-0677-3

Liu, J., Yue, Y., Han, D., Wang, X., Fu, Y., Zhang, L., et al. (2014). A METTL3-METTL14 complex mediates mammalian nuclear RNA N6-adenosine methylation. *Nat. Chem. Biol.* 10, 93–95. doi: 10.1038/nchembio.1432

Livneh, I., Moshitch-Moshkovitz, S., Amariglio, N., Rechavi, G., and Dominissini, D. (2020). The m(6)A epitranscriptome: transcriptome plasticity in brain development and function. *Nat. Rev. Neurosci.* 21, 36–51. doi: 10.1038/s41583-019-0244-z

Lu, Q. R., Sun, T., Zhu, Z., Ma, N., Garcia, M., Stiles, C. D., et al. (2002). Common developmental requirement for Olig function indicates a motor neuron/oligodendrocyte connection. *Cell* 109, 75–86. doi: 10.1016/s0092-8674(02)00678-5

Luo, S., and Tong, L. (2014). Molecular basis for the recognition of methylated adenines in RNA by the eukaryotic YTH domain. *Proc. Natl. Acad. Sci. U.S.A.* 111, 13834–13839. doi: 10.1073/pnas.1412742111

Ma, C., Chang, M., Lv, H., Zhang, Z. W., Zhang, W., He, X., et al. (2018). RNA m(6)A methylation participates in regulation of postnatal development of the mouse cerebellum. *Genome Biol.* 19;68.

Mahar, M., and Cavalli, V. (2018). Intrinsic mechanisms of neuronal axon regeneration. *Nat. Rev. Neurosci.* 19, 323–337. doi: 10.1038/s41583-018-0001-8

Majdan, M., Plancikova, D., Maas, A., Polinder, S., Feigin, V., Theadom, A., et al. (2017). Years of life lost due to traumatic brain injury in Europe: a cross-sectional analysis of 16 countries. *PLoS Med.* 14:e1002331. doi: 10.1371/journal.pmed.1002331

Mauer, J., Luo, X., Blanjoie, A., Jiao, X., Grozhik, A. V., Patil, D. P., et al. (2017). Reversible methylation of m(6)Am in the 5' cap controls mRNA stability. *Nature* 541, 371–375. doi: 10.1038/nature21022

McKenna, M. C., Scafidi, S., and Robertson, C. L. (2015). Metabolic alterations in developing brain after injury: knowns and unknowns. *Neurochem. Res.* 40, 2527–2543. doi: 10.1007/s11064-015-1600-7

Merkurjev, D., Hong, W. T., Iida, K., Oomoto, I., Goldie, B. J., Yamaguti, H., et al. (2018). Synaptic N(6)-methyladenosine (m(6)A) epitranscriptome reveals functional partitioning of localized transcripts. *Nat. Neurosci.* 21, 1004–1014. doi: 10.1038/s41593-018-0173-6

Meyer, K. D., Saletore, Y., Zumbo, P., Elemento, O., Mason, C. E., and Jaffrey, S. R. (2012). Comprehensive analysis of mRNA methylation reveals enrichment in 3' UTRs and near stop codons. *Cell* 149, 1635–1646. doi: 10.1016/j.cell.2012.05.003

Nave, K. A. (2010). Myelination and support of axonal integrity by glia. *Nature* 468, 244–252. doi: 10.1038/nature09614

Park, O. H., Ha, H., Lee, Y., Boo, S. H., Kwon, D. H., Song, H. K., et al. (2019). Endoribonucleolytic cleavage of m(6)A-containing RNAs by RNase P/MRP complex. *Mol. Cell* 74, 494–507.e8.

Patil, D. P., Chen, C. K., Pickering, B. F., Chow, A., Jackson, C., Guttman, M., et al. (2016). m(6)A RNA methylation promotes XIST-mediated transcriptional repression. *Nature* 537, 369–373. doi: 10.1038/nature19342

Patil, D. P., Pickering, B. F., and Jaffrey, S. R. (2018). Reading m(6)A in the transcriptome: m(6)A-binding proteins. *Trends Cell Biol.* 28, 113–127. doi: 10.1016/j.tcb.2017.10.001

Ping, X. L., Sun, B. F., Wang, L., Xiao, W., Yang, X., Wang, W. J., et al. (2014). Mammalian WTAP is a regulatory subunit of the RNA N6-methyladenosine methyltransferase. *Cell Res.* 24, 177–189. doi: 10.1038/cr.2014.3

Puttagunta, R., Tedeschi, A., Soria, M. G., Hervera, A., Lindner, R., Rathore, K. I., et al. (2014). PCAF-dependent epigenetic changes promote axonal regeneration in the central nervous system. *Nat. Commun.* 5:3527.

Ries, R. J., Zaccara, S., Klein, P., Olarerin-George, A., Namkoong, S., Pickering, B. F., et al. (2019). m(6)A enhances the phase separation potential of mRNA. *Nature* 571, 424–428. doi: 10.1038/s41586-019-1374-1

Rottman, F., Shatkin, A. J., and Perry, R. P. (1974). Sequences containing methylated nucleotides at the 5' termini of messenger RNAs: possible implications for processing. *Cell* 3, 197–199. doi: 10.1016/0092-8674(74)90131-7

Roundtree, I. A., Evans, M. E., Pan, T., and He, C. (2017a). Dynamic RNA modifications in gene expression regulation. *Cell* 169, 1187–1200. doi: 10.1016/j.cell.2017.05.045

Roundtree, I. A., Luo, G. Z., Zhang, Z., Wang, X., Zhou, T., Cui, Y., et al. (2017b). YTHDC1 mediates nuclear export of N(6)-methyladenosine methylated mRNAs. *Elife* 6:e31311.

Rowitch, D. H., and Kriegstein, A. R. (2010). Developmental genetics of vertebrate glial-cell specification. *Nature* 468, 214–222. doi: 10.1038/nature09611

Schwartz, S., Mumbach, M. R., Jovanovic, M., Wang, T., Maciag, K., Bushkin, G. G., et al. (2014). Perturbation of m6A writers reveals two distinct classes of mRNA methylation at internal and 5' sites. *Cell Rep.* 8, 284–296. doi: 10.1016/j.celrep.2014.05.048

Shafik, A. M., Zhang, F., Guo, Z., Dai, Q., Pajdzik, K., Li, Y., et al. (2021). N6-methyladenosine dynamics in neurodevelopment and aging, and its potential role in Alzheimer's disease. *Genome Biol.* 22:17.

Shi, H., Wang, X., Lu, Z., Zhao, B. S., Ma, H., Hsu, P. J., et al. (2017). YTHDF3 facilitates translation and decay of N(6)-methyladenosine-modified RNA. *Cell Res.* 27, 315–328. doi: 10.1038/cr.2017.15

Shi, H., Zhang, X., Weng, Y. L., Lu, Z., Liu, Y., Lu, Z., et al. (2018). m(6)A facilitates hippocampus-dependent learning and memory through YTHDF1. *Nature* 563, 249–253. doi: 10.1038/s41586-018-0666-1

Si, W., Li, Y., Ye, S., Li, Z., Liu, Y., Kuang, W., et al. (2020). Methyltransferase 3 mediated miRNA m6A methylation promotes stress granule formation in the early stage of acute ischemic stroke. *Front. Mol. Neurosci.* 13:103. doi: 10.3389/fnmol.2020.00103

Sledz, P., and Jinek, M. (2016). Structural insights into the molecular mechanism of the m(6)A writer complex. *Elife* 5:e18434.

Stoilov, P., Rafalska, I., and Stamm, S. (2002). YTH: a new domain in nuclear proteins. *Trends Biochem. Sci.* 27, 495–497. doi: 10.1016/s0968-0004(02)02189-8

Theler, D., Dominguez, C., Blatter, M., Boudet, J., and Allain, F. H. (2014). Solution structure of the YTH domain in complex with N6-methyladenosine RNA: a reader of methylated RNA. *Nucleic Acids Res.* 42, 13911–13919. doi: 10.1093/nar/gku1116

Visvanathan, A., Patil, V., Arora, A., Hegde, A. S., Arivazhagan, A., Santosh, V., et al. (2018). Essential role of METTL3-mediated m(6)A modification in glioma stem-like cells maintenance and radioresistance. *Oncogene* 37, 522–533. doi: 10.1038/onc.2017.351

Walters, B. J., Mercaldo, V., Gillon, C. J., Yip, M., Neve, R. L., Boyce, F. M., et al. (2017). The role of the RNA demethylase FTO (Fat Mass and Obesity-Associated) and mRNA methylation in hippocampal memory formation. *Neuropsychopharmacology* 42, 1502–1510. doi: 10.1038/npp.2017.31

Wang, C. X., Cui, G. S., Liu, X., Xu, K., Wang, M., Zhang, X. X., et al. (2018). METTL3-mediated m6A modification is required for cerebellar development. *PLoS Biol.* 16:e2004880. doi: 10.1371/journal.pbio.2004880

Wang, D. O., Kim, S. M., Zhao, Y., Hwang, H., Miura, S. K., Sossin, W. S., et al. (2009). Synapse- and stimulus-specific local translation during long-term neuronal plasticity. *Science* 324, 1536–1540. doi: 10.1126/science.1173205

Wang, P., Doxtader, K. A., and Nam, Y. (2016). Structural basis for cooperative function of Mettl3 and Mettl14 methyltransferases. *Mol. Cell* 63, 306–317. doi: 10.1016/j.molcel.2016.05.041

Wang, W., Jiang, B., Sun, H., Ru, X., Sun, D., Wang, L., et al. (2017). Prevalence, incidence, and mortality of stroke in China: results from a nationwide population-based survey of 480 687 adults. *Circulation* 135, 759–771. doi: 10.1161/circulationaha.116.025250

Wang, X., Feng, J., Xue, Y., Guan, Z., Zhang, D., Liu, Z., et al. (2016). Structural basis of N(6)-adenosine methylation by the METTL3-METTL14 complex. *Nature* 534, 575–578. doi: 10.1038/nature18298

Wang, X., Lu, Z., Gomez, A., Hon, G. C., Yue, Y., Han, D., et al. (2014). N6-methyladenosine-dependent regulation of messenger RNA stability. *Nature* 505, 117–120. doi: 10.1038/nature12730

Wang, X., Zhao, B. S., Roundtree, I. A., Lu, Z., Han, D., Ma, H., et al. (2015). N(6)-methyladenosine Modulates Messenger RNA Translation Efficiency. *Cell* 161, 1388–1399. doi: 10.1016/j.cell.2015.05.014

Wang, Y., Li, Y., Yue, M., Wang, J., Kumar, S., Wechsler-Reya, R. J., et al. (2018). N(6)-methyladenosine RNA modification regulates embryonic neural stem cell self-renewal through histone modifications. *Nat. Neurosci.* 21, 195–206. doi: 10.1038/s41593-017-0057-1

Wang, Y., Mao, J., Wang, X., Lin, Y., Hou, G., Zhu, J., et al. (2019). Genome-wide screening of altered m6A-tagged transcript profiles in the hippocampus after traumatic brain injury in mice. *Epigenomics* 11, 805–819. doi: 10.2217/epi-2019-0002

Wei, C. M., Gershowitz, A., and Moss, B. (1975). Methylated nucleotides block 5' terminus of HeLa cell messenger RNA. *Cell* 4, 379–386. doi: 10.1016/0092-8674(75)90158-0

Weng, Y. L., An, R., Cassin, J., Joseph, J., Mi, R., Wang, C., et al. (2017). An intrinsic epigenetic barrier for functional axon regeneration. *Neuron* 94, 337–346.e6.

Weng, Y. L., Wang, X., An, R., Cassin, J., Vissers, C., Liu, Y., et al. (2018). Epitranscriptomic m(6)A regulation of axon regeneration in the adult mammalian nervous system. *Neuron* 97, 313–325.e6.

Widagdo, J., Zhao, Q. Y., Kempen, M. J., Tan, M. C., Ratnu, V. S., Wei, W., et al. (2016). Experience-dependent accumulation of N6-methyladenosine in the prefrontal cortex is associated with memory processes in mice. *J. Neurosci.* 36, 6771–6777. doi: 10.1523/jneurosci.4053-15.2016

Wojtas, M. N., Pandey, R. R., Mendel, M., Homolka, D., Sachidanandam, R., and Pillai, R. S. (2017). Regulation of m(6)A transcripts by the 3'–>5' RNA helicase YTHDC2 is essential for a successful meiotic program in the mammalian germline. *Mol. Cell* 68, 374–387.e12.

Wu, R., Li, A., Sun, B., Sun, J. G., Zhang, J., Zhang, T., et al. (2019). A novel m(6)A reader Prrc2a controls oligodendroglial specification and myelination. *Cell Res.* 29, 23–41. doi: 10.1038/s41422-018-0113-8

Xiao, W., Adhikari, S., Dahal, U., Chen, Y. S., Hao, Y. J., Sun, B. F., et al. (2016). Nuclear m(6)A reader YTHDC1 regulates mRNA splicing. *Mol. Cell* 61, 507–519. doi: 10.1016/j.molcel.2016.01.012

Xu, C., Liu, K., Ahmed, H., Loppnau, P., Schapira, M., and Min, J. (2015). Structural basis for the discriminative recognition of N6-methyladenosine RNA by the human YT521-B homology domain family of proteins. *J. Biol. Chem.* 290, 24902–24913. doi: 10.1074/jbc.m115.680389

Xu, C., Wang, X., Liu, K., Roundtree, I. A., Tempel, W., Li, Y., et al. (2014). Structural basis for selective binding of m6A RNA by the YTHDC1 YTH domain. *Nat. Chem. Biol.* 10, 927–929. doi: 10.1038/nchembio.1654

Xu, H., Dzhashiashvili, Y., Shah, A., Kunjamma, R. B., Weng, Y. L., Elbaz, B., et al. (2020). m(6)A mRNA methylation is essential for oligodendrocyte maturation and CNS myelination. *Neuron* 105, 293–309.e5.

Xu, K., Mo, Y., Li, D., Yu, Q., Wang, L., Lin, F., et al. (2020). N(6)-methyladenosine demethylases Alkbh5/Fto regulate cerebral ischemia-reperfusion injury. *Ther. Adv. Chronic. Dis.* 11:2040622320916024.

Xu, S., Li, Y., Chen, J. P., Li, D. Z., Jiang, Q., Wu, T., et al. (2020). Oxygen glucose deprivation/re-oxygenation-induced neuronal cell death is associated with Lnc-D63785 m6A methylation and miR-422a accumulation. *Cell Death Dis.* 11:816.

Yoon, K. J., Ringeling, F. R., Vissers, C., Jacob, F., Pokrass, M., Jimenez-Cyrus, D., et al. (2017). Temporal control of mammalian cortical neurogenesis by m(6)A methylation. *Cell* 171, 877–889.e17.

Yu, J., Chen, M., Huang, H., Zhu, J., Song, H., Zhu, J., et al. (2018). Dynamic m6A modification regulates local translation of mRNA in axons. *Nucleic Acids Res.* 46, 1412–1423. doi: 10.1093/nar/gkx1182

Zaccara, S., and Jaffrey, S. R. (2020). A unified model for the function of YTHDF proteins in regulating m(6)A-modified mRNA. *Cell* 181, 1582–1595.e18.

Zaccara, S., Ries, R. J., and Jaffrey, S. R. (2019). Reading, writing and erasing mRNA methylation. *Nat. Rev. Mol. Cell. Biol.* 20, 608–624. doi: 10.1038/s41580-019-0168-5

Zhang, C., Wang, Y., Peng, Y., Xu, H., and Zhou, X. (2020). METTL3 regulates inflammatory pain by modulating m(6)A-dependent pri-miR-365-3p processing. *FASEB J.* 34, 122–132. doi: 10.1096/fj.201901555r

Zhang, S., Zhao, B. S., Zhou, A., Lin, K., Zheng, S., Lu, Z., et al. (2017). m(6)A Demethylase ALKBH5 maintains tumorigenicity of glioblastoma stem-like cells by sustaining FOXM1 expression and cell proliferation program. *Cancer Cell* 31, 591–606.e6.

Zhang, Z., Wang, M., Xie, D., Huang, Z., Zhang, L., Yang, Y., et al. (2018). METTL3-mediated N(6)-methyladenosine mRNA modification enhances long-term memory consolidation. *Cell Res.* 28, 1050–1061. doi: 10.1038/s41422-018-0092-9

Zhang, Z., Wang, Q., Zhao, X., Shao, L., Liu, G., Zheng, X., et al. (2020). YTHDC1 mitigates ischemic stroke by promoting Akt phosphorylation through destabilizing PTEN mRNA. *Cell Death Dis.* 11:977.

Zheng, G., Dahl, J. A., Niu, Y., Fedorcsak, P., Huang, C. M., Li, C. J., et al. (2013). ALKBH5 is a mammalian RNA demethylase that impacts RNA metabolism and mouse fertility. *Mol. Cell* 49, 18–29. doi: 10.1016/j.molcel.2012.10.015

Zhou, Q., and Anderson, D. J. (2002). The bHLH transcription factors OLIG2 and OLIG1 couple neuronal and glial subtype specification. *Cell* 109, 61–73. doi: 10.1016/s0092-8674(02)00677-3

Zhuang, M., Li, X., Zhu, J., Zhang, J., Niu, F., Liang, F., et al. (2019). The m6A reader YTHDF1 regulates axon guidance through translational control of Robo3.1 expression. *Nucleic Acids Res.* 47, 4765–4777. doi: 10.1093/nar/gkz157

Conflict of Interest: The authors declare that the research was conducted in the absence of any commercial or financial relationships that could be construed as a potential conflict of interest.

frontiers in Cell and Developmental Biology

ORIGINAL RESEARCH
published: 28 May 2021
doi: 10.3389/fcell.2021.656554

lncRNA Profiles Enable Prognosis Prediction and Subtyping for Esophageal Squamous Cell Carcinoma

Shujun Zhang[1†], Juan Li[1†], Huiru Gao[1], Yao Tong[1], Peilong Li[1], Yunshan Wang[1], Lutao Du[1,2,3] and Chuanxin Wang[1,2,3*]*

[1] Department of Clinical Laboratory, The Second Hospital, Cheeloo College of Medicine, Shandong University, Jinan, China, [2] Shandong Engineering & Technology Research Center for Tumor Marker Detection, Jinan, China, [3] Shandong Provincial Clinical Medicine Research Center for Clinical Laboratory, Jinan, China

OPEN ACCESS

Edited by:
Xuekun Li,
Zhejiang University, China

Reviewed by:
Zhao-Qian Teng,
Institute of Zoology, Chinese Academy of Sciences, China
Feng Wang,
Emory University, United States

***Correspondence:**
Lutao Du
lutaodu@sdu.edu.cn
Chuanxin Wang
cxwang@sdu.edu.cn

[†] These authors have contributed equally to this work and share first authorship

Specialty section:
This article was submitted to Epigenomics and Epigenetics, a section of the journal Frontiers in Cell and Developmental Biology

Received: 21 January 2021
Accepted: 08 April 2021
Published: 28 May 2021

Citation:
Zhang S, Li J, Gao H, Tong Y, Li P, Wang Y, Du L and Wang C (2021) lncRNA Profiles Enable Prognosis Prediction and Subtyping for Esophageal Squamous Cell Carcinoma. Front. Cell Dev. Biol. 9:656554. doi: 10.3389/fcell.2021.656554

Long non-coding RNAs (lncRNAs) have emerged as useful prognostic markers in many tumors. In this study, we investigated the potential application of lncRNA markers for the prognostic prediction of esophageal squamous cell carcinoma (ESCC). We identified ESCC-associated lncRNAs by comparing ESCC tissues with normal tissues. Subsequently, Kaplan–Meier (KM) method in combination with the univariate Cox proportional hazards regression (UniCox) method was used to screen prognostic lncRNAs. By combining the differential and prognostic lncRNAs, we developed a prognostic model using cox stepwise regression analysis. The obtained prognostic prediction model could effectively predict the 3- and 5-year prognosis and survival of ESCC patients by time-dependent receiver operating characteristic (ROC) curves (area under curve = 0.87 and 0.89, respectively). Besides, a lncRNA-based classification of ESCC was generated using k-mean clustering method and we obtained two clusters of ESCC patients with association with race and Barrett's esophagus (BE) (both $P < 0.001$). Finally, we found that lncRNA AC007128.1 was upregulated in both ESCC cells and tissues and associated with poor prognosis of ESCC patients. Furthermore, AC007128.1 could promote epithelial-mesenchymal transition (EMT) of ESCC cells by increasing the activation of MAPK/ERK and MAPK/p38 signaling pathways. Collectively, our findings indicated the potentials of lncRNA markers in the prognosis, molecular subtyping, and EMT of ESCC.

Keywords: ESCC, lncRNAs, prognosis, molecular subtyping, EMT

INTRODUCTION

Esophageal cancer is one of the most common cancers worldwide, and it ranks seventh and sixth in terms of overall incidence and mortality, respectively (Bray et al., 2018). There are two histologic subtypes including esophageal squamous cell carcinoma (ESCC) and esophageal adenocarcinoma (AC) (Short et al., 2017). ESCC occupies over 90% of all esophageal cancer patients and the long-term outcome of ESCC is still limited with 5-year survival rate of 20% (Pennathur et al., 2013; Siegel et al., 2020). In general, prognostic factors may be helpful for better individual risk stratification

and clinical outcome prediction. Traditional prognostic factors mainly depend on clinical and pathologic features, such as the history of drinking and smoking, tumor stage, and lymph node metastasis and so on, which have an effect on the overall survival (OS) in ESCC. However, the clinical course of ESCC patients with the same characteristics might be significantly different (Liu et al., 2012). Discovering new prognostic factors that improve the clinical outcome prediction of patients has been an urgent clinical need in ESCC.

As endogenous RNA transcripts with more than 200 nucleotides, long non-coding RNAs (lncRNAs) lack protein-coding potentials (Djebali et al., 2012; Iyer et al., 2015; Quinn and Chang, 2016). They are now known to act as scaffolds to modulate interactions between proteins and genes, as decoys to bind proteins, and as enhancers to regulate transcription of target genes (Huarte, 2015; Schmitt and Chang, 2016; Yue et al., 2016; Zhang et al., 2018; Blank-Giwojna et al., 2019). The discrepant expressions of lncRNAs, which have been demonstrated in various types of malignancies, possess significant regulatory effects on oncogenesis and tumor progression, indicating their potential oncogenic and tumor-suppressive roles (Hu et al., 2014; Li et al., 2018b; Wang et al., 2018). Growing evidence has suggested that unique lncRNA expression profiles can provide important prognostic information for patients with cancer (Cheng, 2018). Till today, several differentially expressed lncRNAs have been proved to be relevant for ESCC prognosis (Xie et al., 2014; Chen et al., 2015; Hu et al., 2015; Wang et al., 2015). However, previously published studies mainly focused on single lncRNAs as prognostic biomarkers. Little or nothing is known about the multi-lncRNA-based signature associated with OS in ESCC.

Our previous study has shown that the serumal and/or urinary exosome lncRNA profiles can be applied to the diagnosis and prognostic prediction of bladder cancer, colorectal cancer, breast cancer, and lung cancer (Li et al., 2017, 2018a; Xie et al., 2018; Zhan et al., 2018; Zhang et al., 2019). In the present study, we used publicly available The Cancer Genome Atlas (TCGA) RNA-seq expression data and evaluated the potential effectiveness of lncRNA biomarkers for prognosis and subtyping of ESCC. We constructed a prognostic model with selected lncRNA markers and further obtained a lncRNA-based subtype of ESCC by k-means method. Besides, we validated the biological role of lncRNA AC007128.1 by cellular assays in ESCC progression.

MATERIALS AND METHODS

Study Design

In the present study, we were aimed at identifying lncRNA-based model for the prognostic prediction and subtyping of ESCC. Firstly, differential and prognostic lncRNA markers were identified from public TCGA ESCC RNA-seq datasets, and then the prognostic model was constructed by cox stepwise regression analysis. The model was evaluated with cross-validation and time-dependent receiver operating characteristic (ROC) methods and then compared with the clinical characteristics including stage, lymph node metastasis, and distant metastasis. With the lncRNA profiles, two lncRNA ESCC clusters were also constructed via the unsupervised clustering method, and the robustness of subtyping markers in two other datasets was verified. The potential function and mechanism of AC007128.1 were further investigated, which demonstrated high expression in ESCC cells and tissues and could promote cell migration and invasion by MAPK pathway.

Patients Source

Tissue RNA-seq data were obtained from TCGA and Gene Expression Omnibus (GEO) (TCGA-ESCA and GSE53625). Complete clinical and histopathological information are available at TCGA and GEO websites as follows: https://tcga-data.nci.nih.gov/tcga/ and https://www.ncbi.nlm.nih.gov/geo/. The characteristics of ESCC patients are summarized in **Supplementary Table 1**.

Unsupervised Discovery of lncRNA-Based Subtypes

The training dataset (n = 111) was used to discover ESCC subtypes. To narrow down markers and obtain meaningful clustering by lncRNA information, the list was firstly ranked by variance, and the top 1,000 lncRNAs with the larger variance were selected. Secondly, different clustering methods, including hierarchical clustering (HC) (single, complete, average, centroid, and ward) and non-hierarchical clustering (NHC), were compared. Finally, the k-means was chosen to cluster for ESCC. Differentially expressed lncRNA markers were obtained among the new clusters by using the limma package, and the top 50 differential lncRNAs were selected. These 50 marker sets were finally used as the signature to predict ESCC subtypes. Validation was performed on the two predefined validation datasets (n = 51 and 179).

Cell Lines and Cell Culture

Three human ESCC cell lines (KYSE150, EC109, and TE-1) and two normal esophageal epithelial cell lines (Het-1A and HEEC) were bought from the Chinese Academy of Medical Sciences (CAMS), China. KYSE150 and TE-1 cells were cultured in Roswell Park Memorial Institute 1640 (RPMI-1640) medium supplemented with 10% fetal bovine serum (FBS) (Australia Origin, Gibco, Carlsbad, CA, United States) at 37°C in a humidified atmosphere containing 5% CO_2. EC109, Het-1A, and HEEC cells were maintained in Dulbecco's Modified Eagle's Medium (DMEM) supplemented with 10% FBS at 37°C in a humidified atmosphere containing 5% CO_2.

Small Interfering RNAs, Short Hairpin RNAs, Plasmids and Lentivirus Transduction

Small interfering RNAs (siRNAs) or plasmids were transfected into ESCC cells using Lipofectamine 2000 (Invitrogen, United States) following the manufacturer's instructions. The supernatant of the lentivirus-infected cells was substituted with a complete culture medium after 24 h. The stable cell lines were constructed using puromycin. PcDNA3.1-AC007128.1

and pcDNA3.1 empty vector (BoShang, Jinan, China) were extracted using the Endo-Free Plasmid Mini Kit (Omega Bio-Tek, United States). Sequences for short hairpin RNAs (shRNAs) and siRNAs are listed in **Supplementary Table 2**.

Cell Viability Assay

Cell viability was examed using the Cell Counting Kit-8 (CCK-8) assay (Dojindo Labs). The optical density was assessed with a microplate reader (Bio-Rad, Hercules, CA, United States) at a wavelength of 450 nm.

Transwell Invasion and Migration Assays

The transwell invasion assay was done using the transwell (Corning, NY, United States) and matrigel (BD Biosciences, San Jose, CA, United States). Briefly, inserts with 8-μm pores were coated with 8 μL of matrigel. Cells ($\sim 7.5 \times 10^4$) with 200 μL of serum-free medium were added into the upper compartment of the chamber. Subsequently, 600 μL of RPMI-1640 medium or DMEM containing 20% FBS was added into the lower chamber of the chamber as a chemo-attractant. After 36 h of incubation at 37°C in a humidified atmosphere containing 5% CO_2, cells that migrated through the matrigel were fixed with methanol, stained with 0.1% crystal violet, and photographed using a microscope (Zeiss, Axio Observer). The cell number in five randomly selected fields from the central and peripheral regions of the filter was counted. The migration assay was conducted similarly without matrigel coating.

Wound Healing Assay

Wound healing assay was conducted in six-well plates. When cells reached a confluence of 90–100%, a wound was made with a 200-μL pipette tip. Spreading cells between parallel lines were measured by an inverted microscope (Zeiss, Axio Observer) and photographed after 0 and 24 h.

RNA Isolation and Real-Time PCR

Total RNA was obtained from cultured cells with RNA fast 2000 Reagent (Fastagen, Shanghai, China) and quantified with a NanoDrop spectrophotometer (Thermo Fisher Scientific, Waltham, MA, United States). Purified RNA was reversely transcribed into cDNA using oligo-dT and random primers with the PrimeScript™ RT reagent Kit (TaKara, Dalian, China). Real-time PCR was performed on a CFX-96 real-time PCR System (Bio-Rad, Shanghai, China) using TB Green™ Premix Ex Taq™ (TaKara, Dalian China). Glyceraldehyde phosphate dehydrogenase (GAPDH) was employed as a housekeeping gene. The relative expressions of the target genes were calculated using the $2^{-\Delta\Delta CT}$ method and subsequent log2 transformed. Primer sequences are displayed in **Supplementary Table 3**.

Western Blotting Analysis

Total cell lysates were obtained by using the Western/IP lysis buffer (Beyotime, Haimen, China). Equal amounts of proteins were subjected to sodium dodecyl sulfate-polyacrylamide gel electrophoresis (SDS–PAGE) and then transferred onto polyvinylidene fluoride (PVDF) membranes (Millipore, United States). Membranes were immunoblotted with primary antibodies (**Supplementary Table 4**), followed by incubation with peroxidase-conjugated affinipure goat anti-mouse IgG or peroxidase-conjugated affinipure goat anti-rabbit IgG (**Supplementary Table 4**). Immunoreactive bands were visualized using the enhanced chemiluminescence system (Bio-Rad Laboratories). GAPDH was adopted as a loading control.

RNA-seq Library Construction

For RNA-seq experiments with shCtrl and shAC007128.1 in KYSE150 cells, total RNA was isolated from cells with the RNeasy mini kit (Qiagen, Germany). Paired-end libraries were constructed using the TruSeq™ RNA Sample Preparation Kit (Illumina, United States) according to TruSeq™ RNA Sample Preparation Guide. Briefly, the mRNA containing poly-A were purified using poly-T oligo-attached magnetic beads.

After purification, the mRNA was cleaved into small fragments using divalent cations at 94°C for 8 min. The cleaved RNA fragments were amplified into first-strand cDNA using reverse transcriptase and random primers. Second-strand cDNA then was synthesized by DNA polymerase I and RNase H. Next, these cDNA fragments went through an end-repair process, the addition of a single "A" base, and then ligation of the adapters. The products were purified and enriched with PCR to create the final cDNA library. Purified libraries were quantified by Qubit® 2.0 Fluorometer (Life Technologies, United States) and validated by Agilent 2100 bioanalyzer (Agilent Technologies, United States) to confirm the insert size and calculate the molar concentration. Clusters were generated by cBot with the library diluted to 10 pM and then sequenced on the Illumina NovaSeq 6000 (Illumina, United States).

The library was constructed and sequenced at Shanghai Sinomics Corporation.

RNA Sequencing Analysis

Raw reads were preprocessed by filtering out rRNA reads, sequencing adapters, short-fragment reads, and other low-quality reads. Tophat v2.0.9 (Trapnell et al., 2009) was used to map the cleaned reads to the human hg38 reference genome with two mismatches. After mapping, Cufflinks v2.1.1 (Trapnell et al., 2012) was used to generate FPKM values for known gene models. Differentially expressed genes (DEGs) were identified using Cuffdiff (Trapnell et al., 2012). The *p*-value significance threshold in multiple tests was set by the false discovery rate (FDR) (Storey and Tibshirani, 2003). The fold changes (FCs) were also estimated according to the FPKM in each sample. The DEGs were selected using the filter criteria as follows: FDR ≤ 0.05 and FC ≥ 2.

Statistical Analysis

A Cox regression model was applied to build the combined prognosis score (cp-score). Survival analysis was performed by KM curves and log-rank tests with a high-risk and low-risk group assignment relative to the median of cp-score. The time-dependent ROC curve was adopted to compare the performance of cp-score, TNM stage, lymph node metastasis,

distant metastasis, and the combination of all factors. The effects of potential risk factors upon the survival time were assessed by multivariate Cox regression analysis. A P-value < 0.05 was considered statistically significant. Analysis for functional data were presented as mean ± SEM. The comparison between two groups was conducted by the Student's t-test. All statistical analyses were performed using R software (version 3.6.0.), SPSS 17.0 (IBM, SPSS, Chicago, IL, United States) and GraphPad Prism 5.0 (GraphPad Software, LaJolla, CA, United States).

RESULTS

Identification of Differential and Prognostic LncRNAs for ESCC

Based on the RNA-seq data from TCGA database, we extracted lncRNA expression profiles and compared them between 111 ESCC tumor samples and 11 normal samples with DEseq2 package (Love et al., 2014), defined the best cutoff of 2.482 with the mean of absolute log2FC plus standard deviation of absolute log2FC, and found 422 lncRNAs with an FDR less than 0.05, including 257 up-regulated and 165 down-regulated lncRNAs (**Figure 1A**). The heatmap and principal component analysis (PCA) disclosed that ESCC patients and controls could be differentiated by the lncRNA expression profile (**Figures 1B,C**). These selected differential lncRNAs were considered as candidate prognostic markers for ESCC patients.

To select the prognostic lncRNAs, we analyzed 111 ESCC patients from TCGA with a follow-up of more than 1 month. The KM and univariate Cox proportional hazards regression (UniCox) methods were implemented to reduce the dimensionality. We obtained 413 overlapping lncRNAs based on the two algorithms, which were significantly correlated with the ESCC patients' OS (**Figure 1D**). Based on the differential and prognostic lncRNAs, 13 lncRNAs were considered as candidate prognostic biomarkers for ESCC patients (**Figure 1D**).

Meanwhile, we examined the relationship between clinicopathological features and patients' survival time. Patients with late-stage tumors or lymph node metastasis or distant metastasis had a shorter OS than those with early-stage tumors or without lymph node metastasis or distant metastasis (P = 0.00098, 0.02, and 0.00093 respectively, by log-rank test) (**Figures 1E–G**). However, gender, age, race, alcohol, Barrett's esophagus (BE), and T stage were not correlated with the OS (**Supplementary Figures 1A–E**). Furthermore, UniCox showed the same results as the log-rank analysis (**Table 1**). Overall, these results suggested advanced stage, lymph node metastasis, and distant metastasis were related to poor prognosis of patients.

LncRNA-Based Prognostic Prediction Model for ESCC

To construct the prognostic model, the 13 candidate lncRNAs were subjected to cox stepwise regression analysis, and 11 out of 13 lncRNAs were selected to build an optimum prognostic model, with a c-index of 0.73 indicating good discrimination (**Figure 2A**). **Supplementary Table 5** lists the characteristics of 11 prognostic lncRNAs including permutation P-values, hazard ratios, and coefficients and so on. **Figure 3E** and **Supplementary Figures 2A–J** illustrate the KM curves for these lncRNAs. We introduced a cp-score for the prognostic prediction of ESCC according to Luo et al. (2020). The cp-score was obtained according to the coefficients from cox regression and separated the patients into high-risk and low-risk groups. KM curves were performed by using the dichotomized cp-score. The result showed that the low-risk group had significantly better survival time compared with the high-risk group ($P < 0.0001$) (**Figure 2B**). **Figures 2C–E** show the distribution of the risk score, OS status and the corresponding expression profiles of 11 lncRNAs, which were ranked according to the cp-score value. The mortality of high-risk patients was higher than low-risk patients.

Furthermore, we used a time-dependent ROC curve (Heagerty et al., 2000) to characterize the prognostic potential of the cp-score, pathological stage, lymph node metastasis, distant metastasis, and the combination of all above factors. The prognostic prediction model could effectively predict the 3- and 5-year prognosis and survival of ESCC patients by time-dependent ROC curves with area under curve 0.87 and 0.89, respectively (**Figures 2F–G**). Compared with pathological stage, lymph node metastasis, and distant metastasis, the cp-score both showed a better ability to predict prognosis in the 3- and 5-year (**Figures 2F–G**). Besides, the combination of cp-score and clinicopathologic characteristics significantly improved the performance to predict the 5-year prognosis [AUC-ROC:1.00] (**Figure 2G**) compared with the cp-score or clinicopathologic features alone, including TNM stage, lymph node metastasis, and distant metastasis.

Next, we assessed the association between cp-score and the TNM stage, T stage, the presence of lymph node metastasis, and distant metastasis of ESCC. Patients with stage I/II disease had lower cp-scores than those with stage III/IV disease (P = 0.03; **Figure 2H**). Similarly, the cp-scores of patients with lymph node and distant metastasis were significantly higher compared with those without lymph node and distant metastasis (P = 0.014 and 0.0036; **Figures 2I,J**). The cp-scores of patients with T3/4 tumors were moderately higher compared with those with T1/2 tumors (P = 0.18; **Supplementary Figure 2K**). These results demonstrated that the cp-score was correlated with the tumor stage and might be used to predict the TNM stage, lymph node, and distant metastasis. Multivariate Cox regression analysis indicated that the cp-score was an independent prognostic factor for ESCC (**Table 1**).

lncRNA-Based Subtyping of ESCC

We used unsupervised clustering to generate lncRNA-based subtypes of ESCC. **Figure 4A** illustrates the schematic diagram for sample clustering. Firstly, we compared different clustering methods, including HC (single, complete, average, centroid, and ward) and NHC methods (k-means). Ward showed better results among HC methods (**Supplementary Figures 3A–E**). The quality of the single clustering solutions could be assessed with average silhouette width as a measure for clustering quality, so we compare the clustering ability between ward and k-means methods by silhouette plot. The results showed ward method

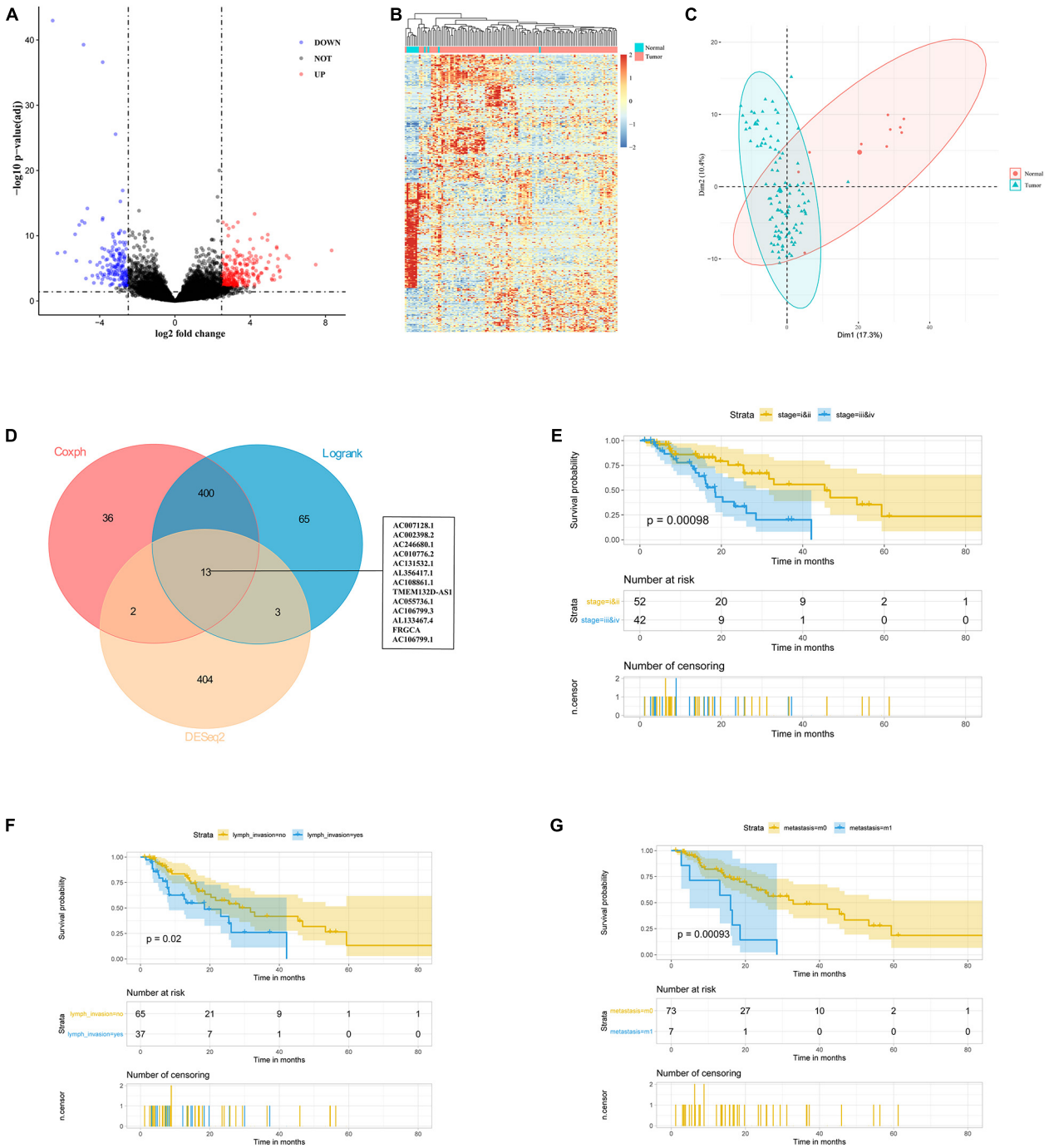

FIGURE 1 | Identification of 13 lncRNAs as candidate prognostic markers for ESCC. **(A)** Volcano plot exhibited differentially expressed lncRNAs. **(B)** Heatmap analysis showed that ESCC patients could be distinguished by dysregulated lncRNAs. **(C)** PCA showed successful segregation between tumor and normal tissues. **(D)** The intersection of differentially expressed and prognostic lncRNAs by DEseq2, log-rank, and cox analysis. **(E–G)** Exploratory KM analysis (log-rank test) of the OS probability (with 95% confidence intervals) in ESCC patients [**(E)** TNM stage; **(F)** lymph node metastasis; and **(G)** distant metastasis].

had a lower silhouette width (0.17) than *k*-means (0.2), which indicated that the clustering quality of ward method was inferior to that of *k*-means (**Supplementary Figures 3G,H**). We finally chose the k-means to cluster for ESCC. Using the 111 ESCC patients as a training dataset, we obtained two clusters with 50 lncRNAs that were different expression between the two clusters and clinical data were indicated by the annotation bars above the heatmap (**Figure 4B**). Silhouette analysis of the clusters showed a good clustering quality with average width 0.54 (**Figure 4C**). We also validated the clusters from residual

TABLE 1 | Univariate and multivariable Cox regression analysis with covariates including cp-score, gender, age, race, alcohol, BE, stage, and T stage, lymph invasion and metastasis for overall survival.

Factor		Univariate coef					Multivariate coef			
		Exp (coef)	SE (coef)	*z*	*P*		Exp (coef)	SE (coef)	*z*	*P*
cp-score: L vs. H	−2.226	0.108	0.451	−4.936	**0.000**	−1.683	0.186	0.564	−2.986	**0.003**
Gender: M vs. F	0.369	1.446	0.525	0.702	0.483					
Age: >=60 vs. <60	−0.265	0.767	0.291	−0.91	0.363					
Race: White vs. Asian	0.322	1.38	0.74	0.435	0.663					
Alcohol_history: Yes vs. No	−0.281	0.755	0.295	−0.953	0.34					
BE: Yes vs. No	0.095	1.1	0.332	0.285	0.775					
Stage: III/IV vs. I/II	1.129	3.094	0.359	3.146	**0.002**	0.478	1.613	0.535	0.893	0.372
T stage: T3/4 vs. T1/2	0.254652	1.290013	0.328613	0.774931	0.43838					
Lymph invasion: Yes vs. No	0.718	2.05	0.314	2.288	**0.022**	−0.096	0.908	0.481	−0.2	0.842
Metastasis: M1 vs. M0	1.345	3.838	0.437	3.076	**0.002**	0.47	1.6	0.521	0.901	0.367

Coef: The regression coefficients; Exp(coef): the exponentiated coefficients, also known as hazard ratios. SE(coef): The standard error of hazard ratios; BE: Barrett's esophagus. The significant differences (P-value < 0.05) were highlighted with the bold values.

57 TCGA ESCC tumor samples with a follow-up of less than 1 month, which showed a strong positive silhouette width (average = 0.61) (**Figures 4D,E**). Furthermore, we also observed the robustness of 50 lncRNAs in another independent dataset from GEO (GSE53625) (**Figures 4F,G**). Taken together, these results indicated that k-means fitted the respective cluster for ESCC. Among these lncRNAs, four were also found in the differential gene list, while none were found in the prognostic marker list (**Supplementary Figure 3I**).

To explore the clinical significance of the two subtypes, we systematically tested the associations between the subtype and clinical characteristics, including TNM stage, distant metastasis, lymph invasion, grade, BE, location, tobacco, alcohol, age, sex, race, and survival outcomes (**Supplementary Table 6**, **Figures 4H,I**, and **Supplementary Figures 3J,K**). There was no survival difference between cluster 1 and cluster 2 in all three datasets (**Supplementary Figures 3J,K**, both $P > 0.05$, log-rank test). Cluster 1 were frequently observed to correlate with the white race and those with BE which was considered as a precancerous lesion (**Figures 4H,I**, both $P < 0.05$, chi-square test). These differences in race and BE with unsupervised lncRNA signatures might implicate the discrepancy of the intrinsic biological processes in each cluster group.

AC007128.1 Is Highly Expressed in ESCC With Poor Prognosis

To explore possible connections between lncRNAs and carcinogenesis and ESCC development, we evaluated the expressions of seven out of 11 prognostic lncRNA markers in ESCC cell lines and normal esophageal epithelial cell lines by RT-qPCR because the expressions of the other four lncRNAs were too low to detect. Of the seven lncRNAs, we found that AC007128.1 had a higher expression in three established ESCC cell lines (KYSE150, TE-1, and EC109) compared with normal cell lines (Het-1A and HEEC), and the expression of AC007128.1 was the highest among the seven lncRNAs (**Figure 3A**). We also detected the level of AC007128.1 in the nuclear and cytoplasmic fractions of KYSE150 and EC109 cells and found that AC007128.1 is mainly enriched in the nucleus (**Supplementary Figures 4A,B**). We also found a higher expression of AC007128.1 in human ESCC samples from three independent datasets (**Figures 3B–D**). Meanwhile, increased AC007128.1 expression was related with a shorter OS in TCGA ESCC samples (**Figure 3E**), which was consistent with a previous study (Liu et al., 2019). These data demonstrated that the expression of AC007128.1 was upregulated in both ESCC tissues and cells, and associated with poor prognosis in ESCC. Therefore, we focused on AC007128.1 for further research.

We further analyzed the correlation between the AC007128.1 expression and the clinicopathologic characteristics of the ESCC patients. The expression of AC007128.1 was associated with the TNM stage ($P = 0.039$), gender ($P = 0.01$), and age ($P = 0.046$) in TCGA dataset (**Supplementary Table 7**). The AC007128.1 expression was associated with grade ($P = 0.013$) in GSE53625 (**Supplementary Table 8**). There was no statistical association between the AC007128.1 expression and other clinical characteristics in the two datasets. Based on these data, we postulated a role for AC007128.1 in ESCC pathology.

Identification of AC007128.1 as a Regulator of ESCC Cell Migration and Invasion

To explore the biological effects of AC007128.1 in the tumorigenesis and development of ESCC, three specific siRNAs targeted to AC007128.1 were used to reduce its expression in two ESCC cell lines, KYSE150 and EC109. We showed that si-AC007128.1-2 exhibited a better silencing efficiency (**Figure 5A**). CCK-8 assay revealed that depletion of AC007128.1 did not affect the proliferation of KYSE150 and EC109 cells ($P > 0.05$; **Supplementary Figures 4C,D**). Next, we assessed the effect of AC007128.1 depletion on cell migration and invasion in ESCC. We found that AC007128.1 depletion dramatically inhibited cell migration, invasion, and wound closure in both KYSE150 and

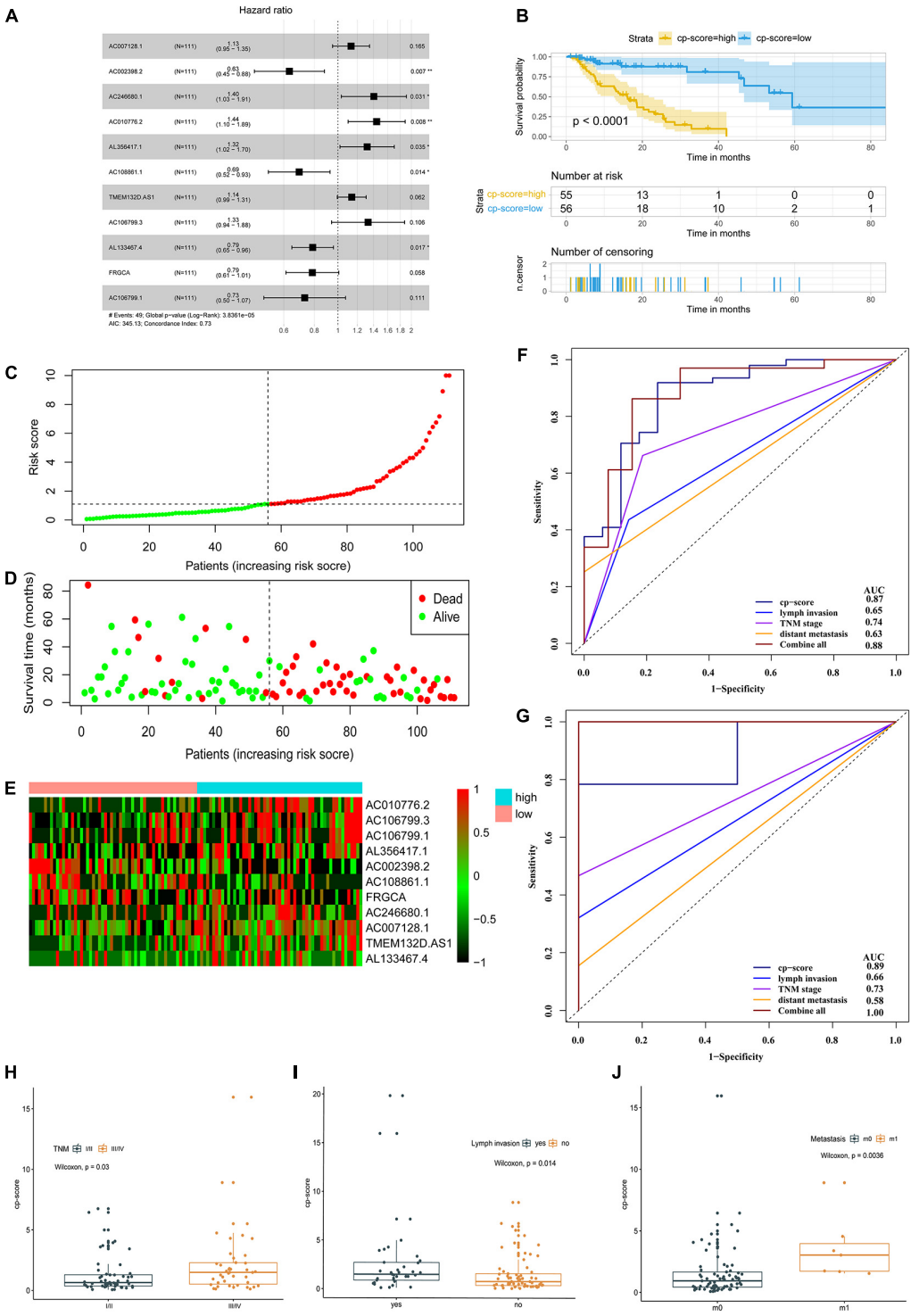

FIGURE 2 | A prognostic model of ESCC survival based on 11 differential and prognostic lncRNAs. **(A)** Forest plot illustrated the HR and 95% CI of the 11 lncRNAs by the multivariate Cox regression. HR, hazard ratio; CI, confidence interval. **(B)** OS curves of ESCC patients with the low and high risk groups according to the cp-score in TCGA cohort. **(C–E)** The distribution of 11-lncRNA risk score **(C)**, OS status **(D)**, and corresponding lncRNA expression profiles **(E)**. The intersection of horizontal and vertical dotted lines represents the risk score of the person ranked in the middle. **(F)** Time-dependent ROC and corresponding AUCs for 3-year survival predicted by cp-score, TNM stage, lymph node metastasis, distant metastasis, and the combination of all these factors. **(G)** ROC and corresponding AUCs for 5-year OS predicted by cp-score, TNM stage, lymph node metastasis, distant metastasis, and the combination of all these factors. **(H)** LncRNA analysis of cp-score of patients with stage I/II and stage III/IV disease. **(I)** cp-score in patients with and without lymph node metastasis. **(J)** cp-score in patients with and without distant metastasis.

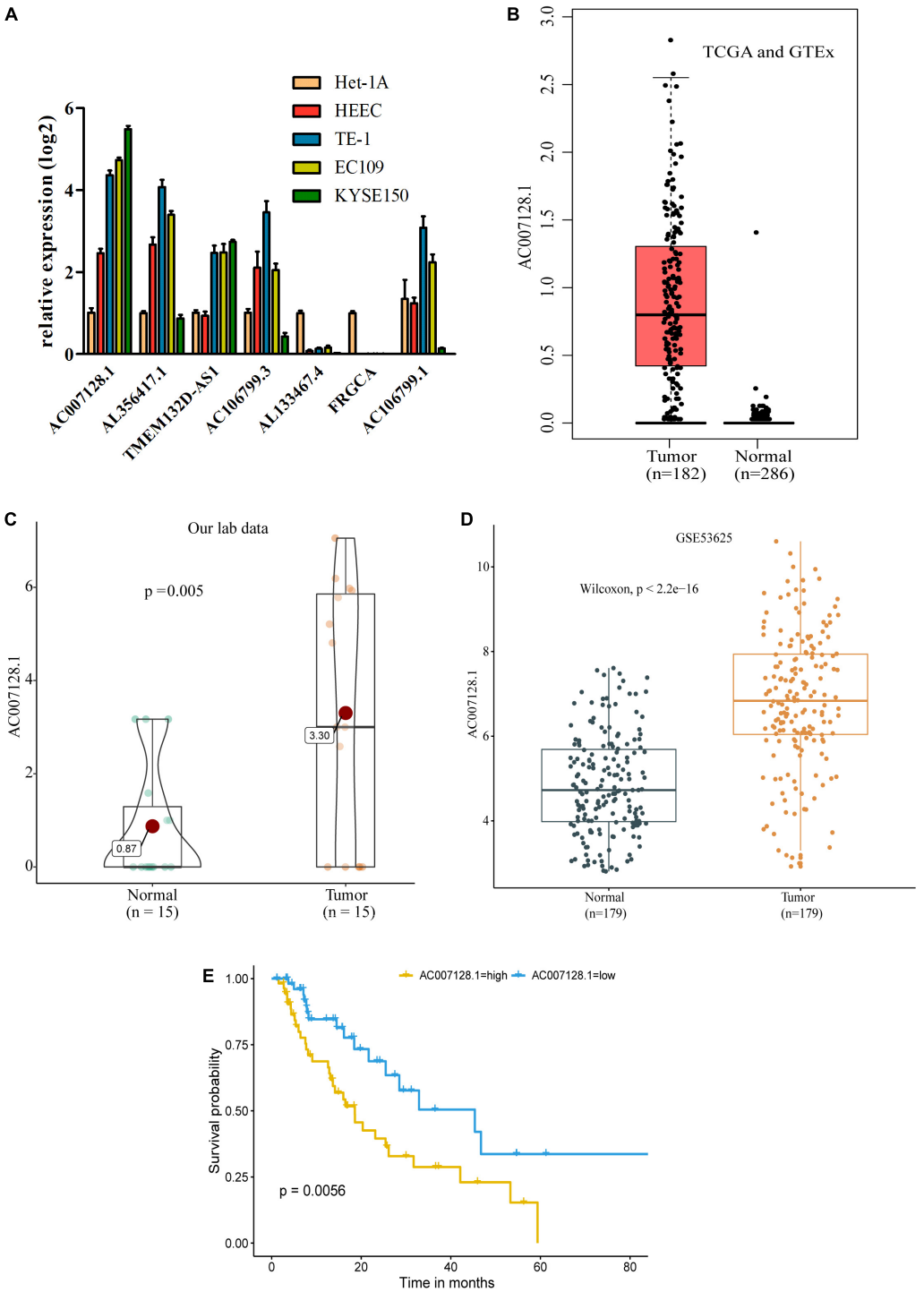

FIGURE 3 | AC007128.1 is up-regulated and linked to poor prognosis in ESCC. **(A)** Comparison of seven lncRNA expressions in ESCC and normal cell lines. Het-1A and HEEC represent normal cell lines, and others represent tumor cell lines. **(B–D)** Relative expression of AC007128.1 in ESCC tissues was analyzed by using GEPIA: http://gepia.cancer-pku.cn **(B)**, our lab **(C)**, and GEO datasets **(D)**. **(E)** KM survival analysis of ESCC patients with high or low AC007128.1 expression (defined by the median) in TCGA. Statistical analysis was performed using the two-sided log-rank test.

EC109 cell lines (**Figures 5B–H**). We also observed the same inhibitory effects on the migration and invasion in TE-1 cells (**Supplementary Figures 4E–G**). Transwell assay (**Figures 5I–M**) and wound healing assay (**Figures 5N–P**) indicated that overexpression of AC007128.1 in EC109 and TE-1 cells dramatically promoted cell migration and invasion. However, it had no

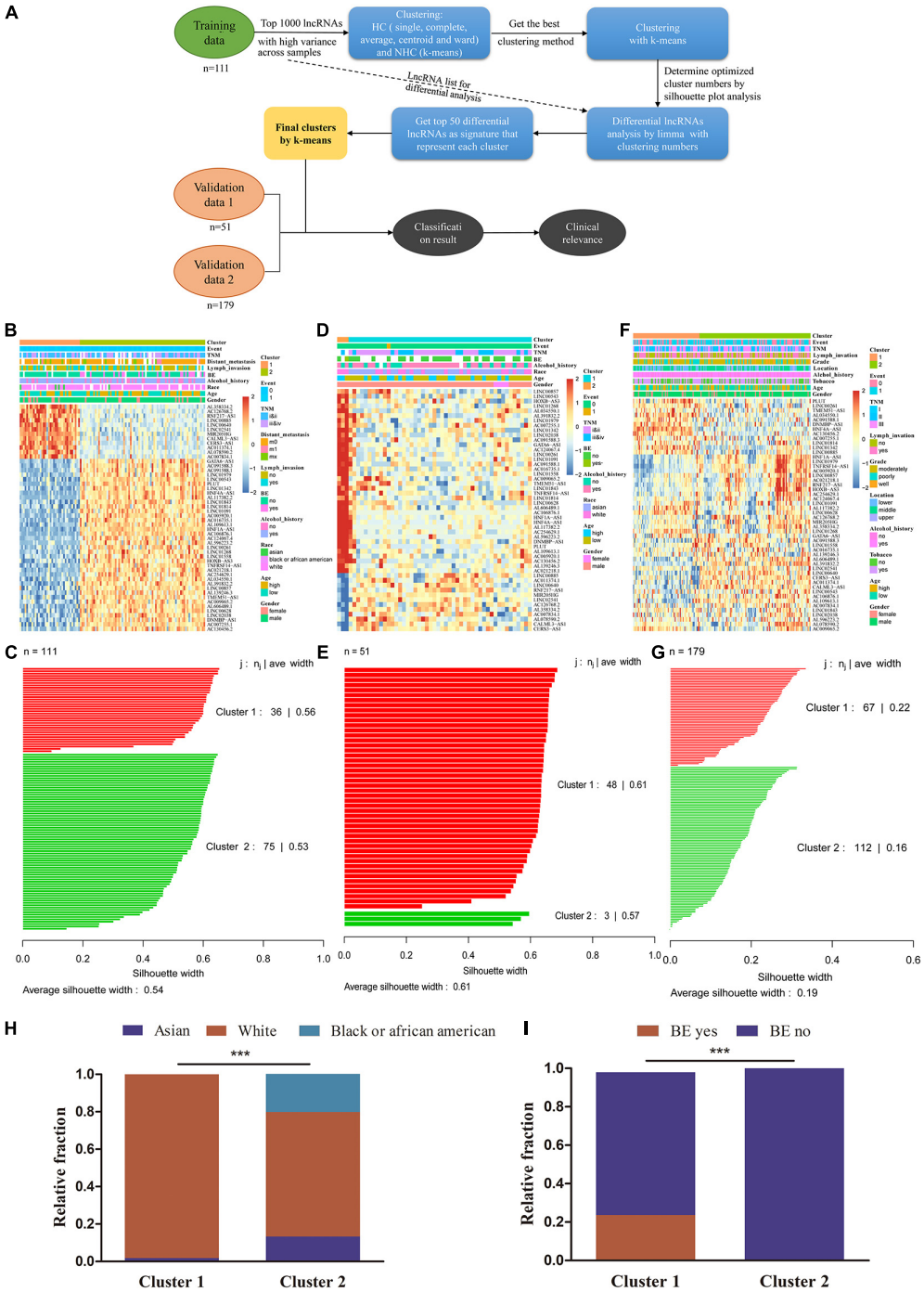

FIGURE 4 | lncRNA subtyping analysis in 341 ESCC patients. **(A)** Schematic diagram for ESCC sample clustering. **(B)** *k*-means clustering of lncRNA markers identified two subtypes in the training cohort. The annotation bars above the heatmap indicate the clinical and molecular features. Patients without related information were colored in white. **(C)** Silhouette analysis of the clusters in the training data. **(D,E)** Subtypes of validation using the 50 markers in other 51 TCGA ESCC samples. **(F,G)** Predicted subtypes/clusters of validation using the 50 markers in 179 independent GEO ESCC samples (GSE53625). **(H)** The proportion of patients with Asian to White or Black ESCC in two clusters (chi-square test, ***$P < 0.001$). **(I)** The proportion of patients with and without BE in two clusters (chi-square test, ***$P < 0.001$). BE, Barrett's esophagus.

significant effect on cell growth (**Supplementary Figures 4H,I**). Collectively, these results suggested that AC007128.1 promoted migration and invasion in ESCC cell lines.

Epithelial-mesenchymal transition (EMT) plays an important role in tumorous migration and invasion (Yang and Weinberg, 2008; De Craene and Berx, 2013; Lamouille et al., 2014;

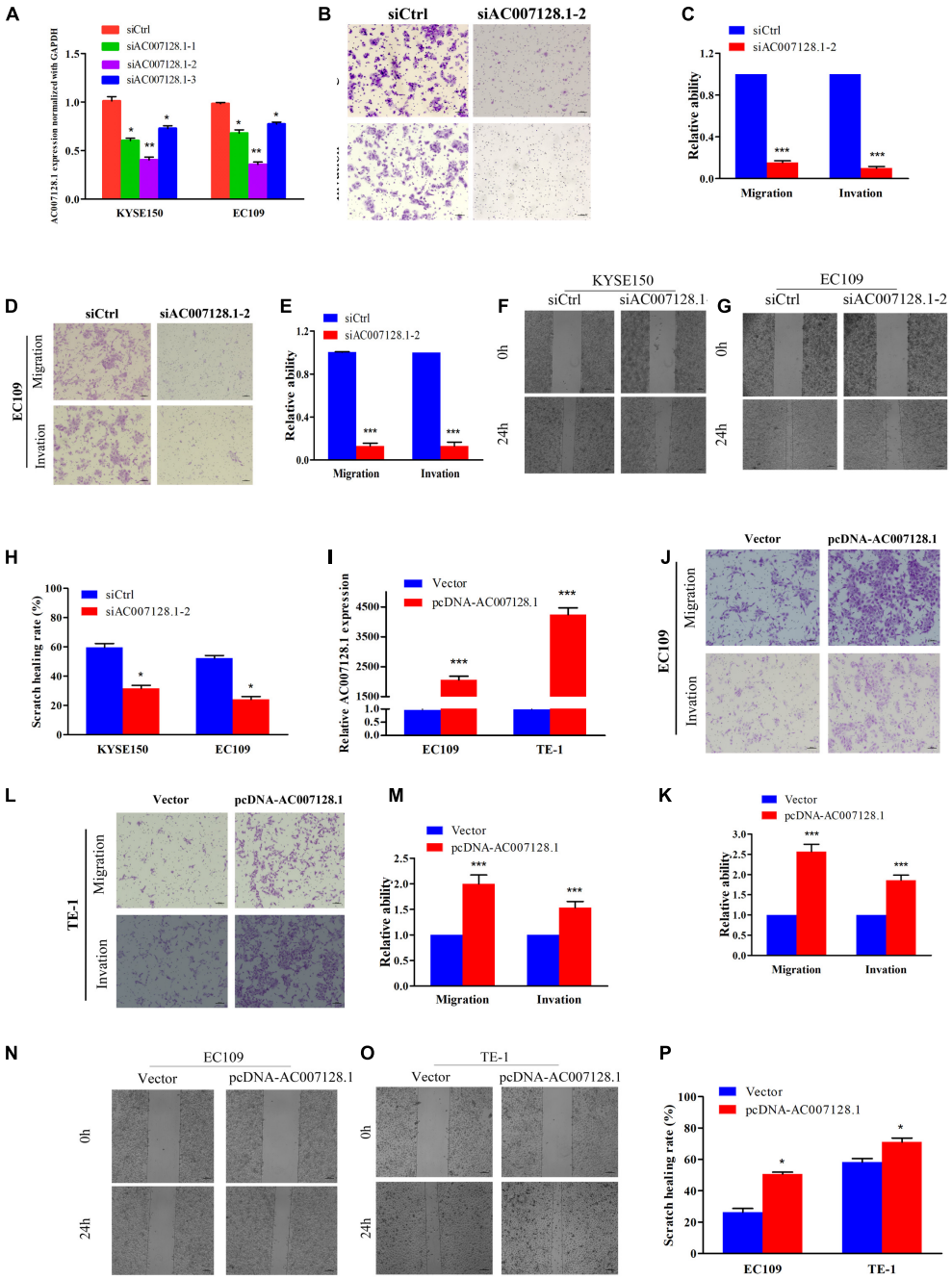

FIGURE 5 | Effects of AC007128.1 expression on ESCC cell aggressiveness. **(A,I)** qPCR analysis of AC007128.1 expression in si-AC007128.1-1, si-AC007128.1-2, si-AC007128.1-3, and pcDNA-AC007128.1-treated ESCC cells. **(B–E)** Representative micrographs of the transwell assay showing the migration and invasiveness of AC007128.1-depleted cells. **(F–H)** Representative micrographs of the wound healing assay showing the motilities of AC007128.1-depleted cells. **(J–M)** Representative micrographs of the transwell assay showing the migration and invasiveness of AC007128.1-overexpressing cells. **(N–P)** Representative micrographs of the wound healing assay showing the motilities of AC007128.1-overexpressing cells. Data represent mean ± SEM from three independent experiments. $^{*}P < 0.05$, $^{**}P < 0.01$, and $^{***}P < 0.001$ by Student's *t*-test as compared with the corresponding control.

Pang et al., 2018; Dongre and Weinberg, 2019). We further detected the expressions of EMT markers, including the epithelial marker E-cadherin and the mesenchymal markers, Vimentin, β-catenin, and Snail in AC007128.1-depleted cells. **Figure 6A** show that depletion of AC007128.1 resulted in a significantly increased expression of E-cadherin at the protein level, while it led to dramatically decreased expressions of Vimentin, β-catenin, and Snail at the protein level. These results indicated that AC007128.1 might promote EMT, thus affecting cell migration and invasion in ESCC.

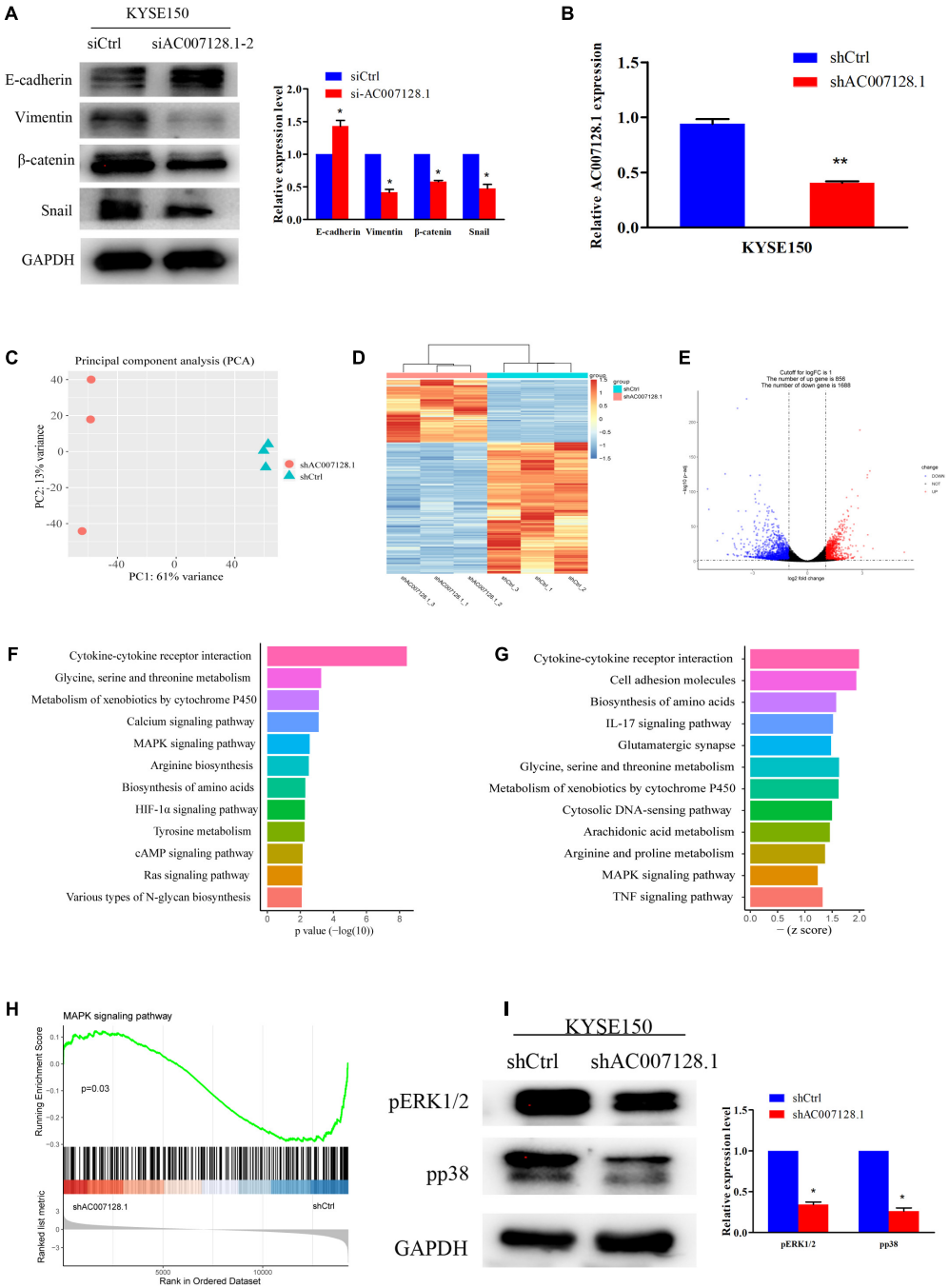

FIGURE 6 | AC007128.1 activates MAPK/ERK and MAPK/p38 signaling pathways. **(A)** AC007128.1 depletion resulted in the increased expression of epithelial marker and decreased expressions of mesenchymal markers. **(B)** qPCR analysis of AC007128.1 expression in shAC007128.1- and shCtrl-treated ESCC cells. **(C)** PCA showed successful segregation between shAC007128.1 and shNC groups. **(D)** Heatmap analysis showed that shAC007128.1 cells could be distinguished by dysregulated lncRNAs. **(E)** Volcano plot exhibited differentially expressed lncRNAs. **(F)** KEGG analysis indicated the down-regulated signaling pathway by repressed genes in AC007128.1-depleted cells. **(G)** GSEA showed the repressed signaling pathway in AC007128.1-depleted cells. **(H)** GSEA indicated that AC007128.1 depletion might inhibit the MAPK signaling pathway. **(I)** Depletion of AC007128.1 obviously decreased the expressions of p-ERK1/2 and p-p38. $^{*}P < 0.05$ and $^{**}P < 0.01$ by Student's t-test as compared with the corresponding control.

AC007128.1 Activated MAPK/ERK and MAPK/p38 Signaling Pathways

To explore the molecular mechanism, through which AC007128.1 promoted migration and invasion of ESCC, we constructed an shRNA specific to human AC007128.1, which was used to successfully reduce the expression of AC007128.1 at the mRNA level (**Figure 6B**), and further performed RNA-sequencing in KYSE150 cells. Global reprogramming of the

ESCC transcriptome was detected in AC007128.1-depleted cells (**Figure 6C**), in which more than 2,500 genes were differentially expressed compared with the shCtrl group (**Figure 6D**), including 856 upregulated genes and 1,688 downregulated genes (**Figure 6E**). The Kyoto Encyclopedia of Genes and Genomes (KEGG) pathway enrichment analysis of the repressed genes showed that these down-regulated genes were mainly enriched in the following pathways including mitogen-activated protein kinase MAPK signaling pathway, cAMP signaling pathway, HIF-1α signaling pathway, Ras signaling pathway, and cytokine-cytokine receptor interaction, which were known to be important in cancer (**Figure 6F**). Moreover, gene set enrichment analysis (GSEA) for all genes revealed that some signaling pathways were depressed, such as MAPK signaling pathway, cell adhesion molecules, IL-17 signaling pathway, TNF signaling pathway, and cytokine-cytokine receptor interaction (**Figure 6G**). The results of KEGG and GSEA indicated that AC007128.1 might contribute to EMT via these signaling pathways in ESCC.

MAPK signaling pathway was identified as inhibited pathway in both KEGG and GSEA analysis when AC007128.1 was depleted in KYSE150 cells (**Figures 6F–H**). Previous studies has been implicated that the MAPK signaling pathway take part in regulating EMT of different cancers, including ESCC (Huang et al., 2004; Hu et al., 2017; Hawsawi et al., 2018; Chen et al., 2019; Peng et al., 2019), Therefore, we hypothesized that AC007128.1 might affect cell EMT by deregulating the MAPK signaling pathway. To test this hypothesis, we explored the effect of AC007128.1 on the activity of MAPK signaling. As expected, we found that depletion of AC007128.1 decreased the expressions of phosphorylated ERK1/2 (p-ERK1/2) and phosphorylated p38 (p-p38) in KYSE150 (**Figure 6I**). It has been shown that ERK1/2 (Wong et al., 2012; Wang et al., 2020; Zhang F. et al., 2020) and p38 (Wang et al., 2012; Ma et al., 2016) pathways are critical in EMT regulation for ESCC. Therefore, we inferred from the above-mentioned results that AC007128.1 affected cell EMT via deregulating MAPK signaling pathway.

DISCUSSION

In recent years, more and more novel lncRNAs have been identified and the roles of lncRNAs in cancer development have been increasingly studied (Yang et al., 2014; Bhan et al., 2017; Peng et al., 2017). In our previous study, we have shown the effectiveness of lncRNA signatures in diagnosis, prognostic prediction, and drug-resistance in four common cancers, namely breast cancer, colorectal cancer, bladder cancer, and lung cancer (Li et al., 2017, 2018a; Xie et al., 2018; Zhan et al., 2018; Zhang et al., 2019). Here, we identified an 11-lncRNA model that was associated with tumor OS in ESCC patients, constructed a lncRNA-based molecular subtype of ESCC, and found that lncRNA AC007128.1 might mediate ESCC EMT through mitogen-activated protein kinases/extracellular signal-regulated kinase (MAPK/ERK) and MAPK/p38 signaling pathways.

In the present study, we developed a prognostic prediction model using 11 selected lncRNA markers from TCGA ESCC RNA-seq dataset and found that this model could effectively distinguish ESCC patients with different prognoses. Moreover, multivariable analysis confirmed that this model was considered as an independent prognostic risk factor. The discrimination potential of the cp-score was superior to other prognostic risk factors (TNM stage, lymph node metastasis, and distant metastasis). We also compared the prognostic ability of this model with those of having been reported prognostic biomarkers for ESCC. The results demonstrated that the 11-lncRNA signature had a higher fidelity than other signatures (Li et al., 2014; Mao et al., 2018; Zhang L. et al., 2020). The combination of cp-score and clinical characteristics improved the 5-year survival prediction, which could identify patients needing more aggressive treatment and surveillance. We also found that the cp-score was correlated with the staging, as well as the lymphatic and distant metastases of ESCC. These results suggested that this model was also useful for detecting staging, lymphatic, and distant metastasis of ESCC. Although the 11-lncRNA model showed potential prognostic biomarkers for esophageal carcinoma, one limitation should be taken into consideration: the present study is short of other independent datasets to show its fidelity as prognostic biomarkers for esophageal carcinoma, and the distribution of clinical features in TCGA dataset might be distinct from those of other datasets, making it unsuitable for other subjects. Therefore, our results should be further validated in other clinical samples in the future.

Molecular subtyping is considered as a favorable source of disease stratification (Guinney et al., 2015; Sjodahl et al., 2017), while similar lncRNA-based subtyping is still lacking. With a k-means clustering analysis (Kakushadze and Yu, 2017), we could divide 111 ESCC patients from TCGA into two molecular subgroups based on 50 lncRNA markers, and its performance was again confirmed in internal and external datasets. The lncRNA-based subtyping showed good clustering capability and could be treated as a potential tool for ESCC molecular subtyping. We further studied the correlation between the lncRNA-based subtyping and clinical factors, including TNM stage, distant metastasis, lymph invasion, grade, BE, tumor site, alcohol, tobacco, age, sex, race, and survival outcomes. We found a relation between lncRNA-based clusters and race, alcohol, BE, and TNM stage in TCGA dataset, which might imply that these clinical variables partially affected the different transcriptions of lncRNAs. However, the study on subtyping was limited by clinical samples that all samples were collected from available public data. Further verification with multi-center clinical samples is still necessary to adequately assess the performance of the lncRNA-based subtype.

We presumed that lncRNA markers in the prognostic model might play important roles in the carcinogenesis and development of ESCC. Therefore, elucidating the underlying mechanism might provide potentially therapeutic targets of ESCC. In this study, we found lncRNA AC007128.1, which was significantly up-regulated in ESCC tissues from

three independent datasets, and correlated with OS of ESCC in TCGA, However, there is one limitation to the validation of lncRNA expression: we didn't detect the expression level of AC007128.1 by RT-qPCR or other method in new ESCC tissue samples due to limited corresponding samples. In view of this limitation, we attempted to prove the reliability of AC007128.1 by detecting the expression in ESCC cell lines and performing functional experiment *in vitro*. The results showed that AC007128.1 was upregulated in ESCC cell lines compared with normal esophageal epithelial cell lines and its depletion could suppress migration and invasion of ESCC cells *in vitro*. EMT is an important biological event during human cancer progression (De Craene and Berx, 2013; Pastushenko et al., 2018; Pastushenko and Blanpain, 2019). Reduced AC007128.1 could increase the expressions of epithelial markers and decreased the expressions of mesenchymal markers. Taken together, these results indicated that AC007128.1 might be closely related to cancer progression and play a tumor progressive role in ESCC.

It is urgently necessary to elucidate the molecular mechanisms underlying ESCC progression. We found that the deletion of AC007128.1 decreased the activation of MAPK/ERK and MAPK/p38 signaling pathways, but the exact mechanism by which AC007128.1 acts on the MAPK signaling pathway requires further study. Several published studies have also shown that the MAPK signaling pathway is activated in the process of tumorigenesis, metastasis, and angiogenesis of multiple human malignancies, including ESCC (Burotto et al., 2014; Hu et al., 2017). We speculated that AC007128.1 might promote migration and invasion of ESCC by increasing the activation of MAPK/ERK and MAPK/p38 signaling pathways.

Collectively, we identified lncRNA markers for prognostic prediction and subtyping of ESCC using lncRNA expression profiles. We also demonstrated a significant up-regulation of AC007128.1 in ESCC tumor tissues and cell lines and found its association with poor survival in ESCC patients. The mechanistic analysis demonstrated that AC007128.1 might promote cancer cell EMT by aberrantly activating the MAPK signaling pathway. These findings provided the possibility that overexpressed AC007128.1 was an important molecule participating in the aberrant activation of the MAPK signaling pathway and could serve as a therapeutic target for ESCC.

DATA AVAILABILITY STATEMENT

The data generated in the manuscript can be found in GEO using accession GSE167345.

AUTHOR CONTRIBUTIONS

SZ and JL designed the experiments. SZ performed the experiments, drafted the figures, and wrote the manuscript. HG and YT helped to perform the experiments. PL and YW provided direction in the experimental design. LD and CW revised the manuscript. All authors contributed to the article and approved the submitted version.

FUNDING

This research was supported by grant from the National Key Research and Development Program of China (2018YFC0114700), the Key Research and Development Program of Shandong Province (2019GHZ003 and 2018YFJH0505), and the Fundamental Research Funds of Shandong University (2082018JC002).

SUPPLEMENTARY MATERIAL

The Supplementary Material for this article can be found online at: https://www.frontiersin.org/articles/10.3389/fcell.2021.656554/full#supplementary-material

Supplementary Figure 1 | (A–E) The correlation between age, gender, alcohol, BE, and T stage and patients' prognosis by KM analysis (log-rank test) (all $P > 0.05$).

Supplementary Figure 2 | (A–J) The association between 10 out 11 prognostic lncRNAs and patients' prognosis by KM analysis (log-rank test) (all $P < 0.05$). **(K)** LncRNA analysis of cp-score of patients with T1/2 and T3/4 ($P = 0.18$).

Supplementary Figure 3 | (A–E) The dendrogram of different HC methods for ESCC patients from TCGA, among which the ward showed the best clustering. **(F)** The silhouette plot showed the optimal number of clusters ($k = 2$). **(G,H)** Silhouette analysis of the ward method **(G)** was slightly inferior to the *k*-means **(H)**. **(I)** Venn diagram showed the intersections of the three lncRNAs from diagnosis, prognosis, and subtyping sections. **(J,K)** OS for each of the lncRNA pattern in each subtype in both the training cohort (TCGA) and validation cohort (GEO) (log-rank test, $P > 0.05$).

Supplementary Figure 4 | (A,B) Level of AC007128.1 in the nuclear and cytoplasmic fractions of KYSE150 and EC109 cells. **(C,D,H,I)** Growth curves of ESCC cells. Numbers of cells were determined at 24 h intervals after transfection with siAC007128.1-2 or pcDNA-AC007128.1 using the CCK-8 assay. **(E)** qPCR analysis of AC007128.1 expression in si-AC007128.1-2 treated TE-1 cells. **(F,G)** Representative micrographs of the transwell assay showing the migration and invasiveness of AC007128.1-depleted TE-1 cells. Data represent mean ± SEM from three independent experiments. $^{**}P < 0.01$ and $^{***}P < 0.001$ by Student's *t*-test as compared with the corresponding control.

REFERENCES

Bhan, A., Soleimani, M., and Mandal, S. S. (2017). Long noncoding RNA and Cancer: a new paradigm. *Cancer Res.* 77, 3965–3981. doi: 10.1158/0008-5472.can-16-2634

Blank-Giwojna, A., Postepska-Igielska, A., and Grummt, I. (2019). lncRNA KHPS1 activates a poised enhancer by triplex-dependent recruitment of epigenomic regulators. *Cell Rep.* 26, 2904–2915.e4.

Bray, F., Ferlay, J., Soerjomataram, I., Siegel, R. L., Torre, L. A., and Jemal, A. (2018). Global cancer statistics 2018: GLOBOCAN estimates of incidence and mortality worldwide for 36 cancers in 185 countries. *CA Cancer J. Clin.* 68, 394–424. doi: 10.3322/caac.21492

Burotto, M., Chiou, V. L., Lee, J. M., and Kohn, E. C. (2014). The MAPK pathway across different malignancies: a new perspective. *Cancer* 120, 3446–3456. doi: 10.1002/cncr.28864

Chen, L., Tian, X. D., Gong, W. C., Sun, B., Li, G. T., Liu, D. M., et al. (2019). Periostin mediates epithelial-mesenchymal transition through the MAPK_ERK

pathway in hepatoblastoma. *Cancer Biol. Med.* 16, 89–100. doi: 10.20892/j.issn.2095-3941.2018.0077

Chen, X. J., Kong, J. Y., Ma, Z. K., Gao, S. G., and Feng, X. S. (2015). Up regulation of the long non-coding RNA NEAT1 promotes esophageal squamous cell carcinoma cell progression and correlates with poor prognosis. *Am. J. Cancer Res.* 5, 2808–2815.

Cheng, P. (2018). A prognostic 3-long noncoding RNA signature for patients with gastric cancer. *J. Cell Biochem.* 119, 9261–9269. doi: 10.1002/jcb.27195

De Craene, B., and Berx, G. (2013). Regulatory networks defining EMT during cancer initiation and progression. *Nat. Rev. Cancer* 13, 97–110. doi: 10.1038/nrc3447

Djebali, S., Davis, C. A., Merkel, A., Dobin, A., Lassmann, T., Mortazavi, A., et al. (2012). Landscape of transcription in human cells. *Nature* 489, 101–108.

Dongre, A., and Weinberg, R. A. (2019). New insights into the mechanisms of epithelial-mesenchymal transition and implications for cancer. *Nat. Rev. Mol. Cell Biol.* 20, 69–84. doi: 10.1038/s41580-018-0080-4

Guinney, J., Dienstmann, R., Wang, X., Reyniès, A. D., Schlicker, A., Soneson, C., et al. (2015). The consensus molecular subtypes of colorectal cancer. *Nat. Med.* 21, 1350–1356.

Hawsawi, O., Henderson, V., Burton, L. J., Dougan, J., Nagappan, P., and Marah, V. O. (2018). High mobility group A2 (HMGA2) promotes EMT via MAPK pathway in prostate cancer. *Biochem. Biophys. Res. Commun.* 504, 196–202. doi: 10.1016/j.bbrc.2018.08.155

Heagerty, P. J., Lumley, T., and Pepe, M. S. (2000). Time-dependent ROC curves for censored survival data and a diagnostic marker. *Biometrics* 56, 337–344. doi: 10.1111/j.0006-341x.2000.00337.x

Hu, L., Wu, Y., Tan, D., Meng, H., Wang, K., Bai, Y., et al. (2015). Up-regulation of long noncoding RNA MALAT1 contributes to proliferation and metastasis in esophageal squamous cell carcinoma. *J. Exp. Clin. Cancer Res.* 34:7. doi: 10.1186/s13046-015-0123-z

Hu, X., Feng, Y., Zhang, D., Zhao, S. D., Hu, Z., Greshock, J., et al. (2014). A functional genomic approach identifies FAL1 as an oncogenic long noncoding RNA that associates with BMI1 and represses p21 expression in cancer. *Cancer Cell* 26, 344–357. doi: 10.1016/j.ccr.2014.07.009

Hu, X. L., Zhai, Y. F., Kong, P. Z., Cui, H. Y., Yan, T., Yang, J., et al. (2017). *FAT*1 prevents epithelial mesenchymal transition (EMT) via MAPK_ERK signaling pathway in esophageal squamous cell cancer. *Cancer Lett.* 397, 83–93. doi: 10.1016/j.canlet.2017.03.033

Huang, C., Jacobson, K., and Schaller, M. D. (2004). MAP kinases and cell migration. *J. Cell Sci.* 117, 4619–4628. doi: 10.1242/jcs.01481

Huarte, M. (2015). The emerging role of lncRNAs in cancer. *Nat. Med.* 21, 1253–1261. doi: 10.1038/nm.3981

Iyer, M. K., Niknafs, Y. S., Malik, R., Singhal, U., Sahu, A., Hosono, Y., et al. (2015). The landscape of long noncoding RNAs in the human transcriptome. *Nat. Genet.* 47, 199–208.

Kakushadze, Z., and Yu, W. (2017). *K-means and cluster models for cancer signatures. *Biomol. Detect. Quantif.* 13, 7–31. doi: 10.1016/j.bdq.2017.07.001

Lamouille, S., Xu, J., and Derynck, R. (2014). Molecular mechanisms of epithelial-mesenchymal transition. *Nat. Rev. Mol. Cell Biol.* 15, 178–196.

Li, J., Chen, Z., Tian, L., Zhou, C., He, M. Y., Gao, Y., et al. (2014). LncRNA profile study reveals a three-lncRNA signature associated with the survival of patients with oesophageal squamous cell carcinoma. *Gut* 63, 1700–1710. doi: 10.1136/gutjnl-2013-305806

Li, P., Zhang, X., Wang, L., Du, L., Yang, Y., Liu, T., et al. (2017). lncRNA HOTAIR contributes to 5FU resistance through suppressing miR-218 and activating NF-kappaB/TS signaling in colorectal Cancer. *Mol. Ther. Nucleic Acids* 8, 356–369. doi: 10.1016/j.omtn.2017.07.007

Li, J., Peng, W., Du, L., Yang, Q., Wang, C., and Mo, Y. Y. (2018a). The oncogenic potentials and diagnostic significance of long non-coding RNA LINC00310 in breast cancer. *J. Cell Mol. Med.* 22, 4486–4495. doi: 10.1111/jcmm.13750

Li, Z., Zhang, J., Liu, X., Li, S., Wang, Q., Di, C., et al. (2018b). The LINC01138 drives malignancies via activating arginine methyltransferase 5 in hepatocellular carcinoma. *Nat. Commun.* 9:1572.

Liu, H., Zhang, Q., Lou, Q., Zhang, X., Cui, Y., Wang, P., et al. (2019). Differential analysis of lncRNA, miRNA and mRNA expression profiles and the prognostic value of lncRNA in esophageal Cancer. *Pathol. Oncol. Res.* 26, 1029–1039. doi: 10.1007/s12253-019-00655-8

Liu, J., Xie, X., Zhou, C., Peng, S., Rao, D., and Fu, J. (2012). Which factors are associated with actual 5-year survival of oesophageal squamous cell carcinoma? *Eur. J. Cardiothorac. Surg.* 41, e7–e11.

Love, M. I., Huber, W., and Anders, S. (2014). Moderated estimation of fold change and dispersion for RNA-seq data with DESeq2. *Genome Biol.* 15:550.

Luo, H. Y., Zhao, Q., Wei, W., Zheng, L. H., Yi, S. H., Li, G., et al. (2020). Circulating tumor DNA methylation profiles enable early diagnosis, prognosis prediction, and screening for colorectal cancer. *Sci. Transl. Med.* 12:eaax7533. doi: 10.1126/scitranslmed.aax7533

Ma, M., Zhao, L.-M., Yang, X.-X., Shan, Y.-N., Cui, W.-X., Chen, L., et al. (2016). p-Hydroxylcinnamaldehyde induces the differentiation of oesophageal carcinoma cells via the cAMP-RhoA-MAPK signalling pathway. *Sci. Rep.* 6:31315.

Mao, Y., Fu, Z., Zhang, Y., Dong, L., Zhang, Y., Zhang, Q., et al. (2018). A seven-lncRNA signature predicts overall survival in esophageal squamous cell carcinoma. *Sci. Rep.* 8:8823.

Pang, A., Carbini, M., Moreira, A. L., and Maki, R. G. (2018). Carcinosarcomas and related Cancers: tumors caught in the act of epithelial-mesenchymal transition. *J. Clin. Oncol.* 36, 210–216. doi: 10.1200/jco.2017.74.9523

Pastushenko, I., and Blanpain, C. (2019). EMT transition states during tumor progression and metastasis. *Trends Cell Biol.* 29, 212–226. doi: 10.1016/j.tcb.2018.12.001

Pastushenko, I., Brisebarre, A., Sifrim, A., Fioramonti, M., Revenco, T., Boumahdi, S., et al. (2018). Identification of the tumour transition states occurring during EMT. *Nature* 556, 463–468. doi: 10.1038/s41586-018-0040-3

Peng, B., He, R., Xu, Q. H., Yang, Y. F., Hu, Q., Hou, H. P., et al. (2019). Ginsenoside 20(S)-protopanaxadiol inhibits triple-negative breast cancer metastasis in vivo by targeting EGFR-mediated MAPK pathway. *Pharmacol. Res.* 142, 1–13. doi: 10.1016/j.phrs.2019.02.003

Peng, W. X., Koirala, P., and Mo, Y. Y. (2017). LncRNA-mediated regulation of cell signaling in cancer. *Oncogene* 36, 5661–5667. doi: 10.1038/onc.2017.184

Pennathur, A., Gibson, M. K., Jobe, B. A., and Luketich, J. D. (2013). Oesophageal carcinoma. *Lancet* 381, 400–412.

Quinn, J. J., and Chang, H. Y. (2016). Unique features of long non-coding RNA biogenesis and function. *Nat. Rev. Genet.* 17, 47–62. doi: 10.1038/nrg.2015.10

Schmitt, A. M., and Chang, H. Y. (2016). Long noncoding RNAs in Cancer pathways. *Cancer Cell* 29, 452–463. doi: 10.1016/j.ccell.2016.03.010

Short, M. W., Burgers, K. G., and Fry, V. T. (2017). Esophageal cancer. *Am. Fam. Phys.* 95, 22–28.

Siegel, R. L., Miller, K. D., and Jemal, A. (2020). Cancer statistics, 2020. *CA Cancer J. Clin.* 70, 7–30.

Sjodahl, G., Eriksson, P., Liedberg, F., and Hoglund, M. (2017). Molecular classification of urothelial carcinoma: global mRNA classification versus tumour-cell phenotype classification. *J. Pathol.* 242, 113–125. doi: 10.1002/path.4886

Storey, J. D., and Tibshirani, R. (2003). Statistical significance for genomewide studies. *Proc. Natl. Acad. Sci. U S A.* 100, 9440–9445. doi: 10.1073/pnas.1530509100

Trapnell, C., Pachter, L., and Salzberg, S. L. (2009). TopHat: discovering splice junctions with RNA-Seq. *Bioinformatics* 25, 1105–1111. doi: 10.1093/bioinformatics/btp120

Trapnell, C., Roberts, A., Goff, L., Pertea, G., Kim, D., Kelley, D. R., et al. (2012). Differential gene and transcript expression analysis of RNA-seq experiments with TopHat and cufflinks. *Nat. Protoc.* 7, 562–578. doi: 10.1038/nprot.2012.016

Wang, X., Lu, N., Niu, B., Chen, X., Xie, J., and Cheng, N. (2012). Overexpression of Aurora-A enhances invasion and matrix metalloproteinase-2 expression in esophageal squamous cell carcinoma cells. *Mol. Cancer Res.* 10, 588–596. doi: 10.1158/1541-7786.mcr-11-0416

Wang, X., Zhao, Y., Fei, X., Lu, Q., Li, Y., Yuan, Y., et al. (2020). LEF1/Id3/HRAS axis promotes the tumorigenesis and progression of esophageal squamous cell carcinoma. *Int. J. Biol. Sci.* 16, 2392–2404. doi: 10.7150/ijbs.47035

Wang, Y., Gu, J., Lin, X., Yan, W., Yang, W., and Wu, G. (2018). lncRNA BANCR promotes EMT in PTC via the Raf/MEK/ERK signaling pathway. *Oncol. Lett.* 15, 5865–5870.

Wang, Y. L., Bai, Y., Yao, W. J., Guo, K., and Wang, Z. M. (2015). Expression of long non-coding RNA ZEB1-AS1 in esophageal squamous cell carcinoma and its correlation with tumor progression and patient survival. *Int. J. Clin. Exp. Pathol.* 8, 11871–11876.

Wong, V. C. L., Chen, H., Ko, J. M. Y., Chan, K. W., Chan, Y. P., Law, S., et al. (2012). Tumor suppressor dual-specificity phosphatase 6 (DUSP6) impairs cell invasion and epithelial-mesenchymal transition (EMT)-associated phenotype. *Int. J. Cancer* 130, 83–95. doi: 10.1002/ijc.25970

Xie, H. W., Wu, Q. Q., Zhu, B., Chen, F. J., Ji, L., Li, S. Q., et al. (2014). Long noncoding RNA SPRY4-IT1 is upregulated in esophageal squamous cell carcinoma and associated with poor prognosis. *Tumour Biol.* 35, 7743–7754. doi: 10.1007/s13277-014-2013-y

Xie, Y., Zhang, Y., Du, L., Jiang, X., Yan, S., Duan, W., et al. (2018). Circulating long noncoding RNA act as potential novel biomarkers for diagnosis and prognosis of non-small cell lung cancer. *Mol. Oncol.* 12, 648–658. doi: 10.1002/1878-0261.12188

Yang, G., Lu, X., and Yuan, L. (2014). LncRNA: a link between RNA and cancer. *Biochim. Biophys. Acta* 1839, 1097–1109. doi: 10.1016/j.bbagrm.2014.08.012

Yang, J., and Weinberg, R. A. (2008). Epithelial-mesenchymal transition: at the crossroads of development and tumor metastasis. *Dev. Cell* 14, 818–829. doi: 10.1016/j.devcel.2008.05.009

Yue, B., Qiu, S., Zhao, S., Liu, C., Zhang, D., Yu, F., et al. (2016). LncRNA-ATB mediated E-cadherin repression promotes the progression of colon cancer and predicts poor prognosis. *J. Gastroenterol. Hepatol.* 31, 595–603. doi: 10.1111/jgh.13206

Zhan, Y., Du, L., Wang, L., Jiang, X., Zhang, S., Li, J., et al. (2018). Expression signatures of exosomal long non-coding RNAs in urine serve as novel non-invasive biomarkers for diagnosis and recurrence prediction of bladder cancer. *Mol. Cancer* 17:142.

Zhang, F., Zhang, Y., Da, J., Jia, Z., Wu, H., and Gu, K. (2020). Downregulation of SPARC expression decreases cell migration and invasion involving epithelial-mesenchymal transition through the p-FAK/p-ERK pathway in esophageal squamous cell carcinoma. *J. Cancer* 11, 414–420. doi: 10.7150/jca.31427

Zhang, G., Li, S., Lu, J., Ge, Y., Wang, Q., Ma, G., et al. (2018). LncRNA MT1JP functions as a ceRNA in regulating FBXW7 through competitively binding to miR-92a-3p in gastric cancer. *Mol. Cancer* 17:87.

Zhang, L., Li, P., Liu, E., Xing, C., Zhu, D., Zhang, J., et al. (2020). Prognostic value of a five-lncRNA signature in esophageal squamous cell carcinoma. *Cancer Cell Int.* 20:386.

Zhang, S., Du, L., Wang, L., Jiang, X., Zhan, Y., Li, J., et al. (2019). Evaluation of serum exosomal LncRNA-based biomarker panel for diagnosis and recurrence prediction of bladder cancer. *J. Cell Mol. Med.* 23, 1396–1405. doi: 10.1111/jcmm.14042

Conflict of Interest: The authors declare that the research was conducted in the absence of any commercial or financial relationships that could be construed as a potential conflict of interest.

frontiers in Genetics

ORIGINAL RESEARCH
published: 28 June 2021
doi: 10.3389/fgene.2021.650863

Integrated Multiomic Analysis Reveals the High-Fat Diet Induced Activation of the MAPK Signaling and Inflammation Associated Metabolic Cascades via Histone Modification in Adipose Tissues

Zhe Wang[1†], Ming Zhu[2†], Meng Wang[2], Yihui Gao[2], Cong Zhang[1], Shangyun Liu[1], Shen Qu[3], Zhongmin Liu[2,4]* and Chao Zhang[1,2]**

[1] Department of Plastic and Reconstructive Surgery, Shanghai Institute of Precision Medicine, Shanghai Ninth People's Hospital, Shanghai Jiao Tong University School of Medicine, Shanghai, China, [2] Translational Medical Center for Stem Cell Therapy and Institute for Regenerative Medicine, Shanghai East Hospital, Shanghai Key Laboratory of Signaling and Disease Research, Frontier Science Center for Stem Cell Research, School of Life Sciences and Technology, Tongji University, Shanghai, China, [3] Department of Endocrinology and Metabolism, National Metabolic Management Center, Shanghai Tenth People's Hospital, School of Medicine, Tongji University, Shanghai, China, [4] Department of Cardiac Surgery, Shanghai East Hospital, School of Medicine, Tongji University, Shanghai, China

Background: The number of diet induced obese population is increasing every year, and the incidence of type 2 diabetes is also on the rise. Histone methylation and acetylation have been shown to be associated with lipogenesis and obesity by manipulating gene expression via the formation of repression or activation domains on chromosomes.

Objective: In this study, we aimed to explore gene activation or repression and related biological processes by histone modification across the whole genome on a high-fat diet (HFD) condition. We also aimed to elucidate the correlation of these genes that modulated by histone modification with energy metabolism and inflammation under both short-term and long-term HFD conditions.

Method: We performed ChIP-seq analysis of H3K9me2 and H3K9me3 in brown and white adipose tissues (WATs; subcutaneous adipose tissue) from mice fed with a standard chow diet (SCD) or HFD and a composite analysis of the histone modification of H3K9me2, H3K9me3, H3K4me1 and H3K27ac throughout the whole genome. We also employed and integrated two bulk RNA-seq and a single-nuclei RNA sequencing dataset and performed western blotting (WB) to confirm the gene expression levels in adipose tissue of the SCD and HFD groups.

Results: The ChIP-seq and transcriptome analysis of mouse adipose tissues demonstrated that a series of genes were activated by the histone modification of H3K9me2, H3K9me3, H3K4me1, and H3K27ac in response to HFD condition. These genes were enriched in Kyoto Encyclopedia of Genes and Genomes (KEGG) pathways

OPEN ACCESS

Edited by:
Shunliang Xu,
Second Hospital of Shandong University, China

Reviewed by:
Giovanni Messina,
Sapienza University of Rome, Italy
Zhao-Qian Teng,
Institute of Zoology, Chinese Academy of Sciences (CAS), China

***Correspondence:**
Shen Qu
qushencn@hotmail.com
Zhongmin Liu
liu.zhongmin@tongji.edu.cn
Chao Zhang
zhangchao@tongji.edu.cn

† These authors have contributed equally to this work

Specialty section:
This article was submitted to Epigenomics and Epigenetics, a section of the journal Frontiers in Genetics

Received: *08 January 2021*
Accepted: *10 May 2021*
Published: *28 June 2021*

Citation:
Wang Z, Zhu M, Wang M, Gao Y, Zhang C, Liu S, Qu S, Liu Z and Zhang C (2021) Integrated Multiomic Analysis Reveals the High-Fat Diet Induced Activation of the MAPK Signaling and Inflammation Associated Metabolic Cascades via Histone Modification in Adipose Tissues. Front. Genet. 12:650863. doi: 10.3389/fgene.2021.650863

involved in lipogenesis, energy metabolism and inflammation. Several genes in the activated mitogen-activated protein kinase (MAPK) pathway might be related to both inflammation and energy metabolism in mice, rats and humans fed with HFD for a short or long term, as showed by bulk RNA-seq and single nuclei RNA-seq datasets. Western blot analyses further confirmed the increased expression of *MET*, *VEGFA* and the enhanced phosphorylation ratio of p44/42 MAPK upon HFD treatment.

Conclusion: This study expanded our understanding of the influence of eating behavior on obesity and could assist the identification of putative therapeutic targets for the prevention and treatment of metabolic disorders in the future.

Keywords: adipose tissue, epigenetics, high-fat diet, inflammation, methylation, obesity

INTRODUCTION

As one of the world's greatest health challenges, obesity is usually accompanied by an increased risk for many chronic diseases, including type 2 diabetes, cardiovascular, hypertension and dyslipidemia. Obesity is a multifactorial disorder that is associated with both genetic and environmental factors, including eating behavior and exercise (Inagaki et al., 2016). As the link between genetic variants and environmental factors, the role of epigenetic modifications in obesity, including histone modifications, DNA methylation and non-coding RNA, had gained much attention in the late decade. Metabolic diseases, such as obesity and diabetes, were found to be tightly associated with epigenetic variation (Ling and Ronn, 2019). Among epigenetic locus, same histone could involve various modifications of several chemical groups, such as methylation and acetylation (Okuno et al., 2013), to activate or repress gene expression. For example, the various degrees of methylation of lysine 9 of histone H3 (H3K9me) are associated with transcriptional repression, whereas H3K4me and H3K27ac are associated with transcriptional activation.

Adipose tissues play vital roles in maintaining energy balance and are classified into white adipose tissue (WAT) and brown adipose tissue (BAT). WAT is responsible for energy storage and obesity syndrome, while BAT consumes fat to generate heat, which is essential for body weight and temperature control (Lee et al., 2014). The differentiation and stimulation of adipose tissue were regulated by various transcription factors and epigenetic modifications (Klose et al., 2006; Tateishi et al., 2009; Ohno et al., 2013; Zhou et al., 2014; Inagaki et al., 2016; Sanchez-Gurmaches et al., 2016; Wang and Seale, 2016; Cheng et al., 2018). For example, previous studies demonstrated the important roles of the methylation modifications of histone H3K9 sites in regulating metabolism of adipose tissue and maintaining homeostasis (Klose et al., 2006; Tateishi et al., 2009; Ohno et al., 2013; Cheng et al., 2018). High levels of H3K9me2 inhibited the expression of *PPARγ* and thereby affected the process of adipogenesis from preadipocytes (Rosen and Spiegelman, 2001; Takada et al., 2009). The deletion of *G9a* with the methylation of H3K9me1 and H3K9me2 in mouse adipose tissues could increase the expression of *PPARγ* and thereby promoted adipogenesis by increasing adipogenic gene expression (Tachibana et al., 2005; Wang et al., 2013). In addition, the histone demethylase *LSD1* (also known as *KDM1*) was essential for the initiation of adipogenesis by decreasing H3K9me2 levels and maintaining H3K4me2 levels at promoter regions (Musri et al., 2010; Duteil et al., 2014). Moreover, high-fat diet (HFD) could stimulate the proliferation of preadipocytes in subcutaneous adipose tissue (Joe et al., 2009). A long term HFD could induce changes in epigenetic modifications in WAT, as demonstrated by decreased levels of H3K4me2 and increased levels of H3K36me2 in mice with HFD induced obesity (Nie et al., 2017). These results suggested that changes in epigenetic states could disrupt the functions of adipose tissue and ultimately led to obesity.

Energy metabolic equilibrium and inflammation of adipose tissues are essential during the establishment of obesity syndrome. Usually, less than 10% of macrophages are located in normal adipose tissues, whereas the development of obesity is associated with increases in the number of macrophages and the polarization of M1 macrophages, which are closely related to energy homeostasis and inflammation (Odegaard and Chawla, 2008; Chawla et al., 2011). Macrophages are the most abundant immune cells and proinflammatory cytokines in obese adipose tissues, that could promote insulin resistance of adipose tissue and result in type 2 diabetes and other metabolic diseases (Odegaard and Chawla, 2008; Chawla et al., 2011). However, little is known on the correlation between genes controlled by histone modification and energy metabolism or inflammation of WAT and BAT in HFD induced obesity syndromes.

In this study, to understand the effect of histone modification on gene expression across the whole genome under high fat diet conditions, we analyzed the methylation modifications of histone H3K9 sites (H3K9me2 and H3K9me3) near the transcription start site and H3K4me1 and H3K27ac histone modifications throughout the genome. Because of the fact that the traditional bulk RNA sequencing cannot identify cell type specific heterogeneity due to the mixture of cell types in the specimen, we additionally integrated two bulk RNA-seq and a single-nuclei adipocyte RNA-seq datasets (SNAP-seq, GSE133486) (Rajbhandari et al., 2019) to identify the correlation between genes activated via histone modification and inflammation associated energy metabolism. In this study, we attempted to address the following questions: (1) Which genes are activated or repressed by histone modification in mouse adipose tissues under a long term HFD? (2) What biological processes are associated with genes that are modulated by HFD induced

histone modifications? (3) Are there any correlations between genes modulated by HFD induced histone modifications and energy metabolism or inflammation under both short- and long-term HFD conditions? Elucidation of these questions will expand our understanding of the influence of eating behavior on obesity and could assist the identification of putative therapeutic targets for the prevention and treatment of metabolic disorders.

MATERIALS AND METHODS

Animal Treatment

All animal experiments were approved by the Institutional Animal Care and Use Committee (IACUC) of the Shanghai Jiao Tong University and the Tongji University. Six-week-old wild-type C57BL/6J mice were fed either a standard chow diet (SCD) or a HFD (D12497, 60 kcal% fat, Research Diets). The body weight was monitored once a week. After 12 weeks, the BAT and WAT of the mice were obtained for subsequent H3K9me2 and H3K9me3 chromatin immunoprecipitation (ChIP-seq) assay.

ChIP-seq of H3K9 Methylation

The BAT and WAT of mice were removed and cleaved into small pieces. Formaldehyde was added to a final concentration of 1% and rotated at room temperature for 8 min. Glycine was added to a final concentration of 125 mM to terminate the cross-linking reaction, and the sample was rotated at room temperature for additional 10 min. H3K9me2 (Anti-Histone H3 (tri methyl K9) antibody, ChIP Grade, ab8898) and H3K9me3 (Anti-Histone H3 (di methyl K9) antibody [mAbcam 1220], ChIP Grade, ab1220) were used for immunoprecipitation assay. Libraries were prepared using the KAPA Hyper Prep Kit following the manufacturer's instructions and sequenced with the Illumina HiSeq X Ten system.

The sequence quality was assessed using FastQC v0.11.9, and adaptors were trimmed using trim_galore v0.6.6. After the data were filtered, the DNA sequences were aligned to the reference genome (mm9) using Bowtie2 (v2.4.2)(Langmead and Salzberg, 2012), and the reads that mapped to multiple sites were removed. Next we performed model-based analysis of ChIP-seq using MACS2 (Zhang et al., 2008) for enriched-region identification (peak calling), and determined the location in the genome with differentially enriched peaks ($P < 0.05$) between the SCD and HFD fed mice. The enriched peaks were annotated with the R package ChIPseeker (Yu et al., 2015). Genes that showed different-sized peaks of H3K9me2 or H3K9me3 in the 3 kb upstream and downstream of the transcription starting sites (defined as the promoter regions) between the SCD and HFD fed mouse adipose tissue were selected for subsequent KEGG enrichment analysis, which was conducted with the R package clusterProfiler (Yu et al., 2012).

Integrated Analysis of H3K4 and H3K27 ChIP-seq Datasets

To clarify the effect of histone modification on gene expression under HFD conditions, we further integrated H3K4me1 and H3K27ac ChIP-seq data (GSE132885) of mouse WAT that was fed with SCD or HFD for 8 weeks (Caputo et al., 2020). From processed data in a published paper (Caputo et al., 2020), we obtained H3K4me1 and H3K27ac enriched regions in subcutaneous adipose tissue of SCD or HFD fed mice using bigWigtoBedGraph v377. The R package edgeR (McCarthy et al., 2012) was used to determine the differences of the number of enriched peaks in gene promoters across the whole genome between SCD and HFD fed mouse adipose tissues. The KEGG enrichment analyses were conducted as mentioned above.

Integrated Analysis of Bulk RNA and Single-Nuclei RNA Sequencing Data of Adipose Tissue

To illustrate the correlation between genes activated by HFD via histone modification and inflammation, we integrated two bulk RNA sequencing datasets (GSE69607 and GSE158627) in this study (Jablonski et al., 2015; Zhang X. et al., 2020). Using data from GSE69607, we compared the differentially expressed genes between M1 and M2 macrophages using the R package limma (Ritchie et al., 2015), and genes with a P-value < 0.05 and logFC > 0.58 were identified as macrophage markers. The genes that served as macrophage markers and also showed differential peaks (in the promoter regions) between SCD and HFD fed mouse WAT (based on H3K9me2 ChIP-seq) were subjected to KEGG enrichment analysis. In addition, using data from GSE158627, we compared the differentially expressed genes between macrophages from WT (Lyz2-Cre) mice fed a SCD and HFD, which might be related to HFD induced inflammation in adipose tissue.

To further illustrate the correlation between genes activated by HFD via histone modification and energy metabolism at single cell resolution, we additionally integrated a single-nuclei adipocyte RNA sequencing dataset (SNAP-seq, GSE133486) in this study (Rajbhandari et al., 2019). We obtained the top 2000 variable genes from the metabolically active adipocyte subtype using the R package Seurat v3 and conducted a KEGG enrichment analysis with the R package clusterProfiler. In addition, we colored several genes (*MAP3K5*, *MAP3K14*, *MET*, and *VEGFA*) on the UMAP dimensional reduction plot to visualize the gene expression level and the number of expressed genes detected in single adipose cell using the R package Seurat v3.

To confirm the activated mitogen-activated protein kinase (MAPK) signaling pathway in adipose tissue of obese rat and human, we analyzed two bulk RNA sequencing datasets from GSE142401 and GSE1813. The differentially expressed genes were calculated as above and the R package pheatmap v1.0.12 and clusterProfiler v3.12 were used for visualization.

Analyses of Western Blot

To confirm the activated MAPK signaling pathway and the increased gene expression in HFD adipose tissues, we further conducted experimental validation using western blot. The adipose tissues of the rats were lysed in RIPA buffer (P0013B, Beyotime, China) supplemented with protease and phosphatase

inhibitor cocktails (C0001 and C0004, Targetmol, United States) on ice. Total lysate was subjected to SDS-PAGE and electro-transferred to a PVDF membrane (IPFL85R, Merck, Germany). The membranes were blocked with 5% BSA, incubated with primary antibody (**Supplementary Table 1**) and HRP-conjugated secondary antibody. Tanon chemiluminescence image detection system (5200S, Tanon, China) was used to detect the luminescent signals. Statistically differences were evaluated by unpaired student's *t* test. GraphPad Prism software (La Jolla, CA, United States) was used for data analysis and visualization.

RESULTS

Various Signaling Pathways Are Activated by Histone Modifications in Mice Adipose Tissues Upon HFD Treatment

Starting at 6-week age, wild type mice were fed with either SCD or HFD, and a significant difference ($P < 0.05$) in body weight began to be observed at week 11 (**Figure 1A**). On week 12, the BAT and WAT of the mice (**Figure 1B**) were dissected to examine the differential methylation modifications of H3K9me2 and H3K9me3. Our results showed that high fold enrichment peaks appeared at the promoter regions (**Figures 1C,D**). Noticeably, the peak fold enrichment of H3K9me2 and H3K9me3 modifications was decreased in both the BAT and WAT of HFD fed mice compared with those of SCD fed mice (**Figures 1C,D**). These results suggested a decreased level of H3K9 methylation crossing the whole genome in HFD fed mice compared with SCD fed group. The KEGG enrichment analysis revealed that the genes with H3K9 demethylation modification in adipose tissue of the HFD-fed mice were enriched in pathways related to lipogenesis, energy metabolism, immunity and inflammation (**Figure 2A**). Among these pathways, the MAPK signaling pathway was enriched with a highest number of genes and had a *P*-value less than 0.001 (**Figure 2**).

We also analyzed published data on histone modifications, including H3K27ac and H3K4me1 ChIP-seq and bulk RNA-seq data (GSE132885). These data showed that compared with the SCD fed mice, many genes in mouse adipose tissue were activated by the consumption of a HFD for 8 weeks. These genes were also enriched in pathways similar to those found for H3K9 (**Figure 2B**), including the MAPK signaling pathway. All of these results suggested that the changes in histone

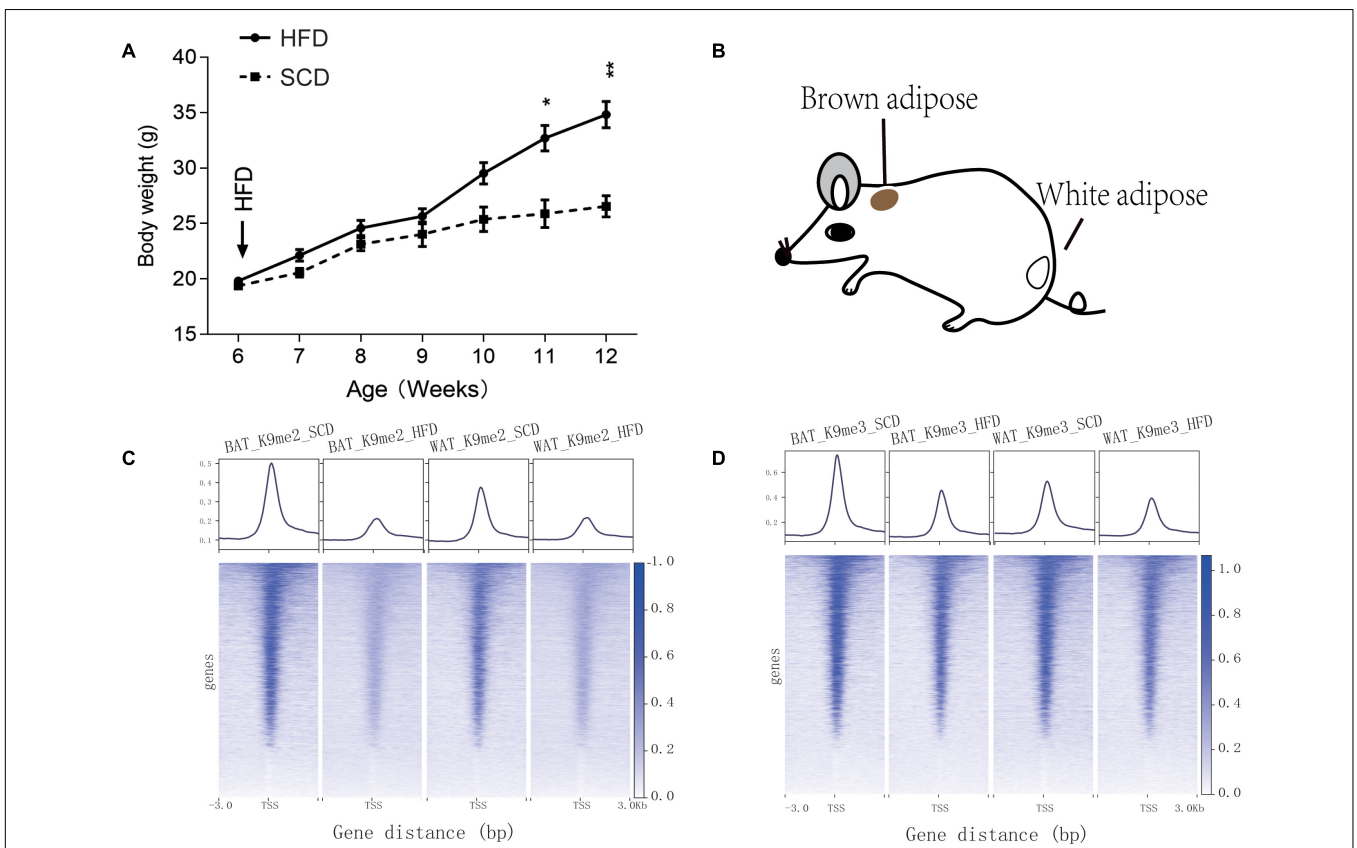

FIGURE 1 | Information of SCD and HFD mice used in this study and peak enrichment of H3K9 methylation. **(A)** Body weight monitoring of mice under control (SCD) and high fat diet (HFD) treatments. *$P < 0.05$, **$P < 0.01$. **(B)** Dissection location of mouse brown adipose tissue and white adipose tissue used for the H3K9me2 and H3K9me3 ChIP-seq experiments. **(C,D)** Peak enrichment at histone H3K9 methylation modification (H3K9me2 and H3K9me3) near the transcription start site (TSS, ±3 kb) of genes.

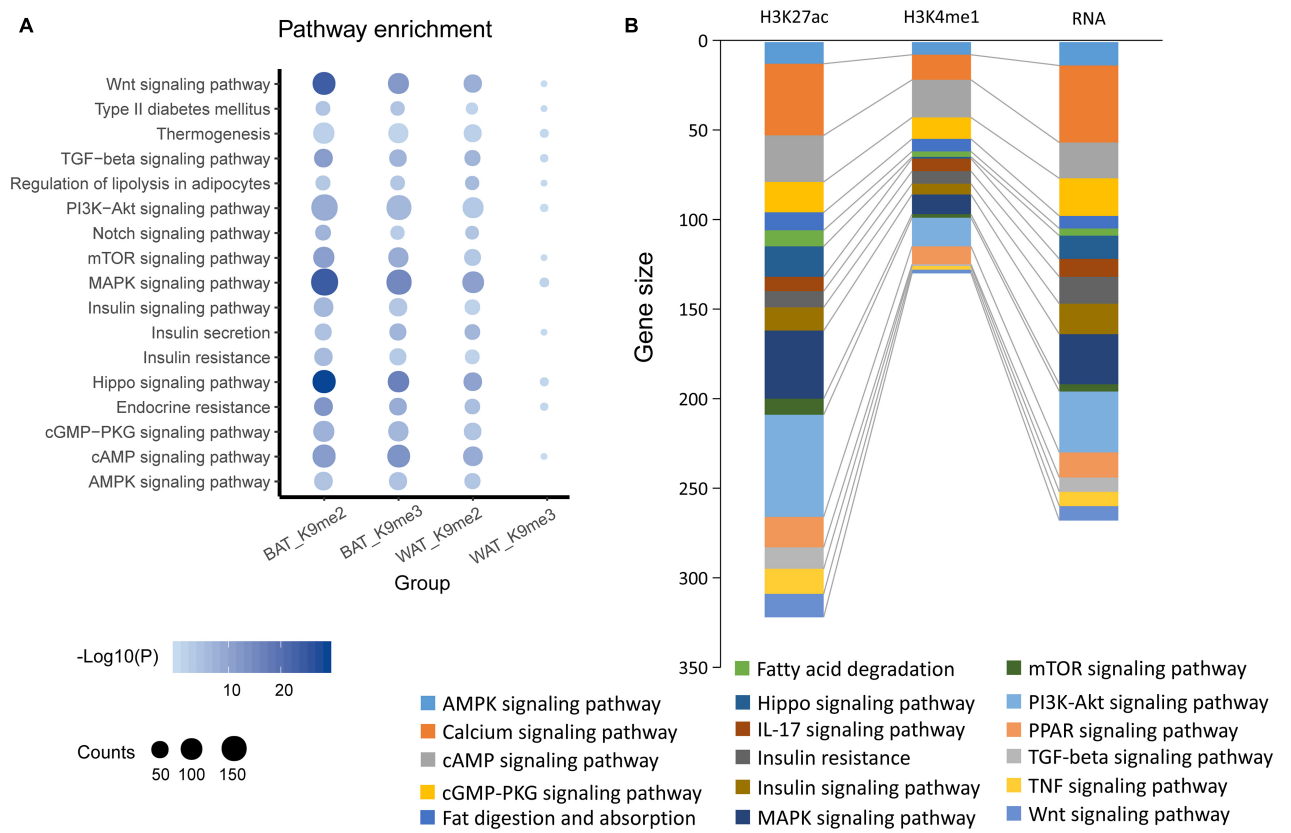

FIGURE 2 | KEGG pathway enrichments of BAT or WAT under SCD and HFD conditions. **(A)** KEGG pathway enrichment by genes showing differential peaks in promoter regions identified by H3K9me2 (K9me2) or H3K9me3 (K9me2) ChIP-seq of mouse brown adipose (BAT) or white adipose tissues (WAT) under HFD condition compared with SCD conditions. **(B)** KEGG pathway enrichment of H3K27ac, H3K4me1 and RNA-activated genes in brown adipose (BAT) or white adipose tissue (scWAT) under HFD condition compared with SCD conditions.

modifications induced by a HFD could activate various genes that are related to the biological processes of lipogenesis, energy metabolism, immunity and inflammation and include the MAPK signaling pathway.

Activation of Genes in the MAPK Signaling Pathway via Histone Modification Are Related to Inflammation and Energy Metabolism

To investigate whether genes with differential peaks caused by histone modification under SCD and HFD conditions exhibited correlations with inflammation and energy metabolism, we integrated two bulk RNA-seq datasets and a SNAP-seq dataset in this study. These RNA sequencing data involved macrophage polarization, which was important for macrophage inflammation and energy metabolism in adipose tissues. First, we found 768 genetic markers of M1 macrophages from the published bulk RNA dataset GSE69607 that showed higher expression levels in M1 macrophages than other types. Among these marker genes, 136 genes were also activated via histone modification in WAT under HFD feeding, as demonstrated by H3K9me2 ChIP-seq (**Figure 3A**). KEGG enrichment analyses showed that the 136 genes were enriched in some pathways, including the MAPK signaling pathway (**Figure 3B**). Among these genes, *Map3k5*, *Ppp3cc*, *Hspa1a*, *Vegfa*, *Dusp2*, and *Met* were also upregulated in macrophages of adipose tissue from HFD fed mice compared with the control group (red squares in **Figure 3B**, GSE158627), suggesting a strong correlation of MAPK signaling to inflammation upon HFD treatment.

In addition, we included a published single-nuclei RNA sequencing data of adipocytes (GSE133486) and defined a metabolic active adipocyte subtype in WAT (Adipose_9 in **Figure 4A**). We obtained the top 2000 variable genes from the metabolically active adipocyte subtype and assessed their enrichment in KEGG pathways, including the AMPK, cAMP, GMP-PKG, and MAPK signaling pathways (**Figure 4B**). We also found that the *Map3k5*, *Met*, and *Vegfa* genes were highly expressed in the metabolic active adipocyte subtype (Adipose_9), as reported in the published study (**Figures 4C–E**). Altogether, these results suggested that the *Map3k5*, *Met*, and *Vegfa* genes in the MAPK signaling pathway activated by HFD induced epigenetic modification might be related to both inflammation and energy metabolism, which pointed out an implication for better understanding of the effect of diet and eating behavior on obesity and energy homeostasis.

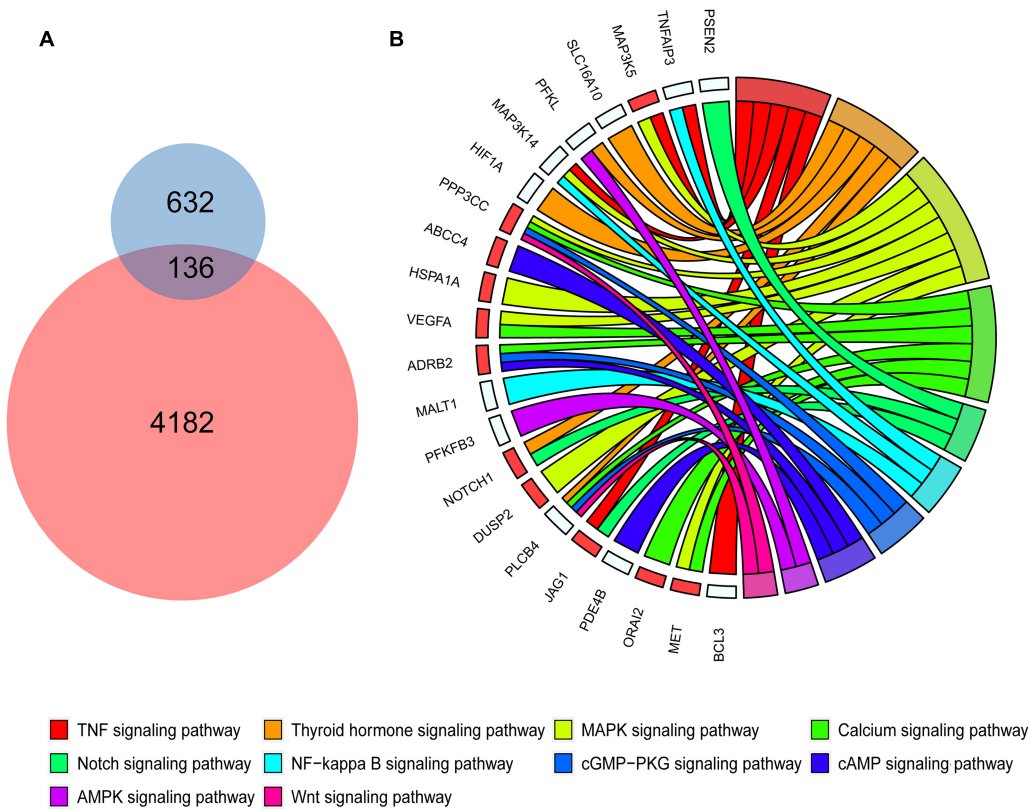

FIGURE 3 | Polarized macrophage marker genes activated by HFD and relevant KEGG pathways. **(A)** The Venn diagrams shows 136 genes shared between the polarized macrophage marker genes and activated genes with differential peaks in the promoter determined by H3K9me2 ChIP-seq data in mouse white adipose tissue of HFD conditions. **(B)** The chord diagrams show the KEGG pathways enriched by the 136 shared genes. The red squares represent the genes shared between the 136 genes and differentially expressed genes of macrophages under SCD and HFD conditions.

Activated MAPK Signaling Pathway in Humans and Rats Under Short- and Long-Term HFD Conditions

Based on the transcriptome of adipose tissue in humans under fasting conditions (0 h) and 4 h post-meal (GSE142401), we found that the genes that were upregulated after the meal were enriched in various KEGG pathways, including the IL-17, NF-kB, MAPK, Toll-like receptor and TNF signaling pathway (**Figure 5A**). In addition, several genes (*MAP3K5*, *MET*, and *VEGFA*) in the MAPK signaling pathway showed relatively higher expression levels after a high-fat meal than fasting condition (**Figure 5B**). Similarly, we found that these genes upregulated in HFD rat were also enriched in MAPK signaling pathway (**Figure 5C**).Furthermore, western blotting (WB) analyses showed increased expression of *Met*, *Vegfa* in WAT from HFD fed rat (**Figures 6A–C**). Additionally, the ratio of p44/42 MAPK phosphorylation was significantly upregulated in the HFD fed group (**Figures 6A,D**), which suggested a relatively activated state of MAPK pathway in obese adipose tissues. All of these results suggested that the MAPK signaling pathway could be activated by histone modification in adipose tissue after both long-term and short-term consumption of a HFD in house mice, rats and humans. The *MAP3K5*, *MET*, and *VEGFA* genes might be involved in inflammation associated energy metabolism via the activation of MAPK signaling cascades.

DISCUSSION

The post-transcriptional modifications of histone tails are essential for the regulation of the chromatin state, which could result in activation or repression of the transcription of the associated genes. For example, the di-methylation and tri-methylation of histone H3 at lysine 9 (H3K9me2 and H3K9me3) are mostly associated with gene repression, whereas histone H3K27 acetylation and H3K4me1 are features of gene activation (Zhang T. et al., 2020). During the growth and differentiation of adipose tissue, histone modifications not only determine the fate of precursor cells but also participate in the regulation of physiological activities and the body's adaptation to the environment. In this study, H3K9me2 and H3K9me3 modification sites were analyzed in the adipose tissue of SCD and HFD fed mice by chromatin immunoprecipitation and high throughput sequencing. Generally, we found a stronger signal of peaks around the transcription start site in SCD fed mice than HFD-fed group (**Figures 1C,D**), suggesting the common

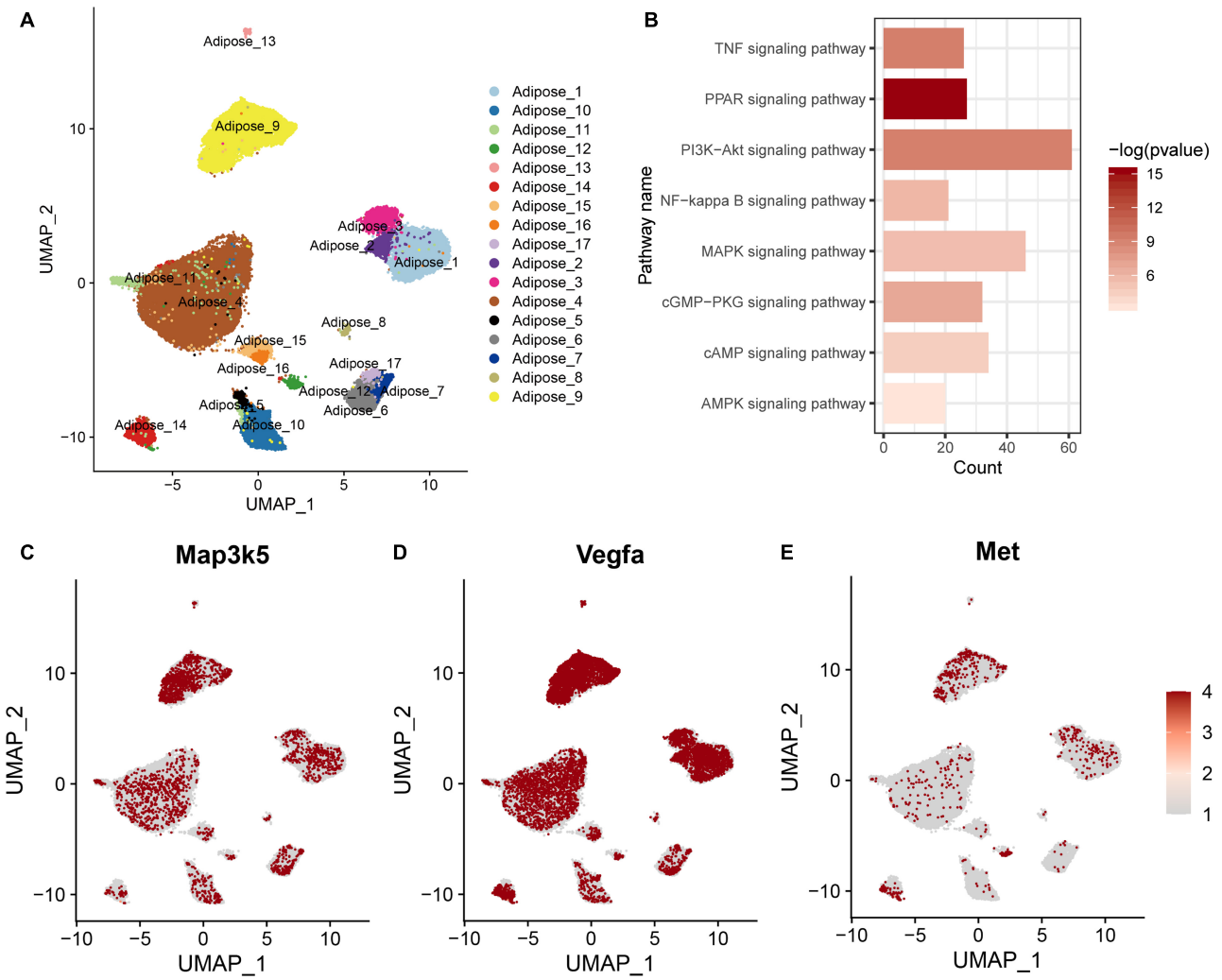

FIGURE 4 | Gene expression and the related KEGG pathway in metabolic active adipocyte subtype by single-nuclei RNA sequencing. **(A)** UMAP plot of single-nuclei RNA sequencing data (GSE133486) illustrating the cell types of adipocytes. **(B)** KEGG pathway enriched by the top 2000 variable genes from the metabolic active adipocyte subtype. **(C–E)** Scaled expression levels of the *Map3k5*, *Met*, and *Vegfa* genes in the adipocyte subtype depicted using a red gradient (gray denotes a lack of expression).

demethylation and activation of transcription through the whole genome induced by HFD.

The KEGG analysis showed that the genes activated by HFD feeding were mainly associated with lipogenesis, energy metabolism and insulin resistance. For example, the Wnt (Bowers and Lane, 2008), mTOR (Caron et al., 2015) and Hippo signaling pathway (Shu et al., 2020) were major regulators of adipogenesis. The mTOR (Caron et al., 2015), cAMP, AMPK, and PI3K-Akt signaling pathway were closely related to energy metabolism.

Notably, we found that the MAPK signaling pathway was enriched with many H3K9me2 and H3K9me3 de-methylation activated genes (**Figure 2A**) as well as H3K4me1, H3K27ac and RNA expression activated genes (**Figure 2B**) upon HFD treatment. MAPK pathways regulated multiple cellular functions, including cell proliferation, migration, differentiation, and apoptosis. A previous study showed that MAPK signaling related genes interacted with dietary factors involved in inflammation and oxidative stress (Slattery et al., 2013). Inflammation of fat adipose tissue could induce insulin resistance and metabolic disease (Acin-Perez et al., 2020), which suggested that activated MAPK might help to improve the understanding of the epigenetic effects of HFD on obesity and metabolic disease.

To illustrate the correlation between obesity, energy metabolism and inflammation, we integrated bulk RNA-seq and single-nuclei RNA-seq dataset of adipocytes from other published study. Single-nuclei RNA-seq could show cell type specific differential gene expression and the results showed that some genes (*Map3k5*, *Met*, and *Vegfa*) in the MAPK signaling pathway activated by a HFD via histone modifications showed high expression levels in the metabolic active adipocyte subtype in WAT though single-nuclei RNA sequencing. These genes might also participate in inflammation (**Figures 4**, **5**) in mice, rat

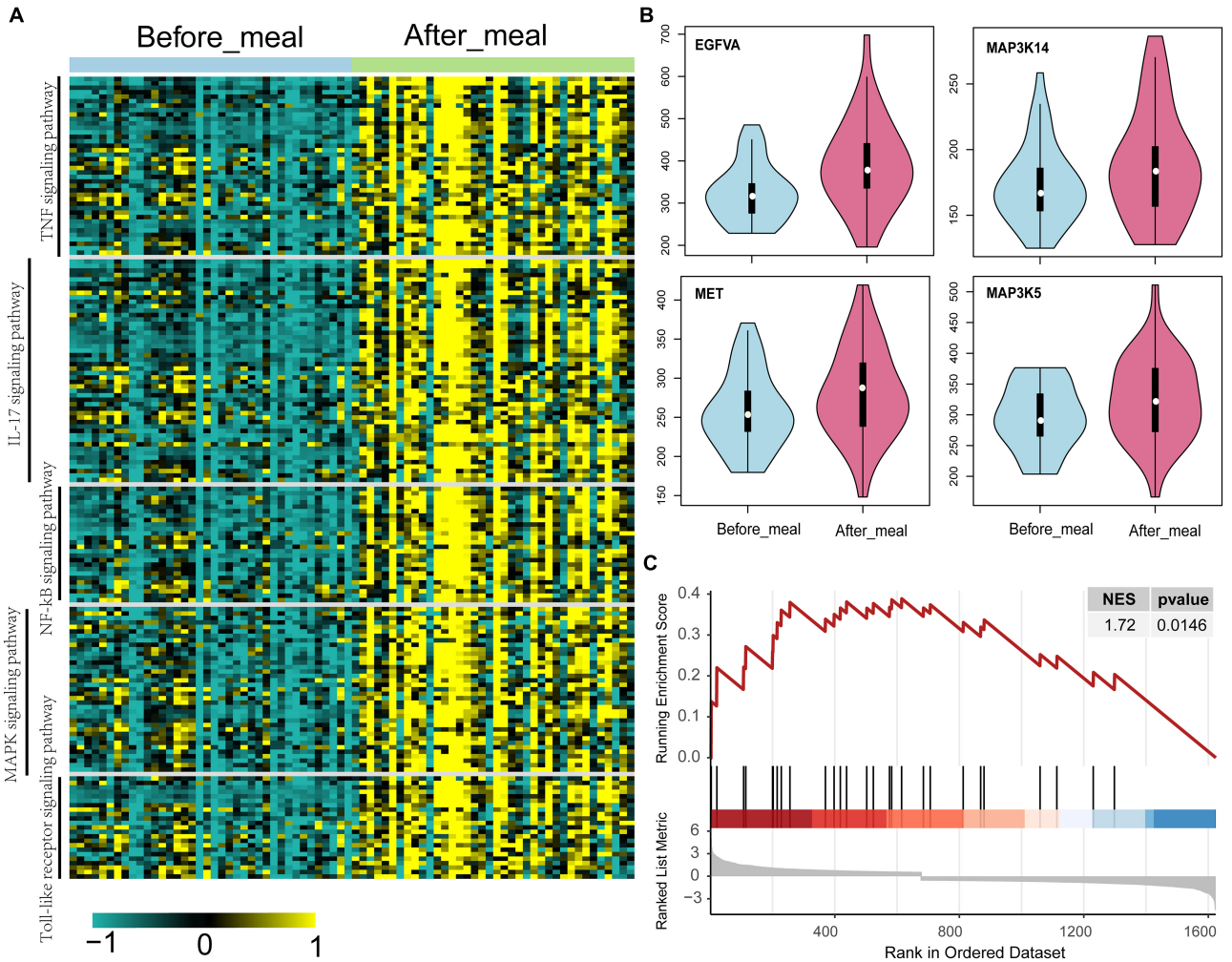

FIGURE 5 | Up-regulated genes and activated KEGG pathways in humans and rats under short- and long-term HFD conditions. **(A)** KEGG pathways of the significantly differentially expressed genes between adipose tissue under fasting (0 h) and at 4 h post-meal condition. **(B)** Violin plots show the level of gene expression in adipose tissue under fasting (0 h) and at 4 h post-meal condition. **(C)** GSEA plot shows the genes upregulated in the adipose tissue of HFD rat are enriched in MAPK signaling pathway.

and humans under short-term or long-term HFD (**Figure 5**). In addition, western blot further confirmed the higher expression of *Met* and *Vegfa* genes and the enhanced ratio of p44/42 MAPK phosphorylation under HFD conditions (**Figure 6**).

Previous studies also showed the potential role of *Map3k5*, *Met*, and *Vegfa* in obesity and metabolic dysregulation (Rudich et al., 2007; Bian et al., 2010; Lu et al., 2012; Elias et al., 2013; Sundaram et al., 2014a,b; Hattori et al., 2016; Haim et al., 2017). For example, Sundaram et al. (2014a,b) found that the expression of *Met* increased in obese mice with breast cancer compared with their lean controls, suggesting that *Met* was potentially associated with obesity and immunity (Sundaram et al., 2014a,b). The *MAP3K5* gene was upregulated in adipose tissues of obese animal (Haim et al., 2017), and a *MAP3K5* mutation that decreased RNA expression was linked to obesity with whole body insulin resistance (Rudich et al., 2007; Bian et al., 2010). In mice, *Map3k5* knockout mice became obese by interfering with brown fat function (Hattori et al., 2016). Vascular endothelial growth factor A (*Vegfa*), a member of the VEGF family, was also highly expressed in adipose tissues (Lu et al., 2012). Lu et al. (2012) found that mice with repressed expression of the *Vegfa* gene presented a lean phenotype and resistance to HFD induced body weight gain (Lu et al., 2012). Elias et al. (2013) showed that *Vegfa* overexpression in adipose tissue could enhance PGC-1α and UCP-1 expression, which resulted in increases in thermogenesis and energy expenditure and decreases in obesity, suggesting the important role of *Vegfa* under HFD conditions (Elias et al., 2013). In addition, increased *Vegfa* expression might be associated with higher inflammation in adipose tissues through its anti-inflammatory role in adipose tissue, which resulted in increases in activated macrophages (Elias et al., 2013; Schlich et al., 2013). Wang et al. (2006) found that the VEGF increased with the stimulation of pro-inflammatory factor TNFα in isolated progenitor cells of the

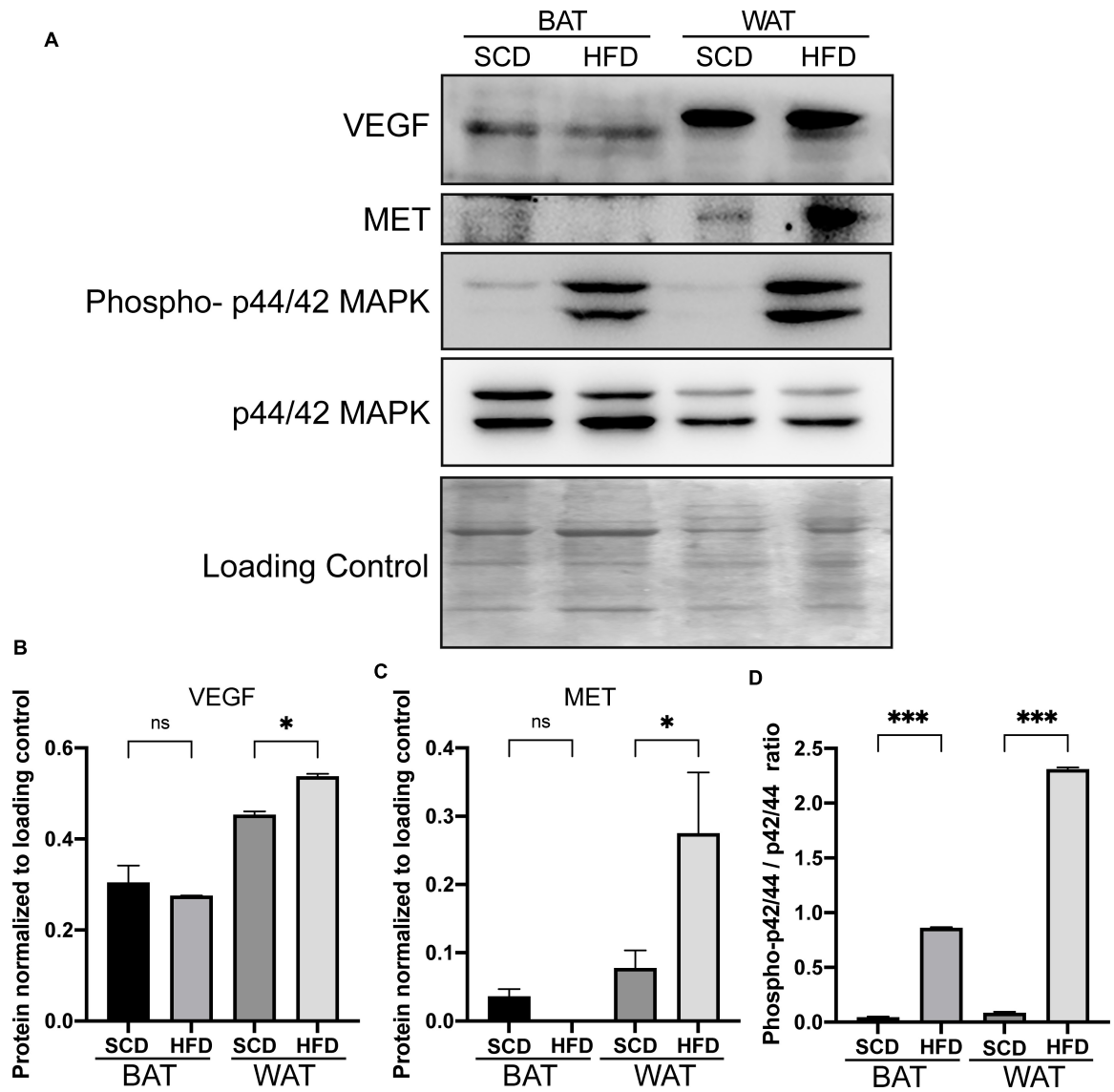

FIGURE 6 | Increased expressions of genes in the adipose tissue of rats under HFD conditions by western blot analysis. Western blot analysis of the increased expressions of *Met* and *Vegfa* gene and the enhanced ratio of phosphorylation of p44/42 MAPK in adipose tissues from HFD rat. **(A)** The protein expression of Met, Vegfa and phospho-p44/42 MAPK in the adipose tissue of rats. **(B–D)** Bar plot of the statistical significance of *Met* and *Vegfa* expression and phosphorylation-p44/42 MAPK ratio in HFD and SCD adipose tissues in rat by unpaired student's *t* tests. Bars represent standard errors. *, **, and *** indicates *P*-value < 0.05, 0.01, and 0.001, respectively. WAT, white adipose tissue; BAT, brown adipose tissue.

human adipose, suggesting the potential roles of VEGF in inflammation. Here our study showed the significantly increased level of the phosphorylation of p42/44 MAPK in both BAT and WAT rat under a HFD condition, suggesting a relatively activated state of MAPK pathway in obesity adipose tissues. Overall, the demethylation activated genes *Map3k5*, *Met* and *Vegfa* in the activated MAPK signaling pathway could participate in inflammation and energy metabolism to lead to obesity, and thus, these genes might be promising markers for the prevention and treatment of metabolic diseases.

In summary, ChIP-seq technology was utilized to assess the changes in the modifications of histone H3 sites in BAT and WAT of mice under SCD or HFD conditions. We found that the HFD decreased the level of H3K9me2 or H3K9me3 level in gene promoters crossing the whole genome. Through integrated analyses of the bulk RNA transcriptome and single-nuclei adipocyte RNA sequencing in mouse, rat and human adipose tissues, we found that a series of genes that were activated by histone modification were also upregulated under both long-term and short-term HFD conditions. These genes, including *MAP3K5*, *MET*, and *VEGFA*, were enriched in KEGG pathways involving lipogenesis, energy metabolism, and inflammation pathways. All these findings would help us to improve the understanding of the influence of diet on obesity and human

metabolic diseases through epigenetic modifications and could assist the identification of putative therapeutic targets for the prevention and treatment of metabolic disorders in the future.

DATA AVAILABILITY STATEMENT

The names of the repository/repositories and accession number(s) can be found below: https://www.ncbi.nlm.nih.gov/genbank/, GSE164530.

ETHICS STATEMENT

All animal experiments were approved by the Institutional Animal Care and Use Committee (IACUC) of the Shanghai Jiao Tong University and the Tongji University.

AUTHOR CONTRIBUTIONS

ZW, MZ, CZh, and ZL conceived and designed the study. ZW, MZ, MW, CZo, SL, YG, and SQ performed the experiments. ZW, MZ, and YG performed the data analysis. All authors participated in data interpretation, manuscript drafting, and approved the final manuscript.

FUNDING

This work was supported by grants from the National Key Research and Development Program of China (grant nos. 2017YFA0103902 and 2019YFA0111400), the Natural Science Foundation of China (31771283), the Fundamental Research Funds for the Central Universities (22120190210), the Innovative Research Team of High-level Local Universities in Shanghai (grant no. SSMU-ZDCX20180700), the Key Laboratory Program of the Education Commission of Shanghai Municipality (ZDSYS14005), and the China Postdoctoral Science Foundation funded project (2020M681380).

SUPPLEMENTARY MATERIAL

The Supplementary Material for this article can be found online at: https://www.frontiersin.org/articles/10.3389/fgene.2021.650863/full#supplementary-material

REFERENCES

Acin-Perez, R., Iborra, S., Marti-Mateos, Y., Cook, E. C. L., Conde-Garrosa, R., Petcherski, A., et al. (2020). Fgr kinase is required for proinflammatory macrophage activation during diet-induced obesity. *Nat. Metab.* 2, 974–988. doi: 10.1038/s42255-020-00273-8

Bian, L., Hanson, R. L., Ossowski, V., Wiedrich, K., Mason, C. C., Traurig, M., et al. (2010). Variants in ASK1 are associated with skeletal muscle ASK1 expression, in vivo insulin resistance, and type 2 diabetes in Pima Indians. *Diabetes* 59, 1276–1282. doi: 10.2337/db09-1700

Bowers, R. R., and Lane, M. D. (2008). Wnt signaling and adipocyte lineage commitment. *Cell Cycle* 7, 1191–1196. doi: 10.4161/cc.7.9.5815

Caputo, T., Tran, V. D. T., Bararpour, N., Winkler, C., Aguileta, G., Trang, K. B., et al. (2020). Anti-adipogenic signals at the onset of obesity-related inflammation in white adipose tissue. *Cell. Mol. Life Sci.* 78, 227–247. doi: 10.1007/s00018-020-03485-z

Caron, A., Richard, D., and Laplante, M. (2015). The roles of mTOR complexes in lipid metabolism. *Annu. Rev. Nutr.* 35, 321–348. doi: 10.1146/annurev-nutr-071714-034355

Chawla, A., Nguyen, K. D., and Goh, Y. P. (2011). Macrophage-mediated inflammation in metabolic disease. *Nat. Rev. Immunol.* 11, 738–749. doi: 10.1038/nri3071

Cheng, Y., Yuan, Q., Vergnes, L., Rong, X., Youn, J., Li, J., et al. (2018). KDM4B protects against obesity and metabolic dysfunction. *Proc. Natl. Acad. Sci. U. S. A.* 115, 5566–5575. doi: 10.1073/pnas.1721814115

Duteil, D., Metzger, E., Willmann, D., Karagianni, P., Friedrichs, N., Greschik, H., et al. (2014). LSD1 promotes oxidative metabolism of white adipose tissue. *Nat. Commun.* 5:4093. doi: 10.1038/ncomms5093

Elias, I., Franckhauser, S., and Bosch, F. (2013). New insights into adipose tissue VEGF-A actions in the control of obesity and insulin resistance. *Adipocyte* 2, 109–112. doi: 10.4161/adip.22880

Haim, Y., Bluher, M., Konrad, D., Goldstein, N., Kloting, N., Harman-Boehm, I., et al. (2017). ASK1 (MAP3K5) is transcriptionally upregulated by E2F1 in adipose tissue in obesity, molecularly defining a human dys-metabolic obese phenotype. *Mol. Metab.* 6, 725–736. doi: 10.1016/j.molmet.2017.05.003

Hattori, K., Naguro, I., Okabe, K., Funatsu, T., Furutani, S., Takeda, K., et al. (2016). ASK1 signalling regulates brown and beige adipocyte function. *Nat. Commun.* 7:11158. doi: 10.1038/ncomms11158

Inagaki, T., Sakai, J., and Kajimura, S. (2016). Transcriptional and epigenetic control of brown and beige adipose cell fate and function. *Nat. Rev. Mol. Cell. Biol.* 17, 480–495. doi: 10.1038/nrm.2016.62

Jablonski, K. A., Amici, S. A., Webb, L. M., Ruiz-Rosado Jde, D., Popovich, P. G., Partida-Sanchez, S., et al. (2015). Novel markers to delineate murine M1 and M2 macrophages. *PLoS One* 10:e0145342. doi: 10.1371/journal.pone.0145342

Joe, A. W., Yi, L., Even, Y., Vogl, A. W., and Rossi, F. M. (2009). Depot-specific differences in adipogenic progenitor abundance and proliferative response to high-fat diet. *Stem Cells* 27, 2563–2570. doi: 10.1002/stem.190

Klose, R., Kallin, E., and Zhang, Y. (2006). JmjC-domain-containing proteins and histone demethylation. *Nat. Rev. Genet.* 7, 715–727. doi: 10.1038/nrg1945

Langmead, B., and Salzberg, S. L. (2012). Fast gapped-read alignment with Bowtie 2. *Nat. Methods* 9, 357–359. doi: 10.1038/nmeth.1923

Lee, Y. H., Mottillo, E. P., and Granneman, J. G. (2014). Adipose tissue plasticity from WAT to BAT and in between. *Biochim. Biophys. Acta* 1842, 358–369. doi: 10.1016/j.bbadis.2013.05.011

Ling, C., and Ronn, T. (2019). Epigenetics in human obesity and type 2 diabetes. *Cell Metab.* 29, 1028–1044. doi: 10.1016/j.cmet.2019.03.009

Lu, X., Ji, Y., Zhang, L., Zhang, Y., Zhang, S., An, Y., et al. (2012). Resistance to obesity by repression of VEGF gene expression through induction of brown-like adipocyte differentiation. *Endocrinology* 153, 3123–3132. doi: 10.1210/en.2012-1151

McCarthy, D. J., Chen, Y., and Smyth, G. K. (2012). Differential expression analysis of multifactor RNA-Seq experiments with respect to biological variation. *Nucleic Acids Res.* 40, 4288–4297. doi: 10.1093/nar/gks042

Musri, M. M., Carmona, M. C., Hanzu, F. A., Kaliman, P., Gomis, R., and Parrizas, M. (2010). Histone demethylase LSD1 regulates adipogenesis. *J. Biol. Chem.* 285, 30034–30041. doi: 10.1074/jbc.M110.151209

Nie, L., Shuai, L., Zhu, M., Liu, P., Xie, Z. F., Jiang, S., et al. (2017). The landscape of histone modifications in a high-fat diet-induced obese (DIO) mouse model. *Mol. Cell Proteomics* 16, 1324–1334. doi: 10.1074/mcp.M117.067553

Odegaard, J. I., and Chawla, A. (2008). Mechanisms of macrophage activation in obesity-induced insulin resistance. *Nat. Clin. Pract. Endocrinol. Metab.* 4, 619–626. doi: 10.1038/ncpendmet0976

Ohno, H., Shinoda, K., Ohyama, K., Sharp, L. Z., and Kajimura, S. (2013). EHMT1 controls brown adipose cell fate and thermogenesis through the PRDM16 complex. *Nature* 504, 163–167. doi: 10.1038/nature12652

Okuno, Y., Ohtake, F., Igarashi, K., Kanno, J., Matsumoto, T., Takada, I., et al. (2013). Epigenetic regulation of adipogenesis by PHF2 histone demethylase. *Diabetes* 62, 1426–1434. doi: 10.2337/db12-0628

Rajbhandari, P., Arneson, D., Hart, S. K., Ahn, I. S., Diamante, G., Santos, L. C., et al. (2019). Single cell analysis reveals immune cell-adipocyte crosstalk regulating the transcription of thermogenic adipocytes. *Elife* 8:e49501. doi: 10.7554/eLife.49501

Ritchie, M. E., Phipson, B., Wu, D., Hu, Y., Law, C. W., Shi, W., et al. (2015). limma powers differential expression analyses for RNA-sequencing and microarray studies. *Nucleic Acids Res.* 43:e47. doi: 10.1093/nar/gkv007

Rosen, E. D., and Spiegelman, B. M. (2001). PPARgamma: a nuclear regulator of metabolism, differentiation, and cell growth. *J. Biol. Chem.* 276, 37731–37734. doi: 10.1074/jbc.R100034200

Rudich, A., Kanety, H., and Bashan, N. (2007). Adipose stress-sensing kinases: linking obesity to malfunction. *Trends Endocrinol. Metab.* 18, 291–299. doi: 10.1016/j.tem.2007.08.006

Sanchez-Gurmaches, J., Hung, C. M., and Guertin, D. A. (2016). Emerging complexities in adipocyte origins and identity. *Trends Cell Biol.* 26, 313–326. doi: 10.1016/j.tcb.2016.01.004

Schlich, R., Willems, M., Greulich, S., Ruppe, F., Knoefel, W. T., Ouwens, D. M., et al. (2013). VEGF in the crosstalk between human adipocytes and smooth muscle cells: depot-specific release from visceral and perivascular adipose tissue. *Mediators Inflamm.* 2013:982458. doi: 10.1155/2013/982458

Shu, Z. P., Yi, G. W., Deng, S., Huang, K., and Wang, Y. (2020). Hippo pathway cooperates with ChREBP to regulate hepatic glucose utilization. *Biochem. Biophys. Res. Commun.* 530, 115–121. doi: 10.1016/j.bbrc.2020.06.105

Slattery, M. L., Lundgreen, A., and Wolff, R. K. (2013). Dietary influence on MAPK-signaling pathways and risk of colon and rectal cancer. *Nutr. Cancer* 65, 729–738. doi: 10.1080/01635581.2013.795599

Sundaram, S., Freemerman, A. J., Galanko, J. A., McNaughton, K. K., Bendt, K. M., Darr, D. B., et al. (2014a). Obesity-mediated regulation of HGF/c-Met is associated with reduced basal-like breast cancer latency in parous mice. *PLoS One* 9:e111394. doi: 10.1371/journal.pone.0111394

Sundaram, S., Le, T. L., Essaid, L., Freemerman, A. J., Huang, M. J., Galanko, J. A., et al. (2014b). Weight loss reversed obesity-induced HGF/c-Met pathway and basal-like breast cancer progression. *Front. Oncol.* 4:175. doi: 10.3389/fonc.2014.00175

Tachibana, M., Ueda, J., Fukuda, M., Takeda, N., Ohta, T., Iwanari, H., et al. (2005). Histone methyltransferases G9a and GLP form heteromeric complexes and are both crucial for methylation of euchromatin at H3-K9. *Genes Dev.* 19, 815–826. doi: 10.1101/gad.1284005

Takada, I., Kouzmenko, A. P., and Kato, S. (2009). Wnt and PPARgamma signaling in osteoblastogenesis and adipogenesis. *Nat. Rev. Rheumatol.* 5, 442–447. doi: 10.1038/nrrheum.2009.137

Tateishi, K., Okada, Y., Kallin, E., and Zhang, Y. (2009). Role of Jhdm2a in regulating metabolic gene expression and obesity resistance. *Nature* 458, 757–761. doi: 10.1038/nature07777

Wang, L., Xu, S., Lee, J. E., Baldridge, A., Grullon, S., Peng, W., et al. (2013). Histone H3K9 methyltransferase G9a represses PPARgamma expression and adipogenesis. *EMBO J.* 32, 45–59. doi: 10.1038/emboj.2012.306

Wang, M., Crisostomo, P. R., Herring, C., Meldrum, K. K., and Meldrum, D. R. (2006). Human progenitor cells from bone marrow or adipose tissue produce VEGF, HGF, and IGF-I in response to TNF by a p38 MAPK-dependent mechanism. *Am. J. Physiol. Regul. Integr. Comp. Physiol.* 291, R880–R884. doi: 10.1152/ajpregu.00280.2006

Wang, W., and Seale, P. (2016). Control of brown and beige fat development. *Nat. Rev. Mol. Cell Biol.* 17, 691–702. doi: 10.1038/nrm.2016.96

Yu, G., Wang, L. G., Han, Y., and He, Q. Y. (2012). clusterProfiler: an R package for comparing biological themes among gene clusters. *OMICS* 16, 284–287. doi: 10.1089/omi.2011.0118

Yu, G., Wang, L. G., and He, Q. Y. (2015). ChIPseeker: an R/Bioconductor package for ChIP peak annotation, comparison and visualization. *Bioinformatics* 31, 2382–2383. doi: 10.1093/bioinformatics/btv145

Zhang, T., Zhang, Z., Dong, Q., Xiong, J., and Zhu, B. (2020). Histone H3K27 acetylation is dispensable for enhancer activity in mouse embryonic stem cells. *Genome Biol.* 21:45. doi: 10.1186/s13059-020-01957-w

Zhang, X., Liu, J., Wu, L., and Hu, X. (2020). MicroRNAs of the miR-17˜9 family maintain adipose tissue macrophage homeostasis by sustaining IL-10 expression. *Elife* 9:e55676. doi: 10.7554/eLife.55676

Zhang, Y., Liu, T., Meyer, C. A., Eeckhoute, J., Johnson, D. S., Bernstein, B. E., et al. (2008). Model-based analysis of ChIP-Seq (MACS). *Genome Biol.* 9:R137. doi: 10.1186/gb-2008-9-9-r137

Zhou, Y., Peng, J., and Jiang, S. (2014). Role of histone acetyltransferases and histone deacetylases in adipocyte differentiation and adipogenesis. *Eur. J. Cell Biol.* 93, 170–177. doi: 10.1016/j.ejcb.2014.03.001

Conflict of Interest: The authors declare that the research was conducted in the absence of any commercial or financial relationships that could be construed as a potential conflict of interest.

frontiers in Cell and Developmental Biology

ORIGINAL RESEARCH
published: 09 August 2021
doi: 10.3389/fcell.2021.654958

Epigenetic Control of Autophagy Related Genes Transcription in Pulpitis via JMJD3

*Bei Yin[1,2], Qingge Ma[1,2], Lingyi Zhao[1,2], Chenghao Song[1,2], Chenglin Wang[1,2], Fanyuan Yu[1,2], Yu Shi[1,2] and Ling Ye[1,2]**

[1] State Key Laboratory of Oral Diseases, West China Hospital of Stomatology, Sichuan University, Chengdu, China, [2] West China School of Stomatology, Sichuan University, Chengdu, China

Autophagy is an intracellular self-cannibalization process delivering cytoplasmic components to lysosomes for digestion. Autophagy has been reported to be involved in pulpitis, but the regulation of autophagy during pulpitis progression is largely unknown. To figure out the epigenetic regulation of autophagy during pulpitis, we screened several groups of histone methyltransferases and demethylases in response to TNFα treatment. It was found JMJD3, a histone demethylase reducing di- and tri-methylation of H3K27, regulated the expression of several key autophagy genes via demethylation of H3K27me3 at the gene promoters. Our study highlighted the epigenetic regulation of autophagy genes during pulpitis, which will potentially provide a novel therapeutic strategy.

Keywords: pulpitis, autophagy, epigenetics, histone methylation, JMJD3

OPEN ACCESS

Edited by:
Yujing Li,
Emory University, United States

Reviewed by:
Sanjay Gupta,
Case Western Reserve University, United States
Abhijit Shukla,
Memorial Sloan Kettering Cancer Center, United States

***Correspondence:**
Ling Ye
yeling@scu.edu.cn

Specialty section:
This article was submitted to Epigenomics and Epigenetics, a section of the journal Frontiers in Cell and Developmental Biology

Received: *18 January 2021*
Accepted: *15 June 2021*
Published: *09 August 2021*

Citation:
Yin B, Ma Q, Zhao L, Song C, Wang C, Yu F, Shi Y and Ye L (2021) Epigenetic Control of Autophagy Related Genes Transcription in Pulpitis via JMJD3. Front. Cell Dev. Biol. 9:654958. doi: 10.3389/fcell.2021.654958

INTRODUCTION

Autophagy is a conserved degradation/self-eating pathway delivering unwanted cytoplasmic components and organelles to lysosomes for digestion. Autophagy ensures organelle renewal and sustains the cellular homeostasis. Excessive or deficient autophagy may contribute to pathogenesis, such as cancers, inflammation, immune diseases and etc.

Autophagy is closely related to inflammation. On the one hand, several proinflammatory cytokines can induce autophagy, such as tumor necrosis factor (TNF) (Mostowy et al., 2011), interleukin1β (IL1β) (Hartman and Kornfeld, 2011) and interferons (Singh et al., 2010). On the other hand, autophagy facilitates the cell autonomous control of inflammation by removing the damaged mitochondria [thus alleviating the release of inflammasome activators such as reactive oxygen species (ROS) or mitochondrial DNA (mtDNA)] (Netea-Maier et al., 2016), degrading the aggregated inflammasomes and interferon regulatory factor 1 (IRF1) (Liang et al., 2019), etc.

Pulp is the only soft tissue in the tooth. It has four principal functions: forming dentin, providing nutrition; sensory function; defense function. Pulpitis is the inflammation of the dental pulp caused by deep caries, trauma, dental fissures, etc. It is one of the most common dental disorders and usually causes severe pain. Generally, the current treatment of pulpitis is root canal therapy in which the dental pulp is cleared away. Loss of the vital pulp may result in postoperative pain, root fracture, secondary infection, leading to a higher incidence of the tooth extraction (Nakashima et al., 2017). In order to preserve the pulp vitality, researchers have focused on studying the underlying regulation mechanisms of the pulpitis pathogenesis. Recently, it was found autophagy was increased

during the inflammation process of dental pulp. Autophagy related genes such as autophagy related 5 (ATG5), ATG7, microtubule associated protein 1 light chain 3 (LC3) and beclin 1 (BECN1) were increased in pulpitis tissue (Qi et al., 2019). The role of autophagy in pulpitis may be dual. Autophagy was induced in odontoblast at the early stage (6 h treatment) of lipopolysaccharide (LPS) stimulation. Autophagy of this stage acted as a protector to conserve cell viability. On the contrary, autophagy was down-regulated in the late-stage (12 h treatment) of LPS treatment, when autopahgy promoted cell death (Pei et al., 2015). Therefore, autophagy may possibly be fine tuned by certain mechanisms to maintain the homeostasis of pulp tissue.

The regulation of autophagy in pulpitis has been studied by several reports. Both the transcription factor forkhead box O3 (FOXO3) and a surface marker CD47 (a "marker of self" distinguishing host cells from foreign invaders) were reported to regulate autophagy (Wang H. et al., 2016; Li et al., 2018). Although epigenetics is one of the most important mechanism linking the extra-cellular signals to the transcription of genes, the epigenetic regulation of autophagy during pulpitis is largely unknown. Histone methylation is an important epigenetic modification for determining the chromatin accessibility and the ensuing transcriptional status. Histone methylation has important effects on the modulation of autophagy induction. Previous studies found histone methylations such as trimethylation of lysine 27 on histone 3 (H3K27me3), trimethylation of lysine 9 on histone 3 (H3K9me3) can affect the transcription of autophagy related genes (de Narvajas et al., 2013; Park et al., 2016). However, it is unknown whether autophagy in pulpitis is regulated by certain histone methylation. To figure out the epigenetic regulation of autophagy during pulpitis, we screened several groups of histone methyltransferases and demethylases in response to TNFα treatment. TNFα is an inflammatory cytokine and TNFα stimulation of HDPCS is often used as an effort to replicate the cell status of pulpitis *in vitro* (Yin et al., 2017). Several studies have reported the suppression of autophagy by TNFα (Dash et al., 2018). In contrast, there are studies reporting the induction of autophagy by TNFα (Chen D. et al., 2016). The effect was TNF on autophagy in HDPCs was unknown, while it was reported that LPS stimulation induced autopahgy in odontoblast. It was found jumonji domain containing 3 (JMJD3), a histone demethylase reducing di- and tri-methylation of H3K27, could regulate the expression of several key autophagy genes by mediating the H3K27 methylation. Our study highlighted the epigenetic regulation of autophagy genes during pulpitis, potentially providing the important clues of therapeutic targets.

MATERIALS AND METHODS

Establishment of Rat Pulpitis Model

The study was approved by the ethics committee of the West China School of Stomatology, Sichuan University. The rat pulpitis model was established as previously (Yin et al., 2017). The pulp chamber of the first molars was opened, so the first molars acted as pulpitis group and the adjacent normal molars acted as healthy control group. The samples were fixed with 4% paraformaldehyde at 4°C for 12 h followed by dehydration, paraffin embedding and slicing.

Immunofluorescent Staining

The samples were dewaxed with xylene, hydrated with graded ethanol, and rinsed with distilled water. Then the sections were subjected to antigen retrieval by pepsin solution at 37°C for 30 min. After treatment with 30% H2O2 and goat serum, the samples were incubated with the primary antibody overnight at 4°C. The sections were successively subjected to a fluorescent secondary antibody and 4′,6-diamidino-2-phenylindole (DAPI). Then the slides were mounted and observed under a Nikon Eclipse300 fluorescence microscope (Compix Inc, Sewickley, PA, United States).

Cell Culture and TNFα Treatment

Primary human dental pulp cells (HDPCs) were cultured and passaged according to our previous study (Yin et al., 2017). The third and fourth passage of the cells were used in our study. For TNFα stimulation, cells were treated with human recombinant tumor necrosis factor α (TNFα) (10 ng/mL) (R&D, Minneapolis, MN, United States) in the presence of GSKJ-4 (Sigma-Aldrich, MO, United States) or DMSO in a serum-free medium for 2 h unless indicated.

Quantitative Real-Time Polymerase Chain Reaction (qRT-PCR)

The total RNA was extracted using the RNeasy mini kit (Qiagen, Valencia, CA, United States). After assessing the concentration and purity of RNA, cDNA was synthesized using the HiScript III SuperMix (Vazyme Biotech, Nanjing, China). Real-time polymerase chain reaction was done using ChamQ Universal SYBR qPCR Master Mix (Vazyme). Conditions for qRT-PCR were as follows: denaturation at 95°C for 30 s, 40 cycles at 95°C 10s and 60°C 30 s. The relative expression level of mRNA is presented as the fold change of the target gene relative to the control calculated by the formula $x = 2^{-\Delta\Delta Ct}$ after glyceraldehyde-3-phosphate dehydrogenase (GAPDH) correction.

Western Blot

The protein was extracted using the Mammalian Protein Extraction Reagent (Thermo Fisher Scientific, Hudson, NH, United States). The loading volume was calculated (20 mg/lane) based on the protein concentration which was determined by a BCA Assay Kit (Beyotime Biotechnology, Beijing, China). The samples were electrophoresed and then transferred to a polyvinylidene fluoride membrane (Millipore, Billerica, MA, United States). The membranes were immersed in 5% BSA for 1 h of blocking and incubated with primary antibodies for JMJD3, FIP200, BECLIN, ATG5, H3K27me3, H3 and GAPDH (all 1:1000) (all from Cell Signaling Technology, Danvers, MA, United States).

The incubation took place at 4°C overnight. Membranes were washed and incubated with appropriate HRP-conjugated immunoglobulin G antibodies (Abcam) before visualizing with High Sensitive ECL Chemiluminescent Substrate (Vazyme).

Infection of Ad-GFP-LC3B

HDPCs of 70% confluence were infected with an adenovirus expressing GFP-LC3B (Ad-GFP-LC3B) (Beyotime). After 24 h of infection, HDPCs underwent the corresponding treatments such as TNFα, GSKJ-4, etc. Then the nuclei were stained with DAPI, photographed by a fluorescence microscope and quantified with Image J.

Small Interfering RNA (siRNA) Transfection

Cells at 90% confluence were transfected according to the manuals of Lipofectamine 3000. JMJD3 stealth siRNA (HSS177200) and negative siRNA (12935200, all from Thermo Fisher) were used in our study. 6 h after transfection, the cells were treated with 10 ng/mL TNFα or phosphatebuffered saline (control) for 2 h before the extraction of RNA and protein.

Chromatin Immunoprecipitation (ChIP)

ChIP experiments were performed using the Magna ChIP™ HiSens (Millipore) based on its protocols. Briefly, the cells were cross-linked with 37% paraformaldehyde and then the cell pellets were lysed with EZ-Zyme™ Lysis Buffer. After that, the EZ-Zyme™ Digestion Buffer containing EZ-Zyme™ Enzymatic Cocktail was used for nuclease digestion. Precipitation reaction was performed at 4°C overnight containing 490 μL SCW buffer, 10 μl resuspended A/G Magnetic Beads, 5 μl antibody (JMJD3, H3K27me3, rabbit IgG) and 5 μl digested chromatin. Then the samples were subjected to de-crosslinking using Proteinase K. The supernatant was collected for qRT-PCR using primers that targeted the promoters of the following genes. The ChIP-qPCR primer sequence was as follows: ATG5: F:5′-AGGCAATGCACCTTAATCCCAC-3′, R:5′-GCAGAAATCCTCACTACAGTGTC-3′; LC3B: F:5′-CTGTAAACCACCCACCACCA-3′, R:5′-CTGAAGTGTGTGTGTGCTGC-3′; FIP200: F:5′-GGTATGAACCAGTCGTTTCTGG-3′, R:5′-TCTGAACTATGCCAGTGATAATCT-3′; ATG12: F:5′-CCCATTCGGGAGGATCAACT-3′, R:5′-TTCTGCTACTCGTGTGTGGT-3′; ATG7: F:5′-GTCCAGGCTGTTCTTGGTCA-3′, R:5′-CCCCTGAATGCCCATTCCTC-3′; BECLIN: F:5′-AGTTATGTGCAAGCACTTTGGAA-3′, R:5′-TGCAATGAAGAGCTGGCTAC-3′.

Statistical Analysis

The SPSS software was used for statistical analysis, and one-way analysis of variance test was done in our study. Statistical difference ($p < 0.05$) and significant statistical difference ($p < 0.01$) were represented as * and ** respectively. Data were presented as the mean ± standard deviation.

RESULTS

Expression of LC3B and Autophagy-Related Genes in Response to TNFα Stimulation

To determine the alteration of autophagy during pulpitis, we established the rat pulpitis model. Hematoxylin-eosin staining was done to verify the infection, that is the infiltration of inflammatory cells (**Figure 1A**). Immunofluoresent staining revealed that LC3B expression was enhanced in pulpitis tissue compared with the adjacent healthy control (**Figure 1B**).

To study the regulation of autophagy *in vitro*, we cultured HDPCs and stimulated them with inflammatory cytokine TNFα. It turned out that the expression of LC3B peaked at 2 h after stimulation of TNFα (**Figure 1C**). The qPCR results showed that the proinflammatory gene IL1β was highly induced after TNFα stimulation for 2 h (**Figure 1D**). Meanwhile, the expression of the autophagy related genes such as autophagy related 7 (ATG7), BECLIN 1, 200-kDa FAK-family interacting protein (FIP200) was enhanced after TNFα treatment (**Figure 1D**). Notedly, the expression of these genes also peaked at 2 h of TNFα stimulation. To observe autophagy vesicles in response to TNFα stimulation, we transfected HDPCs with Ad-GFP-LC3B. GFP-tagged LC3B reporters are widely used for the measure of autophagy. Upon autophagy induction, the cytosolic GFP-LC3-I is conjugated to phosphatidylethanolamine (PE) and thus converted to LC3-II. LC3-II then tethers to the membranes of autophagosomes and thus presents fluorescent puncta signal (Adiseshaiah et al., 2018). Measuring the fluorescent puncta can therefore reflects the autophagosomes. Through this measurement, we found TNFα treatment significantly increased autophagy vesicles (**Figure 1E**).

JMJD3 Expression Was Prominently Induced in Response to TNFα Stimulation

We profiled the expression of several groups of histone lysine methyltransferases in response to TNFα. We found a pronounced level of jumonji domain containing 3 (JMJD3), an H3K27 demethylase, was obviously elicited among these epigenetic regulators (**Figure 2A**). Immunohistochemical staining showed that JMJD3 expression was augmented in human pulpitis tissue (**Figure 2B**). Interestingly, JMJD3 expression also peaked at 2 h stimulation of TNFα treatment (**Figures 2C,D**). And starvation of the HDPCs as a positive control also induced the expression of JMJD3. Conversely, the substrate of JMJD3, H3K27me3, was markedly decreased at 2 h stimulation of TNFα (**Figure 2E**). We noted that the level of H3K27me3 was not always reversely correlated with the level of JMJD3 at various time point. Possibly, the level of H3K27me3 in response to TNFα treatment was affected by both H3K27 methylase EZH2 and H3K27 demethylases, JMJD3 and UTX. EZH2 was reported to increase upon TNFα stimulation in human dental pulp cells (Hui et al., 2014). UTX was also reported to play crucial roles in TNFα signaling in endothelial cells (ECs) (Higashijima et al., 2020). Therefore, the level of H3K27me3 in response to TNFα

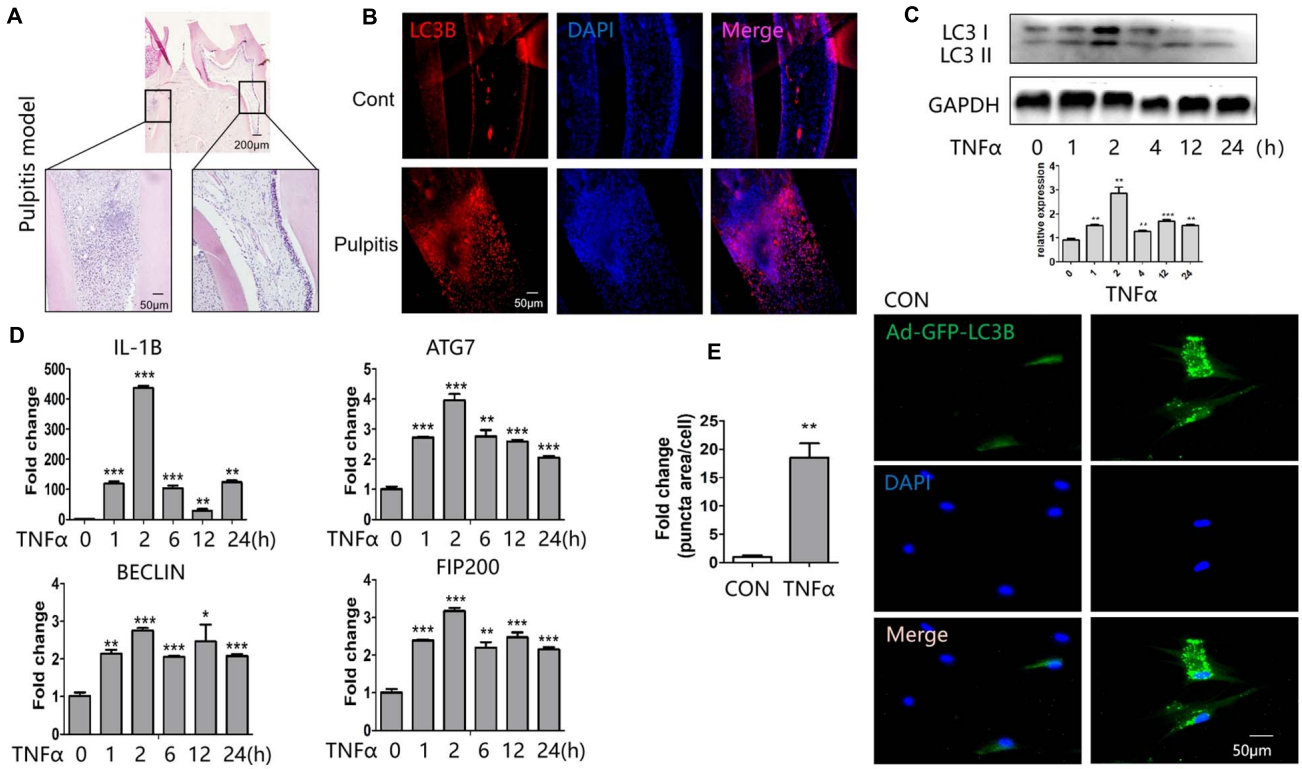

FIGURE 1 | Expression of LC3B and autophagy-related genes in response to TNFα stimulation. **(A)** Hematoxylin-eosin stained sections of healthy (right) and inflamed (left) dental pulp. **(B)** Immunofluorescent staining revealed enhanced expression of LC3B in pulpitis tissue (down) compared with control pulp (up). **(C)** Western blot analysis of LC3B expression at indicated time point of TNFα stimulation in HDPCs. Below was the quantification of the bands relative to the control. **(D)** QPCR analysis of inflammatory and autophagic genes at indicated time point of TNFα stimulation in HDPCs. **(E)** GFP-LC3 puncta was enhanced in response to TNFα stimulation in GFP-LC3B-expressing HDPCs. The relative quantification was on the left side. $^{*}P < 0.05$, $^{**}P < 0.01$, $^{***}P < 0.001$.

stimulation in HDPCs may occur as the result of the coordination of those H3K27 methylases and demethylases.

Since H3K27me3 modification was reported to occur in the promoter regions of several autophagy related genes, we wondered whether JMJD3 played a role in regulating autophagy related gene expression in HDPCs.

GSKJ-4 Mediated the Decrease of Autophagy Genes

GSKJ-4 was the inhibitor of JMJD3. As expected, treatment of GSKJ-4 caused the increase of H3K27me3 (**Figure 3A**). The expression of FIP200, BECLIN, ATG5, ATG7, ATG12 was decreased in mRNA level in response to GSKJ-4 treatment (**Figure 3B**). The western blot revealed that the expression of FIP200, BECLIN, ATG5, LC3B and JMJD3 was enhanced in TNFα group. GSK J-4 treatment led to the decreased expression of JMJD3, ATG5, LC3B, BECLIN and JMJD3 (**Figure 3C**). The decrease of the genes in response to GSKJ-4 was more obvious in the group of TNFα treatment than the group without TNFα stimulation. The P62 is an autophagic adapter sequestering polyubiquitinated proteins and binds directly to LC3. Therefore, P62 acts as an autophagy-specific substrate. Western blot showed that TNFα stimulation led to the decrease of P62, while JMJD3 inhibition resulted in the increase of P62. AdGFP-LC3B infection also revealed that after GSKJ-4 treatment the autophagy vesicles were diminished (**Figure 3D**). Taken together, the results indicated that the enzymatic activity of JMJD3 regulated the autophagy gene expression during pulpitis by mediating the expression of autophagy genes.

JMJD3 siRNA Regulated the Decrease of Autophagy Genes

JMJD3 siRNA was transfected to evaluate whether knockdown of JMJD3 would affect the autophagy process. The expression of JMJD3 was depleted in the siRNA-treated group (**Figure 4A**). The alteration of H3K27me3 level coincided with JMJD3's role as an H3K27 demethylase (**Figure 4B**). Consistent with the GSKJ-4 treatment, JMJD3 suppression decreased the expression of FIP200, BECLIN, ATG5, ATG7, ATG12 with or without TNFα treatment (**Figures 4C,D**). Meanwhile, the LC3 puncta was also decreased in the JMJD3 siRNA-treated group (**Figure 4E**). Furthermore, we used the LPS from P. gingivalis to study the role of JMJD3 in pulpitis. Consistent with TNFα treatment, LPS stimulation also up-regulated the expression FIP200, BECLIN, ATG5 (**Supplementary Figure 1A**). Silencing of JMJD3 decreased their expression in both the protein and RNA

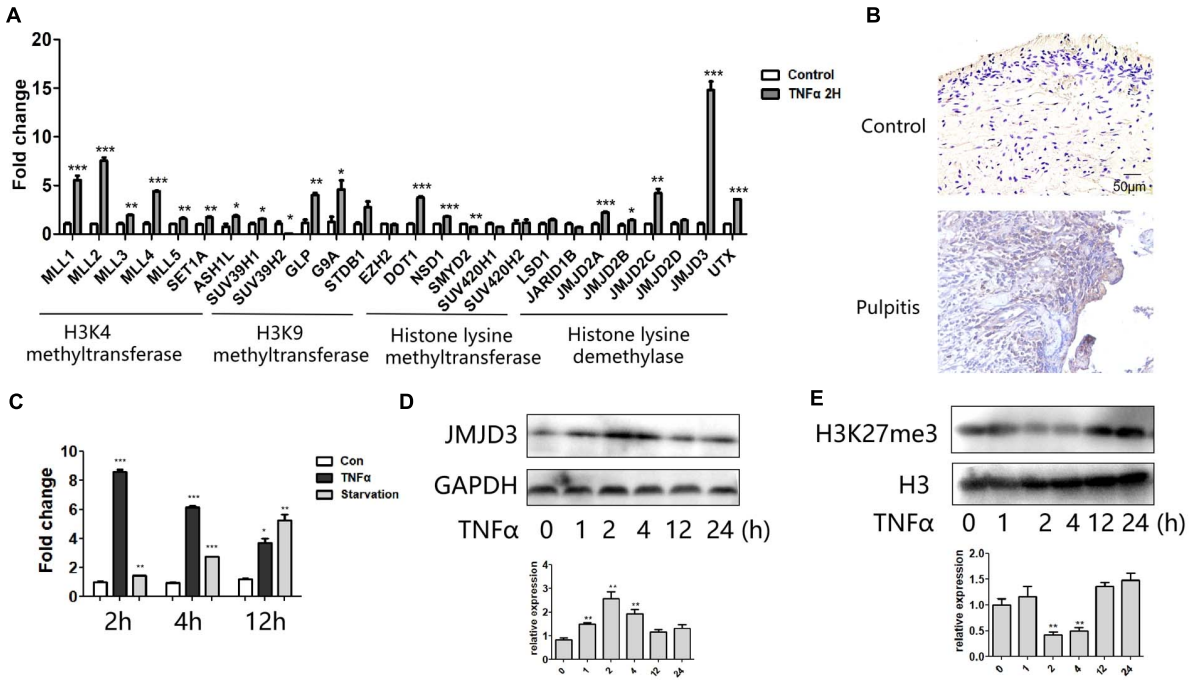

FIGURE 2 | JMJD3 expression was most highly induced in response to TNFα stimulation. **(A)** QPCR analysis of several groups of histone lysine methyltransferase and demethylases in HDPCs with 2 h stimulation of TNFα. **(B)** Immumohistochemical staining of JMJD3 in healthy control pulp tissue (up) and pulpitis tissue (low). **(C)** QPCR analysis of JMJD3 expression in HDPCs with TNFα or starvation stimulation at indicated time. **(D,E)** Western blot analysis of JMJD3 **(D)** and H3K27me3 **(E)** in HDPCs with TNFα stimulation. Below was the relative quantification of the bands. $^{**}P < 0.01$, $^{***}P < 0.001$.

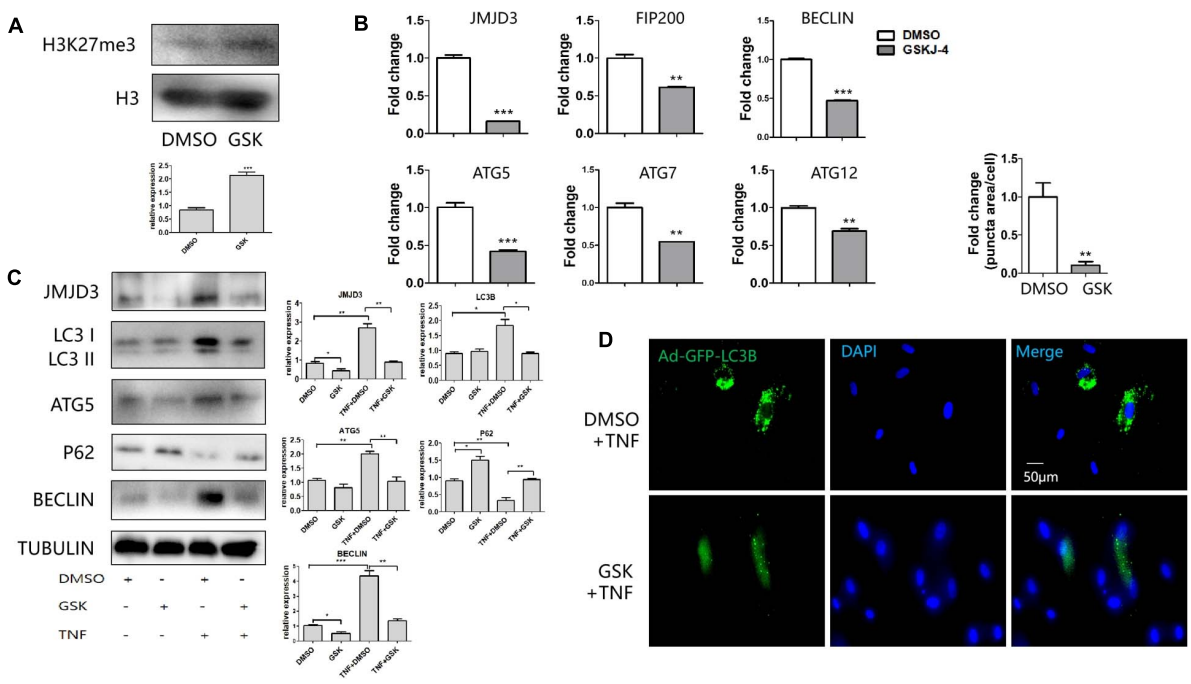

FIGURE 3 | GSKJ-4 mediated the decrease of autophagy genes. **(A)** Western blot analysis of H3K27me3 level in response to GSKJ-4 treatment. Below was the relative quantification of the bands. **(B,C)** QPCR **(B)** and western blot **(C)** analysis of JMJD3 and several autophagic genes after the treatment of GSKJ-4. The relative quantification was on the right. **(D)** GFP-LC3 puncta and the corresponding quantitative analysis (up) in response to GSKJ-4 treatment. The relative quantification was on the upper side. $^{**}P < 0.01$, $^{***}P < 0.001$.

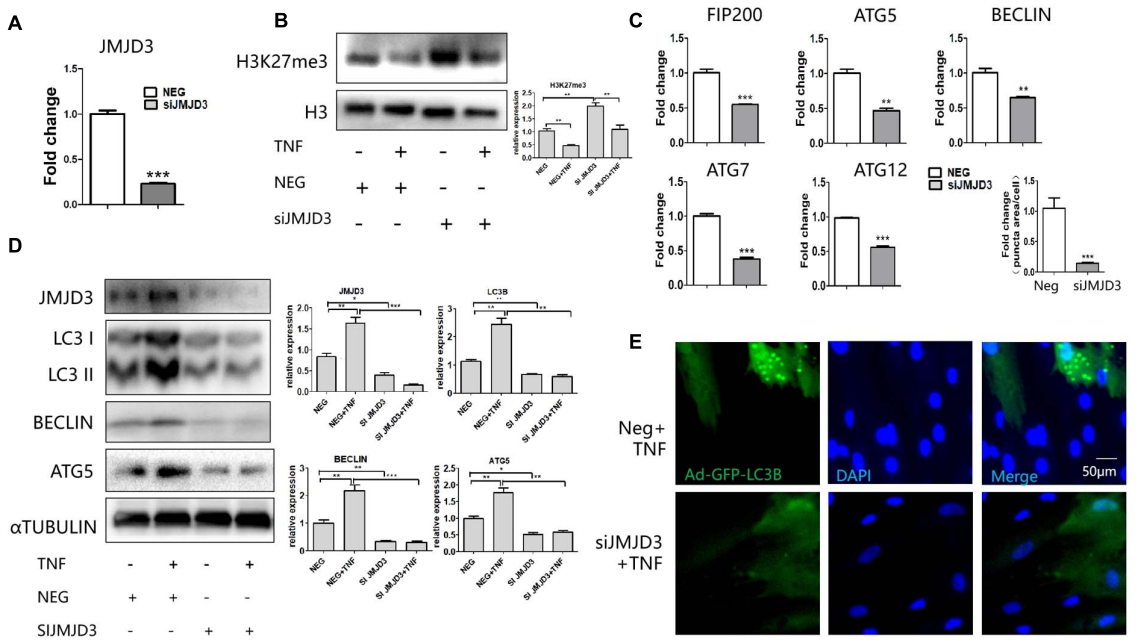

FIGURE 4 | JMJD3 siRNA regulated the decrease of autophagy related genes. **(A)** QPCR analysis of JMJD3 level after JMJD3 siRNA transfection. **(B)** Western blot analysis of H3K27me3 level after the treatment of JMJD3 siRNA. The relative quantification was on the right. **(C,D)** QPCR **(C)** and western blot **(D)** analysis of autophagy related genes in response to JMJD3 siRNA. The relative quantification was on the right. **(E)** GFP-LC3B-expressing HDPCs cells were treated with JMJD3 siRNA for 24 h followed by TNFα or PBS treatment. The relative quantification was on the upper side. $^{**}P < 0.01$, $^{***}P < 0.001$.

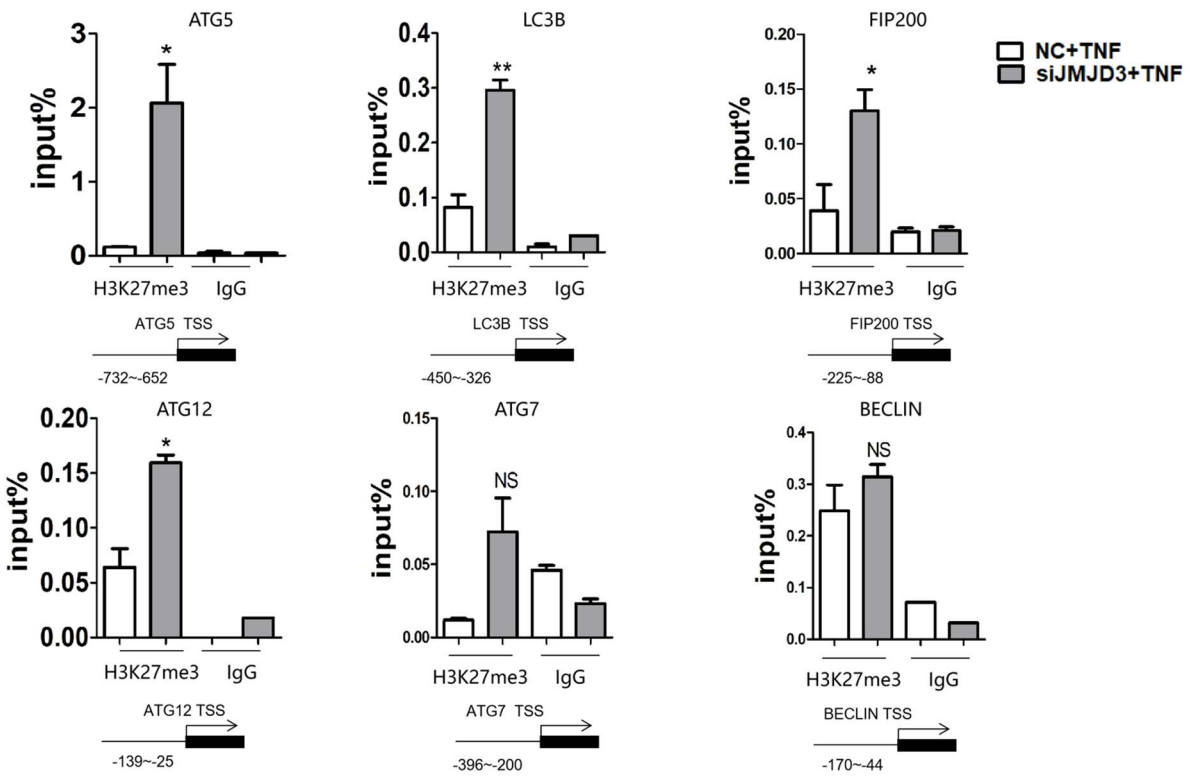

FIGURE 5 | JMJD3 regulated the expression of autophagy-related genes by regulating the H3K27me3 modification. JMJD3 siRNA up-regulated the H3K27me3 level binding to the promoters of ATG5, FIP200, ATG12 and LC3B. $^{*}P < 0.05$, $^{**}P < 0.01$, ns non-significant.

level (**Supplementary Figures 1A,B**). Taken together, JMJD3 knockdown regulated the decrease of autophagy genes.

JMJD3 Regulated the Expression of Autophagy-Related Genes by Regulating the H3K27me3 Modification

To identify whether JMJD3 could regulate the expression of autophagy-related genes directly, we performed ChIP analysis. It turned out that the silencing of JMJD3 upregulated the H3K27me3 level at the promoter region of ATG5, LC3B, FIP200 and ATG12. Although the H3K27me3 modification was present at the BECLIN promoter, JMJD3 silencing didn't alter the H3K27me3 enrichment (**Figure 5**). The H3K27me3 modification on BECLIN gene may be possibly mediated by other H3K27demethylases such as lysine demethylase 6A (KDM6A). As for ATG7 gene, we didn't detect any H3K27me3 modifications at the promoter regions. These findings suggested that JMJD3 could regulate the H3K27me3 modification on ATG5, LC3B, FIP200 and ATG12.

DISCUSSION

Autophagy plays an important role in maintaining cellular homeostasis in teeth. Besides the above-mentioned pulpitis, autophagy is reported to participate in tooth development (Yang et al., 2013a,b) and aging (Murray et al., 2002; Couve and Schmachtenberg, 2011; Couve et al., 2012). Therefore, figuring out the autophagy regulators are of great significance to the teeth homeostasis. Rapamycin is a well-recognized autophagy inducer with great potential for various diseases, but the side effects of hyperglycemia, hyperlipidemia, insulin resistance, etc. motivated the researchers to find alternative therapeutic autophagy inducer (Salmon, 2015). Our study revealed autophagy may be dynamically regulated in pulpitis by using small molecule compound targeting the epigenetic regulators, potentially highlighting a novel therapeutic strategy in the treatment of pulpitis. Our study found GSKJ-4, the small molecule inhibitor of JMJD3, not only changed the H3K27me3 level but decreased the level of JMJD3 as well. Consistent with our results, GSKJ-4 treatment did decrease the expression of JMJD3 in fibroblast-like synoviocytes (Jia et al., 2018), breast cancer stem cells (Yan et al., 2017) and renal interstitial fibroblasts *in vitro* (Yu et al., 2021). Furthermore, GSKJ4 administration by intraperitoneal injection down-regulated JMJD3 level in the kidney *in vivo*. However, in several cells such as endothelial progenitor cells (He et al., 2020) and hepatocytes (Pediconi et al., 2019), GSKJ4 treatment has no impact on the expression of JMJD3. This discrepancy is possibly due to the cell type-dependent responses of transcription factors (TFs) in response to GSK-J4 treatment. GSK-J4 treatment can affect the expression of several TFs including signal transducer and activator of transcription (STAT) (Das et al., 2017). STAT can bind to the JMJD3 promoter and regulates the transcription of JMJD3 (Przanowski et al., 2014; Sherry-Lynes et al., 2017). Therefore, the downregulation of JMJD3 in response to GSK-J4 treatment may be attributed to the GSK-J4-mediated TFs such as STAT.

Our study found TNFα treatment stimulated autophagy in HDPCs, consistent with Serge's study in TNFα-stimulated HeLa cells (Mostowy et al., 2011). We found LC3B puncta were significantly increased in pulpitis tissue compared with the healthy control. Consistently, Wang found LC3 expression could only be detected in caries and pulpitis groups rather than in healthy samples. Possibly, autophagy may be quiescent or less active under normal physiological conditions. Once the external stimuli interrupted the tissue homeostasis, autophagy may be activated elaborately by complicated mechanisms including epigenetics. Mechanismly, we found JMJD3 could regulate the key autophagy genes by decreasing the H3K27me3 modification at the promoters of ATG5, LC3B, FIP200 and ATG12. Consistent with this, Denton found another H3K27 demethylase, KDM6A, was recruited to the promoters of autophagy genes such as ATG5 and LC3B, regulating the enrichment of H3K27me3 on their promoters (Denton et al., 2013). Similarly, the H3K36 demethylase lysine demethylase 4A (KDM4A) was found to repress expression of LC3B and BECLIN1 by H3K36 demethylation (Wang B. et al., 2016). An H3K9 methyltransferase euchromatic histone lysine methyltransferase 2 (EHMT2) also suppressed BECLIN-1 expression by reducing H3K9me2. In addition, other modifications such as H3K4me3, H3K27 acetylation (H3K27ac), H4K16ac and H3K56ac were also correlated with the mRNA expression of several autophagy genes (Füllgrabe et al., 2013; Peeters et al., 2019). Interestingly, several autophagy genes including LC3B possess bivalent modification with high H3K4me3 and H3K9me3 levels. The bivalent modification can poise the chromatin conformation for immediate response to stimuli (Biga et al., 2017). Therefore, the autophagy genes can be dynamically adjusted to the changing environment in the transcription level. Interestingly, it was found JMJD3 interference affected the expression of ATG7 and BECLIN without regulating the H3K27me3 level around their promoters. Possibly, JMJD3 may regulate their expression by targeting the upstream modulators of autophagy. For example, enhancer of zeste 2 polycomb repressive complex 2 subunit (EZH2) can affect the autophagy genes by tuberous sclerosis 2 (TSC2)/mammalian target of rapamyoin (MTOR) pathway (Wei et al., 2015). H3K4 demethylase lysine-specific demethylase 1 (LSD1) can bind to the promoter region of Sestrin2 (SESN2) and regulate autophagy through SESN2/MTOR pathway (Ambrosio et al., 2017).

Apart from mediating histone demethylation, JMJD3 was also reported to regulate non-histone proteins such as the retinoblastoma (RB) protein at the lysine810 residue (K810) (Zhao et al., 2015). Besides, JMJD3 can directly interact with p53 and induce p53 stabilization (Sola et al., 2011). The autophagy components can be modified to dictate the autophagic cascade (Morselli et al., 2011; Lin et al., 2012). For example, ATG3 protein could be acetylated in lysine 19 (K19) and K48, thus affecting the ATG3 and ATG8 interaction (Yi et al., 2012). Several other autophagy components such as ATG5, ATG, ATG8, and ATG12 can also be acetylated (Lee et al., 2008; Lee and Finkel, 2009). It will be intriguing to figure out whether JMJD3 can demethylase autophagy-related proteins directly.

It's worth noting JMJD3 mediation of the autophagy-related genes may potentially have some non-autophagy function. For

example, Gan found FIP200 protected cells from the TNFα-induced apoptosis in an autophagy independent way (Chen S. et al., 2016; Cadwell and Debnath, 2018). Another study found ATG5 decreased the amount of neutrophils during Mycobacterium tuberculosis infection independent of autophagy function (Kimmey et al., 2015). Therefore, further studies are needed to clarify whether ATG5 and FIP200 regulated by JMJD3 may possibly exert the above-mentioned non-autophagic roles in pulpitis.

It would be interesting to study whether combined intervention JMJD3 and other epigenetic factors may present a better way to control autophagy. In fact, it was reported that the inhibitors of histone H3K4 demethylase LSD1 could induce autophagy in multiple mammalian cell lines (Wang et al., 2017). Likely, JMJD3 could coordinate with H3K4 methyltransferases to promote the transcription of autophagy genes in the TNFα-stimulated HDPCs. This coordination may be accomplished by JMJD3 recruiting the Set1/MLL H3K4 methyltransferase complexes (Shi et al., 2014) and incorporating in the MLL complex (De Santa et al., 2007). Taken together, our study highlighted the epigenetic regulation of autophagy genes during pulpitis, potentially providing the important clues of therapeutic targets.

DATA AVAILABILITY STATEMENT

The original contributions presented in the study are included in the article/**Supplementary Material**, further inquiries can be directed to the corresponding author/s.

ETHICS STATEMENT

The animal study was reviewed and approved by The Ethics Committee of the West China School of Stomatology, Sichuan University.

AUTHOR CONTRIBUTIONS

BY: conception and design, collection and assembly of data, and manuscript writing. LZ, QM, CS, and FY: data analysis and interpretation. CW, YS, and LY: final approval of manuscript. All authors contributed to the article and approved the submitted version.

FUNDING

This study was supported by grants from the National Natural Science Foundation of China (81825005, 81873708, and 82001019) and grants from the West China Hospital of Stomatology (RCDWJS2021-5 and RD-02-202008).

SUPPLEMENTARY MATERIAL

The Supplementary Material for this article can be found online at: https://www.frontiersin.org/articles/10.3389/fcell.2021.654958/full#supplementary-material

REFERENCES

Adiseshaiah, P. P., Skoczen, S. L., Rodriguez, J. C., Potter, T. M., Kota, K., and Stern, S. T. (2018). Autophagy monitoring assay II: imaging autophagy induction in LLC-PK1 cells using GFP-LC3 protein fusion construct. *Methods Mol. Biol.* 1682, 211–219. doi: 10.1007/978-1-4939-7352-1_18

Ambrosio, S., Sacca, C. D., Amente, S., Paladino, S., Lania, L., and Majello, B. (2017). Lysine-specific demethylase LSD1 regulates autophagy in neuroblastoma through SESN2-dependent pathway. *Oncogene* 36, 6701–6711. doi: 10.1038/onc.2017.267

Biga, P. R., Latimer, M. N., Froehlich, J. M., Gabillard, J. C., and Seiliez, I. (2017). Distribution of H3K27me3, H3K9me3, and H3K4me3 along autophagy-related genes highly expressed in starved zebrafish myotubes. *Biol. Open* 6, 1720–1725.

Cadwell, K., and Debnath, J. (2018). Beyond self-eating: The control of nonautophagic functions and signaling pathways by autophagy-related proteins. *J. Cell. Biol.* 217, 813–822. doi: 10.1083/jcb.201706157

Chen, D., Liu, J., Lu, L., Huang, Y., Wang, Y., Wang, M., et al. (2016). Emodin attenuates TNF-α-induced apoptosis and autophagy in mouse C2C12 myoblasts though the phosphorylation of Akt. *Int. immunopharmacol.* 34, 107–113. doi: 10.1016/j.intimp.2016.02.023

Chen, S., Wang, C., Yeo, S., Liang, C., Okamoto, T., Sun, S., et al. (2016). Distinct roles of autophagy-dependent and-independent functions of FIP200 revealed by generation and analysis of a mutant knock-in mouse model. *Gene. Dev.* 30, 856–869. doi: 10.1101/gad.276428.115

Couve, E., and Schmachtenberg, O. (2011). Autophagic activity and aging in human odontoblasts. *J. Dent. Res.* 90, 523–528. doi: 10.1177/0022034510393347

Couve, E., Osorio, R., and Schmachtenberg, O. (2012). Mitochondrial autophagy and lipofuscin accumulation in aging odontoblasts. *J. Dental. Res.* 91, 696–701. doi: 10.1177/0022034512449347

Das, A., Arifuzzaman, S., Yoon, T., Kim, S. H., Chai, J. C., Lee, Y. S., et al. (2017). RNA sequencing reveals resistance of TLR4 ligand-activated microglial cells to inflammation mediated by the selective jumonji H3K27 demethylase inhibitor. *Sci. Rep.* 7:6554.

Dash, S., Sarashetti, P., Rajashekar, B., Chowdhury, R., and Mukherjee, S. (2018). TGF-β2-induced EMT is dampened by inhibition of autophagy and TNF-α treatment. *Oncotarget* 9, 6433–6449. doi: 10.18632/oncotarget.23942

de Narvajas, A. A. M., Gomez, T. S., Zhang, J. S., Mann, A. O., Taoda, Y., Gorman, J. A., et al. (2013). Epigenetic regulation of autophagy by the methyltransferase G9a. *Mol. Cell Biol.* 33, 3983–3993.

De Santa, F., Totaro, M. G., Prosperini, E., Notarbartolo, S., Testa, G., and Natoli, G. (2007). The histone H3 lysine-27 demethylase Jmjd3 links inflammation to inhibition of polycomb-mediated gene silencing. *Cell* 130, 1083–1094. doi: 10.1016/j.cell.2007.08.019

Denton, D., Aung-Htut, M. T., Lorensuhewa, N., Nicolson, S., Zhu, W., Mills, K., et al. (2013). UTX coordinates steroid hormone-mediated autophagy and cell death. *Nat. Commun.* 4:2916.

Füllgrabe, J., Lynch-Day, M. A., Heldring, N., Li, W., Struijk, R. B., Ma, Q., et al. (2013). The histone H4 lysine 16 acetyltransferase hMOF regulates the outcome of autophagy. *Nature* 500, 468–471. doi: 10.1038/nature12313

Hartman, M. L., and Kornfeld, H. (2011). Interactions between naive and infected macrophages reduce *Mycobacterium tuberculosis* viability. *PLoS One* 6:e27972. doi: 10.1371/journal.pone.0027972

He, Z., Wang, H., and Yue, L. (2020). Endothelial progenitor cells-secreted extracellular vesicles containing microRNA-93-5p confer protection against sepsis-induced acute kidney injury via the KDM6B/H3K27me3/TNF-α axis. *Exp. Cell Res.* 395:112173. doi: 10.1016/j.yexcr.2020.112173

Higashijima, Y., Matsui, Y., Shimamura, T., Nakaki, R., Nagai, N., Tsutsumi, S., et al. (2020). Coordinated demethylation of H3K9 and H3K27 is required for rapid inflammatory responses of endothelial cells. *EMBO J.* 39:e103949.

Hui, T., Peng, A., Zhao, Y., Wang, C., Gao, B., Zhang, P., et al. (2014). EZH2, a potential regulator of dental pulp inflammation and regeneration. *J. Endodont.* 40, 1132–1138. doi: 10.1016/j.joen.2014.01.031

Jia, W., Wu, W., Yang, D., Xiao, C., Su, Z., Huang, Z., et al. (2018). Histone demethylase JMJD3 regulates fibroblast-like synoviocyte-mediated proliferation and joint destruction in rheumatoid arthritis. *FASEB. J.* 32, 4031–4042. doi: 10.1096/fj.201701483r

Kimmey, J. M., Huynh, J. P., Weiss, L. A., Park, S., Kambal, A., Debnath, J., et al. (2015). Unique role for ATG5 in neutrophil-mediated immunopathology during *M. tuberculosis* infection. *Nature* 528, 565–569. doi: 10.1038/nature16451

Lee, I. H., and Finkel, T. (2009). Regulation of autophagy by the p300 acetyltransferase. *J. Biol. Chem.* 284, 6322–6328. doi: 10.1074/jbc.m807135200

Lee, I. H., Cao, L., Mostoslavsky, R., Lombard, D. B., Liu, J., Bruns, N. E., et al. (2008). A role for the NAD-dependent deacetylase Sirt1 in the regulation of autophagy. *Proc. Natl. Acad. Sci. U.S.A.* 105, 3374–3379. doi: 10.1073/pnas.0712145105

Li, Y., Wang, H., Pei, F., Chen, Z., and Zhang, L. (2018). FoxO3a regulates inflammation-induced autophagy in odontoblast. *J. Endodont.* 44, 786–791. doi: 10.1016/j.joen.2017.12.023

Liang, S., Zhong, Z., Kim, S. Y., Uchiyama, R., Roh, Y. S., Matsushita, H., et al. (2019). Murine macrophage autophagy protects against alcohol-induced liver injury by degrading interferon regulatory factor 1 (IRF1) and removing damaged mitochondria. *J. Biol. Chem.* 294, 12359–12369. doi: 10.1074/jbc.ra119.007409

Lin, S. Y., Li, T. Y., Liu, Q., Zhang, C., Li, X., Chen, Y., et al. (2012). GSK3-TIP60-ULK1 signaling pathway links growth factor deprivation to autophagy. *Science* 336, 477–481. doi: 10.1126/science.1217032

Morselli, E., Mariño, G., Bennetzen, M. V., Eisenberg, T., Megalou, E., Schroeder, S., et al. (2011). Spermidine and resveratrol induce autophagy by distinct pathways converging on the acetylproteome. *J. Cell Biol.* 192, 615–629. doi: 10.1083/jcb.201008167

Mostowy, S., Sancho-Shimizu, V., Hamon, M. A., Simeone, R., Brosch, R., Johansen, T., et al. (2011). p62 and NDP52 proteins target intracytosolic *Shigella* and *Listeria* to different autophagy pathways. *J. Biol. Chem.* 286, 26987–26995. doi: 10.1074/jbc.m111.223610

Murray, P. E., Stanley, H. R., Matthews, J. B., Sloan, A. J., and Smith, A. J. (2002). Age related odontometric changes of human teeth. *Oral Surg. Oral Med. Oral Pathol. Oral Radiol. Endod.* 93, 474–482. doi: 10.1067/moe.2002.120974

Nakashima, M., Iohara, K., Murakami, M., Nakamura, H., Sato, Y., Ariji, Y., et al. (2017). *Stem. Cell Res. Ther.* 8:61.

Netea-Maier, R. T., Plantinga, T. S., van de. Veerdonk, F. L., Smit, J. W., and Netea, M. G. (2016). Modulation of inflammation by autophagy: consequences for human disease. *Autophagy* 12, 245–260. doi: 10.1080/15548627.2015.1071759

Park, S. E., Yi, H. J., Suh, N., Park, Y. Y., Koh, J. Y., Jeong, S. Y., et al. (2016). Inhibition of EHMT2/G9a epigenetically increases the transcription of Beclin-1 via an increase in ROS and activation of NF-κB. *Oncotarget* 7, 39796–39808. doi: 10.18632/oncotarget.9290

Pediconi, N., Salerno, D., Lupacchini, L., Angrisani, A., Peruzzi, G., De Smaele, E., et al. (2019). EZH2, JMJD3, and UTX epigenetically regulate hepatic plasticity inducing retro-differentiation and proliferation of liver cells. *Cell Death. Dis.* 10:518.

Peeters, J. G. C., Picavet, L. W., Coenen, S., Mauthe, M., Vervoort, S. J., Mocholi, E., et al. (2019). Transcriptional and epigenetic profiling of nutrient-deprived cells to identify novel regulators of autophagy. *Autophagy* 15, 98–112. doi: 10.1080/15548627.2018.1509608

Pei, F., Lin, H., Liu, H., Li, L., Zhang, L., and Chen, Z. (2015). Dual role of autophagy in lipopolysaccharide-induced preodontoblastic cells. *J. Dent. Res.* 94, 175–182. doi: 10.1177/0022034514553815

Przanowski, P., Dabrowski, M., Ellert-Miklaszewska, A., Kloss, M., Mieczkowski, J., Kaza, B., et al. (2014). The signal transducers Stat1 and Stat3 and their novel target Jmjd3 drive the expression of inflammatory genes in microglia. *J. Mol. Med.* 92, 239–254. doi: 10.1007/s00109-013-1090-5

Qi, S., Qian, J., Chen, F., Zhou, P., Yue, J., Tang, F., et al. (2019). Expression of autophagy-associated proteins in rat dental irreversible pulpitis. *Mol. Med. Rep.* 19, 2749–2757.

Salmon, A. B. (2015). About-face on the metabolic side effects of rapamycin. *Oncotarget* 6, 2585–2586. doi: 10.18632/oncotarget.3354

Sherry-Lynes, M. M., Sengupta, S., Kulkarni, S., and Cochran, B. H. (2017). Regulation of the JMJD3 (KDM6B) histone demethylase in glioblastoma stem cells by STAT3. *PLoS One* 12:e0174775. doi: 10.1371/journal.pone.0174775

Shi, X., Zhang, Z., Zhan, X., Cao, M., Satoh, T., Akira, S., et al. (2014). An epigenetic switch induced by Shh signalling regulates gene activation during development and medulloblastoma growth. *Nat. Commun.* 5:5425.

Singh, S. B., Ornatowski, W., Vergne, I., Naylor, J., Delgado, M., Roberts, E., et al. (2010). Human IRGM regulates autophagy and cell-autonomous immunity functions through mitochondria. *Nat. Cell Biol.* 12, 1154–1165. doi: 10.1038/ncb2119

Sola, S., Xavier, J. M., Santos, D. M., Aranha, M. M., Morgado, A. L., Jepsenet, K., et al. (2011). p53 interaction with JMJD3 results in its nuclear distribution during mouse neural stem cell differentiation. *PLoS One* 6:e18421. doi: 10.1371/journal.pone.0018421

Wang, B., Fan, X., Ma, C., Lei, H., Long, Q., and Chai, Y. (2016). Downregulation of KDM4A suppresses the survival of glioma cells by promoting autophagy. *J. Mol. Neurosci.* 60, 137–144. doi: 10.1007/s12031-016-0796-6

Wang, H., Pei, F., Chen, Z., Chen, Z., and Zhang, L. (2016). Increased apoptosis of inflamed odontoblasts is associated with CD47 loss. *J. Dent. Res.* 95, 697–703. doi: 10.1177/0022034516633639

Wang, Z., Long, Q. Y., Chen, L., Fan, J., Wang, Z., Li, L., et al. (2017). Inhibition of H3K4 demethylation induces autophagy in cancer cell lines. *Biochim. Biophys. Acta Mol. Cell Res.* 1864, 2428–2437. doi: 10.1016/j.bbamcr.2017.08.005

Wei, F., Cao, Z., Wang, X., Wang, H., Cai, M., Li, T., et al. (2015). Epigenetic regulation of autophagy by the methyltransferase EZH2 through an MTOR-dependent pathway. *Autophagy* 11, 2309–2322. doi: 10.1080/15548627.2015.1117734

Yan, N., Xu, L., Wu, X., Zhang, L., Fei, X., Cao, Y., et al. (2017). GSKJ4, an H3K27me3 demethylase inhibitor, effectively suppresses the breast cancer stem cells. *Exp. Cell Res.* 359, 405–414. doi: 10.1016/j.yexcr.2017.08.024

Yang, J., Wan, C., Nie, S., Jian, S., Sun, Z., Zhang, L., et al. (2013a). Localization of Beclin1 in mouse developing tooth germs: possible implication of the interrelation between autophagy and apoptosis. *J. Mol. Histol.* 44, 619–627. doi: 10.1007/s10735-013-9518-3

Yang, J., Zhu, L., Yuan, G., Chen, Y., Zhang, L., Zhang, L., et al. (2013b). Autophagy appears during the development of the mouse lower first molar. *Histochem. Cell. Biol.* 139, 109–118. doi: 10.1007/s00418-012-1016-2

Yi, C., Ma, M., Ran, L., Zheng, J., Tong, J., Zhu, J., et al. (2012). Function and molecular mechanism of acetylation in autophagy regulation. *Science* 336, 474–477. doi: 10.1126/science.1216990

Yin, B., Hui, T., Yu, F., Luo, H., Liao, X., Yang, J., et al. (2017). ASH1L suppresses matrix metalloproteinase through mitogen-activated protein kinase signaling pathway in pulpitis. *J. Endodont.* 43, 306–314. doi: 10.1016/j.joen.2016.10.020

Yu, C., Xiong, C., Tang, J., Hou, X., Liu, N., Bayliss, G., et al. (2021). Histone demethylase JMJD3 protects against renal fibrosis by suppressing TGFβ and Notch signaling and preserving PTEN expression. *Theranostics* 11:2706. doi: 10.7150/thno.48679

Zhao, L., Zhang, Y., Gao, Y., Geng, P., Lu, Y., Liu, X., et al. (2015). JMJD3 promotes SAHF formation in senescent WI38 cells by triggering an interplay between demethylation and phosphorylation of RB protein. *Cell Death Differ.* 22, 1630–1640. doi: 10.1038/cdd.2015.6

Conflict of Interest: The authors declare that the research was conducted in the absence of any commercial or financial relationships that could be construed as a potential conflict of interest.

Publisher's Note: All claims expressed in this article are solely those of the authors and do not necessarily represent those of their affiliated organizations, or those of the publisher, the editors and the reviewers. Any product that may be evaluated in this article, or claim that may be made by its manufacturer, is not guaranteed or endorsed by the publisher.

frontiers in Cell and Developmental Biology

ORIGINAL RESEARCH
published: 10 August 2021
doi: 10.3389/fcell.2021.671838

Epigenetic Deregulation of the Histone Methyltransferase *KMT5B* Contributes to Malignant Transformation in Glioblastoma

Virginia López[1], Juan Ramón Tejedor[1], Antonella Carella[1], María G. García[1], Pablo Santamarina-Ojeda[1], Raúl F. Pérez[1], Cristina Mangas[1], Rocío G. Urdinguio[1], Aitziber Aranburu[1], Daniel de la Nava[1], María D. Corte-Torres[2], Aurora Astudillo[3], Manuela Mollejo[4], Bárbara Meléndez[4], Agustín F. Fernández[1] and Mario F. Fraga[1]**

[1] Cancer Epigenetics and Nanomedicine Laboratory, Department of Organisms and Systems Biology, Nanomaterials and Nanotechnology Research Center (CINN-CSIC), Health Research Institute of Asturias (ISPA), Institute of Oncology of Asturias (IUOPA), Rare Diseases CIBER (CIBERER) of the Carlos III Health Institute (ISCIII), University of Oviedo, Oviedo, Spain, [2] Biobanco del Principado de Asturias, Hospital Universitario Central de Asturias (HUCA), Oviedo, Spain, [3] Departamento de Anatomía Patológica, Hospital Universitario Central de Asturias (HUCA), Oviedo, Spain, [4] Departamento de Patología, Hospital Virgen de la Salud (CHT), Toledo, Spain

Glioblastoma multiforme (GBM) is the most common and aggressive type of brain tumor in adulthood. Epigenetic mechanisms are known to play a key role in GBM although the involvement of histone methyltransferase *KMT5B* and its mark H4K20me2 has remained largely unexplored. The present study shows that DNA hypermethylation and loss of DNA hydroxymethylation is associated with *KMT5B* downregulation and genome-wide reduction of H4K20me2 levels in a set of human GBM samples and cell lines as compared with non-tumoral specimens. Ectopic overexpression of *KMT5B* induced tumor suppressor-like features *in vitro* and in a mouse tumor xenograft model, as well as changes in the expression of several glioblastoma-related genes. H4K20me2 enrichment was found immediately upstream of the promoter regions of a subset of deregulated genes, thus suggesting a possible role for *KMT5B* in GBM through the epigenetic modulation of key target cancer genes.

Keywords: epigenetics, glioblastoma, histone methyltransferase, histone posttranslational modification, tumor suppressor

OPEN ACCESS

Edited by:
Yujing Li,
Emory University, United States

Reviewed by:
Richard Alan Katz,
Fox Chase Cancer Center, United States
Yingzi Hou,
Emory University, United States

***Correspondence:**
Mario F. Fraga
mffraga@cinn.es
Agustín F. Fernández
agustin.fernandez@cinn.es

Specialty section:
This article was submitted to Epigenomics and Epigenetics, a section of the journal Frontiers in Cell and Developmental Biology

Received: *24 February 2021*
Accepted: *15 July 2021*
Published: *10 August 2021*

Citation:
López V, Tejedor JR, Carella A, García MG, Santamarina-Ojeda P, Pérez RF, Mangas C, Urdinguio RG, Aranburu A, de la Nava D, Corte-Torres MD, Astudillo A, Mollejo M, Meléndez B, Fernández AF and Fraga MF (2021) Epigenetic Deregulation of the Histone Methyltransferase KMT5B Contributes to Malignant Transformation in Glioblastoma. Front. Cell Dev. Biol. 9:671838. doi: 10.3389/fcell.2021.671838

Abbreviations: 5-AZA-dC, 5-aza-2′-deoxycytidine; 5hmC, 5-hydroxymethylcytosine; 5mC, 5-methylcytosine; ATCC, American Type Culture Collection; CFA, colony formation assay; ChIP, chromatin immunoprecipitation; CpGi, CpG island; DMEM, Dulbecco's modified Eagle's medium; DMSO, dimethyl sulfoxide; DNMTs, DNA methyltransferases; ENA, European Nucleotide Archive; FBS, fetal bovine serum; GBM, glioblastoma multiforme; GLM, general linear model; H4K20me, methylation at lysine 20 of histone H4; HDACs, histone deacetylases; hMeDIP, 5-hydroxymethylcytosine immunoprecipitation; KDMs, histone lysine demethylases; KMTs, histone lysine methyltransferases; MTT, 3-(4,5-dimethylthiazol-2-yl)-2,5-diphenyltetrazolium bromide; PCR, polymerase chain reaction; PE, platting efficiency; PI, propidium iodide; RTCA, real time cell analysis system; qRT-PCR, quantitative real-time reverse transcriptase polymerase chain reaction; SAHA, suberoylanilide hydroxamic acid; STR, short tandem repeat; TET, ten–eleven translocation; TMZ, temozolomide; Vit C, vitamin C; WGBS, whole genome bisulfite sequencing.

INTRODUCTION

Glioblastoma multiforme (GBM) is a malignant grade IV glioma which represents the most common and aggressive primary brain tumor among adults. The first line of treatment consists of surgical resection followed by radiotherapy and/or chemotherapy with the alkylating agent temozolomide (TMZ). Nevertheless, the median overall survival after treatment is only 14 months (Weller et al., 2015). Hence there is a critical need to gain a deeper understanding of this frequently fatal and heterogeneous brain cancer, and search for new therapeutic targets.

During tumorigenesis, epigenetic alterations affect different types of cancer-related genes involved in cell cycle control, DNA repair, apoptosis, or cell signaling (Feinberg et al., 2016), among others. Moreover, they can also occur at epigenetic regulator genes, thereby triggering a chain of genome-wide massive epigenetic alterations. As examples of the latter are, on the one hand, epigenetic disruption through the downregulation of different micro RNAs that modulate histone deacetylases (HDACs) expression has been reported in several cancers, such as hepatocellular carcinoma (Yuan et al., 2011), lymphoplasmacytic lymphoma (Roccaro et al., 2010), tongue squamous cell carcinoma (Kai et al., 2014), and breast cancer (Wu et al., 2014). On the other hand, disruption of the methylation signature at the promoter of genes encoding histone deacetylases *HDAC4*, *HDAC5*, and *HDAC9* has been described in papillary thyroid carcinoma (White et al., 2016). In the context of neuroblastoma and glioma, epigenetic inactivation via hypermethylation at promoter CpG island (CpGi) of the histone methyltransferase gene *NSD1* has been defined as the mechanism responsible for the altered histone methylation landscape observed in both types of tumor (Berdasco et al., 2009). In the same vein, it has been shown that DNA methyltransferases (DNMTs) encoded by *DNMT1* and *DNMT3B* are overexpressed in glioma due to, respectively, an aberrant histone code or an aberrant methylation pattern at their promoters (Rajendran et al., 2011). Recently, our laboratory has demonstrated that the expression of the epigenetic enzyme TET3 is aberrantly downregulated in GBM through epigenetic mechanisms, leading to a genome-wide reduction of 5-hydroxymethylcytosine (5hmC) levels (Carella et al., 2020).

Thus, besides genetic features (Brennan et al., 2013), DNA methylation/hydroxymethylation and histone modifications are major epigenetic mechanisms regulating gene expression and genomic stability whose alterations have been widely described in GBM (Hegi et al., 2005; Fernandez et al., 2018; García et al., 2018; Carella et al., 2020). In addition, the brain has a unique DNA methylation/hydroxymethylation landscape, characterized by the highest levels of 5-methylcytosine (5mC) and 5hmC of all human tissues (Nestor et al., 2012). In general terms, 5mC in promoters contributes to create a repressive chromatin environment and decreases gene expression, while 5hmC located within the body of genes may activate transcription (Chen et al., 2016). The balance between the two marks modulates a plethora of biological processes and has been extensively reported to be dysregulated in GBM (Johnson et al., 2016; López et al., 2017; Fernandez et al., 2018; García et al., 2018; Carella et al., 2020). In addition to the epigenetic marks of DNA, many studies have addressed how the modulation of chromatin structure via histone modifications is affected in the context of GBM (Liu et al., 2010). They have mostly focused on the function of histone modifying enzymes, specifically histone lysine demethylases (KDMs) and histone deacetylases (HDACs), and the use of different inhibitors (Singh et al., 2015).

However, to date little attention has been paid to the role of histone lysine methyltransferases (KMTs) in GBM (Gursoy-Yuzugullu et al., 2017). Methylation at lysine 20 of histone H4 (H4K20me) is frequently altered in cancer (Behbahani et al., 2012). However, the contribution of the epigenetic enzymes regulating these histone posttranslational modifications is still not fully understood. A preliminary genome-wide screening of candidate genes altered in GBM revealed that the gene encoding the histone methyltransferase *KMT5B* (alias *SUV420H1*) is frequently hypermethylated and hypo-hydroxymethylated in this tumor type. *KMT5B* employs H4K20me1 as a substrate, giving rise to H4K20me2 (Yang et al., 2008). In the present study we investigated the molecular basis of the deregulation of this epigenetic enzyme as well as its functional consequences and its possible tumoral role in GBM.

MATERIALS AND METHODS

Human Brain and Glioblastoma Samples

Non-tumoral human brain (n = 28) and GBM samples (n = 37) were obtained from the Tumor Bank of the Institute of Oncology of Asturias (Asturias, Spain), the Neurological Tissue Bank of the Clinic Hospital (IDIBAPS, Barcelona, Spain), and the Biobank of the Virgen de la Salud Hospital (BioB-HVS, Toledo, Spain). Informed written consent was obtained from all patients involved in this study. Tissue collection and all analyses were conducted in accordance with the Declaration of Helsinki and approved by the Clinical Research Ethics Committee of the Principality of Asturias (Spain) (date of approval 14/10/2013, project identification code: 116/13).

Culture of Human Glioblastoma Cell Lines and Drug Treatments

The human glioblastoma cell lines LN-18 (RRID: CVCL_0392), LN-229 (RRID: CVCL_0393), U-87MG ATCC (RRID: CVCL_0022), and T98G (RRID: CVCL_0556) were obtained and cultured according to American Type Culture Collection (ATCC) recommendations. Recently (November, 2020), all cell lines were authenticated by short tandem repeat (STR) profiling of an extracted DNA sample using AmpFLSTR™ Identifiler™ Plus PCR Amplification Kit (Applied Biosystems, A26182) at the Scientific and Technological Resources Unit (University of Oviedo, Asturias, Spain). Cells were grown in Dulbecco's Modified Eagle's Medium (DMEM) (Gibco, 41965) supplemented with 10% fetal bovine serum (FBS) (Sigma-Aldrich, F6178), 2% penicillin/streptomycin (Gibco, 15070), and 1% Amphotericin B (Gibco, 15290) at 37°C in a humidified incubator containing 5% CO_2. Cell cultures were regularly tested and verified to be mycoplasma negative with the Mycoplasma Gel Detection kit from Biotools (Biotools, 90.022-4544), and all

experiments were performed with mycoplasma-free cells. For the selection of LN-229 clones overexpressing *KMT5B*, medium was prepared that contained DMEM, 10% FBS, MEM non-essential aminoacids (Sigma-Aldrich, M7145), and Geneticin (G-418, Sigma-Aldrich, A1720) as the selection antibiotic. For the 5-aza-2′-deoxycytidine (5-AZA-dC) and vitamin C treatments, 2×10^6 LN-229 cells were seeded onto P-100 plates and supplemented for 72 h with either 4 μM 5-AZA-dC (Sigma-Aldrich, A3656) alone or in combination with 50 μg/mL vitamin C (Sigma-Aldrich, A7506). Control wells contained the solvent dimethyl sulfoxide (DMSO, Sigma-Aldrich, D5879). For the *KMT5B* inhibitor A-196 treatment (Sigma-Aldrich, SML1565), 2×10^3 stably-transfected LN-229 clone cells were seeded onto 8-well Lab-Tek chamber slides (Thermo Scientific, 177445) and grown for 48 h in selective medium before adding the drug (dissolved in DMSO) at 10 μM for another 48 h, with DMSO alone used in control wells.

DNA Methylation Analysis With High-Density Array and Whole Genome Bisulfite Sequencing

Data corresponding to the oxBS and BS conversion of brain or GBM samples were obtained from our previously reported HumanMethylation 450K array (E-MTAB-6003) (Fernandez et al., 2018). Processed WGBS data were obtained from Arrayexpress (E-MTAB-5171) (Raiber et al., 2017). Both datasets were filtered to highlight the CpG coverage along the *KMT5B* gene. Estimations of 5mC and 5hmC levels were calculated with the R/bioconductor package ENmix (version 1.12.3) using the oxBS.MLE method (Xu et al., 2016).

DNA Extraction

DNA was extracted from freshly frozen GBM, control brains and human GBM cell lines with standard phenol–chloroform-isoamyl alcohol protocol. Samples were stored at −20°C until further analysis.

Bisulfite Pyrosequencing

Bisulfite modification of DNA was performed with the EZ DNA methylation-gold kit (Zymo Research) following the manufacturer's instructions. The set of primers for PCR amplification and sequencing was designed using the specific software PyroMark assay design (version 2.0.01.15) (**Supplementary Table 1**). After PCR amplification, pyrosequencing was performed using Pyro-Mark Q24 reagents, vacuum prep workstation, equipment, and software (Qiagen).

5-Hydroxymethylcytosine Immunoprecipitation and Quantitative Real-Time Polymerase Chain Reaction Assay

EpiQuik Hydroxymethylated DNA Immunoprecipitation Kit (hMeDIP, Epigentek) was used for immunoprecipitation of 5hmC in 11 samples (corresponding to 5 brain samples, 5 GBM samples and LN-229 GBM cell line), according to supplier's protocol. Input, non-specific IgG and 5hmC-enriched fractions were amplified by Quantitative Real-Time Polymerase Chain Reaction (qRT-PCR) in a StepOnePlus™ Real-Time PCR machine (Applied Biosystems) with SYBR Green 2X PCR Master Mix (Applied Biosystems, 4309155) and oligonucleotides for the CpGs in the promoter of *KMT5B* listed in **Supplementary Table 1**. Relative 5hmC enrichment was calculated as a Fold Change relative to Input Ct Mean.

Quantitative Real-Time Reverse Transcriptase Polymerase Chain Reaction

Total RNA was isolated from human samples and GBM cell lines using TRIzol Reagent (Life Technologies, Ref. 15596) according to the manufacturer's instructions. To remove any possible residual genomic DNA, total RNA was treated with DNase I (Turbo DNA-free kit, Ambion-Life Technologies, Ref. AM1906). RNA was quantified both before and after DNase treatment with Nanodrop (ThermoScientific) checking purity as A260/280 ratio. cDNA was synthesized from total RNA using a SuperScript™ III Reverse Transcriptase kit (Invitrogen, Ref. 18080) and following the manufacturer's instructions. Quantitative PCR was carried out in triplicate for each sample, using SYBR Green 2X PCR Master Mix (Applied Biosystems, 4309155) and specific primers detailed in **Supplementary Table 1**. qRT-PCR was performed using the StepOnePlus™ Real-Time PCR System (Applied Biosystems). Gene expression was normalized using *GAPDH* as endogenous control and analyzed by the comparative threshold ($\Delta\Delta$ Ct) method.

KMT5B Transfection

LN-229 cells were stably transfected with either expression vectors encoding human *KMT5B* (pEGFP-*KMT5B*) or with empty vector (pEGFP-C1), kindly provided by Professor Miki Hieda (Ehime Prefectural University of Health Sciences, Matsuyama, Japan) and constructed as described previously (Yokoyama et al., 2014), using Lipofectamine 3000 (Invitrogen, L3000015) according to the manufacturer's instructions. Geneticin-resistant cells were selected 72 h after transfection with 1 mg/mL G-418 (Sigma-Aldrich, A-1720), after which sub-cloning was carried out by limiting dilution, and several clones overexpressing *KMT5B* were obtained. *KMT5B* expression was tested in positive clones by qRT-PCR using specific primers for *KMT5B* transcription variant 1 detection (**Supplementary Table 1**).

Chromatin Immunoprecipitation Assays and Real-Time PCR Quantification (qChIP)

For real-time PCR quantification of H4K20me2-enriched genomic regions (qChIP), LN-229 cells (empty vector, *KMT5B* #3, and *KMT5B* #7) were freshly processed using the SimpleChIP Enzymatic Chromatin IP Kit with magnetic beads (Cell Signaling, 9003). Immunoprecipitations were performed using antibodies against H4K20me2 (ab9052, Abcam), total histone H3 (Abcam, ab1791) as positive control, and IgG antiserum (Abcam, ab46540) as negative control (see **Supplementary Table 2**).

DNA was purified and used for quantitative real-time PCR with SYBR Green 2X PCR Master Mix (Applied Biosystems) and the primers for the gene loci listed in **Supplementary Table 1**. Input chromatin DNA was used to create a standard curve and determine the efficiency of amplification for each primer set in a StepOnePlus™ Real-Time PCR machine (Applied Biosystems). All samples were measured in triplicate. IgG was used as negative control. ChIP data were analyzed and are shown in the results as the percentage relative to the input DNA amount by the equation:

$$\text{Percent input} = 2\% \times 2^{[2\%\ \text{Input}\ Ct - \text{Sample}\ Ct]}$$

Immunohistochemistry

The immunohistochemical analyses of *KMT5B* protein levels in three GBM samples and paired-normal brain tissue were performed using the EnVision FLEX Mini Kit (DAKO, K8024) and Dako Autostainer system. Briefly, paraffin embedded tissue (3–5 μm) was deparaffinized, rehydrated, and then epitopes were retrieved by heat induction (HIER) at 95°C for 20 min at pH 6.0 (DAKO, GV805) in the Pre-Treatment Module, PT-LINK (DAKO). Sections were incubated with anti-*KMT5B* antibody (sc-169462, Santa Cruz) at 1:100 dilution in EnVision™ FLEX Antibody Diluent (DAKO, K8006) for 60 min after blocking endogenous peroxidase with EnVision™ FLEX Peroxidase-Blocking Reagent (DAKO, DM821). Signal was detected using diaminobenzidine chromogen as substrate after incubation with Dako EnVision™ FLEX/HRP (DAKO, DM822). Sections were counterstained with hematoxylin. Appropriate negative and positive controls were also tested. After the complete process, sections were dehydrated and mounted with permanent medium (Dako mounting medium, CS703). Images were captured using a Nikon Eclipse Ci microscope equipped with a 20x objective and a camera (Nikon Instruments Europe B. V.).

Immunofluorescence

For immunofluorescence experiments 2×10^3 cells were seeded onto 8-well Lab-Tek chamber slides (Thermo Scientific, 177445) and grown for 48 h. Samples were fixed with 4% formaldehyde (252931 Panreac) for 15 min at RT, and permeabilized with 1 × PBS/0.1% Triton X-100 (Sigma-Aldrich) for 20 min at RT. Blocking was performed with 1 × PBS/10% BSA (A7906 Sigma-Aldrich) at RT for 1 h, followed by incubation with the corresponding primary antibody _ rabbit anti-H4K20me1 (ab9051, Abcam) or rabbit anti-H4K20me2 (ab9052, Abcam)_ at 1:1,000 dilution (see **Supplementary Table 2**) in antibody diluent (EnVision FLEX DM830 Dako), for 1 h at 4°C. Secondary antibody chicken anti-rabbit IgG Alexa Fluor 488 (A-21441 Invitrogen) at 1:500 dilution was incubated for 1 h at RT protected from light. Finally, slides were mounted using EverBrite mounting medium with DAPI (23002 Biotium). Immunofluorescence images were acquired with a Zeiss microscope, equipped with a 63X/1.4 NA immersion objective and an AxioCam MRm camera (Carl Zeiss). Fluorescence intensity measurements were performed using the ZEN lite software (ZEN lite 2.3 SP1, Carl Zeiss).

Cell Proliferation Assay

Cell proliferation rates were measured using xCELLigence Real Time Cell Analyzer (RTCA, ACEA Biosciences). Quadruplicates of mock or stably-transfected LN-229 clone cells (15×10^3) were seeded onto analyzer specific plates. Cell impedance was measured every 2 h for eight consecutive days through micro-electric biosensors located at the base of the plate wells. Cell proliferation was represented by Cell Index, slope, and doubling time parameters.

Cell Viability Assay

Cell viability of LN-229 clones stably-transfected with *KMT5B* or empty vectors was determined by 3-(4,5-Dimethylthiazol-2-yl)-2,5-Diphenyltetrazolium Bromide (MTT) assay. Briefly, ten replicates of 2×10^3 cells per condition and time point (up to 72 h) were seeded onto 96-well plates. MTT (Sigma-Aldrich, M5655) was added to the corresponding wells (every 24 h for 3 days) to a final concentration of 500 μg/mL, and incubated at 37°C, 5% CO_2 for 3 h. The MTT was then removed and the formazan crystals formed were dissolved in DMSO (Sigma-Aldrich-Aldrich, D5879). Absorbance at 570 nm was measured with an automated microtiter plate reader (Synergy HT, BioTek).

Colony Formation Assay

Colony formation assays of LN-229 clones stably-transfected with *KMT5B* or empty vectors were conducted as described by Franken et al. (2006), with minor modifications. Briefly, cells were seeded at two different densities (100 and 200 cells) onto P-6 wells. After incubation for 14 days, stable colonies were fixed and stained with a mixture of 6.0% glutaraldehyde (Sigma-Aldrich, 340855) and 0.5% crystal violet (Sigma-Aldrich, C3886). After washing, the number of colonies was counted manually. The results were expressed as mean Plating Efficiency (PE), a parameter which represents the ratio between the number of grown colonies versus the number of cells seeded at each different density.

$$\text{PE} = [\text{Number of colonies formed} \div \text{Number of cells seeded}] \times 100$$

Cell Cycle Analysis

Cell cycle analysis of LN-229 clones stably-transfected with *KMT5B* or empty vectors was conducted by flow cytometry using propidium iodide (PI, Sigma-Aldrich, P4170). Briefly, cells were trypsinized, washed with PBS, and fixed with cold absolute ethanol overnight at −20°C. Cells were then washed twice with PBS and dyed with PI, and RNase A for 30 min at 37°C in the dark. The suspension was filtered with a nylon mesh filter and analyzed using a BD FACS Aria Ilu cytometer (BD Biosciences) and FlowJoV10 software.

Tumor Xenografts

For the xenograft experiments, 5-weeks old NU/NU female mice ($n = 4$) were purchased from Charles River Japan Inc. (Kanagawa, Japan). Animal housing and experimental procedures were approved by the Animal Ethics Committee of University

of Oviedo (Asturias, Spain) on 21/06/2018 with the project identification code PROAE 18/2018. Mice were subcutaneously injected in each flank with 1×10^6 LN-229 cells (mock and *KMT5B* stably-transfected clones) suspended in culture medium 1:1 with Matrigel (Corning, Ref 354248). Tumor volumes were measured with a calliper twice a week and calculated using the formula $V = 4/3\pi\ (Rr)^2$, were R is the maximum diameter and r is the minimum diameter. After animal sacrifice, the tumors were excised and weighed.

RNAseq

For RNA-seq, total RNA from three replicates of mock and *KMT5B* stably-transfected clones was isolated using the RNeasy Mini Kit (Cat. No. 74104, Qiagen) according to the manufacturer's instructions, submitted to GeneWiz (Germany) for next-generation sequencing purposes, and to the European Nucleotide Archive (ENA) database (accession number PRJEB39613). Library preparation was performed using the Illumina Poly(A) selection method according to GeneWiz pipeline for standard RNA sequencing. Samples were sequenced using the Illumina HiSeq platform using 2×150 bp configuration mode. Adaptor removal was performed using fastp (v. 0.20.1), and the filtered reads were aligned to the human reference genome GRCh38 using the ultra-fast selective-alignment provided by SALMON (v.1.2.1). A prior step was introduced to generate the gentrome files from the concatenated GENCODE transcriptome and GRCh38 genome primary assembly (V29). The sequencing coverage and quality statistics for each sample are summarized in **Supplementary Table 6**. Differential gene expression analyses were conducted using the DESeq2 R/Bioconductor package (v.1.22.2) using as input the read count matrices obtained from SALMON. Genes with an absolute Log2 fold change = 1 and FDR < 0.05 were considered to be significant for downstream purposes. Subsequent enrichment analyses were performed using the R/Bioconductor package clusterProfiler (v.3.16.0). Significant gene-disease associations were represented using the R/Bioconductor package enrichplot (v.1.8.1).

Statistical Analysis

All statistical analyses were conducted using the R statistical programming language (version 3.4.0). Specific analyses are described in the corresponding section.

RESULTS

KMT5B Shows Altered 5mC/5hmC Pattern in GBM

On the basis of data from our previously reported 450 K Illumina methylation array of 11 GBM and 5 non-tumoral brain samples (Fernandez et al., 2018), we performed a genome-wide screening of candidate genes which are altered in GBM. We found that *KMT5B*, a gene encoding a histone methyltransferase, had altered DNA methylation and hydroxymethylation patterns. Specifically, compared to healthy brain tissue, GBM showed higher levels of 5mC and greatly reduced levels of 5hmC in the CpGi at the promoter and several CpG sites within the *KMT5B* gene body (**Figure 1A** and **Supplementary Table 3**). Comparison with publicly available whole genome bisulfite sequencing (WGBS) data, with a deeper CpG coverage along the *KMT5B* locus (Raiber et al., 2017), confirmed a 5mC/5hmC imbalance in GBM as compared to non-tumoral brain (**Figure 1B** and **Supplementary Table 4**).

We validated 5mC array data by means of the bisulfite pyrosequencing of five representative CpG sites at *KMT5B* promoter in the same specimens included in the array, as well as in a larger set of samples consisting of: 27 GBM, 4 non-tumoral brains, and 4 human GBM cell lines. Pyrosequencing results confirmed the 5mC pattern observed in the array (**Figure 1C** and **Supplementary Table 5**). With respect to 5hmC array data, we validated those results using a different technique that relied not on oxidative bisulfite conversion, but on DNA immunoprecipitation with an antibody against 5hmC. We used an hMeDIP Kit (see "Materials and Methods" section) with 5 GBM, 5 non-tumoral brain samples and the human GBM cell line LN-229. qRT-PCR was used to analyse the samples and the results confirmed the extensive loss of 5hmC affecting the *KMT5B* locus in GBM (Wilcoxon rank sum test, $^{**}p < 0.01$; **Figure 1D**).

KMT5B Expression Is Downregulated in a Subset of Human GBM Samples and in GBM Cell Lines

Next, we wanted to investigate whether the aberrant methylation landscape of *KMT5B* could have an effect at the transcriptional regulation level. In order to determine the expression status of *KMT5B* in GBM, we measured its mRNA levels by means of qRT-PCR in 13 GBM samples, four human GBM cell lines, and 23 non-tumoral control brains (seven corresponding to gray matter and 16 to white matter samples). The results showed that *KMT5B* mRNA expression was significantly downregulated in a subset of GBM samples compared with non-tumoral brains (**Figure 1E**). Comparison with gene expression array data obtained from different brain datasets in ArrayExpress (Günther et al., 2008; Sim et al., 2009; Grzmil et al., 2011) confirmed that downregulation of *KMT5B* affects a subset of GBMs (**Supplementary Figure 1**, **Supplementary Table 8**, and **Supplementary Methods**).

To validate our observations at the protein level, we subjected three GBM samples and their paired non-tumoral brain tissue to immunohistochemistry (IHC). The results were in line with the mRNA expression data and revealed that *KMT5B* protein expression was high in non-tumoral brain tissues and low to absent in GBM (**Figure 1F**).

These findings point to a potential epigenetic silencing of *KMT5B* through the methylation of the promoter and hypo-hydroxymethylation of the gene body in GBM.

Correlation Between Epigenetic Regulation and *KMT5B* Gene Expression

To further explore the possible functional link between the epigenetic alterations described above and *KMT5B* repression, we

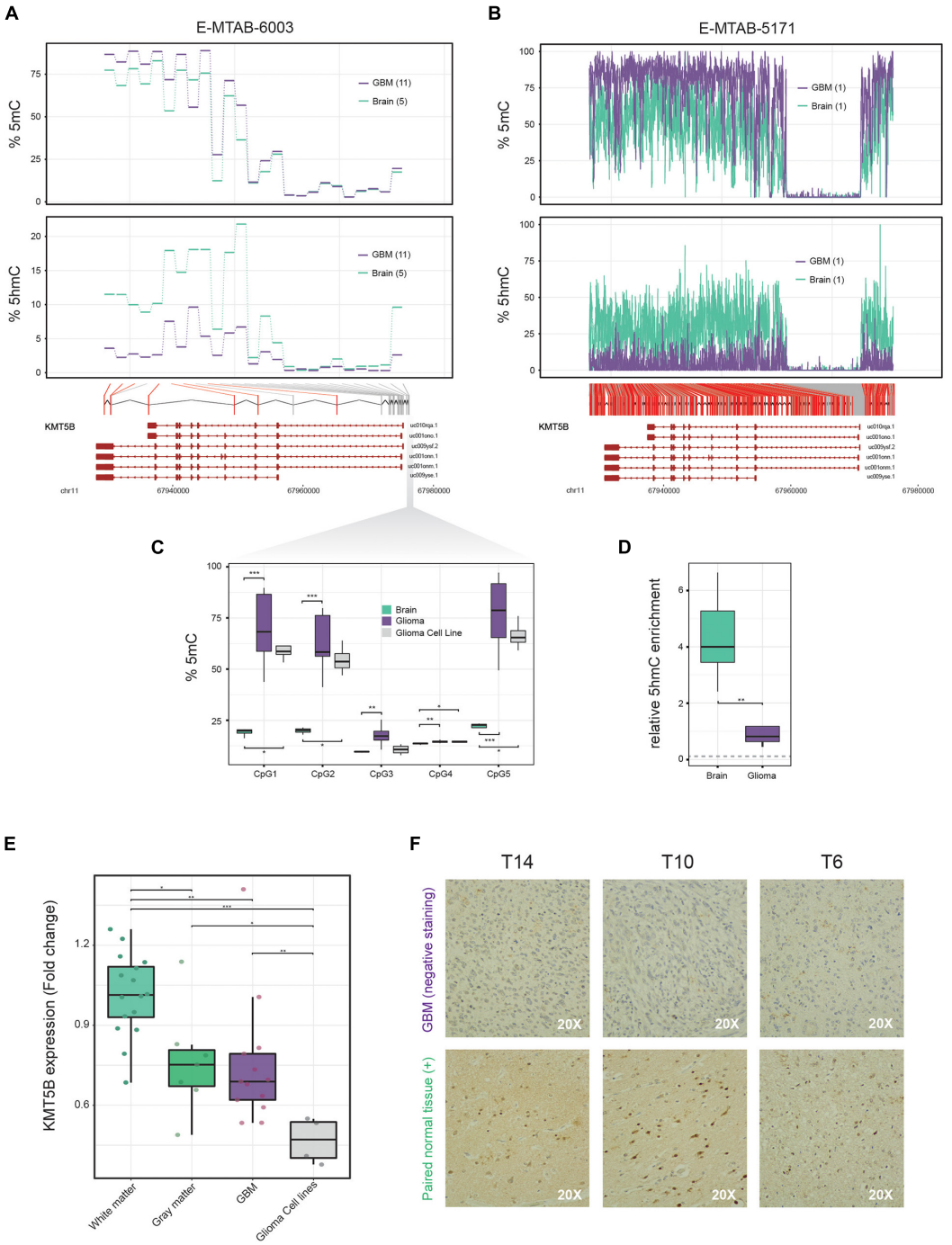

FIGURE 1 | 5mC and 5hmC profiling along the *KMT5B* locus in brain and glioblastoma multiforme (GBM) samples and analysis of *KMT5B* expression in brain, GBM and GBM cell lines. **(A)** Line plots represent percentage of average 5mC (*upper panel*) and 5hmC values (*lower panel*) corresponding to 25 CpG positions in the *KMT5B* gene for five control brain and eleven GBM samples, depicted in blue and violet, respectively. Data were obtained from a genome-wide Illumina HumanMethylation 450 K array (E-MTAB-6003). Welch *t*-tests were applied for each CpG and those that were significant are depicted in red (q-value < 0.05). **(B)** WGBS dataset with high content profiling of 5mC and 5hmC (accession number E-MTAB-5171) confirmed the altered 5mC/5hmC pattern of *KMT5B*. CpGs depicted in red represent those with changes =15%. Lower diagrams in panels **(A,B)** represent the relative location of the analyzed CpG sites along *KMT5B* locus. **(C,D)** Biological validation of the methylation and hydroxymethylation values in five *KMT5B* promoter CpGs using, respectively, bisulfite pyrosequencing and hMeDIP. The gray dotted line in panel **(D)** indicates 5hmC levels in GBM cell line LN-229. Wilcoxon rank sum tests were applied (*$p < 0.05$; **$p < 0.01$; ***$p < 0.001$). **(E)** Box plot represents *KMT5B* mRNA relative expression in 16 white matter and 7 gray matter control brains, 13 GBM samples and 4 GBM cell lines, measured by qRT-PCR in relation to *GAPDH* and represented as Fold Change relative to white-matter control brains. Wilcoxon rank sum tests were applied (*$p < 0.05$; **$p < 0.01$; ***$p < 0.001$). **(F)** Representative images of *KMT5B* protein levels detected in GBM samples and their paired non-tumoral brain tissue by immunohistochemistry (IHC), shown at 20× magnification. Only non-tumoral brain sections showed positive *KMT5B* nuclear staining.

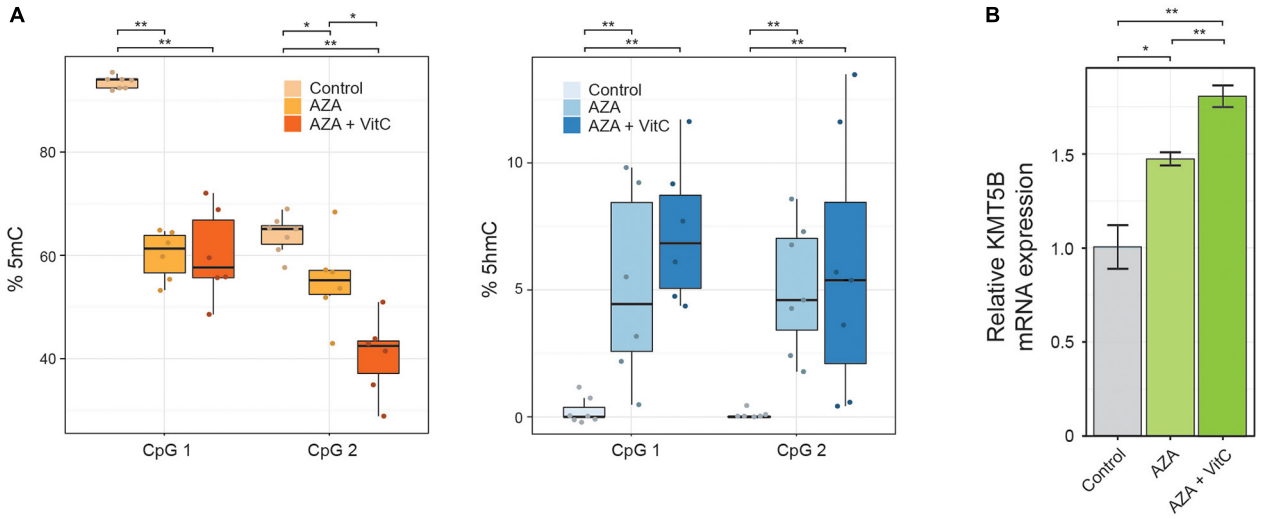

FIGURE 2 | Pharmacological restoration of 5mC/5hmC levels in human GBM cell line LN-229. Cells were treated with demethylating agent 5-AZA-dC, either alone or in combination with vitamin C (Vit C). The effects on 5mC/5hmC levels and on *KMT5B* expression were assessed by **(A)** bisulfite pyrosequencing at two intragenic CpG positions (Wilcoxon rank sum test; $^{*}p < 0.05$; $^{**}p < 0.01$) and **(B)** *KMT5B* mRNA relative expression by means of qRT-PCR. The data are the average ±SEM of three independent experiments (Welch *t*-test; $^{*}p < 0.05$; $^{**}p < 0.01$).

performed a pharmacological restoration of 5mC/5hmC levels in human GBM cell line LN-229. To this end, we incubated LN-229 cells with 5-aza-2′-deoxycytidine (5-AZA-dC) either alone or together with vitamin C. 5-AZA-dC is an epigenetic drug, widely used in clinical practice, that decreases 5mC levels through DNA methyl-transferases (DNMTs) inhibition, and increases 5hmC levels through upregulating the expression of Ten-Eleven-Translocation proteins (TETs) (Sajadian et al., 2015). Vitamin C, a TET cofactor, has been shown to increase intragenic 5hmC levels and to act synergistically with 5-AZA-dC *in vitro* (Sajadian et al., 2016). The treatments carried out here caused a significant decrease in 5mC and an increase in 5hmC levels, as confirmed at two intragenic CpG sites (CpG in the array CG27086672 and the next downstream CpG position) by means of bisulfite pyrosequencing (Wilcoxon rank sum tests, $^{*}p < 0.05$; $^{**}p < 0.01$; **Figure 2A** and **Supplementary Table 5**). At the mRNA level, *KMT5B* expression was also upregulated, especially when both drugs were present (Welch *t*-test, $^{**}p < 0.01$; **Figure 2B**).

Taken together, these data indicate that aberrant epigenetic regulation contributes to *KMT5B* repression in GBM.

Ectopic Expression of *KMT5B* Reduces the Tumorigenic Potential of Glioblastoma Cells *in vitro*

To delve into the possible role of *KMT5B* epigenetic repression in GBM, we stably transfected either a *KMT5B* expression plasmid or an empty vector (mock) into the human GBM cell line LN-229, which exhibits hypo-hydroxymethylation and downregulation of *KMT5B*. Two clones, namely *KMT5B* #3 and *KMT5B* #7, were selected among those that were drug resistant, and the expression of *KMT5B* was confirmed by qRT-PCR (**Figure 3A**). Impedance-based proliferation assays showed that *KMT5B*-transfected clones grew less than control cells (**Figure 3B**). Overexpression of *KMT5B* also reduced the clonogenicity of the clones compared with the mock transfected cells (**Figure 3C**). In addition, an MTT assay demonstrated that *KMT5B* overexpression caused a significant decrease in cell viability (**Figure 3D**). Cell cycle analysis confirmed that *KMT5B* overexpression induced G2/M arrest, as was demonstrated previously by Evertts et al. (2013), thus explaining the decreased cell proliferation and viability of the overexpressing clones (**Supplementary Figure 2**).

As expected, the increased expression of *KMT5B* elevated the levels of its histone mark H4K20me2, concomitantly reducing those of H4K20me1, as seen by immunofluorescence (IF) in stably-transfected clones versus mock (**Figures 4A,B** and **Supplementary Figures 3A,B**). Conversely, inhibition of *KMT5B* enzymatic activity with the selective drug A-196 (Bromberg et al., 2017) increased monomethylated and decreased dimethylated forms of H4K20 in stably-transfected clones, thus recapitulating the histone H4K20 methylation landscape of LN-229 GBM cell line (**Figures 4C,D** and **Supplementary Figures 3C,D**).

KMT5B Overexpression Reduces Tumor Growth in Nude Mice

In light of the above data, we sought to further characterize the role of *KMT5B* expression in GBM *in vivo*. To this end, we subcutaneously injected stably-transfected *KMT5B* or mock LN-229 cells into nude mice. Tumor volume was notably smaller in mice flanks receiving *KMT5B*-overexpressing LN-229 clones compared to those injected with empty vector transfected cells (General linear model, $^{***}p$-value < 0.001; **Figure 5A**). At the time of sacrifice, 56 days after tumor-xenograft implantation, the average weight of tumors generated by *KMT5B*-overexpressing clones was significantly lower than those from control cells (Wilcoxon rank sum tests; $^{*}p < 0.05$; $^{**}p < 0.01$; **Figure 5B**). The

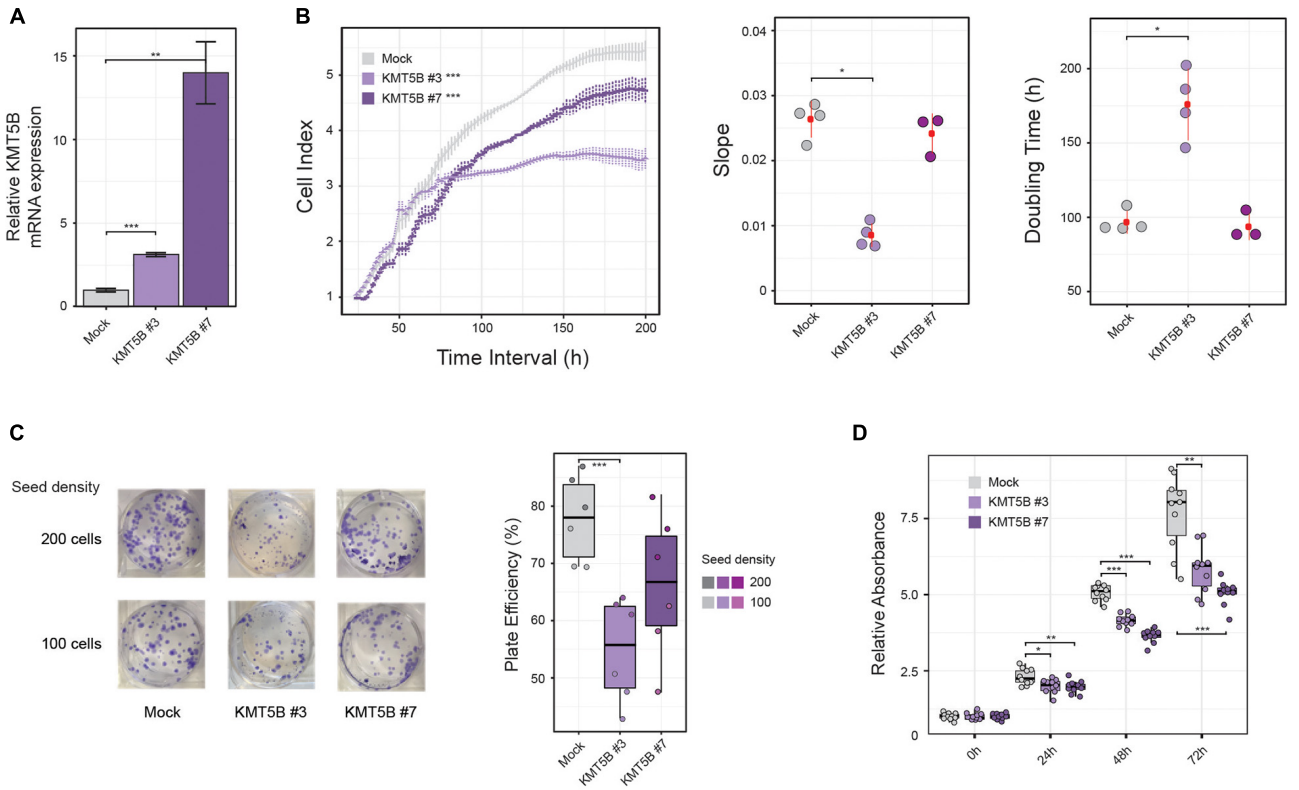

FIGURE 3 | *In vitro* effect of *KMT5B* ectopic expression. Human GBM cell line LN-229 was transfected with an empty (control) or a *KMT5B* expression vector. **(A)** Stable transfectants were obtained after selection with 1 mg/mL G-418, and named mock, *KMT5B* #3, and *KMT5B* #7. *KMT5B* expression was confirmed by qRT-PCR (the data shown are the average ±SEM of three independent experiments. Welch *t*-test; $^{**}p < 0.01$; $^{***}p < 0.001$). **(B)** The proliferation rate of mock and the two *KMT5B* stably-transfected clones was measured by an impedance-based assay and represented as cell index units [General linear model (GLM) $^{***}p$-value < 0.001], slope and doubling time for three to four technical replicates (Wilcoxon rank sum tests; $^{*}p$-value < 0.05). **(C)** On the left, representative image of plates showing colony formation assay. Experiments were done in triplicate for each clone and seeding density. Results are represented in the box plot on the right as plate efficiency (Wilcoxon rank sum tests; $^{***}p$-value < 0.001). **(D)** Cell viability was determined by MTT assay on control and *KMT5B* transfected cells. Box plot represents the average absorbance of ten replicates at several time points, relative to the absorbance at time 0 h for each clone (Wilcoxon rank sum test; $^{*}p < 0.05$; $^{**}p < 0.01$; $^{***}p < 0.001$).

tumor xenografts thereby revealed that *KMT5B* overexpression also slows tumorigenesis *in vivo*, suggesting that *KMT5B* could play a possible role as a putative tumor suppressor in GBM.

Overexpression of *KMT5B* Affects Genome-Wide Gene Expression in GBM Cells

In an attempt to shed light on the molecular pathways and mechanisms by which *KMT5B* decreases GBM tumorigenesis, we subjected our stably-transfected overexpressing or mock LN-229 clones to RNAseq (**Supplementary Table 6**). *KMT5B* has been proposed to impact transcriptional regulation by means of its product H4K20me2 (Miao and Natarajan, 2005; Vakoc et al., 2006). Our results showed that overexpression of *KMT5B* changed the transcriptome of GBM cells through up- or downregulation of hundreds of genes (**Figure 6** and **Supplementary Table 7**). Specifically, for clone *KMT5B*#3 a total of 725 genes were significantly affected, corresponding to 333 upregulated and 392 downregulated ones. Regarding *KMT5B*#7, expression changes implicated a total of 962 genes of which 484 were upregulated and 478 downregulated. The Venn diagram in **Figure 6B** represents the overlap of differentially expressed genes in *KMT5B* clones as compared to the LN-229 control cells (mock). The two clones shared a total of 315 differentially expressed genes. Among the upregulated ones, *CDH11* (*cadherin-11*) has been associated with blocking the invasion of GBM cells *in vitro* (Delic et al., 2012). Interestingly, several of those genes had been previously described to be overexpressed and implicated in GBM tumorigenesis, including: *CA9* (*carbonic anhydrase 9*) (Boyd et al., 2017), *PDL1* (*Programmed Death Ligand 1*, also known as *CD274*) (Jacobs et al., 2009), and *IL13RA2* (*Interleukin 13 Receptor Subunit Alpha 2*). We focused on *IL13RA2* as this gene encodes a monomeric IL4-independent and high grade glioma-associated IL13 receptor (Mintz et al., 2002). IL13RA2 is overexpressed in most patients with GBM but not in normal brain (Brown et al., 2013). As expected, the gene-disease associations platform DisGeNET related the above-mentioned genes with malignant glioma. Interestingly, it also

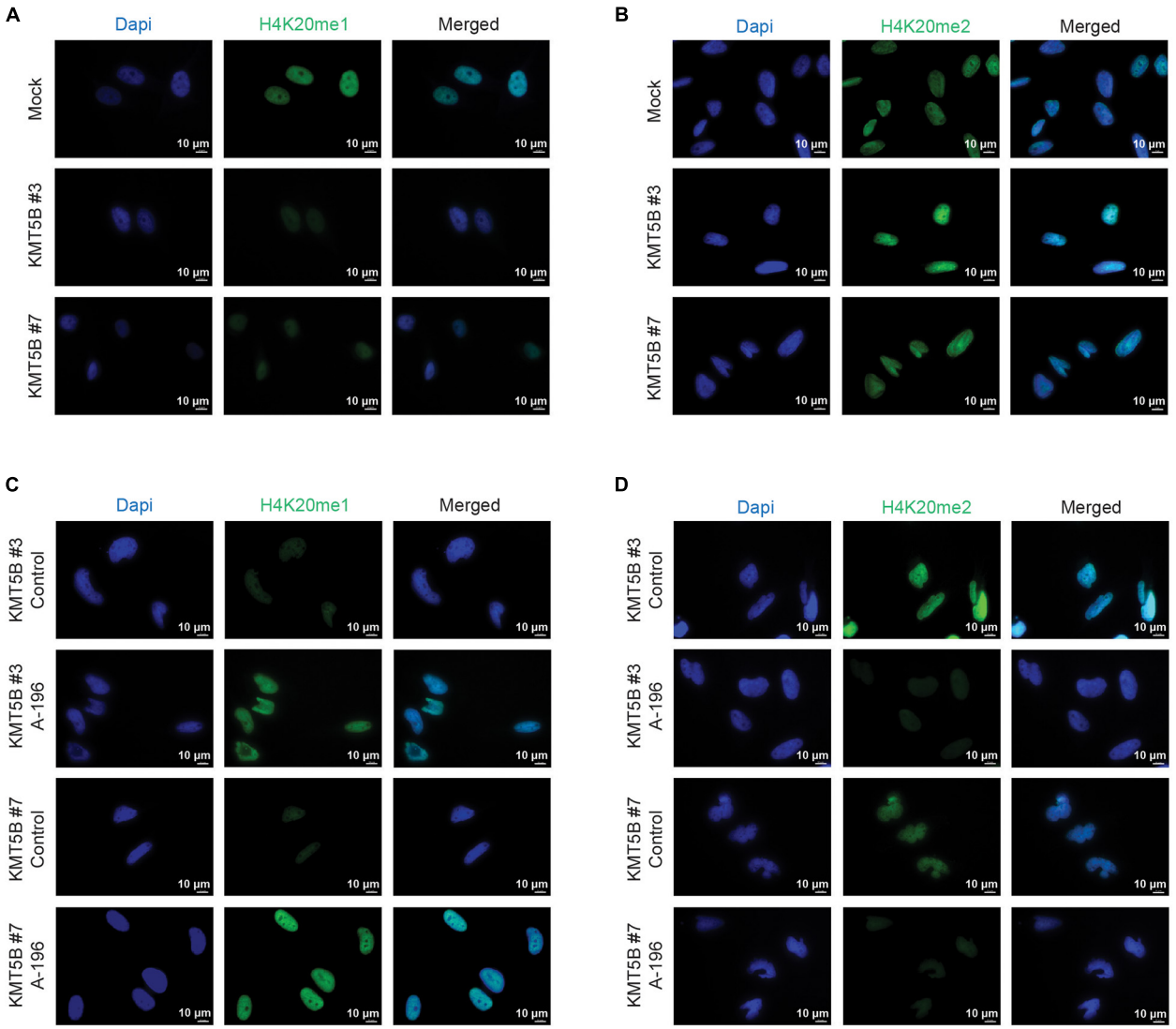

FIGURE 4 | Immunofluorescence analysis of mono- and dimethylation of H4K20. Representative images of mock and *KMT5B*-transfected clones immunostained with **(A)** anti-H4K20me1 or **(B)** anti-H4K20me2 antibodies (green). In panels **(C,D)** representative images of *KMT5B*-transfected clones immunostained with **(C)** anti-H4K20me1 or **(D)** anti-H4K20me2 antibodies (green) after treating the cells with *KMT5B* inhibitor A-196 for 48 h. Nuclei were counterstained with DAPI (blue). Bars: 10 µm.

highlighted the association of certain other genes with both malignant glioma and kidney diseases, thus pointing to a yet-undescribed hypothetical role of *KMT5B* in such renal pathologies (**Figure 6C**).

To verify the RNAseq results and assess the involvement of *KMT5B* and H4K20 methylation in the regulation of *IL13RA2* and *CDH11* expression, we performed a ChIP assay for H4K20me2 in our clones. The analysis of immunoprecipitated DNA by qRT-PCR demonstrated that H4K20me2 is enriched immediately upstream of the *IL13RA2* and *CDH11* transcription start sites in the *KMT5B*-overexpressing clones, but not in mock-transfected GBM cells (**Figure 6D**). Additionally, we conducted pairwise correlation analyses between *KMT5B* and candidate genes using the cBioPortal platform (Cerami et al., 2012) with microarray data obtained from the comprehensive characterization of glioblastoma performed by the TCGA consortium (Cancer Genome Atlas Research Network, 2008). Considering all the samples from the GBM dataset (n = 206), *KMT5B* mRNA expression showed inverse correlation with *IL13RA2* and direct correlation with *CDH11*, which is in line with our RNAseq and qChIP results (**Supplementary Figure 4**, upper panels). When grouping the samples by their corresponding GBM gene expression profile (Classical, Mesenchymal, Neural, and Proneural), we observed a similar trend in correlations across all subtypes, and they were particularly significant in the neural GBM subtype (**Supplementary Figure 4**). Altogether, these data suggest that *IL13RA2* and *CDH11* could represent direct targets of *KMT5B*-mediated gene expression regulation.

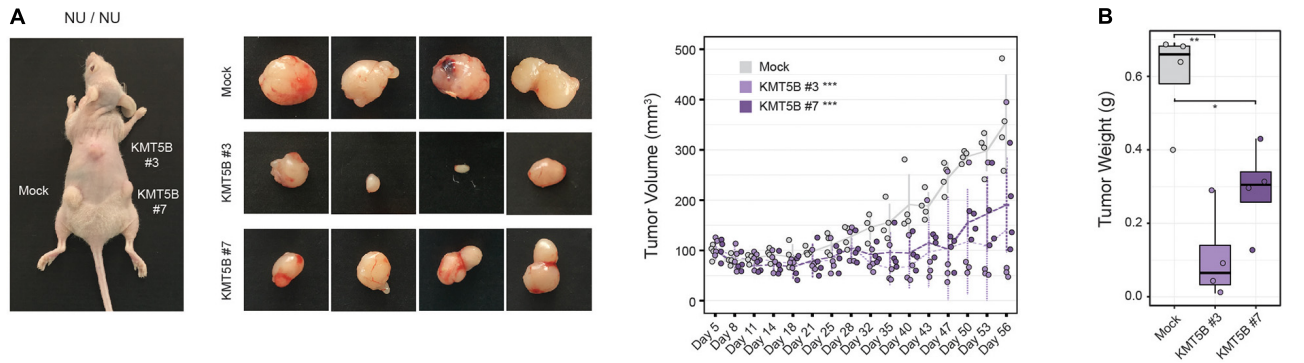

FIGURE 5 | *In vivo* effect of *KMT5B* overexpression. **(A)** Mock or *KMT5B*-transfected LN-229 cells were subcutaneously injected into the flanks or the neck base of 4 nude mice. An image of the tumors excised after animal sacrifice is shown on the left. Tumor growth was monitored for 56 days [General linear model (GLM) ***p-value < 0.001]. **(B)** Box plot represents average tumor weights for the tumors generated by each clone (Wilcoxon rank sum tests; *$p < 0.05$; **$p < 0.01$).

DISCUSSION

The involvement of KMTs in GBM pathogenesis has not as yet been fully elucidated. Referring back to our data from a 450K Infinium Illumina methylation array reported in 2018 (Fernandez et al., 2018), we found that the *KMT5B* gene shows an altered DNA methylation and hydroxymethylation profile in GBM as compared to non-tumoral brain samples. The present study aimed to investigate the contribution of this chromatin modifying gene to the etiology of GBM. We obtained evidence that it could exert an anti-tumoral effect, likely through its histone mark H4K20me2.

Expression analyses revealed that *KMT5B* hypermethylation and hypo-hydroxymethylation correlated with its decreased expression in some of our GBM specimens in comparison with normal brain tissue strongly indicating that the epigenetic downregulation of *KMT5B* might be relevant for a subset of GBM tumors. In fact, gene inactivation by DNA hypermethylation of CpGis at gene promoters is a well-established epigenetic hallmark in cancer (Koch et al., 2018). As for DNA hydroxymethylation, its presence at gene bodies is positively correlated with gene expression (Jin et al., 2011b), while its loss has been described in several cancers, including GBM (Jin et al., 2011a). This was reinforced in this work through the pharmacological reestablishment of 5mC and 5hmC levels, using a DNMTs inhibitor and a TETs cofactor, which successfully rescued *KMT5B* expression in our human GBM cell line LN-229. Nevertheless, unlike Sajadian et al. (2016), we did not find differences in the magnitude of changes in 5mC and 5hmC levels using 5-AZA-dC alone or when in combination with vitamin C. This apparent discrepancy might be explained by the fact that we specifically evaluated the methylation/hydroxymethylation state of two intragenic CpGs rather than considering global levels of those marks as in the study cited.

At the functional level, overexpression *KMT5B* reduced cell proliferation, cell viability and clonogenic potential *in vitro*, and tumor growth *in vivo* in mice xenografts. Interestingly, the loss of proliferative capacity induced by *KMT5B* overexpression in our clones was not related to apoptotic mechanisms, but rather to a G2/M cell cycle blockade. This is in agreement with a previous study showing that *KMT5B* overexpression causes G2 arrest (Evertts et al., 2013), and is consistent with the widely described role of methylated forms of H4K20 in cell cycle progression (Pesavento et al., 2008).

Regarding the histone mark deposited by *KMT5B*, H4K20me2, its levels were confirmed to be diminished in mock-transfected GBM cells, and to recover upon *KMT5B* expression in stably-transfected clones, as demonstrated through immunohistochemical analyses. Concurrently, levels of the histone mark H4K20me1, which serves as *KMT5B* substrate, varied according to the expression of this enzyme, i.e., they were very low in *KMT5B*-expressing clones and higher in mock-transfected ones. We further confirmed the H4K20 patterns by treating the cells with A-196, a drug which causes *KMT5B* enzymatic inhibition. Indeed, the treatment reverted the levels of both marks in *KMT5B* stably-transfected clones, increasing H4K20me1 and decreasing H4K20me2 to a comparable extent as seen in LN-229 GBM cells.

Furthermore, ectopic expression of *KMT5B* was associated with transcriptional changes of several GBM-related genes, as seen by the results of RNAseq analyses. The role of H4K20 monomethylation in gene expression has been controversial for some time due to studies associating this mark with both transcriptional repression (Nishioka et al., 2002) and activation (Talasz et al., 2005; Vakoc et al., 2006). However, more recent works and all the genome-wide ChIP analyses to date have rendered compelling results linking this mark with transcription activation (Barski et al., 2007; Li et al., 2011) and, indeed, it is one of the histone modifications that is most strongly correlated with active transcription (Barski et al., 2007; Karliæ et al., 2010; Veloso et al., 2014). By contrast, to date, the function of H4K20 dimethylation in gene expression has scarcely been addressed. That said, studies carried out in human cells suggest that H4K20me2 could be related to gene silencing (Miao and Natarajan, 2005; Vakoc et al., 2006; Gwak et al., 2016). The results presented here highlight the importance of *KMT5B* epigenetic downregulation in GBM, which leads to a distorted H4K20 methylation pattern. This is in line with the roles for

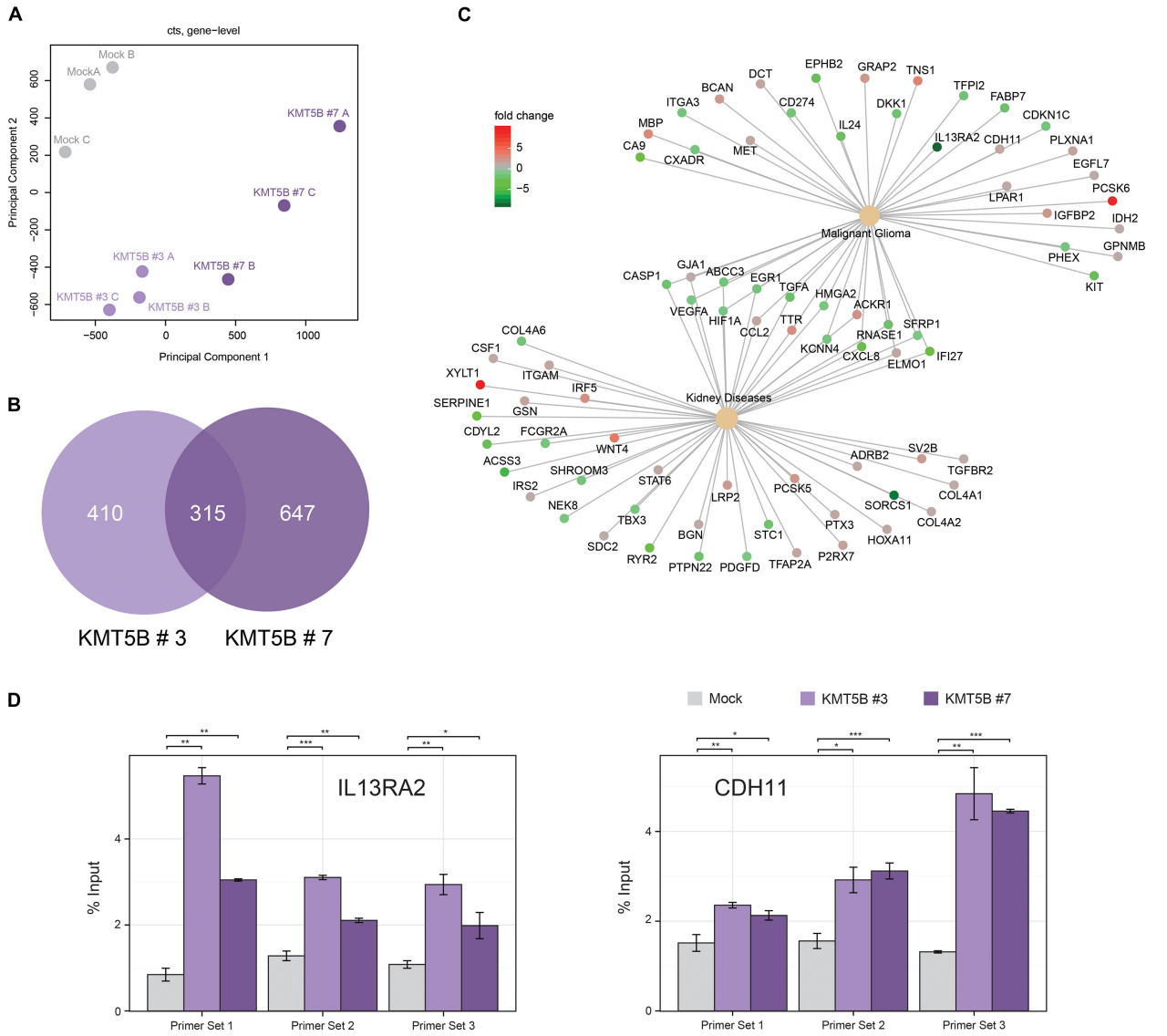

FIGURE 6 | Overexpression of *KMT5B* alters the expression of several genes, including *IL13RA2*. **(A)** Principal component analysis of the three replicates of each clone subjected to RNAseq **(B)** Venn diagram showing differentially expressed genes in *KMT5B*-expressing clones *KMT5B*#3 and *KMT5B*#7. Both comparisons were made independently against the expression profile of the LN-229 control cells (mock). **(C)** Network diagram showing the functional relationships between the genes differentially expressed in the RNAseq analysis and disease ontologies (glioblastoma and renal diseases) obtained from DisGeNET. To facilitate the interpretation of the data, the relationships of genes and ontologies common to both conditions are indicated. Information on the expression levels of the different genes compared to the control (mock) is indicated by the colour scale. **(D)** Enrichment of H4K20me2 upstream of the *IL13RA2* and *CDH11* transcription start sites due to *KMT5B* overexpression. Chromatin immunoprecipitation (ChIP) assays were performed in mock and *KMT5B* stably-transfected LN-229 cells using either anti-H4K20me2 polyclonal antibody or control IgG (see **Supplementary Table 2**). DNA eluted from the ChIP assay was amplified by qRT-PCR with primer sets mapping to *IL13RA2* or *CDH11* promoters (listed in **Supplementary Table 1**). The enrichment of H4K20me2 at the indicated regions in *KMT5B* clones was compared to the same regions in mock control cells (Welch *t*-tests; $*p < 0.05$; $**p < 0.01$; $***p < 0.001$).

H4K20me1 and H4K20me2 in gene expression mentioned above, and tie in with the concept of epigenetic de-repression of oncogenes. While it is well-known that the epigenetic silencing of tumor suppressor genes occurs during tumorogenesis, the role of epigenetic de-repression of oncogenes due to the loss of repressive chromatin marks has remained partially unexplored (Baylin and Jones, 2016). Our experiments showed that the epigenetic downregulation of *KMT5B* impairs the balance between H4K20me species in human GBM cell line LN-229. In turn, this may cause global transcriptomic changes, given our finding that overexpression of *KMT5B* restored H4K20me2 patterns and decreased the expression of several oncogenes, such as *IL13RA2*, a tumor-restricted receptor (Mintz et al., 2002). IL13 is a pleiotropic Th2-derived cytokine implicated in inflammation and immunomodulation, and is known to induce apoptosis in different cell types, including GBM (Hsi et al., 2011).

IL13RA2 binds IL13 with a higher affinity than the physiological IL13RA1/IL4RA receptor but prevents apoptosis as it does not transduce the signal for STAT6 pathway activation (Kawakami et al., 2001). Although the functional significance of IL13RA2 expression is not fully understood, it is considered an inhibitory or decoy receptor in GBM (Rahaman et al., 2002) that contributes to tumor growth (Hsi et al., 2011) and several studies have found that its overexpression is associated with higher glioma grades and poor patient prognosis (Brown et al., 2013; Han and Puri, 2018). Investigations in pancreatic, colorectal, and ovarian cancer have shown that IL13RA2 overexpression promotes tumor migration and invasion (Fujisawa et al., 2009, 2012; Barderas et al., 2012). More recent studies in GBM have also pointed to a role for IL13RA2 in stimulating cell growth and metastasis (Tu et al., 2016). As such, IL13RA2 has become an attractive therapeutic target in GBM, even though the regulatory mechanisms of its expression are currently unknown (Sharma and Debinski, 2018). By means of RNAseq and ChIP experiments, our study suggests that *KMT5B* and its mark H4K20me2 might be involved in IL13RA2 regulation since overexpression of *KMT5B* in our clones caused H4K20me2 deposition upstream of the *IL13RA2* promoter and a concomitant downregulation of *IL13RA2* mRNA.

Notwithstanding, we observed that some genes were upregulated upon *KMT5B* overexpression. Among them *CDH11*, which encodes Cadherin 11, has been previously reported to block GBM cell invasion *in vitro* (Delic et al., 2012). One plausible explanation is that H4K20me2 might function as both transcriptional activator or repressor depending on the cellular context, in concert with other associated histone modifications and readers. That dual role on gene expression modulation would fit with the abundance and ubiquitous distribution of this mark on chromatin (Pesavento et al., 2008; Schotta et al., 2008). Future research is guaranteed in order to elucidate the context dependant function of H4K20me2. Consequently, it is possible that the anti-tumoral effect of *KMT5B* observed in our study would not be due to the overexpression of this epigenetic modifier itself, but rather might be mediated by the re-establishment of levels of its product H4K20me2 in the promoter region of key GBM-related genes, such as *IL13RA2* and *CDH11*.

The dynamic and reversible nature of H4K20me2 opens the possibility of targeting its demethylase (KDM), via small-molecule inhibitors, to restore this histone mark in GBM. Indeed, in recent years, histone modifiers, such as KDMs, are envisaged as attractive druggable targets for GBM therapy (Jones et al., 2016). Although H4K20me2 is the most abundant form of H4K20 in eukaryotic cells (Pesavento et al., 2008), only a H4K20me2 demethylase has been described so far. It is LSD1n, a neuron-specific splicing variant of the flavin-dependent monoamine oxidase LSD1 with acquired new specificity against H4K20me2 and H4K20me1 (Wang et al., 2015). However, caution is needed when considering LSD1n as a potential therapeutic target using a hypothetical specific KDM inhibitor. On the one hand, there is increasing evidence that histone modifications do not act alone, but influence one another. Hence, modulation of H4K20me2 levels via a LSD1n inhibitor could potentially affect the modification status of other histone residues on the vicinity with unknown effects. On the other hand, non-histone targets of LSD1n should also be taken into account. Moreover, it has been reported that LSD1n promotes neuronal activity-regulated gene expression and plays a critical role in neurite morphogenesis, spatial learning, long-term memory formation, and modulation of emotional behavior (Zibetti et al., 2010; Wang et al., 2015; Rusconi et al., 2016). All of the above reveals the challenging pleiotropic consequences and the complexity of the epigenetic regulation via KDM inhibitors within CNS. In the future, a deeper understanding of the roles and LSD1n targets other than histones, as well as the transcriptional networks regulated by H4K20me2, or even the discovery of other yet unknown specific demethylases, could boost the development of novel specific KDM inhibitors and inform novel strategies in cancer therapy.

Taken together, our results suggest that when *KMT5B* expression and its histone mark H4K20me2 are perturbed in GBM through deregulated epigenetic mechanisms, this process has a genome-wide effect on gene transcription and may contribute to malignant transformation.

DATA AVAILABILITY STATEMENT

The datasets presented in this study can be found in online repositories. The names of the repository/repositories and accession number(s) can be found below: ENA, PRJEB39613.

ETHICS STATEMENT

The studies involving human participants were reviewed and approved by Clinical Research Ethics Committee of the Principality of Asturias (Spain). The patients/participants provided their written informed consent to participate in this study. The animal study was reviewed and approved by Animal Ethics Committee of University of Oviedo (Asturias, Spain).

AUTHOR CONTRIBUTIONS

MF and AF: conceptualization, study supervision, and funding acquisition. VL, JT, AC, MG, PS-O, RP, CM, RU, AiA, and DN: development of methodology. VL, MC-T, AuA, MM, and BM: acquisition of data. VL, JT, AF, and MF: analysis and interpretation of data, and writing–review and editing. JT and RP: software analysis. VL: writing–original draft preparation. MF: final approval. All authors have read and agreed to the published version of the manuscript.

FUNDING

This research was funded by the Health Institute Carlos III (Plan Nacional de I+D+I) cofounding FEDER (PI15/00892 and PI18/01527 to MF and AF); the Government of the Principality of Asturias PCTI-Plan de Ciencia, Tecnología e Innovación de Asturias co-funding 2018–2022/FEDER (IDI/2018/146 to MF);

AECC (PROYE18061FERN to MF); FGCSIC (0348_CIE_6_E to MF); Severo Ochoa Program BP17-165 to PS-O and BP17-114 to RP); the Ministry of Economy and Competitiveness of Spain (VL, Juan de la Cierva fellowship IJCI-2015-23316; JT, Juan de la Cierva fellowship FJCI-2015-26965); FICYT (AC and MG); FINBA-ISPA (VL); and IUOPA (VL and CM). The IUOPA is supported by the Obra Social Cajastur-Liberbank, Spain.

ACKNOWLEDGMENTS

We sincerely apologize to all colleagues whose work could not be cited because of space constraints. We would like to thank Miki Hieda (Ehime Prefectural University of Health Sciences, Matsuyama, Japan) for kindly providing the plasmids used in this study. Ronnie Lendrum for editorial assistance. Laura Santos and the Technical Services of University of Oviedo for technical support. All the members of Cancer Epigenetics and Nanomedicine laboratory (FINBA-ISPA, IUOPA, and CINN-CSIC) for their positive feedback and helpful discussions.

SUPPLEMENTARY MATERIAL

The Supplementary Material for this article can be found online at: https://www.frontiersin.org/articles/10.3389/fcell.2021.671838/full#supplementary-material

REFERENCES

Barderas, R., Bartolomé, R. A., Fernandez-Aceñero, M. J., Torres, S., and Casal, J. I. (2012). High expression of IL-13 receptor α2 in colorectal cancer is associated with invasion, liver metastasis, and poor prognosis. *Cancer Res.* 72, 2780–2790. doi: 10.1158/0008-5472.CAN-11-4090

Barski, A., Cuddapah, S., Cui, K., Roh, T.-Y., Schones, D. E., Wang, Z., et al. (2007). High-resolution profiling of histone methylations in the human genome. *Cell* 129, 823–837. doi: 10.1016/j.cell.2007.05.009

Baylin, S. B., and Jones, P. A. (2016). Epigenetic Determinants of Cancer. *Cold Spring Harb. Perspect. Biol.* 8:a019505. doi: 10.1101/cshperspect.a019505

Behbahani, T. E., Kahl, P., von, der Gathen, J., Heukamp, L. C., Baumann, C., et al. (2012). Alterations of global histone H4K20 methylation during prostate carcinogenesis. *BMC Urol.* 12:5. doi: 10.1186/1471-2490-12-5

Berdasco, M., Ropero, S., Setien, F., Fraga, M. F., Lapunzina, P., Losson, R., et al. (2009). Epigenetic inactivation of the Sotos overgrowth syndrome gene histone methyltransferase NSD1 in human neuroblastoma and glioma. *Proc. Natl. Acad. Sci. U. S. A.* 106, 21830–21835. doi: 10.1073/pnas.0906831106

Boyd, N. H., Walker, K., Fried, J., Hackney, J. R., McDonald, P. C., Benavides, G. A., et al. (2017). Addition of carbonic anhydrase 9 inhibitor SLC-0111 to temozolomide treatment delays glioblastoma growth in vivo. *JCI Insight* 2:92928. doi: 10.1172/jci.insight.92928

Brennan, C. W., Verhaak, R. G. W., McKenna, A., Campos, B., Noushmehr, H., Salama, S. R., et al. (2013). The somatic genomic landscape of glioblastoma. *Cell* 155, 462–477. doi: 10.1016/j.cell.2013.09.034

Bromberg, K. D., Mitchell, T. R. H., Upadhyay, A. K., Jakob, C. G., Jhala, M. A., Comess, K. M., et al. (2017). The SUV4-20 inhibitor A-196 verifies a role for epigenetics in genomic integrity. *Nat. Chem. Biol.* 13, 317–324. doi: 10.1038/nchembio.2282

Brown, C. E., Warden, C. D., Starr, R., Deng, X., Badie, B., Yuan, Y.-C., et al. (2013). Glioma IL13Rα2 is associated with mesenchymal signature gene expression and poor patient prognosis. *PLoS One* 8:e77769. doi: 10.1371/journal.pone.0077769

Cancer Genome Atlas Research Network (2008). Comprehensive genomic characterization defines human glioblastoma genes and core pathways. *Nature* 455, 1061–1068. doi: 10.1038/nature07385

Carella, A., Tejedor, J. R., García, M. G., Urdinguio, R. G., Bayón, G. F., Sierra, M., et al. (2020). Epigenetic downregulation of TET3 reduces genome-wide 5hmC levels and promotes glioblastoma tumorigenesis. *Int. J. Cancer* 146, 373–387. doi: 10.1002/ijc.32520

Cerami, E., Gao, J., Dogrusoz, U., Gross, B. E., Sumer, S. O., Aksoy, B. A., et al. (2012). The cBio cancer genomics portal: an open platform for exploring multidimensional cancer genomics data. *Cancer Discov.* 2, 401–404. doi: 10.1158/2159-8290.CD-12-0095

Chen, K., Zhao, B. S., and He, C. (2016). Nucleic acid modifications in regulation of gene expression. *Cell Chem. Biol.* 23, 74–85. doi: 10.1016/j.chembiol.2015.11.007

Delic, S., Lottmann, N., Jetschke, K., Reifenberger, G., and Riemenschneider, M. J. (2012). Identification and functional validation of CDH11, PCSK6 and SH3GL3 as novel glioma invasion-associated candidate genes. *Neuropathol. Appl. Neurobiol.* 38, 201–212. doi: 10.1111/j.1365-2990.2011.01207.x

Evertts, A. G., Manning, A. L., Wang, X., Dyson, N. J., Garcia, B. A., and Coller, H. A. (2013). H4K20 methylation regulates quiescence and chromatin compaction. *Mol. Biol. Cell* 24, 3025–3037. doi: 10.1091/mbc.E12-07-0529

Feinberg, A. P., Koldobskiy, M. A., and Göndör, A. (2016). Epigenetic modulators, modifiers and mediators in cancer aetiology and progression. *Nat. Rev. Genet.* 17, 284–299. doi: 10.1038/nrg.2016.13

Fernandez, A. F., Bayón, G. F., Sierra, M. I., Urdinguio, R. G., Toraño, E. G., García, M. G., et al. (2018). Loss of 5hmC identifies a new type of aberrant DNA hypermethylation in glioma. *Hum. Mol. Genet.* 27, 3046–3059. doi: 10.1093/hmg/ddy214

Franken, N. A. P., Rodermond, H. M., Stap, J., Haveman, J., and van Bree, C. (2006). Clonogenic Assay of Cells in Vitro. *Nat. Protoc.* 1, 2315–2319. doi: 10.1038/nprot.2006.339

Fujisawa, T., Joshi, B., Nakajima, A., and Puri, R. K. (2009). A novel role of interleukin-13 receptor alpha2 in pancreatic cancer invasion and metastasis. *Cancer Res.* 69, 8678–8685. doi: 10.1158/0008-5472.CAN-09-2100

Fujisawa, T., Joshi, B. H., and Puri, R. K. (2012). IL-13 regulates cancer invasion and metastasis through IL-13Rα2 via ERK/AP-1 pathway in mouse model of human ovarian cancer. *Int. J. Cancer* 131, 344–356. doi: 10.1002/ijc.26366

García, M. G., Carella, A., Urdinguio, R. G., Bayón, G. F., Lopez, V., Tejedor, J. R., et al. (2018). Epigenetic dysregulation of TET2 in human glioblastoma. *Oncotarget* 9, 25922–25934. doi: 10.18632/oncotarget.25406

Grzmil, M., Morin, P., Lino, M. M., Merlo, A., Frank, S., Wang, Y., et al. (2011). MAP kinase-interacting kinase 1 regulates SMAD2-dependent TGF-β signaling pathway in human glioblastoma. *Cancer Res.* 71, 2392–2402. doi: 10.1158/0008-5472.CAN-10-3112

Günther, H. S., Schmidt, N. O., Phillips, H. S., Kemming, D., Kharbanda, S., Soriano, R., et al. (2008). Glioblastoma-derived stem cell-enriched cultures form distinct subgroups according to molecular and phenotypic criteria. *Oncogene* 27, 2897–2909. doi: 10.1038/sj.onc.1210949

Gursoy-Yuzugullu, O., Carman, C., Serafim, R. B., Myronakis, M., Valente, V., and Price, B. D. (2017). Epigenetic therapy with inhibitors of histone methylation suppresses DNA damage signaling and increases glioma cell radiosensitivity. *Oncotarget* 8, 24518–24532. doi: 10.18632/oncotarget.15543

Gwak, J., Shin, J. Y., Lee, K., Hong, S. K., Oh, S., Goh, S.-H., et al. (2016). SFMBT2 (Scm-like with four mbt domains 2) negatively regulates cell migration and invasion in prostate cancer cells. *Oncotarget* 7, 48250–48264. doi: 10.18632/oncotarget.10198

Han, J., and Puri, R. K. (2018). Analysis of the cancer genome atlas (TCGA) database identifies an inverse relationship between interleukin-13 receptor α1 and α2 gene expression and poor prognosis and drug resistance in subjects with glioblastoma multiforme. *J. Neurooncol.* 136, 463–474. doi: 10.1007/s11060-017-2680-9

Hegi, M. E., Diserens, A.-C., Gorlia, T., Hamou, M.-F., de Tribolet, N., Weller, M., et al. (2005). MGMT gene silencing and benefit from temozolomide

in glioblastoma. *N. Engl. J. Med.* 352, 997–1003. doi: 10.1056/NEJMoa043331

Hsi, L. C., Kundu, S., Palomo, J., Xu, B., Ficco, R., Vogelbaum, M. A., et al. (2011). Silencing IL-13Rα2 promotes glioblastoma cell death via endogenous signaling. *Mol. Cancer Ther.* 10, 1149–1160. doi: 10.1158/1535-7163.MCT-10-1064

Jacobs, J. F. M., Idema, A. J., Bol, K. F., Nierkens, S., Grauer, O. M., Wesseling, P., et al. (2009). Regulatory T cells and the PD-L1/PD-1 pathway mediate immune suppression in malignant human brain tumors. *Neuro-Oncol.* 11, 394–402. doi: 10.1215/15228517-2008-104

Jin, S.-G., Jiang, Y., Qiu, R., Rauch, T. A., Wang, Y., Schackert, G., et al. (2011a). 5-Hydroxymethylcytosine is strongly depleted in human cancers but its levels do not correlate with IDH1 mutations. *Cancer Res.* 71, 7360–7365. doi: 10.1158/0008-5472.CAN-11-2023

Jin, S.-G., Wu, X., Li, A. X., and Pfeifer, G. P. (2011b). Genomic mapping of 5-hydroxymethylcytosine in the human brain. *Nucleic Acids Res.* 39, 5015–5024. doi: 10.1093/nar/gkr120

Johnson, K. C., Houseman, E. A., King, J. E., von Herrmann, K. M., Fadul, C. E., and Christensen, B. C. (2016). 5-Hydroxymethylcytosine localizes to enhancer elements and is associated with survival in glioblastoma patients. *Nat. Commun.* 7:13177. doi: 10.1038/ncomms13177

Jones, P. A., Issa, J.-P. J., and Baylin, S. (2016). Targeting the cancer epigenome for therapy. *Nat. Rev. Genet.* 17, 630–641. doi: 10.1038/nrg.2016.93

Kai, Y., Peng, W., Ling, W., Jiebing, H., and Zhuan, B. (2014). Reciprocal effects between microRNA-140-5p and ADAM10 suppress migration and invasion of human tongue cancer cells. *Biochem. Biophys. Res. Commun.* 448, 308–314. doi: 10.1016/j.bbrc.2014.02.032

Karlić, R., Chung, H.-R., Lasserre, J., Vlahovicek, K., and Vingron, M. (2010). Histone modification levels are predictive for gene expression. *Proc. Natl. Acad. Sci. U. S. A.* 107, 2926–2931. doi: 10.1073/pnas.0909344107

Kawakami, K., Taguchi, J., Murata, T., and Puri, R. K. (2001). The interleukin-13 receptor alpha2 chain: an essential component for binding and internalization but not for interleukin-13-induced signal transduction through the STAT6 pathway. *Blood* 97, 2673–2679. doi: 10.1182/blood.v97.9.2673

Koch, A., Joosten, S. C., Feng, Z., de Ruijter, T. C., Draht, M. X., Melotte, V., et al. (2018). Analysis of DNA methylation in cancer: location revisited. *Nat. Rev. Clin. Oncol.* 15, 459–466. doi: 10.1038/s41571-018-0004-4

Li, Z., Nie, F., Wang, S., and Li, L. (2011). Histone H4 Lys 20 monomethylation by histone methylase SET8 mediates Wnt target gene activation. *Proc. Natl. Acad. Sci. U. S. A.* 108, 3116–3123. doi: 10.1073/pnas.1009353108

Liu, B., Cheng, J., Zhang, X., Wang, R., Zhang, W., Lin, H., et al. (2010). Global histone modification patterns as prognostic markers to classify glioma patients. *Cancer Epidemiol. Biomark. Prev.* 19, 2888–2896. doi: 10.1158/1055-9965.EPI-10-0454

López, V., Fernández, A. F., and Fraga, M. F. (2017). The role of 5-hydroxymethylcytosine in development, aging and age-related diseases. *Ageing Res. Rev.* 37, 28–38. doi: 10.1016/j.arr.2017.05.002

Miao, F., and Natarajan, R. (2005). Mapping global histone methylation patterns in the coding regions of human genes. *Mol. Cell. Biol.* 25, 4650–4661. doi: 10.1128/MCB.25.11.4650-4661.2005

Mintz, A., Gibo, D. M., Slagle-Webb, B., Christensen, N. D., and Debinski, W. (2002). IL-13Ralpha2 is a glioma-restricted receptor for interleukin-13. *Neoplasia N. Y. N* 4, 388–399. doi: 10.1038/sj.neo.7900234

Nestor, C. E., Ottaviano, R., Reddington, J., Sproul, D., Reinhardt, D., Dunican, D., et al. (2012). Tissue type is a major modifier of the 5-hydroxymethylcytosine content of human genes. *Genome Res.* 22, 467–477. doi: 10.1101/gr.126417.111

Nishioka, K., Rice, J. C., Sarma, K., Erdjument-Bromage, H., Werner, J., Wang, Y., et al. (2002). PR-Set7 is a nucleosome-specific methyltransferase that modifies lysine 20 of histone H4 and is associated with silent chromatin. *Mol. Cell* 9, 1201–1213. doi: 10.1016/s1097-2765(02)00548-8

Pesavento, J. J., Yang, H., Kelleher, N. L., and Mizzen, C. A. (2008). Certain and progressive methylation of histone H4 at lysine 20 during the cell cycle. *Mol. Cell. Biol.* 28, 468–486. doi: 10.1128/MCB.01517-07

Rahaman, S. O., Sharma, P., Harbor, P. C., Aman, M. J., Vogelbaum, M. A., and Haque, S. J. (2002). IL-13R(alpha)2, a decoy receptor for IL-13 acts as an inhibitor of IL-4-dependent signal transduction in glioblastoma cells. *Cancer Res.* 62, 1103–1109. doi: 10.1093/intimm/10.8.1103

Raiber, E.-A., Beraldi, D., Martínez Cuesta, S., McInroy, G. R., Kingsbury, Z., Becq, J., et al. (2017). Base resolution maps reveal the importance of 5-hydroxymethylcytosine in a human glioblastoma. *NPJ Genomic Med.* 2:6. doi: 10.1038/s41525-017-0007-6

Rajendran, G., Shanmuganandam, K., Bendre, A., Muzumdar, D., Mujumdar, D., Goel, A., et al. (2011). Epigenetic regulation of DNA methyltransferases: DNMT1 and DNMT3B in gliomas. *J. Neurooncol.* 104, 483–494. doi: 10.1007/s11060-010-0520-2

Roccaro, A. M., Sacco, A., Jia, X., Azab, A. K., Maiso, P., Ngo, H. T., et al. (2010). microRNA-dependent modulation of histone acetylation in Waldenstrom macroglobulinemia. *Blood* 116, 1506–1514. doi: 10.1182/blood-2010-01-265686

Rusconi, F., Grillo, B., Ponzoni, L., Bassani, S., Toffolo, E., Paganini, L., et al. (2016). LSD1 modulates stress-evoked transcription of immediate early genes and emotional behavior. *Proc. Natl. Acad. Sci. U. S. A.* 113, 3651–3656. doi: 10.1073/pnas.1511974113

Sajadian, S. O., Ehnert, S., Vakilian, H., Koutsouraki, E., Damm, G., Seehofer, D., et al. (2015). Induction of active demethylation and 5hmC formation by 5-azacytidine is TET2 dependent and suggests new treatment strategies against hepatocellular carcinoma. *Clin. Epigenetics* 7:98. doi: 10.1186/s13148-015-0133-x

Sajadian, S. O., Tripura, C., Samani, F. S., Ruoss, M., Dooley, S., Baharvand, H., et al. (2016). Vitamin C enhances epigenetic modifications induced by 5-azacytidine and cell cycle arrest in the hepatocellular carcinoma cell lines HLE and Huh7. *Clin. Epigenetics* 8:46. doi: 10.1186/s13148-016-0213-6

Schotta, G., Sengupta, R., Kubicek, S., Malin, S., Kauer, M., Callén, E., et al. (2008). A chromatin-wide transition to H4K20 monomethylation impairs genome integrity and programmed DNA rearrangements in the mouse. *Genes Dev.* 22, 2048–2061. doi: 10.1101/gad.476008

Sharma, P., and Debinski, W. (2018). Receptor-Targeted Glial Brain Tumor Therapies. *Int. J. Mol. Sci.* 19:9113326. doi: 10.3390/ijms19113326

Sim, F. J., Windrem, M. S., and Goldman, S. A. (2009). Fate determination of adult human glial progenitor cells. *Neuron Glia Biol.* 5, 45–55. doi: 10.1017/S1740925X09990317

Singh, M. M., Johnson, B., Venkatarayan, A., Flores, E. R., Zhang, J., Su, X., et al. (2015). Preclinical activity of combined HDAC and KDM1A inhibition in glioblastoma. *Neuro-Oncol.* 17, 1463–1473. doi: 10.1093/neuonc/nov041

Talasz, H., Lindner, H. H., Sarg, B., and Helliger, W. (2005). Histone H4-lysine 20 monomethylation is increased in promoter and coding regions of active genes and correlates with hyperacetylation. *J. Biol. Chem.* 280, 38814–38822. doi: 10.1074/jbc.M505563200

Tu, M., Wange, W., Cai, L., Zhu, P., Gao, Z., and Zheng, W. (2016). IL-13 receptor α2 stimulates human glioma cell growth and metastasis through the Src/PI3K/Akt/mTOR signaling pathway. *Tumour Biol.* 37, 14701–14709. doi: 10.1007/s13277-016-5346-x

Vakoc, C. R., Sachdeva, M. M., Wang, H., and Blobel, G. A. (2006). Profile of histone lysine methylation across transcribed mammalian chromatin. *Mol. Cell. Biol.* 26, 9185–9195. doi: 10.1128/MCB.01529-06

Veloso, A., Kirkconnell, K. S., Magnuson, B., Biewen, B., Paulsen, M. T., Wilson, T. E., et al. (2014). Rate of elongation by RNA polymerase II is associated with specific gene features and epigenetic modifications. *Genome Res.* 24, 896–905. doi: 10.1101/gr.171405.113

Wang, J., Telese, F., Tan, Y., Li, W., Jin, C., He, X., et al. (2015). LSD1n is an H4K20 demethylase regulating memory formation via transcriptional elongation control. *Nat. Neurosci.* 18, 1256–1264. doi: 10.1038/nn.4069

Weller, M., Wick, W., Aldape, K., Brada, M., Berger, M., Pfister, S. M., et al. (2015). Glioma. *Nat. Rev. Dis. Primer* 1:15017. doi: 10.1038/nrdp.2015.17

White, M. G., Nagar, S., Aschebrook-Kilfoy, B., Jasmine, F., Kibriya, M. G., Ahsan, H., et al. (2016). Epigenetic Alterations and Canonical Pathway Disruption in Papillary Thyroid Cancer: A Genome-wide Methylation Analysis. *Ann. Surg. Oncol.* 23, 2302–2309. doi: 10.1245/s10434-016-5185-4

Wu, M.-Y., Fu, J., Xiao, X., Wu, J., and Wu, R.-C. (2014). MiR-34a regulates therapy resistance by targeting HDAC1 and HDAC7 in breast cancer. *Cancer Lett.* 354, 311–319. doi: 10.1016/j.canlet.2014.08.031

Xu, Z., Taylor, J. A., Leung, Y.-K., Ho, S.-M., and Niu, L. (2016). oxBS-MLE: an efficient method to estimate 5-methylcytosine and 5-hydroxymethylcytosine in

paired bisulfite and oxidative bisulfite treated DNA. *Bioinforma. Oxf. Engl.* 32, 3667–3669. doi: 10.1093/bioinformatics/btw527

Yang, H., Pesavento, J. J., Starnes, T. W., Cryderman, D. E., Wallrath, L. L., Kelleher, N. L., et al. (2008). Preferential dimethylation of histone H4 lysine 20 by Suv4-20. *J. Biol. Chem.* 283, 12085–12092. doi: 10.1074/jbc.M707974200

Yokoyama, Y., Matsumoto, A., Hieda, M., Shinchi, Y., Ogihara, E., Hamada, M., et al. (2014). Loss of histone H4K20 trimethylation predicts poor prognosis in breast cancer and is associated with invasive activity. *Breast Cancer Res. BCR* 16:R66. doi: 10.1186/bcr3681

Yuan, J., Yang, F., Chen, B., Lu, Z., Huo, X., Zhou, W., et al. (2011). The histone deacetylase 4/SP1/microrna-200a regulatory network contributes to aberrant histone acetylation in hepatocellular carcinoma. *Hepatol. Baltim. Md* 54, 2025–2035. doi: 10.1002/hep.24606

Zibetti, C., Adamo, A., Binda, C., Forneris, F., Toffolo, E., Verpelli, C., et al. (2010). Alternative splicing of the histone demethylase LSD1/KDM1 contributes to the modulation of neurite morphogenesis in the mammalian nervous system. *J. Neurosci. Off. J. Soc. Neurosci.* 30, 2521–2532. doi: 10.1523/JNEUROSCI.5500-09.2010

Conflict of Interest: The authors declare that the research was conducted in the absence of any commercial or financial relationships that could be construed as a potential conflict of interest.

frontiers in Cell and Developmental Biology

REVIEW
published: 27 August 2021
doi: 10.3389/fcell.2021.688789

Role of Mitochondria in Neurodegenerative Diseases: From an Epigenetic Perspective

*Sutong Xu[1,2], Xi Zhang[1,2], Chenming Liu[1,2], Qiulu Liu[1,2], Huazhen Chai[1,2], Yuping Luo[1,2] and Siguang Li[1,2]**

[1] Key Laboratory of Spine and Spinal Cord Injury Repair and Regeneration of Ministry of Education, Orthopedic Department of Tongji Hospital, Tongji University School of Medicine, Shanghai, China, [2] Stem Cell Translational Research Center, Tongji Hospital, Tongji University School of Medicine, Shanghai, China

Mitochondria, the centers of energy metabolism, have been shown to participate in epigenetic regulation of neurodegenerative diseases. Epigenetic modification of nuclear genes encoding mitochondrial proteins has an impact on mitochondria homeostasis, including mitochondrial biogenesis, and quality, which plays role in the pathogenesis of neurodegenerative diseases like Alzheimer's disease, Parkinson's disease, Huntington's disease, and amyotrophic lateral sclerosis. On the other hand, intermediate metabolites regulated by mitochondria such as acetyl-CoA and NAD^+, in turn, may regulate nuclear epigenome as the substrate for acetylation and a cofactor of deacetylation, respectively. Thus, mitochondria are involved in epigenetic regulation through bidirectional communication between mitochondria and nuclear, which may provide a new strategy for neurodegenerative diseases treatment. In addition, emerging evidence has suggested that the abnormal modification of mitochondria DNA contributes to disease development through mitochondria dysfunction. In this review, we provide an overview of how mitochondria are involved in epigenetic regulation and discuss the mechanisms of mitochondria in regulation of neurodegenerative diseases from epigenetic perspective.

Keywords: mitochondria, metabolism, mtDNA, epigenetics, neurodegenerative diseases

OPEN ACCESS

Edited by:
Xuekun Li,
Zhejiang University, China

Reviewed by:
Apiwat Mutirangura,
Chulalongkorn University, Thailand
Yujing Li,
Emory University, United States

***Correspondence:**
Siguang Li
siguangli@163.com

Specialty section:
This article was submitted to Epigenomics and Epigenetics, a section of the journal Frontiers in Cell and Developmental Biology

Received: *31 March 2021*
Accepted: *10 August 2021*
Published: *27 August 2021*

Citation:
Xu S, Zhang X, Liu C, Liu Q, Chai H, Luo Y and Li S (2021) Role of Mitochondria in Neurodegenerative Diseases: From an Epigenetic Perspective. Front. Cell Dev. Biol. 9:688789. doi: 10.3389/fcell.2021.688789

INTRODUCTION

Mitochondria originated from *Alphaproteobacteria* with a circular genome packaged into DNA–protein assemblies. The mammalian mitochondrial genome is 16.6 kb and encodes 37 genes, including 2 ribosomal RNAs (12S and 16SrRNA), 22 tRNAs, and 13 core component proteins of the respiratory electron transport chain (ETC). Some miRNAs and lncRNAs are found transcript from mitochondria DNA (mtDNA; Mercer et al., 2011; Rackham et al., 2011). Mitochondrial function is regulated by both nuclear and mitochondrial genome, since most of proteins in mitochondria

are encoded by nuclear and transported into mitochondria leading by mitochondrial targeting sequences. Indeed, next to producing energy, other mitochondrial functions have come into focus. Mitochondria are involved in metabolic processes and modulate several signal transduction pathways. The crosstalk between nucleus and mitochondria is identified as bidirectional micronucleus communication, which is essential for maintaining cell homeostasis and shaping diseases (Quirós et al., 2016; Mottis et al., 2019). Specially, the micronucleus communication is involved in epigenetic regulation (Bellizzi et al., 2012; Quirós et al., 2016). Epigenetic regulation, responding to environmental stimulation to regulate gene expression without changing the genome, is primarily divided into DNA methylation, histone post-translational modification (acetylation, methylation, etc.), chromatin open state and non-coding RNA regulation. Nuclear epigenome can drive changes in mitochondria functions, and in turn, signaling molecules mediated by metabolites can travel from mitochondria to nucleus which may play a role in nuclear epigenetic regulation. Mitochondrial metabolic intermediates, such as acetyl-CoA and NAD^+, are the substrate for acetylation and a cofactor of deacetylation, respectively, (**Figure 1**). *S*-adenosine methionine (SAM) is involved in both DNA and histone methylation. It is produced through the coupling of folate and methionine cycles in the cytoplasm, which is maintained by one-carbon (One-C) metabolism in mitochondria (**Figure 1**). Moreover, α-Ketoglutarate, a key intermediate in the tricarboxylic acid (TCA) cycle of oxidative phosphorylation (OXPHOS), is required for Jumonji C domain demethylases and DNA demethylase translocation (TET) as cofactors (Xu et al., 2011; **Figure 1**). These intermediates may directly or indirectly provide by mitochondria and affect the epigenetic regulation of the nuclear genome. In addition, although the mitochondrial genome lacks histones, mtDNA can be modified by methyltransferase to participate in epigenetic regulation. In recent years, there has been an increasing interest in mtDNA methylation in neurodegenerative diseases.

Mitochondria are bimembranous organelles whose inner membranes fold inwards into a crista-like structure and contain five enzyme complexes OXPHOS (complex I–V). They synthesize ATP through the ETC, which supports the biosynthesis and metabolic demand of cells. Normal integrity and function are very important for the maintenance of cell vitality. Mitochondria are dynamic organelles that can adapt to physiological changes by changing their morphology or number. A number of studies have shown the importance of mitochondrial dysfunction in the pathogenesis of neurodegenerative diseases such as Alzheimer's disease (AD), Parkinson's disease (PD), amyotrophic lateral sclerosis (ALS), and Huntington's disease (HD; Lin and Beal, 2006; Yao et al., 2009; Chaturvedi and Flint Beal, 2013). In these diseases, mitochondria are characterized by decreased activity of respiratory chain enzyme, abnormal morphology, and more mutations in mtDNA (Chaturvedi and Flint Beal, 2013). Regulating mitochondrial function or changing mitochondrial metabolites is a strategy to treat neurodegenerative diseases.

This review will focus on the role of the mitochondria in the epigenetic regulation of neurodegenerative diseases, including how nuclear epigenome affects mitochondrial function and mitochondrial epigenetic regulation.

MITOCHONDRIA ARE INVOLVED IN THE PATHOGENESIS OF SEVERAL NEURODEGENERATIVE DISEASES

The Maintenance of Mitochondrial Homeostasis Determines the Normal Function of Mitochondria

As energy supply station, mitochondria maintain their homeostasis and keep functional in many ways, including mitochondrial biogenesis, mitochondrial dynamics, mitophagy, and apoptosis.

Mitochondria biogenesis is the progress that new mitochondria are producted from existing one. In mammals, mitochondrial transcription begins at D-Loop region where the mitochondrial RNA polymerase (POLRMT) and the mitochondrial transcription factor A (TFAM) interact directly to bind transcription start site to regulate mtDNA transcription. Mitochondrial transcription factor B2 is a key factor assisting POLRMT in promoting mitochondrial RNA transcription initiation. Transcriptional termination is then regulated by Mitochondrial Transcription Termination Factor 1. In addition, the proliferator-activated receptor γ coactivator-1 (PGC1) family (PGC1-α and PGC1-β) and several transcription factors subsequently regulated by PGC1-related cofactor (PRC), including NRF1, NRF2, and YIN-YANG 1 (YY1), affect mitochondrial gene expression (Vercauteren et al., 2006, 2008, 2009; Cunningham et al., 2007; Shao et al., 2010; **Figure 2**).

Mitochondria are highly dynamic organelle undergo continuous fusion and fission events to keep their shape and size normal, which is mediated by GTPases, including dleprotein-like protein 1 (DRP1), mitochondrial fusion protein 1 (MFN1), mitochondrial fusion protein 2 (MFN2), and optic nerve atrophy protein 1 (OPA1). MFN1 and MFN2 are transmitochondrial extramembrane proteins that regulate mitochondria fusion, while DRP1 remains in the cytoplasm until it is recruited to outer mitochondrial membrane (OMM) for fission (Koshiba et al., 2004; **Figure 2**). OPA1 is in the inner mitochondrial membrane (IMM) and plays a role in balancing the fission and fusion of mitochondria (Friedman and Nunnari, 2014; **Figure 2**).

Mitophagy, another form of mitochondrial quality maintenance, is mainly mediated by PINK1 and Parkin (**Figure 2**). PINK1 is a constitutive circulating kinase on the OMM, and Parkin is an E3 ubiquitin ligase which can be phosphorylated at Ser65 in UBL domain by PINK1 and recruited to damaged mitochondria to polyubiquitinates its substrates (Pickrell and Youle, 2015). Autophagy receptor proteins such as SQSTM1/P62 combined with LC3, bind ubiquitinated cargo and connect them to the autophagosome, then the autophagosome is eliminated by lysosome (Pickrell and Youle, 2015).

Reactive oxygen species (ROS)-mediated mitochondrial oxidative stress damage can induce cell apoptosis. ROS such as superoxide anion (O2●-), hydroxyl radical (OH●), and stable

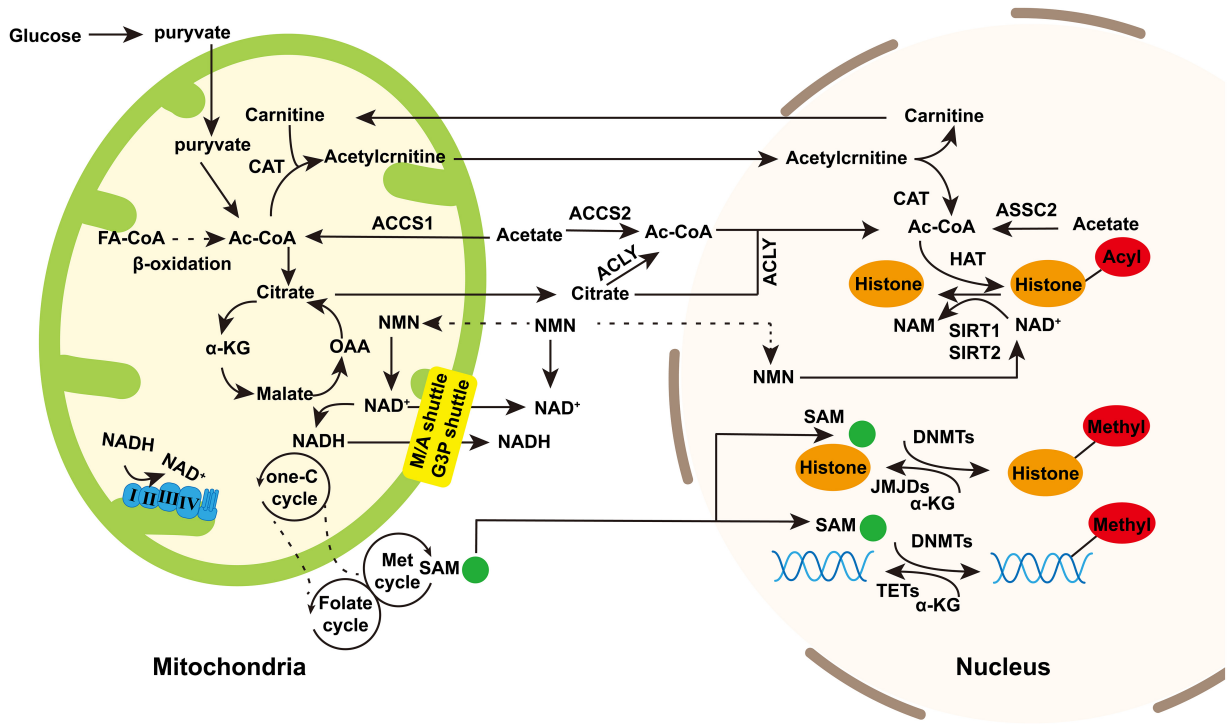

FIGURE 1 | The regulation of mitochondrial intermediate metabolites to nuclear epigenetics. Mitochondria provide substrates for nuclear epigenetics such as DNA or histone methylation and histone acetylation/deacetylation. Acetyl-CoA is the source of acetyl groups used in histone acetylation. It is produced during fatty acid synthesis and glycolysis. Besides, acetate is catalyzed by ASSC1 in mitochondria and ASSC2 in cytoplasm and nucleus to generate acetyl-CoA. Acetyl-CoA in the nucleus and cytoplasm can be exchanged through nuclear pores. Acetyl-CoA enters into TCA cycle to produce citrate in mitochondria which is transported into cytoplasm and then catalyzed by ACLY to regenerate acetyl-CoA. Acetyl-CoA produced in mitochondria can also be regenerated in nucleus trough carnitine/acylcarnitine translocator. NAD^+ is the cofactor of sirtuins in deacetylation. In TCA cycle, NAD^+ is converted into NADH, and then NADH reconverted into NAD^+ by complex I and III in OXPHOS. NAD^+/NADH in mitochondria can be exchanged in cytoplasm and mitochondria through malate/aspartic acid shuttle and glyceraldehyde-3-phosphate shuttle. NAM is potentially transported into mitochondria and nucleus to generate NAD^+. *S*-adenosine methionine (SAM) is generated through the coupling of the folate and methionine cycles in the cytosol and sustained by the one-carbon (one-C) metabolism in mitochondria. SAM can enter into nucleus as the source of methyl group in histone or DNA methylation. α-Ketoglutarate (α-KG), the intermediate of TCA cycle, can enter into nucleus as the cofactor of JMJDs and histone demethylases and TET DNA demethylases. Dashed arrows indicate potentially indirect connections or pathways that need further validation. Abbreviations: FA-CoA, fatty acyl CoA; ac-CoA, acetyl-CoA; CAT, carnitine acetyltransferase; OAA, oxaloacetic acid; ACLY, ATP-citrate lyase; NMN, nicotinamide mononucleotide; M/A shuttle, malate/aspartate shuttle; and G3P shuttle, glyceraldehyde 3-phosphate shuttle.

hydrogen peroxide (H_2O_2) mainly come from ETC where some H^+ leak from the complex I and III and react with dioxygen (Murphy, 2009). The superoxide dismutases (SODs) family, including the mitochondrial MnSOD (SOD2) and the intracellular (SOD1) or extracellular (ECSOD, SOD3) isoforms of Cu/ZnSOD, catalyze the superoxide anions into oxygen and hydrogen peroxide. Then, hydrogen peroxide is converted into water by glutathione peroxidase and catalase, acting as an additional antioxidant defense (Lubos et al., 2011; Dimauro et al., 2020). The imbalance between ROS and the antioxidant defense system causes oxidative stress damage, which is one of the causes of mitochondrial dysfunction and cell apoptosis.

Mitochondria Dysfunction Is Crucial for the Pathogenesis of Neurodegenerative Diseases

Neurodegenerative diseases are complex diseases regulated by heredity and environment, which are characterized by a gradual loss of neuronal function and the gradual deterioration with the progress of neurodegenerative diseases. Imbalance of mitochondrial homeostasis is present in AD, PD, HD, and ALS, which is shown in **Figure 2**.

Alzheimer's disease characterized by a decline in cognitive function is the most common cause of dementia (Battle, 2013). It is divided into early-onset familiar AD and late-onset sporadic AD. The accumulation of beta-amyloid (Aβ) and phosphorylated Tau (pTau) in the brain is a pathological feature of AD (Hyman et al., 2012). Aβ and pTau affect mitochondrial integrity and aggravate mitochondrial dysfunction (Tönnies and Trushina, 2017). Meanwhile, damaged mitochondria induce excessive oxidative stress which promotes the accumulation of these two proteins in turn (Tönnies and Trushina, 2017). The oxidative damage induced by Aβ and pTau leads to the decrease protein levels of PINK1 and Parkin, which inhibits mitochondrial autophagy, thereby increasing the amount of Aβ and pTau (Kerr et al., 2017). Aβ and pTau induce the enlargement of mitochondrial permeability transition pore

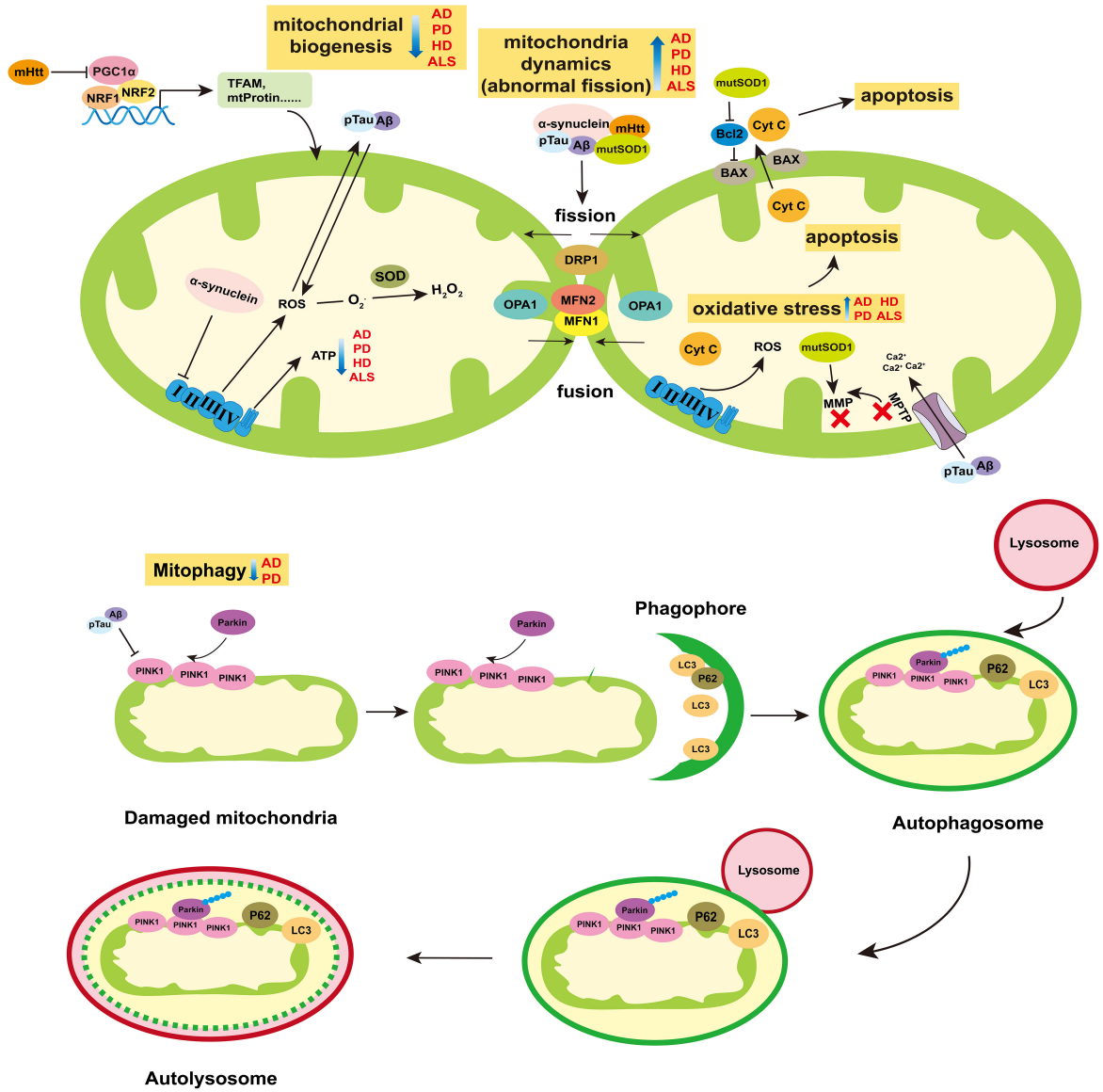

FIGURE 2 | Role of mitochondria in neurodegenerative diseases. The breakdown of mitochondrial homeostasis is considered to play crucial role in the pathogenesis of neurodegenerative diseases. Mitochondrial biogenesis, dynamics, mitophagy, and ROS-mediated cell apoptosis are ways for mitochondria to maintain homeostasis. The ability of mitochondrial biogenesis is reduced in AD, PD, HD, and ALS. Particularly, the mHtt can suppress the activity of PGC1α, which is the main cause of mitochondria dysfunction in HD. Abnormal mitochondrial division appear in AD, PD, HD, and ALS. The pTau and Aβ of AD, α-synuclein of PD, mHtt of HD and mutSOD of ALS can increase the protein levels of mitochondria fission (DRP1), and reduce mitochondria fusion (MFN1/2 and OPA1). The release of ROS increases in those four diseases, which can induce oxidative stress and then mediate cell apoptosis. In AD and PD, mitophagy is blocked, which prevents the damaged mitochondria from being removed effectively. Moreover, α-synuclein can inhibit the activity of complex I of ETC. pTau and Aβ can enlarge the MPTP to decrease the MMP, which can reduce the synthesis of ATP. Besides, the mutSOD can destroy the MMP and have impair on mitochondria functions. Abbreviations: AD, Alzheimer's disease; PD, Parkinson's disease; HD, Huntington's disease; ALS, amyotrophic lateral sclerosis; Aβ, β-Amyloid protein; pTau, phosphorylated Tau; mHtt, mutation Htt protein; mutSOD, mutation SOD protein; MMP, mitochondrial membrane potential; and MPTP, Mitochondrial Permeability Transition Pore.

(mPTP), destroy the permeation barrier of IMM, and lead to the decrease of intermembrane potential (Szeto, 2014; Quntanilla and Tapia-Monsalves, 2020). At the same time, cyt C and other pro-apoptotic proteins escape into the cytoplasm through mPTP and trigger cell apoptosis and death (Szeto, 2014). In addition, abnormal mitochondrial fission and decreased expression of mitochondrial biogenesis-related proteins (PGC-1α, TFAM, and NRF2) were found in AD patients, AD mouse models and AD cell models, which indicates that mitochondria dynamic and biogenesis are impaired (Manczak et al., 2011; Rice et al., 2014). On the other hand, mutations in amyloid precursor protein (APP), presenilin-1 (PS1), and presenilin-2 loci contribute to the early onset of familial AD, which is considered to predispose to greater

mitochondrial dysfunction (Manczak et al., 2011; Hyman et al., 2012; Rice et al., 2014).

Parkinson's disease is characterized by cardinal motor manifestations of tremor and bradykinesia, the signature clinical manifestation of which is a decrease in dopamine neurons and dopamine level in the substantia nigra pars compacta (Samii et al., 2004). It is divided into familiar PD and sporadic PD. The causes of PD include mitochondrial dysfunction, abnormal protein aggregation, chronic inflammation, and oxidative imbalance (Subramaniam and Chesselet, 2013; Bose and Beal, 2016; Rocha et al., 2018). Reduced activity of ETC complex I is found in PD substantia nigra (SN). Interestingly, the neurotoxin 1-Methyl-4-phenyl-1,2,3,6-tetrahydropyridine (MPTP), which targets mitochondrial complex I, induces animal phenotypes similar to PD (Ballard et al., 1985). In dopamine neurons, mitochondrial dysfunction is an important cause of oxidative stress which plays an important role in the production of neurotoxins. Besides, α-synuclein aggregates to form Lewy bodies or Lewy neurites, which are also one of the pathological features of PD (Gorbatyuk et al., 2008; Volpicelli-Daley et al., 2011, 2014). The accumulation of α-synuclein in the outer membrane may interfere with the protein import mechanism (Rocha et al., 2018). And growing evidence show that α-synuclein can affect mitochondrial dynamics, particularly by disrupting the mitochondrial fusion (Kamp et al., 2010; Nakamura et al., 2011; Fabian and Sonenberg, 2012). In addition, there are several pathogenic genes of familial PD. For example, SCNA and LRRK2 control autosomal dominant PD, while Parkin, PINK1 and ATP13A2 control autosomal recessive PD.

Huntington's disease is characterized by the presence of aggregation of Huntington mutated protein (mHtt), and the main clinical symptoms of HD are cognitive decline, progressive dyslexia, and psychiatric disorders. MHtt binds to DRP1 to trigger mitochondrial abnormal fission. The mRNA levels of DRP1 and FIS1 increase with the progression of HD, but the expression of MFN1/2 does the opposite (Kim et al., 2010; Shirendeb et al., 2011; Song et al., 2011). MHtt interacts with autophagy receptors, preventing them from binding to damaged mitochondria and preventing autophagosomes from engorging abnormal mitochondria (Martinez-Vicente et al., 2010). Particularly, mHtt can inhibit PGC-1α and reduce mitochondrial biogenesis, which is a common root cause of mitochondrial dysfunction in HD (Chaturvedi et al., 2009; Johri et al., 2013).

Amyotrophic lateral sclerosis is characterized by progressive neurodegeneration in brain and spinal cord (Kwong et al., 2006). Oxidative stress caused by the production and accumulation of ROS is one of the main factors of ALS pathology (Cozzolino et al., 2008). Mutation of Cu/Zn SOD1 gene is the main manifestation of ALS (Rosen, 1993). The accumulation of mutated SOD (mutSOD) protein in mitochondria may cause mitochondrial dysfunction through a variety of ways. It damages the mitochondrial membrane, resulting in reduced mitochondrial membrane potential (MMP), mitochondrial swelling, and vacuolar degeneration (Wong et al., 1995; Kong and Xu, 1998). The mutSOD binds to the apoptotic regulator Bcl-2 to alter the electrical conductivity of voltage dependent anionchannel, reduce ATP production, and increase calcium accumulation (Guégan et al., 2001; Takeuchi et al., 2002; Kirkinezos et al., 2005; Ferri et al., 2006). Formation of the toxic mutSOD1/Bcl-2 complex leads to conformational changes in Bcl-2, as well as mitochondrial dysfunction, including altered mitochondrial morphology, disruption of mitochondrial membrane integrity, and increased release of cyt C (Pedrini et al., 2010). Moreover, expression of mutSOD1 in neurons decreased the expression level of OPA1 and increased the level of phosphorylated DRP1, which induces abnormal mitochondrial fragmentation (Ferri et al., 2010).

MITOCHONDRIA ARE INVOLVED IN NUCLEAR EPIGENETIC REGULATION IN NEURODEGENERATIVE DISEASES

DNA methylation means that DNA is methylated by adding a methyl group at the 5′ position of the cytosine to produce 5-methylcytosine (5mC), which usually occurs at cytosine-phosphate-guanine (CpG) islands. The key step of methylation is mediated by three DNA methyltransferases (DNMT): DNMT1, DNMT3A, and DNMT3B. DNMT1 preferentially methylates hemimethylated DNA and maintains genomic DNA methylation patterns following DNA replication, while DNMT3A and DNMT3B have the responsible to *de novo* methylation of DNA (Pradhan et al., 1999; Ramsahoye et al., 2000).

Data from several studies suggest that nuclear genomic DNA methylation can affect the development of PD by regulating mitochondria functions. Previous studies have shown no PARK2 (Parkin) differential DNA methylation in the brains of PD patients and healthy controls (De Mena et al., 2013). Recently, the methylation levels of parkin promoter were significantly reduced in early-onset Parkinson's disease patients shown in the epigenome-wide association study (Eryilmaz et al., 2017). Moreover, in SN of sporadic PD, DNA hypermethylation was found in the promoter of PGC-1α, an important transcription factor that regulates the mitochondria biological functions (Su et al., 2015).

Mitochondria can indirectly regulate the production of SAM and affect the nuclear epigenome (**Figure 1**). SAM, a methionine metabolite, is a source of methyl groups used in the nucleus for histone and DNMT. One-C metabolism includes the folate cycle and the methionine cycle. 5-methyl-THF (5-MTHF), an intermediate product of the folate cycle in the cytoplasm, participates in methylation of homocysteine to methionine, which enters the methionine cycle to produce SAM (Ormazabal et al., 2015). The connection between mitochondria and cytoplasm is through the exchange of One-C donors such as serine and glycine (Tibbetts and Appling, 2010). Mitochondria are unable to synthesize SAM due to lack of methionine adenosyltransferase activity, so the SAM synthesized in cytoplasmic is transferred into mitochondria through methionine carriers/transporters (Agrimi et al., 2004). The mitochondrial One-C cycle and ATP maintain the synthesis of SAM in the cytoplasm. SAM is used by DNMTs and then it converted into *S*-adenosine homocysteine (SAH;

Chiang et al., 1996). SAH rapidly hydrolyzes to Homocysteine (Hcy), which is then catabolized or remethylated to methionine (Medina et al., 2001). Changes in carbon metabolism can directly affect DNA methylation through SAM and SAH levels and regulation of methyltransferase activity. Late-onset AD is associated with hyperhomocysteinemia which is influenced by diet (vitamin B6, vitamin B12, and folic acid; Fuso et al., 2008). Vitamin B deficiency induced the accumulation of Hcy and SAH, thus impeding methyltransferase activity (Fuso et al., 2011). Specific demethylation of PS1 promoter sites resulted in overexpression of PS1 and upregulation of γ-secretase activity, which might promote overproduction of Aβ (Li et al., 2015). Folic acid deficiency increased the protein levels of APP, PS1, and Aβ proteins in hippocampus (Li et al., 2015). After folic acid supplementation, APP and PS1 promoter methylation rates increased and APP, PS1, and Aβ protein levels decreased (Li et al., 2015).

MITOCHONDRIA GENOME METHYLATION IS INVOLVED IN NEURODEGENERATIVE DISEASES

Methyltransferases Are Diverse in Mitochondria

The present of mtDNA methylation is controversial because of imperfect detection methods (van der Wijst and Rots, 2015). Although the earliest studies reported that mtDNA was not methylated, subsequent studies found low levels of CpG dinucleotide methylation in mitochondria of several species (Nass, 1973; Number et al., 1983; Pollack et al., 1984). In human colon carcinoma cells (HCT116) and mouse embryonic fibroblasts cells (MEFs), DNMT1 transcriptional variants were found to translocated to mitochondria driven by mitochondrial targeting sequences and bound to a unique non-coding region called D-Loop (Shock et al., 2011). D-Loop is the start of mitochondrial DNA replication and transcription, where has two promoters, namely heavy chain promoter (HSP) and light chain promoter. DNMT3A was not found in MEFs and HCT116 cell lines, however, according to further studies, it was found in motor neurons (Chestnut et al., 2011; Shock et al., 2011). It indicates that these methyltransferases in mitochondria may be tissue specific. In addition, DNMT1 and low expression level of DNMT3B were observed in the mitochondria of mouse 3T3-L1 and HeLa cells, and inactivation of these two transmethylase could reduce methylation levels at CpG site (Bellizzi et al., 2013).

The demethylation pathway may play a role in mitochondria. One of DNA demethylation mechanisms is initiated by the oxidation of 5mC to 5-hydroxymethylcytosine (5hmC) by ten-eleven translocation (TET) enzymes (Ito et al., 2011). Both TET1 and TET2 are showed in the mitochondria, along with the presence of 5hmC in the D-Loop (Bellizzi et al., 2013). Additionally, evidence presented that 5mC and 5hmC existed stably at cytosine without guanine base in mtDNA, suggesting the role of non-CpG methylation in mtDNA (Bellizzi et al., 2013). CpG and non-CpG methylation sites are in HSP promoter regions and conserved sequence blocks, thus the epigenetic modifications may adjust mtDNA copy and transcription (Ito et al., 2011).

The Extent of mtDNA Methylation Varies Among Neurodegenerative Diseases Compared With Controls

The methylation level of mtDNA changes dynamically with the development of AD. Initial dot blot analysis showed that mitochondrial 5hmC levels in superior and middle temporal gyrus of preclinical AD and late-stage AD subjects were elevated, but it remained further verification due to the small number of samples used (Bradley-Whitman and Lovell, 2013). A later study found that mitochondrial 5mC levels in D-Loop region of mtDNA in the entorhinal cortex were increased in human postmortem brains with AD-related pathology (stages I to II and stages III to IV of Braak and Braak) compared with control cases, and the methylation levels were higher in early stages (stages I/II) than in later stages (stages III/IV; Blanch et al., 2016). Whereas, another study showed the mitochondrial D-Loop methylation levels in peripheral blood of late-onset Alzheimer's disease patients were significantly lower than those of healthy controls (Stoccoro et al., 2017). The reason about the differences in results may be that the samples used in studies represent different phenotype classification of PD and came from different tissues.

Mitochondria DNA methylation levels may be reduced in ALS caused by superoxide dismutase-1 (SOD1) mutation. In postmortem ALS patients, DNMT1 and DNMT3A were observed at the nucleus and mitochondria of the motor cortex, and increased levels of DNMT3A protein were detected at the nuclear, soluble, and mitochondrial fractions (Chestnut et al., 2011). DNMT3A was also observed in mitochondria of adult mouse CNS, skeletal muscle and testis, and adult human cerebral cortex (Wong et al., 2013). The mitochondrial DNMT3A protein levels were significantly reduced in skeletal muscle and spinal cord at presymptomatic or early stage of disease in human *SOD1* transgenic mouse models of ALS (Wong et al., 2013). Subsequent studies reported that ALS patients, especially those with *SOD1* and Chromosome 9 Open Reading Frame 72 (*C9ORF72*) mutations, had an inverse correlation between the D-Loop methylation levels and mtDNA copy number (Stoccoro et al., 2018). However, only *SOD1* mutations resulted in a significant decrease in D-Loop methylation levels, suggesting that demethylation in the D-Loop region may represent a compensatory mechanism of mtDNA upregulation to counteract oxidative stress in ALS-linked *SOD1* mutation carriers (Stoccoro et al., 2018). The latest finding further confirmed this result. Patients with *SOD1* mutation and sporadic ALS patients showed lower levels of D-Loop methylation, while *C9ORF72*-ALS patients showed no significant difference in levels of D-Loop methylation compared with controls (Stoccoro et al., 2020). Therefore, the pattern of mtDNA methylation varies among diseases and mtDNA methylation levels may change along with the progression of the neurodegenerative

diseases. However, further research is needed to identify the accurate mitochondrial gene methylation sites and elucidate their biological significance.

MITOCHONDRIA ARE INDIRECTLY INVOLVED IN HISTONE ACETYLATION/DEACETYLATION VIA ACETYL-CoA AND NAD$^+$ IN NEURODEGENERATIVE DISEASES

Acetyl-CoA Provided by Mitochondria Indirectly Affects Histone Acetylation and Benefits for AD Treatment

Histone acetyl transferases (Hats) transfer an acetyl group from acetyl-CoA to lysine ε-amino residues, which relaxes chromatin and increases the binding potential of transcriptional activators. Acetyl-CoA, the only donor of histone acetylation, is dynamically correlated with the acetylation levels of histones and transcription factors (Cai et al., 2011; Pietrocola et al., 2015; Shi and Tu, 2015). The acetyl-CoA levels are positively regulated by energy state in cells. When energy production is abundant, levels of acetyl-CoA are increased to promote histone acetylation and gene expression, and conversely, low energy reduces acetyl-CoA levels, thereby decreasing histone acetylation and inhibiting gene expression through chromatin concentration (Menzies et al., 2016).

Acetyl-CoA can be produced in cytoplasm, mitochondria and nucleus, and there are interactions between different pool of acetyl-COA. In mitochondria, acetyl-CoA is primarily synthesized by three pathways, including: (1) glycolysis; (2) β-oxidation of fatty acids (Rufer et al., 2009); and (3) the catabolism of branched amino acids (Harris et al., 2005). Besides, the mitochondrial enzyme acetyl-CoA synthetase short-chain family member 1 (ACSS1) can employ acetate to generate acetyl-CoA (Fujino et al., 2001; **Figure 1**). Acetyl-CoA synthesized in mitochondria cannot penetrate the mitochondrial membrane to reach the cytoplasm. Nevertheless, acetyl-CoA usually enters the TCA cycle to generate free CoA and citrate which can be exported from mitochondria via the mitochondrial tricarboxylate transporter (SLC25A1) and then catalyzed by ATP-citrate lyase (ACLY) to produce acetyl-CoA in cytosol and nucleus (Wellen et al., 2009; Zaidi et al., 2012; Pietrocola et al., 2015; **Figure 1**). Alternatively, the acetylcarnitine formed in the mitochondria is transported to cytoplasm by carnitine/acylcarnitine translocator and then enters the nucleus where acetylcarnitine is converted into acetyl-CoA by nuclear carnitine acetyltransferase (Madiraju et al., 2009; **Figure 1**). In cytosol and nucleus, acetyl-CoA can be generated from acetate by short-chain family member 2, a cytosolic counterpart of ACSS1 (Schug et al., 2015; **Figure 1**). Besides, acetyl-CoA synthesized in the cytoplasm can enter the nucleus directly (**Figure 1**).

The kinetics of histone acetylation largely depends on the concentration of acetyl-CoA, especially the ratio of acetyl-CoA to free CoA (Pietrocola et al., 2015). Studies suggest that the level of acetyl-CoA in mitochondria may influence histone acylation, though this requires direct evidence. For example, TP53 inducible glycolysis and apoptosis regulator (TIGAR), an endogenous inhibitor of glycolysis, was significantly increased during brain development as neural differentiation proceeding, especially in a rapid growth period of NSC differentiation (Zhou et al., 2019). Knocking out TIGAR could reduce the mRNA level of *ACLY* as well as acetyl-CoA production in mitochondria (Zhou et al., 2019). Simultaneously, levels of acetyl-CoA and H3K9 acetylation were also decreased at the promoter of NSC differentiation-related genes such as *Gfap*, *Neurod*, and *Ngn1* (Zhou et al., 2019). CMS12 and J147, two AD drug candidates, maintain mitochondrial homeostasis by regulating acetyl-CoA metabolism. They played a neuroprotective role by increasing acetyl-CoA production and increasing H3K9 acetylation in aging accelerated mouse tendency 8 (SAMP8) mice (Currais et al., 2019). Thus, increasing the level of acetyl-CoA can also be used as a drug target of inducing NSC differentiation and treating AD, but more evidence is needed to confirm it.

NAD$^+$ Provided by Mitochondria Indirectly Affects Histone Deacetylation Through Sirtuins

Histone deacetylases (HDACs) remove acetyl groups, resulting in chromatin contraction and gene transcription suppression. Sirtuins (SIRT1–SIRT7) are the only type of HDACs whose activities require NAD$^+$ and are affected by the fluctuation of NAD$^+$/NADH (Haigis and Sinclair, 2010). NAD$^+$ is a cofactor of sirtuin deacetylase, which removes the acetyl group from the lysine residue of protein in an NAD$^+$-dependent manner to produce nicotinamide (NAM) and acyl-ADP-ribose (Lautrup et al., 2019; **Figure 1**).

The sources of NAD$^+$ in cells include diet, tryptophan synthesis and NAD$^+$ depletion and recovery (Verdin, 2015; Lautrup et al., 2019). NAD$^+$ distributes in the nucleus, cytoplasm and mitochondria, maintaining a constant balance between depletion and recycling. The cytoplasmic and nuclear NAD$^+$ pools may be balanced by diffusion through the nuclear pore (Cantó et al., 2015). Since the mitochondrial membrane is impermeable to both NAD$^+$ and NADH, a transport mechanism is required for their exchange between cytoplasmic and mitochondria (Stein and Imai, 2012). During glycolysis in cytoplasm, NAD$^+$ is convert to NADH which is transferred to mitochondrial matrix via malate/aspartic acid shuttle and glyceraldehyde-3-phosphate shuttle (Madiraju et al., 2009; **Figure 1**). In mitochondria, NAD$^+$ is reduced in the TCA cycle to produce multiple NADHs, and then NADHs are oxidized by complex I in ETC to produce NAD$^+$ (Verdin, 2015; **Figure 1**). Although NAD$^+$ is spread over in different compartments, the level of it in the cell may be limited (Pittelli et al., 2011). In yeast, malate-aspartic acid shuttle balances the NAD$^+$/NADH ratio between the cytoplasm and the mitochondrial pool. The increase ratio of mitochondrial NAD$^+$/NADH leads to the production of aspartic acid from malate via malate dehydrogenase (Mdh1) and asparagine (Aat1).

Aspartic acid is transported to the cytoplasm via the AGC1 carrier, and then aspartic acid converted to malic acid by cytoplasmic malate dehydrogenase (Mdh2) and asparagine (Aat2), resulting in an increased cytoplasmic NAD^+/NADH ratio (Easlon et al., 2008). It was also reported later that exogenous NAD^+ could make the NAD^+ level higher in mitochondria than in cytoplasmic, which indicated that the precursor or intermediate of NAD^+ could penetrate the mitochondrial membrane (Pittelli et al., 2011). NR, the NAD^+ precursor nicotinamide ribose, is likely to be converted into nicotinamide mononucleotide (NMN) in the cytoplasm, and NMN may pass through the mitochondrial membrane via nicotinamide mononucleotide adenosine transferase 1 (NMNAT) to produce NAD^+ (Yang et al., 2007). It was interesting that NR increased proliferation and induces neurogenesis in the hippocampal dentate gyrus and the subventricular zones of aged mice (Zhang H. et al., 2016). Thus, mitochondria are one of NAD^+ metabolism compartmentalization that may indirectly affect NAD^+ concentrations in the nucleus and cytoplasm.

The sirtuins protein family is distributed in different compartments of the cells, including nucleus (SIRT1, SIRT6, and SIRT7), cytoplasm (SIRT2), and mitochondria (SIRT3-5; Haigis and Sinclair, 2010). SIRT1-3 showed strong deacetyl kinase activity, while the activities of SIRT4–7 were weak *in vitro* (Michishita et al., 2005). SIRT1 and SIRT2 could acetylate histones or non-histone proteins, and they were able to travel between nucleus and cytoplasm, while SIRT3 primarily performed post-translational modification of proteins in mitochondria (Tanno et al., 2007; Jing and Lin, 2015). SIRT1 and SIRT2 were the most abundant sirtuins in cultured cells isolated from normal adult brain tissues (Jayasena et al., 2016). The expression level of SIRT1 was the highest in neurons, and SIRT2 was highly enriched in adult human frontal lobes (Jayasena et al., 2016).

SIRT1 and SIRT2 Play an Opposite Role in PD Under Mitochondria Dysfunction

In the PD cell model induced by rotenone, an inhibition of respiratory chain complex I, SIRT1 bound to H3K9 in the p53 promoter region, resulting in decreased H3K9 acetylation and increased H3K9 trimethylation, thereby inhibiting p53 gene transcription and reducing rotenone-induced apoptosis (Feng et al., 2015). 1-methyl-4-phenylpyridinium (MPP^+) is also an inhibitor of respiratory chain complex I, which may induce ROS production and increase HIF-1α expression in SH-SY5Y cells. Inhibiting SIRT1 expression could significantly increase H3K14 acetylation in the HIF-1α promoter region, leading to transcriptional activation (Dong et al., 2016). It was found in earlier years that the direct binding of α-synuclein to histones, which reduced the level of histone H3 acetylation in cultured cells and maybe cause the nuclear toxicity of α-synuclein (Kontopoulos et al., 2006). Further study demonstrated that HDAC inhibitor of SIRT2 could save the toxicity of α-synuclein in a PD cell model (Outeiro et al., 2007). A similar phenomenon was observed that oxidative stress induced the relocalization of α-synuclein into nucleus (Siddiqui et al., 2012). Then α-synuclein subsequently bound to the PGC1-α promoter, which resulted in histone deacetylation, thereby reducing the expression of PGC1-α and impaired mitochondrial function (Siddiqui et al., 2012). Therefore, in PD, increasing SIRT1 can repair mitochondrial dysfunction and plays a neuroprotective role. On the other hand, inhibiting SIRT2 can alleviate the toxicity of α-synuclein and may enhance mitochondrial function.

NON-CODING RNAS ARE INVOLVED IN NEURODEGENERATIVE DISEASES BY REGULATION MITOCHONDRIA FUNCTIONS

MiRNA, siRNA, piRNA, lncRNA, and circRNA are non-coding RNAs involved in epigenetic regulation (Panni et al., 2020). In mitochondria, non-coding RNAs are derived from nuclear or mitochondria genome. However, mitochondrial-encoded non-coding RNAs are rarely reported in the study of neurodegenerative diseases. And the process about how nuclear-encoded non-coding RNAs enter into mitochondria is unclear beside miRNA. One of hypotheses about how miRNAs enter into mitochondria is that the complex of AGO2 and miRNA crosses the OMM via SAM50 and TOM20 and then they are translocated into mitochondrial matrix through the IMM (Macgregor-Das and Das, 2018; **Figure 3**). Several miRNAs were found altered in mitochondrial fractions of hippocampal tissue after controlled cortical impact injury in rats, which suggested the regulation of mitochondrial miRNAs to cerebral nerve injury (Wang et al., 2015, 2021). It implies the possibility of mitochondrial miRNAs regulating neurodegenerative diseases, but the related research is still sparse.

The regulation of nuclear-encoded non-coding RNAs on mitochondrial function plays a crucial role in the onset or treatment of neurodegenerative diseases (Wu and Kuo, 2020). In this review, we will focus on the regulatory mechanisms of non-coding RNAs on mitochondrial homeostasis in neurodegenerative diseases.

MiRNAs Regulate Neurodegenerative Diseases by Targeting Genes Associated With Mitochondria Functions

MiRNAs are short non-coding RNAs regulating gene expression at post-transcription level. In cytoplasm, miRNAs, after being processed by Dicer, interact with Argonaute (AGO) proteins and assemble into RNA-induced silencing complex and then bind to the 3′ UTR region of mRNA to promote mRNA degradation or inhibit protein translation (Fabian and Sonenberg, 2012; **Figure 3**). MiRNAs can be transported between various cell compartments such as nucleus, cytoplasm and mitochondria to regulate the target mRNA translation or even transcriptional rate (Makarova et al., 2016). In addition, miRNAs can be secreted extracellularly as signaling molecules to mediate intercellular communication (O'Brien et al., 2018).

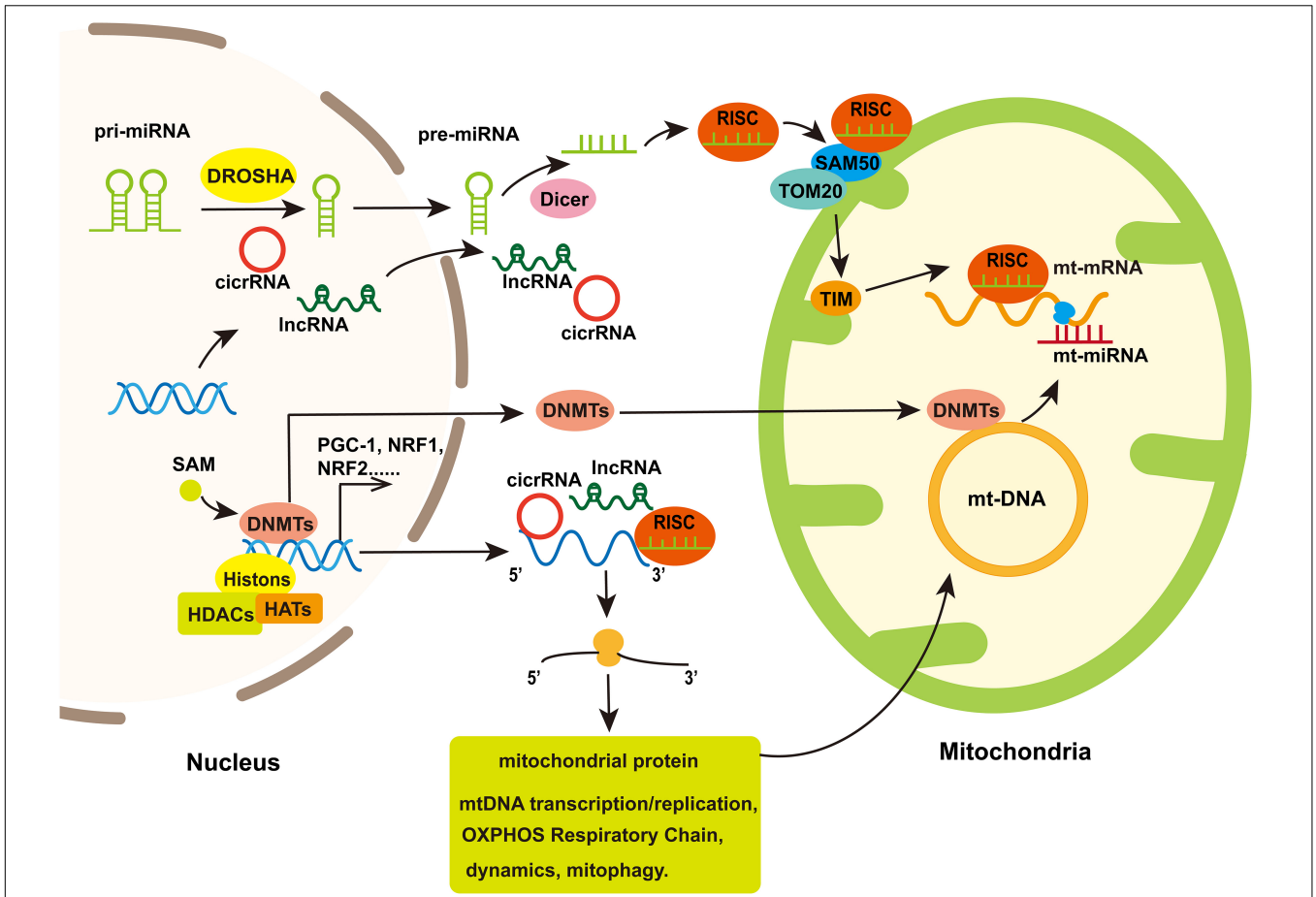

FIGURE 3 | The involvement of mitochondria in nuclear epigenetic regulation and mtDNA methylation. Mitochondrial genomes can be modified by methyltransferases which are transport from nuclear to mitochondria. Simultaneously, Histone acetylation/deacetylation and DNA methylation participate in the expression of nuclear-encoded genes regulated mitochondrial function including some transcription factor that regulated genes associated with mitochondrial biogenesis. Non-coding RNA, including miRNA, lncRNA, and cicrRNA, coded by nucleus genome or several miRNAs coded by mt-DNA, can regulate genes encoding part of proteins in mitochondria to influence mitochondria biogenesis, mitochondrial dynamics, mitophagy, and cell apoptosis. In addition, the nuclear-encoded miRNAs assemble with Ago to form the RNA-induced silencing complex (RISC), which is improved into the mitochondria through protein channels in mitochondria membrane and thereby regulate mt-mRNA translation.

MiRNAs targeting genes associated with mitochondria biogenesis and ECT activity have neuroprotective effects on diseases and provide potential therapeutic strategies for patients. The up-regulated expression of miR-590-3p and miR-144-3p in AD and PD disease models, respectively, to improve mitochondrial function by increasing the expression levels of PGC-1α, NRF1, and TFAM (Li et al., 2016; Wang J. et al., 2016). In AD, the innate immune system activated by oligomeric amyloid β42 (oAβ42) was likely to trigger chronic neuroinflammation (Salminen et al., 2009). *In vitro* study showed that oAβ42 stimulated the production of TNF-α in mitochondria, increased the expression level of miR-34a, and reduced the expression of five key proteins in the mitochondrial ETC, including NDUFC2 in complex I, SDHC in complex II, UQCRB and UQCRQ in complex III, COX10 in complex V (Russell and N Doll, 2016). 11 miRNAs families in the frontal cortex of PD patients might influence the mitochondrial biogenesis by potentially targeting *PGC1*-α or its upstream regulators (Thomas et al., 2012). In ALS, miR-23a was discovered to inhibit the activity of PGC1-α in skeletal muscle (Russell et al., 2013).

Increasing mitochondrial fusion has a protective effect on the onset and escalation of neurodegenerative diseases. The expression of MFN2 was decreased in the hippocampus and cortical neurons of AD patients (Manczak et al., 2011; Wang H. et al., 2019). In a phenotypic SAMP8 model similar to the symptoms of late-onset and age-related sporadic AD patients, miR-195 targeted and inhibited *MFN2* expression in the mice hippocampus, reduced the MMP and caused mitochondrial dysfunction (Zhang R. et al., 2016). Another study also found that increasing mitochondrial fusion was beneficial to preventing AD. Mutations in the APP are able to trigger AD. In APP mutant cells, the mRNA and protein levels of mitochondrial biogenesis (PGC1-α, NRF1, NRF2, and TFAM) and synaptic genes (synaptophysin and PSD95) were reduced, and upregulating of miR-455-3p could rescued the decreased expression of these genes (Kumar et al., 2019). In HD patients, the

protein levels of DRP1 and FIS1 were increased while the protein levels of MFN1, MFN2, OPA1, and TOMM40 were decreased (Shirendeb et al., 2011). Exogenous expression of miR-214 could inhibit MFN2 expression, increase mitochondrial fragment distribution, and alter cell distribution at different stages of the cell cycle, which might interfere with the pathogenesis of HD (Bucha et al., 2015).

MiRNA can participate in regulating mitophagy to maintain the mitochondrial quality. Mutations in *PINK1* and *Parkin* are the common cause of autosomal recessive PD (Pickrell and Youle, 2015). miR-27a/b could target *PINK1* to decrease its translational level, which led to the inhibition of the accumulation of PINK1, parkin transportation and the expression of LC3II after mitochondrial injury (Kim et al., 2016). Simultaneously, autophagy of lysosomal clearance in damaged mitochondria was inhibited (Kim et al., 2016). In the PD mouse model and SH-SY5Y cell model, the expression levels of miR-103A-3p were increased, which inhibited *Parkin* expression and the clearance of damaged mitochondria (Zhou et al., 2020). Rat treated with rotenone resulted in an oxidative imbalance in the brain and activation of NF-Kβ. Activated NF-Kβ induced miR-146a transcription by banding to miR-146a promoter region, thereby downregulating Parkin protein levels and causing mitochondrial damage and dysfunction (Jauhari et al., 2020).

The damaged mitochondria undergo autophagy and eventually degradation in the lysosome, which is a key to control mitochondrial quality. MiR-5701 was able to reduce the mRNA levels of genes involved in lysosomal biogenesis and mitochondrial quality control, such as *VCP*, *LAPTM4a,* and *ATP6V0D1* (Prajapati et al., 2018). The decreased expression of those gene led to mitochondrial dysfunction, defective autophagy flux and further made SH-SY5Y cells sensitive to the neurotoxin 6-hydroxydopamine (6-OHDA) -induced cell death (Prajapati et al., 2018).

MiRNAs are involved in regulating ROS-induced apoptosis in neurodegenerative diseases. Bax is a proapoptotic member of BCl-2 family. The production of ROS resulted in the formation of pores at mitochondrial membranes, which could recruit Bax, promote the release of Cyt c, and activate caspase-mediated cascade amplification reaction to induce apoptosis of mitochondrial pathway (Orrenius et al., 2007; Sinha et al., 2013). However, antiapoptotic proteins of Bcl-2 family such as Bcl-2 and Bcl-X_L inhibited the activity of these proapoptotic proteins by preventing oligomerization (Orrenius et al., 2007). MiR-7 and miR-153 were able to regulate mitochondrial ROS-mediated α-synuclein protein synthesis and reduce MPP^+ -mediated α-synuclein level (Je and Kim, 2017). MiR-7 overexpression inhibited the release of ROS and Cyt c responding to MPP^+ in human neuroblastoma SH-SY5Y cells (Chaudhuri et al., 2016). Bim enhanced Bax mitochondrial translocation by activating JNK/c-Jun, which induced Cyt c release and led to the apoptosis of dopaminergic neurons (Perier et al., 2007). MiR-124 was able to suppress Bax translocation to mitochondria by inhibiting Bim in MPTP-treated mice. Morever, upregulating the expression of miR-124 could alleviate the characteristics of MPP^+-intoxicated SH-SY5Y cells, such as impaired autophagy process, autophagosome accumulation and lysosomal depletion (Wang H. et al., 2016). In the PD cell model induced by 6-OHDA, inhibiting miR-410 reduced the viability of neuronal cells and increased capase-3 activity, ROS production and apoptosis (Ge et al., 2019).

LncRNAs and CircRNAs Regulate Neurodegenerative Diseases by Targeting Genes Associated With Mitochondria Functions

In addition to miRNAs, some lncRNAs and circRNAs have also been found to regulate mitochondrial function and play a role in the progression of neurodegenerative diseases. LncRNAs is long non-coding RNAs that directly interact with transcription factors, functional RNA and chromatin remodeling modifiers to regulate gene expression at the transcriptional, post-transcriptional and epigenetic levels, respectively, (Kopp and Mendell, 2018). CircRNAs are characterized by covalently closed loop structures. They can act as miRNA sponges to reduce the inhibition of miRNAs to target genes (Du et al., 2017).

In PD studies, a decrease in the level of lncRNA AL049437 was able to increase cell viability, MMP, mitochondrial mass, and tyrosine hydroxylase secretion, on the contrary, knocking out AK021630 had the opposite effect (Ni et al., 2017). Hence, it was speculated that lncRNA AL049437 may cause the risk of PD, and lncRNA AK021630 might inhibit the development of PD (Ni et al., 2017). LncRNA MALAT1 was highly expressed in the brains of MPTP-induced PD mouse model and LPS/ATP-induced mouse BV2 microglia. Knockdown of MALAT1 inhibited the expression of NRF2, thereby inhibiting inflammasome activation and ROS production (Cai et al., 2020). The expression of circDLGAP4 was reduced both in the MPTP-induced PD mouse model and MPP^+-induced PD cell model (Feng et al., 2020). *In vitro* study have shown that circDLGAP4 promoted cell viability, reduced apoptosis, mitochondrial damage, and enhanced autophagy, which reduced the neurotoxic effect of MPP^+ in SH-SY5Y and MN9D cells (Feng et al., 2020).

In $A\beta_{25-35}$-induced AD model of PC12 cells, the silence long non-coding RNA brain-derived neurotrophic factor antisense inhibited $A\beta_{25-35}$-induced apoptosis by inhibiting the release of Cyt c, which increased the expression of Bcl-2 and reduced the expression of caspase-3 and Bax (Guo et al., 2018). In SH-SY5Y and HPN cells, lncRNA SNHG15 reduction partially rescued the effects of $A\beta_{25-35}$ treatment on cell viability, apoptosis, MMP, caspase-3 activity and apoptosis-related protein levels (Wang H. et al., 2019). LncRNA NEAT1 with elevated expression level interacted with NEDD4L and promoted the ubiquitination of PINK1 to impair PINK1-dependent autophagy in animal model of AD (Huang et al., 2020). Another research in AD showed that overexpression of lncRNA WT-AS inhibited the expression of transcription factor WT which suppressed the expression of miR-375 and SIX4 (Wang et al., 2020). And lncRNA WT-AS could inhibit the pTau protein and promote the production of ATP and therefore play

a role in the regulation of mitochondrial structure and function (Wang et al., 2020).

THE INVOLVEMENT OF MITOCHONDRIA IN EPIGENETIC REGULATION CAN PROVIDE NEW STRATEGIES FOR NEURODEGENERATIVE DISEASES TREATMENT

Treatment or diagnosis of diseases based on epigenetic regulation included epigenetic modified biomarkers, chemical drugs and miRNA-targeting drugs (mimics or inhibitors). The causes of majority of neurodegenerative diseases are hereditary, thus pathogenic genes or single nucleotide polymorphisms can be used as early diagnostic markers (Gotovac et al., 2014). In addition, neurodegenerative diseases have sporadic cases, and the influence of environmental factors on the onset of diseases cannot be ignored. Therefore, epigenetic biomarkers have attracted attention. Many studies on DNA methylation markers of neurodegenerative diseases have been recognized (Fetahu et al., 2019; Wang C. et al., 2019; Vasanthakumar et al., 2020). Currently, mitochondria have attracted increasing attention in the field of epigenetics. Fluctuations in mtDNA methylation levels have been observed in AD, PD, and ALS compared with normal population, suggesting that mtDNA methylation studies has therapeutic potential in neurodegenerative diseases. However, due to the lack of functional studies on mtDNA methylation, it has not entered the clinical application stage.

The effects of drugs and compounds targeting mitochondria of neurodegenerative diseases are mainly antioxidant, improving mitochondrial biogenesis and increasing energy generation (Stanga et al., 2020). Some drugs targeting DNA methylation have been shown to be effective on mtDNA. For instance, valproic acid, a histone deacetylase inhibitor, is an anticonvulsant and mood stabilizer and a pharmacological tool used in the study of nuclear epigenetics, such as DNA methylation. After few days of treatment with valproic acid in mouse 3T3-L1 cells, it was observed a decrease in 5hmC levels of mtDNA, while 5mC level was not affected (Chen et al., 2012). In addition to drugs, overall methylation levels can be improved by regulating nutritional supplement. For example, One-C metabolism in mitochondria can regulate the production of SAM, and external nutrients such as vitamin B12 and folic acid can promote the production of SAM and thus enhance DNA methylation (Li et al., 2015; Román et al., 2019). Moreover, NAD^+ and NR are used to treat AD and ALS. Their main role is to enhance mitochondrial biogenesis and inhibit ROS (Chaturvedi et al., 2009; Li et al., 2015; Cenini and Voos, 2019; Carrera-Juliá et al., 2020). NAD^+ is a co-regulator

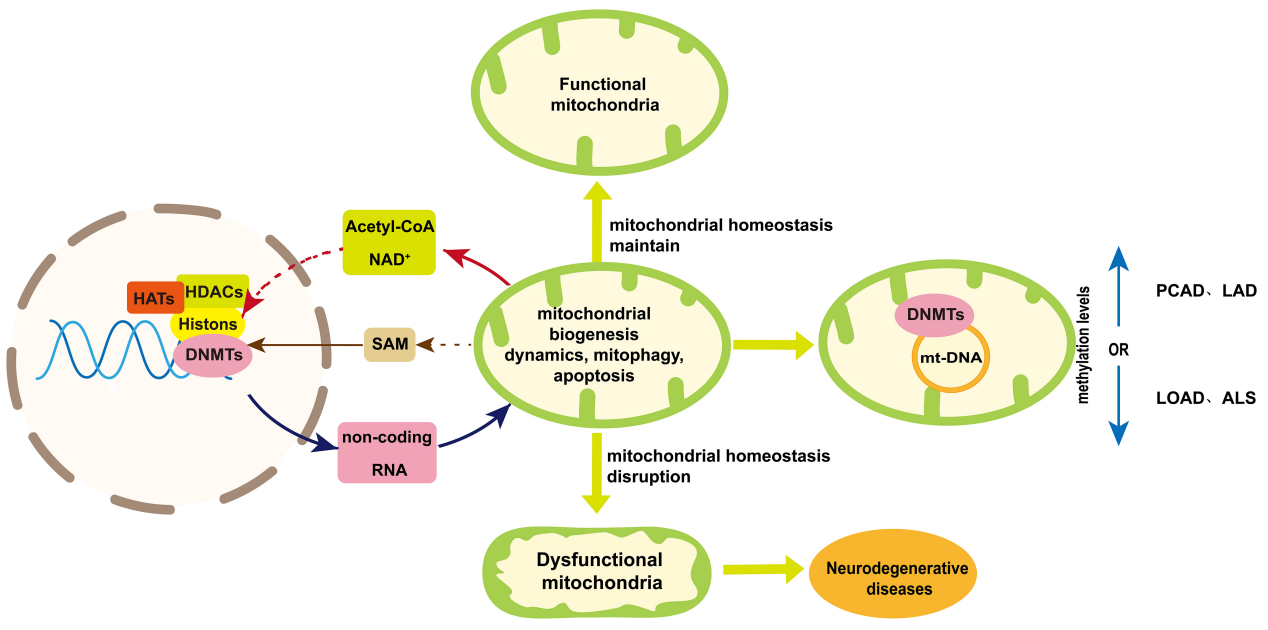

FIGURE 4 | A schematic diagram of mtDNA methylation and the bidirectional communication between mitochondria and nuclear in epigenetic regulation. Mitochondria maintain their homeostasis in several ways including mitochondrial biogenesis, dynamic, mitophagy and apoptosis. Disruption of mitochondrial homeostasis will result in impaired mitochondrial function, which may contribute to neurodegenerative diseases. Mitochondria are involved in the epigenetic regulation from two aspects. One is mtDNA methylation, the extent of which varies among neurodegenerative diseases. The other is the bidirectional communication between mitochondria and nuclear, which is essential to maintain mitochondria homeostasis and can play a role in nuclear epigenetic regulation of neurogenerative diseases. Acetyl-CoA and NAD^+ provided by mitochondria indirectly play a role in histone acetylation and deacetylation, respectively, to influencing mitochondria homeostasis. Mitochondria can influence the production of SAM that regulated nuclear DNA methylation. On the other hand, non-coding RNAs coded by nuclear genome can regulate neurogenerative diseases by influencing mitochondria homeostasis. Dashed arrows indicate pathways that need further validation. Abbreviations: PCAD, preclinical Alzheimer's disease; LAD, late-stage Alzheimer's disease; LOAD late-onset Alzheimer's disease; ALS, amyotrophic lateral sclerosis; and SAM, S-adenosyl methionine.

of histone acetylation. Whether exogenous NAD^+ can improve disease by regulating histone acetylation remains to be studied. Similarly, acetyl-CoA, a metabolic intermediate of mitochondria, is the acetyl group donor for histone acetylation. At present, there are two AD drugs that can enhance the methylation of histone H3K9 by increasing the level of acetyl-CoA, maintain mitochondrial homeostasis and play a neuroprotective role (Currais et al., 2019).

Since miRNAs can regulate the expression of endogenous genes and biological pathways, taking miRNA as a target for the treatment of diseases has become a very interesting research direction (Junn and Mouradian, 2012). Anti-miRNA drugs or miRNA analogs can be delivered to the body as a personalized therapy using viral vectors, lipids, nanoparticles, and exosomes (Lakhal and Wood, 2011; Zhao et al., 2016; Paul et al., 2020). However, there are still many problems to be solved. As more and more miRNAs have been shown to improve disease traits by regulating mitochondrial function, it is likely that miRNA will become a targeted therapeutic strategy in the future.

In general, although the involvement of mitochondria in epigenetic regulation have provided the potential strategies for neurodegenerative diseases, more in-depth studies are required to research and development of mitochondria-specific drugs.

CONCLUSION AND FUTURE PERSPECTIVES

In this review, we discuss the role of mtDNA, metabolic intermediate (SAM, acetyl-CoA and NAD^+) and non-coding RNAs in the epigenetic regulation of neurodegenerative diseases (**Figure 4**). The regulation of nuclear-encoded non-coding RNAs is able to improve neurodegenerative diseases by enhancing mitochondria biogenesis, maintaining mitochondria quality and reducing apoptosis (Je and Kim, 2017; Ni et al., 2017; Kumar et al., 2019; Feng et al., 2020; Zhou et al., 2020). On the other hand, the extent of mtDNA methylation varies among neurodegenerative diseases (Blanch et al., 2016; Stoccoro et al., 2020). But the mechanism of mitochondrial DNA methylation in neurodegenerative diseases requires further study. Available literatures indicate acetyl-CoA and NAD^+ provided by mitochondria may indirectly affect the histone acetylation and deacetylation, respectively, in the research of neurodegenerative diseases. The level of SAM can be increase by taking vitamin B12 and folic acid to enhance the methylation level for neurodegenerative disease treatment. However, the sources of acyl-CoA and NAD^+ participated in histone modification are needed to be tracked to elucidate the role of mitochondrial metabolites involved in epigenetic regulation (Trefely et al., 2020). And a deeper understanding of the relationship between mitochondrial metabolism and epigenetics in neurodegenerative diseases is required in order to provide new treatment strategies.

AUTHOR CONTRIBUTIONS

SX, YL, and SL conceived the manuscript. SX, XZ, and CL wrote the manuscript. QL and HC contributed to crafting figures. YL and SL reviewed and edited the manuscript. All authors listed have made a substantial, direct and intellectual contribution to work, and approved it for publication.

FUNDING

This project was supported by grants from the National Key R&D Program of China (2017YFE9126600), National Natural Science Foundation of China (31830111 and 81771333), and Key Research and Innovation Program of Shanghai Municipal Education Commission (2019-01-07-00-07-E00040).

REFERENCES

Agrimi, G., Di Noia, M. A., Marobbio, C. M. T., Fiermonte, G., Lasorsa, F. M., and Palmieri, F. (2004). Identification of the human mitochondrial S-adenosylmethionine transporter: bacterial expression, reconstitution, functional characterization and tissue distribution. *Biochem. J.* 379, 183–190. doi: 10.1042/BJ20031664

Ballard, P. A., Tetrud, J. W., and Langston, J. W. (1985). Permanent human parkinsonism due to 1-methyl-4-phenyl-1,2,3,6-tetrahydropyridine (MPTP): seven cases. *Neurology* 35, 949–956. doi: 10.1212/wnl.35.7.949

Battle, D. E. (2013). Diagnostic and statistical manual of mental disorders (DSM). *CoDAS* 25, 191–192. doi: 10.1590/s2317-17822013000200017

Bellizzi, D., Daquila, P., Giordano, M., Montesanto, A., and Passarino, G. (2012). Global DNA methylation levels are modulated by mitochondrial DNA variants. *Epigenomics* 4, 17–27. doi: 10.2217/epi.11.109

Bellizzi, D., D'aquila, P., Scafone, T., Giordano, M., Riso, V., Riccio, A., et al. (2013). The control region of mitochondrial DNA shows an unusual CpG and non-CpG methylation pattern. *DNA Res.* 20, 537–547. doi: 10.1093/dnares/dst029

Blanch, M., Mosquera, J. L., Ansoleaga, B., Ferrer, I., and Barrachina, M. (2016). Altered mitochondrial DNA methylation pattern in Alzheimer disease-related pathology and in Parkinson disease. *Am. J. Pathol.* 186, 385–397. doi: 10.1016/j.ajpath.2015.10.004

Bose, A., and Beal, M. F. (2016). Mitochondrial dysfunction in Parkinson's disease. *J. Neurochem.* 139, 216–231. doi: 10.1111/jnc.13731

Bradley-Whitman, M. A., and Lovell, M. A. (2013). Epigenetic changes in the progression of Alzheimer's disease. *Mech. Ageing Dev.* 134, 486–495. doi: 10.1016/j.mad.2013.08.005

Bucha, S., Mukhopadhyay, D., and Bhattacharyya, N. P. (2015). Regulation of mitochondrial morphology and cell cycle by microRNA-214 targeting Mitofusin2. *Biochem. Biophys. Res. Commun.* 465, 797–802. doi: 10.1016/j.bbrc.2015.08.090

Cai, L., Sutter, B. M., Li, B., and Tu, B. P. (2011). Acetyl-CoA induces cell growth and proliferation by promoting the acetylation of histones at growth genes. *Mol. Cell* 42, 426–437. doi: 10.1016/j.molcel.2011.05.004

Cai, L. J., Tu, L., Huang, X. M., Huang, J., Qiu, N., Xie, G. H., et al. (2020). LncRNA MALAT1 facilitates inflammasome activation via epigenetic suppression of Nrf2 in Parkinson's disease. *Mol. Brain* 13, 130. doi: 10.1186/s13041-020-00656-8

Cantó, C., Menzies, K. J., and Auwerx, J. (2015). NAD(+) metabolism and the control of energy homeostasis: a balancing act between mitochondria and the nucleus. *Cell Metab.* 22, 31–53. doi: 10.1016/j.cmet.2015.05.023

Carrera-Juliá, S., Moreno, M. L., Barrios, C., de la Rubia Ortí, J. E., and Drehmer, E. (2020). Antioxidant alternatives in the treatment of amyotrophic lateral sclerosis: a comprehensive review. *Front. Physiol.* 11:63. doi: 10.3389/fphys.2020.00063

Cenini, G., and Voos, W. (2019). Mitochondria as potential targets in alzheimer disease therapy: an update. *Front. Pharmacol.* 10:902. doi: 10.3389/fphar.2019.00902

Chaturvedi, R. K., Adhihetty, P., Shukla, S., Hennessy, T., Calingasan, N., Yang, L., et al. (2009). Impaired PGC-1alpha function in muscle in Huntington's disease. *Hum. Mol. Genet.* 18, 3048–3065. doi: 10.1093/hmg/ddp243

Chaturvedi, R. K., and Flint Beal, M. (2013). Mitochondrial diseases of the brain. *Free Radic. Biol. Med.* 63, 1–29. doi: 10.1016/j.freeradbiomed.2013.03.018

Chaudhuri, A. D., Choi, D. C., Kabaria, S., Tran, A., and Junn, X. E. (2016). MicroRNA-7 regulates the function of mitochondrial permeability transition pore by targeting vdac1 expression. *J. Biol. Chem.* 291, 6483–6493. doi: 10.1074/jbc.M115.691352

Chen, H., Dzitoyeva, S., and Manev, H. (2012). Effect of valproic acid on mitochondrial epigenetics. *Eur. J. Pharmacol.* 690, 51–59. doi: 10.1016/j.ejphar.2012.06.019

Chestnut, B. A., Chang, Q., Price, A., Lesuisse, C., Wong, M., and Martin, L. J. (2011). Epigenetic regulation of motor neuron cell death through DNA methylation. *J. Neurosci.* 31, 16619–16636. doi: 10.1523/JNEUROSCI.1639-11.2011

Chiang, P. K., Gordon, R. K., Tal, J., Zeng, G. C., Doctor, B. P., Pardhasaradhi, K., et al. (1996). S-Adenosylmethionine and methylation. *FASEB J. Off. Publ. Fed. Am. Soc. Exp. Biol.* 10, 471–480.

Cozzolino, M., Ferri, A., and Carrì, M. T. (2008). Amyotrophic lateral sclerosis: from current developments in the laboratory to clinical implications. *Antioxid. Redox Signal.* 10, 405–443. doi: 10.1089/ars.2007.1760

Cunningham, J. T., Rodgers, J. T., Arlow, D. H., Vazquez, F., Mootha, V. K., and Puigserver, P. (2007). mTOR controls mitochondrial oxidative function through a YY1-PGC-1α transcriptional complex. *Nature* 450, 736–740. doi: 10.1038/nature06322

Currais, A., Huang, L., Goldberg, J., Petrascheck, M., Ates, G., Pinto-Duarte, A., et al. (2019). Elevating acetyl-CoA levels reduces aspects of brain aging. *Elife* 8:e47866. doi: 10.7554/eLife.47866

De Mena, L., Cardo, L. F., Coto, E., and Alvarez, V. (2013). No differential DNA methylation of PARK2 in brain of Parkinson's disease patients and healthy controls. *Mov. Disord.* 28, 2032–2033. doi: 10.1002/mds.25593

Dimauro, I., Paronetto, M. P., and Caporossi, D. (2020). Exercise, redox homeostasis and the epigenetic landscape. *Redox Biol.* 35:101477. doi: 10.1016/j.redox.2020.101477

Dong, S. Y., Guo, Y. J., Feng, Y., Cui, X. X., Kuo, S. H., Liu, T., et al. (2016). The epigenetic regulation of HIF-1α by SIRT1 in MPP+ treated SH-SY5Y cells. *Biochem. Biophys. Res. Commun.* 470, 453–459. doi: 10.1016/j.bbrc.2016.01.013

Du, W. W., Zhang, C., Yang, W., Yong, T., Awan, F. M., and Yang, B. B. (2017). Identifying and characterizing circRNA-protein interaction. *Theranostics* 7, 4183–4191. doi: 10.7150/thno.21299

Easlon, E., Tsang, F., Skinner, C., Wang, C., and Lin, S. J. (2008). The malate-aspartate NADH shuttle components are novel metabolic longevity regulators required for calorie restriction-mediated life span extension in yeast. *Genes Dev.* 22, 931–944. doi: 10.1101/gad.1648308

Eryilmaz, I. E., Cecener, G., Erer, S., Egeli, U., Tunca, B., Zarifoglu, M., et al. (2017). Epigenetic approach to early-onset Parkinson's disease: low methylation status of SNCA and PARK2 promoter regions. *Neurol. Res.* 39, 965–972. doi: 10.1080/01616412.2017.1368141

Fabian, M. R., and Sonenberg, N. (2012). The mechanics of miRNA-mediated gene silencing: a look under the hood of miRISC. *Nat. Struct. Mol. Biol.* 19, 586–593. doi: 10.1038/nsmb.2296

Feng, Y., Liu, T., Dong, S. Y., Guo, Y. J., Jankovic, J., Xu, H., et al. (2015). Rotenone affects p53 transcriptional activity and apoptosis via targeting SIRT1 and H3K9 acetylation in SH-SY5Y cells. *J. Neurochem.* 134, 668–676. doi: 10.1111/jnc.13172

Feng, Z., Zhang, L., Wang, S., and Hong, Q. (2020). Circular RNA circDLGAP4 exerts neuroprotective effects via modulating miR-134-5p/CREB pathway in Parkinson's disease. *Biochem. Biophys. Res. Commun.* 522, 388–394. doi: 10.1016/j.bbrc.2019.11.102

Ferri, A., Cozzolino, M., Crosio, C., Nencini, M., Casciati, A., Gralla, E. B., et al. (2006). Familial ALS-superoxide dismutases associate with mitochondria and shift their redox potentials. *Proc. Natl. Acad. Sci. U.S.A.* 103, 13860–13865. doi: 10.1073/pnas.0605814103

Ferri, A., Fiorenzo, P., Nencini, M., Cozzolino, M., Pesaresi, M. G., Valle, C., et al. (2010). Glutaredoxin 2 prevents aggregation of mutant SOD1 in mitochondria and abolishes its toxicity. *Hum. Mol. Genet.* 19, 4529–4542. doi: 10.1093/hmg/ddq383

Fetahu, I. S., Ma, D., Rabidou, K., Argueta, C., Smith, M., Liu, H., et al. (2019). Epigenetic signatures of methylated DNA cytosine in Alzheimer's disease. *Sci. Adv.* 5:eaaw2880. doi: 10.1126/sciadv.aaw2880

Friedman, J. R., and Nunnari, J. (2014). Mitochondrial form and function. *Nature* 505, 335–343. doi: 10.1038/nature12985

Fujino, T., Kondo, J., Ishikawa, M., Morikawa, K., and Yamamoto, T. T. (2001). Acetyl-CoA Synthetase 2, a mitochondrial matrix enzyme involved in the oxidation of acetate. *J. Biol. Chem.* 276, 11420–11426. doi: 10.1074/jbc.M008782200

Fuso, A., Nicolia, V., Cavallaro, R. A., Ricceri, L., D'Anselmi, F., Coluccia, P., et al. (2008). B-vitamin deprivation induces hyperhomocysteinemia and brain S-adenosylhomocysteine, depletes brain S-adenosylmethionine, and enhances PS1 and BACE expression and amyloid-beta deposition in mice. *Mol. Cell. Neurosci.* 37, 731–746. doi: 10.1016/j.mcn.2007.12.018

Fuso, A., Nicolia, V., Cavallaro, R. A., and Scarpa, S. (2011). DNA methylase and demethylase activities are modulated by one-carbon metabolism in Alzheimer's disease models. *J. Nutr. Biochem.* 22, 242–251. doi: 10.1016/j.jnutbio.2010.01.010

Ge, H., Yan, Z., Zhu, H., and Zhao, H. (2019). MiR-410 exerts neuroprotective effects in a cellular model of Parkinson's disease induced by 6-hydroxydopamine via inhibiting the PTEN/AKT/mTOR signaling pathway. *Exp. Mol. Pathol.* 109, 16–24. doi: 10.1016/j.yexmp.2019.05.002

Gorbatyuk, O. S., Li, S., Sullivan, L. F., Chen, W., Kondrikova, G., Manfredsson, F. P., et al. (2008). The phosphorylation state of Ser-129 in human alpha-synuclein determines neurodegeneration in a rat model of Parkinson disease. *Proc. Natl. Acad. Sci. U.S.A.* 105, 763–768. doi: 10.1073/pnas.0711053105

Gotovac, K., Hajnšek, S., Pašiæ, M. B., Pivac, N., and Boroveèki, F. (2014). Personalized medicine in neurodegenerative diseases: how far away? *Mol. Diagn. Ther.* 18, 17–24. doi: 10.1007/s40291-013-0058-z

Guégan, C., Vila, M., Rosoklija, G., Hays, A. P., and Przedborski, S. (2001). Recruitment of the mitochondrial-dependent apoptotic pathway in amyotrophic lateral sclerosis. *J. Neurosci.* 21, 6569–6576. doi: 10.1523/JNEUROSCI.21-17-06569.2001

Guo, C. C., Jiao, C. h, and Gao, Z. M. (2018). Silencing of LncRNA BDNF-AS attenuates Aβ25-35-induced neurotoxicity in PC12 cells by suppressing cell apoptosis and oxidative stress. *Neurol. Res.* 40, 795–804. doi: 10.1080/01616412.2018.1480921

Haigis, M. C., and Sinclair, D. A. (2010). Mammalian sirtuins: biological insights and disease relevance. *Annu. Rev. Pathol.* 5, 253–295. doi: 10.1146/annurev.pathol.4.110807.092250

Harris, R. A., Joshi, M., Jeoung, N. H., and Obayashi, M. (2005). Overview of the molecular and biochemical basis of branched-chain amino acid catabolism. *J. Nutr.* 135(6 Suppl), 1527S–1530S. doi: 10.1093/jn/135.6.1527s

Huang, Z., Zhao, J., Wang, W., Zhou, J., and Zhang, J. (2020). Depletion of LncRNA NEAT1 rescues mitochondrial dysfunction through NEDD4L-Dependent PINK1 degradation in animal models of alzheimer's disease. *Front. Cell. Neurosci.* 14:28. doi: 10.3389/fncel.2020.00028

Hyman, B. T., Phelps, C. H., Beach, T. G., Bigio, E. H., Cairns, N. J., Carrillo, M. C., et al. (2012). National Institute on Aging-Alzheimer's Association guidelines for the neuropathologic assessment of Alzheimer's disease. *Alzheimers. Dement.* 8, 1–13. doi: 10.1016/j.jalz.2011.10.007

Ito, S., Shen, L., Dai, Q., Wu, S. C., Collins, L. B., Swenberg, J. A., et al. (2011). Tet proteins can convert 5-methylcytosine to 5-formylcytosine and 5-carboxylcytosine. *Science* 333, 1300–1303. doi: 10.1126/science.1210597

Jauhari, A., Singh, T., Mishra, S., Shankar, J., and Yadav, S. (2020). Coordinated action of miR-146a and parkin gene regulate rotenone-induced neurodegeneration. *Toxicol. Sci.* 176, 433–445. doi: 10.1093/toxsci/kfaa066

Jayasena, T., Poljak, A., Braidy, N., Zhong, L., Rowlands, B., Muenchhoff, J., et al. (2016). Application of targeted mass spectrometry for the quantification of sirtuins in the central nervous system. *Sci. Rep.* 6:35391. doi: 10.1038/srep35391

Je, G., and Kim, Y. S. (2017). Mitochondrial ROS-mediated post-transcriptional regulation of α-synuclein through miR-7 and miR-153. *Neurosci. Lett.* 661, 132–136. doi: 10.1016/j.neulet.2017.09.065

Jing, H., and Lin, H. (2015). Sirtuins in epigenetic regulation. *Chem. Rev.* 115, 2350–2375. doi: 10.1021/cr500457h

Johri, A., Chandra, A., and Flint Beal, M. (2013). PGC-1α, mitochondrial dysfunction, and Huntington's disease. *Free Radic. Biol. Med.* 62, 37–46. doi: 10.1016/j.freeradbiomed.2013.04.016

Junn, E., and Mouradian, M. M. (2012). MicroRNAs in neurodegenerative diseases and their therapeutic potential. *Pharmacol. Ther.* 133, 142–150. doi: 10.1016/j.pharmthera.2011.10.002

Kamp, F., Exner, N., Lutz, A. K., Wender, N., Hegermann, J., Brunner, B., et al. (2010). Inhibition of mitochondrial fusion by α-synuclein is rescued by PINK1, Parkin and DJ-1. *EMBO J.* 29, 3571–3589. doi: 10.1038/emboj.2010.223

Kerr, J. S., Adriaanse, B. A., Greig, N. H., Mattson, M. P., Cader, M. Z., Bohr, V. A., et al. (2017). Mitophagy and Alzheimer's Disease: cellular and molecular mechanisms. *Trends Neurosci.* 40, 151–166. doi: 10.1016/j.tins.2017.01.002

Kim, J., Fiesel, F. C., Belmonte, K. C., Hudec, R., Wang, W. X., Kim, C., et al. (2016). MiR-27a and miR-27b regulate autophagic clearance of damaged mitochondria by targeting PTEN-induced putative kinase 1 (PINK1). *Mol. Neurodegener.* 11:55. doi: 10.1186/s13024-016-0121-4

Kim, J., Moody, J. P., Edgerly, C. K., Bordiuk, O. L., Cormier, K., Smith, K., et al. (2010). Mitochondrial loss, dysfunction and altered dynamics in Huntington's disease. *Hum. Mol. Genet.* 19, 3919–3935. doi: 10.1093/hmg/ddq306

Kirkinezos, I. G., Bacman, S. R., Hernandez, D., Oca-Cossio, J., Arias, L. J., Perez-Pinzon, M. A., et al. (2005). Cytochrome c association with the inner mitochondrial membrane is impaired in the CNS of G93A-SOD1 mice. *J. Neurosci.* 25, 164–172. doi: 10.1523/JNEUROSCI.3829-04.2005

Kong, J., and Xu, Z. (1998). Massive mitochondrial degeneration in motor neurons triggers the onset of amyotrophic lateral sclerosis in mice expressing a mutant SOD1. *J. Neurosci.* 18, 3241–3250. doi: 10.1523/JNEUROSCI.18-09-03241.1998

Kontopoulos, E., Parvin, J. D., and Feany, M. B. (2006). α-synuclein acts in the nucleus to inhibit histone acetylation and promote neurotoxicity. *Hum. Mol. Genet.* 15, 3012–3023. doi: 10.1093/hmg/ddl243

Kopp, F., and Mendell, J. T. (2018). Functional classification and experimental dissection of long noncoding RNAs. *Cell* 172, 393–407. doi: 10.1016/j.cell.2018.01.011

Koshiba, T., Detmer, S. A., Kaiser, J. T., Chen, H., McCaffery, J. M., and Chan, D. C. (2004). Structural basis of mitochondrial tethering by mitofusin complexes. *Science* 305, 858–862. doi: 10.1126/science.1099793

Kumar, S., Reddy, A. P., Yin, X., and Reddy, P. H. (2019). Novel MicroRNA-455-3p and its protective effects against abnormal APP processing and amyloid beta toxicity in Alzheimer's disease. *Biochim. Biophys. Acta - Mol. Basis Dis.* 1865, 2428–2440. doi: 10.1016/j.bbadis.2019.06.006

Kwong, J. Q., Beal, M. F., and Manfredi, G. (2006). The role of mitochondria in inherited neurodegenerative diseases. *J. Neurochem.* 97, 1659–1675. doi: 10.1111/j.1471-4159.2006.03990.x

Lakhal, S., and Wood, M. J. A. (2011). Exosome nanotechnology: an emerging paradigm shift in drug delivery: exploitation of exosome nanovesicles for systemic in vivo delivery of RNAi heralds new horizons for drug delivery across biological barriers. *Bioessays* 33, 737–741. doi: 10.1002/bies.201100076

Lautrup, S., Sinclair, D. A., Mattson, M. P., and Fang, E. F. (2019). NAD(+) in brain aging and neurodegenerative disorders. *Cell Metab.* 30, 630–655. doi: 10.1016/j.cmet.2019.09.001

Li, K., Zhang, J., Ji, C., and Wang, L. (2016). MiR-144-3p and its target gene β-amyloid precursor protein regulate 1-methyl-4-phenyl-1,2-3,6-tetrahydropyridine-induced mitochondrial dysfunction. *Mol. Cells* 39, 543–549. doi: 10.14348/molcells.2016.0050

Li, W., Liu, H., Yu, M., Zhang, X., Zhang, M., Wilson, J. X., et al. (2015). Folic acid administration inhibits amyloid β-peptide accumulation in APP/PS1 transgenic mice. *J. Nutr. Biochem.* 26, 883–891. doi: 10.1016/j.jnutbio.2015.03.009

Lin, M. T., and Beal, M. F. (2006). Mitochondrial dysfunction and oxidative stress in neurodegenerative diseases. *Nature* 443, 787–795. doi: 10.1038/nature05292

Lubos, E., Loscalzo, J., and Handy, D. E. (2011). Glutathione peroxidase-1 in health and disease: from molecular mechanisms to therapeutic opportunities. *Antioxidants Redox Signal.* 15, 1957–1997. doi: 10.1089/ars.2010.3586

Macgregor-Das, A. M., and Das, S. (2018). A microRNA's journey to the center of the mitochondria. *Am. J. Physiol. Hear. Circ. Physiol.* 315, H206–H215. doi: 10.1152/ajpheart.00714.2017

Madiraju, P., Pande, S. V., Prentki, M., and Madiraju, S. R. M. (2009). Mitochondrial acetylcarnitine provides acetyl groups for nuclear histone acetylation. *Epigenetics* 4, 399–403. doi: 10.4161/epi.4.6.9767

Makarova, J. A., Shkurnikov, M. U., Wicklein, D., Lange, T., Samatov, T. R., Turchinovich, A. A., et al. (2016). Intracellular and extracellular microRNA: an update on localization and biological role. *Prog. Histochem. Cytochem.* 51, 33–49. doi: 10.1016/j.proghi.2016.06.001

Manczak, M., Calkins, M. J., and Reddy, P. H. (2011). Impaired mitochondrial dynamics and abnormal interaction of amyloid beta with mitochondrial protein Drp1 in neurons from patients with Alzheimer's disease: implications for neuronal damage. *Hum. Mol. Genet.* 20, 2495–2509. doi: 10.1093/hmg/ddr139

Martinez-Vicente, M., Talloczy, Z., Wong, E., Tang, G., Koga, H., Kaushik, S., et al. (2010). Cargo recognition failure is responsible for inefficient autophagy in Huntington's disease. *Nat. Neurosci.* 13, 567–576. doi: 10.1038/nn.2528

Medina, M., Urdiales, J. L., and Amores-Sánchez, M. I. (2001). Roles of homocysteine in cell metabolism: old and new functions. *Eur. J. Biochem.* 268, 3871–3882. doi: 10.1046/j.1432-1327.2001.02278.x

Menzies, K. J., Zhang, H., Katsyuba, E., and Auwerx, J. (2016). Protein acetylation in metabolism-metabolites and cofactors. *Nat. Rev. Endocrinol.* 12, 43–60. doi: 10.1038/nrendo.2015.181

Mercer, T. R., Neph, S., Dinger, M. E., Crawford, J., Smith, M. A., Shearwood, A. M. J., et al. (2011). The human mitochondrial transcriptome. *Cell* 146, 645–658. doi: 10.1016/j.cell.2011.06.051

Michishita, E., Park, J. Y., Burneskis, J. M., Barrett, J. C., and Horikawa, I. (2005). Evolutionarily conserved and nonconserved cellular localizations and functions of human SIRT proteins. *Mol. Biol. Cell* 16, 4623–4635. doi: 10.1091/mbc.E05-01-0033

Mottis, A., Herzig, S., and Auwerx, J. (2019). Mitocellular communication: shaping health and disease. *Science* 366, 827–832. doi: 10.1126/science.aax3768

Murphy, M. P. (2009). How mitochondria produce reactive oxygen species. *Biochem. J.* 417, 1–13. doi: 10.1042/BJ20081386

Nakamura, K., Nemani, V. M., Azarbal, F., Skibinski, G., Levy, J. M., Egami, K., et al. (2011). Direct membrane association drives mitochondrial fission by the Parkinson disease-associated protein alpha-synuclein. *J. Biol. Chem.* 286, 20710–20726. doi: 10.1074/jbc.M110.213538

Nass, M. M. K. (1973). Differential methylation of mitochondrial and nuclear DNA in cultured mouse, hamster and virus-transformed hamster cells *In vivo* and *in vitro* methylation. *J. Mol. Biol.* 80, 155–175. doi: 10.1016/0022-2836(73)90239-8

Ni, Y., Huang, H., Chen, Y., Cao, M., Zhou, H., and Zhang, Y. (2017). Investigation of long non-coding RNA expression profiles in the Substantia Nigra of Parkinson's Disease. *Cell. Mol. Neurobiol.* 37, 329–338. doi: 10.1007/s10571-016-0373-0

Number, G., Reis, R. J. S., and Goldstein, S. (1983). Mitochondrial DNA in mortal and immortal human cells. *J. Biol. Chem.* 258, 9078–9085.

O'Brien, J., Hayder, H., Zayed, Y., and Peng, C. (2018). Overview of MicroRNA biogenesis, mechanisms of actions, and circulation. *Front. Endocrinol. (Lausanne).* 9:402. doi: 10.3389/fendo.2018.00402

Ormazabal, A., Casado, M., Molero-Luis, M., Montoya, J., Rahman, S., Aylett, S.-B., et al. (2015). Can folic acid have a role in mitochondrial disorders? *Drug Discov. Today* 20, 1349–1354. doi: 10.1016/j.drudis.2015.07.002

Orrenius, S., Gogvadze, V., and Zhivotovsky, B. (2007). Mitochondrial oxidative stress: implications for cell death. *Annu. Rev. Pharmacol. Toxicol.* 47, 143–183. doi: 10.1146/annurev.pharmtox.47.120505.105122

Outeiro, T. F., Kontopoulos, E., Altmann, S. M., Kufareva, I., Strathearn, K. E., Amore, A. M., et al. (2007). Sirtuin 2 inhibitors rescue α-synuclein-mediated toxicity in models of Parkinson's disease. *Science* 317, 516–519. doi: 10.1126/science.1143780

Panni, S., Lovering, R. C., Porras, P., and Orchard, S. (2020). Non-coding RNA regulatory networks. *Biochim. Biophys. acta. Gene Regul. Mech.* 1863:194417. doi: 10.1016/j.bbagrm.2019.194417

Paul, S., Bravo Vázquez, L. A., Pérez Uribe, S., Roxana Reyes-Pérez, P., and Sharma, A. (2020). Current status of microRNA-based therapeutic approaches in neurodegenerative disorders. *Cells* 9:1698. doi: 10.3390/cells9071698

Pedrini, S., Sau, D., Guareschi, S., Bogush, M., Brown, R. H. J., Naniche, N., et al. (2010). ALS-linked mutant SOD1 damages mitochondria by promoting conformational changes in Bcl-2. *Hum. Mol. Genet.* 19, 2974–2986. doi: 10.1093/hmg/ddq202

Perier, C., Bové, J., Wu, D. C., Dehay, B., Choi, D. K., Jackson-Lewis, V., et al. (2007). Two molecular pathways initiate mitochondria-dependent dopaminergic neurodegeneration in experimental Parkinson's disease. *Proc. Natl. Acad. Sci. U.S.A.* 104, 8161–8166. doi: 10.1073/pnas.0609874104

Pickrell, A. M., and Youle, R. J. (2015). The roles of PINK1, parkin, and mitochondrial fidelity in Parkinson's disease. *Neuron* 85, 257–273. doi: 10.1016/j.neuron.2014.12.007

Pietrocola, F., Galluzzi, L., Bravo-San Pedro, J. M., Madeo, F., and Kroemer, G. (2015). Acetyl coenzyme A: a central metabolite and second messenger. *Cell Metab.* 21, 805–821. doi: 10.1016/j.cmet.2015.05.014

Pittelli, M., Felici, R., Pitozzi, V., Giovannelli, L., Bigagli, E., Cialdai, F., et al. (2011). Pharmacological effects of exogenous NAD on mitochondrial bioenergetics, DNA repair, and apoptosis. *Mol. Pharmacol.* 80, 1136–1146. doi: 10.1124/mol.111.073916

Pollack, Y., Kasir, J., Shemer, R., Metzger, S., and Szyf, M. (1984). Methylation pattern of mouse mitochondrial DNA. *Nucleic Acids Res.* 12, 4811–4824. doi: 10.1093/nar/12.12.4811

Pradhan, S., Bacolla, A., Wells, R. D., and Roberts, R. J. (1999). Recombinant human DNA (cytosine-5) methyltransferase. I. Expression, purification, and comparison of novo and maintenance methylation. *J. Biol. Chem.* 274, 33002–33010. doi: 10.1074/jbc.274.46.33002

Prajapati, P., Sripada, L., Singh, K., Roy, M., Bhatelia, K., Dalwadi, P., et al. (2018). Systemic analysis of miRNAs in PD Stress Condition: miR-5701 modulates mitochondrial–lysosomal cross talk to regulate neuronal death. *Mol. Neurobiol.* 55, 4689–4701. doi: 10.1007/s12035-017-0664-6

Quirós, P. M., Mottis, A., and Auwerx, J. (2016). Mitonuclear communication in homeostasis and stress. *Nat. Rev. Mol. Cell Biol.* 17, 213–226. doi: 10.1038/nrm.2016.23

Quntanilla, R. A., and Tapia-Monsalves, C. (2020). The role of mitochondrial impairment in alzheimer's disease neurodegeneration: the tau connection. *Curr. Neuropharmacol.* 18, 1076–1091. doi: 10.2174/1570159X18666200525020259

Rackham, O., Shearwood, A. M. J., Mercer, T. R., Davies, S. M. K., Mattick, J. S., and Filipovska, A. (2011). Long noncoding RNAs are generated from the mitochondrial genome and regulated by nuclear-encoded proteins. *RNA* 17, 2085–2093. doi: 10.1261/rna.029405.111

Ramsahoye, B. H., Biniszkiewicz, D., Lyko, F., Clark, V., Bird, A. P., and Jaenisch, R. (2000). Non-CpG methylation is prevalent in embryonic stem cells and may be mediated by DNA methyltransferase 3a. *Proc. Natl. Acad. Sci. U.S.A.* 97, 5237–5242. doi: 10.1073/pnas.97.10.5237

Rice, A. C., Keeney, P. M., Algarzae, N. K., Ladd, A. C., Thomas, R. R., and Bennett, J. P. J. (2014). Mitochondrial DNA copy numbers in pyramidal neurons are decreased and mitochondrial biogenesis transcriptome signaling is disrupted in Alzheimer's disease hippocampi. *J. Alzheimers. Dis.* 40, 319–330. doi: 10.3233/JAD-131715

Rocha, E. M., De Miranda, B., and Sanders, L. H. (2018). Alpha-synuclein: pathology, mitochondrial dysfunction and neuroinflammation in Parkinson's disease. *Neurobiol. Dis.* 109, 249–257. doi: 10.1016/j.nbd.2017.04.004

Román, G. C., Mancera-Páez, O., and Bernal, C. (2019). Epigenetic factors in late-onset alzheimer's disease: MTHFR and CTH gene polymorphisms, metabolic transsulfuration and methylation pathways, and B Vitamins. *Int. J. Mol. Sci.* 20:319. doi: 10.3390/ijms20020319

Rosen, D. R. (1993). Mutations in Cu/Zn superoxide dismutase gene are associated with familial amyotrophic lateral sclerosis. *Nature* 364:362. doi: 10.1038/364362c0

Rufer, A. C., Thoma, R., and Hennig, M. (2009). Structural insight into function and regulation of carnitine palmitoyltransferase. *Cell. Mol. Life Sci.* 66, 2489–2501. doi: 10.1007/s00018-009-0035-1

Russell, A. E., and N Doll, D. (2016). TNF-α and beyond: rapid mitochondrial dysfunction mediates TNF-α-Induced Neurotoxicity. *J. Clin. Cell. Immunol.* 7:467. doi: 10.4172/2155-9899.1000467

Russell, A. P., Wada, S., Vergani, L., Hock, M. B., Lamon, S., Léger, B., et al. (2013). Disruption of skeletal muscle mitochondrial network genes and miRNAs in amyotrophic lateral sclerosis. *Neurobiol. Dis.* 49, 107–117. doi: 10.1016/j.nbd.2012.08.015

Salminen, A., Ojala, J., Kauppinen, A., Kaarniranta, K., and Suuronen, T. (2009). Inflammation in Alzheimer's disease: amyloid-β oligomers trigger innate immunity defence via pattern recognition receptors. *Prog. Neurobiol.* 87, 181–194. doi: 10.1016/j.pneurobio.2009.01.001

Samii, A., Nutt, J. G., and Ransom, B. R. (2004). Parkinson's disease. *Lancet (London, England)* 363, 1783–1793. doi: 10.1016/S0140-6736(04)16305-8

Schug, Z. T., Peck, B., Jones, D. T., Zhang, Q., Grosskurth, S., Alam, I. S., et al. (2015). Acetyl-CoA synthetase 2 promotes acetate utilization and maintains cancer cell growth under metabolic stress. *Cancer Cell* 27, 57–71. doi: 10.1016/j.ccell.2014.12.002

Shao, D., Liu, Y., Liu, X., Zhu, L., Cui, Y., Cui, A., et al. (2010). PGC-1β-Regulated mitochondrial biogenesis and function in myotubes is mediated by NRF-1 and ERRα. *Mitochondrion* 10, 516–527. doi: 10.1016/j.mito.2010.05.012

Shi, L., and Tu, B. P. (2015). Acetyl-CoA and the regulation of metabolism: mechanisms and consequences. *Curr. Opin. Cell Biol.* 33, 125–131. doi: 10.1016/j.ceb.2015.02.003

Shirendeb, U., Reddy, A. P., Manczak, M., Calkins, M. J., Mao, P., Tagle, D. A., et al. (2011). Abnormal mitochondrial dynamics, mitochondrial loss and mutant huntingtin oligomers in Huntington's disease: implications for selective neuronal damage. *Hum. Mol. Genet.* 20, 1438–1455. doi: 10.1093/hmg/ddr024

Shock, L. S., Thakkar, P. V., Peterson, E. J., Moran, R. G., and Taylor, S. M. (2011). DNA methyltransferase 1, cytosine methylation, and cytosine hydroxymethylation in mammalian mitochondria. *Proc. Natl. Acad. Sci. U.S.A.* 108, 3630–3635. doi: 10.1073/pnas.1012311108

Siddiqui, A., Chinta, S. J., Mallajosyula, J. K., Rajagopolan, S., Hanson, I., Rane, A., et al. (2012). Selective binding of nuclear alpha-synuclein to the PGC1alpha promoter under conditions of oxidative stress may contribute to losses in mitochondrial function: implications for Parkinson's disease. *Free Radic. Biol. Med.* 53, 993–1003. doi: 10.1016/j.freeradbiomed.2012.05.024

Sinha, K., Das, J., Pal, P. B., and Sil, P. C. (2013). Oxidative stress: the mitochondria-dependent and mitochondria-independent pathways of apoptosis. *Arch. Toxicol.* 87, 1157–1180. doi: 10.1007/s00204-013-1034-4

Song, W., Chen, J., Petrilli, A., Liot, G., Klinglmayr, E., Zhou, Y., et al. (2011). Mutant huntingtin binds the mitochondrial fission GTPase dynamin-related protein-1 and increases its enzymatic activity. *Nat. Med.* 17, 377–382. doi: 10.1038/nm.2313

Stanga, S., Caretto, A., Boido, M., and Vercelli, A. (2020). Mitochondrial dysfunctions: a red thread across neurodegenerative diseases. *Int. J. Mol. Sci.* 21:3719. doi: 10.3390/ijms21103719

Stein, L. R., and Imai, S. (2012). The dynamic regulation of NAD metabolism in mitochondria. *Trends Endocrinol. Metab.* 23, 420–428. doi: 10.1016/j.tem.2012.06.005

Stoccoro, A., Mosca, L., Carnicelli, V., Cavallari, U., Lunetta, C., Marocchi, A., et al. (2018). Mitochondrial DNA copy number and D-loop region methylation in carriers of amyotrophic lateral sclerosis gene mutations. *Epigenomics* 10, 1431–1443. doi: 10.2217/epi-2018-0072

Stoccoro, A., Siciliano, G., Migliore, L., and Coppedè, F. (2017). Decreased methylation of the mitochondrial D-Loop region in late-onset Alzheimer's Disease. *J. Alzheimer's Dis.* 59, 559–564. doi: 10.3233/JAD-170139

Stoccoro, A., Smith, A. R., Mosca, L., Marocchi, A., Gerardi, F., Lunetta, C., et al. (2020). Reduced mitochondrial D-loop methylation levels in sporadic amyotrophic lateral sclerosis. *Clin. Epigenetics* 12:137. doi: 10.1186/s13148-020-00933-2

Su, X., Chu, Y., Kordower, J. H., Li, B., Cao, H., Huang, L., et al. (2015). PGC-1α promoter methylation in Parkinson's disease. *PLoS One* 10:e0134087. doi: 10.1371/journal.pone.0134087

Subramaniam, S. R., and Chesselet, M.-F. (2013). Mitochondrial dysfunction and oxidative stress in Parkinson's disease. *Prog. Neurobiol.* 106–107, 17–32. doi: 10.1016/j.pneurobio.2013.04.004

Szeto, H. H. (2014). First-in-class cardiolipin-protective compound as a therapeutic agent to restore mitochondrial bioenergetics. *Br. J. Pharmacol.* 171, 2029–2050. doi: 10.1111/bph.12461

Takeuchi, H., Kobayashi, Y., Ishigaki, S., Doyu, M., and Sobue, G. (2002). Mitochondrial localization of mutant superoxide dismutase 1 triggers caspase-dependent cell death in a cellular model of familial amyotrophic lateral sclerosis. *J. Biol. Chem.* 277, 50966–50972. doi: 10.1074/jbc.M209356200

Tanno, M., Sakamoto, J., Miura, T., Shimamoto, K., and Horio, Y. (2007). Nucleocytoplasmic shuttling of the NAD+-dependent histone deacetylase SIRT1. *J. Biol. Chem.* 282, 6823–6832. doi: 10.1074/jbc.M609554200

Thomas, R. R., Keeney, P. M., and Bennett, J. P. (2012). Impaired complex-I mitochondrial biogenesis in parkinson disease frontal cortex. *J. Parkinsons. Dis.* 2, 67–76. doi: 10.3233/JPD-2012-11074

Tibbetts, A. S., and Appling, D. R. (2010). Compartmentalization of Mammalian folate-mediated one-carbon metabolism. *Annu. Rev. Nutr.* 30, 57–81. doi: 10.1146/annurev.nutr.012809.104810

Tönnies, E., and Trushina, E. (2017). Oxidative stress, synaptic dysfunction, and alzheimer's disease. *J. Alzheimers. Dis.* 57, 1105–1121. doi: 10.3233/JAD-161088

Trefely, S., Lovell, C. D., Snyder, N. W., and Wellen, K. E. (2020). Compartmentalised acyl-CoA metabolism and roles in chromatin regulation. *Mol. Metab.* 38:100941. doi: 10.1016/j.molmet.2020.01.005

van der Wijst, M. G. P., and Rots, M. G. (2015). Mitochondrial epigenetics: an overlooked layer of regulation? *Trends Genet.* 31, 353–356. doi: 10.1016/j.tig.2015.03.009

Vasanthakumar, A., Davis, J. W., Idler, K., Waring, J. F., Asque, E., Riley-Gillis, B., et al. (2020). Harnessing peripheral DNA methylation differences in the Alzheimer's Disease Neuroimaging Initiative (ADNI) to reveal novel biomarkers of disease. *Clin. Epigenetics* 12:84. doi: 10.1186/s13148-020-00864-y

Vercauteren, K., Gleyzer, N., and Scarpulla, R. C. (2008). PGC-1-related coactivator complexes with HCF-1 and NRF-2β in mediating NRF-2(GABP)-dependent respiratory gene expression. *J. Biol. Chem.* 283, 12102–12111. doi: 10.1074/jbc.M710150200

Vercauteren, K., Gleyzer, N., and Scarpulla, R. C. (2009). Short hairpin RNA-mediated silencing of PRC (PGC-1-related coactivator) results in a severe respiratory chain deficiency associated with the proliferation of aberrant mitochondria. *J. Biol. Chem.* 284, 2307–2319. doi: 10.1074/jbc.M806434200

Vercauteren, K., Pasko, R. A., Gleyzer, N., Marino, V. M., and Scarpulla, R. C. (2006). PGC-1-related coactivator: immediate early expression and characterization of a CREB/NRF-1 binding domain associated with cytochrome c promoter occupancy and respiratory growth. *Mol. Cell. Biol.* 26, 7409–7419. doi: 10.1128/mcb.00585-06

Verdin, E. (2015). NAD+ in aging, metabolism, and neurodegeneration. *Science* 350, 1208–1213. doi: 10.1126/science.aac4854

Volpicelli-Daley, L. A., Luk, K. C., and Lee, V. M.-Y. (2014). Addition of exogenous α-synuclein preformed fibrils to primary neuronal cultures to seed recruitment of endogenous α-synuclein to Lewy body and Lewy neurite-like aggregates. *Nat. Protoc.* 9, 2135–2146. doi: 10.1038/nprot.2014.143

Volpicelli-Daley, L. A., Luk, K. C., Patel, T. P., Tanik, S. A., Riddle, D. M., Stieber, A., et al. (2011). Exogenous α-synuclein fibrils induce Lewy body pathology leading to synaptic dysfunction and neuron death. *Neuron* 72, 57–71. doi: 10.1016/j.neuron.2011.08.033

Wang, C., Chen, L., Yang, Y., Zhang, M., and Wong, G. (2019). Identification of potential blood biomarkers for Parkinson's disease by gene expression and DNA methylation data integration analysis. *Clin. Epigenetics* 11:24. doi: 10.1186/s13148-019-0621-5

Wang, H., Lu, B., and Chen, J. (2019). Knockdown of lncRNA SNHG1 attenuated Aβ25-35-inudced neuronal injury via regulating KREMEN1 by acting as a ceRNA of miR-137 in neuronal cells. *Biochem. Biophys. Res. Commun.* 518, 438–444. doi: 10.1016/j.bbrc.2019.08.033

Wang, H., Ye, Y., Zhu, Z., Mo, L., Lin, C., Wang, Q., et al. (2016). MiR-124 regulates apoptosis and autophagy process in MPTP model of Parkinson's disease by targeting to bim. *Brain Pathol.* 26, 167–176. doi: 10.1111/bpa.12267

Wang, J., Le, T., Wei, R., and Jiao, Y. (2016). Knockdown of JMJD1C, a target gene of hsa-miR-590-3p, inhibits mitochondrial dysfunction and oxidative stress in MPP+-treated MES23.5 and SH-SY5Y cells. *Cell. Mol. Biol.* 62, 39–45. doi: 10.14715/cmb/2016.62.3.8

Wang, Q., Ge, X., Zhang, J., and Chen, L. (2020). Effect of lncRNA WT1-AS regulating WT1 on oxidative stress injury and apoptosis of neurons in Alzheimer's disease via inhibition of the miR-375/SIX4 axis. *Aging (Albany. NY)* 12, 23974–23995. doi: 10.18632/aging.104079

Wang, W. X., Prajapati, P., Vekaria, H., Spry, M., Cloud, A., Sullivan, P., et al. (2021). Temporal changes in inflammatory mitochondria-enriched microRNAs following traumatic brain injury and effects of miR-146a nanoparticle delivery. *Neural Regen. Res.* 16, 514–522. doi: 10.4103/1673-5374.293149

Wang, W. X., Visavadiya, N. P., Pandya, J. D., Nelson, P. T., Sullivan, P. G., and Springer, J. E. (2015). Mitochondria-associated microRNAs in rat hippocampus following traumatic brain injury. *Exp. Neurol.* 265, 84–93. doi: 10.1016/j.expneurol.2014.12.018

Wellen, K. E., Hatzivassiliou, G., Sachdeva, U. M., Bui, T. V., Cross, J. R., and Thompson, C. B. (2009). ATP-citrate lyase links cellular metabolism to histone acetylation. *Science* 324, 1076–1080. doi: 10.1126/science.1164097

Wong, M., Gertz, B., Chestnut, B. A., and Martin, L. J. (2013). Mitochondrial DNMT3A and DNA methylation in skeletal muscle and CNS of transgenic mouse models of ALS. *Front. Cell. Neurosci.* 7:279. doi: 10.3389/fncel.2013.00279

Wong, P. C., Pardo, C. A., Borchelt, D. R., Lee, M. K., Copeland, N. G., Jenkins, N. A., et al. (1995). An adverse property of a familial ALS-linked SOD1 mutation causes motor neuron disease characterized by vacuolar degeneration of mitochondria. *Neuron* 14, 1105–1116. doi: 10.1016/0896-6273(95)90259-7

Wu, Y.-Y., and Kuo, H.-C. (2020). Functional roles and networks of non-coding RNAs in the pathogenesis of neurodegenerative diseases. *J. Biomed. Sci.* 27:49. doi: 10.1186/s12929-020-00636-z

Xu, W., Yang, H., Liu, Y., Yang, Y., Wang, P., Kim, S. H., et al. (2011). Oncometabolite 2-hydroxyglutarate is a competitive inhibitor of α-ketoglutarate-dependent dioxygenases. *Cancer Cell* 19, 17–30. doi: 10.1016/j.ccr.2010.12.014

Yang, H., Yang, T., Baur, J. A., Perez, E., Matsui, T., Carmona, J. J., et al. (2007). Nutrient-Sensitive Mitochondrial NAD+ levels dictate cell survival. *Cell* 130, 1095–1107. doi: 10.1016/j.cell.2007.07.035

Yao, J., Irwin, R. W., Zhao, L., Nilsen, J., Hamilton, R. T., and Brinton, R. D. (2009). Mitochondrial bioenergetic deficit precedes Alzheimer's pathology in female mouse model of Alzheimer's disease. *Proc. Natl. Acad. Sci. U.S.A.* 106, 14670–14675. doi: 10.1073/pnas.0903563106

Zaidi, N., Swinnen, J. V., and Smans, K. (2012). ATP-citrate lyase: a key player in cancer metabolism. *Cancer Res.* 72, 3709–3714. doi: 10.1158/0008-5472.CAN-11-4112

Zhang, H., Ryu, D., Wu, Y., Gariani, K., Wang, X., Luan, P., et al. (2016). NAD+ repletion improves mitochondrial and stem cell function and enhances life span in mice. *Science* 352, 1436–1443. doi: 10.1126/science.aaf2693

Zhang, R., Zhou, H., Jiang, L., Mao, Y., Cui, X., Xie, B., et al. (2016). MiR-195 dependent roles of mitofusin2 in the mitochondrial dysfunction of hippocampal neurons in SAMP8 mice. *Brain Res.* 1652, 135–143. doi: 10.1016/j.brainres.2016.09.047

Zhao, Y., Alexandrov, P. N., and Lukiw, W. J. (2016). Anti-microRNAs as novel therapeutic agents in the clinical management of alzheimer's disease. *Front. Neurosci.* 10:59. doi: 10.3389/fnins.2016.00059

Zhou, J., Zhao, Y., Li, Z., Zhu, M., Wang, Z., Li, Y., et al. (2020). miR-103a-3p regulates mitophagy in Parkinson's disease through Parkin/Ambra1 signaling. *Pharmacol. Res.* 160:105197. doi: 10.1016/j.phrs.2020.105197

Zhou, W., Zhao, T., Du, J., Ji, G., Li, X., Ji, S., et al. (2019). TIGAR promotes neural stem cell differentiation through acetyl-CoA-mediated histone acetylation. *Cell Death Dis.* 10:198. doi: 10.1038/s41419-019-1434-3

Conflict of Interest: The authors declare that the research was conducted in the absence of any commercial or financial relationships that could be construed as a potential conflict of interest.

Publisher's Note: All claims expressed in this article are solely those of the authors and do not necessarily represent those of their affiliated organizations, or those of the publisher, the editors and the reviewers. Any product that may be evaluated in this article, or claim that may be made by its manufacturer, is not guaranteed or endorsed by the publisher.

frontiers in Cell and Developmental Biology

REVIEW
published: 30 August 2021
doi: 10.3389/fcell.2021.719247

Long Non-coding RNAs in Pathogenesis of Neurodegenerative Diseases

*Shiyue Zhou[1], Xiao Yu[2], Min Wang[1], Yujie Meng[3], Dandan Song[3], Hui Yang[1], Dewei Wang[1], Jianzhong Bi[1] and Shunliang Xu[1]**

[1] Department of Neurology, The Second Hospital, Cheeloo College of Medicine, Shandong University, Jinan, China, [2] Department of Nutrition, The Second Hospital, Cheeloo College of Medicine, Shandong University, Jinan, China, [3] Cheeloo College of Medicine, Shandong University, Jinan, China

Emerging evidence addresses the link between the aberrant epigenetic regulation of gene expression and numerous diseases including neurological disorders, such as Alzheimer's disease (AD), Parkinson's disease (PD), amyotrophic lateral sclerosis (ALS), and Huntington's disease (HD). LncRNAs, a class of ncRNAs, have length of 200 nt or more, some of which crucially regulate a variety of biological processes such as epigenetic-mediated chromatin remodeling, mRNA stability, X-chromosome inactivation and imprinting. Aberrant regulation of the lncRNAs contributes to pathogenesis of many diseases, such as the neurological disorders at the transcriptional and post-transcriptional levels. In this review, we highlight the latest research progress on the contributions of some lncRNAs to the pathogenesis of neurodegenerative diseases *via* varied mechanisms, such as autophagy regulation, Aβ deposition, neuroinflammation, Tau phosphorylation and α-synuclein aggregation. Meanwhile, we also address the potential challenges on the lncRNAs-mediated epigenetic study to further understand the molecular mechanism of the neurodegenerative diseases.

Keywords: long non-coding RNAs, neurodegenerative diseases, Alzheimer's disease, Parkinson's disease, Huntington's disease, amyotrophic lateral sclerosis

OPEN ACCESS

Edited by:
Mojgan Rastegar, University of Manitoba, Canada

Reviewed by:
Serge Weis, Kepler University Hospital GmbH, Austria
Graziano Pesole, University of Bari Aldo Moro, Italy

****Correspondence:***
Shunliang Xu
slxu@live.com

Specialty section:
This article was submitted to Epigenomics and Epigenetics, a section of the journal Frontiers in Cell and Developmental Biology

Received: *02 June 2021*
Accepted: *11 August 2021*
Published: *30 August 2021*

Citation:
Zhou S, Yu X, Wang M, Meng Y, Song D, Yang H, Wang D, Bi J and Xu S (2021) Long Non-coding RNAs in Pathogenesis of Neurodegenerative Diseases. Front. Cell Dev. Biol. 9:719247. doi: 10.3389/fcell.2021.719247

INTRODUCTION

Epigenetics literally refers to regulation of gene expression due to external modifications to DNA and histones without altering DNA sequence. Caused by a variety of factors inside / outside of organisms, such as hormones, metabolism, diet, temperature, light, drugs, air pollution, age and so on, epigenetic changes could alter growth, development, reproduction and aging, and even contribute to pathogenesis of diseases such as neurological disorders. Significant efforts have been made in study of the epigenetic basis of neurodegenerative diseases (Thompson et al., 2020), such as Alzheimer's disease (AD), Parkinson's disease (PD), amyotrophic lateral sclerosis (ALS), Huntington's disease (HD), and so on.

Epigenetic modifications could be classified into three main categories including DNA modifications, histone modifications, and non-coding RNAs (ncRNAs)-mediated modifications (Hwang et al., 2017; Thompson et al., 2020). Of the DNA methylation modifications, 5-methylcytosine (5-mC), 5-hydroxymethylcytosine (5-hmC), and N^6-methyladenosine (m6A) have been identified and characterized as important epigenetic markers involved in regulation of gene

expression in complicated mechanisms (Dermentzaki and Lotti, 2020; Pizzorusso and Tognini, 2020). In a broad sense, the ncRNAs are widely defined as all types of RNAs that are not translated into proteins due to the lack of an open reading frame (ORF).

Based on the length with 200 nt as cutoff value (Elling et al., 2016), ncRNAs could be classified into small ncRNAs (sncRNAs) and long ncRNAs (lncRNAs). Typical sncRNAs include microRNAs (miRNAs), piwi interacting RNAs (piRNAs), endogenous small interference RNAs (esiRNAs), micronucleus RNAs (snRNAs), small nucleolus RNAs (snoRNAs) and so on (Sosinska et al., 2015; Elling et al., 2016; Wu and Kuo, 2020).

It has been estimated that there are more than 50,000 of lncRNAs in the human genome (Managadze et al., 2013). Based on the genomic location of lncRNAs relative to protein coding genes, lncRNAs could be classified into five categories (**Figure 1**): (1) long intergenic non-coding RNAs (LincRNAs), consisting of independent transcriptional units located between but not overlapped with protein codes; (2) intron transcripts located in the intron region of protein coding genes (sense or antisense); (3) Sense lncRNAs are transcribed by the sense chain of the protein-coding gene, which overlaps with at least one exon of the protein-coding gene on the same chain and has the same transcriptional direction. The sense lncRNAs may partially overlap with the protein coding gene, or it may cover the entire sequence of the protein coding gene; (4) Antisense lncRNAs are transcribed by a complementary DNA chain of protein-encoded genes, they are transcribed in the opposite direction and overlaps with at least one exon of the positive gene; (5) bidirectional lncRNAs (bilncRNAs) transcribed from different bidirectional promoters (Quan et al., 2017; Liu et al., 2021).

Structurally, majority lncRNAs are very similar to but different from mRNAs. In terms of the similarity, they are transcribed from RNA polymerase II (POLII) from genomic sites in a chromatin-like state; usually 5-capped, spliced, and polyglandular. However, there is still a general trend to distinguish lncRNAs from mRNAs: lncRNAs tends to be shorter than mRNAs, with fewer but longer exons, failing to translate due to lacking in open reading frame, relatively low expression level and poor conservation of primary sequences (Quinn and Chang, 2015).

LncRNA could regulate expression of genes located in other genomic loci on different chromosomes at the transcriptional and posttranscriptional levels, such as RNA processing and translation (Elling et al., 2016). Most lncRNAs are located in the nucleus, thereby acting as scaffolds for chromatin modifiers by interacting with chromatin modification complexes or performing their regulatory functions as transcription co-regulators *via* binding to transcription factors (Ulitsky and Bartel, 2013). For example, LncRNA-XIST is a well-studied *cis*-acting LncRNA, which performs the critical developmental process of dosage compensation in females (Cerase et al., 2015). It suppresses the expression of the entire chromosome by inhibition the deposition of chromatin markers and relocating this inactive X chromosome to the periphery of the nucleus (Cerase et al., 2015). In the cytoplasm, lncRNAs usually act as regulators of RNA processing, such as RNA editing, splicing, and miRNA-mediated mRNA expression. LncRNAs also bind to other coding or ncRNAs to regulate transcription as competing endogenous RNAs (ceRNAs) (Salmena et al., 2011). LncRNAs can be used as a molecular sponge of miRNAs and titrate their levels, thereby increasing the expression of mRNAs targeted by these miRNAs (Salmena et al., 2011).

PHYSIOLOGICAL FUNCTION OF LncRNAs IN THE CENTRAL NERVOUS SYSTEM

It is estimated that about 40% of LncRNAs are specifically expressed in brain tissue, and their number far exceeds that of protein-coding genes (Derrien et al., 2012). And compared with other tissues, LncRNAs are more conservative in brain tissue. In addition, in brain tissue, lncRNAs show stronger temporal and spatial specificity than mRNAs (Ponjavic et al., 2009). For example, LncRNAs have significant differences in different brain tissues (brain cortex, hippocampus, etc.) and in different age groups (Kadakkuzha et al., 2015). For example, human acceleration region 1 (HAR1), which is part of the overlapping lncRNA gene HAR1F (HAR1A). The gene is specifically expressed in Cajal–Retzius neurons in the developing human cerebral cortex (Pollard et al., 2006). LncRNAs are related to neural differentiation. In proliferative stem cells / progenitor cells, lncRNAs control the sequential activation of cell type-specific gene regulatory programs, thus promoting the development from pluripotent cells in early embryos to the terminal cell types evident in the brain of mature mammals (Zimmer-Bensch, 2019). LncRNA_DALI promotes neural differentiation by driving the expression of necessary neuronal differentiation genes in neuroblastoma cells through a variety of mechanisms. It promotes the expression of Pou3f3 in *cis*, forms a *trans*-acting regulatory complex with DALI, and regulates the expression of neural differentiation genes (Chalei et al., 2014). LncRNAs are related to neurite outgrowth, synaptogenesis and synaptic plasticity (Yang et al., 2021). Neurite outgrowth, synaptogenesis and synaptic plasticity all require complex gene expression regulation and signal transduction, in which lncRNA plays an important role (Modarresi et al., 2012; Mateos-Aparicio and Rodriguez-Moreno, 2019). Brain-derived neurotrophic factor (BDNF) is related to synaptogenesis and neurite outgrowth (Modarresi et al., 2012). BDNF-AS, the antisense LncRNA of BDNF, suppresses the BDNF growth factor gene by recruiting PRC2 to the BDNF site, thus affecting BDNF-mediated axonal growth, proliferation and apoptosis (Modarresi et al., 2012).

LncRNAs AND AD

Alzheimer's disease is the most common, irreversible, and progressive neurodegenerative disorder, accounting for 60% of all dementia cases (Ryan et al., 2018), particularly the people over 65 years old. Among the more than 50 million cases of dementia patients worldwide in 2018, AD patients accounted for 50.75%. Statistically, the global cost of dementia reached United States $957.56 billion in 2015 and will continue increasing

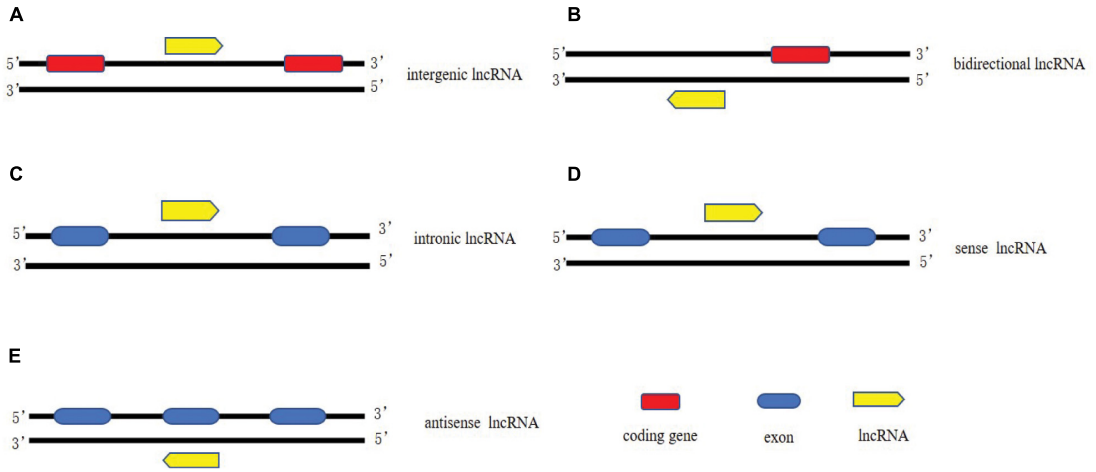

FIGURE 1 | Classification of lncRNAs. **(A)** long intergenic non-coding RNAs, consisting of independent transcriptional units located between but not overlapped with protein codes; **(B)** bidirectional lncRNAs transcribed from different bidirectional promoters. **(C)** intron lncRNAs located in the intron region of protein coding genes (sense or antisense); **(D)** Sense lncRNAs are transcribed by the sense chain of the protein-coding gene, which overlaps with at least one exon of the protein-coding gene on the same chain and has the same transcriptional direction; **(E)** Antisense lncRNAs are transcribed by a complementary DNA chain of protein-encoded genes, they are transcribed in the opposite direction and overlaps with at least one exon of the positive gene.

to United States $9.12 trillion in 2050 as estimated. The main pathological features of AD include β-amyloid plaque deposition, neurofibrillary tangles caused by hyperphosphorylated tau protein, and neuronal loss in specific areas of the brain (Lashley et al., 2018). Despite the high prevalence of AD, the etiology of AD remains to be unclear.

Emerging data have correlated the imbalance of lncRNA expression with a variety of human diseases, such as cardiovascular diseases, cerebrovascular diseases, malignant tumors and neurodegenerative diseases. Indeed, expression disorder of many lncRNAs has been detected in AD (Luo and Chen, 2016), mainly involved in A β deposition, Tau protein hyperphosphorylation, oxidative stress, neuroinflammation, mitochondrial dysfunction, autophagy regulation and other pathological processes (**Table 1**).

Aβ Plaque Formation

Previous studies have proven the contribution of lncRNAs to formation of the Aβ plaques derived from the proteolytic cleavage of Aβ precursor protein (APP) by β-position APP cleaving enzyme 1 (BACE1) and γ secretase. Indeed, dysregulation of BACE1 leads to overproduction of Aβ, contributing to pathogenesis of AD (Modarresi et al., 2011). Basically, lncRNA BACE1-AS is transcribed by RNA polymerase II from the antisense strand of the BACE1 locus located on chromosome 11. It was clear that BACE1-AS is highly expressed in brains of the AD patients and APP transgenic mice, regulates the expression of BACE1 mRNA and increases the production of Aβ (Cortini et al., 2019). The loss of BACE1 in animal models led to physical and behavioral defects, such as decreased learning ability, memory and emotional loss (Ma et al., 2007). The siRNA-based silencing of BACE1-AS in mouse brains significantly decreased the BACE1 mRNA levels in cortex, central and dorsal hippocampal regions (Faghihi et al., 2008). Mechanistically, high level expression of BACE1-AS could promote the stability of BACE1mRNA, which in turn enhances the processing ability of APP and consequently promotes Aβ deposition

TABLE 1 | Main dysregulated long non-coding RNAs in Alzheimer's disease.

LncRNA	Target mRNA	AD-related process	Biological function	References
BACE1-AS	*BACE1*	Aβ deposition	Upregulating *BACE1* mRNA stability	Faghihi et al., 2008; Shah et al., 2012; Cortini et al., 2019
XIST	*BACE1*	Aβ deposition	Upregulating *BACE1* mRNA stability	Zhu et al., 2018; Yue et al., 2019
51A	*SORL1*	Aβ deposition	Downregulating *SORL1* variant A	Ciarlo et al., 2013
Linc00507	*MAPT / TTBK1*	Tau hyperphosphorylation	Regulating the expression of MAPT and TTBK1	Yan et al., 2020
NEAT1	*FZD3*	Tau hyperphosphorylation	Impairing the FZD3/GSK3β/p-tau signaling pathway	Zhao et al., 2020
MALAT1	*IL-10/ SOC1*	Neuroinflammation	Regulating the expression of IL-10 and SOC1	Masoumi et al., 2019; Ma et al., 2019
EBF3-AS	*EBF3*	Neuronal apoptosis	Promoting neuronal apoptosis in AD	Magistri et al., 2015; Gu et al., 2018
SNHG1	*KRENEN1*	Neuronal apoptosis	Target miR-137 to inhibit KREMEN1	Causeret et al., 2016; Wang et al., 2019

(Faghihi et al., 2008). Some epigenetic factors could regulate the expression of BACE1-AS. For example, stress response stimulates the expression of the BACE1-AS, accelerating development of AD (Shah et al., 2012).

Another important lncRNA essentially involved in the pathogenesis of AD is XIST, one of the most extensively characterized lncRNA, which plays important roles in cancer and cardiovascular diseases as well (Sun et al., 2017; Kong et al., 2018; Zhou et al., 2019). Expression of the XIST was upregulated in AD model mice and N2a cells in response to H_2O_2 oxidative stress. Bioinformatic analysis predicted a binding site between miR-124 and XIST as well as between miR-124 and BACE1. Expression of XIST was negatively correlated with miR-124 but positively with BACE1. Consistently, knockdown of XIST upregulated expression of miR-124 but downregulated the expression of BACE1 in N2a cells. The direct interactions between XIST and miR-124, as well as BACE1 and miR-124 were further confirmed by using luciferase reporter assay (Zhu et al., 2018). Altogether, it could be concluded that silencing of XIST could attenuate alteration of the AD-related BACE1 *via* the miR-124 / BACE1 signaling pathway (Yue et al., 2019). Besides BACE1-AS and XIST, lnc-51A has been acknowledged as an important factor for Aβ deposition. Upregulation of the lnc-51A was detected in plasma of sporadic AD patients. Furthermore, expression of lnc-51A was negatively correlated with disease progression assessed by MMSE score most probably because the upregulation of lnc-51A altered splicing mode of SORL1, thereby causing damage to APP processing and leading to promotion of the Aβ deposition (Ciarlo et al., 2013). These results suggest that the lnc-51A may serve as a stable diagnostic biomarker of AD as well.

Tau Hyperphosphorylation

As another important possible pathogenesis of AD, Tau plays an important role in inducing Aβ deposition. Hyperphosphorylation of Tau leads to tau aggregation, exerting neurotoxicity that destroys neuronal function and thereby inducing AD (Clavaguera et al., 2009; Zempel and Mandelkow, 2015). So far, several lncRNAs have been identified to be involved in Tau hyperphosphorylation, such as linc-00507, lncRNA SOX21-AS1, and NEAT1. Expression of linc-00507 was significantly upregulated in hippocampus, cerebral cortex, and AD SH-SY5Y-like cells of APP/PS transgenic mice. The linc-00507 could regulate the expression of microtubule-associated proteins Tau (MAPT) and tau-tubulin protein kinase 1 (TTBK1) *via* two mechanisms: as competitive endogenous RNA (ceRNA) to bind miR181c-5p, as enhancer of hyperphosphorylation of tau protein by activating P25/P35 /GSK3β signaling pathway (Yan et al., 2020).

Upregulation of SOX21-AS1 was also observed in SH-SY5Y and SK-N-SH cells treated with Aβ 1–42. Essentially, the SOX21-AS1 functions as a sponge for miR-107 in SH-SY5Y and SK-N-SH cells. Silencing of SOX21-AS1 could attenuate the level of Tau phosphorylation mediated by Aβ 1–42 in SHSY5Y and SK-N-SH cells. Consistently, the SOX21-AS1 knockdown reversed the level of p-Tau mediated by miR107 inhibition (Xu et al., 2020a). More importantly, SOX21-AS1 silencing could inhibit hippocampal neuronal apoptosis and enhance memory and learning ability in AD mice (Zhang et al., 2019a), suggesting that SOX21-AS1 could serve as a potential biomarker for AD patient.

Similarly, NEAT1 was upregulated in SH-SY5Y cells and primary neurons of the AD model, and downregulation of NEAT1 promoted Tau protein phosphorylation through FZD3/GSK3 β / p-tau pathway (Zhao et al., 2020).

Neuroinflammation

The neuroinflammation has been acknowledged as one of the key features in AD with a primary role in exacerbation of Aβ plaques and tau hyperphosphorylation, contributing to AD pathology. So far, some lncRNAs have been identified to be involved in the neuroinflammation, such as MALAT1.

Downregulation of MALAT1 promotes the polarization of macrophages to M1 phenotype and induces the proliferation of T cells in multiple sclerosis (MS), indicating the potential anti-inflammatory effect of MALAT1 on MS (Masoumi et al., 2019). Stimulation of SD rat embryonic PC12 cells and primary cortical neurons with nerve growth factor (NGF) inhibited apoptosis of neurons in PC12 AD model and primary neuronal AD model mediated by lncMALAT1 and promoted growth of neurites in primary neuronal AD model. To further explain the mechanism of MALAT1 on neuroinflammation in AD, it was found that MALAT1 downregulated expression of IL-6 and TNF-α in PC12AD model and primary neuronal AD model, but enhanced expression of IL-10. These results suggest that MALAT1 contributes to the pathogenesis of AD by regulating inflammation response. Further study demonstrated that MALAT1 may inhibit several inflammation-related miRNAs, such as miR-125b and miR-155. These miRNAs targets to the genes involved in many signaling pathways, such as JAK signal transduction and activator of transcription (STAT) pathway, nuclear factor- kB (NF-kB) signaling pathway, JNK pathway and p38 signaling pathway, thereby inhibiting neuroinflammation of AD (Ma et al., 2019).

LncRNA MEG3 (maternally expressed gene 3) plays important roles in cell proliferation, learning, and memory (Guo et al., 2016; Zhang et al., 2016a). The expression of MEG3 was downregulated in the hippocampus of rats with AD. It has been found that MEG3 upregulation could improve the spatial learning and memory ability of AD rats. MEG3 can reduce the deposition of Aβ 25–35 and oxidative stress in the hippocampus of rats with AD, and reduce the inflammatory injury by downregulating IL-1 β, IL-6 and TNF- α. In addition, the overexpression of MEG3 inhibits the activation of astrocytes in the hippocampus of patients with AD by inhibiting PI3K/Akt signal pathway (Yi et al., 2019).

Neuronal Apoptosis

LncRNA-mediated neuronal apoptosis has been linked to pathogenesis of AD. Knockout of SNHG1 could increase cell viability and inhibit apoptosis in SH-SY5Y and HPN cells treated with Aβ 25–35. The SNHG1 could protect SH-SY5Y and HPN cells treated with Aβ 25–35 from neuronal apoptosis *via*

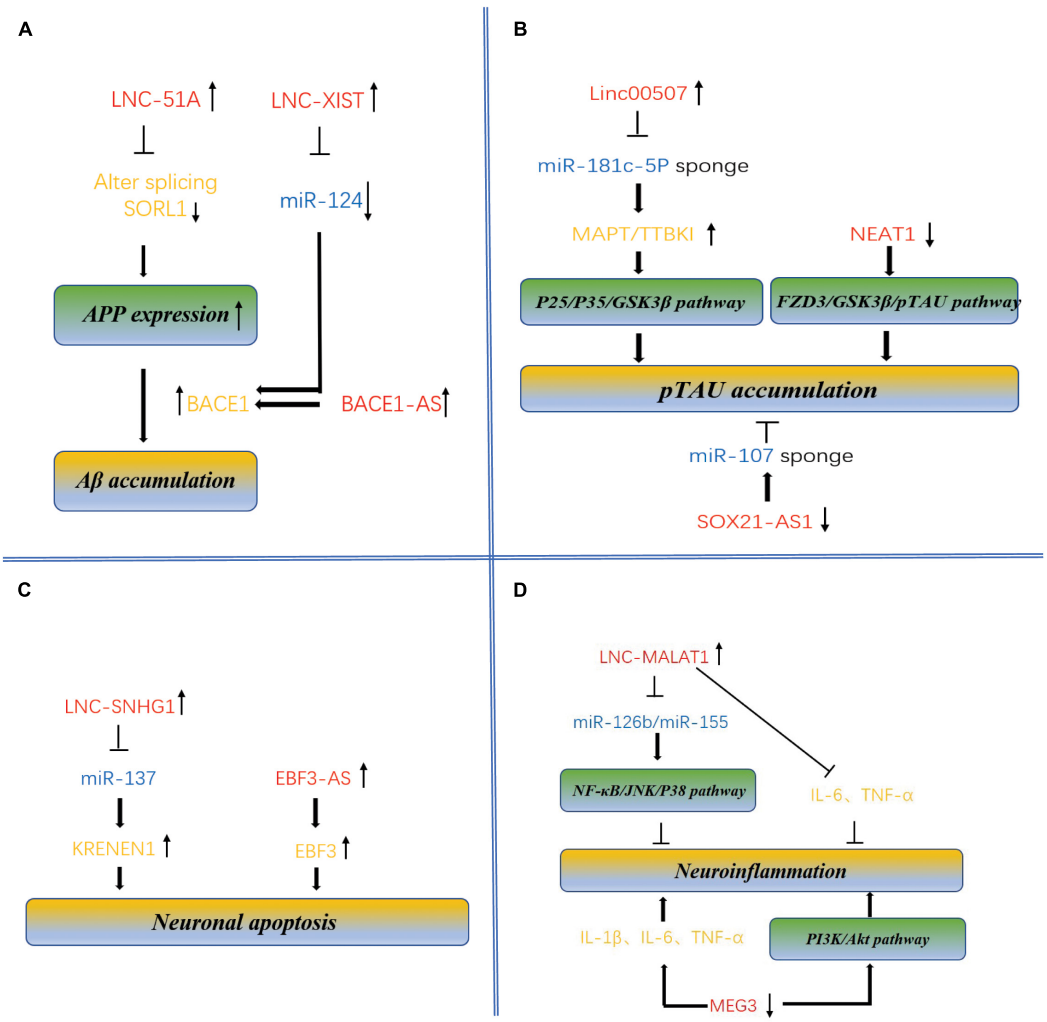

FIGURE 2 | Molecular mechanism of lncRNAs and miRNAs mediated accumulation of Aβ plaques and pTAU, neuronal apoptosis and neuroinflammation in AD. **(A)** Dysregulation of BACE1-AS, XIST, and lnc-51A leads to overproduction of Aβ, contributing to pathogenesis of AD. BACE1-AS, XIST, and lnc-51A are highly expressed in brains of the AD patients and APP transgenic mice, regulates the expression of BACE1 mRNA and increases the production of Aβ. Enhanced expression of lnc-51A in AD patient altered splicing mode of SORL1, thereby causing damage to APP processing and leading to promotion of the A β deposition. XIST and BACE1 are targets of miR-124 because there is a binding site in these two targets. The XIST-miR-124-BACE1 axis regulates the expression of BACE1 in AD, determining the formation of Aβ. **(B)** LncRNAs regulate pTAU accumulation. Linc-00507, SOX21-AS1, and NEAT1 have been characterized to be involved in Tau hyperphosphorylation. Significantly upregulated expression of linc-00507 downregulates miR181c-5p, thereby elevating the levels of MAPT and TTBK1 and consequently enhancing hyperphosphorylation of tau protein by activating P25/P35 /GSK3β signaling pathway. On the other hand, silencing of SOX21-AS1 could attenuate the level of Tau phosphorylation mediated by miR107 inhibition. Similarly, downregulation of NEAT1 promoted Tau protein phosphorylation *via* FZD3/GSK3 β / p-tau pathway. **(C)** LncRNAs regulate neuronal apoptosis. LncRNA-SNHG1, lnc-EBF3-AS, and MEG3 have been identified to be involved in neuronal apoptosis, linking to pathogenesis of AD. SNHG1 silencing inhibited miR-137, therefore repressing KRENEN1 expression and increasing cell viability and inhibiting apoptosis. was maladjusted in late-onset AD patients (Magistri et al., 2015), its upregulation of lnc-EBF3-AS stimulated the expression of EBF3, thus promoting the apoptosis of neurons in AD. **(D)** LncRNAs regulate neuroinflammation. Some lncRNAs, and miRNAs such as MALAT1 and MEG3, have been identified to be involved in the neuroinflammation. Upregulation of MALAT1 downregulated expression several inflammation-related miRNAs, such as miR-125b and miR-155. These miRNAs target to the genes involved in many signaling pathways, such as JAK signal transduction and activator of transcription (STAT) pathway, nuclear factor –kB (NF-kB) signaling pathway, JNK pathway and p38 signaling pathway, thereby inhibiting neuroinflammation of AD. downregulated expression of MEG3 promoting the occurrence of inflammation.

inhibiting miR-137. KREMEN1 belongs to the dickkopf (Dkk) family of Wnt antagonists. Wnt-independent way plays a role in promoting apoptosis in cells (Causeret et al., 2016). Further study showed that knockdown of SNHG1 exerts its neuronal protective effect through the inhibition of KRENEN1 by ceRNA miR-137 (Wang et al., 2019).

Lnc-EBF3-AS was maladjusted in late-onset AD patients (Magistri et al., 2015), its upregulation was detected to stimulate the expression of EBF3 in the hippocampus of the AD transgenic mouse model, thus promoting the apoptosis of neurons in AD (Gu et al., 2018). This study suggests the potential role of the lnc-EBF3-AS in the pathogenesis of AD (**Figure 2**).

LncRNAs AND PD

Parkinson's disease is an anther age-related progressive neurodegenerative disease, affecting 1% of people mainly over the age of 65. Compared with effect on memory, thinking and cognition in AD, PD mainly affects the motor system. The two typical features of PD include loss of dopaminergic neurons in the substantia nigra and accumulation of a-synuclein (Calabresi et al., 2013; Bose and Beal, 2016). Despite decades of research, our understanding to the pathophysiology and diagnosis of PD is still at infancy stage. Accordingly, so far, there is no efficient strategy for therapy of the disease albeit the current dopamine replacement strategies and surgical interventions can provide symptom relief, still failing to prevent or reverse the underlying pathology (Hegarty et al., 2020; **Table 2**).

Dopaminergic Neuron Loss

Efforts have been made to elucidate the mechanisms of the lncRNA-mediated dopaminergic neuron loss in AD (Jiang et al., 2020). H19, among the first lncRNAs identified, has been considered as one of the major players in embryonic development, cancer, and PD *via* regulating proliferation, differentiation and cell motility through controlling DNA methylation and intracellular miRNA pattern being both a sponge for miRNAs and miRNA reservoir.

H19 is located in the imprinted gene cluster H19-IGF2 (Li et al., 2016), whereas the IGF2- proinsulin precursor (INS)-TH gene cluster located at the telomere end of chromosome 11 has been reported to encode various proteins important for homeostasis in dopamine neurons (Sutherland et al., 2008). Therefore, this gene cluster is associated with the risk of PD (Sutherland et al., 2008). Level of the H19 significantly decreased in the 6-hydroxydopa (6-OHDA)-induced PD mice. Consistently, overexpression of the H19 could prevent dopaminergic neuron loss in the 6-OHDA-induced PD model by activating HPRT1-mediated Wnt/β catenin signaling pathway *via* impairing miR-301b-3p-targeted repression of HPRT1 transcription (Jiang et al., 2020). Indeed, significant upregulation of miR-301b in the pars compacta of substantia nigra of PD mouse model downregulates HPRT1 expression. Thus, by serving as sponge of miR-301b-3p, H19 could reduce the loss of dopaminergic neurons and eventually slow down the degeneration of striatum nigra (SN) (Jiang et al., 2020).

NEAT1 upregulation in dopaminergic neurons of PD may protect dopaminergic neurons from LRRK2-mediated damage under the oxidative stress. Highly variable expression level of NEAT1 in SN may reflect its response to multiple factors. Due to the estrogen-associated high expression of NEAT1 in female, dopaminergic neurons in the SN could be protected, potentially explaining why the incidence of PD in women is significantly lower than in men (Chakravarty et al., 2014; Bastias-Candia et al., 2019). However, significant upregulation of NEAT1 expression does not always protect dopaminergic neurons for any PD patients. Instead, it is in a patient (such as gender and carriers of LRRK2 mutations) dependent manner. For example, the enhanced NEAT1 expression in simvastatin and fenofibrate was harmful for certain PD patients, such as carriers of LRRK2 mutations. Altogether suggest that certain drugs that could alter the expression of NEAT1 in SN might potentially function as prevention or therapy of PD for a specific subpopulations of PD patients (Simchovitz et al., 2019).

Another important lncRNA that could be potentially involved in Dopaminergic neuron loss is SNHG14, its expression is upregulated in brain tissue of PD mouse model induced by rotenone. Binding affinity of the transcription factor SP-1 to SNHG14 promoter was enhanced, leading to upregulation of SNHG14 expression in the rotenone induced PD model of MN9D cells. Consistently, knockdown of SNHG14 expression in MN9D cells could alleviate the damage induced by rotenone in dopaminergic neurons through activation of the miR-133b inhibited by SNHG14, whereas miR-133b targets to 3′UTR of α-synuclein that contributes to PD pathogenesis. Similarly, the silencing of SNHG14 reduced the neuronal damage in the PD mouse model as well. Therefore, silencing of SNHG14 reduces the damage of dopaminergic neurons by downregulating α-synuclein *via* miR-133b, improving the symptoms of PD (Zhang et al., 2019b).

TABLE 2 | Main dysregulated long non-coding RNAs in Parkinson's disease.

LncRNA	Target mRNA	AD-related process	Biological function	References
H19	*HPRT1*	Dopaminergic neuron loss	Upregulating *HPRT1* mRNA stability	Li et al., 2016; Jiang et al., 2020
NEAT1	*LRRK2*	Dopaminergic neuron loss	Regulation of oxidative stress in dopaminergic neurons	Bastias-Candia et al., 2019; Simchovitz et al., 2019
SNHG1	*SIAH1*	α-synuclein aggregation	Promoting the ubiquitination of α-synuclein	Lee et al., 2008; Chen et al., 2018
LincRNA-p21	*α-Synuclein*	α-synuclein aggregation	Transcription repressor	Xu et al., 2018
GAS5	*NLPR3*	Neuroin flammation	Promoting inflammation of microglia	Xu et al., 2020b
HAGLROS	*PI3K*	Autophagy	Regulating the PI3K/AKT/mTOR signaling pathway	Peng et al., 2019

α-Synuclein Aggregation

The α-synuclein, a presynaptic neuron protein, is a major component of Lewy bodies and has been linked to several neurodegenerative diseases (Bennett, 2005). Mutations in the α-synuclein gene are associated with the pathophysiology of PD. The abnormally soluble oligomeric conformation of α-synuclein is considered to be a toxic, leading to neuronal death and disruption of cell homeostasis. Targeting α-synuclein is generally considered as a potential strategy for PD therapy (Dehay et al., 2015).

As mentioned above, MALAT1 confers neuroinflammation in AD. However, in PD, instead of leading to neuroinflammation, MALAT1 was related to the aggregation of α-synuclein. The expression of MALAT1 is upregulated in the midbrain of MALAT1 -induced PD mouse model and in SH-SY5Y cells exposed to MPP+, suggesting that MALAT1 may play an

important role in the pathogenesis of PD. MALAT1 binds to α-synuclein to enhance its stability, resulting in high abundance of α-synuclein. It is well known that β-asarone plays a neuroprotective role by mediating the downregulation of α-synuclein and MALAT1. In a *in vivo* PD model, β-asarone could increase the number of TH+ cells and downregulate expression of α-synuclein, while the overexpression of MALAT1 could reverse its effect (Zhang et al., 2016b). To understand the pathophysiology of PD models induced by MPP+ and MPTP, miRNA profiling was conducted and found that miR-15b-5p expression was downregulated in response to MPP+ and MPTP accompanied by upregulation of SNHG1 expression.

On another hand, it has been reported that SIAH1 interacts with the brain-rich E2 ubiquitin-binding enzyme UbcH8 to promote the ubiquitination of α-synuclein, thereby promoting the aggregation and toxicity of α-synuclein (Lee et al., 2008) in neurons. Interestingly, SIAH1 serves as one of the downstream targets of miR-15b5p, and upregulation of miR-15b-5p repressed the accumulation of α-synuclein and inhibited apoptosis induced by α-synuclein in SH-SY5Y cells. In contrast, overexpression of SIAH1 or downregulation of miR-15b-5p reversed the protective effect of siSNHG1 on SH-SY5Y cells due to α-synuclein aggregation. Therefore, it is further concluded that SNHG1 promotes the aggregation and toxicity of α-synuclein through activating SIAH1 in SH-SY5Y cells *via* downregulating miR-15b-5p (Chen et al., 2018). In addition to SNHG1, a long intergenic non-coding RNA-p21 (lincRNA-p21) with a length of 3,100 nt located on chromosome 6, also play a part in cell proliferation, metabolism and reprogramming, and lincRNA-p21 is considered as a potential diagnostic marker for many diseases (Chen et al., 2017). The lincRNA-p21 is a p53-dependent transcriptional target gene that functions as a transcriptional inhibitor and triggers apoptosis (Huarte et al., 2010). In the MPTP-induced PD mice and the MPP+-treated SH-SY5Y cells, lincRNA-p21 expression was significantly upregulated, in accordance with inhibition of cell viability and induction of apoptosis associated with downregulation of miR-1277-5p and upregulation of α-synuclein protein (Xu et al., 2018). Altogether addresses the regulation of α-synuclein aggregation and toxicity by axis of SNHG1-miR15b-5p- SIAH1-linc-p21- miR-1277-5p-α-synuclein aggregation.

Neuroinflammation

Neuroinflammation is considered to promote the development of PD (Kaur et al., 2017). As the main immune cells of CNS, microglia are activated in PD models in response to MPTP or lipopolysaccharide (LPS) (More and Choi, 2017), mediating the immune response in the brain and triggering the release of pro-inflammatory cytokines such as tumor necrosis factor-α (TNFα), IL-1β and IL-6, and consequently leading to apoptosis and death of DA neurons in the midbrain (Tang and Le, 2016).

Some lncRNAs are involved in activation of microglia such as SNHG1 and lnc-GAS5. Upregulation of SNHG1 has been observed in both LPS-stimulated BV2 microglia and MPTP-induced PD mice, suggesting that this lncRNA is related to LPS-induced activation and inflammation of BV2 microglia. In the MCS metastasis model, downregulation of SNHG1 could prevent the apoptosis of activated microglia and reduce the activation of microglia and the loss of dopaminergic neurons in PD mice induced by MPTP. Moreover, SNHG1 as the ceRNA of miR-7, regulates the expression of NLRP3, leading to the activation of NLRP3 inflammatory bodies (Cao et al., 2018). More data showed that by spongifying miR223-3p, the GAS5 could also promote microglial inflammation in PD *via* regulation of NLRP3 pathway (Xu et al., 2020b).

Autophagy

Increasingly emerged evidence supports the view that autophagy dysfunction contributes to occurrence or development of PD (Ghavami et al., 2014). For example, overexpression of transcription factor EB (TFEB), a key autophagy regulator, helps to clean the α-synuclein aggregation and to prevent neuronal loss in PD (Decressac et al., 2013).

After death autopsy showed significant upregulation of the SNHG1 in PD patient brain samples (Kraus et al., 2017). Consistent with PD patients, substantial increase of SNHG1 expression *in vivo* and *in vitro* were detected the MPP+-treated MN9D cells. Bioinformatic analysis confirmed a common miR-221/222 response element specifically for SNHG1. Interestingly, overexpression of miR-221/222 promoted the level of LC3-II and reduced the neurotoxicity induced by MPP+, in consistence with the increased the level of LC3-II in MN9D cells under SNHG1 silencing, thereby preventing cytotoxicity and suggesting the regulation of SNHG1 through miR-221/222. In MPP+-treated MN9D cells, miR221 or miR-222 inhibitors reversed siRNA-SNHG1-induced p-mTOR inhibition, which was consistent with the effect of silencing p27. This experiment finally confirmed that lncRNA-SNHG1 regulates the expression of p27/mTOR through competitive interaction with miR-221/222 members in MPP+-treated MN9D cells (Qian et al., 2019).

Another lncRNA HAGLROS is considered to be involved in occurrence and development of PD. Upregulated expression of HAGLROS in PD mouse model induced by MPTP and SH-SY5Y cells poisoned by MPP, is in consistence with the reduction of apoptosis and autophagy in response to silencing of lnc-HAGLROS. Further *in vitro* studies showed that HAGLROS negatively regulated the expression of miR-100, and that HAGLROS enhanced apoptosis and autophagy of SH-SY5Y cells exposed to MPP through downregulation of sponge-like miR-100. These findings indicated that the inhibition of HAGLROS could alleviate the MPP induced damage of SH-SY5Y cells by activating PI3K/AKT/mTOR pathway, suggesting the essential role of lnc-HAGLROS in PD (Peng et al., 2019).

Instead of promoting MPP+-induced apoptosis as did the HAGLROS, upregulation of NORAD could protect the apoptosis and mitochondrial dysfunction, while the downregulation of NORAD could reverse the protection (Tatton et al., 2003). To further understand the protection mechanism of the NORAD, *in vitro* cytotoxicity assays were conducted by generating stable SHSY5Y cell lines that silence or overexpress NORAD mediated by lentivirus in the SHSY5Y cells. Overexpression of NORAD could significantly protect SH-SY5Y cells from the MPP+-induced cytotoxicity, while the down-regulation enhanced the cytotoxicity in a MPP+ dose and time dependent manner (Song et al., 2019) (**Figure 3**).

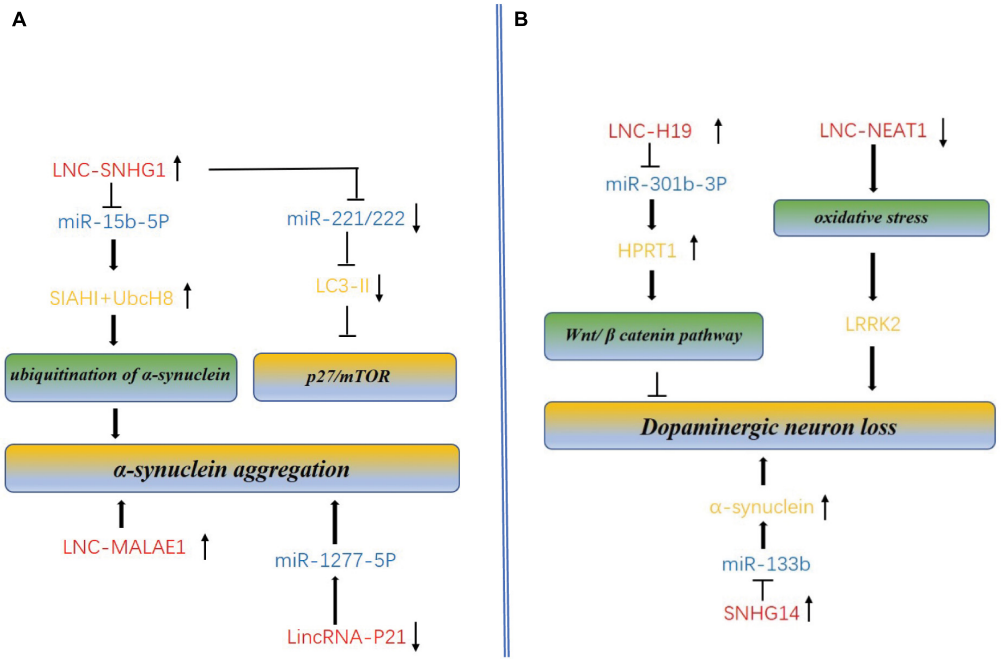

FIGURE 3 | Molecular mechanism of lncRNAs and miRNAs mediated accumulation of dopaminergic neuron loss, α-synuclein aggregation and autophagy in PD. **(A)** LncRNAs regulate α-synuclein aggregation and autophagy. SNHG1 and lnc-MALAE1 are highly expressed in AD, promotes the α-synuclein aggregation. SNHG1 also can inhibit autophagy by reducing the expression of mTOR. Linc-P21 is down-expressed in PD and promotes aggregation through overexpression of miR-1277-5P. **(B)** LncRNAs regulate dopaminergic neuron loss. Overexpression of the H19 could prevent dopaminergic neuron loss in the 6-OHDA-induced PD model by activating HPRT1-mediated Wnt/β catenin signaling pathway *via* impairing miR-301b-3p-targeted repression of HPRT1 transcription. NEAT1 upregulation in dopaminergic neurons of PD may protect dopaminergic neurons from LRRK2-mediated damage under the oxidative stress. Overexpression of the ln_SNHG14 could promote dopaminergic neuron loss.

LncRNAs AND ALS

As a common and serious adult-onset neuromuscular disease, ALS affects motor neurons in the spinal cord, brainstem and motor cortex. Sporadic ALS(SALS) accounts for up to 90% of ALS cases and the other 10% have a strong genetic component also called as familial ALS (FALS). Mutations in more than 20 genes contribute to FALS (Renton et al., 2014). TDP-43, a multifunctional RNA binding protein encoded by TARDBP gene, is considered to be the main component involved in ALS. TDP-43 mutations contribute to about 95% of SALS cases, while FALS cases are caused by C9ORF72 gene mutations. However, the pathological boundary is not that clear between SALS and FALS. For example, dozens of TARDBP mutations have been found in both FALS and SALS patients. Further characterization of all these TDP-43 mutation cases *via* loss of TDP-43 from the nucleus and cytoplasmic and gain of TDP-43 function suggests that this protein is related to ALS (Shelkovnikova et al., 2018; **Table 3**).

LncRNAs Interactive With TDP-43

Transcriptomic profiling conducted in 30 patients with SALS and 30 matched normal persons, led to identification of 293 of lncRNAs differentially expressed (DE) in the SALS patients. Of the DE lnc-RNAs, 183 out of 293 (62.5%) were upregulated, while 184 out of 293 (62.8%) belong to antisense RNAs and 81 out of 293 (27.7%) were reported as real DE lincRNAs (Gagliardi et al., 2018), suggesting the lncRNAs mediated regulation of ALS.

NEAT1 containing a sequence rich in GpCs, mainly expressed in spinal motoneurons at the early stage of ALS and contributed to pathogenesis of ALS. The NEAT1 mainly binds to TDP43 in the brain tissue of ALS patients and cultured cells (HeLa and SH-SY5Y) (Tollervey et al., 2011). Both TDP-43 and fused in sarcoma/translocated in liposarcoma (FUS/TLS) are considered to be necessary components for the formation of normal accessory spots *via* direct protein-protein interactions (Hutchinson et al., 2007). The frequency of accessory spot formation increased dramatically at the early stage of ALS. Therefore, NEAT1 was considered to be the scaffold of RNA binding proteins in the motor neuron nuclei of ALS patients. As a component of Paraspeckles, FUS significantly promotes their stability by regulating the steady-state level of NEAT1 and maintaining the structure of the nucleosome (Naganuma et al., 2012). More detailed analysis showed that NEAT1 was highly enriched in neurons of the anterior horn of the spinal cord and in the cortex of ALS patients (Tollervey et al., 2011; Shelkovnikova et al., 2018). Given that the formation of accessory spots in the spinal cord of SALS and FALS patients is much more than that in the healthy people, it is plausible to speculate that the accessory spot formation might be a common feature of ALS patient (Shelkovnikova et al., 2018).

Other lncRNAs are involved in ALS mostly *via* interaction with proteins related to ALS pathogenesis, such as TDP-43 or FUS. The expression of the MALAT1 was significantly upregulated in the cortex of sporadic FTD patients and binds to

TABLE 3 | Main dysregulated long non-coding RNAs in Huntington's disease and amyotrophic lateral sclerosis.

Disease	LncRNA	Target mRNA	Biological function	References
Amyotrophic lateral sclerosis	*NEAT1/ MALAT1*	TDP-43	Improving toxicity of TDP-43	Hutchinson et al., 2007; Tollervey et al., 2011; Militello et al., 2018
	MEG3	Hox	promotes the formation of PRC2-Jarid2 complexes	Yen et al., 2018; Vangoor et al., 2020
	C9ORF72-AS	C9ORF72	Regulates repetition of (G4C2)n in C9ORF72	Kovanda et al., 2015; DeJesus-Hernandez et al., 2017; Shelkovnikova et al., 2018
Huntington's disease	*NEAT1*	HTT/TP53	Reducing the expression of endogenous HTT and TP53.	Chanda et al., 2018
	TUG1	P53	Regulates P53 transcriptional regulatory pathway in HD	Khalil et al., 2009

TDP-43 that interacts with several other lncRNAs, including lnc-BDNFOS and lnc-TFEB α (in SHSY5Y cells) and lnc-Myolinc (in muscle cells) (Militello et al., 2018). The expression of heat shock rna ω (hsr ω) in lncRNA is positively regulated by TDP-43 *via* direct interaction with hsr ω. Upregulated expression of hsr ω is detected in both human FTD patients and cellular model of TDP-43 overexpression (Chung et al., 2018). The ALS-related mutations in FUS affect expression of several lncRNAs in mESC- MN. For example, relative to wild type FUS-/- MNS, mutation FUSP517L/517L could upregulate lnc-Lhx1os specifically, while both lnc-MN-1 (2610316D01Rik) and lnc-MN2 (5330434G04Rik) were downregulated, indicating that the loss of FUS function altered the expression of several lncRNAs.

Evolutionally, lnc-Lhx1os, lnc-MN-1 and lnc-MN2 are conserved between mice and humans, and their expressions levels are elevated during the differentiation of human MN *in vitro* (Biscarini et al., 2018). The homologous gene dFU in Drosophila and human FUS both interact with hsr ω, and its deletion could lead to cytoplasmic dislocation and loss of nuclear dFU function. In addition, knockout of MN-specific hsr ω impaired the movement of larvae and adults of Drosophila melanogaster, and also led to the anatomical defects of MN presynaptic terminals. In view of the different interactions between TDP-43 / FUS and lncRNAs, the cytoplasmic mislocalization and dysfunction of TDP-43 and FUS in ALS may affect the distribution, expression and / or function of lncRNAs, thereby leading to degeneration and ALS of MN (Lo Piccolo and Yamaguchi, 2017).

LncRNAs Derived From C9ORF72 Antisense Transcript

Expansion of (GGGGCC)n (G4C2) repeats in 5′UTR of the C9ORF72 gene has been acknowledged as one of the most common genetic factors in ALS (Shelkovnikova et al., 2018). Three transcript variants were detected in the expansion of the (G4C2)n repeats in C9ORF72, including variants 1 and 3 located in intron 1, and variant 2 in the promoter region (Balendra and Isaacs, 2018). The (G4C2)n repeats in C9ORF72 were observed in nearly 40% of FALS and FTD cases and in up to 8% of SALS, respectively (Majounie et al., 2012; DeJesus-Hernandez et al., 2017). As for the (G4C2)n repeat number, healthy persons carry as many as 20–30 repeats, while the repeat number was expanded to hundreds even thousands in ALS (DeJesus-Hernandez et al., 2017). The C9ORF72-associated ALS cases (C9-ALS) are associated with loss of C9ORF72 function and acquisition of toxic function mediated by expansion of (G4C2)n repeats. C9ORF72 antisense transcript (C9ORF72-AS) is a kind of lncRNA named as lnc-C9ORF72-AS transcribed from intron 1 of the C9ORF72 gene (Mori et al., 2013). Although C9ORF72 and its corresponding proteins have been extensively investigated, the functional correlation of lnc-C9ORF72-AS remains poorly understood. C9ORF72-S can form a G-quadruple known to regulate gene expression (Reddy et al., 2013; Haeusler et al., 2014). Theoretically, C-rich C9ORF72-AS repeats may not form a similar structure. On the contrary, the expansion of (G2C4)n repeats in lnc-C9ORF72-AS may form a C-rich sequence (Kovanda et al., 2015), thereby potentially affecting the stability and transcription of the genome. Furthermore, it was found that these could rescue disease-specific transcriptional changes in iPSC-derived neurons by using antisense oligodeoxynucleotides (ASO) against C9ORF72 in Drosophila model (Sareen et al., 2013; Zhang et al., 2015).

LncRNAs AND HUNTINGTON'S DISEASE

Huntington's disease is a neurodegenerative disease characterized by autosomal dominant inheritance, cognitive impairment, dance motor disorder and mental disorder. Selective loss of intermediate spinous neurons in caudate nucleus and putamen is a typical pathological feature of HD (Labbadia and Morimoto, 2013). The abnormal expansion of (CAG)n in HT protein gene leads to the formation of mutant HT proteins containing the expanded polyglutamine region. The mutant HT protein induces neurodegeneration through a variety of mechanisms such as transcriptional disorders, clearance of misfolded proteins, toxic N-terminal fragments, mitochondrial dysfunction and oxidative stress (Ross and Tabrizi, 2011; Sunwoo et al., 2017). Given that HT protein is widely expressed in different cell types at all developmental stages of the body, the pathogenesis of HD may begin early and last for a lifelong process (Bassi et al., 2017; **Table 3**).

Previous studies have confirmed the contribution of ncRNAs to HD pathogenesis. 12 of ncRNAs were identified and characterized in the brains of HD mice, eight of which are human homologs. Of the identified ncRNAs, MEG3, NEAT1 and XIST

showed a sustained and significant increase in HD cells and animal models. Knockdown of MEG3 and NEAT1 in HD cell model resulted in a significant decrease in the aggregation of mutant HT protein and a downregulation of endogenous Tp53 expression (Chanda et al., 2018). Upregulation of MEG3 was observed at the early stage (6 weeks) and lasted to late stage (8 weeks) in R6/2 mice as well as in other HD cell models. However, downregulation of MEG3 was also reported in the brains of HD patients (Johnson, 2012).

Previous studies reported elevation of the NEAT1 levels in both GEO data mining, HD models, and autopsy samples of HD patients (Brochier et al., 2008; Makhlouf et al., 2014). However, no information is available for the alteration of XIST levels in HD (Chanda et al., 2018). Other studies have shown that NEAT1 physically interact with loci of other genes located on the active chromatin sites near the Tp53 gene (Yang et al., 2013). Tp53 directly regulates the transcription of NEAT1 by binding to the promoter region of the gene (West et al., 2014; Sunwoo et al., 2017). Therefore, the level of NEAT1 and Tp53 is controlled by the feedback loop. Given that inhibition of proteasome degradation could increase levels of NEAT1, cytoplasmic and nuclear polymers containing ubiquitin proteins are expected to be identified as well (Idogawa et al., 2017). In view of the fact that proteasome degradation is affected in HD (Hirose et al., 2014; Hyrskyluoto et al., 2014) and that NEAT1 level is elevated in HD (Makhlouf et al., 2014), it could be inferred that Neat1 may affect proteasome degradation in HD. Aberrant expression of lncRNAs was observed in the postmortem brain of human HD and the brain of R6Unix2 mice, such as upregulation of NEAT1. Transfection of the short isomer of NEAT1 into N2a cells significantly reduced cell death caused by H_2O_2 oxidative stress, revealing the functional correlation of NEAT1 and neuroprotective mechanism in the pathogenesis of HD (Sunwoo et al., 2017).

MEG3, NEAT1, and XIST may interact with many miRNAs through sequence complementarity, potentially reducing the efficiency of binding to their target mRNAs by acting as "sponges" or competitors. Reduced levels of miR-9, miR-125b, miR-132, miR-146a and miR-150, miR-221, and miR-222 have been reported in various HD cells, HD models as well as in postmortem HD tissues (Sinha et al., 2012; Blume et al., 2015). Therefore, it is reasonable to speculate that the interaction of lncRNAs and miRNAs may contribute to the reduced levels of these miRNAs, thereby promoting the occurrence and development of HD.

Many other lncRNAs, such as BACE1-AS,TUG1, and HAR1, ware also involved in the occurrence and development of HD although no evidence to show that they interact with miRNAs. For example, BACE1 antisense transcripts (BACE1-AS) positively regulate BACE1 mRNA levels in the brain of HD patients. It is worth of noting that knocking down of BACE1-AS,could reduce the stable mRNA level of the justice gene (Johnson, 2012). Another up-regulatedTUG1 has been reported to target p53 target (Khalil et al., 2009), a known transcriptional regulatory pathway in HD driven by the pathological activation of P53 tumor suppressor proteins. Different from BACE1-AS and TUG1, the HAR1 expression was downregulated in two brain regions cortex (Brodman region 7/9) and striatum comparing the HD autopsy to the control persons. More specifically, significant reductions in the levels of both HAR1F and HAR1R were observed in the striatum of HD patients, but not in the cortex compared with the Brodman7/9 region. Furthermore, HAR1 was considered as the target of REST, but no evidence could support this thought in a way that disruption of REST failed to downregulate HAR1 level in mice (Johnson et al., 2010).

CONCLUSION

Although significant efforts have been made in dissection of pathology for the neurodegenerative disorders such as AD, PD, HD, and ALS, our understanding is still very limited. Excitingly, dramatic breakthroughs in high throughput sequencing technologies in recent years significantly speeds up our understanding on epigenetic contribution to pathogenesis of neurodegenerative disorders. Accumulated evidence has enabled us to acknowledge that lncRNAs could suppress or promote the neurodegenerative disorders *via* epigenetically regulating expression of genes crucially involved in the pathogenesis at both transcriptional and posttranscriptional levels. In the nucleus, lncRNAs can inhibit or promote gene expression through act either in *cis* or in *trans* (Wang et al., 2011). XIST is the most extensively investigated *cis*-acting lncRNA, which inactivate the whole X chromosome by inhibiting the deposition of chromatin markers and relocating this chromosome to the periphery of the nucleus (Cerase et al., 2015). LncRNA HOTAIR interacts with polycomb repressive complex2 (PRC2), leading to H3K27me3-mediated gene silencing at HOXD locus in *trans* (Rinn et al., 2007). However, the exact mechanisms of how these lncRNAs affect the onset and progression of neurodegenerative diseases remains largely unknown. On one hand, some studies on lncRNAs lack biological repeats or conducted only *in vitro*, without confirmation *in vivo*. On the other hand, although some lncRNAs are differentially expressed in in the patients and normal persons, they lack tissue specificity. For example, MEG3 has been demonstrated to be differently expressed in AD, ALS, HD and some malignant tumors. This poses a great challenge for identification of the CNS-specific lncRNAs as biomarkers. More importantly, the ceRNA theory has become the main hypothesis of how lncRNAs function as ceRNA in neurodegenerative diseases. However, it is still skeptical about whether the physiological expression level of a single lncRNA is sufficient to alter the expression level of miRNAs, because a single lncRNA represent only a very small fraction of the total miRNA targets (Denzler et al., 2014; Thomson and Dinger, 2016). Besides, since most databases were generated by using a variety of miRNA prediction algorithms, biochemical and gene expression data, hard to determine the reliability of the ceRNA interactions established from these different prediction methods (Thomson et al., 2011). In terms of the experimental strategy, the models were generated *via* ceRNA overexpression or silencing. Thus, the concern is that overexpression of miRNAs or ceRNAs at the physiological level is experimentally challenging (Liu et al., 2021). As mentioned above, most of the lncRNA studies are conducted

in vitro, failing to mimick the *in vivo* patients. Therefore, mouse models or human brain organoids should be used as more relevant physiological model.

It is well known that a plurality of lncRNAs can target a miRNA and a single lncRNA targets multiple miRNAs simultaneously, making the interplay of miRNAs and lncRNAs extremely complicated. In this context, it is essential for the future study to investigate all the genes crucially involved in the pathogenesis as well as their regulation elements such as ncRNAs (miRNAs and lncRNAs) genetically, epigenetically, molecularly, and biochemically. Understanding the interaction networks and orchestration of all the ncRNAs and target genes could help us identify the biomarkers for diagnosis and therapy.

Antisense oligonucleotides (ASOs) have been confirmed to target lncRNAs in the nucleus more effectively than siRNAs. Furthermore, ASOs based study in disease animal models as well as the clinical trials have been conducted for some disease such as cancer. For example, specific ASO can act on specific lncRNA to alleviate the production of A β in the AD animal model (Massone et al., 2012). Moreover, Clinical trials using ASO to treat malignant tumors (Adams et al., 2017) and intrathecal injection of ASO for the therapy of ASL (Chiriboga et al., 2016) have been carried out. These studies shed light on the expectation that lncRNAs could potentially become new biomarkers for diagnosis and clinical therapy of ND, meanwhile the promising results inspire the scientists to make greater efforts to reach this goal. However, there is distance to go to identify and characterize the specific lncRNAs that contribute to the pathogenesis of neurodegenerative diseases. To this end, the animal ND models, the cell-based assays, the human brain organoids derived from ND patients and normal persons, the patients' samples (brain tissues and blood) should be employed for analysis and validation of the specific ncRNAs. The cell-based assays and animal models such as mouse could be employed for fast and primary screening. It is worthy of noting that the large evolutionary distance between mouse and human lead to a discrepancy in genetic, anatomic, and physiological basis between animal models and humans. In addition, human brain organoids are a miniaturized and simplified version of brain organ generated *in vitro* but could recapitulate key features brain development. Thus, candidate lncRNAs identified in animal models should be further validated in human organoids even human tissues.

To sum up, further study on lncRNAs in CNSNDs will contribute to further understanding of brain function and the pathogenesis as well as the development of the promising therapeutic strategies for the CNSNDs.

AUTHOR CONTRIBUTIONS

SX designed the topic and conceived the structure of the manuscript. SZ, XY, YM, DS, HY, and DW collected the articles, and made the tables and figures. SZ wrote the manuscript. SX, MW, and JB revised the manuscript. All authors contributed to the manuscript.

FUNDING

This work was supported by the Shandong Provincial Natural Science Foundation China #ZR2015HM024 and # 2019GSF108066; IIFDU #11681701 and SFR for ROCS, SEM.

ACKNOWLEDGMENTS

We would like to thank Dr. He Chen and Dr. Yujing for editing our manuscript.

REFERENCES

Adams, B. D., Parsons, C., Walker, L., Zhang, W. C., and Slack, F. J. (2017). Targeting noncoding RNAs in disease. *J. Clin. Invest.* 127, 761–771. doi: 10.1172/JCI84424

Balendra, R., and Isaacs, A. M. (2018). C9orf72-mediated ALS and FTD: multiple pathways to disease. *Nat. Rev. Neurol.* 14, 544–558. doi: 10.1038/s41582-018-0047-2

Bassi, S., Tripathi, T., Monziani, A., Di Leva, F., and Biagioli, M. (2017). Epigenetics of huntington's disease. *Adv. Exp. Med. Biol.* 978, 277–299. doi: 10.1007/978-3-319-53889-1_15

Bastias-Candia, S., Zolezzi, J. M., and Inestrosa, N. C. (2019). Revisiting the paraquat-induced sporadic Parkinson's disease-like model. *Mol. Neurobiol.* 56, 1044–1055. doi: 10.1007/s12035-018-1148-z

Bennett, M. C. (2005). The role of alpha-synuclein in neurodegenerative diseases. *Pharmacol. Ther.* 105, 311–331. doi: 10.1016/j.pharmthera.2004.10.010

Biscarini, S., Capauto, D., Peruzzi, G., Lu, L., Colantoni, A., Santini, T., et al. (2018). Characterization of the lncRNA transcriptome in mESC-derived motor neurons: Implications for FUS-ALS. *Stem Cell Res.* 27, 172–179. doi: 10.1016/j.scr.2018.01.037

Blume, C. J., Hotz-Wagenblatt, A., Hullein, J., Sellner, L., Jethwa, A., Stolz, T., et al. (2015). p53-dependent non-coding RNA networks in chronic lymphocytic leukemia. *Leukemia* 29, 2015–2023. doi: 10.1038/leu.2015.119

Bose, A., and Beal, M. F. (2016). Mitochondrial dysfunction in Parkinson's disease. *J. Neurochem.* 139(Suppl. 1), 216–231. doi: 10.1111/jnc.13731

Brochier, C., Gaillard, M. C., Diguet, E., Caudy, N., Dossat, C., Segurens, B., et al. (2008). Quantitative gene expression profiling of mouse brain regions reveals differential transcripts conserved in human and affected in disease models. *Physiol. Genomics* 33, 170–179. doi: 10.1152/physiolgenomics.00125.2007

Calabresi, P., Castrioto, A., Di Filippo, M., and Picconi, B. (2013). New experimental and clinical links between the hippocampus and the dopaminergic system in Parkinson's disease. *Lancet Neurol.* 12, 811–821. doi: 10.1016/S1474-4422(13)70118-2

Cao, B., Wang, T., Qu, Q., Kang, T., and Yang, Q. (2018). Long Noncoding RNA SNHG1 promotes neuroinflammation in Parkinson's disease via regulating miR-7/NLRP3 pathway. *Neuroscience* 388, 118–127. doi: 10.1016/j.neuroscience.2018.07.019

Causeret, F., Sumia, I., and Pierani, A. (2016). Kremen1 and Dickkopf1 control cell survival in a Wnt-independent manner. *Cell Death Differ.* 23, 323–332. doi: 10.1038/cdd.2015.100

Cerase, A., Pintacuda, G., Tattermusch, A., and Avner, P. (2015). Xist localization and function: new insights from multiple levels. *Genome Biol.* 16:166. doi: 10.1186/s13059-015-0733-y

Chakravarty, D., Sboner, A., Nair, S. S., Giannopoulou, E., Li, R., Hennig, S., et al. (2014). The oestrogen receptor alpha-regulated lncRNA NEAT1 is a

critical modulator of prostate cancer. *Nat. Commun.* 5:5383. doi: 10.1038/ncomms6383

Chalei, V., Sansom, S. N., Kong, L., Lee, S., Montiel, J. F., Vance, K. W., et al. (2014). The long non-coding RNA Dali is an epigenetic regulator of neural differentiation. *Elife* 3:e04530. doi: 10.7554/eLife.04530

Chanda, K., Das, S., Chakraborty, J., Bucha, S., Maitra, A., Chatterjee, R., et al. (2018). Altered levels of long NcRNAs Meg3 and neat1 in cell and animal models of huntington's disease. *RNA Biol.* 15, 1348–1363. doi: 10.1080/15476286.2018.1534524

Chen, S., Liang, H., Yang, H., Zhou, K., Xu, L., Liu, J., et al. (2017). LincRNa-p21: function and mechanism in cancer. *Med. Oncol.* 34:98. doi: 10.1007/s12032-017-0959-5

Chen, Y., Lian, Y. J., Ma, Y. Q., Wu, C. J., Zheng, Y. K., and Xie, N. C. (2018). LncRNA SNHG1 promotes alpha-synuclein aggregation and toxicity by targeting miR-15b-5p to activate SIAH1 in human neuroblastoma SH-SY5Y cells. *Neurotoxicology* 68, 212–221. doi: 10.1016/j.neuro.2017.12.001

Chiriboga, C. A., Swoboda, K. J., Darras, B. T., Iannaccone, S. T., Montes, J., De Vivo, D. C., et al. (2016). Results from a phase 1 study of nusinersen (ISIS-SMN(Rx)) in children with spinal muscular atrophy. *Neurology* 86, 890–897. doi: 10.1212/WNL.0000000000002445

Chung, C. Y., Berson, A., Kennerdell, J. R., Sartoris, A., Unger, T., Porta, S., et al. (2018). Aberrant activation of non-coding RNA targets of transcriptional elongation complexes contributes to TDP-43 toxicity. *Nat. Commun.* 9:4406. doi: 10.1038/s41467-018-06543-0

Ciarlo, E., Massone, S., Penna, I., Nizzari, M., Gigoni, A., Dieci, G., et al. (2013). An intronic ncRNA-dependent regulation of SORL1 expression affecting Abeta formation is upregulated in post-mortem Alzheimer's disease brain samples. *Dis. Model Mech.* 6, 424–433. doi: 10.1242/dmm.009761

Clavaguera, F., Bolmont, T., Crowther, R. A., Abramowski, D., Frank, S., Probst, A., et al. (2009). Transmission and spreading of tauopathy in transgenic mouse brain. *Nat. Cell Biol.* 11, 909–913. doi: 10.1038/ncb1901

Cortini, F., Roma, F., and Villa, C. (2019). Emerging roles of long non-coding RNAs in the pathogenesis of Alzheimer's disease. *Ageing Res. Rev.* 50, 19–26. doi: 10.1016/j.arr.2019.01.001

Decressac, M., Mattsson, B., Weikop, P., Lundblad, M., Jakobsson, J., and Bjorklund, A. (2013). TFEB-mediated autophagy rescues midbrain dopamine neurons from alpha-synuclein toxicity. *Proc. Natl. Acad. Sci. U.S.A.* 110, E1817–E1826. doi: 10.1073/pnas.1305623110

Dehay, B., Bourdenx, M., Gorry, P., Przedborski, S., Vila, M., Hunot, S., et al. (2015). Targeting alpha-synuclein for treatment of Parkinson's disease: mechanistic and therapeutic considerations. *Lancet Neurol.* 14, 855–866. doi: 10.1016/S1474-4422(15)00006-X

DeJesus-Hernandez, M., Finch, N. A., Wang, X., Gendron, T. F., Bieniek, K. F., Heckman, M. G., et al. (2017). In-depth clinico-pathological examination of RNA foci in a large cohort of C9ORF72 expansion carriers. *Acta Neuropathol.* 134, 255–269. doi: 10.1007/s00401-017-1725-7

Denzler, R., Agarwal, V., Stefano, J., Bartel, D. P., and Stoffel, M. (2014). Assessing the ceRNA hypothesis with quantitative measurements of miRNA and target abundance. *Mol. Cell* 54, 766–776. doi: 10.1016/j.molcel.2014.03.045

Dermentzaki, G., and Lotti, F. (2020). New insights on the role of N (6)-Methyladenosine RNA methylation in the physiology and pathology of the nervous system. *Front. Mol. Biosci.* 7:555372. doi: 10.3389/fmolb.2020.555372

Derrien, T., Johnson, R., Bussotti, G., Tanzer, A., Djebali, S., Tilgner, H., et al. (2012). The GENCODE v7 catalog of human long noncoding RNAs: analysis of their gene structure, evolution, and expression. *Genome Res.* 22, 1775–1789. doi: 10.1101/gr.132159.111

Elling, R., Chan, J., and Fitzgerald, K. A. (2016). Emerging role of long noncoding RNAs as regulators of innate immune cell development and inflammatory gene expression. *Eur. J. Immunol.* 46, 504–512. doi: 10.1002/eji.201444558

Faghihi, M. A., Modarresi, F., Khalil, A. M., Wood, D. E., Sahagan, B. G., Morgan, T. E., et al. (2008). Expression of a noncoding RNA is elevated in Alzheimer's disease and drives rapid feed-forward regulation of beta-secretase. *Nat. Med.* 14, 723–730. doi: 10.1038/nm1784

Gagliardi, S., Zucca, S., Pandini, C., Diamanti, L., Bordoni, M., Sproviero, D., et al. (2018). Long non-coding and coding RNAs characterization in peripheral blood mononuclear cells and spinal cord from amyotrophic lateral sclerosis patients. *Sci. Rep.* 8:2378. doi: 10.1038/s41598-018-20679-5

Ghavami, S., Shojaei, S., Yeganeh, B., Ande, S. R., Jangamreddy, J. R., Mehrpour, M., et al. (2014). Autophagy and apoptosis dysfunction in neurodegenerative disorders. *Prog. Neurobiol.* 112, 24–49. doi: 10.1016/j.pneurobio.2013.10.004

Gu, C., Chen, C., Wu, R., Dong, T., Hu, X., Yao, Y., et al. (2018). Long Noncoding RNA EBF3-AS promotes neuron apoptosis in alzheimer's disease. *DNA Cell Biol.* 37, 220–226. doi: 10.1089/dna.2017.4012

Guo, Q., Qian, Z., Yan, D., Li, L., and Huang, L. (2016). LncRNA-MEG3 inhibits cell proliferation of endometrial carcinoma by repressing Notch signaling. *Biomed. Pharmacother.* 82, 589–594. doi: 10.1016/j.biopha.2016.02.049

Haeusler, A. R., Donnelly, C. J., Periz, G., Simko, E. A., Shaw, P. G., Kim, M. S., et al. (2014). C9orf72 nucleotide repeat structures initiate molecular cascades of disease. *Nature* 507, 195–200. doi: 10.1038/nature13124

Hegarty, S. V., Green, H. F., Niclis, J., O'Keeffe, G. W., and Sullivan, A. M. (2020). Editorial: the role of stem cells, epigenetics and MicroRNAs in Parkinson's Disease. *Front. Neurosci.* 14:515. doi: 10.3389/fnins.2020.00515

Hirose, T., Virnicchi, G., Tanigawa, A., Naganuma, T., Li, R., Kimura, H., et al. (2014). NEAT1 long noncoding RNA regulates transcription via protein sequestration within subnuclear bodies. *Mol. Biol. Cell* 25, 169–183. doi: 10.1091/mbc.E13-09-0558

Huarte, M., Guttman, M., Feldser, D., Garber, M., Koziol, M. J., Kenzelmann-Broz, D., et al. (2010). A large intergenic noncoding RNA induced by p53 mediates global gene repression in the p53 response. *Cell* 142, 409–419. doi: 10.1016/j.cell.2010.06.040

Hutchinson, J. N., Ensminger, A. W., Clemson, C. M., Lynch, C. R., Lawrence, J. B., and Chess, A. (2007). A screen for nuclear transcripts identifies two linked noncoding RNAs associated with SC35 splicing domains. *BMC Genomics* 8:39. doi: 10.1186/1471-2164-8-39

Hwang, J. Y., Aromolaran, K. A., and Zukin, R. S. (2017). The emerging field of epigenetics in neurodegeneration and neuroprotection. *Nat. Rev. Neurosci.* 18, 347–361. doi: 10.1038/nrn.2017.46

Hyrskyluoto, A., Bruelle, C., Lundh, S. H., Do, H. T., Kivinen, J., Rappou, E., et al. (2014). Ubiquitin-specific protease-14 reduces cellular aggregates and protects against mutant huntingtin-induced cell degeneration: involvement of the proteasome and ER stress-activated kinase IRE1alpha. *Hum. Mol. Genet.* 23, 5928–5939. doi: 10.1093/hmg/ddu317

Idogawa, M., Ohashi, T., Sasaki, Y., Nakase, H., and Tokino, T. (2017). Long non-coding RNA NEAT1 is a transcriptional target of p53 and modulates p53-induced transactivation and tumor-suppressor function. *Int. J. Cancer* 140, 2785–2791. doi: 10.1002/ijc.30689

Jiang, J., Piao, X., Hu, S., Gao, J., and Bao, M. (2020). LncRNA H19 diminishes dopaminergic neuron loss by mediating microRNA-301b-3p in Parkinson's disease via the HPRT1-mediated Wnt/beta-catenin signaling pathway. *Aging (Albany NY)* 12, 8820–8836. doi: 10.18632/aging.102877

Johnson, R. (2012). Long non-coding RNAs in Huntington's disease neurodegeneration. *Neurobiol. Dis.* 46, 245–254. doi: 10.1016/j.nbd.2011.12.006

Johnson, R., Richter, N., Jauch, R., Gaughwin, P. M., Zuccato, C., Cattaneo, E., et al. (2010). Human accelerated region 1 noncoding RNA is repressed by REST in Huntington's disease. *Physiol. Genomics* 41, 269–274. doi: 10.1152/physiolgenomics.00019.2010

Kadakkuzha, B. M., Liu, X. A., McCrate, J., Shankar, G., Rizzo, V., Afinogenova, A., et al. (2015). Transcriptome analyses of adult mouse brain reveal enrichment of lncRNAs in specific brain regions and neuronal populations. *Front. Cell Neurosci.* 9:63. doi: 10.3389/fncel.2015.00063

Kaur, K., Gill, J. S., Bansal, P. K., and Deshmukh, R. (2017). Neuroinflammation - A major cause for striatal dopaminergic degeneration in Parkinson's disease. *J. Neurol. Sci.* 381, 308–314. doi: 10.1016/j.jns.2017.08.3251

Khalil, A. M., Guttman, M., Huarte, M., Garber, M., Raj, A., Rivea Morales, D., et al. (2009). Many human large intergenic noncoding RNAs associate with chromatin-modifying complexes and affect gene expression. *Proc. Natl. Acad. Sci. U.S.A.* 106, 11667–11672. doi: 10.1073/pnas.0904715106

Kong, Q., Zhang, S., Liang, C., Zhang, Y., Kong, Q., Chen, S., et al. (2018). LncRNA XIST functions as a molecular sponge of miR-194-5p to regulate MAPK1 expression in hepatocellular carcinoma cell. *J. Cell Biochem.* 119, 4458–4468. doi: 10.1002/jcb.26540

Kovanda, A., Zalar, M., Sket, P., Plavec, J., and Rogelj, B. (2015). Anti-sense DNA d(GGCCCC)n expansions in C9ORF72 form i-motifs and protonated hairpins. *Sci. Rep.* 5:17944. doi: 10.1038/srep17944

Kraus, T. F. J., Haider, M., Spanner, J., Steinmaurer, M., Dietinger, V., and Kretzschmar, H. A. (2017). Altered long noncoding RNA expression precedes the course of Parkinson's Disease-a preliminary report. *Mol. Neurobiol.* 54, 2869–2877. doi: 10.1007/s12035-016-9854-x

Labbadia, J., and Morimoto, R. I. (2013). Huntington's disease: underlying molecular mechanisms and emerging concepts. *Trends Biochem. Sci.* 38, 378–385. doi: 10.1016/j.tibs.2013.05.003

Lashley, T., Schott, J. M., Weston, P., Murray, C. E., Wellington, H., Keshavan, A., et al. (2018). Molecular biomarkers of Alzheimer's disease: progress and prospects. *Dis. Model Mech.* 11:dmm031781. doi: 10.1242/dmm.031781

Lee, J. T., Wheeler, T. C., Li, L., and Chin, L. S. (2008). Ubiquitination of alpha-synuclein by Siah-1 promotes alpha-synuclein aggregation and apoptotic cell death. *Hum. Mol. Genet.* 17, 906–917. doi: 10.1093/hmg/ddm363

Li, C., Wang, X., Cai, H., Fu, Y., Luan, Y., Wang, W., et al. (2016). Molecular microevolution and epigenetic patterns of the long non-coding gene H19 show its potential function in pig domestication and breed divergence. *BMC Evol. Biol.* 16:87. doi: 10.1186/s12862-016-0657-5

Liu, S. J., Dang, H. X., Lim, D. A., Feng, F. Y., and Maher, C. A. (2021). Long noncoding RNAs in cancer metastasis. *Nat. Rev. Cancer* 21, 446–460. doi: 10.1038/s41568-021-00353-1

Lo Piccolo, L., and Yamaguchi, M. (2017). RNAi of arcRNA hsromega affects subcellular localization of *Drosophila* FUS to drive neurodiseases. *Exp. Neurol.* 292, 125–134. doi: 10.1016/j.expneurol.2017.03.011

Luo, Q., and Chen, Y. (2016). Long noncoding RNAs and Alzheimer's disease. *Clin. Interv. Aging* 11, 867–872. doi: 10.2147/CIA.S107037

Ma, H., Lesne, S., Kotilinek, L., Steidl-Nichols, J. V., Sherman, M., Younkin, L., et al. (2007). Involvement of beta-site APP cleaving enzyme 1 (BACE1) in amyloid precursor protein-mediated enhancement of memory and activity-dependent synaptic plasticity. *Proc. Natl. Acad. Sci. U.S.A.* 104, 8167–8172. doi: 10.1073/pnas.0609521104

Ma, P., Li, Y., Zhang, W., Fang, F., Sun, J., Liu, M., et al. (2019). Long Non-coding RNA MALAT1 inhibits neuron apoptosis and neuroinflammation while stimulates neurite outgrowth and its correlation With MiR-125b Mediates PTGS2, CDK5 and FOXQ1 in Alzheimer's Disease. *Curr. Alzheimer Res.* 16, 596–612. doi: 10.2174/1567205016666190725130134

Magistri, M., Velmeshev, D., Makhmutova, M., and Faghihi, M. A. (2015). Transcriptomics profiling of alzheimer's disease reveal neurovascular defects, altered amyloid-beta homeostasis, and deregulated expression of long noncoding RNAs. *J. Alzheimers Dis.* 48, 647–665. doi: 10.3233/JAD-150398

Majounie, E., Renton, A. E., Mok, K., Dopper, E. G., Waite, A., Rollinson, S., et al. (2012). Frequency of the C9orf72 hexanucleotide repeat expansion in patients with amyotrophic lateral sclerosis and frontotemporal dementia: a cross-sectional study. *Lancet Neurol.* 11, 323–330. doi: 10.1016/S1474-4422(12)70043-1

Makhlouf, M., Ouimette, J. F., Oldfield, A., Navarro, P., Neuillet, D., and Rougeulle, C. (2014). A prominent and conserved role for YY1 in Xist transcriptional activation. *Nat. Commun.* 5:4878. doi: 10.1038/ncomms5878

Managadze, D., Lobkovsky, A. E., Wolf, Y. I., Shabalina, S. A., Rogozin, I. B., and Koonin, E. V. (2013). The vast, conserved mammalian lincRNome. *PLoS Comput. Biol.* 9:e1002917. doi: 10.1371/journal.pcbi.1002917

Masoumi, F., Ghorbani, S., Talebi, F., Branton, W. G., Rajaei, S., Power, C., et al. (2019). Malat1 long noncoding RNA regulates inflammation and leukocyte differentiation in experimental autoimmune encephalomyelitis. *J. Neuroimmunol.* 328, 50–59. doi: 10.1016/j.jneuroim.2018.11.013

Massone, S., Ciarlo, E., Vella, S., Nizzari, M., Florio, T., Russo, C., et al. (2012). NDM29, a RNA polymerase III-dependent non coding RNA, promotes amyloidogenic processing of APP and amyloid beta secretion. *Biochim. Biophys. Acta* 1823, 1170–1177. doi: 10.1016/j.bbamcr.2012.05.001

Mateos-Aparicio, P., and Rodriguez-Moreno, A. (2019). The impact of studying brain plasticity. *Front. Cell Neurosci.* 13:66. doi: 10.3389/fncel.2019.00066

Militello, G., Hosen, M. R., Ponomareva, Y., Gellert, P., Weirick, T., John, D., et al. (2018). A novel long non-coding RNA Myolinc regulates myogenesis through TDP-43 and Filip1. *J. Mol. Cell Biol.* 10, 102–117. doi: 10.1093/jmcb/mjy025

Modarresi, F., Faghihi, M. A., Lopez-Toledano, M. A., Fatemi, R. P., Magistri, M., Brothers, S. P., et al. (2012). Inhibition of natural antisense transcripts in vivo results in gene-specific transcriptional upregulation. *Nat. Biotechnol.* 30, 453–459. doi: 10.1038/nbt.2158

Modarresi, F., Faghihi, M. A., Patel, N. S., Sahagan, B. G., Wahlestedt, C., and Lopez-Toledano, M. A. (2011). Knockdown of BACE1-AS nonprotein-coding transcript modulates beta-amyloid-related hippocampal neurogenesis. *Int. J. Alzheimers Dis.* 2011:929042. doi: 10.4061/2011/929042

More, S., and Choi, D. K. (2017). Neuroprotective role of Atractylenolide-I in an *In Vitro* and *In Vivo* model of Parkinson's disease. *Nutrients* 9:451. doi: 10.3390/nu9050451

Mori, K., Weng, S. M., Arzberger, T., May, S., Rentzsch, K., Kremmer, E., et al. (2013). The C9orf72 GGGGCC repeat is translated into aggregating dipeptide-repeat proteins in FTLD/ALS. *Science* 339, 1335–1338. doi: 10.1126/science.1232927

Naganuma, T., Nakagawa, S., Tanigawa, A., Sasaki, Y. F., Goshima, N., and Hirose, T. (2012). Alternative 3'-end processing of long noncoding RNA initiates construction of nuclear paraspeckles. *EMBO J.* 31, 4020–4034. doi: 10.1038/emboj.2012.251

Peng, T., Liu, X., Wang, J., Liu, Y., Fu, Z., Ma, X., et al. (2019). Long noncoding RNA HAGLROS regulates apoptosis and autophagy in Parkinson's disease via regulating miR-100/ATG10 axis and PI3K/Akt/mTOR pathway activation. *Artif. Cells Nanomed. Biotechnol.* 47, 2764–2774. doi: 10.1080/21691401.2019.1636805

Pizzorusso, T., and Tognini, P. (2020). Interplay between metabolism, nutrition and epigenetics in shaping brain DNA methylation, neural function and behavior. *Genes (Basel)* 11:742. doi: 10.3390/genes11070742

Pollard, K. S., Salama, S. R., Lambert, N., Lambot, M. A., Coppens, S., Pedersen, J. S., et al. (2006). An RNA gene expressed during cortical development evolved rapidly in humans. *Nature* 443, 167–172. doi: 10.1038/nature05113

Ponjavic, J., Oliver, P. L., Lunter, G., and Ponting, C. P. (2009). Genomic and transcriptional co-localization of protein-coding and long non-coding RNA pairs in the developing brain. *PLoS Genet.* 5:e1000617. doi: 10.1371/journal.pgen.1000617

Qian, C., Ye, Y., Mao, H., Yao, L., Sun, X., Wang, B., et al. (2019). Downregulated lncRNA-SNHG1 enhances autophagy and prevents cell death through the miR-221/222 /p27/mTOR pathway in Parkinson's disease. *Exp. Cell Res.* 384, 111614. doi: 10.1016/j.yexcr.2019.111614

Quan, Z., Zheng, D., and Qing, H. (2017). Regulatory roles of long non-coding RNAs in the central nervous system and associated neurodegenerative diseases. *Front. Cell. Neurosci.* 11:175. doi: 10.3389/fncel.2017.00175

Quinn, J. J., and Chang, H. Y. (2015). Unique features of long non-coding RNA biogenesis and function. *Nat. Rev. Genet.* 17, 47–62. doi: 10.1038/nrg.2015.10

Reddy, K., Zamiri, B., Stanley, S. Y., Macgregor, R. B. Jr., and Pearson, C. E. (2013). The disease-associated r(GGGGCC)n repeat from the C9orf72 gene forms tract length-dependent uni- and multimolecular RNA G-quadruplex structures. *J. Biol. Chem.* 288, 9860–9866. doi: 10.1074/jbc.C113.452532

Renton, A. E., Chio, A., and Traynor, B. J. (2014). State of play in amyotrophic lateral sclerosis genetics. *Nat. Neurosci.* 17, 17–23. doi: 10.1038/nn.3584

Rinn, J. L., Kertesz, M., Wang, J. K., Squazzo, S. L., Xu, X., Brugmann, S. A., et al. (2007). Functional demarcation of active and silent chromatin domains in human HOX loci by noncoding RNAs. *Cell* 129, 1311–1323. doi: 10.1016/j.cell.2007.05.022

Ross, C. A., and Tabrizi, S. J. (2011). Huntington's disease: from molecular pathogenesis to clinical treatment. *Lancet Neurol.* 10, 83–98. doi: 10.1016/S1474-4422(10)70245-3

Ryan, P., Patel, B., Makwana, V., Jadhav, H. R., Kiefel, M., Davey, A., et al. (2018). Peptides, peptidomimetics, and carbohydrate-peptide conjugates as amyloidogenic aggregation inhibitors for alzheimer's disease. *ACS Chem. Neurosci.* 9, 1530–1551. doi: 10.1021/acschemneuro.8b00185

Salmena, L., Poliseno, L., Tay, Y., Kats, L., and Pandolfi, P. P. (2011). A ceRNA hypothesis: the Rosetta Stone of a hidden RNA language? *Cell* 146, 353–358. doi: 10.1016/j.cell.2011.07.014

Sareen, D., O'Rourke, J. G., Meera, P., Muhammad, A. K., Grant, S., Simpkinson, M., et al. (2013). Targeting RNA foci in iPSC-derived motor neurons from ALS patients with a C9ORF72 repeat expansion. *Sci. Transl. Med.* 5:208ra149. doi: 10.1126/scitranslmed.3007529

Shah, K., Desilva, S., and Abbruscato, T. (2012). The role of glucose transporters in brain disease: diabetes and Alzheimer's Disease. *Int. J. Mol. Sci.* 13, 12629–12655. doi: 10.3390/ijms131012629

Shelkovnikova, T. A., Kukharsky, M. S., An, H., Dimasi, P., Alexeeva, S., Shabir, O., et al. (2018). Protective paraspeckle hyper-assembly downstream of TDP-43 loss of function in amyotrophic lateral sclerosis. *Mol. Neurodegener.* 13:30. doi: 10.1186/s13024-018-0263-7

Simchovitz, A., Hanan, M., Niederhoffer, N., Madrer, N., Yayon, N., Bennett, E. R., et al. (2019). NEAT1 is overexpressed in Parkinson's disease substantia nigra and confers drug-inducible neuroprotection from oxidative stress. *FASEB J.* 33, 11223–11234. doi: 10.1096/fj.201900830R

Sinha, M., Mukhopadhyay, S., and Bhattacharyya, N. P. (2012). Mechanism(s) of alteration of micro RNA expressions in Huntington's disease and their possible contributions to the observed cellular and molecular dysfunctions in the disease. *Neuromolecular. Med.* 14, 221–243. doi: 10.1007/s12017-012-8183-0

Song, Q., Geng, Y., Li, Y., Wang, L., and Qin, J. (2019). Long noncoding RNA NORAD regulates MPP+-induced Parkinson's disease model cells. *J. Chem. Neuroanat.* 101:101668. doi: 10.1016/j.jchemneu.2019.101668

Sosinska, P., Mikula-Pietrasik, J., and Ksiazek, K. (2015). The double-edged sword of long non-coding RNA: the role of human brain-specific BC200 RNA in translational control, neurodegenerative diseases, and cancer. *Mutat. Res. Rev. Mutat. Res.* 766, 58–67. doi: 10.1016/j.mrrev.2015.08.002

Sun, J., Pan, L. M., Chen, L. B., and Wang, Y. (2017). LncRNA XIST promotes human lung adenocarcinoma cells to cisplatin resistance via let-7i/BAG-1 axis. *Cell Cycle* 16, 2100–2107. doi: 10.1080/15384101.2017.1361071

Sunwoo, J. S., Lee, S. T., Im, W., Lee, M., Byun, J. I., Jung, K. H., et al. (2017). Altered expression of the long noncoding RNA NEAT1 in huntington's disease. *Mol. Neurobiol.* 54, 1577–1586. doi: 10.1007/s12035-016-9928-9

Sutherland, G., Mellick, G., Newman, J., Double, K. L., Stevens, J., Lee, L., et al. (2008). Haplotype analysis of the IGF2-INS-TH gene cluster in Parkinson's disease. *Am. J. Med .Genet. B Neuropsychiatr. Genet.* 147B, 495–499. doi: 10.1002/ajmg.b.30633

Tang, Y., and Le, W. (2016). Differential roles of M1 and M2 microglia in neurodegenerative diseases. *Mol. Neurobiol.* 53, 1181–1194. doi: 10.1007/s12035-014-9070-5

Tatton, W. G., Chalmers-Redman, R., Brown, D., and Tatton, N. (2003). Apoptosis in Parkinson's disease: signals for neuronal degradation. *Ann. Neurol.* 53 Suppl 3, S61–S70. doi: 10.1002/ana.10489

Thompson, C., Otero, P., Srinageshwar, B., Petersen, R. B., Dunbar, G. L., and Rossignol, J. (2020). Possible roles of epigenetics in stem cell therapy for Parkinson's disease. *Epigenomics* 12, 647–656. doi: 10.2217/epi-2019-0347

Thomson, D. W., Bracken, C. P., and Goodall, G. J. (2011). Experimental strategies for microRNA target identification. *Nucleic Acids Res.* 39, 6845–6853. doi: 10.1093/nar/gkr330

Thomson, D. W., and Dinger, M. E. (2016). Endogenous microRNA sponges: evidence and controversy. *Nat. Rev. Genet.* 17, 272–283. doi: 10.1038/nrg.2016.20

Tollervey, J. R., Curk, T., Rogelj, B., Briese, M., Cereda, M., Kayikci, M., et al. (2011). Characterizing the RNA targets and position-dependent splicing regulation by TDP-43. *Nat. Neurosci.* 14, 452–458. doi: 10.1038/nn.2778

Ulitsky, I., and Bartel, D. P. (2013). lincRNAs: genomics, evolution, and mechanisms. *Cell* 154, 26–46. doi: 10.1016/j.cell.2013.06.020

Vangoor, V. R., Gomes-Duarte, A., and Pasterkamp, R. J. (2020). Long non-coding RNAs in motor neuron development and disease. *J. Neurochem.* 156, 777–801. doi: 10.1111/jnc.15198

Wang, H., Lu, B., and Chen, J. (2019). Knockdown of lncRNA SNHG1 attenuated Abeta25-35-inudced neuronal injury via regulating KREMEN1 by acting as a ceRNA of miR-137 in neuronal cells. *Biochem. Biophys. Res. Commun.* 518, 438–444. doi: 10.1016/j.bbrc.2019.08.033

Wang, K. C., Yang, Y. W., Liu, B., Sanyal, A., Corces-Zimmerman, R., Chen, Y., et al. (2011). A long noncoding RNA maintains active chromatin to coordinate homeotic gene expression. *Nature* 472, 120–124. doi: 10.1038/nature09819

West, J. A., Davis, C. P., Sunwoo, H., Simon, M. D., Sadreyev, R. I., Wang, P. I., et al. (2014). The long noncoding RNAs NEAT1 and MALAT1 bind active chromatin sites. *Mol. Cell* 55, 791–802. doi: 10.1016/j.molcel.2014.07.012

Wu, Y. Y., and Kuo, H. C. (2020). Functional roles and networks of non-coding RNAs in the pathogenesis of neurodegenerative diseases. *J. Biomed. Sci.* 27:49. doi: 10.1186/s12929-020-00636-z

Xu, W., Li, K., Fan, Q., Zong, B., and Han, L. (2020a). Knockdown of long non-coding RNA SOX21-AS1 attenuates amyloid-beta-induced neuronal damage by sponging miR-107. *Biosci. Rep.* 40:BSR20194295. doi: 10.1042/BSR20194295

Xu, W., Zhang, L., Geng, Y., Liu, Y., and Zhang, N. (2020b). Long noncoding RNA GAS5 promotes microglial inflammatory response in Parkinson's disease by regulating NLRP3 pathway through sponging miR-223-3p. *Int. Immunopharmacol.* 85:106614. doi: 10.1016/j.intimp.2020.106614

Xu, X., Zhuang, C., Wu, Z., Qiu, H., Feng, H., and Wu, J. (2018). LincRNA-p21 inhibits cell viability and promotes cell apoptosis in Parkinson's Disease through Activating alpha-Synuclein expression. *Biomed. Res. Int.* 2018:8181374. doi: 10.1155/2018/8181374

Yan, Y., Yan, H., Teng, Y., Wang, Q., Yang, P., Zhang, L., et al. (2020). Long non-coding RNA 00507/miRNA-181c-5p/TTBK1/MAPT axis regulates tau hyperphosphorylation in Alzheimer's disease. *J. Gene Med.* 22:e3268. doi: 10.1002/jgm.3268

Yang, J. H., Li, J. H., Jiang, S., Zhou, H., and Qu, L. H. (2013). ChIPBase: a database for decoding the transcriptional regulation of long non-coding RNA and microRNA genes from ChIP-Seq data. *Nucleic Acids Res.* 41, D177–D187. doi: 10.1093/nar/gks1060

Yang, S., Yang, H., Luo, Y., Deng, X., Zhou, Y., and Hu, B. (2021). Long non-coding RNAs in neurodegenerative diseases. *Neurochem. Int.* 148:105096. doi: 10.1016/j.neuint.2021.105096

Yen, Y. P., Hsieh, W. F., Tsai, Y. Y., Lu, Y. L., Liau, E. S., Hsu, H. C., et al. (2018). Dlk1-Dio3 locus-derived lncRNAs perpetuate postmitotic motor neuron cell fate and subtype identity. *Elife* 7:38080. doi: 10.7554/eLife.38080

Yi, J., Chen, B., Yao, X., Lei, Y., Ou, F., and Huang, F. (2019). Upregulation of the lncRNA MEG3 improves cognitive impairment, alleviates neuronal damage, and inhibits activation of astrocytes in hippocampus tissues in Alzheimer's disease through inactivating the PI3K/Akt signaling pathway. *J. Cell Biochem.* 120, 18053–18065. doi: 10.1002/jcb.29108

Yue, D., Guanqun, G., Jingxin, L., Sen, S., Shuang, L., Yan, S., et al. (2019). Silencing of long noncoding RNA XIST attenuated Alzheimer's disease-related BACE1 alteration through miR-124. *Cell Biol. Int.* 44, 630–636. doi: 10.1002/cbin.11263

Zempel, H., and Mandelkow, E. M. (2015). Tau missorting and spastin-induced microtubule disruption in neurodegeneration: alzheimer disease and hereditary spastic paraplegia. *Mol. Neurodegener.* 10:68. doi: 10.1186/s13024-015-0064-1

Zhang, J., Yao, T., Wang, Y., Yu, J., Liu, Y., and Lin, Z. (2016a). Long noncoding RNA MEG3 is downregulated in cervical cancer and affects cell proliferation and apoptosis by regulating miR-21. *Cancer Biol. Ther.* 17, 104–113. doi: 10.1080/15384047.2015.1108496

Zhang, K., Donnelly, C. J., Haeusler, A. R., Grima, J. C., Machamer, J. B., Steinwald, P., et al. (2015). The C9orf72 repeat expansion disrupts nucleocytoplasmic transport. *Nature* 525, 56–61. doi: 10.1038/nature14973

Zhang, L., Fang, Y., Cheng, X., Lian, Y. J., and Xu, H. L. (2019a). Silencing of long noncoding RNA SOX21-AS1 relieves neuronal oxidative stress injury in mice with alzheimer's disease by upregulating FZD3/5 via the Wnt signaling pathway. *Mol. Neurobiol.* 56, 3522–3537. doi: 10.1007/s12035-018-1299-y

Zhang, L. M., Wang, M. H., Yang, H. C., Tian, T., Sun, G. F., Ji, Y. F., et al. (2019b). Dopaminergic neuron injury in Parkinson's disease is mitigated by interfering lncRNA SNHG14 expression to regulate the miR-133b/ alpha-synuclein pathway. *Aging (Albany NY)* 11, 9264–9279. doi: 10.18632/aging.102330

Zhang, Q. S., Wang, Z. H., Zhang, J. L., Duan, Y. L., Li, G. F., and Zheng, D. L. (2016b). Beta-asarone protects against MPTP-induced Parkinson's disease via regulating long non-coding RNA MALAT1 and inhibiting alpha-synuclein protein expression. *Biomed. Pharmacother.* 83, 153–159. doi: 10.1016/j.biopha.2016.06.017

Zhao, Y., Wang, Z., Mao, Y., Li, B., Zhu, Y., Zhang, S., et al. (2020). NEAT1 regulates microtubule stabilization via FZD3/GSK3beta/P-tau pathway in SH-SY5Y cells and APP/PS1 mice. *Aging (Albany NY)* 12, 23233–23250. doi: 10.18632/aging.104098

Zhou, T., Qin, G., Yang, L., Xiang, D., and Li, S. (2019). LncRNA XIST regulates myocardial infarction by targeting miR-130a-3p. *J. Cell Physiol.* 234, 8659–8667. doi: 10.1002/jcp.26327

Zhu, J., Zhang, R., Yang, D., Li, J., Yan, X., Jin, K., et al. (2018). Knockdown of long non-coding RNA XIST inhibited doxorubicin resistance in colorectal cancer by upregulation of miR-124 and Downregulation of SGK1. *Cell Physiol. Biochem.* 51, 113–128. doi: 10.1159/000495168

Zimmer-Bensch, G. (2019). Emerging roles of long non-coding RNAs as drivers of brain evolution. *Cells* 8:1399. doi: 10.3390/cells8111399

Conflict of Interest: The authors declare that the research was conducted in the absence of any commercial or financial relationships that could be construed as a potential conflict of interest.

Publisher's Note: All claims expressed in this article are solely those of the authors and do not necessarily represent those of their affiliated organizations, or those of the publisher, the editors and the reviewers. Any product that may be evaluated in this article, or claim that may be made by its manufacturer, is not guaranteed or endorsed by the publisher.

frontiers in Cell and Developmental Biology

REVIEW
published: 06 September 2021
doi: 10.3389/fcell.2021.689962

Epigenetic Regulation of Angiogenesis in Development and Tumors Progression: Potential Implications for Cancer Treatment

Veronica Mădălina Aspriţoiu[1], Ileana Stoica[1], Coralia Bleotu[1,2] and Carmen Cristina Diaconu[2]*

[1] Faculty of Biology, University of Bucharest, Bucharest, Romania, [2] Romanian Academy, Stefan S. Nicolau Institute of Virology, Bucharest, Romania

Angiogenesis is a multi-stage process of new blood vessel development from pre-existing vessels toward an angiogenic stimulus. The process is essential for tissue maintenance and homeostasis during embryonic development and adult life as well as tumor growth. Under normal conditions, angiogenesis is involved in physiological processes, such as wound healing, cyclic regeneration of the endometrium, placental development and repairing certain cardiac damage, in pathological conditions, it is frequently associated with cancer development and metastasis. The control mechanisms of angiogenesis in carcinogenesis are tightly regulated at the genetic and epigenetic level. While genetic alterations are the critical part of gene silencing in cancer cells, epigenetic dysregulation can lead to repression of tumor suppressor genes or oncogene activation, becoming an important event in early development and the late stages of tumor development, as well. The global alteration of the epigenetic spectrum, which includes DNA methylation, histone modification, chromatin remodeling, microRNAs, and other chromatin components, is considered one of the hallmarks of cancer, and the efforts are concentrated on the discovery of molecular epigenetic markers that identify cancerous precursor lesions or early stage cancer. This review aims to highlight recent findings on the genetic and epigenetic changes that can occur in physiological and pathological angiogenesis and analyze current knowledge on how deregulation of epigenetic modifiers contributes to tumorigenesis and tumor maintenance. Also, we will evaluate the clinical relevance of epigenetic markers of angiogenesis and the potential use of "epi-drugs" in modulating the responsiveness of cancer cells to anticancer therapy through chemotherapy, radiotherapy, immunotherapy and hormone therapy as anti-angiogenic strategies in cancer.

Keywords: epigenetic regulation, angiogenesis, development, tumors progression, cancer treatment

OPEN ACCESS

Edited by:
Shunliang Xu,
Second Hospital of Shandong University, China

Reviewed by:
David D. Eisenstat,
Royal Children's Hospital, Australia
Maria Pia Bozzetti,
University of Salento, Italy

****Correspondence:***
Coralia Bleotu
cbleotu@yahoo.com

Specialty section:
This article was submitted to Epigenomics and Epigenetics, a section of the journal Frontiers in Cell and Developmental Biology

Received: *01 April 2021*
Accepted: *16 August 2021*
Published: *06 September 2021*

Citation:
Aspriţoiu VM, Stoica I, Bleotu C and Diaconu CC (2021) Epigenetic Regulation of Angiogenesis in Development and Tumors Progression: Potential Implications for Cancer Treatment. Front. Cell Dev. Biol. 9:689962. doi: 10.3389/fcell.2021.689962

INTRODUCTION

Angiogenesis is a multi-stage process defined as new blood vessels development that originates from pre-existing vessels, which usually grow toward an angiogenic stimulus (Adair and Montani, 2010). The process is essential for tissue maintenance and homeostasis during embryonic development and adult life as well as tumor growth. Under physiological conditions, angiogenesis is involved

in physiological processes, such as placental development, cyclic regeneration of endometrium, wound healing and repairing the damage inflicted by ischemia or cardiac failure (Ferrara and Alitalo, 1999). However, aberrations of the phenomenon may constitute the pathogenetic basis of diseases such as cancer, an essential condition for the early stages of tumoral maintenance and development of vascular networks that support metastases in the advanced stages of the disease. Angiogenesis is necessary for cancer growth and metastasis and, therefore, an imperative goal for cancer research. In cancer biology, vessels network are crucial for nutrients and oxygen supply for the tumor, and new blood circuits are essential for the maintenance of tumor cells, ensuring nutrients and removing metabolic waste from tumor sites (Tonini et al., 2003). The regulatory mechanisms in physiological angiogenesis are coordinated, well balanced, and strictly regulated by pro and anti-angiogenic factors. In contrast, tumor angiogenesis is characterized by the excess of pro-angiogenic factors that lead to uncoordinated endothelial cell (EC) proliferation and supportive cell migration (Pozzi and Zent, 2009).

Unlike normal blood vessels, the structure and function of the tumor vasculature are abnormally characterized by the affectation of pericytes and basement membrane (BM), small vessel diameter, heterogeneous vascular density and high permeability to large molecules (Tonini et al., 2003). These abnormalities contribute to an abnormal microenvironment, characterized by the pressure generated in growing tumors which compresses the intratumoral blood and lymphatic vessels leading to an inadequate blood supply, interstitial hypertension, hypoxia, and acidosis (Padera et al., 2004). On the other hand, the hypoxic microenvironment is a precondition for tumor drug resistance. A possible explanation of resistance to radiotherapy may be that oxygen is mandatory for the cytotoxic effects of ionizing radiation. Furthermore, resistance to chemotherapy is often characterized by an insufficient drug supply in the treated tumor (Vaupel et al., 2001). Specific anti-angiogenic agents can adjust tumor angiogenesis, normalize of tumor vasculature, and improve blood flow and tumor perfusion, reducing vascular permeability and interstitial fluid pressure (Jain, 2001). This hypothesis was supported by several preclinical and clinical studies in which anti-angiogenic therapy was combined with chemotherapy and/or radiotherapy for glioblastoma, ovarian, breast, colorectal, and pancreatic cancer. Unfortunately for these patients, the progression-free survival and overall survival were only for few months, and new therapeutic strategies are under exploration to improve survival for patients with cancer (Montemagno and Pagès, 2020).

Considering that all organisms need to adapt quickly to environmental changes, epigenetic regulation of genes is the mechanism through which organisms rapidly adapt to these changes. Thus, the analysis of the epigenetic status of different modified genes, chromatin regions, histone and miRNA in various pathologies was developed, leading to the discovery of many useful epigenetic biomarkers. For example, the DNA methylation signature in a tumor sample may have additional medical value by being used as prognostic and diagnostic biomarkers in different cancer types. Using methylation data, it was concluded that patients with a higher methylation grade at CpG islands who showed aberrant hypermethylation at target genes had poorer results than patients with a lower methylation grade. Hence, methylation can be a good indicator of survival prediction and of response to therapies (Shen et al., 2010). In addition, it has been observed that epigenetic agents inhibit the development of latent cancer cells that express anti-angiogenic genes. These genes are reduced during switching to active growth by changes in DNA methylation and histone changes (Lyu et al., 2013).

In this review, we have summarized information about the non-pathological angiogenic process but also the implications of angiogenic agents in the development and progression of tumors, by addressing vascular cooption and intussusception, sprouting angiogenesis and/or vasculogenic mimicry to meet the needs of supplementary vasculature. Moreover, we have presented important epigenetic agents and their role in carcinogenesis that can be used as treatment targets in various pathologies. Epigenetic changes have reversible effects and in general epigenetic agents have lower toxicity, having potential in antiangiogenic treatments or as adjuvants.

ANGIOGENESIS MECHANISMS

Angiogenesis is described as microvascular growth under an angiogenic stimulus (**Figure 1A**; Risau and Flamme, 1995). As a general mechanism, the process involves a structural alteration of the basement membrane (BM) and dilated vessel. After partial degradation of the basement membrane, endothelial cell migrates maintaining their basal-luminal polarity forming interendothelial junctions. The new growing vessel elongates toward angiogenic factors while BM is deposited continuously by the endothelial cell, and pericytes are recruited for the new vessel coverage (**Figure 2A**; Paku and Paweletz, 1991).

Several ways to develop new blood vessels have been described: sprouting angiogenesis, intussusception, vascular mimicry and cooption and using endothelial progenitor cells or angioblasts. Sprouting angiogenesis is the process by which specialized endothelial tip cells migrate from preexisting vessels and invade surrounding avascular tissue. The process starts with sprouts composed of specific and proliferative endothelial cells (ECs), which usually grow toward an angiogenic stimulus (**Figure 1A**; Adair and Montani, 2010; Groppa et al., 2018).

Non-sprouting vessels can be intussusceptive or splitting angiogenesis (**Figure 1D**), through which the intraluminal walls are divided longitudinally from the pre-existing vessels into new smaller ones (Gianni-Barrera et al., 2011; Ribatti and Crivellato, 2012). In addition, two models were observed during tumor development: vascular mimicry and vascular cooption with implication on tumor progression (**Figures 1B,C**). It was observed that angioblasts isolated from human peripheral blood and differentiated in ECs *in vitro*, have the ability to be incorporated into active sites of angiogenesis. This may be an important fact in the normalization of tumor vasculature, supplementing vessel growth in therapeutic angiogenesis (Asahara et al., 1997).

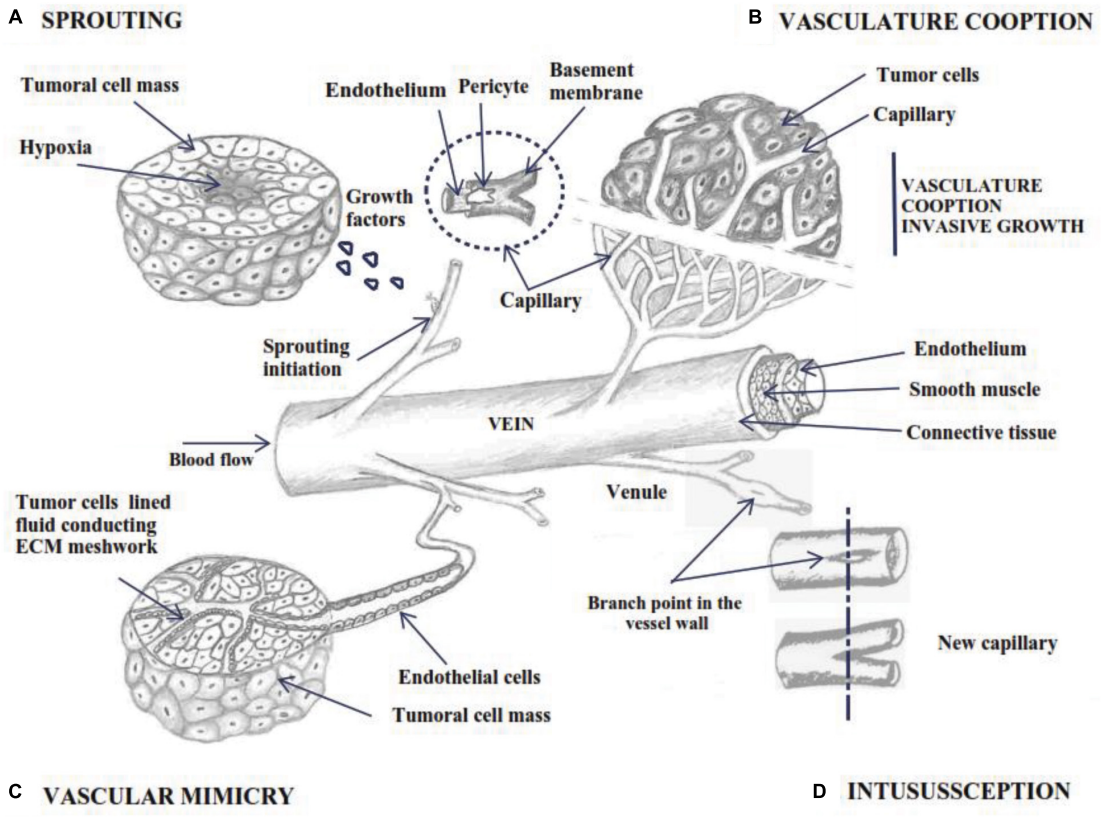

FIGURE 1 | Schematic outline of angiogenesis by 4 different mechanisms; **(A)** sprouting angiogenesis: bud initiation from capillary wall under growth factor signaling; **(B)** vascular cooption of nearby tissue vessels as its own source of nutrients; **(C)** vascular mimicry – the tumor cells adopt endothelial phenotype and form a vasculogenic-like network **(D)** vessel intussusception involves the splitting of pre-existing vessels into two new vascular structures.

Quiescence and Sprouting: Regulation of Tip and Stalk Cell

Endothelial cells cover the vessels' inner surface, an intricate network nourishing all organism tissues. In embryonic development, *de novo* vessels appear by assembling endothelial precursors that differentiate to form a primitive vascular system (vasculogenesis) (Potente et al., 2011). Upcoming vessel sprouting by angiogenesis creates new blood vessels that originate from pre-existing ones and requires pericytes and vascular smooth muscle cells for covering nascent EC (Adair and Montani, 2010; Carmeliet and Jain, 2011). In healthy adults, vessels are quiescent, but their constitutive ECs maintain their plasticity to sense and respond to angiogenic stimuli. Thus, under pro-angiogenic signals influences, ECs become motile and invade the surrounding sites (Carmeliet and Jain, 2011). Tip cells, the ECs located at the tip of the sprout, are migratory and polarized cells with minimal proliferation rate, leading to new-formed vessels. Using their many phyllopods, they sense endogenous stimuli from the environment and guide the angiogenic sprout toward the direction of stimuli (**Figures 2B,C**; del Toro et al., 2010).

In contrast, stalk cell proliferates during sprout extension behind the leading tip cell and forms the nascent vascular lumen cells by maintaining their position and connection to the parent vasculature. Stalk cells shape the branches and organize the vascular lumen of the new routes near the sprout (Gerhardt et al., 2003), constitute cell-cell junctions with adjacent cells, and synthesize components for the basement membrane (Phng and Gerhardt, 2009). During maturation, stalk cells transform into phalanx cells (De Spiegelaere et al., 2012). The proliferation rate of the phalanx cells is slower than the stalk cells. They resemble resting ECs, but forms the basement membrane continuously and strengthens the tight junctions forming a tight barrier between the blood and the surrounding tissue (De Smet et al., 2009).

Quiescent ECs are non-proliferating cells with long half-lives, which are maintained by factors like vascular endothelial growth factor (VEGF), NOTCH, angiopoietin-1 (ANG-1) and fibroblast growth factors (FGFs) (Carmeliet and Jain, 2011). The quiescent phenotype is adopted for vessel integrity through increased cell adhesion. Phalanx cells are immobile cells, which line the newly established perfused vessel. They are closely connected by tight junctions and adherens junctions, strengthening the blood vessel wall and forming a lumenized barrier between blood and surrounding tissues that control fluid exchange and immune cell infiltration (Potente et al., 2011).

Cell-cell adhesion between ECs and neighboring cells is regulated at the adherent junctions at the endothelium level

by transmembrane adhesive proteins, VE-cadherin N-cadherin, as well as claudin, occludin, nectins, and junctional adhesion molecules (JAMs). Tight junction molecules maintain and regulate paracellular permeability (Gavard and Gutkind, 2008). VE-cadherin interacts with the cytoskeleton and controls EC adhesion by solidifying the wall or facilitating EC separation and movement. In a complex with VEGFR2, VE-cadherin sustains EC quiescence by recruiting phosphatases, as VE-PTP (Vascular Endothelial Protein Tyrosine Phosphatase) and DEP-1, that remove the phosphate group from the VEGFR2 level, thus limiting VEGF signaling. In addition, activation of TIE2 by ANG1 protects the vessels wall from VEGF-induced cellular mobility by blocking the capability of VEGF to induce VE-cadherin endocytosis (Potente et al., 2011). The main function of VEGF functions in angiogenesis are presented in **Box 1**.

Initiation of sprouting involves endothelial cell specification into three different subtypes bearing different morphologies

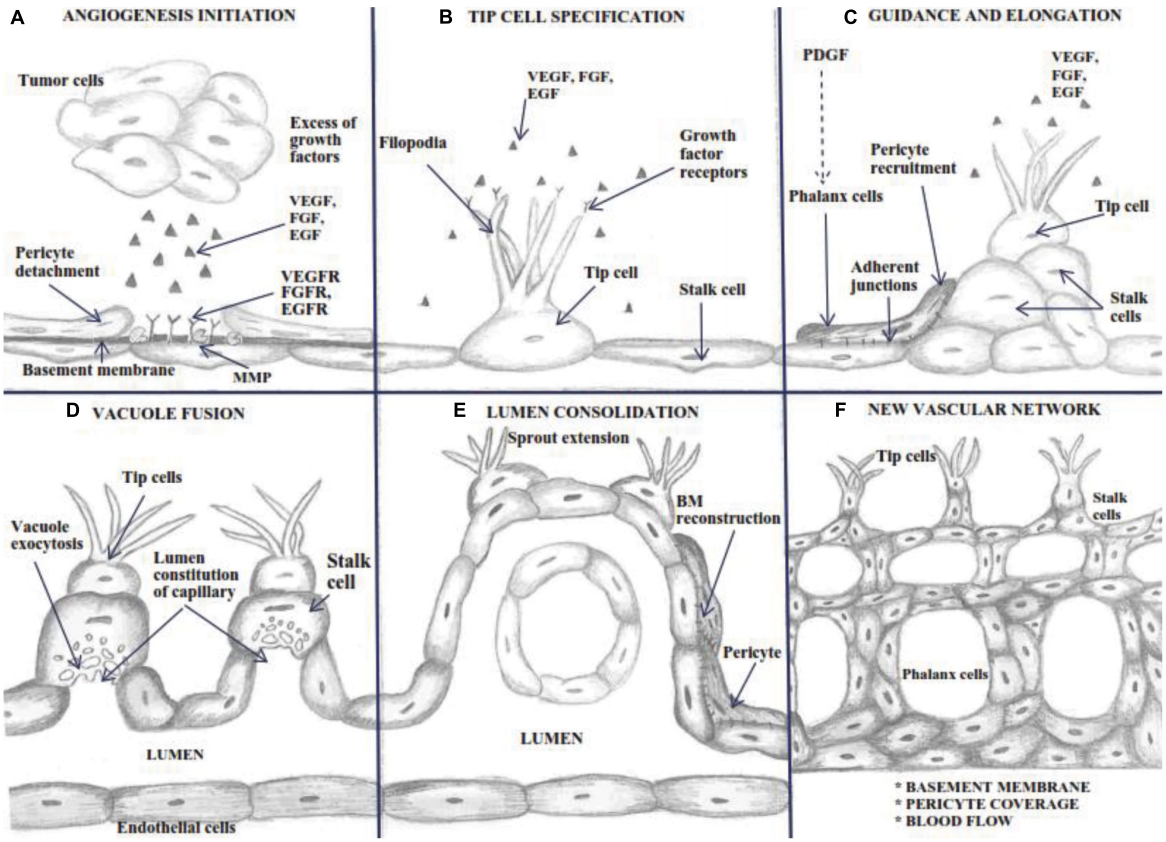

FIGURE 2 | Schematic outline of the Sprouting process. Angiogenesis is a complex process involving: **(A)** a basement membrane alteration produced by MMP, which expose growth factors receptors, characterized by a dilated mother vessel projecting ECs into the connective tissue; **(B)** tip cell specification and filopodia extension determined by growth factors amount-dependent arising from the growing capillary bud; **(C)** ECs migrate in parallel establishing a lumen and sealed by integral endothelial junctions and pericyte recruitment; **(D)** stalk cells display vacuole exocytosis for lumen constitution; **(E)** polarized ECs continuously deposit the basement membrane, and the proliferating pericytes migrate through the basement membrane of the capillary sprout, resulting in the entire constitution of the new vessel wall; **(F)** complete BM reconstitution and the restoration of blood flow.

BOX 1 | The functions of the VEGF family members.

Each of the six homologous genes from the vascular endothelial growth factors family, the VEGF-A, VEGF-B, VEGF-C, VEGF-D and placental growth factors (PlGF1–4), resulting from alternative splicing, plays a significant role in various contexts of vascular growth, from embryonic vasculogenesis to blood and lymphatic angiogenesis in parenchymal tissues (Ferrara, 2004). VEGF-A is the main component of the family. It plays a fundamental role in physiological and pathological angiogenesis by signaling through the VEGF-2 receptor (VEGFR-2, also known as FLK1). VEGFR-2 is a tyrosine kinase receptor expressed by ECs, positively conducting mitogenic and chemotactic signaling in this type of cells correlated with VEGF concentrations (Ribatti and Crivellato, 2012). VEGFR-1 is predominantly expressed in stalk cells, with major importance in guiding and inhibiting tip cell formation, using NOCH signaling that reduces the availability of VEGF ligand and prevents external migration of the tip cell (Chappell et al., 2009). VEGFR-3 is essential in vasculogenesis and is strongly expressed in the leading tip cell, being a fundamental regulator of the development of new lymphatic and blood vessels. VEGFR-3 is tip cell marker. In stalk cell it is down-regulated by NOTCH signaling pathway during sprouting angiogenesis (Ribatti and Crivellato, 2012). Also, VEGFR3 is highly expressed in endothelial lymphocytes. In addition to its promotion of vascular ECs proliferation, VEGF has also been reported to promote vascular permeability through the phosphorylation of VE-cadherin conditioned by VEGF-induced initiation of Rac, which weaken cell-cell interaction in ECs (Gerwins et al., 2000).

and functional properties: filopodia-rich migratory tip cells, highly proliferating stalk cells and quiescent phalanx cells (**Table 1**). Sprouting angiogenesis is initiated through oxygen-sensing mechanisms that detect a hypoxia level and initiates the formation of new blood vessels that meet the metabolic requirements of tumor or somatic cells (**Figure 1A**). Oxygen levels are heterogeneous inside of solid tumors and can range from 2–0.1% O_2 (Hammond et al., 2014). These cells respond to the hypoxic environment by producing and secreting pro-angiogenic growth or proteolytically liberated angiogenic factors from the extracellular matrix (ECM) molecules (Adair and Montani, 2010).

The balance between pro-angiogenic factors (especially the ones involved in NOTCH pathway) is implicated in the reversibility of transiently specification as tip or stalk cells ECs. In the endothelial tip, cells were observed with low NOTCH signaling activity levels and high levels of expression of DLL4 and VEGFR2 during sprouting (Gerhardt et al., 2003). The increase of motility and sprout formation is due to EphrinB2, located in tip cells' filopodia, where it increases endocytosis and activates VEGF-R2 and VEGF-R3, without affecting endothelial proliferation (Sawamiphak et al., 2010). The EphrinB2 receptor, EphB4 is not present at the tip cells level, but instead, it is expressed on ECs after the vessel's growth, being found predominantly in large blood vessels. Its overexpression suppresses sprouting and switch vascular growth to circumferential enlargement (Erber et al., 2006).

In contrast with tip cells which express NOTCH ligand DLL4 for sprout guidance, stalk cells express lower DLL4, but with high NOTCH signaling activity by downregulating VEGFR2, VEGFR3, and neuropilin 1 (NRP1) concomitant with up-regulating VEGFR1 (del Toro et al., 2010). The NOTCH ligand JAGGED1 (JAG1) is expressed primarily by stalk cells being involved in activating NOTCH 1 and maintaining differential NOTCH activity by antagonizing DLL4 that signals back to tip cells (Potente et al., 2011). JAG1- NOTCH signaling pathways promote the sprouting process, unlike DLL4- NOTCH signaling, which inhibits angiogenic sprouting (Bridges et al., 2011).

As the master regulator of angiogenesis, the VEGF pathway comprehensively directs the process of angiogenesis, comprising endothelial cell sprouting, lumen development, vessel enlargement and permeability, and the microarchitecture of vascular networks (Ribatti and Crivellato, 2012). During vascular sprouting, VEGF induces endothelial cell polarization and determination of tip cell formation (Gerhardt et al., 2003). At the same time, adjacent cells to stalk cells are converted by NOTCH signaling leading to VEGF receptor expression (Hellström et al., 2007; Potente et al., 2011).

At the vascular front, ECs' phenotypic specialization as tip or stalk cells is defined as a transient and reversible process determined by the equilibrium between pro-angiogenic factors. The high level VEGF exposure of ECs selects them to become tip cells and regulates migration outward from the parent vessel up the gradient (Ribatti and Crivellato, 2012). In tip cells, VEGF induces the formation and extension of filopodia abundant in VEGFR-2. Filopodia guides the migration of the sprout in the nearby tissue to form a "bond" with other tip or stalk cells, moving toward each other and developing a new vessel (**Figures 2B–D**; De Smet et al., 2009). In a brief description, in response to a VEGF gradient, tip cells up-regulate the expression of ligand DLL4, leading to activation of NOTCH in stalk cells which further inhibit VEGFR-2 expression. Therefore stalk cells become less responsive to VEGF (that regulates proliferation of stalk cells), thereby ensuring tip cell activation (Adair and Montani, 2010). Concomitantly, VEGFR2 signaling up-regulates GLUT1 and PFKFB3 (6-Phosphofructo-2-Kinase/Fructose-2,6-Biphosphatase 3), thus increasing filopodia activity in tip cells (Fitzgerald et al., 2018). NOTCH inactivation is associated with disruption of the vascular hierarchy because the tip cells are not equipped to strengthen stable junctional complexes, explaining why inhibition of NOTCH in tumors results in suppressing tumor growth despite a high number of ECs and sprouts (Adair and Montani, 2010). NOTCH activation consists of proteolytic cleavage of NOTCH receptors and release of the intracellular domain (NICD). The NICD is translocated to the nucleus and interacts with the transcription factor CBF1 and Mastermind-like proteins leading to the activation of target gene expression and p300 histone acetyltransferases to turn on the expression of NOTCH target genes (Phng and Gerhardt, 2009). Acetylation on lysines of NCID enhances NOTCH activity by interfering with turnover of NICD, while associated SIRT1- NICD functions as a deacetylase that opposes NICD stabilization, thus restricting NOTCH activity (Guarani et al., 2011).

Endothelial tip cell filopodia are projected against the direction of interstitial flow or in the direction of an increasing VEGF gradient (Song and Munn, 2011). ECs equipped with

TABLE 1 | The main cells involved in angiogenesis process.

Cells types	Main function during angiogenesis
Endothelial cells	Line blood vessels having a quiescent behavior in normal conditions
Tip cells	Cells leading to the formation of new vessel branches. They are motile, invasive, highly polarized with a large number of long filopodial protrusions which can extend, lead and guide endothelial sprouts in their environment
Stalk cells	Form a lumenized tube growing behind the tip cells, proliferate, elongate the sprouts and construct blood circulation under suitable conditions.
Phalanx cells	Emerge in the final step during angiogenesis by lining vessels once the new vessel branches have been consolidated and also are engaged in optimizing blood flow, tissue perfusion, and oxygenation
Mural cells: pericytes and smooth muscle cells	Contribute to vessel lumen formation by strong cell-cell adhesion and tight junctions, are embedded in a thick basement membrane, and remain attached.

guidance receptors at the filopodia level, which determines the back and forth movement for migration of ECs. For instance, ROBO4 is actively involved in filopodia constitution by remodeling and regulating the actin cytoskeleton (Sheldon et al., 2009). Also, ROBO4 maintains vessel integrity by activating and determining filopodia retraction of ECs (Larrivée et al., 2001). Similarly, PLEXIN-D1 is critical in limiting tip cells by modulating the ratio between tip and stalk cells in response to the VEGF gradient and modulating filopodia's retraction. NRP and EPH family members are also involved in sprouting dynamics managing bidirectional signaling in tip cells by expressing the receptor or the ligand (Sawamiphak et al., 2010).

At the commencement of sprouting, a branch point in the vessel wall is produced by the degradation of BM and ECM from nearby capillaries. The structural alteration of the BM on the side of the enlarged mother vessel placed close to the angiogenic stimulus allows pro-angiogenic factors to discharge from the ECM (Tonini et al., 2003). ECs junctions become altered, and the space created in the matrix is invaded by ECs that initiate migration and proliferate within the somatic or tumor mass (Theocharis et al., 2016). ECM is the space between the tissue and vessels containing interstitial fluid, collagen, elastin, fibronectin, laminins, several other glycoproteins, and connective tissue cells (macrophages, fibroblasts, and plasma cells (Theocharis et al., 2016). Very low or high values of matrix densities (due to contents in collagen, elastin, etc.) will not allow the migration and proliferation of ECs only with an intermediate optimal matrix density (Bazmara et al., 2015). As heterodimeric receptors involved in adhesion to the ECM, integrins play a key role in regulating ECs' sprouting ability by determining whether they can survive and adhere to a particular microenvironment (Humphries et al., 2006). Integrins control the adhesion and migration of ECs, as well as the proliferation and cells survival. The integrins, αvβ3 and αvβ5 are involved in promoting distinct pathways of angiogenesis: αvβ3 is required to initiate vessel growing through basic fibroblast growth factor (bFGF) or tumor necrosis factor α (TNF-α) and αvβ5 integrins by VEGF or transforming growth factor α (TGF-α) signaling pathways (see **Box 2**) (Weis and Cheresh, 2011).

Box 3 Tumor cells and the supporting cells secrete matrix metalloproteinases (MMPs) that can modulate angiogenesis by several mechanisms through direct cleavage of cell surface molecules or by exposing cryptic cell-binding sites in the ECM (Deryugina and Quigley, 2015). MMPs release pro-angiogenic growth factors that are sequestered in the matrix, such as VEGF and FGF and generate anti-angiogenic molecules (such as tumstatin and angiostatin) by dividing plasma proteins, matrix molecules, or proteases themselves to inhibit the angiogenesis process or coordinate branching (Arroyo and Iruela-Arispe, 2010). The inhibition of MMP functions is performed by tissue inhibitors of the matrix metalloproteinase (TIMPs) secreted by tumor or somatic cells. TIMP-1 binds to MMP-9 and inhibits its active form by binding to the zymogen forms of the enzyme (Deryugina and Quigley, 2015).

Patterning of Vascular Networks and Vessel Maturation

After the migration of ECs into the surrounding matrix, the angiogenesis process continues with the re-organization of newly formed ECs to form tubules and create a new basement membrane for vascular stability (Tonini et al., 2003). New vessel circuits ascend when a tip cell contact other tip cells, and the BM is constantly deposited by the polarized ECs. Single sprouts headed by tip cells extending long filopodia direct the migration of the sprout in the nearby tissue. After forming anastomosis and blood flow in the capillaries, it starts to create shear stress, decreasing the VEGF-induced activity of ECs (Bazmara et al., 2015). Once vascularization of the tissue is reestablished, the pro-angiogenic factors are down-regulated, and ECs institute a quiescent phenotype, stable and highly interconnected with strong vessels walls, secreting VE-cadherins (Potente et al., 2011). Vascular maturation is induced by blood perfusion that determines pericyte recruitment and maturation and BM deposition (**Figures 2E,F**; Potente et al., 2011). However, loop capillary survival, elongation, and stabilization depend on blood flow pressure and changes in capillary diameter. Uncontrolled capillary blood flow and shear stress will determine the collapse of new loop formation (Bazmara et al., 2015). Pericytes covering the vessels support newly developed vessel structures and prevent their collapse, allowing the lumen to accommodate the size and volume of tumor cell aggregates and blood flow (Goel et al., 2011). This is a necessary ability of tumor angiogenic vasculature to sustain metastasis (Raza et al., 2010).

An essential feature for the proper function of vessels is maturation and coverage by mural cells (pericyte and vascular smooth muscle cells). Some growth factors, such as PDGFs, angiopoietins and TGF-β, contribute to this process. In capillaries and newly formed vessels, pericytes create direct contact with ECs, whereas arteries and veins are consolidated by layers of smooth muscle cells and a matrix (Bergers and Song, 2005). The interaction between ECs

BOX 2 | Fibroblast Growth Factor (FGF).

FGF, an angiogenic growth factor as heparin-binding protein, has a strong stimulatory effect in endothelial cell migration and proliferation. This is placed in the vascular BM and is up-regulated in the course of active angiogenesis. The most common fibroblast growth factors are FGF-2 or basic FGF (bFGF) and FGF-1 or acidic FGF (aFGF), which binds to their complementary receptors FGFR-1 or FGFR-2 (Gerwins et al., 2000). FGF2 stimulates angiogenesis by directly binding to FGFR1, increasing EC migration, promoting capillary morphogenesis (Presta et al., 2005). Also, FGF-2 up-regulate the expression of matrix metalloproteases (MMPs) and urokinase-type plasminogen activator (uPA) and stimulate degradation of the ECM and the stimulation of collagen, fibronectin and proteoglycans synthesis by ECs (see **Box 3**) (Lu et al., 2011). The lack of FGF2 determines integrity defects in ECs, required for sustaining endothelial cell proliferation and vessels restoration in damaged tissues. Also, FGF5 stimulate blood flow and enhanced vessel formation into the injured myocardium. FGF2 is critical for inducing angiogenesis in the presence of VEGF-A, treatment of ECs with FGF2 inhibitors causes the formation of vessels with abnormal architecture, including prominent filopodia suggesting that FGF2 has an important role in vascular integrity during angiogenesis (Seo et al., 2016).

BOX 3 | MMP family members roles in angiogenesis.
MMP family members, zinc-dependent endopeptidases, can be organized into several groups, characterized by different substrate specificities such as gelatinases, collagenases, stromelysins, matrilysins and membrane-type MMPs (Nagase et al., 2006). MMP1 (a collagenase, enriched in tip cells) and MMP2 (a gelatinase) are expressed during angiogenesis and act to degrade extracellular matrix components. MMP-9 plays an important role in cancer cell invasion and tumor metastases (Hao, 2015). MMP-9 acts directly by degrading ECM proteins and activates cytokines and chemokines to regulate tissue remodeling in a large spectrum of physiologic and pathophysiologic processes (Yabluchanskiy et al., 2013). MMP-9 protein contains a catalytic domain that contains fibronectin type II domains, essential for substrate binding and degradation (Vandooren et al., 2013). MMP-9 interacts with substrates with hemopexin-like domain required for specific substrate recognition. ECM degradation initiated by MMP9 is succeeded by activation of VEGF and FGF-2. Also, in matrix remodeling and tumors stromal invasion MMP9 is increased by EGF/EGFR signaling (Deryugina and Quigley, 2015). MMP-9 stimulates macrophages, neutrophils and mast cells to initiate angiogenesis and, therefore, pathogenesis and intensify disease progression by MMP9-mediated activation of VEGF (Huang, 2018).

and pericytes for the vessel's consolidation and stabilization involves the angiopoietin–Tie2 signaling pathway. Pericytes migrate and proliferate on the sprouting site and release TGFβ and angiopoietin-1 in a paracrine manner to suppress ECs proliferation and lead to endothelial layer maturation (Bergers and Song, 2005). TGF-β has considerable angiogenesis activities, starting with coordinating adjustment from vascular inhibition to pro-angiogenic activity depending on the context (Ferrari et al., 2012). It was noted that maintaining an endothelial quiescence state by TGF-β signaling through the TGFBR1/ALK5 receptor inhibits angiogenesis initiation while signaling through the ACVRL1/ALK1 receptor stimulates EC proliferation and migration (Gaengel et al., 2009).

Survival and Vessel Perfusion

Blood flow and fluid shear stress strongly inhibit cell apoptosis and act as survival indicators for ECs (Rostama et al., 2014). Shear stress and pressure are essential to coordinate vessel diameters along with blood flow (Pries et al., 2010). Newly formed vessels regulate their form to fulfill oxygen demands from tissues by activating HIFs (Hypoxia Inducible Factor) that respond to changes in oxygen tension in ECs. HIF activity is regulated by prolyl hydroxylase domain proteins (PHD), which can sense the concentration of oxygen (Fan et al., 2014). Under normoxia, PHDs bind the oxygen molecules to hydroxylate HIFs, and hydroxylated HIF is recognized by the ubiquitin E3 ligase, and eliminated by proteasomal degradation. In hypoxic conditions, oxygen sensors become inactive and HIFs escape from degradation, leading to increased soluble VEGFR1 and VE-cadherin levels, thus allowing ECs to readjust vessel shape to their function of oxygen delivery dynamically. Particularly, in hypoxic conditions, oxygen sensors regulate in a feedback loop the expression of VE-cadherin to optimize vessel perfusions due to insufficient oxygen supply (Mazzone et al., 2009).

During maturation, the EC maintains the integrity of the microvessels lining and protects the vessel wall from environmental stresses by autocrine and paracrine survival signals. Differentiated pericytes produce VEGF as a survival factor for EC in vessels, so that inhibition of VEGF induces apoptosis in endothelial and mesenchymal cell cocultures (Darland et al., 2003). VEGF activates the PI3K/AKT survival pathway of ECs in physiological conditions. VEGF activity also has a paracrine activity in angiogenesis stimulation, such that inhibition of VEGF in ECs does not affect vascular development (Duffy et al., 2000). Endothelial cell communication with vascular smooth muscle cells is mediated via NOTCH signaling on adjacent cells. NOTCH signaling sustains vascular homeostasis due to its ability to establish mature vessels that promote perfusion and relieve tissue hypoxia. Mural cells promote vessel stability through NOTCH – DLL4 signaling by sustaining the accumulation of BM components (Rostama et al., 2014).

Vascular Modeling in Angiogenesis

Modeling and development of blood vessels is a multi-step process that involves different mechanisms of angiogenesis. The initial stages of vascular growth in expanding tissue are mainly promoted by sprouting angiogenesis. Remodeling of the vascular network is performed by splitting angiogenesis, described as intussusceptive angiogenesis, vascular cooption and vascular mimicry (De Spiegelaere et al., 2012).

Intussusceptive Angiogenesis (IA)

Intussusceptive microvascular growth is a fast process (hours or even minutes) that occurs without ECs proliferation and without interfering with the local physiological conditions with relatively lower metabolic cost (**Figure 1D**). As an intravascular growth mechanism, vessel intussusception involves the division of pre-existing vessels into two new vasoformations (De Spiegelaere et al., 2012; Zuazo-Gaztelu and Casanovas, 2018), remodeling through vascular reduction and increased tissue volume, developing the capillary network without a high metabolic demand (Phng and Gerhardt, 2009). This process requires the interaction between two ECs on the opposite walls that form a cell bridge, based on the endothelial bilayer with cell-cell junctions and the interstitial pillar. The process includes the recruitment of pericytes and mural cells that cover the wall, which is further enlarged, allowing the retraction of ECs and developing two connected but separate vessels (Zuazo-Gaztelu and Casanovas, 2018).). The degree of vascular enlargement is proportional to VEGF dose. Both low and high VEGF expression initiates intraluminal pillar formation, but excessive diameters lead to the failure of the formation of a normal vasculature, leading to the failure of division and atypical blood vessels separated by collagen fibers (Ozawa et al., 2004). In order to stabilize nascent vascular structures, pericyte recruitment is crucial. Loss of pericytes layers by incomplete angiogenesis in adult tissue leads to persistent proliferation of ECs and increased fragile vascular structures (Banfi et al., 2012). The molecular mechanism of the switch among normal and abnormal angiogenesis by VEGF dose is associated with the EphrinB2-EphB4 pathway. Specific VEGF doses regulate EphB4 to control endothelial proliferation, size of the initial vascular enlargement,

and modulating its downstream signaling through MAPK/ERK. While EphrinB2 sustain tip cell migration in sprouting by the VEGF pathway, EphB4 diminishes endothelial proliferation during intussusceptive angiogenesis by VEGF-induced ERK1/2 phosphorylation (Groppa et al., 2018).

Vascular Cooption in Tumor Tissue

Some highly vascularized primary and metastatic tumors use pre-existing host tissue vessels as their blood supply by expressing a mixed phenotype with co-opted vessels and angiogenesis (**Figure 1B**). Also, they can grow to an assured level without causing a specific angiogenic response (Donnem et al., 2013). Faster as an angiogenic response by sprouting, tumors connect with the host vessels in the stroma and with increasing size of cellular mass, the blood vessels become completely embedded in the tumor (Küsters et al., 2002). Co-opted blood vessels are commonly detected in highly vascularized tissue such as the brain, lung, liver, and lymph nodes (Donnem et al., 2013; Kuczynski et al., 2019). The key players for ECs survival during cooption are VEGF and ANG-1, which supports tumor vessel maintenance. Shortly after that, tumor coopted vessels begin to fail as a host defense mechanism by overexpressing ANG-2 that disrupts the interaction between ANG-1 and Tie-2 and causes destabilization of capillary walls (Holash et al., 1999). Vessel cooption is implicated in patient outcomes and resistance to cancer therapies and is a valid target of new therapeutic strategies (Kuczynski et al., 2019). In some cases, it was observed that anti-angiogenic treatment is less operative in the tumor periphery, meaning that vessel cooption is located at the edge of tumors (Donnem et al., 2013). Oder tumors with a profound central devascularized upon sunitinib treatment continued to be well vascularized at the upper edge of these aggressive tumors (Welti et al., 2012).

Vasculogenic Mimicry (VM) in Tumor Tissue

This mechanism refers to the tumor cells that adopt an endothelial phenotype and determine *de novo* development of the matrix infused vasculogenic-like system as alternative mechanisms for re-vascularization (**Figure 1C**; De Spiegelaere et al., 2012). The vascular mimicry process results in a capillary network completely composed of tumor cells or mosaic vessels alternating tumoral cells and ECs in the vascular walls (Angara et al., 2017). It reflects the plasticity of aggressive behavior and easily metastasizes toward distant sites, which express vascular cell markers and line the tumor vasculature. Therapeutic strategies that target ECs do not affect tumor cells that engage in VM (Zhang et al., 2007). The morphological, clinical and molecular characterization of vasculogenic mimicry has been described in almost all carcinogenic mass types and was linked to unfavorable outcomes of malignancies (Ge and Luo, 2018). Vasculogenic mimicry describes tumor cells' ability to undergo epithelial-mesenchymal transition (EMT) and achieve cancer stem cells like phenotypes. Those cells are transdifferentiated into endothelial-like cells that support the ECM formation, which is CD31 negative and express PAS-positive patterned vasculogenic networks. The new networks are connected to the mother vessel but with distinct microvessels that provide suitable nutrient supply and contribute to tumor progression (Folberg et al., 2000). For example, in aggressive melanomas, the tumor cells adopt an endothelial-like phenotype characterized by overexpression of specific endothelial genes (Folberg et al., 2000) and meticulously reproduce vasculogenesis starting from dedifferentiated tumor cells. While VE-cadherin is considered specific for ECs, it has been detected in tumoral cells with aggressive phenotypes except for benign masses, and also its down-regulation is conductive to the loss of VM formation in melanoma (Ge and Luo, 2018). Usually, anti-angiogenic drugs target ECs by initiating endothelial cell apoptosis and proliferation inhibition to reduce tumor vascularization. The incidence of vascular mimicry may complicate common anti-angiogenic strategies to treat certain tumors, because the vasculature can be adjusted to another angiogenic phenotype (De Spiegelaere et al., 2012). Remaining malignant cells at a tumoral site can form VM channels, providing oxygen and nutrients that sustain cancer progression. On the other hand, resistance to anti-angiogenic therapies leads to cancer recurrence. Taken together, VM channels increase intratumoral therapeutic agent delivery but with a reduction of drug efficacy of conventional chemotherapeutic agents (Lezcano et al., 2014; Ge and Luo, 2018). Therefore, the development of novel chemotherapies is urgently needed to abolish VM structures and improve tumor therapy.

Endothelial Progenitor Cells Promote Angiogenesis

In some cases, endothelial progenitor cells or angioblasts that are a CD34-enriched subpopulation of mononuclear blood cells, are able to adapt to an adherent endothelial phenotype. This model supposes that new vessels can also grow by recruiting endothelial progenitor cells (EPCs) circulating in the blood (Asahara et al., 1997). Recruitment and integration of EPCs into angiogenesis is a coordinated process that includes chemoattraction and cell arrest in the vessel wall, interstitial migration and incorporation into the vasculature, and endothelial cell differentiation (Hillen and Griffioen, 2007). The recruitment of EPCs is produced under physiological trauma or stress and tumor growth. It starts with the activation of MMP9, detachment of the progenitor cells (c-kit positive) from the bone marrow niche and release of EPCs from the bone marrow into the circulation (Heissig et al., 2002). Angiogenic factors like PLGF, VEGF, MMP9, SDF1, ANG-1, selectin and integrins are essential for the active arrest of EPCs to the vasculature and transendothelial migration (Hillen and Griffioen, 2007). The EPCs undergo a change in specific markers from EPCs endothelial-like such as CD14, CD34, CD31, Tie-2 and VEGFR2 (Kalka et al., 2000) toward a mature endothelial cell pattern (VE-cadherin, von Willebrand factor and eNOS) (Hillen and Griffioen, 2007). However, the characterization of EPC subpopulations is yet to be fully elucidated, and the exact molecular pathways involved in the mobilization and recruiting of EPCs are complex and still under investigation.

ANGIOGENESIS IN DISEASE PROGRESSION

In physiological angiogenesis, cells located more than 200 μm from a blood vessel determine new blood oxygen and nutrients source's recruitment and remove waste products.

Solid tumors development involves synchronization between the neovascularization process and tumor cells proliferation, a process regulated by endogenous activators and the angiogenic process's inhibitor (Tonini et al., 2003). The progressive expansion of the tumor exceeds the capacity to support the existing vasculature and is limited to the tumor's periphery, leading to low oxygenation (hypoxia) and tumor progression (Krock et al., 2011; Dulloo et al., 2015).

Hypoxia induces pro-angiogenic factors in excess, creating a local imbalance that leads to new blood vessels recruitment. These can be poorly organized, fragile, with low functionality, causing low oxygen areas in the tumor that generate a persistent angiogenic signal (Vaupel et al., 2001; Krock et al., 2011). Initially, the hypoxic condition promotes cell death in the tumor mass, but in this way, it provides constant angiogenic signals, allowing survival in the absence of oxygen. In these hypoxic microregions, the resistant cells are selected based on their ability to survive and contribute to a potent tumor mass with very malignant characteristics (Wouters et al., 2003). HIF-1, the oxygen-sensitive transcription factor, acts as heterodimer containing β subunit that is constitutively expressed and one of three alpha subunits (HIF-1α, HIF-2α, or HIF-3α). HIF activity is regulated mainly by post-translational changes in various amino acid residues of its alpha subunits. Both β and α subunits belong to the group of the basic helix-loop-helix (bHLH)-PER-ARNT-SIM (PAS) protein class (Zhang et al., 2011). HIF function is mainly regulated by a stabilized HIF-1α subunit, which is translocated to the nucleus upon hypoxic induction, where it dimerizes with HIF-1β via bHLH and PAS motifs. The activity of HIF-1 is controlled mainly by regulating protein levels at various amino acid residues of the α subunit (Lee et al., 2004). The HIF-1α subunit becomes stable and recruits co-activators such as p300/CBP and HIF-1β to control its transcriptional activity and change transcriptional levels of a hypoxia-specific miR-210 (Wang et al., 2007). Thus HIF-1α is tightly regulated to protect itself against degradation by the tumor suppressor von Hippel-Lindau in hypoxic conditions (Lee et al., 2004). Moreover, HIF-1 is a master modulator for hypoxic gene expression and signaling that can simultaneously induce the transcriptional expression of both proangiogenic factors, VEGF and MMP-9 in a coordinated fashion (Deryugina and Quigley, 2015). The high expression of HIF-1α level in tumor tissues can up-regulate VEGF expression and determine loss of E-cadherin expression, thus reducing cell-cell adhesion and facilitating tumor cell metastasis (Vaupel et al., 2001).

Pro- and Anti-angiogenic Factors in Tumor Angiogenesis

A balance between angiogenic inductors and inhibitors results in quiescent vasculature in normal adult tissue. Similarly, angiogenesis is dormant in small tumors that start as avascular masses, depending on their microenvironment vasculature (Baeriswyl and Christofori, 2009). Disturbance of balance in physiological angiogenesis generates wound healing, but in pathological angiogenesis, it results in an outgrowing vascularized tumor and eventually to malignant tumor progression (Huang and Bao, 2003). In addition to vessel growth, HIF1 is induced as an essential gene expression regulator, when tumor tissues exceed the oxygen diffusion limit (Dulloo et al., 2015) and induce pro-angiogenic compounds targeting tumor vascular supply, disturbing the existing vessels (**Table 2**). These facts activate the "angiogenic switch," which sustains tumor growth and metastasis process (Huang and Bao, 2003). Therefore, hypoxic tumor cells around the necrotic nucleus overexpress VEGF, which controls the formation of new blood vessels from the existing normal vasculature adjacent to the hypoxic site. The onset of angiogenesis involves both endothelial cell proliferation and increased vascular permeability. Endothelial progenitor cells derived from bone marrow or mesenchymal or hematopoietic stem cells that migrate from the systemic circulation to tumors are also recruited to form blood vessels (Das and Marsden, 2013).

In general, tumor blood vessels are considered leaky and inefficient in oxygenation, raising hypoxia, including the generation of growth factors and cytokines by the surrounding tumor cells. This, in turn, promotes tumor invasion and metastasis. Therefore, the concept of vessel "normalization" has gained significant attention in order to control the tumor vasculature to improve drug delivery (Warren and Iruela-Arispe, 2010).

Tumors Micro-Environment

The tumor microenvironment consists of a mixture of cells (tumoral cells, ECs, immune cells, fibroblasts) and extracellular matrix surrounding or infiltrating tumor tissues. Meanwhile, tumor stroma can produce factors to acquire blood vessels for proper supplies of oxygen, nutrients, and waste disposal. Therefore tumoral angiogenesis is considered to be essential for tumor progression and metastatic dissemination (Bhome et al., 2015). The tumor microenvironment comprises several pro-angiogenic factors, including VEGF, bFGF, PDGF, MMP and inflammatory cytokines secreted by tumor cells or tumor-infiltrating lymphocytes or macrophages. These tumoral cells may increase a pre-existing invasion program activity, activate pro-angiogenic gene expression, and stimulate angiogenesis, ensuring tumor cell motility, invasion, and metastasis (Goel et al., 2011).

EPIGENETIC CONTROL OF ANGIOGENESIS IN TUMOR DEVELOPMENT

The suppression of tumor suppressor genes or the activation of oncogenes induced by tumor development and progression is associated with reversible epigenetic dysregulation. Global alteration of epigenetic modification is considered one of the hallmarks of cancer. While it is known that genetic changes (DNA mutations, insertions, deletions, chromosomal rearrangement) have an essential role in the altering of target genes in cancer cells, the importance of epigenetic mechanisms becomes an important event in the early development and late stages of tumor development. Epigenetic modification of tumor cells includes diverse reinforcing and converging signals, including DNA

TABLE 2 | Pro- and antiangiogenic their importance in the angiogenesis process.

Angiogenic factors	Major function in angiogenesis process	References
Pro-angiogenic factors		
VEGF-A, PlGF, VEGF-B, VEGF-C, VEGF-D, VEGF-E	Vasculature formation; Formation of primitive endothelial tubes; Induce proliferation, migration, and differentiation of EC	Kazemi et al., 2002
aFGF, bFGF	Development and maintenance of a mature vascular network	Eguchi et al., 1992; Lee et al., 2000
MMP-9; MMP-14	Direct degradation of ECM proteins; overexpression of MMP-14 increases VEGF production and angiogenesis in glioblastomas	Deryugina and Quigley, 2015
Angiogenin	Support endothelial survival and proliferation, endothelial tube development	Miyake et al., 2015
FGF2, FGF5	Induce cell sprouting elongated morphology with prominent filopodia; endothelial cell growth and movement	Seo et al., 2016
TGFα/β, PDGF, TNFα, HGF/SF, COX-2	Induce differentiation of EC, proliferation and migration	Yoo and Kwon, 2013
NPAS4	Regulates VE-cadherin expression and regulates sprouting angiogenesis and tip cell formation	Esser et al., 2015
TBX3	Its overexpression drives angiogenesis and tumor expansion *in vivo*	Krstic et al., 2020
Nuclear factor 90	Sustain tube formation and cell migration of HUVECs and expression of VEGF-A induced by hypoxia in cancer	Zhang et al., 2018
TSLP	Promotes angiogenesis in cervical cancer	Zhou et al., 2017
TXNDC5	Down-regulate SERPINF1 and TRAF1 expression; sustain atypical angiogenesis, vasculogenic mimicry and metastasis	Xu et al., 2017
IL-1, IL-5, IL-6, IL-8, IL-17	Pro-inflammatory chemokines secreted by leukocytes and macrophages. Induce endothelial cell tube formation and vascularization	Ribatti, 2018
LAPTM4B	Promote tumor angiogenesis through the HIF-1α and VEGF pathway	Meng et al., 2015
CD146	New coreceptor for VEGFR-2; EMT inducer; promotes endothelial cell migration and angiogenesis and human tumor growth	Jiang et al., 2012
Anti-angiogenic factors		
Angiopoietin: ANG-1 ANG-2	Stabilization of existing vessels, control the interaction between ECs and the surrounding environment; ANG-1 suppresses ICAM-1, VCAM-1 and E-selectin; ANG-2 is an antagonist for ANG-1 and inhibits blood vessels maturation	Huang and Bao, 2003
TSP-1, TSP-2	Suppresses migration and induces endothelial cell apoptosis by blocking angiogenic factor access to co-receptors on the endothelial cell surface	Huang and Bao, 2003
TIMP1	Inhibit MMP9 or uPA activity; binds to MMP-9 to inhibit its active form	Yabluchanskiy et al., 2013
Angiostatin	Directly inhibit neutrophil migration and neutrophil-mediated angiogenesis	Benelli et al., 2002
Endostatin	Inhibition of ECs proliferation and migration, tube formation	Ergün et al., 2010
Vasostatin	Angiogenesis inhibitor that specifically targets proliferating ECs	Pike et al., 1998
Interferon-alpha	IFN α – decrease VEGF gene expression	von Marschall et al., 2003
Interleukins: IL-1β, IL-4, IL-10, IL-12, IL-18, IL-23, IL-25, IL-27	Inhibits endothelial cell proliferation	Ribatti, 2018
TGF -beta	Suppresses VEGFA-mediated angiogenesis and tumor progression and metastasis	Geng et al., 2013
SEMA3A	Endogenous inhibitor expressed in premalignant lesions that disappear during tumor progression.	Maione et al., 2009

Cox-2, cyclooxygenase-2; PlGF, placental growth factor; NPAS4, neuronal PAS domain protein 4; TBX3, T-box transcription factor 3; HGF/SF, hepatocyte growth factor/scatter factor; TSLP, thymic stromal lymphopoietin; TXNDC5, thioredoxin domain-containing protein 5; CD146, cluster of differentiation 146; ANG, angiopoietin; ICAM-1, intercellular adhesion molecule-1; VCAM-1, vascular cell adhesion molecule-1; TSP, thrombospondin; TIMP1, TIMP metallopeptidase inhibitor 1; SEMA3A, semaphorin 3A.

methylation, covalent modifications of histones, nucleosome-DNA interactions and small inhibitory RNA molecules.

DNA Methylation of Anti-angiogenic Factors

Angiogenesis initiation marks the conversion process from a dormant cellular state to active growth of ECs, a common disease progression feature. DNA methylation occurs as modification of cytosines nucleotides placed within CpG dinucleotides. Methylation abnormalities commonly occur in many pathological disorders in the form of hypermethylation of CpGs within promoter regions of genes, and therefore these tumor suppressors are silenced. In contrast, global genomic hypomethylation or demethylation has been found in many types of tumors and is associated with activation of proto-oncogenes and generation of chromosomal instability (Hellebrekers et al., 2007).

The most common epigenetic changes in tumoral cells include hypermethylation of anti-angiogenic factors, a mechanism of the tumor to promote angiogenic pathways. For example, methylation-induced silencing gene expression of the angiogenesis inhibitor thrombospondin 1 (THBS-1) inhibits the secretion of TGFß, which was correlated with increased metastasis, invasion, and poor prognosis in several types of cancers (Buysschaert et al., 2008). Also, hypermethylation of proteases with anti-angiogenic properties, such as ADAMTS-8, tissue inhibitor of MMP2 and MMP3 (TIMP-2 and –3), was observed in various tumors (Hellebrekers et al., 2007).

Vascular endothelial growth factor, its receptors and eNOS, essential genes critical for angiogenesis promotion, also are controlled by their gene promoter methylation status. VEGF and eNOS expressions were downregulated via Methyl-CpG–Binding Domain Protein 2 (MBD2) binding, the protein readers of methylation that regulate endothelial function in both physiological and disease states (Rao et al., 2011). In physiological conditions, ECs expressed moderate levels of MBD2, but the lack of MBD2 significantly enriched angiogenesis and secured ECs from H_2O_2-induced apoptosis. Reduced expression of MBD2 determines a higher ERK1/2 activity in ECs, which promotes apoptosis by increasing the expression of BCL-2. In ischemic insults, the essential endothelial genes such as eNOS and VEGFR 2 undergo a DNA methylation turnover, and MBD2 reads DNA methylation changes signals for mediating gene silencing (Rao et al., 2011). MBD2 overexpression has been detected in various solid tumors and promotes cancer progression by mediating silencing of tumor suppressor genes (Gong et al., 2020). MBD2 binds to the gene promoter of brain angiogenesis inhibitor 1 (BAI1) and inhibits its antiangiogenic and antitumorigenic properties in glioma cells. 5-Aza-dC treatment released MBD2 led to reactivation of functional activity of BAI1 *in vitro* and *in vivo* (Zhu et al., 2011). However, MBD2 has dynamic activity and functions in a cell, and tissue-specific way and its expression is associated with malignancy and poor prognosis in solid tumors. In lung cancer, reduced expression of MBD2 was associated with disease progression metastasis and severe patient prognosis (Pei et al., 2019). MBD2 is component of Mi-2/NuRD (Nucleosome Remodeling Deacetylase) complex which reveals nucleosome remodeling and histone deacetylation activities. MBD2/NuRD complex deacetylates the nucleosomes surrounding the targeting site. MBD2 and MBD3 appear to have both activating and repressive roles when complexed with NuRD/Mi-2 in a context-dependent manner (Menafra and Stunnenberg, 2014).

Histone Modifications Defining Angiogenesis

Eukaryotic DNA is tightly packaged into chromosomes around histone protein complexes, forming nucleosomes folded into chromatin structures, and for gene regulation, the histone amino (N)-terminal tails extending from the nucleosomal cores are acetylated and deacetylated at ε-acetyllysine residues by histone acetyltransferases (HATs) and histone deacetylases (HDACs) respectively. HATs sustain gene transcription through acetylation of histones, influencing the charge neutralization and relaxing nucleosomes structure, and HDACs modulate chromatin structure by promoting histones' deacetylation and suppressing transcription by condensing the chromatin (Sasaki and Matsui, 2008).

Histone deacetylases are involved in maintaining vascular integrity due to the association of endothelial growth and vascular morphogenesis with increases in HDAC1 activity and its export from the nucleus (**Table 3**). Also, inhibition of HDAC1 diminishes endothelial morphogenesis and MMP14 gene expression, potentially through its role as a transcriptional regulator (Bazou et al., 2016). HDAC1 also regulates VEGF expression in normal keratinocytes (Reynoso-Roldan et al., 2012). It was shown that HDAC1 supplements and amplifies the VEGF signaling pathway and activate angiogenesis when interstitial flow signals are existent in angiogenic sprouting (Bazou et al., 2016). Overexpression of HDAC1 inhibits p53 and von Hippel-Lindau tumor suppressor gene expression and promotes angiogenesis under hypoxic conditions (Kim et al., 2001).

G9a

G9a, also known as EHMT2 (Euchromatic histone-lysine N-methyltransferase 2) a nuclear lysine histone methyltransferase that mainly catalyzes histone H3 lysine 9 (H3K9), is involved in cancer invasion and metastasis. Generally, G9a involves reversible modification of transcriptional gene silencing, but its activity is associated with tumoral angiogenesis and poor patient outcome (Pirola et al., 2018). A higher expression of G9a in aggressive cervical cancer than in normal epithelium cells was correlated with increased angiogenesis in cervical cancer (Chen et al., 2017). Inhibition of G9a histone methyltransferase significantly inhibits angiogenic factors like VEGF, interleukin-8 and angiogenin (Chen et al., 2017). In tumor angiogenesis, increased H3K9 acetylation was related to over-expression of TIMP3 inhibiting growth of carcinoma cells, while decreased H3K27me3 resulted in the upregulation of TIMP3 and re-expression of anti-angiogenic genes in dormant cells. In addition, an increase in both H3K4me3 and H3K9 was associated with higher CDH1 expression during dormancy. TIMP3 and CDH1 are overexpressed during the dormancy of cancer cells having antiangiogenic properties and are inhibited in the course of the conversion to active development by epigenetic changes (Lyu et al., 2013).

DOT1L

DOT1L is an H3K79 histone methyltransferase studied in embryogenesis, hematopoiesis, cardiac function, cycle regulation, DNA damage response and leukemia (Nguyen and Zhang, 2011).

TABLE 3 | The enzymes that modify histones in angiogenesis.

Enzyme	Activity	Target	References
G9a	Histone methyltransferase	Histone H3 lysine 9 (H3-K9) methylation	Pirola et al., 2018
DOT1L	Histone methyltransferase	H3K79 methylation, H3K9 dimethylation and H4K20 tri-methylation	Jones et al., 2008
SET7	Histone methyltransferase	Methylates H3K4	Zhang et al., 2016
JMJD1A	Histone demethylases	Demethylates Histone 3 lysine 9 (H3K9)	Osawa et al., 2013
LSD1	Histone demethylases	H3k4me1/2, h3k9me1/2	Perillo et al., 2020

DOT1, like histone lysine methyltransferase; JMJD1A, jumonji domain containing 1A; LSD1, lysine-specific demethylase 1A.

Knockout of DOT1L results in embryonic death during organogenesis due to abnormal cardiac morphogenesis and angiogenesis defects in the yolk sac. It plays an important role in heterochromatin formation, as DOT1L-deficient stem cells have low levels of H3K9 dimethylation and H4K20 tri-methylation in centromeres and telomeres and also show an overall loss of H3K79 methylation (Jones et al., 2008). In human umbilical vein endothelial cells (HUVECs), silencing of DOT1L decreases ECs viability and migration, tube formation and sprout development, and cannot establish a functional vascular network. The pro-angiogenic role of DOT1L, was also supported by the observation that DOT1L work together with the ETS-1 proto-oncogene to activate VEGFR2 expression, which further activates the ERK1/2 and AKT signaling pathways in order to achieve angiogenesis (Duan et al., 2013).

SET7

SET7 is a histone methyltransferase that specifically methylates H3K4 in humans, involved in angiogenesis by cooperating with the transcription factor GATA1, which promotes transcriptional up-regulation of VEGF and angiogenesis initiation. SET7 inhibition in breast cancer showed decreased VEGF secretion *in vitro* and *in vivo*, leading to lower proliferation rates, migration and tube formation of HUVECs and also inhibition of breast cancer development in nude mice. Also, GATA1 and SET7 were upregulated and associated with poor prognosis in breast cancer samples (Zhang et al., 2016). On the other hand, SET7/9 is highly expressed in breast tumoral tissues and cancer cell lines. Moreover, a recent study confirms the association between unfavorable prognosis in breast cancer with upregulated SET7/9 expression, describing a carcinogenicity mechanism of SET7/9 through activation of Runt-related transcription factor 2 (RUNX2). The same study showed that SET7/9 is negatively regulated by tripartite motif-containing protein 21 (TRIM21) through a proteasome-dependent mechanism and increased ubiquitination (Si et al., 2020).

Enhancer of Zeste Homolog 2

Enhancer of zeste homolog 2 (EZH2) promotes angiogenesis in a paracrine manner by methylating and silencing vasohibin1 (VASH1) (Lu et al., 2010). High EZH2 expression and low VASH1 in intrahepatic cholangiocarcinoma were associated with tumor angiogenesis initiation, poor disease-free survival, and poor overall survival (Nakagawa et al., 2018). Also, miR-101 was reported to target EZH2 in glioblastoma cells directly. *In vitro* and *in vivo* inhibition of EZH2 attenuated endothelial tubule formation, tumoral migration and invasion, resulting in generally reduced tumor growth (Smits et al., 2010).

JMJD1A

JMJD1A an epigenetic regulator that demethylates Histone 3 lysine 9 (H3K9), is expressed as a response to the cooperative action of hypoxia and nutrient starvation in cancer cells by promoting angiogenesis and macrophage infiltration. JMJD1A inhibition suppresses tumor growth and angiogenesis and sensitizes cancer cells to VEGF and VEGFR inhibitors by suppressing FGF2, HGF, and ANG2. Moreover, inhibition of JMJD1A sustained the antitumoral properties of two anti-angiogenic treatments (bevacizumab and sunitinib), limiting tumor resistance (Osawa et al., 2013).

LSD1

LSD1 remove methyl groups of H3K4me1/2, H3K9me1/2, and some non-histone substrates that mediate many cellular signaling pathways that are highly overexpressed in different types of cancers (Perillo et al., 2020). It also controls the turnover of HIF-1α as a cellular response to hypoxia. LSD1 promotes protein stability and tumor angiogenesis by demethylating the K391 residue and inhibiting HIF-1α downregulation with H_2O_2 production, which inhibits the hydroxylating activity of PHD_2 on HIF-1α with its subsequent ubiquitination (Lee J. Y. et al., 2017).

MicroRNAs (miRNAs) as Modulators in the Development of Angiogenesis

An essential role in regulating the angiogenesis process has been attributed to microRNAs. These are non-protein-coding RNA, small molecules with around 22 nucleotides. miRNAs regulate the expression of the target protein by two effects: *complete* matching the miRNA 5′ end with 3′ untranslated regions (3′-UTR) of target mRNA conduct to the reduction of targeted messenger mRNA and subsequently, their translation, or *incomplete* by repressing target protein translation without affecting mRNA stability (Schwerk and Savan, 2005).

MicroRNAs, generated from independent transcription units, can be either in polycistronic clusters or located within an intron of a protein-coding gene (Bartel, 2004; Suárez et al., 2008). The discovery of miRs that mediate post-transcriptional silencing of target genes has exposed exactly how non-coding RNAs play complex roles in angiogenesis. Initial evidence for the importance of miRs in regulating angiogenesis emerged from several experiments using a mutation in the Dicer gene, which is a ribonuclease essential for microRNA biogenesis (Kuehbacher et al., 2007; Suárez et al., 2008). EC-specific Dicer inactivation in mice reveals embryonic lethality and fails to determine a vasculogenic phenotype. With weakened angiogenic capacity and reduced endothelial tube development, the mouse embryo showed an alteration of proangiogenic factors genes and reduced angiogenic response (Yin et al., 2015). An increasing number of endothelial miRNAs have been reported to control the angiogenesis signaling pathways, thus controlling endothelial proliferation, migration and vascular integrity (**Table 4**; Yin et al., 2015).

Hypoxia-induced angiogenesis up-regulates the expressions of let-7 and miR-103/107 via activation of HIFs. These miRs suppress argonaute 1 (*AGO1*), which is required for the microRNA-induced silencing complex (miRISC) to silence VEGF mRNA, resulting in the translational de-suppression of VEGF (Chen et al., 2013). In ECs, miR-210 and other miRs regulated under hypoxic conditions directly down-modulate the expression of Ephrin-A3, a receptor protein-tyrosine kinase with effects on tubulogenesis and chemotaxis (Fasanaro et al., 2008). As well as proteins, there are some anti-and pro-angiogenic effects on the angiogenesis process regulating genes and oncogenes. They are presented below (**Table 2**).

TABLE 4 | Pro-angiogenic and anti-angiogenic miRNAs and their role in the angiogenesis process.

microRNA	Suppression of target genes	Role in angiogenesis	References
Pro angiogenic miRNAs			
miR-222	c-kit, eNOS p27	Induce proliferation and cell cycle progression Inhibit p27 and increase cells clonogenicity	Fish et al., 2008; Ding et al., 2017
miR-17-5p, -18a, -19a, -20a, -19b, and -92a	TIMP1, TSP-1 PTEN, CTGF, TGFβ, SMAD3	Promotes ECs proliferation, survival and cord formation and angiogenesis Induce tumor angiogenesis, better-perfused tumors *in vivo* Supress c-Myc, which upregulate VEGF and downregulate TSP1 Direct repression of TSP-1 and CTGF	Knies-Bamforth et al., 2004; Fox et al., 2013
miR-424	VEGFA	Functions to promote VEGF signaling in glioma	Sun et al., 2020
miR-130a	MEOX2, HOXA5	Antagonizes the inhibitory effects of MEOX2 or HOXA5 on ECs tube formation	Chen and Gorski, 2008
miR-210	EphrinA3, HGF NPTX1, HOXA1, HOXA9, HOXA3, E3F3	Stimulates tube formation and migration of ECs in hypoxia Decrease proapoptotic signaling in a hypoxic tumor environment. VEGF-induced chemotaxis, HUVEC tubulogenesis and development of capillary-like structures	Fasanaro et al., 2008; Wang Z. et al., 2017; Fan et al., 2018
miR-296	HGF	Mediate tube formation and ECs migration and tumoral angiogenesis; Inhibit HGF which lead to VEGFR2 and PDGFR expression.	Würdinger et al., 2008
miR-378	Sufu, Fus-1	Promotes cell survival tumor growth and angiogenesis by reducing expression of tumor suppressor both Sufu and Fus-1	Lee et al., 2007
miR-126	SPRED1, VCAM1 and PIK3R2	Endothelial cell migration, re-organization of the cytoskeleton, capillary network stability and cell survival	Fish et al., 2008
miR-21	PTEN	Promote tumor angiogenesis by activating partially AKT and ERK and over-expression of HIF-1 and VEGF.	Liu et al., 2011
Anti-angiogenic miRNAs			
miR-221, 222	c-kit, eNOS, ZEB2	Reduces capilary tube formation, EC migration and angiogenesis	Celic et al., 2017
miR-15, miR-15b miR-16	VEGF, Bcl2	Induces apoptosis, cell cycle regulation and reduce tumor induced angiogenesis	Cimmino et al., 2005
miR-92a	Integrin α5	Inhibit VEGFA and integrin subunit alpha5	Bonauer et al., 2009
miR-27a/b	SEMA6A	Inhibit SEMA6A antiangiogenic activity, which controls the repulsion of adjacent ECs	Urbich et al., 2012
miRNA-29c	VEGF MMP2	Inhibits angiogenesis by downregulating VEGF and increase MMP-2 levels	Fan et al., 2013
miRNA-199a-3p	VEGFA, VEGFR1, VEGFR2, HGF MMP2	Overexpression suppressed cancer growth, angiogenesis and lung metastasis and HCC	Ghosh et al., 2017
miRNA-497 miR-29b	VEGFR2, VEGFA	Cell proliferation and migration during sprouting angiogenesis.	Rosano et al., 2020
miRNA-519c	HIF-1α, HIF-2α,	Inhibiting angiogenesis and metastasis of neuroblastoma	Cha et al., 2010
miR-543	ANG2	Inhibit angiogenesis in osteosarcoma	Wang L. H. et al., 2017
miRNA-9	MMP14, Stathmin	Inhibit vascular mimicry in glioma cell	Song et al., 2013
miRNA-181-5p	MMP14	Attenuating breast cancer cell migration, invasion and angiogenesis	Li et al., 2015
miRNA-135a	FAK	Inhibits ECs migration and invasion by targeting FAK pathway	Cheng et al., 2017
miRNA-218	ROBO1	Disturbed the tubular structure and inhibited the migration of ECs	Zhang et al., 2017
miR-9, miR-135a, miR-181a/b, miR-199b and miR-204	SIRT1	Downregulate SIRT1 and defective blood vessel formation	Saunders et al., 2010
miR-874	STAT3/VEGFA	Inhibit angiogenesis through STAT3/VEGFA pathway in gastric cancer	Zhang et al., 2015

ZEB2, zinc finger E-Box binding homeobox2; PTEN, phosphatase and tensin homolog deleted on chromosome ten; CTGF, connective tissue growth factor; HGF, hepatocyte growth factor; SMAD3, SMAD family member 3; SPRED1, sprouty related EVH1 domain containing 1; PIK3R2, phosphoinositide-3-kinase regulatory subunit 2; HOXA5, homeobox A5; MEOX2, mesenchyme homeobox 2; NPTX1, neuronal pentraxin 1; FUS1, nuclear fusion protein; Robo1, Roundabout1; SIRT1, Sirtuins 1.

Epigenetic Compounds

Epigenetic inhibitors that affect the expression of angiogenic factors secreted into the tumor microenvironment have gained interest in developing anti-angiogenic agents. VEGF-induced angiogenesis was analyzed in correlation with HDAC inhibitors known to relieve gene silencing (**Table 5**).

Trichostatin A

Trichostatin A (TSA) has anti-cancer and antifungal effects that selectively inhibits histone deacetylases (HDACs). TSA considerably inhibits the transcription of endothelial receptors such as VEGFR1, VEGFR2 and neuropilin-1, along with the upregulation of SEMA3 (semaphorin 3) in ECs (Deroanne et al., 2002). SEMA3 inhibits angiogenesis and metastatic dissemination of tumor cells by interfering with neuropilin-1-mediated VEGF signaling (Neufeld et al., 2012). It was observed that in the human tongue, squamous cell carcinoma cells have a robust anti-angiogenic activity by reducing HIF-1α protein accumulation and the levels of VEGF mRNA and protein expression (Kang et al., 2012). TSA treatment promotes the stabilization of HIF-1α under normal oxygen conditions, leading to VEGF overexpression. HIF-1α is stabilized and translocated into the nucleus to activate the VEGF promoter by TSA-mediated acetylation at lysine (K) 674. The effectiveness of TSA is reduced

by overexpression of HIF-1α or hypoxic conditions, which leads to drug resistance in tumor cells (Lee J. W. et al., 2017). Moreover, it seems that under normoxic conditions, TSA treatment has a concomitant effect on drug resistance and anticancer effects by HIF-1α acetylation (Geng et al., 2011). Trichostatin A is mainly used in clinical trials and also in a phase I clinical trial investigating the safety and tolerability of trichostatin A in adults with relapsed or refractory hematologic malignancies.

Suberoylanilide Hydroxamic Acid

Suberoylanilide hydroxamic acid (SAHA) inhibits the histone deacetylases activity of class I and II (HDACs). SAHA selectively inhibits of the pathological development of a variety of transformed cells with relatively little toxicity (Marks, 2007). Several studies have shown that SAHA has an important role in regulating the expression of the VEGFs pathway. It was noted that in lung cancer cell lines, inhibition of HDACs by SAHA and TSA leads to vascular receptors expression reductions such as VEGFR1 and VEGFR2 and their co-receptors neuropilin1 (NP1) and neuropilin2 (NP2). Also, in breast cancer, the HDAC inhibitor SAHA reduces VEGF-C expression in a dose-dependent manner (Cheng and Hung, 2003). Several studies have shown that SAHA sustains autophagy, tumoral cell viability reduction and demonstrates a strong anti-proliferative activity in tumoral cells (Butler et al., 2002; Lee et al., 2012). SAHA exerts selectivity toward HDAC6 and HDAC3. In breast cancer cells, HDAC6 has played a vital role in survivin deacetylation and nuclear export, which is an essential anti-apoptotic agent and thus increases the sensitivity of cells to chemotherapeutic drugs (Lee et al., 2016).

Valproic Acid

Valproic acid (VPA) is a HDAC inhibitor, is evaluated for its anti-cancer properties due to its anti-angiogenic potential, inhibits *in vitro* and *in vivo* angiogenesis, involving a reduction in eNOS expression preceded by HDAC inhibition (Michaelis et al., 2004). VPA-treatment significantly inhibits endothelial tube formation and stabilization, nitric oxide production, proliferation, and migration in ECs by promoting EMT states in cancer cells regulating the mesenchymal markers Vimentin-cadherin (Murugavel et al., 2018). Besides the antitumor effect, VPA affects the immune cells by suppressing the inflammatory response mediated by cytokines and oxidative stress molecules (ROS, NO) (Soria-Castro et al., 2019). VPA has an inhibitory effect on pathological retinal angiogenesis in mice through HDAC inhibition, which reduces VEGF expression. In the mouse retina, the mammalian target of rapamycin complex 1 (mTORC1) is activated by VEGF, determining ECs proliferation, leading to angiogenesis (Iizuka et al., 2018).

TABLE 5 | The most important epigenetic compounds that can affect angiogenesis.

Compounds	Function	References
Trichostatin A	Inhibits histone deacetylases	Deroanne et al., 2002
Suberoylanilide hydroxamic acid	Inhibits histone deacetylases	Marks, 2007
Valproic acid	HDAC inhibitor	Michaelis et al., 2004
Sodium butyrate	HDAC inhibitor	Pellizzaro et al., 2002
5-azacytidine and 5-aza-2′deoxycytidine	DNMT inhibitors	Hellebrekers et al., 2006
Zebularine	DNA methylation inhibitor	Patnaik and Anupriya, 2019
GSK343	Inhibits histone H3K27 methylation	Yu et al., 2017
Panobinostat	Induces acetylation of histone H3	Zhi-Gang et al., 2017
Curcumin	Inhibitor of DNMTs	Hassan et al., 2019
Sulforaphane	Suppress HDACs	Shankar et al., 2008

Sodium Butyrate

Sodium butyrate (NaB) induces cell cycle arrest, cancer cell differentiation and apoptosis in colon cancer cells by modulating the expression of VEGF and HIF-1α in a dose-dependent manner (Pellizzaro et al., 2002). NaB suppresses hTERT gene expression and, therefore contributes to a low telomerase activity in human prostate cancer cells (Rahman and Grundy, 2011). NaB is an HDAC inhibitor that reactivates epigenetically silenced genes in cancer cells by promoting apoptosis via p53 and Bax activation and cell-cycle arrest by induction of p21 (Dashwood and Ho, 2007). On the other hand, the inhibition of HDAC by NaB had an anti-inflammatory effect by suppressing nuclear factor κB (NFkB) activation and inhibition of interferon γ production (Hamer et al., 2008).

5-Azacytidine and 5-aza-2′Deoxycytidine

5-Azacytidine and 5-aza-2′deoxycytidine are both nucleoside analogs and DNMT inhibitors which show less toxicity than TSA. 5-Aza-2′-deoxycytidine and TSA reactivate angiogenesis by inhibiting antiangiogenic agents by direct methylation to the promoter of TSP1, JUNB, and IGFBP3 genes, which are suppressed in tumor-conditioned ECs. The effect of these inhibitors is only antiproliferative without affecting ECs, apoptosis and migration and also supporting their angiostatic activity (Hellebrekers et al., 2006).

Zebularine

Zebularine is a DNA methylation inhibitor that cooperates with DNMT creating a covalent complex. It shows antiangiogenic activity and significantly reduces vessel development in tumors (Hellebrekers et al., 2006). It has a good correlation between low toxicity and high efficacy, with potential contribution as an adjuvant agent for anticancer treatments and low-dose administration for a prolonged period (Patnaik and Anupriya, 2019).

GSK343

GSK343 inhibits histone H3K27 methylation and increases expression of E-cadherin, p21 and PTEN. Also, this drug suppresses the proliferation and tumoral invasion by inhibiting the expression of EZH2 (Yu et al., 2017). The treatment of human umbilical cord blood-derived cells with GSK343 decreases levels of H3K27me2/3 in a time and dose-dependent manner without affecting other histones, including H3K27me1,

H3K4me3, H3K9me3 or H4K20me3, which further improves the pro-angiogenic functions (Fraineau et al., 2017).

Panobinostat or LBH589

Panobinostat or LBH589 inhibits proliferation and angiogenesis of glioblastoma cells by increasing degradation of HIF-1a mediated by the Hsp90/HDAC6 complex under hypoxic conditions (Zhi-Gang et al., 2017). LBH589 induces acetylation of histone H3 and alpha-tubulin protein on ECs, leading to tumor angiogenesis inhibition. LBH589 represses endothelial tube formation and invasion and inhibits AKT expression, ERK1/2 and CXCR4 *in vitro*. Complementary, in mice LBH589 treatment reduced angiogenesis and tumoral development (Qian et al., 2006).

Curcumin (Diferuloylmethane)

Curcumin (diferuloylmethane) is well known as an anti-inflammatory agent, which also exhibits antiangiogenic properties, including downregulation of the proangiogenic factors VEGF, MMP-9, down-regulation of growth factor receptors (EGFR, HER2, etc.) and inhibiting endothelial cell migration and invasion. The epigenetic regulatory roles consist in the inhibition of DNMTs, regulation of HATs, HDACs and miRNA. Curcumin is useful as an agent in cancer chemoprevention in the form of dietary phytochemicals, having the potential role of reversing epigenetic changes and efficient regulation of gene expression that causes tumorigenesis (Hassan et al., 2019). Curcumin is a safe compound with indicated no dose-limiting toxicity at 10 g/day. As a disadvantage, curcumin has poor solubility and a low absorption rate in the gastrointestinal tract after ingestion (Aggarwal et al., 2003).

Sulforaphane

Sulforaphane (SFN) is a natural compound found in cruciferous vegetables, which express antitumor effects without any toxic effect, inhibiting tumor growth, metastasis, and angiogenesis. SFN suppress HDACs and mediate epigenetic regulation of apoptosis, cell cycle and inflammation in various cancers (Alumkal et al., 2015). Emerging evidence suggests that SFN downregulate MMP-1, MMP-2, MMP-7, and MMP-9 and therefore intervenes in cancer cells invasion and angiogenesis (Shankar et al., 2008).

ANTIANGIOGENIC APPROACHES

Currently approved anti-angiogenic therapies includes several agents approved for clinical use (**Figure 3**). Angiogenesis inhibitors were extensively studied in the past decade and resulted in a modest increase in cancer cases' overall survival when used as monotherapies. Anti-angiogenic therapies focused on VEGF signaling pathways are demonstrating clinical benefits for an increasing number of cancer types. The difference in clinical benefits of treatment practice is manifested when is using multiple chemotherapy drugs. However, only a proportion of patients have a prolonged favorable response to therapy, indicating treatment resistance in some cases (Bergers and Hanahan, 2010).

For a long time, the development of antiangiogenic drugs has focused on VEGF inhibition and its receptors (**Figure 3**). Bevacizumab is the first FDA approved monoclonal antibody against VEGF-A, which increased the overall survival of patients with metastatic colorectal cancer after 8 months of bevacizumab supplementation in chemotherapy (Cao et al., 2019). Also, sorafenib and sunitinib, tyrosine kinase inhibitors, have shown positive results in liver and kidney cancers (Motzer et al., 2006; Ben Mousa, 2008). In some cases, anti-angiogenic strategies showed no benefit or induced initial responses followed by disease progression, thereby giving limited survival benefit (Bergers and Hanahan, 2010). The failure of this therapeutic approach due to the acquired resistance of the tumors led to an increased understanding of VEGF-independent angiogenesis. Inhibition of VEGF/VEGFR2 has led to the activation of other signaling pathways that support angiogenesis by alternative signaling pathways (Lu et al., 2012). In an attempt to abolish acquired resistance to treatment, trebananib has been proposed as an adjunctive therapy that indirectly inhibits angiogenesis by blocking the interaction between Ang1/Ang2 and the Tie2 receptor. Similarly, cabozantinib can inhibit both the VEGF and c-Met in various solid tumors (Bueno et al., 2017). Moreover, anti-angiogenic therapy may lead to the onset of hypoxia, resulting in the activation of HIF1a in tumor cells with a consequence of tumor cell adaptation to hypoxia and the promotion of tumor angiogenesis (Bergers and Hanahan, 2010).

Clinical findings from bevacizumab, sunitinib, and sorafenib provide valuable information for angiogenesis research, with survival benefits in some aggressive tumors, but in other cases failing to produce lasting clinical responses in most patients including those with metastatic cancer (Mitchell and Bryan, 2010). Treatment failure frequently occurs in patients with metastatic cancer due to various mechanisms that support pathological angiogenesis and acquired resistance, phenomena in which the tumor microenvironment and communication between tumor cells and adjacent non-malignant cells play an essential role (Bueno et al., 2017). Elimination of resistance to therapeutic agents should be evaluated as a dynamic multifactorial process and inhibition of angiogenesis should be optimized by inhibiting alternative signaling pathways and integrating interaction changes between the tumor microenvironment and stromal cells. The incidence of VEGF-resistant tumors targets alternative pathways, which include ANG-1, EGF, FGF, PDGF, and SDF-1 (Bottsford-Miller et al., 2012). Thus, complementary methodologies have been studied, such as combining VEGF inhibitors with agents that target alternative blood vessel formation mechanisms (**Figure 3**). Volociximab inhibits angiogenesis by blocking the interaction between α5β1 and its ligand fibronectin (Almokadem and Belani, 2012). Bortezomib, the first proteasome inhibitor targeting the ubiquitin-proteasome pathway, has shown a positive clinical benefit both alone and in combination therapy to produce tumor sensitization or to avoid drug resistance for multiple myeloma and mantle cell lymphoma. Bortezomib up-regulate the pro-apoptotic protein NOXA, which interacts with Bcl-2 and results in apoptosis in malignant cells (Chen et al., 2011). Nintedanib, a selective inhibitor of tumor angiogenesis by

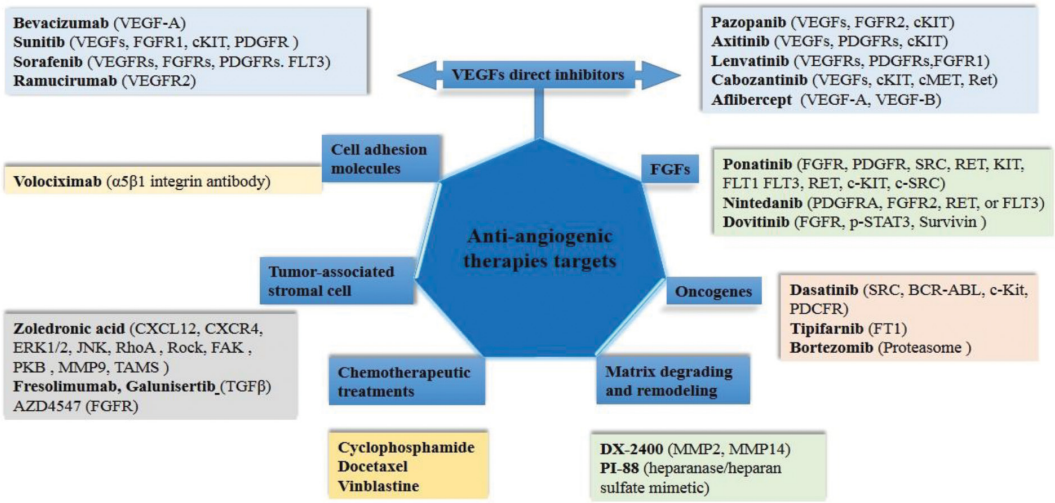

FIGURE 3 | Schematic representation of currently approved anti-angiogenic inhibitors and their targets. Here we delimit the direct VEGF inhibitors and other targets from others, such as FGFs, oncogenes, remodeling and ECM degradation, cell adhesion molecules and conventional chemotherapeutic treatment.

blocking receptors activities such as VEGFR1–3, PDGFR-α and -β, and FGFR1–3, was proposed to treat non–small cell lung adenocarcinoma and idiopathic lung fibrosis (Hilberg et al., 2018). Also, as a new targeted strategic approach, nanotechnology medical applications have been intensively studied to deliver anti-angiogenic drugs into the tumoral specific sites using nanomaterials as cerium oxide, gold, silver, copper, silica, based on carbon or hyaluronic acid and others (Mukherjee and Patra, 2016).

CONCLUSION AND FUTURE DIRECTIONS

Besides their role in normal tissue maintenance, angiogenesis initiation may indicate a shift from tumor latency to malignant active growth and recurrence of the disease. The precise functions of pro- and anti-angiogenic factors and the interactions between them in tumor angiogenesis are not fully understood and the important question is how anti-angiogenic medicine can be improved. However, the mechanisms of induction of vascularization and subsequent development from precancerous lesions to micrometastases achieved by angiogenic strategies for vessel recruitment are not yet fully elucidated in all pathological cases. Specific agents that can block tumor vascularization are required to inhibit angiogenesis and tumor growth.

This review summarizes angiogenic factors involved in each step of vessel development to present an integrated overview of tumor vascularization models (such as cooption, intussusception, sprouting angiogenesis, vasculogenic mimicry, and angioblasts) which, depending on the context, can be helpful for targeted or combined anti-angiogenic therapies. Moreover, we present the epigenetic changes in cancer which in contrast with genetic changes, are potentially reversible, increasing the prospect that epigenetic therapy will be able to mediate tumor fate. In addition to more disease-specific biomarkers, an important issue remains optimization of the dose and frequency of delivery of anti-angiogenic drugs. Current efforts for biomarker discovery in cancer have primarily focused on multi-gene expression patterns, but complementary analysis of DNA methylation signatures may lead to diagnostic and prognostic improvement and better cancer therapy strategies.

The major limitations of drug delivery systems remain the lack of specificity. However, drug-specific therapies that use a lower dose of epi-drugs could improve the effectiveness and tolerability of treatments. Another approach that might improve cancer therapy is the optimization of the dose and duration of release of anti-angiogenic drugs, with potential to alleviate colateral damage that conventional treatments that are toxic to both tumor and normal cells might produce. Future directions for these treatments may include combined drug delivery systems that might target several types of anti-angiogenic factors for synergistic or additive therapeutic effects, and might increase the efficacy and specificity along with reduction of side effects.

AUTHOR CONTRIBUTIONS

VA and CD were involved in study conception. IS and CB were involved in study design. VA wrote the manuscript with support from IS, CB, and CD. All authors reviewed and approved the final version of the manuscript.

ACKNOWLEDGMENTS

We gratefully acknowledge the funding from the project Competitiveness Operational Programme (COP) A1.1.4. ID: P_37_798 MyeloAL-EDiaProT, Contract 149/26.10.2016, (SMIS: 106774) MyeloAL Project.

REFERENCES

Adair, T. H., and Montani, J. P. (2010). *Chapter 1, Overview of Angiogenesis. Angiogenesis*. San Rafael, CA: Morgan & Claypool Life Sciences.

Aggarwal, B. B., Kumar, A., and Bharti, A. C. (2003). Anticancer potential of curcumin: preclinical and clinical studies. *Anticancer Res.* 23, 363–398.

Almokadem, S., and Belani, C. P. (2012). Volociximab in cancer. *Expert. Opin. Biol. Ther.* 12, 251–257. doi: 10.1517/14712598.2012.646985

Alumkal, J. J., Slottke, R., Schwartzman, J., Cherala, G., Munar, M., Graff, J. N., et al. (2015). A phase II study of sulforaphane-rich broccoli sprout extracts in men with recurrent prostate cancer. *Invest. New Drugs* 33, 480–489. doi: 10.1007/s10637-014-0189-z

Angara, K., Borin, T. F., and Arbab, A. S. (2017). A novel neovascularization mechanism driving anti-angiogenic therapy (AAT) resistance in glioblastoma. *Transl. Oncol.* 10, 650–660. doi: 10.1016/j.tranon.2017.04.007

Arroyo, A. G., and Iruela-Arispe, M. L. (2010). Extracellular matrix, inflammation, and the angiogenic response. *Cardiovasc. Res.* 86, 226–235. doi: 10.1093/cvr/cvq049

Asahara, T., Murohara, T., Sullivan, A., Silver, M., van der Zee, R., Li, T., et al. (1997). Isolation of putative progenitor endothelial cells for angiogenesis. *Science* 275, 964–967. doi: 10.1126/science.275.5302.964

Baeriswyl, V., and Christofori, G. (2009). The angiogenic switch in carcinogenesis. *Semin. Cancer Biol.* 19, 329–337. doi: 10.1016/j.semcancer.2009.05.003

Banfi, A., von Degenfeld, G., Gianni-Barrera, R., Reginato, S., Merchant, M. J., McDonald, D. M., et al. (2012). Therapeutic angiogenesis due to balanced single-vector delivery of VEGF and PDGF-BB. *FASEB J.* 26, 2486–2497. doi: 10.1096/fj.11-197400

Bartel, D. P. (2004). MicroRNAs: genomics, biogenesis, mechanism, and function. *Cell* 116, 281–297. doi: 10.1016/s0092-8674(04)00045-5

Bazmara, H., Soltani, M., Sefidgar, M., Bazargan, M., Mousavi Naeenian, M., and Rahmim, A. (2015). The vital role of blood flow-induced proliferation and migration in capillary network formation in a multiscale model of angiogenesis. *PLoS One* 10:e0128878. doi: 10.1371/journal.pone.0128878

Bazou, D., Ng, M. R., Song, J. W., Chin, S. M., Maimon, N., and Munn, L. L. (2016). Flow-induced HDAC1 phosphorylation and nuclear export in angiogenic sprouting. *Sci. Rep.* 6:34046. doi: 10.1038/srep34046

Ben Mousa, A. (2008). Sorafenib in the treatment of advanced hepatocellular carcinoma. *Saudi J. Gastroenterol.* 14, 40–42. doi: 10.4103/1319-3767.37808

Benelli, R., Morini, M., Carrozzino, F., Ferrari, N., Minghelli, S., Santi, L., et al. (2002). Neutrophils as a key cellular target for angiostatin: implications for regulation of angiogenesis and inflammation. *FASEB J.* 16, 267–269. doi: 10.1096/fj.01-0651fje

Bergers, G., and Hanahan, D. (2010). Modes of resistance to anti-angiogenic therapy. *Nat. Rev. Cancer.* 8, 592–603. doi: 10.1038/nrc2442

Bergers, G., and Song, S. (2005). The role of pericytes in blood-vessel formation and maintenance. *Neuro Oncol.* 7, 452–464. doi: 10.1215/S1152851705000232

Bhome, R., Bullock, M. D., Al Saihati, H. A., Goh, R. W., Primrose, J. N., Sayan, A. E., et al. (2015). A top-down view of the tumor microenvironment: structure, cells and signaling. *Front. Cell. Dev. Biol.* 3:33. doi: 10.3389/fcell.2015.00033

Bonauer, A., Carmona, G., Iwasaki, M., Mione, M., Koyanagi, M., Fischer, A., et al. (2009). MicroRNA-92a controls angiogenesis and functional recovery of ischemic tissues in mice. *Science* 324, 1710–1713. doi: 10.1126/science.1174381

Bottsford-Miller, J. N., Coleman, R. L., and Sood, A. K. (2012). Resistance and escape from antiangiogenesis therapy: clinical implications and future strategies. *J. Clin. Oncol.* 30, 4026–4034. doi: 10.1200/JCO.2012.41.9242

Bridges, E., Oon, C. E., and Harris, A. (2011). Notch regulation of tumor angiogenesis. *Future Oncol.* 7, 569–588. doi: 10.2217/fon.11.20

Bueno, M. J., Mouron, S., and Quintela-Fandino, M. (2017). Personalising and targeting antiangiogenic resistance: a complex and multifactorial approach. *Br. J. Cancer.* 116, 1119–1125. doi: 10.1038/bjc.2017.69

Butler, L. M., Zhou, X., Xu, W. S., Scher, H. I., Rifkind, R. A., Marks, P. A., et al. (2002). The histone deacetylase inhibitor SAHA arrests cancer cell growth, up-regulates thioredoxin-binding protein-2, and down-regulates thioredoxin. *Proc. Natl. Acad. Sci. U.S.A.* 99, 11700–11705. doi: 10.1073/pnas.182372299

Buysschaert, I., Schmidt, T., Roncal, C., Carmeliet, P., and Lambrechts, D. (2008). Genetics, epigenetics and pharmaco-(epi)genomics in angiogenesis. *J. Cell. Mol. Med.* 12, 2533–2551. doi: 10.1111/j.1582-4934.2008.00515.x

Cao, D., Zheng, Y., Xu, H., Ge, E. W., and Xu, X. (2019). Bevacizumab improves survival in metastatic colorectal cancer patients with primary tumor resection: a meta-analysis. *Sci. Rep.* 9:20326. doi: 10.1038/s41598-019-56yb528-2

Carmeliet, P., and Jain, R. K. (2011). Molecular mechanisms and clinical applications of angiogenesis. *Nature* 473, 298–307. doi: 10.1038/nature10144

Celic, T., Metzinger-Le Meuth, V., Six, I., Massy, Z. A., and Metzinger, L. (2017). The mir-221/222 cluster is a key player in vascular biology via the fine-tuning of endothelial cell physiology. *Curr. Vasc. Pharmacol.* 15, 40–46. doi: 10.2174/1570161114666160914175149

Cha, S. T., Chen, P. S., Johansson, G., Chu, C. Y., Wang, M. Y., and Jeng, Y. M. (2010). MicroRNA-519c suppresses hypoxia-inducible factor-1alpha expression and tumor angiogenesis. *Cancer Res.* 70, 2675–2685. doi: 10.1158/0008-5472.CAN-09-2448

Chappell, J. C., Taylor, S. M., Ferrara, N., and Bautch, V. L. (2009). Local guidance of emerging vessel sprouts requires soluble Flt-1. *Dev. Cell* 17, 377–386. doi: 10.1016/j.devcel.2009.07.011

Chen, D., Frezza, M., Schmitt, S., Kanwar, J., and Dou, Q. P. (2011). Bortezomib as the first proteasome inhibitor anticancer drug: current status and future perspectives. *Curr. Cancer Drug Targets* 11, 239–253. doi: 10.2174/156800911794519752

Chen, R., Shun, C., Yen, M., Chou, C., and Lin, M. (2017). Methyltransferase G9a promotes cervical cancer angiogenesis and decreases patient survival. *Oncotarget* 8, 62081–62098. doi: 10.18632/oncotarget.19060

Chen, Y., and Gorski, D. H. (2008). Regulation of angiogenesis through a microRNA (miR-130a) that down-regulates antiangiogenic homeobox genes GAX and HOXA5. *Blood* 111, 1217–1226. doi: 10.1182/blood-2007-07-104133

Chen, Z., Lai, T. C., Jan, Y. H., Lin, F. M., Wang, W. C., and Xiao, H. (2013). Hypoxia-responsive miRNAs target argonaute 1 to promote angiogenesis. *J. Clin. Invest.* 123, 1057–1067. doi: 10.1172/JCI65344

Cheng, H. T., and Hung, W. C. (2003). Inhibition of lymphangiogenic factor VEGF-C expression and production by the histone deacetylase inhibitor suberoylanilide hydroxamic acid in breast cancer cells. *Oncol. Rep.* 29, 1238–1244. doi: 10.3892/or.2012.2188

Cheng, Z., Liu, F., Zhang, H., Li, X., Li, Y., Li, J., et al. (2017). miR-135a inhibits tumor metastasis and angiogenesis by targeting FAK pathway. *Oncotarget* 8, 31153–31168. doi: 10.18632/oncotarget.16098

Cimmino, A., Calin, G. A., Fabbri, M., Iorio, M. V., Ferracin, M., and Shimizu, M. (2005). miR-15 and miR-16 induce apoptosis by targeting BCL2. *Proc. Natl. Acad. Sci. U.S.A.* 103:2464.

Darland, D. C., Massingham, L. J., Smith, S. R., Piek, E., Saint-Geniez, M., and D'Amore, P. A. (2003). Pericyte production of cell-associated VEGF is differentiation-dependent and is associated with endothelial survival. *Dev. Biol.* 264, 275–288. doi: 10.1016/j.ydbio.2003.08.015

Das, S., and Marsden, P. A. (2013). Angiogenesis in glioblastoma. *N. Engl. J. Med.* 369, 1561–1563. doi: 10.1056/NEJMcibr1309402

Dashwood, R. H., and Ho, E. (2007). Dietary histone deacetylase inhibitors: from cells to mice to man. *Semin. Cancer Biol.* 17, 363–369. doi: 10.1016/j.semcancer.2007.04.001

De Smet, F., Segura, I., De Bock, K., Hohensinner, P. J., and Carmeliet, P. (2009). Mechanisms of vessel branching: filopodia on endothelial tip cells lead the way. *Arterioscler. Thromb. Vasc. Biol.* 29, 639–649. doi: 10.1161/ATVBAHA.109.185165

De Spiegelaere, W., Casteleyn, C., Van den Broeck, W., Plendl, J., Bahramsoltani, M., Simoens, P., et al. (2012). Intussusceptive angiogenesis: a biologically relevant form of angiogenesis. *J. Vasc. Res.* 49, 390–404. doi: 10.1159/000338278

del Toro, R., Prahst, C., Mathivet, T., Siegfried, G., Kaminker, J. S., Larrivee, B., et al. (2010). Identification and functional analysis of endothelial tip cell-enriched genes. *Blood* 116, 4025–4033. doi: 10.1182/blood-2010-02-270819

Deroanne, C. F., Bonjean, K., Servotte, S., Devy, L., Colige, A., Clausse, N., et al. (2002). Histone deacetylases inhibitors as anti-angiogenic agents altering vascular endothelial growth factor signaling. *Oncogene* 21, 427–436. doi: 10.1038/sj.onc.1205108

Deryugina, E. I., and Quigley, J. P. (2015). Tumor angiogenesis: MMP-mediated induction of intravasation- and metastasis-sustaining neovasculature. *Matrix Biol.* 44-46, 94–112. doi: 10.1016/j.matbio.2015.04.004

Ding, S., Huang, H., Xu, Y., Zhu, H., and Zhong, C. (2017). MiR-222 in cardiovascular diseases: physiology and pathology. *Biomed. Res. Int.* 2017:4962426. doi: 10.1155/2017/4962426

Donnem, T., Hu, J., Ferguson, M., Adighibe, O., Snell, C., Harris, A. L., et al. (2013). Vessel co-option in primary human tumors and metastases: an obstacle

to effective anti-angiogenic treatment? *Cancer Med.* 2, 427–436. doi: 10.1002/cam4.105

Duan, Y., Wu, X., Zhao, Q., Gao, J., Huo, D., Liu, X., et al. (2013). DOT1L promotes angiogenesis through cooperative regulation of VEGFR2 with ETS-1. *Oncotarget* 7, 69674–69687. doi: 10.18632/oncotarget.11939

Duffy, A. M., Bouchier-Hayes, D. J., and Harmey, J. H. (2000). *Vascular Endothelial Growth Factor (VEGF) and Its Role in Non-Endothelial Cells: Autocrine Signalling by VEGF. Madame Curie Bioscience Database*. Austin, TX: Landes Bioscience.

Dulloo, I., Phang, B. H., Othman, R., Tan, S. Y., Vijayaraghavan, A., Goh, L. K., et al. (2015). Hypoxia-inducible TAp73 supports tumorigenesis by regulating the angiogenic transcriptome. *Nat. Cell Biol.* 7, 511–523. doi: 10.1038/ncb3130

Eguchi, J., Nomata, K., Kanda, S., Igawa, T., Taide, M., Koga, S., et al. (1992). Gene expression and immunohistochemical localization of basic fibroblast growth factor in renal cell carcinoma. *Biochem. Biophys. Res. Commun.* 183, 937–944. doi: 10.1016/s0006-291x(05)80280-3

Erber, R., Eichelsbacher, U., Powajbo, V., Korn, T., Djonov, V., Lin, J., et al. (2006). EphB4 controls blood vascular morphogenesis during postnatal angiogenesis. *EMBO J.* 25, 628–641. doi: 10.1038/sj.emboj.7600949

Ergün, S., Kilic, N., Wurmbach, J. H., Ebrahimnejad, A., Fernando, M., Sevinc, S., et al. (2010). Endostatin inhibits angiogenesis by stabilization of newly formed endothelial tubes. *Angiogenesis* 4, 193–206. doi: 10.1023/a:1014027218980

Esser, J. S., Charlet, A., Schmidt, M., Heck, S., Allen, A., Lother, A., et al. (2015). The neuronal transcription factor NPAS4 is a strong inducer of sprouting angiogenesis and tip cell formation. *Cardiovasc. Res.* 113, 222–223. doi: 10.1093/cvr/cvw248

Fan, L., Li, J., Yu, Z., Dang, X., and Wang, K. (2014). The hypoxia-inducible factor pathway, prolyl hydroxylase domain protein inhibitors, and their roles in bone repair and regeneration. *Biomed. Res. Int.* 2014:239356. doi: 10.1155/2014/239356

Fan, Y. C., Mei, P. J., Chen, C., Miao, F. A., Zhang, H., and Li, Z. L. (2013). MiR-29c inhibits glioma cell proliferation, migration, invasion and angiogenesis. *J. Neurooncol.* 115, 179–188. doi: 10.1007/s11060-013-1223-2

Fan, Z. G., Qu, X. L., Chu, P., Gao, Y. L., Gao, X. F., Chen, S. L., et al. (2018). MicroRNA-210 promotes angiogenesis in acute myocardial infarction. *Mol. Med. Rep.* 17, 5658–5665. doi: 10.3892/mmr.2018.8620

Fasanaro, P., D'Alessandra, Y., Di Stefano, V., Melchionna, R., Romani, S., Pompilio, G., et al. (2008). MicroRNA-210 modulates endothelial cell response to hypoxia and inhibits the receptor tyrosine kinase ligand ephrin-A3. *J. Biol. Chem.* 283, 15878–15883. doi: 10.1074/jbc.M800731200

Ferrara, N. (2004). Vascular endothelial growth factor: basic science and clinical progress. *Endocr. Rev.* 25, 581–611. doi: 10.1210/er.2003-0027

Ferrara, N., and Alitalo, K. (1999). Clinical applications of angiogenic growth factors and their inhibitors. *Nat. Med.* 5, 1359–1364. doi: 10.1038/70928

Ferrari, G., Terushkin, V., Wolff, M. J., Zhang, X., Valacca, C., Poggio, P., et al. (2012). TGF-β1 induces endothelial cell apoptosis by shifting VEGF activation of p38(MAPK) from the prosurvival p38β to proapoptotic p38α. *Mol. Cancer Res.* 10, 605–614. doi: 10.1158/1541-7786.MCR-11-0507

Fish, J. E., Santoro, M. M., Morton, S. U., Yu, S., Yeh, R. F., Wythe, J. D., et al. (2008). miR-126 regulates angiogenic signaling and vascular integrity. *Dev. Cell* 15, 272–284. doi: 10.1016/j.devcel.2008.07.008

Fitzgerald, G., Soro-Arnaiz, I., and De Bock, K. (2018). The warburg effect in endothelial cells and its potential as an anti-angiogenic target in cancer. *Front. Cell Dev. Biol.* 6:100. doi: 10.3389/fcell.2018.00100

Folberg, R., Hendrix, M. J., and Maniotis, A. J. (2000). Vasculogenic mimicry and tumor angiogenesis. *Am. J. Pathol.* 156, 361–381. doi: 10.1016/S0002-9440(10)64739-6

Fox, J. L., Dews, M., Minn, A. J., and Thomas-Tikhonenko, A. (2013). Targeting of TGFβ signature and its essential component CTGF by miR-18 correlates with improved survival in glioblastoma. *RNA* 19, 177–190. doi: 10.1261/rna.036467.112

Fraineau, S., Palii, C. G., McNeill, B., Ritso, M., Shelley, W. C., Prasain, N., et al. (2017). Epigenetic activation of pro-angiogenic signaling pathways in human endothelial progenitors increases vasculogenesis. *Stem Cell Rep.* 9, 1573–1587. doi: 10.1016/j.stemcr.2017.09.009

Gaengel, K., Genové, G., Armulik, A., and Betsholtz, C. (2009). Endothelial-mural cell signaling in vascular development and angiogenesis. *Arterioscler. Thromb. Vasc. Biol.* 29, 630–638. doi: 10.1161/ATVBAHA.107.161521

Gavard, J., and Gutkind, J. S. (2008). VE-cadherin and claudin-5: it takes two to tango. *Nat. Cell Biol.* 10, 883–885. doi: 10.1038/ncb0808-883

Ge, H., and Luo, H. (2018). Overview of advances in vasculogenic mimicry – a potential target for tumor therapy. *Cancer Manag. Res.* 10, 2429–2437. doi: 10.2147/CMAR.S164675

Geng, H., Harvey, C. T., Pittsenbarger, J., Liu, Q., Beer, T. M., Xue, C., et al. (2011). HDAC4 protein regulates HIF1α protein lysine acetylation and cancer cell response to hypoxia. *J. Biol. Chem.* 286, 38095–38102. doi: 10.1074/jbc.M111.257055

Geng, L., Chaudhuri, A., Talmon, G., Wisecarver, J. L., and Wang, J. (2013). TGF-beta suppresses VEGFA-mediated angiogenesis in colon cancer metastasis. *PLoS One* 8:e59918. doi: 10.1371/journal.pone.0059918

Gerhardt, H., Golding, M., Fruttiger, M., Ruhrberg, C., Lundkvist, A., Abramsson, A., et al. (2003). VEGF guides angiogenic sprouting utilizing endothelial tip cell filopodia. *J. Cell Biol.* 161, 1163–1177. doi: 10.1083/jcb.200302047

Gerwins, P., Sköldenberg, E., and Claesson-Welsh, L. (2000). Function of fibroblast growth factors and vascular endothelial growth factors and their receptors in angiogenesis. *Crit. Rev. Oncol. Hematol.* 34, 185–194. doi: 10.1016/s1040-8428(00)00062-7

Ghosh, A., Dasgupta, D., Ghosh, A., Roychoudhury, S., Kumar, D., Gorain, M., et al. (2017). MiRNA199a-3p suppresses tumor growth, migration, invasion and angiogenesis in hepatocellular carcinoma by targeting VEGFA, VEGFR1, VEGFR2, HGF and MMP2. *Cell Death Dis.* 8:e2706.

Gianni-Barrera, R., Trani, M., Reginato, S., and Banfi, A. (2011). To sprout or to split? VEGF, Notch and vascular morphogenesis. *Biochem. Soc. Trans.* 39, 1644–1648. doi: 10.1042/BST20110650

Goel, S., Duda, D. G., Xu, L., Munn, L. L., Boucher, Y., Fukumura, D., et al. (2011). Normalization of the vasculature for treatment of cancer and other diseases. *Physiol. Rev.* 91, 1071–1121. doi: 10.1152/physrev.00038.2010

Gong, W., Ni, M., Chen, Z., and Zheng, Z. (2020). Expression and clinical significance of methyl-CpG binding domain protein 2 in high-grade serous ovarian cancer. *Oncol. Lett.* 20, 2749–2756. doi: 10.3892/ol.2020.11836

Groppa, E., Brkic, S., Uccelli, A., Wirth, G., Korpisalo-Pirinen, P., Filippova, M., et al. (2018). EphrinB2/EphB4 signaling regulates non-sprouting angiogenesis by VEGF. *EMBO Rep.* 19:e45054. doi: 10.15252/embr.201745054

Guarani, V., Deflorian, G., Franco, C. A., Krüger, M., Phng, L. K., Bentley, K., et al. (2011). Acetylation-dependent regulation of endothelial Notch signalling by the SIRT1 deacetylase. *Nature* 473, 234–238. doi: 10.1038/nature09917

Hamer, H. M., Jonkers, D., Venema, K., Vanhoutvin, S., Troost, F. J., and Brummer, R. J. (2008). Review article: the role of butyrate on colonic function. *Aliment Pharmacol. Ther.* 27, 104–119. doi: 10.1111/j.1365-2036.2007.03562.x

Hammond, E. M., Asselin, M. C., Forster, D., O'Connor, J. P., Senra, J. M., and Williams, K. J. (2014). The meaning, measurement and modification of hypoxia in the laboratory and the clinic. *Clin. Oncol. (R Coll. Radiol.)* 26, 277–288. doi: 10.1016/j.clon.2014.02.002

Hao, H. (2015). Matrix metalloproteinase-9 (MMP-9) as a cancer biomarker and MMP-9 biosensors: recent advances. *Sensors* 18:3249.

Hassan, F. U., Rehman, M. S., Khan, M. S., Ali, M. A., Javed, A., Nawaz, A., et al. (2019). Curcumin as an alternative epigenetic modulator: mechanism of action and potential effects. *Front. Genet.* 10:514. doi: 10.3389/fgene.2019.00514

Heissig, B., Hattori, K., Dias, S., Friedrich, M., Ferris, B., Hackett, N. R., et al. (2002). Recruitment of stem and progenitor cells from the bone marrow niche requires MMP-9 mediated release of kit-ligand. *Cell* 109, 625–637. doi: 10.1016/s0092-8674(02)00754-7

Hellebrekers, D. M., Griffioen, A. W., and van Engeland, M. (2007). Dual targeting of epigenetic therapy in cancer. *Biochim. Biophys. Acta* 1775, 76–91. doi: 10.1016/j.bbcan.2006.07.003

Hellebrekers, D. M., Jair, K. W., Viré, E., Eguchi, S., Hoebers, N. T., Fraga, M. F., et al. (2006). Angiostatic activity of DNA methyltransferase inhibitors. *Mol. Cancer Ther.* 5, 467–475. doi: 10.1158/1535-7163.MCT-05-0417

Hellström, M., Phng, L. K., Hofmann, J. J., Wallgard, E., Coultas, L., Lindblom, P., et al. (2007). Dll4 signalling through Notch1 regulates formation of tip cells during angiogenesis. *Nature* 445, 776–780. doi: 10.1038/nature05571

Hilberg, F., Tontsch-Grunt, U., Baum, A., Le, A. T., Doebele, R. C., Lieb, S., et al. (2018). Triple angiokinase inhibitor nintedanib directly inhibits tumor cell growth and induces tumor shrinkage via blocking oncogenic receptor tyrosine kinases an external file that holds a picture, illustration, etc. *J. Pharmacol. Exp. Ther.* 364, 494–503. doi: 10.1124/jpet.117.244129

Hillen, F., and Griffioen, A. W. (2007). Tumour vascularization: sprouting angiogenesis and beyond. *Cancer Metastasis Rev.* 26, 489–502. doi: 10.1007/s10555-007-9094-7

Holash, J., Maisonpierre, P. C., Compton, D., Boland, P., Alexander, C. R., Zagzag, D., et al. (1999). Vessel cooption, regression, and growth in tumors mediated by angiopoietins and VEGF. *Science* 284, 1994–1998. doi: 10.1126/science.284.5422.1994

Huang, H. (2018). Matrix metalloproteinase-9 (MMP-9) as a cancer biomarker and mmp-9 biosensors: recent advances. *Sensors* 18:3249. doi: 10.3390/s18103249

Huang, Z., and Bao, S. D. (2003). Roles of main pro- and anti-angiogenic factors in tumor angiogenesis. *World J. Gastroenterol.* 10, 463–470. doi: 10.3748/wjg.v10.i4.463

Humphries, J. D., Byron, A., and Humphries, M. J. (2006). Integrin ligands at a glance. *J. Cell Sci.* 119(Pt 19), 3901–3903. doi: 10.1242/jcs.03098

Iizuka, N., Morita, A., Kawano, C., Mori, A., Sakamoto, K., Kuroyama, M., et al. (2018). Anti-angiogenic effects of valproic acid in a mouse model of oxygen-induced retinopathy. *J. Pharmacol. Sci.* 138, 203–208. doi: 10.1016/j.jphs.2018.10.004

Jain, R. K. (2001). Normalizing tumor vasculature with anti-angiogenic therapy: a new paradigm for combination therapy. *Nat. Med.* 7, 987–989. doi: 10.1038/nm0901-987

Jiang, T., Zhuang, J., Duan, H., Luo, Y., Zeng, Q., Fan, K., et al. (2012). CD146 is a coreceptor for VEGFR-2 in tumor angiogenesis. *Blood* 120, 2330–2339. doi: 10.1182/blood-2012-01-406108

Jones, B., Su, H., Bhat, A., Lei, H., Bajko, J., Hevi, S., et al. (2008). The histone H3K79 methyltransferase Dot1L is essential for mammalian development and heterochromatin structure. *PLoS Genet.* 4:e1000190. doi: 10.1371/journal.pgen.1000190

Kalka, C., Masuda, H., Takahashi, T., Kalka-Moll, W. M., Silver, M., Kearney, M., et al. (2000). Transplantation of ex vivo expanded endothelial progenitor cells for therapeutic neovascularization. *Proc. Natl. Acad. Sci. U.S.A* 97, 3422–3427. doi: 10.1073/pnas.070046397

Kang, F. W., Que, L., Wu, M., Wang, Z. L., and Sun, J. (2012). Effects of trichostatin A on HIF-1α and VEGF expression in human tongue squamous cell carcinoma cells in vitro. *Oncol. Rep.* 28, 193–199. doi: 10.3892/or.2012.1784

Kazemi, S., Wenzel, D., Kolossov, E., Lenka, N., Raible, A., Sasse, P., et al. (2002). Differential role of bFGF and VEGF for vasculogenesis. *Cell Physiol. Biochem.* 12, 55–62.

Kim, M. S., Kwon, H. J., Lee, Y. M., Baek, J. H., Jang, J. E., Lee, S. W., et al. (2001). Histone deacetylases induce angiogenesis by negative regulation of tumor suppressor genes. *Nat. Med.* 7, 437–443. doi: 10.1038/86507

Knies-Bamforth, U. E., Fox, S. B., Poulsom, R., Evan, G. I., and Harris, A. L. (2004). c-Myc interacts with hypoxia to induce angiogenesis in vivo by a vascular endothelial growth factor-dependent mechanism. *Cancer Res.* 64, 6563–6570. doi: 10.1158/0008-5472.CAN-03-3176

Krock, B. L., Skuli, N., and Simon, M. C. (2011). Hypoxia-induced angiogenesis: good and evil. *Genes Cancer* 2, 1117–1133. doi: 10.1177/1947601911423654

Krstic, M., Hassan, H. M., Kolendowski, B., Hague, M. N., Anborgh, P. H., Postenka, C. O., et al. (2020). Isoform-specific promotion of breast cancer tumorigenicity by TBX3 involves induction of angiogenesis. *Lab Invest.* 100, 400–413. doi: 10.1038/s41374-019-0326-6

Kuczynski, E. A., Vermeulen, P. B., Pezzella, F., Kerbel, R. S., and Reynolds, A. R. (2019). Vessel co-option in cancer. *Nat. Rev. Clin. Oncol.* 6, 469–493. doi: 10.1038/s41571-019-0181-9

Kuehbacher, A., Urbich, C., Zeiher, A. M., and Dimmeler, S. (2007). Role of dicer and drosha for endothelial microRNA expression and angiogenesis. *Circ. Res.* 101, 59–68. doi: 10.1161/CIRCRESAHA.107.153916

Küsters, B., Leenders, W. P., Wesseling, P., Smits, D., Verrijp, K., Ruiter, D. J., et al. (2002). Vascular endothelial growth factor-A(165) induces progression of melanoma brain metastases without induction of sprouting angiogenesis. *Cancer Res.* 62, 341–345.

Larrivée, B., Freitas, C., Trombe, M., Lv, X., Delafarge, B., Yuan, L., et al. (2001). Activation of the UNC5B receptor by Netrin-1 inhibits sprouting angiogenesis. *Genes Dev.* 21, 2433–2447. doi: 10.1101/gad.437807

Lee, D. Y., Deng, Z., Wang, C. H., and Yang, B. B. (2007). MicroRNA-378 promotes cell survival, tumor growth, and angiogenesis by targeting SuFu and Fus-1 expression. *Proc. Natl. Acad. Sci. U.S.A* 104, 20350–20355. doi: 10.1073/pnas.0706901104

Lee, J. W., Bae, S. H., Jeong, J. W., Kim, S. H., and Kim, K. W. (2004). Hypoxia-inducible factor (HIF-1)alpha: its protein stability and biological functions. *Exp. Mol. Med.* 36, 1–12. doi: 10.1038/emm.2004.1

Lee, J. W., Yang, D. H., Park, S., Han, H. K., Park, J. W., Kim, B. Y., et al. (2017). Trichostatin A resistance is facilitated by HIF-1α acetylation in HeLa human cervical cancer cells under normoxic conditions. *Oncotarget* 9, 2035–2049. doi: 10.18632/oncotarget.23327

Lee, J. Y., Kuo, C. W., Tsai, S. L., Cheng, S. M., Chen, S. H., Chan, H. H., et al. (2016). Inhibition of HDAC3- and HDAC6-promoted survivin expression plays an important role in saha-induced autophagy and viability reduction in breast cancer cells. *Front. Pharmacol.* 7:81. doi: 10.3389/fphar.2016.00081

Lee, J. Y., Park, J. H., Choi, H. J., Won, H. Y., Joo, H. S., Shin, D. H., et al. (2017). LSD1 demethylates HIF1α to inhibit hydroxylation and ubiquitin-mediated degradation in tumor angiogenesis. *Oncogene* 36, 5512–5521. doi: 10.1038/onc.2017.158

Lee, S. H., Schloss, D. J., and Swain, J. L. (2000). Maintenance of vascular integrity in the embryo requires signaling through the fibroblast growth factor receptor. *J. Biol. Chem.* 275, 33679–33687.

Lee, Y. J., Won, A. J., Lee, J., Jung, J. H., Yoon, S., Lee, B. M., et al. (2012). Molecular mechanism of SAHA on regulation of autophagic cell death in tamoxifen-resistant MCF-7 breast cancer cells. *Int. J. Med. Sci.* 9, 881–893. doi: 10.7150/ijms.5011

Lezcano, C., Kleffel, S., Lee, N., Larson, A. R., Zhan, Q., DoRosario, A., et al. (2014). Merkel cell carcinoma expresses vasculogenic mimicry: demonstration in patients and experimental manipulation in xenografts. *Lab Invest.* 94, 1092–1102. doi: 10.1038/labinvest.2014.99

Li, Y., Kuscu, C., Banach, A., Zhang, Q., Pulkoski-Gross, A., Kim, D., et al. (2015). miR-181a-5p inhibits cancer cell migration and angiogenesis via downregulation of matrix metalloproteinase-14. *Cancer Res.* 75, 2674–2685. doi: 10.1158/0008-5472.CAN-14-2875

Liu, L. Z., Li, C., Chen, Q., Jing, Y., Carpenter, R., Jiang, Y., et al. (2011). MiR-21 induced angiogenesis through AKT and ERK activation and HIF-1α expression. *PLoS One* 6:e19139. doi: 10.1371/journal.pone.0019139

Lu, C., Han, H. D., Mangala, L. S., Ali-Fehmi, R., Newton, C. S., Ozbun, L., et al. (2010). Regulation of tumor angiogenesis by EZH2. *Cancer Cell* 18, 185–197. doi: 10.1016/j.ccr.2010.06.016

Lu, K. V., Chang, J. P., Parachoniak, C. A., Pandika, M. M., Aghi, M. K., Meyronet, D., et al. (2012). VEGF inhibits tumor cell invasion and mesenchymal transition through a MET/VEGFR2 complex. *Cancer Cell* 22, 21–35. doi: 10.1016/j.ccr.2012.05.037

Lu, P., Takai, K., Weaver, V. M., and Werb, Z. (2011). Extracellular matrix degradation and remodeling in development and disease. *Cold Spring Harb. Perspect. Biol.* 3:a005058. doi: 10.1101/cshperspect.a005058

Lyu, T., Jia, N., Wang, J., Yan, X., Yu, Y., Lu, Z., et al. (2013). Expression and epigenetic regulation of angiogenesis-related factors during dormancy and recurrent growth of ovarian carcinoma. *Epigenetics* 8, 1330–1346. doi: 10.4161/epi.26675

Maione, F., Molla, F., Meda, C., Latini, R., Zentilin, L., Giacca, M., et al. (2009). Semaphorin 3A is an endogenous angiogenesis inhibitor that blocks tumor growth and normalizes tumor vasculature in transgenic mouse models. *Clin. Invest.* 119, 3356–3372. doi: 10.1172/JCI36308

Marks, P. A. (2007). Discovery and development of SAHA as an anticancer agent. *Oncogene* 26, 1351–1356. doi: 10.1038/sj.onc.1210204

Mazzone, M., Dettori, D., de Oliveira, R. L., Loges, S., Schmidt, T., Jonckx, B., et al. (2009). Heterozygous deficiency of PHD2 restores tumor oxygenation and inhibits metastasis via endothelial normalization. *Cell* 136, 839–851. doi: 10.1016/j.cell.2009.01.020

Menafra, R., and Stunnenberg, H. G. (2014). MBD2 and MBD3: elusive functions and mechanisms. *Front. Genet.* 5:428. doi: 10.3389/fgene.2014.00428

Meng, F., Chen, X., Song, H., and Lou, G. (2015). LAPTM4B down regulation inhibits the proliferation, invasion and angiogenesis of HeLa cells in vitro. *Cell Physiol. Biochem.* 37, 890–900. doi: 10.1159/000430216

Michaelis, M., Michaelis, U. R., Fleming, I., Suhan, T., Cinatl, J., Blaheta, R. A., et al. (2004). Valproic acid inhibits angiogenesis in vitro and in vivo. *Mol. Pharmacol.* 65, 520–527. doi: 10.1124/mol.65.3.520

Mitchell, D. C., and Bryan, B. A. (2010). Anti-angiogenic therapy: adapting strategies to overcome resistant tumors. *J. Cell Biochem.* 111, 543–553. doi: 10.1002/jcb.22764

Miyake, M., Goodison, S., Lawton, A., Gomes-Giacoia, E., and Rosser, C. J. (2015). Angiogenin promotes tumoral growth and angiogenesis by regulating matrix metallopeptidase-2 expression via the ERK1/2 pathway. *Oncogene.* 34, 890–901. doi: 10.1038/onc.2014.2

Montemagno, C., and Pagès, G. (2020). Resistance to anti-angiogenic therapies: a mechanism depending on the time of exposure to the drugs front. *Cell. Dev. Biol.* 8:584. doi: 10.3389/fcell.2020.00584

Motzer, R. J., Rini, B. I., Bukowski, R. M., Curti, B. D., George, D. J., Hudes, G. R., et al. (2006). Sunitinib in patients with metastatic renal cell carcinoma. *JAMA* 295, 2516–2524. doi: 10.1001/jama.295.21.2516

Mukherjee, S., and Patra, C. R. (2016). Therapeutic application of anti-angiogenic nanomaterials in cancers. *Nanoscale* 8, 12444–12470. doi: 10.1039/c5nr07887c

Murugavel, S., Bugyei-Twum, A., Matkar, P. N., Al-Mubarak, H., Chen, H. H., Adam, M., et al. (2018). Valproic acid induces endothelial-to-mesenchymal transition-like phenotypic switching. *Front. Pharmacol.* 9:737. doi: 10.3389/fphar.2018.00737

Nagase, H., Visse, R., and Murphy, G. (2006). Structure and function of matrix metalloproteinases and TIMPs. *Ardiovasc. Res.* 3, 562–573. doi: 10.1016/j.cardiores.2005.12.002

Nakagawa, S., Okabe, H., Ouchi, M., Tokunaga, R., Umezaki, N., Higashi, T., et al. (2018). Enhancer of zeste homolog 2 (EZH2) regulates tumor angiogenesis and predicts recurrence and prognosis of intrahepatic cholangiocarcinoma. *HPB* 20, 939–948. doi: 10.1016/j.hpb.2018.03.018

Neufeld, G., Sabag, A. D., Rabinovicz, N., and Kessler, O. (2012). Semaphorins in angiogenesis and tumor progression. *Cold Spring Harb. Perspect. Med.* 2:a006718. doi: 10.1101/cshperspect.a006718

Nguyen, A. T., and Zhang, Y. (2011). The diverse functions of Dot1 and H3K79 methylation. *Genes Dev.* 25, 1345–1358. doi: 10.1101/gad.2057811

Osawa, T., Tsuchida, R., Muramatsu, M., Shimamura, T., Wang, F., Suehiro, J., et al. (2013). Inhibition of histone demethylase JMJD1A improves anti-angiogenic therapy and reduces tumor-associated macrophages. *Cancer Res.* 73, 3019–3028. doi: 10.1158/0008-5472.CAN-12-3231

Ozawa, C. R., Banfi, A., Glazer, N. L., Thurston, G., Springer, M. L., Kraft, P. E., et al. (2004). Microenvironmental VEGF concentration, not total dose, determines a threshold between normal and aberrant angiogenesis. *Clin. Invest.* 113, 516–527. doi: 10.1172/JCI18420

Padera, T. P., Stoll, B. R., Tooredman, J. B., Capen, D., di Tomaso, E., and Jain, R. K. (2004). Pathology: cancer cells compress intratumour vessels. *Nature* 427, 695. doi: 10.1038/427695a

Paku, S., and Paweletz, N. (1991). First steps of tumor-related angiogenesis. *Lab. Invest.* 65, 334–346.

Patnaik, S., and Anupriya, T. (2019). Drugs targeting epigenetic modifications and plausible therapeutic strategies against colorectal cancer. *Front. Pharmacol.* 10:588. doi: 10.3389/fphar.2019.00588

Pei, Y. F., Xu, X. N., Wang, Z. F., Wang, F. W., Wu, W. D., Geng, J. F., et al. (2019). Methyl-CpG binding domain protein 2 inhibits the malignant characteristic of lung adenocarcinoma through the epigenetic modulation of 10 to 11 translocation 1 and miR-200s. *Am. J. Pathol.* 189, 1065–1076. doi: 10.1016/j.ajpath.2019.01.010

Pellizzaro, C., Coradini, D., and Daidone, M. G. (2002). Modulation of angiogenesis-related proteins synthesis by sodium butyrate in colon cancer cell line HT29. *Carcinogenesis* 23, 735–740. doi: 10.1093/carcin/23.5.735

Perillo, B., Tramontano, A., Pezone, A., and Migliaccio, A. (2020). Lysine-specific histone demethylase 1 (LSD1). *Exp. Mol. Med.* 52, 1936–1947. doi: 10.1038/s12276-020-00542-2

Phng, L. K., and Gerhardt, H. (2009). Angiogenesis: a team effort coordinated by notch. *Dev. Cell* 16, 196–208. doi: 10.1016/j.devcel.2009.01.015

Pike, S. E., Yao, L., Jones, K. D., Cherney, B., Appella, E., Sakaguchi, K., et al. (1998). Vasostatin, a calreticulin fragment, inhibits angiogenesis and suppresses tumor growth. *J. Exp. Med.* 188, 2349–2356. doi: 10.1084/jem.188.12.2349

Pirola, L., Ciesielski, O., and Balcerczyk, A. (2018). The methylation status of the epigenome: its emerging role in the regulation of tumor angiogenesis and tumor growth, and potential for drug targeting. *Cancers* 10:268. doi: 10.3390/cancers10080268

Potente, M., Gerhardt, H., and Carmeliet, P. (2011). Basic and therapeutic aspects of angiogenesis. *Cell* 146, 873–887. doi: 10.1016/j.cell.2011.08.039

Pozzi, A., and Zent, R. (2009). Regulation of endothelial cell functions by basement membrane- and arachidonic acid-derived products. *Wiley Interdiscip. Rev. Syst. Biol. Med.* 1, 254–272. doi: 10.1002/wsbm.7

Presta, M., Dell'Era, P., Mitola, S., Moroni, E., Ronca, R., and Rusnati, M. (2005). Fibroblast growth factor/fibroblast growth factor receptor system in angiogenesis. *Cytokine Growth Factor Rev.* 16, 159–178. doi: 10.1016/j.cytogfr.2005.01.004

Pries, A. R., Höpfner, M., Le Noble, F., Dewhirst, M. W., and Secomb, T. W. (2010). The shunt problem: control of functional shunting in normal and tumour vasculature. *Nat. Rev. Cancer* 10, 587–593. doi: 10.1038/nrc2895

Qian, D. Z., Kato, Y., Shabbeer, S., Wei, Y., Verheul, H. M., Salumbides, B., et al. (2006). Targeting tumor angiogenesis with histone deacetylase inhibitors: the hydroxamic acid derivative LBH589. *Clin. Cancer Res.* 12, 634–642. doi: 10.1158/1078-0432.CCR-05-1132

Rahman, R., and Grundy, R. (2011). Histone deacetylase inhibition as an anticancer telomerase-targeting strategy. *Int. J. Cancer* 129, 2765–2774. doi: 10.1002/ijc.26241

Rao, X., Zhong, J., Zhang, S., Zhang, Y., Yu, Q., Yang, P., et al. (2011). Loss of methyl-CpG–binding domain protein 2 enhances endothelial angiogenesis and protects mice against hind-limb ischemic injury. *Circulation* 123, 2964–2974. doi: 10.1161/CIRCULATIONAHA.110.966408

Raza, A., Franklin, M. J., and Dudek, A. Z. (2010). Pericytes and vessel maturation during tumor angiogenesis and metastasis. *Am. J. Hematol.* 85, 593–598. doi: 10.1002/ajh.21745

Reynoso-Roldan, A., Roldan, M. L., Cancino-Diaz, J. C., Rodriguez-Martinez, S., and Cancino-Diaz, M. E. (2012). Vascular endothelial growth factor production is induced by histone deacetylase 1 and suppressed by von Hippel-Lindau protein in HaCaT cells. *Clin. Invest. Med.* 35, E340–E350. doi: 10.1186/1471-2407-12-293

Ribatti, D. (2018). Interleukins as modulators of angiogenesis and anti-angiogenesis in tumors. *Cytokine* 118, 3–7. doi: 10.1016/j.cyto.2018.10.022

Ribatti, D., and Crivellato, E. (2012). "Sprouting angiogenesis", a reappraisal. *Dev. Biol.* 372, 157–165. doi: 10.1016/j.ydbio.2012.09.018

Risau, W., and Flamme, I. (1995). Annual review of cell and developmental biology. *Vasculogenesis* 11, 73–91. doi: 10.1146/annurev.cb.11.110195.000445

Rosano, S., Corà, D., Parab, S., Zaffuto, S., Isella, C., Porporato, R., et al. (2020). A regulatory microRNA network controls endothelial cell phenotypic switch during sprouting angiogenesis. *Elife* 9:e48095. doi: 10.7554/eLife.48095

Rostama, B., Peterson, S. M., Vary, C. P., and Liaw, L. (2014). Notch signal integration in the vasculature during remodeling. *Vascul. Pharmacol.* 63, 97–104. doi: 10.1016/j.vph.2014.10.003

Sasaki, H., and Matsui, Y. (2008). Epigenetic events in mammalian germ-cell development: reprogramming and beyond. *Nat. Rev. Genet.* 9, 129–140. doi: 10.1038/nrg2295

Saunders, L. R., Sharma, A. D., Tawney, J., Nakagawa, M., Okita, K., Yamanaka, S., et al. (2010). miRNAs regulate SIRT1 expression during mouse embryonic stem cell differentiation and in adult mouse tissues. *Aging* 2, 415–431. doi: 10.18632/aging.100176

Sawamiphak, S., Seidel, S., Essmann, C. L., Wilkinson, G. A., Pitulescu, M. E., Acker, T., et al. (2010). Ephrin-B2 regulates VEGFR2 function in developmental and tumour angiogenesis. *Nature* 65, 487–491. doi: 10.1038/nature08995

Schwerk, J., and Savan, R. (2005). Translating the untranslated region. *J. Immunol.* 195, 2963–2971. doi: 10.4049/jimmunol.1500756

Seo, H. R., Jeong, H. E., Joo, H. J., Choi, S. C., Park, C. Y., Kim, J. H., et al. (2016). Intrinsic FGF2 and FGF5 promotes angiogenesis of human aortic endothelial cells in 3D microfluidic angiogenesis system. *Sci. Rep.* 6:28832. doi: 10.1038/srep28832

Shankar, S., Ganapathy, S., and Srivastava, R. K. (2008). Sulforaphane enhances the therapeutic potential of TRAIL in prostate cancer orthotopic model through regulation of apoptosis, metastasis, and angiogenesis. *Clin. Cancer Res.* 14, 6855–6866. doi: 10.1158/1078-0432.CCR-08-0903

Sheldon, H., Andre, M., Legg, J. A., Heal, P., Herbert, J. M., Sainson, R., et al. (2009). Active involvement of Robo1 and Robo4 in filopodia formation and endothelial cell motility mediated via WASP and other actin nucleation-promoting factors. *FASEB J.* 23, 513–522. doi: 10.1096/fj.07-098269

Shen, L., Kantarjian, H., Guo, Y., Lin, E., Shan, J., Huang, X., et al. (2010). DNA methylation predicts survival and response to therapy in patients with myelodysplastic syndromes. *J. Clin. Oncol.* 28, 605–613. doi: 10.1200/JCO.2009.23.4781

Si, W., Zhou, J., Zhao, Y., Zheng, J., and Cui, L. (2020). SET7/9 promotes multiple malignant processes in breast cancer development via RUNX2 activation and is

negatively regulated by TRIM21. *Cell Death Dis.* 11:151. doi: 10.1038/s41419-020-2350-2

Smits, M., Nilsson, J., Mir, S. E., van der Stoop, P. M., Hulleman, E., Niers, J. M., et al. (2010). miR-101 is down-regulated in glioblastoma resulting in EZH2-induced proliferation, migration, and angiogenesis. *Oncotarget* 1, 710–720. doi: 10.18632/oncotarget.205

Song, J. W., and Munn, L. L. (2011). Fluid forces control endothelial sprouting. *Proc. Natl. Acad. Sci. U.S.A* 108, 15342–15347. doi: 10.1073/pnas.1105316108

Song, Y., Mu, L., Han, X., Li, Q., Dong, B., Li, H., et al. (2013). MicroRNA-9 inhibits vasculogenic mimicry of glioma cell lines by suppressing stathmin expression. *J. Neurooncol.* 115, 381–390. doi: 10.1007/s11060-013-1245-9

Soria-Castro, R., Schcolnik-Cabrera, A., Rodríguez-López, G., Campillo-Navarro, M., Puebla-Osorio, N., Estrada-Parra, S., et al. (2019). Exploring the drug repurposing versatility of valproic acid as a multifunctional regulator of innate and adaptive immune cells. *J. Immunol. Res.* 2019:9678098. doi: 10.1155/2019/9678098

Suárez, Y., Fernández-Hernando, C., Yu, J., Gerber, S. A., Harrison, K. D., Pober, J. S., et al. (2008). Dicer-dependent endothelial microRNAs are necessary for postnatal angiogenesis. *Proc. Natl. Acad. Sci. U.S.A.* 105, 14082–14087. doi: 10.1073/pnas.0804597105

Sun, S. L., Shu, Y. G., and Tao, M. Y. (2020). LncRNA CCAT2 promotes angiogenesis in glioma through activation of VEGFA signalling by sponging miR-424. *Mol. Cell Biochem.* 468, 69–82. doi: 10.1007/s11010-020-03712-y

Theocharis, A. D., Skandalis, S. S., Gialeli, C., and Karamanos, N. K. (2016). Extracellular matrix structure. *Adv. Drug Deliv. Rev.* 97, 4–27. doi: 10.1016/j.addr.2015.11.001

Tonini, T., Rossi, F., and Claudio, P. (2003). Molecular basis of angiogenesis and cancer. *Oncogene* 22, 6549–6556. doi: 10.1038/sj.onc.1206816

Urbich, C., Kaluza, D., Frömel, T., Knau, A., Bennewitz, K., Boon, R. A., et al. (2012). MicroRNA-27a/b controls endothelial cell repulsion and angiogenesis by targeting semaphorin 6A. *Blood* 119, 1607–1616. doi: 10.1182/blood-2011-08-373886

Vandooren, J., Van den Steen, P. E., and Opdenakker, G. (2013). Biochemistry and molecular biology of gelatinase B or matrix metalloproteinase-9 (MMP-9): the next decade. *Crit. Rev. Biochem. Mol. Biol.* 48, 222–272. doi: 10.3109/10409238.2013.770819

Vaupel, P., Kelleher, D. K., and Höckel, M. (2001). Oxygen status of malignant tumors: pathogenesis of hypoxia and significance for tumor therapy. *Semin. Oncol.* 28(2 Suppl. 8), 29–35. doi: 10.1016/s0093-7754(01)90210-6

von Marschall, Z., Scholz, A., Cramer, T., Schäfer, G., Schirner, M., Oberg, K., et al. (2003). Effects of interferon alpha on vascular endothelial growth factor gene transcription and tumor angiogenesis. *J. Natl. Cancer Inst.* 95, 437–448. doi: 10.1093/jnci/95.6.437

Wang, L. H., Tsai, H. C., Cheng, Y. C., Lin, C. Y., Huang, Y. L., Tsai, C. H., et al. (2017). CTGF promotes osteosarcoma angiogenesis by regulating miR-543/angiopoietin 2 signaling. *Cancer Lett.* 391, 28–37. doi: 10.1016/j.canlet.2017.01.013

Wang, Z., Deng, M., Liu, Z., and Wu, S. (2007). Hypoxia-induced miR-210 promoter demethylation enhances proliferation, autophagy and angiogenesis of schwannoma cells. *Oncol. Rep.* 37, 3010–3018.

Wang, Z., Deng, M., Liu, Z., and Wu, S. (2017). Hypoxia-induced miR-210 promoter demethylation enhances proliferation, autophagy and angiogenesis of schwannoma cells. *Oncol. Rep.* 37, 3010–3018. doi: 10.3892/or.2017.5511

Warren, C. M., and Iruela-Arispe, M. L. (2010). Signaling circuitry in vascular morphogenesis. *Curr. Opin. Hematol.* 17, 213–218. doi: 10.1097/MOH.0b013e32833865d1

Weis, S. M., and Cheresh, D. A. (2011). αV integrins in angiogenesis and cancer. *Cold Spring Harb. Perspect. Med.* 1:a006478. doi: 10.1101/cshperspect.a006478

Welti, J. C., Powles, T., Foo, S., Gourlaouen, M., Preece, N., Foster, J., et al. (2012). Contrasting effects of sunitinib within in vivo models of metastasis. *Angiogenesis* 15, 623–641. doi: 10.1007/s10456-012-9291-z

Wouters, B. G., Koritzinsky, M., Chiu, R. K., Theys, J., Buijsen, J., and Lambin, P. (2003). Modulation of cell death in the tumor microenvironment. *Semin. Radiat. Oncol.* 13, 31–41. doi: 10.1053/srao.2003.50004

Würdinger, T., Tannous, B. A., Saydam, O., Skog, J., Grau, S., Soutschek, J., et al. (2008). miR-296 regulates growth factor receptor overexpression in angiogenic endothelial cells. *Cancer Cell* 14, 382–393. doi: 10.1016/j.ccr.2008.10.005

Xu, B., Li, J., Liu, X., Li, C., and Chang, X. (2017). TXNDC5 is a cervical tumor susceptibility gene that stimulates cell migration, vasculogenic mimicry and angiogenesis by down-regulating SERPINF1 and TRAF1 expression. *Oncotarget* 8, 91009–91024. doi: 10.18632/oncotarget.18857

Yabluchanskiy, A., Ma, Y., Iyer, R. P., Hall, M. E., and Lindsey, M. L. (2013). Matrix Metalloproteinase-9: many shades of function in cardiovascular disease. *Physiology* 28, 391–403. doi: 10.1152/physiol.00029.2013

Yin, K. J., Hamblin, M., and Chen, Y. E. (2015). Angiogenesis-regulating microRNAs and ischemic stroke. *Curr. Vasc. Pharmacol.* 13, 352–365. doi: 10.2174/15701611113119990016

Yoo, S. Y., and Kwon, S. M. (2013). Angiogenesis and its therapeutic opportunities. *Mediators Inflamm.* 2013:127170. doi: 10.1155/2013/127170

Yu, T., Wang, Y., Hu, Q., Wu, W., Wu, Y., Wei, W., et al. (2017). The EZH2 inhibitor GSK343 suppresses cancer stem-like phenotypes and reverses mesenchymal transition in glioma cells. *Oncotarget* 8, 98348–98359. doi: 10.18632/oncotarget.21

Zhang, S., Zhang, D., and Sun, B. (2007). Vasculogenic mimicry: current status and future prospects. *Cancer Lett.* 254, 157–164. doi: 10.1016/j.canlet.2006.12.036

Zhang, W., Xiong, Z., Wei, T., Li, Q., Tan, Y., Ling, L., et al. (2018). Nuclear factor 90 promotes angiogenesis by regulating HIF-1α/VEGF-A expression through the PI3K/Akt signaling pathway in human cervical cancer. *Cell Death Dis.* 9:276. doi: 10.1038/s41419-018-0334-2

Zhang, X., Dong, J., He, Y., Zhao, M., Liu, Z., Wang, N., et al. (2017). miR-218 inhibited tumor angiogenesis by targeting ROBO1 in gastric cancer. *Gene* 615, 42–49. doi: 10.1016/j.gene.2017.03.022

Zhang, X., Tang, J., Zhi, X., Xie, K., Wang, W., Li, Z., et al. (2015). miR-874 functions as a tumor suppressor by inhibiting angiogenesis through STAT3/VEGF-A pathway in gastric cancer. *Oncotarget* 6, 1605–1617. doi: 10.18632/oncotarget.2748

Zhang, Y., Liu, J., Lin, J., Zhou, L., Song, Y., Wei, B., et al. (2016). The transcription factor GATA1 and the histone methyltransferase SET7 interact to promote VEGF-mediated angiogenesis and tumor growth and predict clinical outcome of breast cancer. *Oncotarget* 7, 9859–9875. doi: 10.18632/oncotarget.7126

Zhang, Z., Yan, J., Chang, Y., ShiDu Yan, S., and Shi, H. (2011). Hypoxia Inducible Factor-1 as a target for neurodegenerative diseases. *Curr. Med. Chem.* 18, 4335–4343. doi: 10.2174/092986711797200426

Zhi-Gang, Y., Wen-Huan, L., Fang, H., Hong-Xia, C., Miao-Qing, Z., Xi-Chao, S., et al. (2017). LBH589 Inhibits glioblastoma growth and angiogenesis through suppression of HIF-1α expression. *J. Neuropathol. Exp. Neurol.* 76, 1000–1007. doi: 10.1093/jnen/nlx088

Zhou, W. J., Yang, H. L., Chang, K. K., Meng, Y., Wang, M. Y., Yuan, M. M., et al. (2017). Human thymic stromal lymphopoietin promotes the proliferation and invasion of cervical cancer cells by downregulating microRNA-132 expression. *Oncol. Lett.* 14, 7910–7916. doi: 10.3892/ol.2017.7260

Zhu, D., Hunter, S. B., Vertino, P. M., and Van Meir, E. G. (2011). Overexpression of MBD2 in glioblastoma maintains epigenetic silencing and inhibits the antiangiogenic function of the tumor suppressor gene BAI1. *Cancer Res.* 71, 5859–5870. doi: 10.1158/0008-5472.CAN-11-1157

Zuazo-Gaztelu, I., and Casanovas, O. (2018). Unraveling the role of angiogenesis in cancer ecosystems. *Front. Oncol.* 8:248. doi: 10.3389/fonc.2018.00248

Conflict of Interest: The authors declare that the research was conducted in the absence of any commercial or financial relationships that could be construed as a potential conflict of interest.

Publisher's Note: All claims expressed in this article are solely those of the authors and do not necessarily represent those of their affiliated organizations, or those of the publisher, the editors and the reviewers. Any product that may be evaluated in this article, or claim that may be made by its manufacturer, is not guaranteed or endorsed by the publisher.

frontiers in Genetics

ORIGINAL RESEARCH
published: 13 September 2021
doi: 10.3389/fgene.2021.696840

Whole-Genome Methylation Analysis Revealed ART-Specific DNA Methylation Pattern of Neuro- and Immune-System Pathways in Chinese Human Neonates

Zongzhi Liu[1,3,8†], Wei Chen[4,5,6,7†], Zilong Zhang[3,8,9†], Junyun Wang[3,8†], Yi-Kun Yang[2†], Luo Hai[1†], Yuan Wei[4,5,6], Jie Qiao[4,7] and Yingli Sun[1,3,8*]*

[1] Central Laboratory, National Cancer Center/National Clinical Research Center for Cancer/Cancer Hospital & Shenzhen Hospital, Chinese Academic of Medical Sciences and Peking Union Medical College, Shenzhen, China, [2] Department of Thoracic Surgery, National Cancer Center/National Clinical Research Center for Cancer/Cancer Hospital & Shenzhen Hospital, Chinese Academy of Medical Sciences and Peking Union Medical College, Shenzhen, China, [3] University of Chinese Academy of Sciences, Beijing, China, [4] Center for Reproductive Medicine, Department of Obstetrics and Gynecology, Peking University Third Hospital, Beijing, China, [5] Key Laboratory of Assisted Reproduction, Ministry of Education, Beijing, China, [6] Beijing Key Laboratory of Reproductive Endocrinology and Assisted Reproduction, Beijing, China, [7] Peking-Tsinghua Center for Life Sciences, Peking University, Beijing, China, [8] CAS Key Laboratory of Genome Sciences and Information, Beijing Institute of Genomics, Chinese Academy of Sciences/China National Center for Bioinformation, Beijing, China, [9] Tianjin Novogene Bioinformatic Technology Co., Ltd., Tianjin, China

The DNA methylation of human offspring can change due to the use of assisted reproductive technology (ART). In order to find the differentially methylated regions (DMRs) in ART newborns, cord blood maternal cell contamination and parent DNA methylation background, which will add noise to the real difference, must be removed. We analyzed newborns' heel blood from six families to identify the DMRs between ART and natural pregnancy newborns, and the genetic model of methylation was explored, meanwhile we analyzed 32 samples of umbilical cord blood of infants born with ART and those of normal pregnancy to confirm which differences are consistent with cord blood data. The DNA methylation level was lower in ART-assisted offspring at the whole genome-wide level. Differentially methylated sites, DMRs, and cord blood differentially expressed genes were enriched in the important pathways of the immune system and nervous system, the genetic patterns of DNA methylation could be changed in the ART group. A total of three imprinted genes and 28 housekeeping genes which were involved in the nervous and immune systems were significant different between the two groups, six of them were detected both in heel blood and cord blood. We concluded that there is an ART-specific DNA methylation pattern involved in neuro- and immune-system pathways of human ART neonates, providing an epigenetic basis for the potential long-term health risks in ART-conceived neonates.

Keywords: human offspring, differentially methylated regions, housekeeping gene, assisted reproductive technology, DNA methylation pattern, imprinted gene

OPEN ACCESS

Edited by:
Zhao-Qian Teng,
Institute of Zoology, Chinese Academy of Sciences (CAS), China

Reviewed by:
Daniel Vaiman,
Institut National de la Santé et de la Recherche Médicale (INSERM), France
Xuekun Li,
Zhejiang University, China

****Correspondence:***
Yingli Sun
yinglisun37@126.com
Jie Qiao
jie.qiao@263.net

† These authors have contributed equally to this work

Specialty section:
This article was submitted to Epigenomics and Epigenetics, a section of the journal Frontiers in Genetics

Received: *18 April 2021*
Accepted: *08 July 2021*
Published: *13 September 2021*

Citation:
Liu Z, Chen W, Zhang Z, Wang J, Yang Y-K, Hai L, Wei Y, Qiao J and Sun Y (2021) Whole-Genome Methylation Analysis Revealed ART-Specific DNA Methylation Pattern of Neuro- and Immune-System Pathways in Chinese Human Neonates. Front. Genet. 12:696840. doi: 10.3389/fgene.2021.696840

INTRODUCTION

Assisted reproductive technology (ART) involves fertilizing a human egg *in vitro* and the transplantation of the resulting embryo into the uterus for conception (Van Voorhis, 2007; Belva et al., 2016; Boulet et al., 2016; De Geyter et al., 2018). Decades after the first successful application of ART in humans, over 8 million infants have been born with ART assistance worldwide (Wade et al., 2015; Rao et al., 2018; Fauser, 2019; Leaver and Wells, 2019). ART has become well-accepted and popular in recent years (Liu et al., 2015; Simopoulou et al., 2018; Gleicher et al., 2019). Epidemiological and animal experiments show that the early stage of fetal development is particularly sensitive to changes in the environment and that the environmental abnormalities suffered during this period may lead to problems later in life (Faulk and Dolinoy, 2011; Hanson and Gluckman, 2014; Grandjean et al., 2015; Heindel et al., 2017; Li T. et al., 2019). During this sensitive period, adverse environmental stimulation may affect cell proliferation and lineage differentiation by affecting normal epigenetic reprogramming processes, leading to abnormal epigenetic modification levels and permanent changes in gene expression patterns (Yamazaki et al., 2003; Hanson and Gluckman, 2014; Nelissen et al., 2014; Koot et al., 2016). ART treatments, such as exposure to culture medium and gamete or embryo freezing, may affect DNA methylation reprogramming and embryonic development (de Waal et al., 2015; Canovas et al., 2017b; Mani and Mainigi, 2018; Argyraki et al., 2019). Zoological and embryological studies have revealed that ART can affect the DNA methylation pattern and the expression of imprinted genes in mouse, pig, and bovine embryos (Wright et al., 2011; de Waal et al., 2014; Anckaert and Fair, 2015; Salilew-Wondim et al., 2015; Canovas et al., 2017a; Hattori et al., 2019). Additionally, epidemiological studies have reported the abnormal development of the immune system (Tan et al., 2016; Kollmann et al., 2017; Pathare et al., 2017), increased risk of neurological diseases, the presence of metabolic abnormalities, and the presence of congenital anomalies in ART-assisted human offspring, including autism spectrum disorders, intellectual disability, specific congenital heart defects, cardiovascular disease, and metabolic disorder (Sandin et al., 2013; Tararbit et al., 2013; Guo et al., 2017; Liu et al., 2017).

More and more observations of rising health risks in ART-conceived neonates have linked ART technology to potential epigenetic abnormities (Tararbit et al., 2013; Guo et al., 2017). Previous works only focused on the epigenetic influence of ART on a limited numbers of genes. Recent works reported the impact of ART on genome-wide DNA methylation. Nevertheless, the DNA methylation of ART processes has not been fully elucidated, and parental background has not been considered. Several studies showed that ART was associated with diverse DNA methylation changes in human offspring (Melamed et al., 2015; Castillo-Fernandez et al., 2017; DeAngelis et al., 2018; Menezo et al., 2019). However, these observations were primary and these studies analyzed DNA methylation from cord blood data, which contained maternal cell contamination (Lo et al., 1996, 2000) affecting the results of the methylation data analyses (Houseman et al., 2012; Bakulski et al., 2016; Jones et al., 2017; Lin et al., 2018). Therefore, a mixture of cord blood samples may result in high background and unclear data of DNA methylation.

Herein, as shown in **Figure 1A**, by using the heel blood of the ART-conceived newborns and removing the background DNA methylation level of parents, we are able to perform a more accurate and reliable analysis of DNA methylation with low background noise. Heel prick blood sampling enables us to identify ART-specific DNA methylation pattern changes precisely, objectively, and accurately.

MATERIALS AND METHODS

Editorial Policies and Ethical Considerations

All samples were obtained in the Center for Reproductive Medicine, Peking University Third Hospital. All blood samples were obtained after written informed patient consent and were fully anonymized. The studies involving human participants were reviewed and approved by The Reproductive Study Ethics Committee of Peking University Third Hospital (approved protocol no. 201752-044). The participants' parents and legal guardians provided written informed consent to participate in this study.

Participants and Study Design

We collected information on three families who had assisted reproductive pregnancies and three families who normal pregnancies. All families had twins by cesarean birth. The heel blood of neonates was collected 3 days after birth. The peripheral blood of parents was stored in an EDTA blood collection vessel. The Illumina Methylation 450K array was performed on all samples. Meanwhile, we analyzed the RNA-seq data we recently uploaded to the GEO database which we collected from umbilical cord blood of 32 newborns who underwent IVF-ET, IVF-FET, ICSI-ET, ICSI-FET, and normal pregnancy.

Characteristics of the ART and Control Groups

The gestational age of the newborns at birth was 34–38 weeks. All the newborns in the three ART families and three control families were delivered by cesarean section. Neither parent had a history of familial hereditary diseases, these details are shown in **Table 1**.

DNA Extraction

Genomic DNA was extracted using the QIAamp DNA Mini Kit (QIAGEN 51304, Germany) according to the manufacturer's instructions.

Methylation Microarray Analysis

Genomic DNA (1 μg) was bisulfite-converted using the EZ DNA Methylation-Gold Kit (ZYMO RESEARCH, D5005, FosterCity, California, United States). Then DNA was whole-genome-amplified, enzymatically fragmented, purified, and applied to

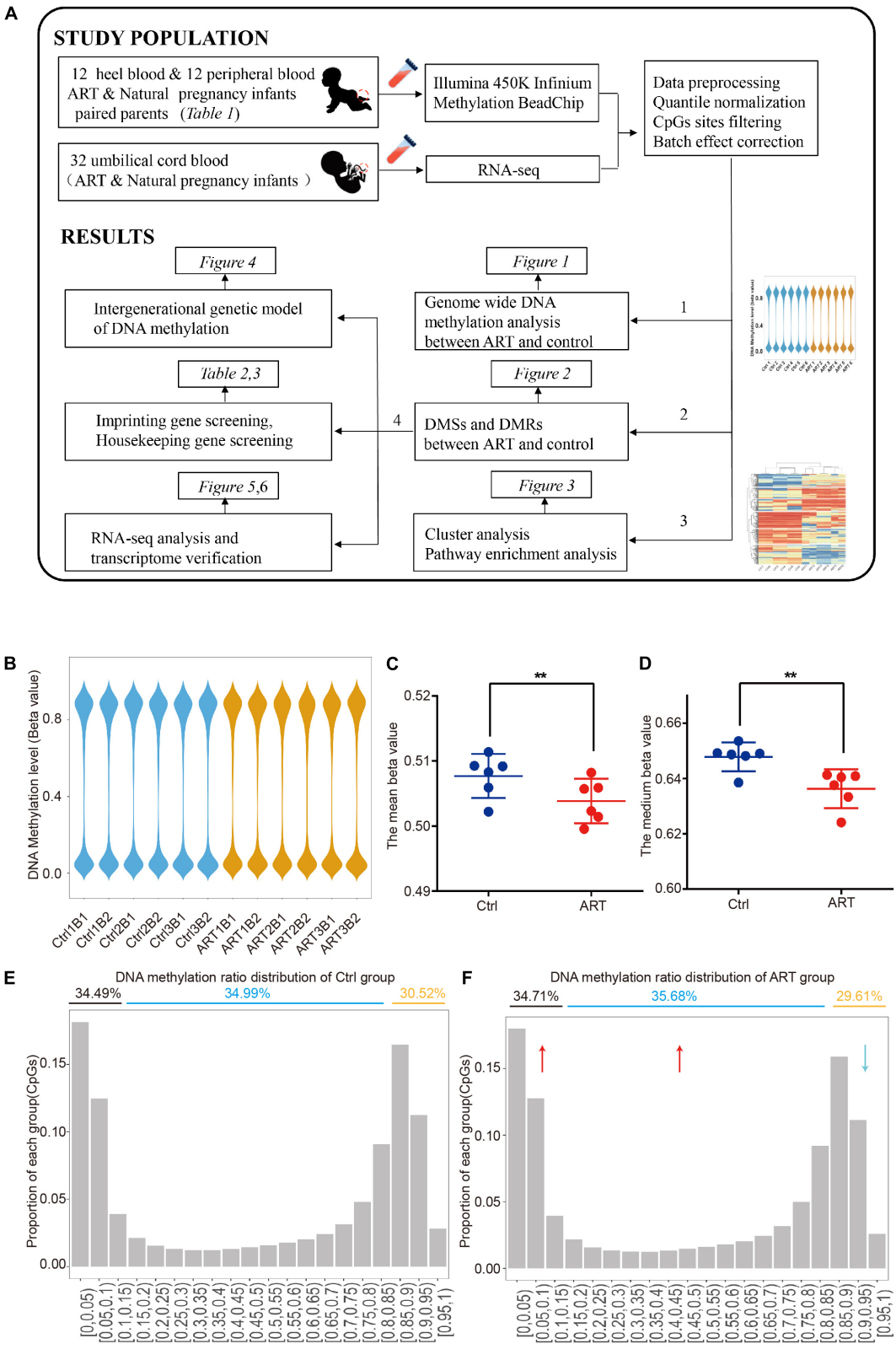

FIGURE 1 | Genome-wide DNA hypomethylation pattern in assisted reproductive technology (ART)-conceived infants. **(A)** Graphical overview of the study design. **(B)** The distribution of DNA methylation showed that the two groups had a similar pattern at the genome level. Mean **(C)** and median **(D)** DNA methylation levels. DNA methylation ratio distribution of the control **(E)** and ART group **(F)**.

TABLE 1 | Detailed information on Control and assisted reproductive technology (ART) samples.

	Control 1	Control 2	Control 3	Control 4	Control 5	Control 6	ART1	ART2	ART3	ART4	ART5	ART6
Family ID	Control Family 1	Control Family 1	Control Family 2	Control Family 2	Control Family 3	Control Family 3	ART Family 1	ART Family 1	ART Family 2	ART Family 2	ART Family 3	ART Family 3
Cesarean birth	Yes	Yes	Yes	Yes	Yes	Yes	Yes	Yes	Yes	Yes	Yes	Yes
Gestational age	36	36	37	37	34	34	37	37	38	38	34	34
Infant body length	47 cm	47 cm	48 cm	48 cm	43 cm	41 cm	47 cm	45 cm	49 cm	48 cm	44 cm	44 cm
Infant weight	2560 g	2600 g	2600 g	2810 g	2250 g	1810 g	2740 g	2220 g	2940 g	2830 g	1980 g	2010 g
Sex	Female	Female	Male	Male	Male	Male	Female	Female	Female	Female	Male	Male
Father's age	–	–	–	–	26	26	40	40	33	33	–	–
Mother's age	28	28	30	30	25	25	38	38	32	32	27	27
Mother's weight	82 kg	82 kg	66.5 kg	66.5 kg	82 kg	82 kg	68 kg	68 kg	74.5 kg	74.5 kg	77 kg	77 kg
Mother's height	161 cm	161 cm	163 cm	163 cm	172 cm	172 cm	167 cm	167 cm	169 cm	169 cm	162 cm	162 cm
Weight gain during pregnancy	18.5 kg	18.5 kg	18.5 kg	18.5 kg	20 kg	20 kg	7.5 kg	7.5 kg	15 kg	15 kg	18 kg	18 kg
Hereditary diseases	None	None	None	None	None	None	None	None	None	None	None	None

the Illumina Infinium Methylation 450K array according to the Illumina methylation protocol.

Analysis of the Methylation Microarray Data

DNA methylation files were processed and normalized by R software packages using the "Illumina Methylation Analyzer (IMA)" package. For each of the samples, CpG sites with a detection *p*-value less than 0.05 were excluded from the analysis. In addition, probes with SNPs or their single base extension, X chromosome and Y chromosome at the CpG site were excluded. Differences in global DNA methylation levels between the ART and control groups were analyzed by the Wilcoxon test. The standard DMSs between the ART and control groups were δ beta$| > 0.2$ and $p < 0.05$ (Wilcoxon test). DMRs analysis used QDMR Tutorial software (Zhang et al., 2011).

Chromosome distribution differences were analyzed by the Wilcoxon test. Cluster analysis and visualization were performed using pheatmap (R package). Heel blood DNA methylation pathway enrichment analysis was performed by IPA. Information on imprinted genes was obtained from the gene imprint website.[1] Information on housekeeping genes was obtained from Eisenberg and Levanon (2013).

Analysis of RNA-Seq Data

Downloaded raw fastq data were firstly processed using Trimmomatic (version 0.36) to remove the library adapter, low-quality bases, and reads smaller than 50 bases. The retained reads were mapped to the Homo sapiens reference genome (human GRCh38/hg38) using STAR (version 2.5.3a) with the default parameters, and read counting was performed using featureCounts (version 1.6.3). Finally, DEseq2 (version 1.26.0) was used to obtain the normalized count matrix for all samples. GO enrichment analysis was carried out using the R/Bioconductor package ChIPseeker (Houseman et al., 2012; version 1.10.3).

[1]http://www.geneimprint.com/site/gene

RESULTS

The Whole Genome-Wide Methylation Differences in ART-Conceived and Naturally Conceived Neonates

In order to compare the differences of global methylation level between ART and naturally conceived newborns, we first analyzed the genome-wide methylation patterns. The overall DNA methylation beta value showed similar distribution patterns among all samples (**Figure 1B** and **Supplementary Figure 1**). However, the global DNA methylation level was lower in the ART group ($\bar{\beta}$ART = 0.504 ± 0.003 versus $\bar{\beta}$ctrl = 0.508 ± 0.003). Further analysis of the mean (**Figure 1C**) and median (**Figure 1D**) DNA methylation beta values of individuals confirmed this observation.

After the methylation beta level (0–1) was divided into approximately 20 intervals, the results revealed that such hypomethylation in the ART group was mainly caused by the decreased ratio in CpG sites with high DNA methylation levels (methylation beta level > 0.85), with 29.61% in the ART group and 30.52% in the control group, and the increased ratio in the CpG site with low and medium DNA methylation levels (methylation beta level < 0.85), with 70.39% in the ART group and 69.48% in the control group (**Figures 1E,F**).

Differential Methylation Sites Were Enriched in Important Pathways of the Immune and Nervous Systems

As shown in **Figure 2A**, a total of 301 differential methylation sites (DMSs) were screened as described in the "Materials and Methods" part. The number of hypomethylated DMSs counted for 178, and the number of hypermethylated DMSs was 123 (59 versus 41%; **Figure 2B**), which was consistent with the analysis of demethylation at the genome-wide level mentioned. The beta value analysis of the DMSs for each sample showed this tendency more clearly. The mean beta values of differential hypomethylation sites in the ART group were 0.418 ± 0.032 and 0.730 ± 0.007 in the control group (**Figure 2C**). The mean beta

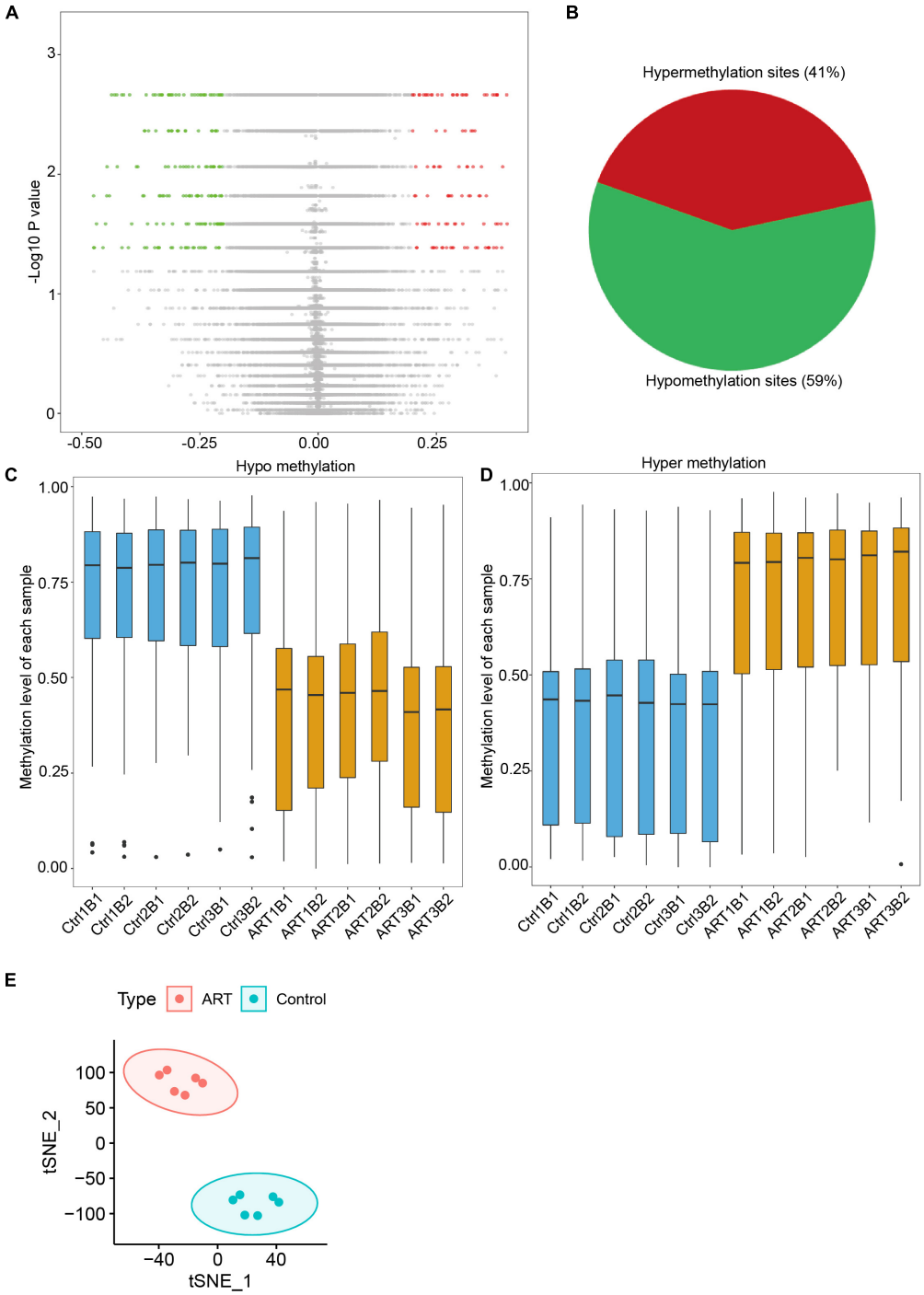

FIGURE 2 | Differential methylation analysis showed that the number of hypomethylation sites in ART-conceived infants was significantly higher than the number of hypermethylation sites. **(A)** Distribution of differences in DNA methylation levels between the two groups of infants. **(B)** The ratio of sites with hypomethylation differences and hypermethylation differences was 59:41. Distribution of methylation levels at different sites of hypomethylation **(C)** and hypermethylation **(D)**. **(E)** tSNE analysis of differentially methylated sites (DMSs).

values of differential hypermethylation sites in the ART group were 0.702 ± 0.018 and 0.372 ± 0.0124 in the control group (**Figure 2D**). Through t-SNE analysis, the DMSs can significantly divide the ART and control infants into two groups (**Figure 2E**).

DMSs were significantly enriched in the S shelf and open sea based on their relationship with CpG islands (**Figures 3A,B**) and gene bodies and intergenic regions based on the nearest genes (**Figures 3C,D**). Specifically, they were represented in the CpG

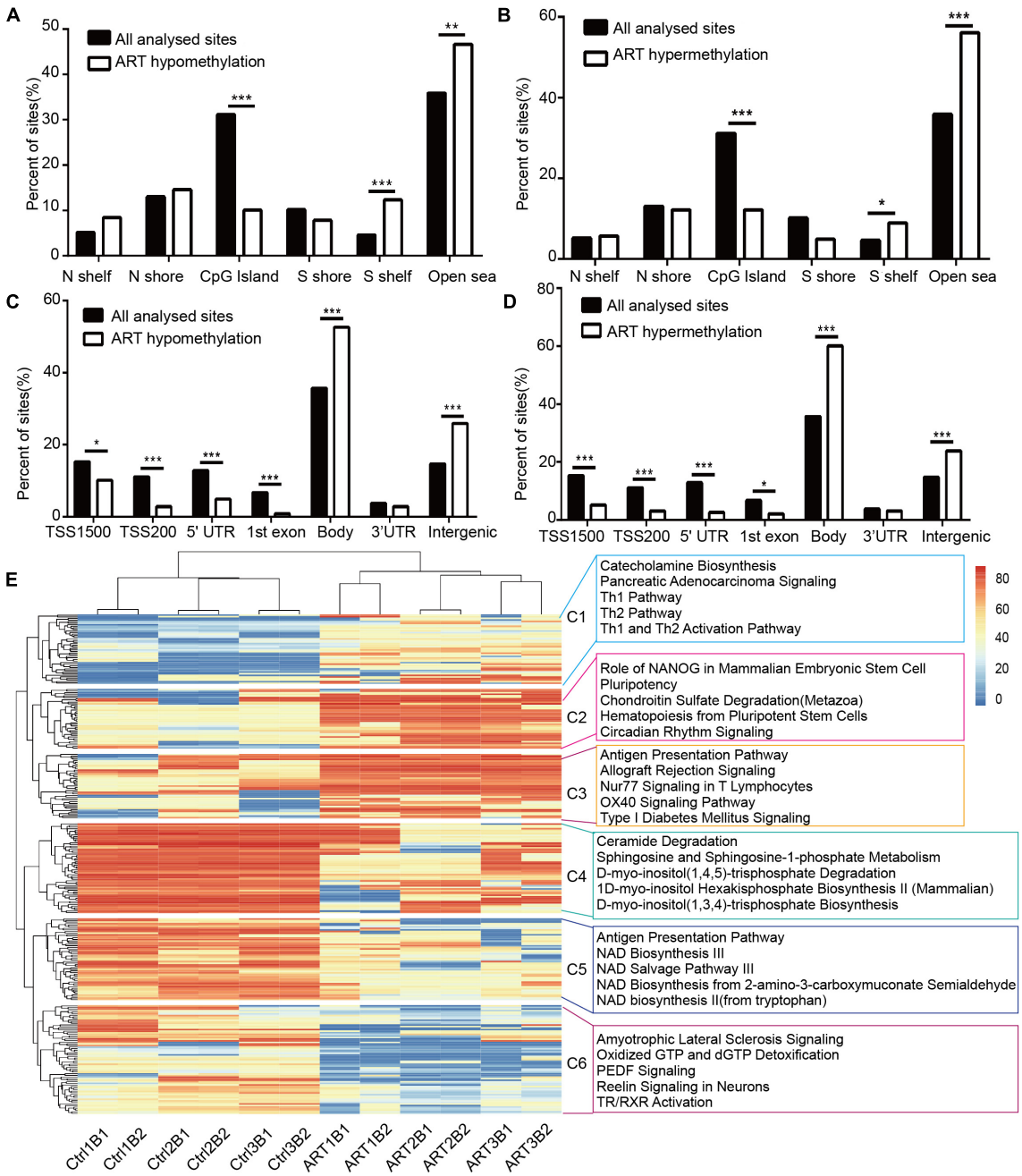

FIGURE 3 | Non-randomized effects of ART on DNA methylation patterns were associated with early infant development. The distribution of hypomethylated **(A)** and hypermethylated DMSs **(B)** affected by ART in relation to the nearest CpG island. The distribution of hypomethylated **(C)** and hypermethylated DMSs **(D)** affected by ART in relation to the nearest genes. **(E)** Heatmap derived from supervised cluster analysis of DMSs. The red color in the heatmap indicates hypermethylation values, and blue indicates hypomethylation values.

islands, TSS1500, TSS200, 5′UTR, and 1st exon. These findings further indicated that the ART-assisted and control groups shared similar methylation patterns with specific differences.

Furthermore, the DMSs we identified could be used to classify the ART group and control group by supervised cluster analysis. Six ART infants were clustered together, and six control infants were grouped together at the top of the cluster tree (**Figure 3E**). Further, we discovered several consistent patterns when DMSs were clustered into six subgroups (C1–C6) based on supervised clusters. The methylation levels of DMSs in the C1, C4, and C5 subgroups were relatively conservative in all six control infants (C1: hypomethylation in nearly all sites, C4 and C5: hypermethylation in nearly all sites) but with high randomness and diversity in the six ART infants (different

samples had different methylation levels at the same site). In contrast, the methylation levels of DMSs in the C2, C3, and C6 subgroups were greatly heterogeneous among the six control infants (different samples had different methylation levels at the same site) but with high consistency in the six ART infants (C2 and C3: hypermethylation in nearly all sites, C6: hypomethylation in nearly all sites). Additionally, all loci were statistically analyzed for the degree of dispersion to confirm our results. In parts C1, C4, and C5, the scattering degree (SD) value of the ART group was larger, while that of the control group was more conservative. In parts C2, C3, and C6, the SD value of the ART group was smaller, while that of the control group was larger (**Supplementary Table 1**). Furthermore, ingenuity pathway analysis (IPA) showed that DMSs were enriched in key pathways, e.g., (1) the "Ceramide Degradation" and "Catecholamine Biosynthesis" pathways were well associated with nervous system development and nerve signals transfer; (2) the "Antigen Presentation Pathway," "Th1 Pathway," and "Th2 Pathway" were important pathways related to immune system establishment; (3) "NAD Biosynthesis III," "NAD Salvage Pathway III," and "NAD Biosynthesis" played key roles in metabolic development. Importantly, the pathway analysis results were consistent with clinical manifestations, such as with a cognitive development problem and a higher risk of autism in ART-conceived infants (Fountain et al., 2015; Rumbold et al., 2017; Berntsen et al., 2019).

Immune- and Nervous-System Pathways Were Identified by Differential Methylation Regions Analysis and Cord Blood RNA-Seq

DNA methylation usually functioned in a region, we identified differentially methylated regions (DMRs) to find their functional association. Interestingly, DMRs analysis showed similar results with DMSs. The obtained DMRs were highly enriched in the regulation of neuron differentiation processes, antigen presentation, and other important developmental pathways (**Supplementary Figure 2**). Moreover, 10 of the 301 DMSs with the most remarkable differences in methylation beta values could be used to divide the two groups in the principal component analysis (PCA) (**Supplementary Figure 3**). These 10 most susceptible sites included 7 genes, namely, *ZNF137*, *TAP2*, *RBM28*, *NUDT1*, *NMNAT3*, *EIF3E*, and *AFAP1* (**Supplementary Table 2**). Among the above genes, four genes were involved in neurological and immune-related functions: (1) *TAP2* was related to the expression of major histocompatibility complex (MHC) class I molecules and the development of insulin-dependent diabetes mellitus (Qu et al., 2007; Qiu et al., 2015; Praest et al., 2018); (2) *RBM28* was related to progressive neurological defects and endocrinopathy (Nousbeck et al., 2008); (3) NUDT1 was related to neurodegeneration (Pudelko et al., 2017; Haruyama et al., 2019); (4) *NMNAT3* encoded a member of the nicotinamide/nicotinic acid mononucleotide adenylyltransferase family and played a neuroprotective role as a molecular chaperone (Galindo et al., 2017). Collectively, these results suggested that DNA methylation in ART offspring could be changed and that these changes were enriched in development-related pathways, particularly in the nervous, immune, and metabolic systems.

The Opposite Genetic Pattern of DNA Methylation Between ART and Normal Pregnancy Infants

We have confirmed that the DNA methylation pattern of ART infants was different from that of normal pregnant infants through DMSs, DMRs, and DEGs analyses, further, we want to confirm whether these epigenetic differences are influenced by parental heredity. As shown in **Figure 4**, we analyzed C1–C6 separately and combined them with their parents, then we found that the difference of DNA methylation pattern between ART and natural pregnancy infants also existed in their parents (heatmap, C1–C6), however, the genetic pattern of ART infants was opposite compared to normal pregnancy infants (boxplot, C1–C6 and histogram C1–C6). When we removed the background DNA methylation level of parents, we found that in C1–C3 (**Figure 4A**) the methylation level of normal pregnancy infants tended toward hypomethylation compared with their parents, however, there was a trend of hypermethylation in ART infants compared with their parents. In C4–C6 (**Figure 4B**), the methylation level of normal pregnancy infants tended toward hypermethylation compared with their parents, however, there was a trend of hypomethylation in ART infants compared with their parents. All the opposite genetic patterns had significant statistical difference ($p < 0.001$).

The Discovery of Imprinted Genes and Housekeeping Genes Changes Can Be Found in RNA-Seq of Cord Blood

As described above, ART could specifically affect the conservativeness of the DNA methylation pattern. Imprinted genes and housekeeping genes were conserved in genetic processes and played important roles in development. In a comparison involving the imprinted and housekeeping gene database, we identified 3 DMSs located in 2 imprinted genes (**Table 2**) and 28 DMSs located in 26 housekeeping genes (**Table 3**). The two imprinted genes included: (1) *NTM*, which encoded a protein of the IgLON family with specific expression in the brain that promotes neurite outgrowth and adhesion via a homophilic mechanism (Li et al., 2015; Maruani et al., 2015); (2) *BRUNOL4*, which was related to variable splicing of precursor RNA and its editing and normal function of the nervous system (Wang et al., 2016; An et al., 2019). Among the housekeeping genes, *CASP7*, *RBM28*, and *FEZ2* were associated with the maintenance of nerve function (Nousbeck et al., 2008; Choudhury et al., 2015; Hapairai et al., 2017). CMPK1 and INPP5A were related to metabolic function (Zhu et al., 2018; Li G. et al., 2019). *GALNS* and *TAPBP* were involved in the innate immune system and MHC class I-mediated antigen processing and presentation (Williams et al., 2000, 2002; Park et al., 2004; Tamarozzi et al., 2014).

To further verify the above imprinted and housekeeping gene, we used our recently published RNA-sequencing data

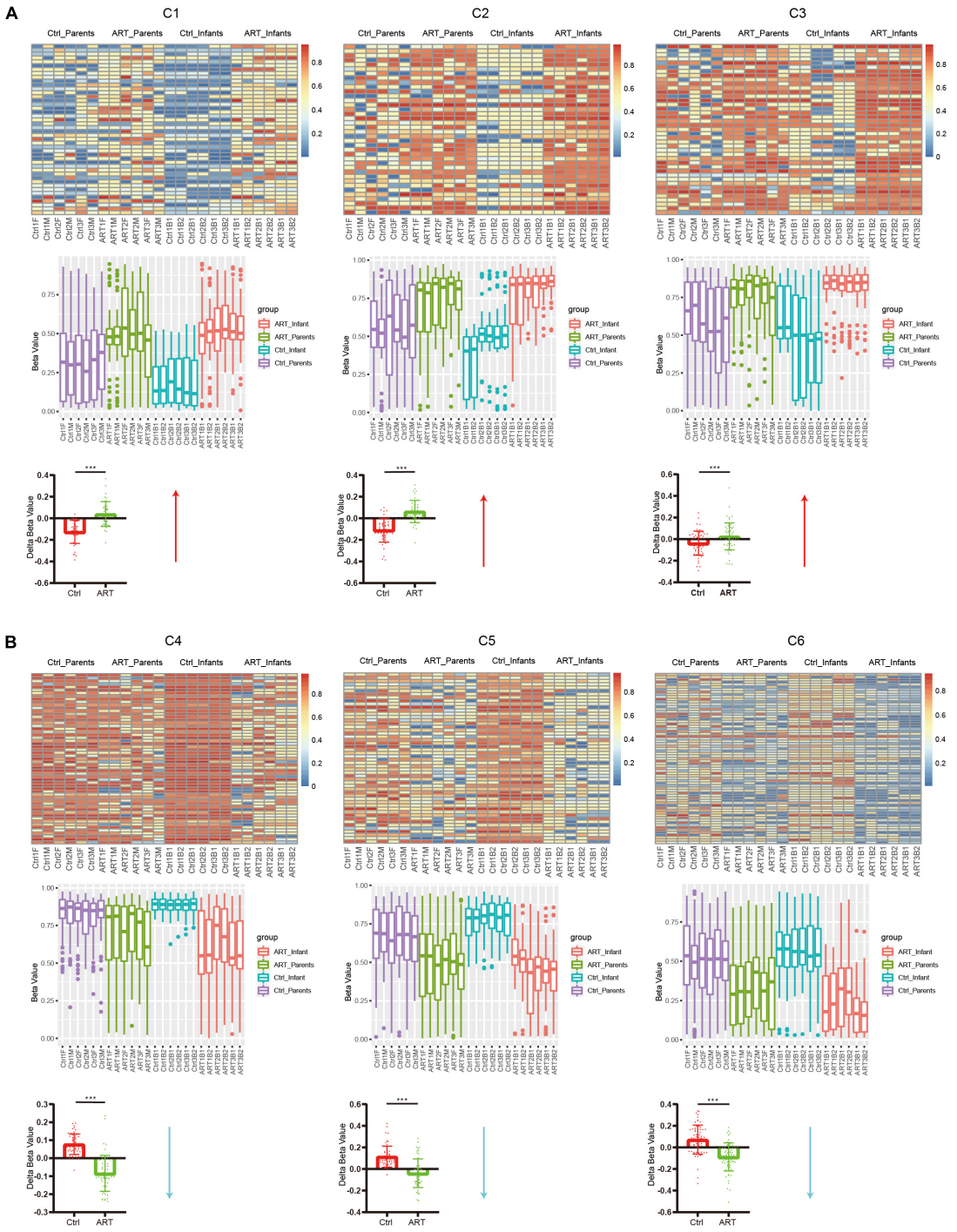

FIGURE 4 | The opposite genetic pattern of DNA methylation between ART and normal pregnancy infants. **(A)** In C1–C3, the methylation level of normal pregnancy infants tended toward hypomethylation compared with their parents, however, there was a trend of hypermethylation in ART infants compared with their parents. **(B)** In C4–C6, the methylation level of normal pregnancy infants tended toward hypermethylation compared with their parents, however, there was a trend of hypomethylation in ART infants compared with their parents. All the opposite genetic patterns had significant statistical difference ($p < 0.001$).

(GSE136849) to analyze the gene expression. The ART-conceived pregnancy families were further divided into four subgroups based on the type of ART applied, including the *in vitro* fertilization-embryo transfer (IVF-ET), *in vitro* fertilization and frozen-thawed embryo transfer (IVF-FET), intracytoplasmic sperm injection-embryo transfer (ICSI-ET), and intracytoplasmic sperm injection and frozen-thawed embryo transfer (ICSI-FET) subgroups. Each ART subgroup had its

TABLE 2 | Analysis of imprinted genes affected in ART.

Target ID	CHR	MAPINFO	Gene name	Diff (ART-N)	*P*-value
cg09663736	11	131554122	*NTM*	−0.20	0.026
cg13077366	18	34908626	*BRUNOL4*	−0.22	0.004
cg20094343	18	34917603	–	−0.27	0.015

TABLE 3 | Analysis of housekeeping genes affected in ART.

Target ID	CHR	MAPINFO	Gene name	Diff (ART-N)	*P*-value
cg12501287	10	134411480	*INPP5A*	0.20	0.015
cg16645815	10	134556992	*INPP5A*	−0.25	0.004
cg16542356	7	1121190	*C7orf50*	−0.20	0.026
cg23496178	7	1142861	*C7orf50*	−0.26	0.041
cg00023507	6	33276465	*TAPBP*	−0.33	0.002
cg00999163	1	47799638	*CMPK1*	0.26	0.041
cg01128042	10	115465924	*CASP7*	−0.47	0.041
cg02379549	6	36887307	*C6orf89*	0.31	0.026
cg03119308	7	127950724	*RBM28*	0.68	0.002
cg05385718	2	242693323	*D2HGDH*	0.28	0.015
cg05398700	14	102677141	*WDR20*	−0.23	0.015
cg06314883	6	5404958	*FARS2*	0.21	0.041
cg08136432	16	88902276	*GALNS*	0.38	0.026
cg08603678	8	109235928	*EIF3E*	0.69	0.002
cg08912652	11	130779479	*SNX19*	0.31	0.041
cg12604331	1	156906485	*ARHGEF11*	0.29	0.002
cg13143872	2	200778865	*C2orf69*	−0.31	0.002
cg14060113	19	18054643	*CCDC124*	−0.34	0.041
cg14497649	4	528497	*PIGG*	−0.30	0.002
cg14609104	10	111989324	*MXI1*	0.41	0.009
cg1542132	5	153372524	*FAM114A2*	−0.53	0.002
cg16241932	6	157876915	*ZDHHC14*	0.35	0.026
cg17004290	4	108853384	*CYP2U1*	−0.45	0.015
cg24976563	14	24587638	*DCAF11*	0.36	0.041
cg25282454	1	1158325	*SDF4*	0.31	0.002
cg25465065	1	156198365	*PMF1*	−0.36	0.026
cg26303777	1	230311676	*GALNT2*	−0.24	0.026
cg06634576	2	36782386	*FEZ2*	−0.32	0.015

technical details, but they all intervened on embryonic cells *in vitro*. As shown in **Figure 5** and **Supplementary Figure 4**, the gene expression pattern of the above four ART subgroups was different from that of the control group. Among them, six genes were significantly different from the control group in all ART subgroups, namely *GALNT2*, *GALNS*, *EIF3E*, *C2ORF69*, *CYP2U1*, and *CASP7*, respectively. Among the above genes, *GALNT2* was involved in glucose and lipid metabolism; *EIF3E* was highly associated with the survival of human glioblastoma cells; *CYP2U1* transcripts were most abundant in the thymus and the brain, indicating a specific physiological role for *CYP2U1* in these tissues. Next, we did hierarchical cluster analysis on the transcriptome (**Figure 6A**), PCA results showed that that the expression profiles of the control group and ART newborns could be significantly divided into two groups (**Figure 6B**), the number of DEGs between the IVF frozen and natural pregnancy groups was relatively large (**Figure 6C**). They were highly enriched in pathways involving autophagy and sialic acid secretion (**Figure 6D**). At the same time, we found that the immune and nervous system-related pathways also had significant statistical differences, which justifies the results of our heel blood methylation pathway analysis (**Supplementary Figure 5**).

DISCUSSION

ART treatment can affect the epigenomes of offspring, such as aberrant DNA methylation (Tan et al., 2016; Castillo-Fernandez et al., 2017; El Hajj et al., 2017; Ghosh et al., 2017), most of the studies addressing these changes use the cord blood, which has an unwanted maternal background. Moreover, most of these studies are not whole genome-wide. To demonstrate the specific effect caused by ART, we used heel blood to compare the DNA methylation patterns of ART and naturally conceived newborns.

Our main findings were as follows: (1) ART can affect the conservation of DNA methylation in specific genomic regions, and the DMSs are mainly enriched in the function of the nervous system and immune system; (2) our discovery of DMSs can be confirmed by the difference of DMRs, RNA expression level of imprinted genes, and housekeeping genes in ART babies.

Our study reveals that ART infants show a similar global DNA methylation pattern with naturally conceived infants, which is consistent with the results of NirMelamed's study (Melamed et al., 2015). However, by using cord blood, which adds background noise from the maternal cells, the above work fails to show the specific methylation difference in ART-assisted babies. We screened 301 DMSs in the heel blood of ART-assisted samples. Although the number of loci screened out was relatively small, it actually reflects the real difference in methylation levels between the ART and control groups. It can be explained by the fact that our sample contains only the methylation information of newborns with no environmental influence, and we set up a strict standard for screening. Previous works do not reveal the genes annotated from all 301 DMSs (**Supplementary Figure 6**; Melamed et al., 2015; Castillo-Fernandez et al., 2017; El Hajj et al., 2017). The differential genes we found were consistent with the gene found by Juan et al., and there have been very few common discoveries among previous works. Furthermore, our data demonstrate that ART shows a specific effect on the reprogramming of DNA methylation patterns in human offspring.

The pathway analysis of DMSs and DMRs shows that the altered DNA methylation patterns are mainly enriched in key pathways in early-stage developmental pathways, such as neurotransmitter secretion, immune system establishment, and NAD metabolism. Quite a few previous works of clinical studies suggest an increased risk of autism spectrum disorders, intellectual disability, specific congenital heart defects, cardiovascular disease, and metabolic disorder in late-stage ART-assisted infants (Sandin et al., 2013; Guo et al., 2017; Liu et al., 2017). It is reasonable to hypothesize that abnormal DNA methylation in ART-assisted offspring is rooted in the effect of DNA methylation reprogramming in the early developmental

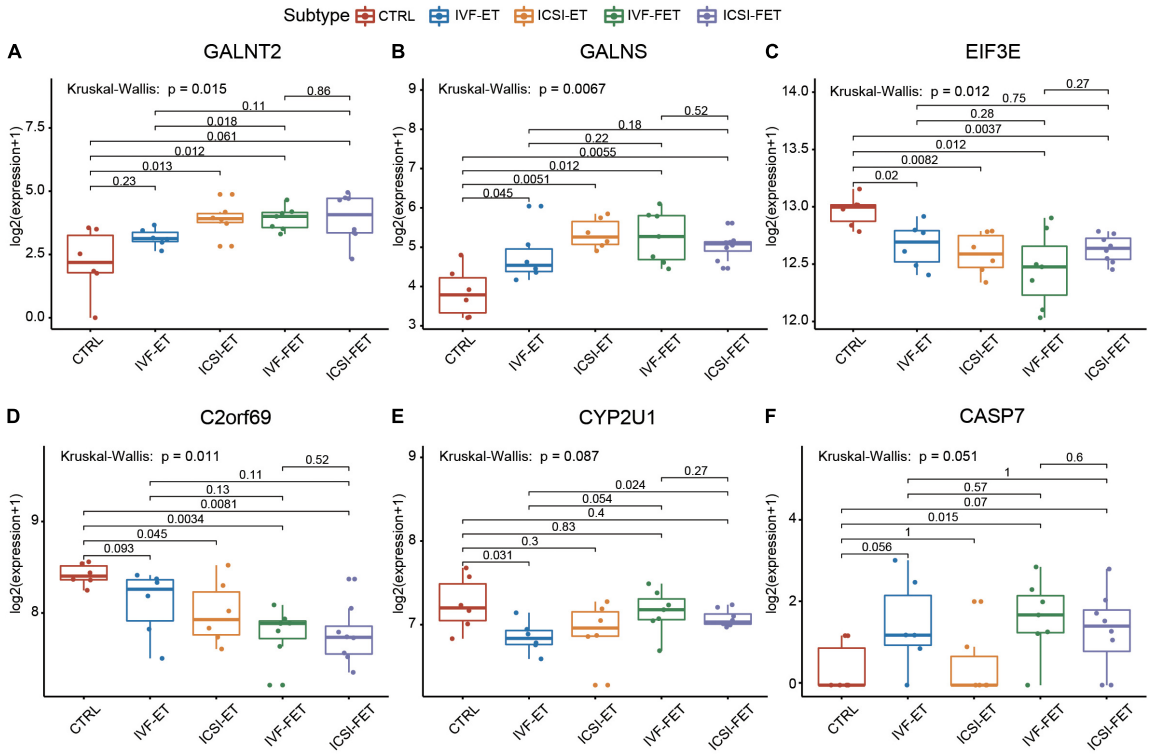

FIGURE 5 | The housekeeping genes and imprinting genes in DMSs was confirmed by RNA-seq. The expression profiles of imprinted genes and housekeeping genes in the four ART subgroups: IVF-ET, IVF-FET, ICSI-ET, and ICSI-FET, six genes had significant differences in all ART subgroups.

stage, as suggested by the Developmental Origins of Health and Disease (DOHaD) theory (Berntsen et al., 2019).

Although we used the blood sample analysis differences of DNA methylation between ART infants and natural pregnancy infants, it is reasonable that ART may have an impact on the development of nervous and immune systems. Heel blood contains a large number of white blood cells, it is easier to understand why the results of heel blood would be enriched in the immune system. Meanwhile, analysis pathway in blood and predating the dysregulation of brain tissue is comprehensively used in many different fields. The results of W Esther show that blood can serve as a surrogate marker for the brain. There is a large correlation between blood DNA methylation and brain diseases, a proportion that, although small, was significantly greater than prediction by chance. A subset of peripheral data may represent the methylation status of brain tissue. The results of Chuang et al. (2017) also showed that DNA methylation levels in human blood and saliva is associated with Parkinson's disease (Walton et al., 2016; Edgar et al., 2017; Zhang et al., 2017). Although we are not yet able to know the mental and nervous system development of these children in the future, our pathway research shows that it is consistent with current known clinical research phenomena.

We also identify three significant DMSs-located imprinted genes and 28 significant DMSs-located housekeeping genes, and these are key genes related to the development and echo the results of pathway enrichment analysis. These results collectively suggest that the ART process potentially influenced the development of the nervous system in progenies, not only by the co-effect of multiple genes of the nerve gene signaling pathway but also by influencing the methylation status of imprinted genes and housekeeping genes. These six genes, *GALNT2*, *GALNS*, *EIF3E*, *C2ORF69*, *CYP2U1*, and *CASP7*, may be the key genes affected by ART technology, the significant differences can be seen in heel blood and umbilical cord blood at the same time in all kinds of ART technology (IVF-ET, IVF-FET, ICSI-ET, and ICSI-FET), meanwhile, they are related to the nervous system and immune system.

Our findings are highly consistent with previous clinical epidemiology data and highlight the epigenetic impact of ART on the nervous system and the immune system during development. Since the first DNA methylation reprogramming starts from the two-cell stage, it may be influenced by the *in vitro* environment. Further investigation to compare the multi-cell stage embryo may help to uncover the underlying mechanism. Due to the great heterogeneity among populations (such as living habits, genetic background, reproductive age, and health status of the parents), a larger cohort is needed to systematically assess and confirm the above-mentioned epigenetic risk in ART-assisted children. At the same time, our research also has some areas that can be further optimized. For example, we can further control the homozygote and heterozygote of the sampling to ensure that our data are more accurate and reliable and expand our sample size to provide better evidence for our conclusion. Also, since the heel blood

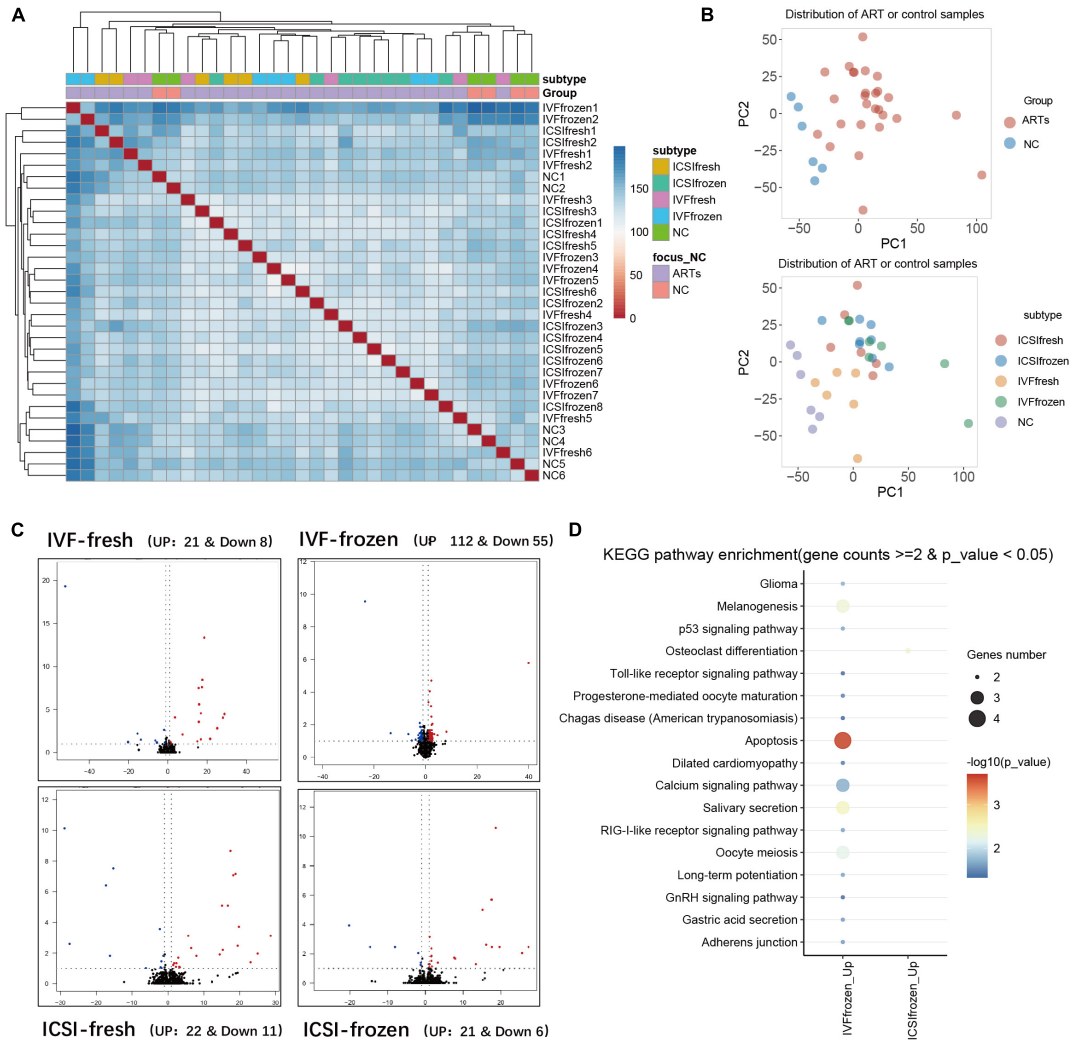

FIGURE 6 | Analysis of RNA-seq in umbilical cord blood of different types of ART and natural pregnancy infants. **(A)** Hierarchical clustering analysis of RNA seq data. **(B)** Principal component analysis (PCA) analysis of ART and natural pregnancy infants. **(C)** Differentially expressed genes (DEGs) analysis of IVF-fresh and IVF-frozen. **(D)** KEGG pathway analysis of IVF-frozen and ICSI-frozen.

was harvested 3 days post-natal, there could be some differential methylation marks added to the baby epigenetic marks. At the same time, we can ensure the quality of blood collection as much as possible, so that we can carry out multi-omics analysis of DNA methylation and transcriptome of the same infant to verify the conclusion of our heel blood data and explore the effect of ART technology on DNA methylation and the genetic pattern of newborns more accurately.

CONCLUSION

In summary, we found DMRs between ART-assisted and naturally conceived human offspring at the whole genome-wide level. These DNA methylation variations were enriched in important pathways of the immune system and nervous system.

DATA AVAILABILITY STATEMENT

The datasets presented in this study can be found in online repositories. The names of the repository/repositories and accession number(s) can be found below: https://www.ncbi.nlm.nih.gov/, GSE142554 https://www.ncbi.nlm.nih.gov/, GSE136849.

AUTHOR CONTRIBUTIONS

ZL participated in sample collection, data analysis, and manuscript writing. WC participated in sample collection and manuscript writing. YW participated in sample collection. ZZ, LH, and Y-KY participated in data analysis. JW, JQ, and YS designed the experiment and revised the article. All authors read and approved the final manuscript.

FUNDING

This work was supported by the National Natural Science Foundation of China (Grant No. 81702796), the Precision Medicine Research Program of the Chinese Academy of Sciences (Grant No. KJZD-EW-L14), the Sanming Project of Medicine in Shenzhen (Grant No. SZSM201812062), the National Key Research and Development Program of China (Grant No. 2019YFC1315701), the Cancer Hospital and Shenzhen Hospital, Chinese Academy of Medical Sciences and Peking Union Medical College (Grant No. SZ2020ZD004), and the Sanming Project of Medicine in Shenzhen (Grant No. SZSM201812062).

ACKNOWLEDGMENTS

We are sincerely grateful to the family for providing samples and offering us their trust. We also sincerely thank Shuangyan Tan and Wenxin Zhang for their help in blood sampling.

SUPPLEMENTARY MATERIAL

The Supplementary Material for this article can be found online at: https://www.frontiersin.org/articles/10.3389/fgene.2021.696840/full#supplementary-material

Supplementary Figure 1 | Correlation analysis of DNA methylation in the heel blood of the two groups of newborns. The *X*-axis represents the methylation value of each site in the ART group, and the *Y*-axis represents the methylation value of each point in the control group. Two groups have a significant correlationship $r^2 = 0.9973796$, $p = 2.2e\text{-}16$.

Supplementary Figure 2 | Differentially methylated regions (DMRs) pathway analysis. DMRs pathway analysis showed the main different pathways, which were enriched in key pathways of immune-system and neuro-system, such as the Antigen Presentation Pathway, OX40 Signaling Pathway, Neuroprotective Role of THOP1 in Alzheimer's Disease et al.

Supplementary Figure 3 | Assisted reproductive technology (ART)-conceived and naturally conceived infants could be divided into two groups by the ten most susceptible DNA methylation sites. The two components could be divided into two groups by the principal component analysis: yellow represents the ART group; Blue represents the control group.

Supplementary Figure 4 | House keeping genes and imprinting genes in DMSs was confirmed by RNA-seq. The expression profiles of *GALNT2*, *GALNS*, *EIF3E*, *C2ORF69*, *CYP2U1*, and *CASP7* in the four ART subgroups: IVF-ET, IVF-FET, ICSI-ET, and ICSI-FET, these six genes had significant differences in all ART subgroups.

Supplementary Figure 5 | Differentially expressed genes (DEGs) pathway analysis of different types of ART and natural pregnancy infants. DEGs pathway analysis showed the main different pathways, which were enriched in key pathways of immune-system and neuro-system, such as regulation of T cell activation, regulation of neural precursor cell proliferation and neuroblast proliferation et al.

Supplementary Figure 6 | Venn diagram showing the relationship with the reported genes. Venn diagram showed there were few overlaps in the differently methylated genes that have been reported.

REFERENCES

An, L., Chen, Z., Zhang, N., Ren, D., Yuan, F., Yuan, R., et al. (2019). Genetic association between CELF4 rs1557341 polymorphism and neuroticism in Chinese Han population. *Psychiatry Res.* 279, 138–139.

Anckaert, E., and Fair, T. (2015). DNA methylation reprogramming during oogenesis and interference by reproductive technologies: studies in mouse and bovine models. *Reprod. Fertil. Dev.* 27, 739–754. doi: 10.1071/rd14333

Argyraki, M., Damdimopoulou, P., Chatzimeletiou, K., Grimbizis, G. F., Tarlatzis, B. C., Syrrou, M., et al. (2019). In-utero stress and mode of conception: impact on regulation of imprinted genes, fetal development and future health. *Hum. Reprod. Update* 25, 777–801. doi: 10.1093/humupd/dmz025

Bakulski, K. M., Feinberg, J. I., Andrews, S. V., Yang, J., Brown, S., L McKenney, S., et al. (2016). DNA methylation of cord blood cell types: applications for mixed cell birth studies. *Epigenetics* 11, 354–362. doi: 10.1080/15592294.2016.1161875

Belva, F., Bonduelle, M., Roelants, M., Michielsen, D., Van Steirteghem, A., Verheyen, G., et al. (2016). Semen quality of young adult ICSI offspring: the first results. *Hum. Reprod.* 31, 2811–2820. doi: 10.1093/humrep/dew245

Berntsen, S., Soderstrom-Anttila, V., Wennerholm, U. B., Laivuori, H., Loft, A., Oldereid, N. B., et al. (2019). The health of children conceived by ART: 'the chicken or the egg?'. *Hum. Reprod. Update* 25, 137–158. doi: 10.1093/humupd/dmz001

Boulet, S. L., Kirby, R. S., Reefhuis, J., Zhang, Y., Sunderam, S., Cohen, B., et al. (2016). Assisted reproductive technology and birth defects among liveborn infants in Florida, Massachusetts, and Michigan, 2000-2010. *JAMA Pediatr.* 170:e154934. doi: 10.1001/jamapediatrics.2015.4934

Canovas, S., Ivanova, E., Romar, R., Garcia-Martinez, S., Soriano-Ubeda, C., Garcia-Vazquez, F. A., et al. (2017a). DNA methylation and gene expression changes derived from assisted reproductive technologies can be decreased by reproductive fluids. *Elife* 6:e23670.

Canovas, S., Ross, P. J., Kelsey, G., and Coy, P. (2017b). DNA methylation in embryo development: epigenetic impact of ART (assisted reproductive technologies). *BioEssays* 39.

Castillo-Fernandez, J. E., Loke, Y. J., Bass-Stringer, S., Gao, F., Xia, Y., Wu, H., et al. (2017). DNA methylation changes at infertility genes in newborn twins conceived by in vitro fertilisation. *Genome Med.* 9:28.

Choudhury, S., Liu, Y., Clark, A. F., and Pang, I. H. (2015). Caspase-7: a critical mediator of optic nerve injury-induced retinal ganglion cell death. *Mol. Neurodegener.* 10:40.

Chuang, Y. H., Paul, K. C., Bronstein, J. M., Bordelon, Y., Horvath, S., and Ritz, B. (2017). Parkinson's disease is associated with DNA methylation levels in human blood and saliva. *Genome Med.* 9:76.

De Geyter, C., Calhaz-Jorge, C., Kupka, M. S., Wyns, C., Mocanu, E., Motrenko, T., et al. (2018). ART in Europe, 2014: results generated from European registries by ESHRE: the European IVF-monitoring Consortium (EIM) for the European society of human reproduction and embryology (ESHRE). *Hum. Reprod.* 33, 1586–1601.

de Waal, E., Mak, W., Calhoun, S., Stein, P., Ord, T., Krapp, C., et al. (2014). In vitro culture increases the frequency of stochastic epigenetic errors at imprinted genes in placental tissues from mouse concepti produced through assisted reproductive technologies. *Biol. Reprod.* 90:22.

de Waal, E., Vrooman, L. A., Fischer, E., Ord, T., Mainigi, M. A., Coutifaris, C., et al. (2015). The cumulative effect of assisted reproduction procedures on placental development and epigenetic perturbations in a mouse model. *Hum. Mol. Genet.* 24, 6975–6985.

DeAngelis, A. M., Martini, A. E., and Owen, C. M. (2018). Assisted reproductive technology and epigenetics. *Semin. Reprod. Med.* 36, 221–232. doi: 10.1055/s-0038-1675780

Edgar, R. D., Jones, M. J., Meaney, M. J., Turecki, G., and Kobor, M. S. (2017). BECon: a tool for interpreting DNA methylation findings from blood in the context of brain. *Transl. Psychiatry* 7:e1187. doi: 10.1038/tp.2017.171

Eisenberg, E., and Levanon, E. Y. (2013). Human housekeeping genes, revisited. *Trends Genet.* 29 569–574. doi: 10.1016/j.tig.2013.05.010

El Hajj, N., Haertle, L., Dittrich, M., Denk, S., Lehnen, H., Hahn, T., et al. (2017). DNA methylation signatures in cord blood of ICSI children. *Hum. Reprod.* 32, 1761–1769. doi: 10.1093/humrep/dex209

Faulk, C., and Dolinoy, D. C. (2011). Timing is everything: the when and how of environmentally induced changes in the epigenome of animals. *Epigenetics* 6, 791–797. doi: 10.4161/epi.6.7.16209

Fauser, B. C. (2019). Towards the global coverage of a unified registry of IVF outcomes. *Reprod. Biomed. Online* 38, 133–137.

Fountain, C., Zhang, Y., Kissin, D. M., Schieve, L. A., Jamieson, D. J., Rice, C., et al. (2015). Association between assisted reproductive technology conception and autism in California, 1997-2007. *Am. J. Public Health* 105, 963–971. doi: 10.2105/ajph.2014.302383

Galindo, R., Banks Greenberg, M., Araki, T., Sasaki, Y., Mehta, N., Milbrandt, J., et al. (2017). NMNAT3 is protective against the effects of neonatal cerebral hypoxia-ischemia. *Ann. Clin. Transl. Neurol.* 4, 722–738. doi: 10.1002/acn3.450

Ghosh, J., Coutifaris, C., Sapienza, C., and Mainigi, M. (2017). Global DNA methylation levels are altered by modifiable clinical manipulations in assisted reproductive technologies. *Clin. Epigenetics* 9:14.

Gleicher, N., Kushnir, V. A., and Barad, D. H. (2019). Worldwide decline of IVF birth rates and its probable causes. *Hum. Reprod. Open* 2019:hoz017.

Grandjean, P., Barouki, R., Bellinger, D. C., Casteleyn, L., Chadwick, L. H., Cordier, S., et al. (2015). Life-long implications of developmental exposure to environmental stressors: new perspectives. *Endocrinology* 156, 3408–3415.

Guo, X. Y., Liu, X. M., Jin, L., Wang, T. T., Ullah, K., Sheng, J. Z., et al. (2017). Cardiovascular and metabolic profiles of offspring conceived by assisted reproductive technologies: a systematic review and meta-analysis. *Fertil. Steril.* 107, 622–631.e5.

Hanson, M. A., and Gluckman, P. D. (2014). Early developmental conditioning of later health and disease: physiology or pathophysiology? *Physiol. Rev.* 94, 1027–1076. doi: 10.1152/physrev.00029.2013

Hapairai, L. K., Mysore, K., Chen, Y., Harper, E. I., Scheel, M. P., Lesnik, A. M., et al. (2017). Lure-and-Kill yeast interfering RNA larvicides targeting neural genes in the human disease vector mosquito *Aedes aegypti*. *Sci. Rep.* 7:13223.

Haruyama, N., Sakumi, K., Katogi, A., Tsuchimoto, D., De Luca, G., Bignami, M., et al. (2019). 8-Oxoguanine accumulation in aged female brain impairs neurogenesis in the dentate gyrus and major island of Calleja, causing sexually dimorphic phenotypes. *Prog. Neurobiol.* 180:101613. doi: 10.1016/j.pneurobio.2019.04.002

Hattori, H., Hiura, H., Kitamura, A., Miyauchi, N., Kobayashi, N., Takahashi, S., et al. (2019). Association of four imprinting disorders and ART. *Clin. Epigenet.* 11:21.

Heindel, J. J., Blumberg, B., Cave, M., Machtinger, R., Mantovani, A., Mendez, M. A., et al. (2017). Metabolism disrupting chemicals and metabolic disorders. *Reprod. Toxicol.* 68, 3–33.

Houseman, E. A., Accomando, W. P., Koestler, D. C., Christensen, B. C., Marsit, C. J., Nelson, H. H., et al. (2012). DNA methylation arrays as surrogate measures of cell mixture distribution. *BMC Bioinformatics* 13:86. doi: 10.1186/1471-2105-13-86

Jones, M. J., Islam, S. A., Edgar, R. D., and Kobor, M. S. (2017). Adjusting for Cell type composition in DNA methylation data using a regression-based approach. *Methods Mol. Biol.* 1589, 99–106. doi: 10.1007/7651_2015_262

Kollmann, Z., Schneider, S., Fux, M., Bersinger, N. A., and von Wolff, M. (2017). Gonadotrophin stimulation in IVF alters the immune cell profile in follicular fluid and the cytokine concentrations in follicular fluid and serum. *Hum. Reprod.* 32, 820–831. doi: 10.1093/humrep/dex005

Koot, Y. E., van Hooff, S. R., Boomsma, C. M., van Leenen, D., Groot Koerkamp, M. J., Goddijn, M., et al. (2016). An endometrial gene expression signature accurately predicts recurrent implantation failure after IVF. *Sci. Rep.* 6:19411.

Leaver, M., and Wells, D. (2019). Non-invasive preimplantation genetic testing (niPGT): the next revolution in reproductive genetics? *Hum. Reprod. Update*

Li, C., Bazzano, L. A., Rao, D. C., Hixson, J. E., He, J., Gu, D., et al. (2015). Genome-wide linkage and positional association analyses identify associations of novel AFF3 and NTM genes with triglycerides: the GenSalt study. *J. Genet. Genomics* 42, 107–117. doi: 10.1016/j.jgg.2015.02.003

Li, G., Xie, C., Wang, Q., Wan, D., Zhang, Y., Wu, X., et al. (2019). Uridine/UMP metabolism and their function on the gut in segregated early weaned piglets. *Food Funct.* 10, 4081–4089. doi: 10.1039/c9fo00360f

Li, T., Liu, Y., Yue, S., Liao, Z., Luo, Z., Wang, M., et al. (2019). Analyzing the effects of intrauterine hypoxia on gene expression in oocytes of rat offspring by single cell transcriptome sequencing. *Front. Genet.* 10:1102. doi: 10.3389/fgene.2019.01102

Lin, X., Tan, J. Y. L., Teh, A. L., Lim, I. Y., Liew, S. J., MacIsaac, J. L., et al. (2018). Cell type-specific DNA methylation in neonatal cord tissue and cord blood: a 850K-reference panel and comparison of cell types. *Epigenetics* 13, 941–958. doi: 10.1080/15592294.2018.1522929

Liu, H., Zhang, Y., Gu, H. T., Feng, Q. L., Liu, J. Y., Zhou, J., et al. (2015). Association between assisted reproductive technology and cardiac alteration at age 5 years. *JAMA Pediatr.* 169, 603–605. doi: 10.1001/jamapediatrics.2015.0214

Liu, L., Gao, J., He, X., Cai, Y., Wang, L., and Fan, X. (2017). Association between assisted reproductive technology and the risk of autism spectrum disorders in the offspring: a meta-analysis. *Sci. Rep.* 7:46207.

Lo, Y. M., Lau, T. K., Chan, L. Y., Leung, T. N., and Chang, A. M. (2000). Quantitative analysis of the bidirectional fetomaternal transfer of nucleated cells and plasma DNA. *Clin. Chem.* 46, 1301–1309. doi: 10.1093/clinchem/46.9.1301

Lo, Y. M., Lo, E. S., Watson, N., Noakes, L., Sargent, I. L., Thilaganathan, B., et al. (1996). Two-way cell traffic between mother and fetus: biologic and clinical implications. *Blood* 88, 4390–4395.

Mani, S., and Mainigi, M. (2018). Embryo culture conditions and the epigenome. *Semin. Reprod. Med.* 36, 211–220. doi: 10.1055/s-0038-1675777

Maruani, A., Huguet, G., Beggiato, A., ElMaleh, M., Toro, R., Leblond, C. S., et al. (2015). 11q24.2-25 micro-rearrangements in autism spectrum disorders: relation to brain structures. *Am. J. Med. Genet. A* 167A, 3019–3030.

Melamed, N., Choufani, S., Wilkins-Haug, L. E., Koren, G., and Weksberg, R. (2015). Comparison of genome-wide and gene-specific DNA methylation between ART and naturally conceived pregnancies. *Epigenetics* 10, 474–483. doi: 10.4161/15592294.2014.988041

Menezo, Y., Clement, P., and Dale, B. (2019). DNA Methylation patterns in the early human embryo and the epigenetic/imprinting problems: a plea for a more careful approach to human assisted reproductive technology (ART). *Int. J. Mol. Sci.* 20:1342. doi: 10.3390/ijms20061342

Nelissen, E. C., Dumoulin, J. C., Busato, F., Ponger, L., Eijssen, L. M., Evers, J. L., et al. (2014). Altered gene expression in human placentas after IVF/ICSI. *Hum. Reprod.* 29, 2821–2831. doi: 10.1093/humrep/deu241

Nousbeck, J., Spiegel, R., Ishida-Yamamoto, A., Indelman, M., Shani-Adir, A., Adir, N., et al. (2008). Alopecia, neurological defects, and endocrinopathy syndrome caused by decreased expression of RBM28, a nucleolar protein associated with ribosome biogenesis. *Am. J. Hum. Genet.* 82, 1114–1121.

Park, B., Kim, Y., Shin, J., Lee, S., Cho, K., Fruh, K., et al. (2004). Human cytomegalovirus inhibits tapasin-dependent peptide loading and optimization of the MHC class I peptide cargo for immune evasion. *Immunity* 20, 71–85. doi: 10.1016/s1074-7613(03)00355-8

Pathare, A. D. S., Zaveri, K., and Hinduja, I. (2017). Downregulation of genes related to immune and inflammatory response in IVF implantation failure cases under controlled ovarian stimulation. *Am. J. Reprod. Immunol.* 78.

Praest, P., Luteijn, R. D., Brak-Boer, I. G. J., Lanfermeijer, J., Hoelen, H., Ijgosse, L., et al. (2018). The influence of TAP1 and TAP2 gene polymorphisms on TAP function and its inhibition by viral immune evasion proteins. *Mol. Immunol.* 101, 55–64.

Pudelko, L., Rouhi, P., Sanjiv, K., Gad, H., Kalderen, C., Hoglund, A., et al. (2017). Glioblastoma and glioblastoma stem cells are dependent on functional MTH1. *Oncotarget* 8, 84671–84684. doi: 10.18632/oncotarget.19404

Qiu, Y. H., Deng, F. Y., Tang, Z. X., Jiang, Z. H., and Lei, S. F. (2015). Functional relevance for type 1 diabetes mellitus-associated genetic variants by using integrative analyses. *Hum. Immunol.* 76, 753–758. doi: 10.1016/j.humimm.2015.09.033

Qu, H. Q., Lu, Y., Marchand, L., Bacot, F., Frechette, R., Tessier, M. C., et al. (2007). Genetic control of alternative splicing in the TAP2 gene: possible implication in the genetics of type 1 diabetes. *Diabetes* 56, 270–275. doi: 10.2337/db06-0865

Rao, M., Zeng, Z., and Tang, L. (2018). Maternal physical activity before IVF/ICSI cycles improves clinical pregnancy rate and live birth rate: a systematic review and meta-analysis. *Reprod. Biol. Endocrinol.* 16:11.

Rumbold, A. R., Moore, V. M., Whitrow, M. J., Oswald, T. K., Moran, L. J., Fernandez, R. C., et al. (2017). The impact of specific fertility treatments on cognitive development in childhood and adolescence: a systematic review. *Hum. Reprod.* 32, 1489–1507. doi: 10.1093/humrep/dex085

Salilew-Wondim, D., Fournier, E., Hoelker, M., Saeed-Zidane, M., Tholen, E., Looft, C., et al. (2015). Genome-wide DNA methylation patterns of bovine blastocysts developed in vivo from embryos completed different stages of development in vitro. *PLoS One* 10:e0140467. doi: 10.1371/journal.pone.0140467

Sandin, S., Nygren, K. G., Iliadou, A., Hultman, C. M., and Reichenberg, A. (2013). Autism and mental retardation among offspring born after in vitro fertilization. *JAMA* 310, 75–84. doi: 10.1001/jama.2013.7222

Simopoulou, M., Sfakianoudis, K., Antoniou, N., Maziotis, E., Rapani, A., Bakas, P., et al. (2018). Making IVF more effective through the evolution of prediction models: is prognosis the missing piece of the puzzle? *Syst. Biol. Reprod. Med.* 64, 305–323. doi: 10.1080/19396368.2018.1504347

Tamarozzi, E. R., Torrieri, E., Semighini, E. P., and Giuliatti, S. (2014). In silico analysis of mutations occurring in the protein N-acetylgalactosamine-6-sulfatase (GALNS) and causing mucopolysaccharidosis IVA. *Genet. Mol. Res.* 13, 10025–10034. doi: 10.4238/2014.november.28.7

Tan, K., Zhang, Z., Miao, K., Yu, Y., Sui, L., Tian, J., et al. (2016). Dynamic integrated analysis of DNA methylation and gene expression profiles in in vivo and in vitro fertilized mouse post-implantation extraembryonic and placental tissues. *Mol. Hum. Reprod.* 22, 485–498. doi: 10.1093/molehr/gaw028

Tararbit, K., Lelong, N., Thieulin, A. C., Houyel, L., Bonnet, D., Goffinet, F., et al. (2013). The risk for four specific congenital heart defects associated with assisted reproductive techniques: a population-based evaluation. *Hum. Reprod.* 28, 367–374. doi: 10.1093/humrep/des400

Van Voorhis, B. J. (2007). Clinical practice. In vitro fertilization. *N. Engl. J. Med.* 356, 379–386.

Wade, J. J., MacLachlan, V., and Kovacs, G. (2015). The success rate of IVF has significantly improved over the last decade. *Austr. N. Z. J. Obstet. Gynaecol.* 55, 473–476. doi: 10.1111/ajo.12356

Walton, E., Hass, J., Liu, J., Roffman, J. L., Bernardoni, F., Roessner, V., et al. (2016). Correspondence of DNA methylation between blood and brain tissue and its application to schizophrenia research. *Schizophr. Bull.* 42, 406–414. doi: 10.1093/schbul/sbv074

Wang, X., Sun, C. L., Quinones-Lombrana, A., Singh, P., Landier, W., Hageman, L., et al. (2016). CELF4 variant and anthracycline-related cardiomyopathy: a children's oncology group genome-wide association study. *J. Clin. Oncol.* 34, 863–870. doi: 10.1200/jco.2015.63.4550

Williams, A. P., Bevan, S., Bunce, M., Houlston, R., Welsh, K. I., and Elliott, T. (2000). Identification of novel Tapasin polymorphisms and linkage disequilibrium to MHC class I alleles. *Immunogenetics* 52, 9–11. doi: 10.1007/s002510000244

Williams, A. P., Peh, C. A., Purcell, A. W., McCluskey, J., and Elliott, T. (2002). Optimization of the MHC class I peptide cargo is dependent on tapasin. *Immunity* 16, 509–520. doi: 10.1016/s1074-7613(02)00304-7

Wright, K., Brown, L., Brown, G., Casson, P., and Brown, S. (2011). Microarray assessment of methylation in individual mouse blastocyst stage embryos shows that in vitro culture may have widespread genomic effects. *Hum. Reprod.* 26, 2576–2585. doi: 10.1093/humrep/der201

Yamazaki, Y., Mann, M. R., Lee, S. S., Marh, J., McCarrey, J. R., Yanagimachi, R., et al. (2003). Reprogramming of primordial germ cells begins before migration into the genital ridge, making these cells inadequate donors for reproductive cloning. *Proc. Natl. Acad. Sci. U. S. A.* 100, 12207–12212. doi: 10.1073/pnas.2035119100

Zhang, Y., Liu, H., Lv, J., Xiao, X., Zhu, J., Liu, X., et al. (2011). QDMR: a quantitative method for identification of differentially methylated regions by entropy. *Nucleic Acids Res.* 39:e58. doi: 10.1093/nar/gkr053

Zhang, Y., Wilson, R., Heiss, J., Breitling, L. P., Saum, K. U., Schöttker, B., et al. (2017). DNA methylation signatures in peripheral blood strongly predict all-cause mortality. *Nat. Commun.* 8:14617.

Zhu, K. W., Chen, P., Zhang, D. Y., Yan, H., Liu, H., Cen, L. N., et al. (2018). Association of genetic polymorphisms in genes involved in Ara-C and dNTP metabolism pathway with chemosensitivity and prognosis of adult acute myeloid leukemia (AML). *J. Transl. Med.* 16:90.

Conflict of Interest: ZZ was employed by the company Tianjin Novogene Bioinformatic Technology Co., Ltd., China.

The remaining authors declare that the research was conducted in the absence of any commercial or financial relationships that could be construed as a potential conflict of interest.

Publisher's Note: All claims expressed in this article are solely those of the authors and do not necessarily represent those of their affiliated organizations, or those of the publisher, the editors and the reviewers. Any product that may be evaluated in this article, or claim that may be made by its manufacturer, is not guaranteed or endorsed by the publisher.

frontiers in Cell and Developmental Biology

REVIEW
published: 11 October 2021
doi: 10.3389/fcell.2021.753931

Interactions Among lncRNA/circRNA, miRNA, and mRNA in Musculoskeletal Degenerative Diseases

Yi-Li Zheng[1†], Ge Song[1†], Jia-Bao Guo[2], Xuan Su[1], Yu-Meng Chen[1], Zheng Yang[1], Pei-Jie Chen[1] and Xue-Qiang Wang[1,3*]*

[1] Department of Sport Rehabilitation, Shanghai University of Sport, Shanghai, China, [2] The Second School of Clinical Medicine, Xuzhou Medical University, Xuzhou, China, [3] Department of Rehabilitation Medicine, Shanghai Shangti Orthopaedic Hospital, Shanghai, China

OPEN ACCESS

Edited by:
Zhao-Qian Teng,
Institute of Zoology, Chinese Academy of Sciences (CAS), China

Reviewed by:
Lei Zhao,
University of Wisconsin-Madison, United States
Jun Zou,
Soochow University, China

***Correspondence:**
Pei-Jie Chen
chenpeijie@sus.edu.cn
Xue-Qiang Wang
wangxueqiang@sus.edu.cn

[†] These authors have contributed equally to this work and share first authorship

Specialty section:
This article was submitted to Epigenomics and Epigenetics, a section of the journal Frontiers in Cell and Developmental Biology

Received: 05 August 2021
Accepted: 22 September 2021
Published: 11 October 2021

Citation:
Zheng Y-L, Song G, Guo J-B, Su X, Chen Y-M, Yang Z, Chen P-J and Wang X-Q (2021) Interactions Among lncRNA/circRNA, miRNA, and mRNA in Musculoskeletal Degenerative Diseases. Front. Cell Dev. Biol. 9:753931. doi: 10.3389/fcell.2021.753931

Musculoskeletal degenerative diseases (MSDDs) are pathological conditions that affect muscle, bone, cartilage, joint and connective tissue, leading to physical and functional impairments in patients, mainly consist of osteoarthritis (OA), intervertebral disc degeneration (IDD), rheumatoid arthritis (RA) and ankylosing spondylitis (AS). Long non-coding RNAs (lncRNAs) and circular RNAs (circRNAs) are novel regulators of gene expression that play an important role in biological regulation, involving in chondrocyte proliferation and apoptosis, extracellular matrix degradation and peripheral blood mononuclear cell inflammation. Research on MSDD pathogenesis, especially on RA and AS, is still in its infancy and major knowledge gaps remain to be filled. The effects of lncRNA/circRNA-miRNA-mRNA axis on MSDD progression help us to fully understand their contribution to the dynamic cellular processes, provide the potential OA, IDD, RA and AS therapeutic strategies. Further studies are needed to explore the mutual regulatory mechanisms between lncRNA/circRNA regulation and effective therapeutic interventions in the pathology of MSDD.

Keywords: degenerative musculoskeletal disorders, aging, age-related disease, non-coding RNAs, miRNA, circRNA, lncRNA

INTRODUCTION

Musculoskeletal degenerative diseases (MSDDs) are pathological conditions that affect muscle, bone, cartilage, joint and connective tissue, leading to physical and functional impairment in patients (Chen Y. et al., 2017; Huo et al., 2018). With the acceleration of the global aging process, the prevalence of MSDD is increasing. This is a huge challenge for patients and healthcare workers, and adds to the global healthcare burden (Li and Chen, 2019). The main MSDD consists of osteoarthritis (OA), intervertebral disc degeneration (IDD), rheumatoid arthritis (RA), and ankylosing spondylitis (AS) (Vinatier et al., 2016; Huo et al., 2018; Loef et al., 2018). OA is a chronic age-related MSDD, featuring for subchondral bone thickening, articular cartilage degradation, and osteophyte formation (Loeser et al., 2012; Hunter and Bierma-Zeinstra, 2019). IDD is also age-related and is caused by progressive degeneration of the disk (Yang S. et al., 2020), causing loss of disk height, reduced hydration and decreased potential to absorb load (Samartzis et al., 2011; Cooper et al., 2016). RA is an autoimmune disease characterized by aggressive arthritis that can

lead to joint deformities and loss of function (Smolen et al., 2016). AS, a rare but clear cause of chronic back pain, is an inflammatory disease involving the spine, sacroiliac joints and other joints (Taurog et al., 2016). OA and IDD became mainly responsible for MSDD. Their common character is the broken dynamic equilibrium between catabolism and anabolism in the extracellular matrix (ECM). On the one hand, chondrocytes is only resident cells in the articular system, the ECM degeneration in OA is leaded by chondrocytes' catabolic and abnormal differentiation (Zhou Z.B. et al., 2019). Cartilage cellularity is reduced in OA because of chondrocyte death. On the other hand, ECM breakdown and abnormal matrix synthesis in IDD is responsible by nucleus pulposus (NP) cells, which are predominant cells in the NP tissue (Fontana et al., 2015). Excessive apoptosis of NP cells could accelerate IDD progression (Zhao et al., 2006). Meanwhile, endplate cartilage degeneration is another risk factor of IDD (Iwakura et al., 2013) due to its irreplaceable nutrition supplement of intervertebral disk (Yuan et al., 2015). Although multiple factors are involved in the pathogenesis of MSDD (Li and Chen, 2019), the development of molecular mechanism of MSDD is still poor. Thus, it is urgent to discover new biomarkers to optimize MSDD early diagnosis and treatment.

With the development of sequencing technology, recent advances have shown that about 98% of the human genome is composed of non-coding RNAs (ncRNAs). In the past, ncRNAs were thought to act as 'evolutionary junk.' However, an increasing amount of evidence reported that ncRNAs play an important role in biological regulation (Beermann et al., 2016; Vieira et al., 2018). The main types of ncRNAs include long non-coding RNA (lncRNA), circular RNA (circRNA) and microRNA (miRNA) (Beermann et al., 2016). Recently, extensive evidence suggested that ncRNAs play a vital role in the development of MSDD (Chen W.K. et al., 2017; Yu and Sun, 2018; Wang J. et al., 2019). Moreover, circRNA and lncRNA can interact with miRNA to further regulate downstream target mRNA in the MSDD and play regulatory roles in numerous biological functions, such as proliferation, apoptosis and inflammation. In this review, we focused on the role of lncRNA/circRNA-miRNA-mRNA axis in the development of MSDD and further explored related molecular mechanism of MSDD.

INTERACTIONS BETWEEN lncRNA/circRNA and miRNA

Interactions Between lncRNA and miRNA

MicroRNAs are encoded by endogenous genes, are approximately 20 nucleotides in length and are non-coding single-stranded RNA molecules (Beermann et al., 2016). Since they were first described in *Caenorhabditis elegans*, the number of miRNAs that have been found in mammals increased (Lee et al., 1993). miRNA is evolutionarily conserved and regulates gene expression at the post-transcriptional level by interfering with mRNA translation and degradation (Zhang et al., 2020b). With the iteration of gene chip and sequencing technology, numerous miRNAs have been found to play important roles in MSDD and can be used as biomarkers for clinical diagnosis and treatment (Satoshi Yamashita, 2012; Seeliger et al., 2016; Moran-Moguel et al., 2018). lncRNAs refers to non-protein-coding transcripts with the lengths of more than 200 nucleotides (Beermann et al., 2016). According to the position of the protein-encoding genes in the genome, lncRNAs are divided into five types, namely, intronic, intergenic, bidirectional, sense and antisense (Wang J. et al., 2019). More and more evidence argues that lncRNAs can act as an enhancer or suppressor to regulate the immune response at the epigenetic level, function as scaffold molecules through interactions with RNA-binding proteins in chromatin remodeling complexes (Mathy and Chen, 2017), and then, are involved in many cellular and biological processes in MSDD, such as proliferation, apoptosis, differentiation, inflammation and ECM degradation (Jiang et al., 2017; Li Z. et al., 2018; Abbasifard et al., 2020). Thus, it is important to develop lncRNA as a biomarker and therapeutic target for MSDD.

In recent years, extensive evidence has shown that lncRNAs can interact with miRNAs through several post-transcriptional mechanisms, and the four mechanisms of interaction are as follows. (1) lncRNAs act as miRNA sponges. The lncRNA that can prevent miRNA from acting on mRNA is called competing endogenous RNAs (ceRNAs). These lncRNAs have similar miRNA targets, and they can act as sponges of miRNA, thereby reducing the expression of miRNA and enhancing the translation of target mRNA. lncRNA AK048451 was first considered as an endogenous sponge of miR-489 that can combine with and inhibit the expression of miR-489 (Huang, 2018). (2) Several lncRNAs could directly compete with miRNAs to bind with mRNAs, thereby removing the regulatory roles of miRNAs on mRNAs. For example, lncRNA BACE1AS competes with miR-485-5p to combine with BACE1 mRNA. Thus, the degradation of BACE1 induced by miR-485-5p was inhibited (Faghihi et al., 2010). (3) miRNAs aim at lncRNAs to decrease the stability of lncRNAs and affect the abundance of lncRNAs. It has been verified that lncRNA-p21 was modulated by miRNA let-7b. Upregulation of let-7b promoted the degradation of RNA, leading to the instability of lncRNA-p21 (Deng et al., 2016). (4) Several lncRNAs could generate miRNAs. For instance, lncRNA H19 can generate miR-675 (Deng et al., 2016). To achieve a better understanding of the molecular mechanisms in MSDD progression, in-depth studies about the effects of lncRNAs and their potential downstream miRNA regulators have been performed in recent years.

Interactions Between circRNA and miRNA

As endogenous RNAs, circRNAs are characterize by covalent loop structures without 5′–3′ polarity nor a polya- denylated tail (Zhou et al., 2018). Different from linear RNA, circRNAs are inherently conserved due to their closed covalent structure and resistance to exonuclides; they are considered to be stable in exosomes (Haque and Harries, 2017). circRNAs are classified into four

types according to their origin, namely, exonic circRNAs, exon-intron circRNAs, intronic circRNAs and intergenic circRNAs (Deng et al., 2016). A growing number of studies indicate that circRNAs exist miRNA complementary binding sites to interact with miRNAs, thereby playing regulatory roles in diseases and effecting in many biological processes, such as inflammation, apoptosis and ECM degradation, by participating in the modulation of transcriptional and post-transcriptional levels (Rong et al., 2017; Verduci et al., 2019). The mechanisms included circRNAs acting as miRNAs sponges and miRNAs regulating circRNAs (Kulcheski et al., 2016). For instance, the circAnks1a could regulate VEGFB (vascular endothelial growth factor-B) expression to suppress the excitability of spinal cord by sponging miR-324-3p in neuropathic pain (Zhang S.B. et al., 2019). Pan et al. (2019) elucidated that the miR-1224 could mediate circRNA-Filip1l expression through regulating Ubr5 in the spinal cord of chronic inflammatory pain mice. Although circRNAs are generally considered as ncRNAs because of non-linear structure, several circRNAs, such as CircFBXW7 (Ye et al., 2019) and Circ-EGFR (Liu et al., 2021), are proved to have translation functions due to its translatable open reading frame containing a start codon. The cap-independent translation pathway is thought to be the main mechanism of circRNA translation to encode protein (He et al., 2021). Combined with the above explanation, currently known that circRNAs can interact with proteins or act as miRNA sponges and regulate the expression of upstream gene to participate in the process of diseases development. In recent years, circRNAs have become a research hotspot in MSDD and showed great potential as biomarkers and therapeutic targets (Li H.Z. et al., 2018; Lei B. et al., 2019; Wu et al., 2019).

INTERACTIONS AMONG lncRNA, miRNA, AND mRNA IN DEGENERATIVE MUSCULOSKELETAL DISEASES

Osteoarthritis

In the past decade, quite number of studies have shown that the interaction between lnRNAs and miRNAs is involved in the multiple biological processes of OA, such as inflammation, proliferation, apoptosis, autophagy, cell viability and ECM degradation (**Table 1**). The major interaction mechanism between lncRNA and miRNA in OA was that lncRNAs as ceRNAs acts as miRNAs sponges. Wang Q. et al. (2017) reported that the expressions of lncRNA OPN and NEAT1 significantly increased, whereas that of miR-181c decreased. According to luciferase assays, miR-181c could combine with NEAT1 and 3′UTR of OPN in synoviocytes, leading to NEAT1 competing with OPN for binding with miR-181c and further enhancing the level of OPN. Chen Y. et al. (2020) showed that lncRNA HOTAIR (HOX transcript antisense intergenic RNA) and mRNA PTEN (phosphatase and tensin homolog) was significantly increased in the OA mice, whereas miR-20b decreased. HOTAIR was involved in the process of apoptosis and ECM degradation by sponging miR-20b and regulating the downstream target PTEN. Lu and Zhou (2020) revealed that lncRNA00662 was downregulated in the cartilage of OA rats. The expression of miR-15b-5p was negative with lncRNA00662, whereas the expression of GPR120 was positively correlated with lncRNA00662. lncRNA00662 regulated GPR120 in apoptosis by serving as a sponge for miR-15b-5p. Sun P. et al. (2020) also studied the effect of XIST on OA patients and showed that XIST upregulated SGTB and inhibited the depression on SGTB induced by miR-142-5p through sponging miR-142-5p. Another study reported that the level of lnc00623 and HRAS was downregulated, whereas miR-101 was increased in OA tissues compared with normal tissues (Lü et al., 2020). Based on luciferase reporter, miR-101 could combine with lnc00623 and HRAS. lnc00623 sponges miR-101 through competing with HRAS, thereby preventing the miR-101-induced depression on HRAS. Some other lncRNAs act as miRNAs sponges in OA and more detailed information is presented in **Table 1**.

Intervertebral Disk Degeneration

The mechanism by which lncRNA and miRNA act on IDD that has been most studied is as follows: lncRNA acts as the sponge of miRNA to modulate target genes (**Figure 1**). Xi et al. (2017) demonstrated that lncRNA HCG18 was upregulated in the IDD and plays the sponge roles of miR-146a-5p in NP cells. HCG18 is involved in the progression of cell proliferation and apoptosis in NP cells via the miR-146a-5p/TARF6/NF-κB axis. Compared with normal NP tissues, lncRNA SNHG1 (small nucleolar RNA host gene 1) expression was boosted and miR-326, a target gene of SNHG1, was reduced in IDD samples (Tan et al., 2018). Moreover, miR-326 could directly bind with Cyclin D1 (CCND1), and the level of CCND1 in the NP cells markedly increased. Thus, Tan et al. (2018) observed that SNHG1 modulates NP cells proliferation via sponging miR-326 and further regulating CCND1. Another study reported that lncRNA H19 was upregulated in the IDD tissues and could activate Wnt/β-catenin signaling pathway (Wang et al., 2018d). Moreover, miR-326 could directly bind with Cyclin D1 (CCND1), and the level of CCND1 in the NP cells markedly increased. Thus, Tan et al. (2018) observed that SNHG1 modulates NP cells proliferation via sponging miR-326 and further regulating CCND1. Another study reported that lncRNA H19 was upregulated in the IDD tissues and could activate Wnt/β-catenin signaling pathway (Shao et al., 2019). Another research suggested that LINC00641 level increased in NP tissues, whereas miR-153-3p level decreased. ATG5 (autophagy-related gene 5) was a downstream gene of miR-153-3p and upregulated in NP cells (Wang J. et al., 2019). Moreover, LINC00641 could sponge miR-153-3p, and thereby regulate the level of ATG5, cell death and the progression of IDD. Yang Y. et al. (2019) elucidated that lncRNA lincRNA-SLC20A1 (SLC20A1) was overexpressed in IDD patients, and SLC20A1 could induce ECM degradation via sponging miR-31-5p and further modulating the downstream target gene MMP3. Another study established that the level of lncRNA PART1 and mRNA matrix metallopeptidase 2 (MMP2) in NP tissues were significantly higher than those in the control groups, whereas

TABLE 1 | lncRNA/miRNA/mRNA networks in osteoarthritis.

	Species	Diseases	Region	lncRNA	Change	miRNA	Expression	Target gene	Change	Functions	References
(1)	Human	OA	Cartilage	H19	Up	miR-675	Up	COL2A1	Up	Inflammation	Steck et al., 2012
(2)	Human, mice	OA	Cartilage, chondrocyte	GAS5	Up	miR-21	Down	MMPs, ADAMTS-4	Up	Cell apoptosis and autophagy	Song et al., 2014
(3)	Human	OA	Cartilage, chondrocyte	lncRNA-MSR	Up	miRNA-152	Down	TMSB4	Up	ECM degradation	Liu et al., 2016a
(4)	Human	OA	Cartilage, chondrocyte	UFC1	Down	miR-34a	Up	–	–	Cell proliferation and apoptosis	Zhang et al., 2016
(5)	Human	OA	Chondrocyte, C28/I2 cells	HOTAIR	Up	miR-17-3p	Down	ETV1	Up	Cell apoptosis and inflammation	Chen H. et al., 2017
(6)	Human	OA	Cartilage, chondrocyte	lncRNA PVT1	Up	miR-488-3p	Down	–	–	Cell apoptosis	Li Y. et al., 2017
(7)	Human	OA	Cartilage, chondrocyte	lncRNA CIR	Up	miR-27	Down	MMP13	Up	ECM degradation	Li Y.F. et al., 2017
(8)	Human	OA	Cartilage, chondrocyte	lncRNA -UCA1	Up	miR-204-5p	Down	MMP13	Up	Cell proliferation	Wang G. et al., 2017
(9)	Human	OA	Synovium tissues, synoviocytes	NEAT1	Up	miR-181c	Down	OPN	Up	Cell proliferation	Wang Q. et al., 2017
(10)	Rats	OA	Cartilage, chondrocyte	lncRNA MEG3	Down	miR-16	Up	SMAD7	Down	Cell proliferation and apoptosis	Xu and Xu, 2017
(11)	Human	OA	Cartilage, chondrocyte	lncRNA FOXD2-AS1	Up	miR-206	Down	CCND1	Up	Cell proliferation and apoptosis	Cao et al., 2018
(12)	Human	OA	Cartilage, chondrocyte	DANCR	Up	miR-577	Down	SphK2	Up	Cell proliferation and apoptosis	Fan et al., 2018
(13)	Human	OA	Cartilage, chondrocyte	HOTAIR	Up	miR-17-5p	Down	FUT2	Up	Cell proliferation, apoptosis and ECM degradation	Hu et al., 2018
(14)	Human	OA	Cartilage, chondrocyte	XIST	Up	miR-211	Down	CXCR4	Up	Cell proliferation and apoptosis	Mohammadi et al., 2018
(15)	Human	OA	Cartilage, chondrocyte	MALAT1	Up	miR-127-5p	Down	PI3K/Akt	Up	Cell proliferation	Liang et al., 2018
(16)	Mice	OA	Cartilage, chondrocyte	lncRNA-KLF3-AS1	Up	miR-206	Down	GIT1	Up	Cell proliferation and apoptosis	Liu et al., 2018
(17)	Human	OA	Cartilage, chondrocyte	lncRNA CIR	Up	miR-130a	Down	Bim	Up	Cell apoptosis and inflammation	Lu Z. et al., 2019
(18)	Murine	OA	Chondrogenic ATDC5 cells	MALAT1	Up	miR-19b	Down	Wnt/β-catenin and NF-κB pathways	Up	Cell apoptosis and inflammation	Pan et al., 2018
(19)	Human	OA	Cartilage, chondrocyte	lncRNA SNHG5	Down	miR-26a	Up	SOX2	Down	Cell proliferation	Shen et al., 2018
(20)	Human	OA	Human cartilage ATDC5 cells	lncRNA RP11-445H22.4	Up	miR-301a	Down	CXCR4	Up	Cell viability, apoptosis and inflammation	Sun et al., 2018
(21)	Human	OA	Cartilage, chondrocyte	lncRNA -p21	Up	miR-451	Down	–	–	Cell apoptosis	Tang L. et al., 2018
(22)	Human	OA	Cartilage, chondrocyte	lncRNA TUG1	Up	miR-195	Down	MMP13	Up	ECM degradation	Tang L.P. et al., 2018
(23)	Human	OA	ATDC5 cell	MEG3	Down	miR-203	Up	Sirt1	Up	Cell viability, apoptosis and inflammation	Wang et al., 2018e
(24)	Human	OA	Cartilage, chondrocyte	lncRNA DANCR	Up	miR-216a-5p	Down	JAK2/STAT3 signal pathway	Up	Cell proliferation, apoptosis and inflammation	Zhang et al., 2018
(25)	Human	OA	Cartilage, chondrocyte	PVT1	Up	miR-149	Down	–	–	Inflammation	Zhao et al., 2018
(26)	Human	OA	Cartilage, chondrocyte	lncRNA DNM3OS	Down	miR-126	Up	IGF1	Down	Cell proliferation and apoptosis	Ai and Yu, 2019
(27)	Rats	OA	Cartilage, chondrocyte	MEG3	Down	miR-93	Up	TGFBR2	Down	Cell proliferation, apoptosis and ECM degradation	Chen et al., 2019

(Continued)

TABLE 1 | (Continued)

	Species	Diseases	Region	lncRNA	Change	miRNA	Expression	Target gene	Change	Functions	References
(28)	Human	OA	Cartilage, ATDC5 cells	lncRNA-HULC	Down	miR-101	Up	NF-κB and p38MAPK signaling pathways	Down	Inflammation	Chu et al., 2019
(29)	Human	OA	Synovial fluid, chondrocytes	MCM3AP-AS1	Up	miR-142-3p	Down	HMGB1	Up	Cell apoptosis	Gao et al., 2019
(30)	Human	OA	LPS-treated C28/I2 cells	H19	Up	miR-130a	Down	–	–	Cell viability, apoptosis, and inflammation	Hu et al., 2019
(31)	Human	OA	Cartilage, chondrocyte	TNFSF10	Up	miR-376-3p	Down	FGFR1	Up	Cell proliferation, apoptosis, and inflammation	Huang et al., 2019
(32)	Human	OA	Chondrocyte	lncRNA SNHG1	Down	miR-16-5p	Up	p38MAPK and NF-κB Signaling Pathways	Down	Inflammation	Lei J. et al., 2019
(33)	Human	OA	LPS-treated ATDC5 cells	MIAT	Up	miR-132	Down	NF-κB and JNK pathways	Up	Cell apoptosis and inflammation	Li et al., 2019a
(34)	Rats	OA	LPS-treated chondrocytes	MALAT1	Down	miR-146a	Up	PI3K	Down	ECM degradation, inflammation and apoptosis	Li et al., 2019b
(35)	Human	OA	Cartilage, synoviocytes	lncRNA-ANRIL	Up	miR-122-5p	Down	DUSP4	Up	Cell proliferation and apoptosis	Li et al., 2019c
(36)	Human	OA	LPS-treated ATDC5 cells	PMS2L2	Down	miR-203	Up	MCL-1	Down	Cell viability, apoptosis, and inflammation	Li et al., 2019d
(37)	Human	OA	Cartilage, chondrocytes	lncRNA-TM1P3	Up	miR-22	Down	ALK1	Up	ECM degradation	Li et al., 2019e
(38)	Human	OA	IL-1β-induced chondrocytes	MALAT1	Up	miR-145	Down	ADAMTS5	Up	ECM degradation	Liu C. et al., 2019
(39)	Murine	OA	LPS-induced ATDC5 cells	THRIL	Up	miR-125b	Down	JAK1/STAT3 and NF-κB pathways	Up	Inflammation	Liu G. et al., 2019
(40)	Human	OA	Cartilages, chondrocytes	PART-1	Down	miR-590-3p	Up	TGFBR2, Smad3	Down	Cell viability and apoptosis	Lu C. et al., 2019
(41)	Human	OA	hMSC, cartilage, chondrocytes	HOTTIP	Up	miR-455-3p	Down	CCL3	Up	Cartilage degradation	Mao et al., 2019
(42)	Human	OA	Chondrocytes	Nespas	Up	miR-291a-3p, miR-196a-5p, miR-23a-3p, miR-24-3p, miR-let-7a-5p	Down	ACSL6	Up	Lipid metabolism	Park et al., 2019
(43)	Human	OA	Synovial fluid, chondrogenic cell line CHON-001	CAIF	Down	miR-1246	Up	IL-6	Up	Cell apoptosis	Qi et al., 2019
(44)	Human	OA	Cartilage, chondrocyte	MEG3	Down	miR-361-5p	Up	FOXO1	Down	Cell proliferation, apoptosis and ECM degradation	Wang A. et al., 2019
(45)	Human, rats	OA	Chondrocyte (Human) cartilage (rat)	XIST	Up	miR-1277-5p	Down	MMP-13, ADAMTS5	Up	ECM degradation	Wang T. et al., 2019
(46)	Human	OA	Cartilage, chondrocyte	FOXD2-AS1	Up	miR-27a-3p	Down	TLR4	Up	Cell proliferation, inflammation and ECM degradation	Wang Y. et al., 2019
(47)	Human	OA	Synovium, chondrocyte	NEAT1	Down	miR-181a	Up	GPD1L	Down	Cell proliferation, apoptosis and inflammation	Wang Z. et al., 2019
(48)	Human	OA	Cartilages, mesenchymal stem cells (MSCs)	HOTAIRM1-1	Down	miR-125b	Up	BMPR2	Down	Cell viability, apoptosis and differentiation	Xiao et al., 2019

(Continued)

TABLE 1 | (Continued)

	Species	Diseases	Region	lncRNA	Change	miRNA	Expression	Target gene	Change	Functions	References
(49)	Human	OA	Cartilages, chondrocyte	LINC00341	Down	miR-141	Up	YAF2	Down	Cell apoptosis	Yang Q. et al., 2019
(50)	Murine	OA	LPS-induced ATDC5 cells	lncRNA-ATB	Down	miR-223	Up	MyD88/NF-κB and p38MAPK pathways	Up	Cell viability, apoptosis and inflammation	Ying et al., 2019
(51)	Mice	OA	IL-6-induced ATDC5 cells	CHRF	Up	miR-146a	Down	/	/	Cell viability, apoptosis and inflammation	Yu et al., 2019
(52)	Human	OA	Cartilage, chondrocyte	H19	Up	miR-106a-5p	Down	/	/	Cell proliferation and apoptosis	Zhang X. et al., 2019
(53)	Human	OA	Cartilage, chondrocyte	MALAT1	Up	miR-150-5p	Down	AKT3	Up	Cell proliferation, apoptosis and ECM degradation	Zhang Y. et al., 2019
(54)	Human	OA	Cartilage, chondrocyte	PART1	Up	miR-373-3p	Down	SOX4	Up	Cell proliferation, apoptosis and ECM degradation	Zhu and Jiang, 2019
(55)	Mice	OA	Cartilage, chondrocytes	HOTAIR	Up	miR-20b	Down	PTEN	Up	Cell apoptosis and ECM degradation	Chen Y. et al., 2020
(56)	Human	OA	Cartilage, chondrocytes	HOTAIR	Up	miR-130A-3p	Down	–	–	Cell apoptosis	He and Jiang, 2020
(57)	Human	OA	Cartilage, chondrocyte	GAS5	Up	miR-34a	Down	Bcl-2	Up	Cell apoptosis	Ji Q. et al., 2020
(58)	Rat	OA	BMSCs	BLACAT1	Up	miR-142-5p	Down	–	–	Cell proliferation and differentiation	Ji Y. et al., 2020
(59)	Human	OA	Cartilage, chondrocyte	NEAT1	Up	miR-16-5p	Up	–	–	Cell proliferation and apoptosis	Li D. et al., 2020
(60)	Human	OA	Cartilage, chondrocyte	XIST	Up	miR-376c-5p	Down	OPN	Up	Cell apoptosis	Li L. et al., 2020
(61)	Human	OA	Cartilage, chondrocyte	NEAT1	Up	miR-193a-3p	Down	SOX5	Up	Cell apoptosis, inflammation and ECM degradation	Liu et al., 2020
(62)	Human	OA	Cartilage, chondrocyte	LINC00623	Down	miR-101	Up	HRAS	Down	Cell apoptosis, senescence and ECM degradation	Lü et al., 2020
(63)	Rat	OA	Cartilage, chondrocyte	LINC00662	Down	miR-15b-5p	Up	GPR120	Down	Cell apoptosis	Lu and Zhou, 2020
(64)	Human	OA	Cartilage, LPS-treated C28/I2 cells	MFI2-AS1	Up	miR-130a-3p	Down	TCF4	Up	Cell viability, apoptosis, inflammation and ECM degradation	Luo et al., 2020
(65)	Human	OA	Cartilage, chondrocyte	XIST	Up	miR-142-5p	Down	SGTB	Up	Cell growth, proliferation and apoptosis	Sun P. et al., 2020
(66)	Human	OA	Synovial fluid, chondrocyte	CASC2	Up	miR-93-5p	Down	–	–	Cell apoptosis	Sun Y. et al., 2020
(67)	Human, Rats	OA	Cartilage (human), chondrocyte (rats)	H19	Down	miR-106b-5p	Up	TIMP2	Down	Cell proliferation, migration and ECM degradation	Tan et al., 2020
(68)	Human	OA	Cartilage, chondrocyte	SNHG7	Down	miR-34a-5p	Up	SYVN1	Down	Cell proliferation, apoptosis and autophagy	Tian et al., 2020
(69)	Human	OA	Cartilage, chondrocyte	NKILA	Down	miR-145	Up	SP1	Down	Cell proliferation, apoptosis and inflammation	Xue et al., 2020
(70)	Human	OA	Synovial fluid, chondrocytes	CTBP1-AS2	Up	miR-130A	Down	–	–	Cell proliferation	Zhang et al., 2020a
(71)	Human	OA	Peripheral Blood, THP-1 cell	IGHCγ1	Up	miR-6891-3p	Down	TLR4	Up	Inflammation	Zhang et al., 2020c

(Continued)

TABLE 1 | (Continued)

	Species	Diseases	Region	lncRNA	Change	miRNA	Expression	Target gene	Change	Functions	References
(72)	Human	OA	Cartilage, chondrocyte	SNHG15	Down	miR-141-3p	Up	BCL2L13	Down	Cell proliferation, apoptosis and ECM degradation	Zhang et al., 2020e
(73)	Human	OA	Cartilage, chondrocyte	LINC00461	Up	miR-30a-5p	Down	–	–	Cell proliferation, cell cycle progression, inflammation, and ECM degradation	Zhang et al., 2020g
(74)	Human	OA	Cartilage, chondrocyte	OIP5-AS1	Down	miR-29b-3p	Up	PGRN	Down	Cell proliferation, migration, apoptosis and inflammation	Zhi et al., 2020

ACSL6, acyl-CoA synthetase 6; ADAMTSs, a disintegrin and metalloprotease with thrombospondin motifs; ALK1, activin receptor-like kinase 1; ANRIL, antisense non-coding RNA in the INK4 locus; ATB, activated by transforming growth factor beta; BCL2L13, Bcl2-like 13; Bim, B-cell lymphoma 2 interacting mediators of cell death; BMPR2, bone morphogenetic protein receptor 2; BMSCs, bone marrow stromal stem cells; CASC2, Cancer Susceptibility 2; CCND1, Cyclin D1; CHRF, cardiac hypertrophy-related factor; CIR, cartilage injury–related; CXCR4, C-X-C chemokine receptor-4; DANCR, differentiation antagonizing non-protein coding RNA; DNM3OS, dynamin 3 opposite strand; ECM, extracellular matrix; ETV1, Erythroblast transformation-specific translocation variant 1; FGFR1, fibroblast growth factor receptor 1; FUT2, fucosyltransferase 2; GAS5, Growth Arrest-Specific 5; GIT1, G-protein- coupled receptor kinase interacting protein-1; GPD1L, glycerol-3-phosphate dehydrogenase 1-like; GPR120, G protein—coupled receptor 120; HMGB1, high mobility group protein B1; hMSC, human mesenchymal stem cell; HOTAIRM1-1, HOX antisense intergenic RNA myeloid 1 variant 1; HULC, highly up-regulated in liver cancer; IGF1, insulin-like growth factor-1; JAK1, c-Jun N-terminal kinase 1; LPS, lipopolysaccharide; MALAT1, metastasis associated lung adenocarcinoma transcript 1; MCM3AP-AS1, Minichromosome Maintenance Complex Component 3 Associated Protein Antisense RNA 1; MEG3, maternally expressed gene 3; MEG3, maternally expressed gene 3; MFI2-AS1, melanotransferrin antisense RNA; MIAT, myocardial infarction associated transcript; MMP, matrix metalloproteinase; MSCs, mesenchymal stem cells; MSR, mechanical stress; NEAT1, nuclear enriched abundant transcript 1; NF-κB, nuclear factor κB; OA, osteoarthritis; OIP5-AS1, OIP5 antisense RNA 1; OPN, osteopontin; PART-1, prostate androgen-regulated transcript-1; PGRN, progranulin; PI3K, Phosphoinositide 3-kinase; PMS2L2, PMS1 Homolog 2, Mismatch Repair System Component Pseudogene 2; PVT1, plasmacytoma variant translocation 1; SGTB, small glutamine rich tetratricopeptide repeat containing beta; SNHG, small nucleolar RNA host gene; SOX4, SRY-related high-mobility group box 4; SOX5, Sex-determining region Y-box protein 5; STAT3, signal transducer and activator of transcription 3; TCF4, transcription factor 4; TGFBR2, Transforming growth factor-beta receptor type 2; THRIL, TNF and hnRNPL related immune-regulatory lincRNA; TMSB4, Thymosin β-4; TUG1, taurine upregulated gene 1; UCA1, urothelial carcinoma associated 1; XIST, X-inactive-specific transcript; YAF2, YY1-associated factor 2.

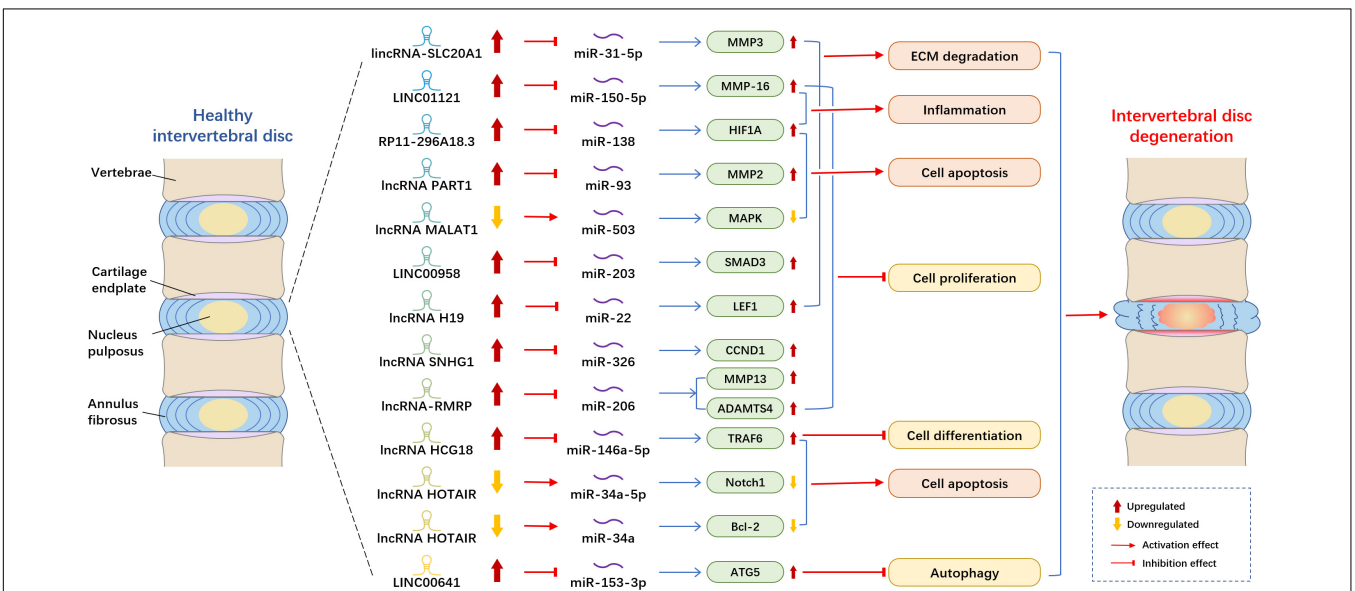

FIGURE 1 | Example of altered lncRNA expression patterns and their biological effects in intervertebral disk degeneration. lncRNA, long non-coding RNA; ECM, extracellular matrix; MMP, matrix metallopeptidase; MAPK, mitogen-activated protein kinase; SMAD3, SMAD family member 3; LEF1, lymphoid enhancing factor-1; CCND1, cyclin D1; ADAMTS4, A disintegrin and metalloproteinase with thrombospondin motifs 4; TRAF6, tumor necrosis factor receptor-associated factor 6; Notch1, Notch Receptor 1; Bcl-2, B cell lymphoma 2; ATG5, autophagy-related gene 5.

the levels of miR-93 were lower (Gao et al., 2020). Through dual-luciferase reporter assay, they proved that PART1 acts as miR-93 sponges in NP tissues and cells to suppress the expression of miR-93 and to further regulate MMP2. Zheng et al. (2020) showed that MALAT1 was reduced in NP cells, and upregulation of MALAT1 could relieve cell proliferation and apoptosis *in vitro* and inhibit the degree of INN *in vivo*. Moreover, they found that MALAT1 plays pivotal roles in IDD through sponging miR-503, and thereby modulate downstream MAPK signaling pathways.

Several studies indicated that lncRNAs plays roles in IDD by modulating miRNA and their target genes. Wang et al. (2018b) showed that the level of lncRNA-RMRP in degenerated NP tissues was higher than that in normal NP tissues, whereas the expression of miR-206 was lower. They indicated that lncRNA-RMRP could promote cell proliferation via modulating miR-206, thereby regulating downstream target gene MMP13 and ADAMTS4. lncRNA HOTAIR was downregulated in NP tissues and cells, whereas miR-34a expression was negatively correlated with HOTAIR and the expression of Bcl-2 was positively connected with HOTAIR (Yu et al., 2018). HOTAIR could inhibit NP cell apoptosis through regulating miR-34a/Bcl-2 axis. A study found that LINC00958 and mRNA SMAD3 were upregulated in NP tissues, whereas miR-203 was downregulated. Ectopic expression of miR-203 could suppress cell growth and ECM degradation (Zhao et al., 2019). Therefore, LINC00958 participates in the cell process by regulating miR-203 and SMAD3. Another study reported that the expression levels of LINC01121 and MMP-16 significantly increased in NP cells, whereas the level of miR-150-5p decreased (Chen X. et al., 2020). They demonstrated that LINC01121 could enhance the cell process of IDD, such as cell growth, ECM degradation and inflammation by regulating miR-150-5p and MMP-16.

Rheumatoid Arthritis

In RA disease, the most studied mechanism of lncRNA and miRNA is that lncRNA acts as the miRNA sponge to modulate downstream genes (**Table 2**). lncRNA PVT1 (plasmacytoma variant translocation 1) and SCUBE2 (signal peptide-CUB-EGF-like containing protein 2) were upregulated, whereas miR-543 was downregulated in synovial tissues of RA rats and patients (Wang et al., 2020). Wang et al. (2020) found that the overexpression of PVT1 or the suppression of miR-543 elevated the level of SCUBE2. Moreover, the knockdown of PVT1 could suppress proliferation and induce apoptosis of RA through hindering the expression of SCUBE2 by sponging miR-543 (Wang et al., 2020). lncRNA LINC-PINT (long intergenic non-protein encoding long-chain RNA p53-induced transcript) was reduced in RA tissues and cells (Wang and Zhao, 2020). Through bioinformatics techniques and RNA Binding Protein Immunoprecipitation (RIP) assay, they found that miR-155-5p could interact with LINC-PINT, and SOCS1 was the target mRNA of miR-155-5p. LINC-PINT could inhibit cell proliferation and invasion via sponging miR-155-5p and regulating the level of SOCS1. Yan et al. (2019) revealed that the level of lncRNA HIX003209 in the peripheral blood mononuclear cells (PBMCs) and macrophages of RA samples and the expression of TLR4 was positively correlated with HIX003209. lncRNA HIX003209 directly targeted miR-6089 and was involved in the regulation of inflammation through acting as miR-6089 sponge via the TLR4/NF-κB signaling pathway.

Ankylosing Spondylitis

That lncRNA acts as the sponge of miRNA to modulate target genes is the most studied mechanism of lncRNA and miRNA acting on AS (**Table 2**). Li Y. et al. (2020) reported the role of MEG3 (maternally expressed gene 3) in the inflammation of AS. They observed that the expression level of MEG3 in the serum of AS patients was significantly downregulated compared with that in normal people, and MEG3 could inhibit inflammatory responses. However, the expression of miR-146a was upregulated in the AS patients and miR-146a could directly bind with MEG3 (Li Y. et al., 2020). Li Y. et al. (2020) assumed that MEG3 may played a vital role in the repression of inflammation factors in AS through sponging miR-146a, thereby exploring a novel potential treatment target for AS patients. Zhang et al. (2020f) found that lncRNA H19 was highly expressed in the AS patients and elevated the expression level of IL-17A and IL-23 inflammation factors. H19 could directly modulate miR-22-5p and miR-675-5p, and VDR (vitamin D receptor) was the target mRNAs of these two miRNAs. Among them, the level of miR-22-5p was negatively correlated with H19, while miR-675-5p and VDR was positively with H19 in AS patients. H19 plays regulatory roles in inflammatory reaction in AS through binding with VDR by sponging miR-22-5p and interacting with miR-675-5p (Zhang et al., 2020f).

INTERACTIONS AMONG circRNA, miRNA, AND mRNA IN DEGENERATIVE MUSCULOSKELETAL DISEASES

Osteoarthritis

Circular RNAs acting as miRNA sponges is the one of the most studied mechanisms (**Figure 2**). Compared with normal cartilage, circRNA-CER (circRNA_100876) was overexpressed and increased with IL-1 (interleukin-1) and TNF-α (tumor necrosis factor-alpha) in OA chondrocytes. circRNA-CER regulated matrix-degrading matrix metalloproteinase (MMP)-13 expression to participated in the process of chondrocyte ECM degradation by sponging miR-136 (Liu et al., 2016b). According to the research of Zhou et al. (2018), overexpressed circRNA_Atp9b sponge miR-138-5p and then mediate ECM catabolism and inflammation to regulates OA progression in chondrocytes by targeting MMP13. circ_0136474 was also verified by the research of Li et al. (2019f) to sponge miR-127-5p to regulate MMP13 in human OA chondrocytes, then, it suppressed cell proliferation and enhanced cell apoptosis during OA progression. The results were in line with those obtained in a study performed by Zhou Z.B. et al. (2019), who found that circRNA.33186/miR-127-5p/MMP13 axis contributes to OA pathogenesis. Furthermore, circSERPINE2 overexpression could slow down the pace of human chondrocytes apoptosis and promote ECM anabolism by sponging miR-1271-5p and thereby targeting ERG (E26 transformation-specific-related gene) to alleviate OA (Shen et al., 2019). In OA blood samples, the downregulation of ciRS-7 and the upregulation of miR-7 were observed (Zhou X. et al., 2019). ciRS-7 was verified to act as a miR-7 sponge to mediate OA progression. Increased cirM3 expression in OA cartilage tissue and cells could serve as a sponge of miR-296-5p to slow down the proliferation and differentiation of OA chondrocytes, thus involving in regulating the occurrence

TABLE 2 | lncRNA/miRNA/mRNA networks in rheumatoid arthritis and ankylosing spondylitis.

	Species	Diseases	Region	lncRNA	Change	miRNA	Expression	Target gene	Change	Functions	References
(1)	Rat	RA	Synovial tissues	PVT1	Up	miR-543	Down	SCUBE2	Up	Cell proliferation and apoptosis	Wang et al., 2020
(2)	Human	RA	Synovial tissues	LINC-PINT	Down	miR-155-5p	Up	SOCS1	Down	Cell proliferation and invasion	Wang and Zhao, 2020
(3)	Human	RA	Serum	HIX003209	Up	miR-6089	Down	TLR4	Up	Inflammation	Yan et al., 2019
(4)	Human	AS	Serum, fibroblast-like synovial cells	lncRNA MEG3	Down	miR-146a	Up	–	–	Inflammation	Li Y. et al., 2020
(5)	Human	AS	Peripheral blood mononuclear cells	H19	Up	miR675-5p/miR22-5p	miR675-5p up; miR22-5p down	VDR	Up	Inflammation	Zhang et al., 2020f

AS, ankylosing spondylitis; MEG3, maternally expressed gene 3; PINT, p53-induced transcript; PVT1, plasmacytoma variant translocation 1; RA, rheumatoid arthritis; SCUBE2, signal peptide-CUB-EGF-like containing protein 2; SOCS1, cytokine signaling 1.

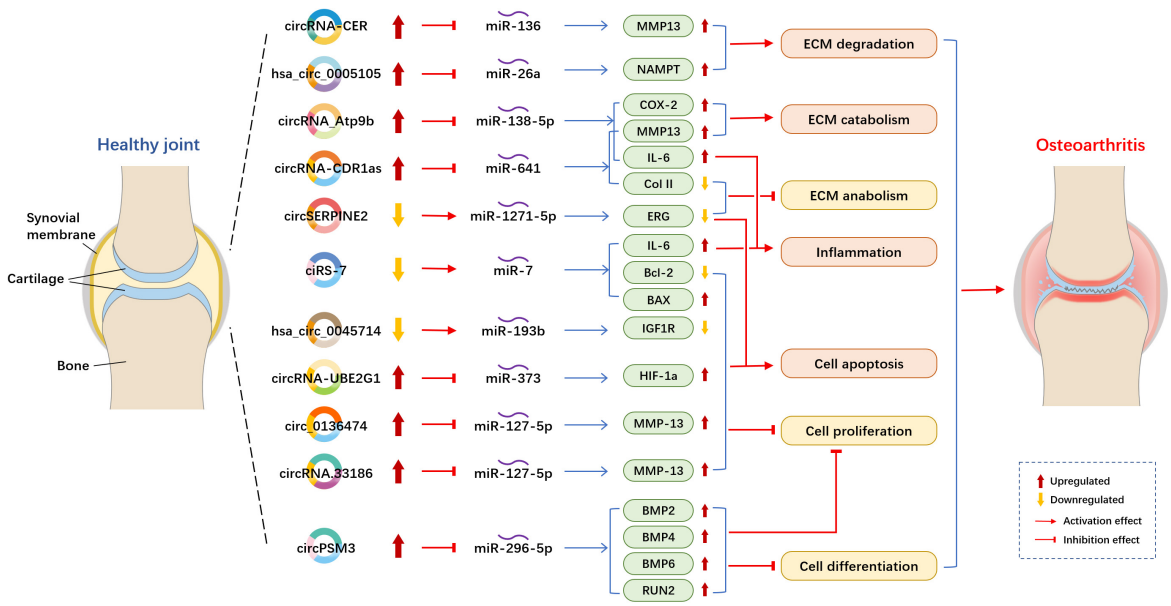

FIGURE 2 | Example of altered circRNA expression patterns and their biological effects in osteoarthritis. circRNA, circular RNA; ECM, extracellular matrix; MMP, matrix metallopeptidase; NAMPT, Nicotinamide phosphoribosyltransferase; COX-2, cyclooxygenase-2; IL-6, interleukin-6; Col II, type II collagen; ERG, E26 transformation-specific-related gene; BAX, BCL2 associated X, apoptosis regulator; Bcl-2, B cell lymphoma 2; IGF1R, insulin-like growth factor 1 receptor; HIF, hypoxia inducible factor; BMP, bone morphogenetic protein.

and development of OA chondrocytes (Ni et al., 2020). The overexpression of circRNA-CDR1as regulated OA progression via reducing Col II level but increased IL-6 and MMP13 contents to modulate inflammation and ECM metabolism by sponging miR-641 (Zhang et al., 2020d).

Several circRNA studies showed that circRNAs act as ceRNAs to competitively bind to miRNAs in OA. Hsa_circ_0045714 expression was downregulated (Liu et al., 2016b; Li B.F. et al., 2017). Furthermore, Li B.F. et al. (2017) determined that hsa_circ_0045714 promoted the expression of miR-193b target gene IGF1R (insulin-like growth factor 1 receptor) to regulate chondrocytes proliferation, apoptosis and ECM synthesis. Otherwise, hsa_circ_0005105 expression is significantly enhanced in OA chondrocytes and can promote ECM degradation by mediating the expression of miR-26a target NAMPT (Nicotinamide phosphoribosyltransferase) (Wu et al., 2017). In the lipopolysaccharide (LPS)-induced OA cell model, the expression levels of circRNA-UBE2G1 was significantly increased and bound to miR-373 as ceRNAs to aggravate the OA progression by targeting hypoxia-inducible factor (HIF)-1a (Chen G. et al., 2020).

Intervertebral Disk Degeneration

Over the past years, some circRNAs have merged as molecular drivers to serve as miRNA sponges or ceRNAs in circRNA/miRNA/mRNA networks in the pathogenesis of IDD (**Figure 3**). Compared with normal NP tissues, circVMA21 (hsa_circ_0091702) was downregulated in NP tissues and NP

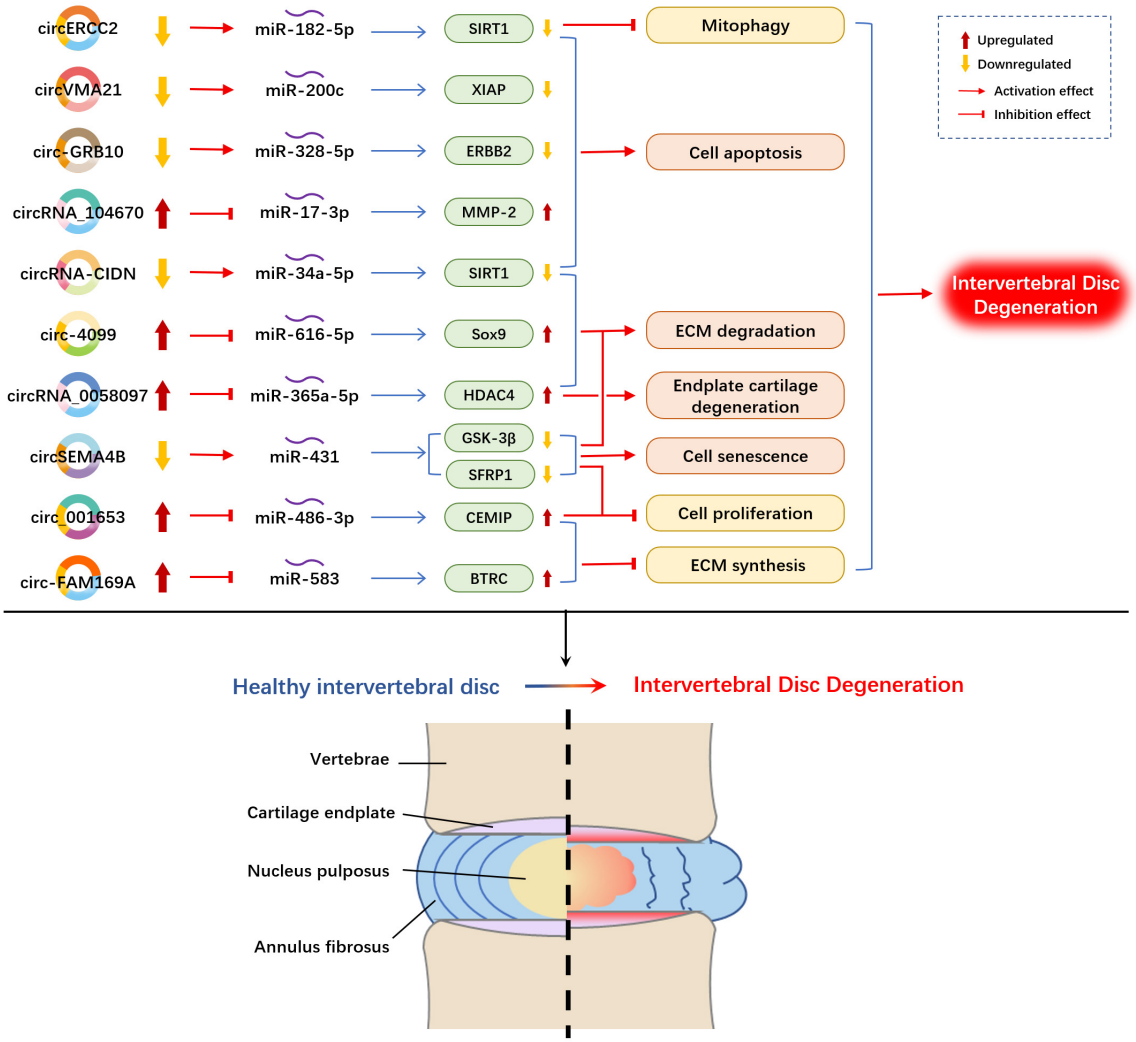

FIGURE 3 | Example of altered circRNA expression patterns and their biological effects in intervertebral disk degeneration. circRNA, circular RNA; ECM, extracellular matrix; SIRT1, silent mating type information regulation 2 homolog 1; XIAP, X linked inhibitor of-apoptosis protein; ERBB2, erb-b2 receptor tyrosine kinase 2; MMP, matrix metallopeptidase; Sox9, SRY-Box transcription factor 9; HDAC4, histone deacetylase 4; GSK-3β, glycogen synthase kinase-3β; SFRP1, secreted frizzled-related protein 1; CEMIP, cell migration-inducing hyaluronan binding protein; BTRC, beta-transducin repeat-containing protein.

TABLE 3 | circRNA/miRNA/mRNA networks in rheumatoid arthritis.

	Species	Diseases	Region	circRNA	Change	miRNA	Change	Target gene	Change	Functions	References
(1)	Human	RA	Synovial tissues	hsa_circ_0001859	Up	miR-204/211	Down	ATF2	Up	Inflammation	Li B. et al., 2018
(2)	Mice	RA	Peripheral blood mononuclear cells	circRNA_09505	Up	miR-6089	Down	AKT1/NF-κB signaling pathway	Up	Inflammation	Yang J. et al., 2020

AKT1, threonine kinase 1; ATF2, activating transcription factor 2; NF-κB: nuclear factor κB; RA, rheumatoid arthritis.

cells in IDD and alleviated NP cell apoptosis by targeting miR-200c and XIAP (X linked inhibitor-of-apoptosis protein) (Cheng et al., 2018). Similarly, circ-GRB10 was downregulated during IDD progression, and competitively bound to miR-328-5p to regulate NP cell apoptosis by targeting erb-b2 receptor tyrosine kinase 2 (ERBB2) in the ErbB signaling pathway (Guo et al., 2018). circRNA_104670 was selected via microarray analysis because of its large multiplier expression in IDD tissues (Song et al., 2018). A study reported that circRNA_104670 acted as a ceRNA that binds to miR-17-3p, downregulated circRNA_104670-suppressed MMP-2 expression through circRNA_104670/miR-17-3p/MMP-2 axis, reduced cell apoptosis

and increased ECM formation. According to another microarray assay made by Wang et al. (2018a), they selected circ-4099 among 72 upregulated circRNAs in degenerated NP tissues for further analysis. They demonstrated that circ-4099 competitively sponged miR-616-5p, which reversed the suppression of Sox9 by miR-616-5p. Wang et al. (2018c) verified that circSEMA4B was downregulated in IDD specimens, and circSEMA4B served as a miR-431 sponge to compete with SFRP1 or GSK-3β, which are two inhibitory regulators of Wnt signaling, for miR-431 binding, thereby alleviating IL-1β-induced degenerative process in NP cells. circRNA-CIDN was downregulated during IDD progression and bound to miR-34a-5p as a miRNA sponge. Upregulation of miR-34a-5p repressed SIRT1 (silent mating type information regulation 2 homolog 1) to enhance the compression-induced damage of NP cells (Xiang et al., 2020). circERCC2 was also downregulated in IDD NP tissues and NP cells. Furthermore, circERCC2 was associated with the alleviation of IDD through miR-182-5p/SIRT1 axis by activating mitophagy and inhibiting apoptosis (Xie et al., 2019). The expression of circ-FAM169A in IDD samples was significantly upregulated with enhanced ECM catabolism and suppressed ECM anabolism in NP cells. The overexpressed circ-FAM169A competitively bound to miR-583, thus upregulating BTRC (an inducer of the NF-κB signaling pathway) (Guo et al., 2020). circ-FAM169A promoted IDD development via miR-583/BTRC signaling. In addition, circ_001653 could be another novel therapeutic target for IDD that functions by regulating miR-486-3p expression to upregulate CEMIP (cell migration-inducing hyaluronan binding protein) (Cui and Zhang, 2020). circ_001653 downregulation could potentially promote cell proliferation and ECM synthesis through the miR486-3p/CEMIP axis.

Human NP tissues and human endplate tissues were collected to detect differentially expressed circRNAs during IDD progression. Xiao et al. (2020) induced circRNA expression profile changes in endplate chondrocytes, and results reported that 17 circRNAs were upregulated and 12 circRNAs were downregulated (with fold changes higher than 1.5). circRNA_0058097 was selected for further analysis. circRNA_0058097 increased the expression of HDAC4 (histone deacetylase 4) by sponging miR-365a-5p, which intensified the morphological changes of endplate chondrocytes, and aggravated endplate cartilage and ECM degradation.

Rheumatoid Arthritis and Ankylosing Spondylitis

Rheumatoid arthritis and AS are both characterized by chronic inflammatory disease (van der Heijde et al., 2019; Zhou Y. et al., 2019). However, only a limited number of studies have been conducted on circRNAs in RA and AS (**Table 3**). Li B. et al. (2018) identified circRNAs in RA synovial tissues and suggested that hsa_circ_0001859 regulated ATF2 expression by competitively sponging miR-204/211. Knockdown of hsa_circ_0001859 suppressed ATF2 expression and decreased inflammatory activity. Hsa_circ_0001859/miR-204/211/ATF2 axis may be used as an approach for treating RA. Another circRNA/miRNA/mRNA network study in RA was conducted by Yang J. et al. (2020), They reported that circRNA_09505 is upregulated in PBMCs from RA patients and mice. The knockdown of circRNA_09505 inhibits macrophage proliferation and alleviates arthritis and inflammation. miR-6089 functions as a ceRNA that is being competitively sponged by circRNA_09505 to regulated macrophage inflammatory response. Furthermore, circRNA_09505 was detected to promote AKT1 expression, which is a direct target of miR-6089, to mediate IκBα/NF-κB signaling pathway. To sum up, circRNA_09505 can sponge miR-6089 and regulate inflammation via miR-6089/AKT1/NF-κB axis in arthritis mice model. Combined with RNA-seq data and RT-qPCR validation of PBMCs from RA patients, the results of Ouyang et al. (2017) showed several upregulated circRNAs (circRNA_101873, circRNA_003524, circRNA_104871, and circRNA_103047), and Wen et al. (2020) proved three upregulated hsa-circRNAs (hsa_circ_0001200, hsa_circ_0001566, and hsa_circ_0003972) and one downregulated hsa_circRNAs (hsa_circ_0008360), but without downstream gene detection to establish circRNA/miRNA/mRNA networks.

At present, studies on circRNA and miRNA interaction mechanism on AS are lacking. The roles of circRNAs in AS remain unclear. Only one profiling and bioinformatics analysis showed differentially expressed circRNAs in AS patients (sampled form spinal ligament tissues), reported the presence of 57 upregulated circRNAs and 66 downregulated circRNAs in AS spinal ligament tissues (Kou et al., 2020).

Taken together, the study about the interactions among circRNA, miRNA and mRNA in RA and AS may have a great clinical prospect.

CONCLUSION AND FUTURE PROSPECT

Recent advances in gene expression of lncRNAs and circRNAs, coupled with the ability to interact with the miRNA, mRNA or signaling pathway, have started to expose the different molecular consequence associated with RNA transcriptions and the roles they play in the development of MSDDs (including OA, IDD, RA, and AS) that involve chondrocyte proliferation and apoptosis, ECM degradation and PBMCs inflammation. The effects of ncRNA/circRNA-miRNA-mRNA axis on MSDD progression elucidated their contribution to the dynamic cellular processes and provided the potential OA, IDD, RA and AS therapeutic strategies. The altered expression of lncRNAs or circRNAs refers to diverse biological processes of MSDD, thereby indicating that lncRNAs/circRNAs may be developed as biomarkers and therapeutic targets. Despite the large numbers of ncRNAs, including lncRNAs and circRNAs, determined to be differentially expressed during these pathogenic processes, only a small portion of them has been elucidated. Research on MSDD pathogenesis, especially on RA and AS, is still in its infancy and major knowledge gaps remain to be filled. Therefore, the interactions among lncRNA/circRNA, miRNA and mRNA in MSDD to present the potential pathogenesis is required. Further studies are needed to explore the mutual regulatory mechanisms

between lncRNA/circRNA regulation and effective therapeutic interventions in the pathology of MSDD.

AUTHOR CONTRIBUTIONS

X-QW and P-JC: conceptualization and methodology. J-BG, XS, Y-MC, and ZY: investigation. Y-LZ and GS: writing – original draft preparation and writing – review and editing. All authors contributed to the article and approved the submitted version.

FUNDING

This work was supported by the National Natural Science Foundation of China (81871844); Shuguang Program supported by Shanghai Education Development Foundation and Shanghai Municipal Education Commission (18SG48); the Shanghai Municipal Commission of Health and Family Planning (201840346); the Shanghai Key Lab of Human Performance (Shanghai University of Sport) (11DZ2261100); and Shanghai Frontiers Science Research Base of Exercise and Metabolic Health.

REFERENCES

Abbasifard, M., Kamiab, Z., Bagheri-Hosseinabadi, Z., and Sadeghi, I. (2020). The role and function of long non-coding RNAs in osteoarthritis. *Exp. Mol. Pathol.* 114:104407. doi: 10.1016/j.yexmp.2020.104407

Ai, D., and Yu, F. (2019). LncRNA DNM3OS promotes proliferation and inhibits apoptosis through modulating IGF1 expression by sponging MiR-126 in CHON-001 cells. *Diagn. Pathol.* 14:106.

Beermann, J., Piccoli, M. T., Viereck, J., and Thum, T. (2016). Non-coding RNAs in development and disease: background, mechanisms, and therapeutic approaches. *Physiol. Rev.* 96, 1297–1325. doi: 10.1152/physrev.00041.2015

Cao, L., Wang, Y., Wang, Q., and Huang, J. (2018). LncRNA FOXD2-AS1 regulates chondrocyte proliferation in osteoarthritis by acting as a sponge of miR-206 to modulate CCND1 expression. *Biomed. Pharmacother.* 106, 1220–1226. doi: 10.1016/j.biopha.2018.07.048

Chen, G., Liu, T., Yu, B., Wang, B., and Peng, Q. (2020). CircRNA-UBE2G1 regulates LPS-induced osteoarthritis through miR-373/HIF-1a axis. *Cell Cycle* 19, 1696–1705. doi: 10.1080/15384101.2020.1772545

Chen, H., Qi, J., Bi, Q., and Zhang, S. (2017). Expression profile of long noncoding RNA (HOTAIR) and its predicted target miR-17-3p in LPS-induced inflammatory injury in human articular chondrocyte C28/I2 cells. *Int. J. Clin. Exp. Pathol.* 10, 9146–9157.

Chen, K., Zhu, H., Zheng, M. Q., and Dong, Q. R. (2019). LncRNA MEG3 inhibits the degradation of the extracellular matrix of chondrocytes in osteoarthritis via targeting miR-93/TGFBR2 axis. *Cartilage* 1947603519855759. doi: 10.1177/1947603519855759 [Published online ahead of print]

Chen, W. K., Yu, X. H., Yang, W., Wang, C., He, W. S., Yan, Y. G., et al. (2017). lncRNAs: novel players in intervertebral disc degeneration and osteoarthritis. *Cell Prolif.* 50:e12313. doi: 10.1111/cpr.12313

Chen, X., Li, Z., Xu, D., and Li, S. (2020). LINC01121 induced intervertebral disc degeneration via modulating miR-150-5p/MMP16 axis. *J. Gene Med.* 22:e3231.

Chen, Y., Huang, J., Tang, C., Chen, X., Yin, Z., Heng, B. C., et al. (2017). Small molecule therapeutics for inflammation-associated chronic musculoskeletal degenerative diseases: past, present and future. *Exp. Cell Res.* 359, 1–9. doi: 10.1016/j.yexcr.2017.07.027

Chen, Y., Zhang, L., Li, E., Zhang, G., Hou, Y., Yuan, W., et al. (2020). Long-chain non-coding RNA HOTAIR promotes the progression of osteoarthritis via sponging miR-20b/PTEN axis. *Life Sci.* 253:117685. doi: 10.1016/j.lfs.2020.117685

Cheng, X., Zhang, L., Zhang, K., Zhang, G., Hu, Y., Sun, X., et al. (2018). Circular RNA VMA21 protects against intervertebral disc degeneration through targeting miR-200c and X linked inhibitor-of-apoptosis protein. *Ann. Rheum. Dis.* 77, 770–779. doi: 10.1136/annrheumdis-2017-212056

Chu, P., Wang, Q., Wang, Z., and Gao, C. (2019). Long non-coding RNA highly up-regulated in liver cancer protects tumor necrosis factor-alpha-induced inflammatory injury by down-regulation of microRNA-101 in ATDC5 cells. *Int. Immunopharmacol.* 72, 148–158. doi: 10.1016/j.intimp.2019.04.004

Cooper, N. A., Scavo, K. M., Strickland, K. J., Tipayamongkol, N., Nicholson, J. D., Bewyer, D. C., et al. (2016). Prevalence of gluteus medius weakness in people with chronic low back pain compared to healthy controls. *Eur. Spine J.* 25, 1258–1265. doi: 10.1007/s00586-015-4027-6

Cui, S., and Zhang, L. (2020). circ_001653 silencing promotes the proliferation and ECM synthesis of NPCs in IDD by downregulating miR-486-3p-mediated CEMIP. *Mol. Ther. Nucleic Acids* 20, 385–399. doi: 10.1016/j.omtn.2020.01.026

Deng, K. Y., Wang, H., Guo, X. Q., and Xia, J. Z. (2016). The cross talk between long, non-coding RNAs and microRNAs in gastric cancer. *Acta Biochim. Biophys. Sin.* 48, 111–116. doi: 10.1093/abbs/gmv120

Faghihi, M. A., Zhang, M., Huang, J., Modarresi, F., Van Der Brug, M. P., Nalls, M. A., et al. (2010). Evidence for natural antisense transcript-mediated inhibition of microRNA function. *Genome Biol.* 11:R56.

Fan, X., Yuan, J., Xie, J., Pan, Z., Yao, X., Sun, X., et al. (2018). Long non-protein coding RNA DANCR functions as a competing endogenous RNA to regulate osteoarthritis progression via miR-577/SphK2 axis. *Biochem. Biophys. Res. Commun.* 500, 658–664. doi: 10.1016/j.bbrc.2018.04.130

Fontana, G., See, E., and Pandit, A. (2015). Current trends in biologics delivery to restore intervertebral disc anabolism. *Adv. Drug Deliv. Rev.* 84, 146–158. doi: 10.1016/j.addr.2014.08.008

Gao, D., Hao, L., and Zhao, Z. (2020). Long non-coding RNA PART1 promotes intervertebral disc degeneration through regulating the miR-93/MMP2 pathway in nucleus pulposus cells. *Int. J. Mol. Med.* 46, 289–299.

Gao, Y., Zhao, H., and Li, Y. (2019). LncRNA MCM3AP-AS1 regulates miR-142-3p/HMGB1 to promote LPS-induced chondrocyte apoptosis. *BMC Musculoskelet. Disord.* 20:605. doi: 10.1186/s12891-019-2967-4

Guo, W., Mu, K., Zhang, B., Sun, C., Zhao, L., Dong, Z. Y., et al. (2020). The circular RNA FAM169A functions as a competitive endogenous RNA and regulates intervertebral disc degeneration by targeting miR-583 and BTRC. *Cell Death Dis.* 11:315.

Guo, W., Zhang, B., Mu, K., Feng, S. Q., Dong, Z. Y., Ning, G. Z., et al. (2018). Circular RNA GRB10 as a competitive endogenous RNA regulating nucleus pulposus cells death in degenerative intervertebral disk. *Cell Death Dis.* 9:319.

Haque, S., and Harries, L. W. (2017). Circular RNAs (circRNAs) in health and disease. *Genes* 8:353. doi: 10.3390/genes8120353

He, B., and Jiang, D. (2020). HOTAIR-induced apoptosis is mediated by sponging miR-130a-3p to repress chondrocyte autophagy in knee osteoarthritis. *Cell Biol. Int.* 44, 524–535. doi: 10.1002/cbin.11253

He, L., Man, C., Xiang, S., Yao, L., Wang, X., and Fan, Y. (2021). Circular RNAs' cap-independent translation protein and its roles in carcinomas. *Mol. Cancer* 20:119.

Hu, J., Wang, Z., Shan, Y., Pan, Y., Ma, J., and Jia, L. (2018). Long non-coding RNA HOTAIR promotes osteoarthritis progression via miR-17-5p/FUT2/β-catenin axis. *Cell Death Dis.* 9:711.

Hu, Y., Li, S., and Zou, Y. (2019). Knockdown of LncRNA H19 relieves LPS-induced damage by modulating miR-130a in osteoarthritis. *Yonsei. Med. J.* 60, 381–388. doi: 10.3349/ymj.2019.60.4.381

Huang, B., Yu, H., Li, Y., Zhang, W., and Liu, X. (2019). Upregulation of long noncoding TNFSF10 contributes to osteoarthritis progression through the miR-376-3p/FGFR1 axis. *J. Cell Biochem.* 120, 19610–19620. doi: 10.1002/jcb.29267

Huang, Y. (2018). The novel regulatory role of lncRNA-miRNA-mRNA axis in cardiovascular diseases. *J. Cell Mol. Med.* 22, 5768–5775. doi: 10.1111/jcmm.13866

Hunter, D. J., and Bierma-Zeinstra, S. (2019). Osteoarthritis. *Lancet* 393, 1745–1759.

Huo, J. Z., Ji, X. H., Su, Z. Y., Shang, P., and Gao, F. (2018). Association of ADAMTS4 and ADAMTS5 polymorphisms with musculoskeletal degenerative diseases: a systematic review and meta-analysis. *Biosci. Rep.* 38:BSR20181619.

Iwakura, T., Inui, A., and Reddi, A. H. (2013). Stimulation of superficial zone protein accumulation by hedgehog and Wnt signaling in surface zone bovine articular chondrocytes. *Arthritis Rheum.* 65, 408–417.

Ji, Q., Qiao, X., Liu, Y., Wang, D., and Yan, J. (2020). Silencing of long-chain non-coding RNA GAS5 in osteoarthritic chondrocytes is mediated by targeting the miR-34a/Bcl-2 axis. *Mol. Med. Rep.* 21, 1310–1319.

Ji, Y., Fang, Q. Y., Wang, S. N., Zhang, Z. W., Hou, Z. J., Li, J. N., et al. (2020). LncRNA BLACAT1 regulates differentiation of bone marrow stromal stem cells by targeting miR-142-5p in osteoarthritis. *Eur. Rev. Med. Pharmacol. Sci.* 24, 2893–2901.

Jiang, S. D., Lu, J., Deng, Z. H., Li, Y. S., and Lei, G. H. (2017). Long noncoding RNAs in osteoarthritis. *Joint Bone Spine* 84, 553–556.

Kou, J., Liu, G., Liu, X., Li, T., Wei, Y., Sun, Y., et al. (2020). Profiling and bioinformatics analysis of differentially expressed circRNAs in spinal ligament tissues of patients with ankylosing spondylitis. *BioMed Res. Int.* 2020:7165893.

Kulcheski, F. R., Christoff, A. P., and Margis, R. (2016). Circular RNAs are miRNA sponges and can be used as a new class of biomarker. *J. Biotechnol.* 238, 42–51. doi: 10.1016/j.jbiotec.2016.09.011

Lee, R. C., Feinbaum, R. L., and Ambros, V. (1993). The C. elegans heterochronic gene lin-4 encodes small RNAs with antisense complementarity to lin-14. *Cell* 75, 843–854. doi: 10.1016/0092-8674(93)90529-y

Lei, B., Xuan, X. Y., and Fan, W. P. (2019). Progress in research on role of CircRNA in autoimmune diseases. *Chin. J. Biol.* 32, 347–350.

Lei, J., Fu, Y., Zhuang, Y., Zhang, K., and Lu, D. (2019). LncRNA SNHG1 alleviates IL-1β-induced osteoarthritis by inhibiting miR-16-5p-mediated p38 MAPK and NF-κB signaling pathways. *Biosci. Rep.* 39:BSR20191523.

Li, B., and Chen, D. (2019). Degenerative musculoskeletal diseases: pathology and treatments. *J. Orthop. Translat.* 17, 1–2. doi: 10.1016/j.jot.2019.05.001

Li, B., Li, N., Zhang, L., Li, K., Xie, Y., Xue, M., et al. (2018). Hsa_circ_0001859 Regulates ATF2 expression by functioning as an MiR-204/211 sponge in human rheumatoid arthritis. *J. Immunol. Res.* 2018:9412387.

Li, B. F., Zhang, Y., Xiao, J., Wang, F., Li, M., Guo, X. Z., et al. (2017). Hsa_circ_0045714 regulates chondrocyte proliferation, apoptosis and extracellular matrix synthesis by promoting the expression of miR-193b target gene IGF1R. *Hum. Cell* 30, 311–318. doi: 10.1007/s13577-017-0177-7

Li, C., Pan, S., Song, Y., Li, Y., and Qu, J. (2019a). Silence of lncRNA MIAT protects ATDC5 cells against lipopolysaccharides challenge via up-regulating miR-132. *Artif. Cells Nanomed. Biotechnol.* 47, 2521–2527. doi: 10.1080/21691401.2019.1626410

Li, D., Sun, Y., Wan, Y., Wu, X., and Yang, W. (2020). LncRNA NEAT1 promotes proliferation of chondrocytes via down-regulation of miR-16-5p in osteoarthritis. *J. Gene Med.* 22:e3203.

Li, H., Xie, S., Li, H., Zhang, R., and Zhang, H. (2019b). LncRNA MALAT1 mediates proliferation of LPS treated-articular chondrocytes by targeting the miR-146a-PI3K/Akt/mTOR axis. *Life Sci.* 254:116801. doi: 10.1016/j.lfs.2019.116801

Li, H. Z., Lin, Z., Xu, X. H., Lin, N., and Lu, H. D. (2018). The potential roles of circRNAs in osteoarthritis: a coming journey to find a treasure. *Biosci. Rep.* 38:BSR20180542.

Li, L., Lv, G., Wang, B., and Kuang, L. (2020). XIST/miR-376c-5p/OPN axis modulates the influence of proinflammatory M1 macrophages on osteoarthritis chondrocyte apoptosis. *J. Cell Physiol.* 235, 281–293. doi: 10.1002/jcp.28968

Li, X., Huang, T. L., Zhang, G. D., Jiang, J. T., and Guo, P. Y. (2019c). LncRNA ANRIL impacts the progress of osteoarthritis via regulating proliferation and apoptosis of osteoarthritis synoviocytes. *Eur. Rev. Med. Pharmacol. Sci.* 23, 9729–9737.

Li, X., Yu, M., Chen, L., Sun, T., Wang, H., Zhao, L., et al. (2019d). LncRNA PMS2L2 protects ATDC5 chondrocytes against lipopolysaccharide-induced inflammatory injury by sponging miR-203. *Life Sci.* 217, 283–292. doi: 10.1016/j.lfs.2018.12.020

Li, Y., Li, S., Luo, Y., Liu, Y., and Yu, N. (2017). LncRNA PVT1 regulates chondrocyte apoptosis in osteoarthritis by acting as a sponge for miR-488-3p. *DNA Cell Biol.* 36, 571–580. doi: 10.1089/dna.2017.3678

Li, Y., Li, Z., Li, C., Zeng, Y., and Liu, Y. (2019e). Long noncoding RNA TM1P3 is involved in osteoarthritis by mediating chondrocyte extracellular matrix degradation. *J. Cell Biochem.* 120, 12702–12712. doi: 10.1002/jcb.28539

Li, Y., Zhang, S., Zhang, C., and Wang, M. (2020). LncRNA MEG3 inhibits the inflammatory response of ankylosing spondylitis by targeting miR-146a. *Mol. Cell Biochem.* 466, 17–24. doi: 10.1007/s11010-019-03681-x

Li, Y. F., Li, S. H., Liu, Y., and Luo, Y. T. (2017). Long noncoding RNA CIR promotes chondrocyte extracellular matrix degradation in osteoarthritis by acting as a sponge for Mir-27b. *Cell Physiol. Biochem.* 43, 602–610. doi: 10.1159/000480532

Li, Z., Li, X., Jiang, C., Qian, W., Tse, G., Chan, M. T. V., et al. (2018). Long non-coding RNAs in rheumatoid arthritis. *Cell Prolif.* 51:e12404.

Li, Z., Yuan, B., Pei, Z., Zhang, K., Ding, Z., Zhu, S., et al. (2019f). Circ_0136474 and MMP-13 suppressed cell proliferation by competitive binding to miR-127-5p in osteoarthritis. *J. Cell Mol. Med.* 23, 6554–6564. doi: 10.1111/jcmm.14400

Liang, J., Xu, L., Zhou, F., Liu, A. M., Ge, H. X., Chen, Y. Y., et al. (2018). MALAT1/miR-127-5p regulates osteopontin (OPN)-mediated proliferation of human chondrocytes through PI3K/Akt pathway. *J. Cell Biochem.* 119, 431–439. doi: 10.1002/jcb.26200

Liu, C., Ren, S., Zhao, S., and Wang, Y. (2019). LncRNA MALAT1/MiR-145 adjusts IL-1β-induced chondrocytes viability and cartilage matrix degradation by regulating ADAMTS5 in human osteoarthritis. *Yonsei Med. J.* 60, 1081–1092. doi: 10.3349/ymj.2019.60.11.1081

Liu, F., Liu, X., Yang, Y., Sun, Z., Deng, S., Jiang, Z., et al. (2020). NEAT1/miR-193a-3p/SOX5 axis regulates cartilage matrix degradation in human osteoarthritis. *Cell Biol Int* 44, 947–957. doi: 10.1002/cbin.11291

Liu, G., Wang, Y., Zhang, M., and Zhang, Q. (2019). Long non-coding RNA THRIL promotes LPS-induced inflammatory injury by down-regulating microRNA-125b in ATDC5 cells. *Int. Immunopharmacol.* 66, 354–361. doi: 10.1016/j.intimp.2018.11.038

Liu, Q., Hu, X., Zhang, X., Dai, L., Duan, X., Zhou, C., et al. (2016a). The TMSB4 pseudogene LncRNA functions as a competing endogenous RNA to promote cartilage degradation in human osteoarthritis. *Mol. Ther.* 24, 1726–1733. doi: 10.1038/mt.2016.151

Liu, Q., Zhang, X., Hu, X., Dai, L., Fu, X., Zhang, J., et al. (2016b). Circular RNA related to the chondrocyte ECM regulates MMP13 expression by functioning as a MiR-136 'Sponge' in human cartilage degradation. *Sci. Rep.* 6:22572.

Liu, Y., Li, Z., Zhang, M., Zhou, H., Wu, X., Zhong, J., et al. (2021). Rolling-translated EGFR variants sustain EGFR signaling and promote glioblastoma tumorigenicity. *Neuro. Oncol.* 23, 743–756. doi: 10.1093/neuonc/noaa279

Liu, Y., Lin, L., Zou, R., Wen, C., Wang, Z., and Lin, F. (2018). MSC-derived exosomes promote proliferation and inhibit apoptosis of chondrocytes via lncRNA-KLF3-AS1/miR-206/GIT1 axis in osteoarthritis. *Cell Cycle* 17, 2411–2422. doi: 10.1080/15384101.2018.1526603

Loef, M., Van Beest, S., Kroon, F. P. B., Bloem, J. L., Dekkers, O. M., Reijnierse, M., et al. (2018). Comparison of histological and morphometrical changes underlying subchondral bone abnormalities in inflammatory and degenerative musculoskeletal disorders: a systematic review. *Osteoarthritis Cartilage* 26, 992–1002. doi: 10.1016/j.joca.2018.05.007

Loeser, R. F., Goldring, S. R., Scanzello, C. R., and Goldring, M. B. (2012). Osteoarthritis: a disease of the joint as an organ. *Arthritis Rheum.* 64, 1697–1707. doi: 10.1002/art.34453

Lu, C., Li, Z., Hu, S., Cai, Y., and Peng, K. (2019). LncRNA PART-1 targets TGFBR2/Smad3 to regulate cell viability and apoptosis of chondrocytes via acting as miR-590-3p sponge in osteoarthritis. *J. Cell Mol. Med.* 23, 8196–8205. doi: 10.1111/jcmm.14690

Lü, G., Li, L., Wang, B., and Kuang, L. (2020). LINC00623/miR-101/HRAS axis modulates IL-1β-mediated ECM degradation, apoptosis and senescence of osteoarthritis chondrocytes. *Aging (Albany NY)* 12, 3218–3237. doi: 10.18632/aging.102801

Lu, M., and Zhou, E. (2020). Long noncoding RNA LINC00662-miR-15b-5p mediated GPR120 dysregulation contributes to osteoarthritis. *Pathol. Int.* 70, 155–165. doi: 10.1111/pin.12875

Lu, Z., Luo, M., and Huang, Y. (2019). lncRNA-CIR regulates cell apoptosis of chondrocytes in osteoarthritis. *J. Cell. Biochem.* 120, 7229–7237. doi: 10.1002/jcb.27997

Luo, X., Wang, J., Wei, X., Wang, S., and Wang, A. (2020). Knockdown of lncRNA MFI2-AS1 inhibits lipopolysaccharide-induced osteoarthritis progression by miR-130a-3p/TCF4. *Life Sci.* 240:117019. doi: 10.1016/j.lfs.2019.117019

Mao, G., Kang, Y., Lin, R., Hu, S., Zhang, Z., Li, H., et al. (2019). Long non-coding RNA HOTTIP promotes CCL3 expression and induces cartilage degradation by sponging miR-455-3p. *Front. Cell Dev. Biol.* 7:161. doi: 10.3389/fcell.2019.00161

Mathy, N. W., and Chen, X. M. (2017). Long non-coding RNAs (lncRNAs) and their transcriptional control of inflammatory responses. *J. Biol. Chem.* 292, 12375–12382. doi: 10.1074/jbc.r116.760884

Mohammadi, A., Kelly, O. B., Filice, M., Kabakchiev, B., Smith, M. I., and Silverberg, M. S. (2018). Differential expression of microRNAs in peripheral blood mononuclear cells identifies autophagy and TGF-Beta-related signatures aberrantly expressed in inflammatory bowel disease. *J. Crohns Colitis* 12, 568–581. doi: 10.1093/ecco-jcc/jjy010

Moran-Moguel, M. C., Petarra-Del Rio, S., Mayorquin-Galvan, E. E., and Zavala-Cerna, M. G. (2018). Rheumatoid arthritis and miRNAs: a critical review through a functional view. *J. Immunol. Res.* 2018:2474529.

Ni, J. L., Dang, X. Q., and Shi, Z. B. (2020). CircPSM3 inhibits the proliferation and differentiation of OA chondrocytes by targeting miRNA-296-5p. *Eur. Rev. Med. Pharmacol. Sci.* 24, 3467–3475.

Ouyang, Q., Wu, J., Jiang, Z., Zhao, J., Wang, R., Lou, A., et al. (2017). Microarray expression profile of circular RNAs in peripheral blood mononuclear cells from rheumatoid arthritis patients. *Cell Physiol. Biochem.* 42, 651–659. doi: 10.1159/000477883

Pan, L., Liu, D., Zhao, L., Wang, L., Xin, M., and Li, X. (2018). Long noncoding RNA MALAT1 alleviates lipopolysaccharide-induced inflammatory injury by upregulating microRNA-19b in murine chondrogenic ATDC5 cells. *J. Cell Biochem.* 119, 10165–10175.

Pan, Z., Li, G. F., Sun, M. L., Xie, L., Liu, D., Zhang, Q., et al. (2019). MicroRNA-1224 splicing circularRNA-Filip1l in an Ago2-dependent manner regulates chronic inflammatory pain via targeting Ubr5. *J. Neurosci.* 39, 2125–2143. doi: 10.1523/jneurosci.1631-18.2018

Park, S., Lee, M., Chun, C. H., and Jin, E. J. (2019). The lncRNA, Nespas, Is associated with osteoarthritis progression and serves as a potential new prognostic biomarker. *Cartilage* 10, 148–156. doi: 10.1177/1947603517725566

Qi, K., Lin, R., Xue, C., Liu, T., Wang, Y., Zhang, Y., et al. (2019). Long non-coding RNA (LncRNA) CAIF is downregulated in osteoarthritis and inhibits LPS-induced interleukin 6 (IL-6) upregulation by downregulation of MiR-1246. *Med. Sci. Monit.* 25, 8019–8024. doi: 10.12659/msm.917135

Rong, D., Sun, H., Li, Z., Liu, S., Dong, C., Fu, K., et al. (2017). An emerging function of circRNA-miRNAs-mRNA axis in human diseases. *Oncotarget* 8, 73271–73281. doi: 10.18632/oncotarget.19154

Samartzis, D., Karppinen, J., Mok, F., Fong, D. Y., Luk, K. D., and Cheung, K. M. (2011). A population-based study of juvenile disc degeneration and its association with overweight and obesity, low back pain, and diminished functional status. *J. Bone Joint Surg. Am.* 93, 662–670. doi: 10.2106/jbjs.i.01568

Satoshi Yamashita, H. A. (2012). miRNA functions in arthritis. *Curr. Rheumatol. Rev.* 8, 98–102. doi: 10.2174/157339712802083786

Seeliger, C., Balmayor, E. R., and Van Griensven, M. (2016). miRNAs related to skeletal diseases. *Stem Cells Dev.* 25, 1261–1281. doi: 10.1089/scd.2016.0133

Shao, T., Hu, Y., Tang, W., Shen, H., Yu, Z., and Gu, J. (2019). The long noncoding RNA HOTAIR serves as a microRNA-34a-5p sponge to reduce nucleus pulposus cell apoptosis via a NOTCH1-mediated mechanism. *Gene* 715:144029. doi: 10.1016/j.gene.2019.144029

Shen, H., Wang, Y., Shi, W., Sun, G., Hong, L., and Zhang, Y. (2018). LncRNA SNHG5/miR-26a/SOX2 signal axis enhances proliferation of chondrocyte in osteoarthritis. *Acta Biochim. Biophys. Sin. (Shanghai)* 50, 191–198. doi: 10.1093/abbs/gmx141

Shen, S., Wu, Y., Chen, J., Xie, Z., Huang, K., Wang, G., et al. (2019). CircSERPINE2 protects against osteoarthritis by targeting miR-1271 and ETS-related gene. *Ann. Rheum. Dis.* 78, 826–836. doi: 10.1136/annrheumdis-2018-214786

Smolen, J. S., Aletaha, D., and Mcinnes, I. B. (2016). Rheumatoid arthritis. *Lancet* 388, 2023–2038.

Song, J., Ahn, C., Chun, C. H., and Jin, E. J. (2014). A long non-coding RNA, GAS5, plays a critical role in the regulation of miR-21 during osteoarthritis. *J. Orthop. Res.* 32, 1628–1635. doi: 10.1002/jor.22718

Song, J., Wang, H. L., Song, K. H., Ding, Z. W., Wang, H. L., Ma, X. S., et al. (2018). CircularRNA_104670 plays a critical role in intervertebral disc degeneration by functioning as a ceRNA. *Exp. Mol. Med.* 50:94.

Steck, E., Boeuf, S., Gabler, J., Werth, N., Schnatzer, P., Diederichs, S., et al. (2012). Regulation of H19 and its encoded microRNA-675 in osteoarthritis and under anabolic and catabolic in vitro conditions. *J. Mol. Med. (Berl)* 90, 1185–1195. doi: 10.1007/s00109-012-0895-y

Sun, P., Wu, Y., Li, X., and Jia, Y. (2020). miR-142-5p protects against osteoarthritis through competing with lncRNA XIST. *J. Gene Med.* 22:e3158.

Sun, T., Yu, J., Han, L., Tian, S., Xu, B., Gong, X., et al. (2018). Knockdown of long non-coding RNA RP11-445H22.4 alleviates LPS-induced injuries by regulation of MiR-301a in osteoarthritis. *Cell Physiol. Biochem.* 45, 832–843. doi: 10.1159/000487175

Sun, Y., Kang, S., Pei, S., Sang, C., and Huang, Y. (2020). MiR93-5p inhibits chondrocyte apoptosis in osteoarthritis by targeting lncRNA CASC2. *BMC Musculoskelet. Disord.* 21:26. doi: 10.1186/s12891-019-3025-y

Tan, F., Wang, D., and Yuan, Z. (2020). The fibroblast-like synoviocyte derived exosomal long non-coding RNA H19 alleviates osteoarthritis progression through the miR-106b-5p/TIMP2 axis. *Inflammation* 43, 1498–1509. doi: 10.1007/s10753-020-01227-8

Tan, H., Zhao, L., Song, R., Liu, Y., and Wang, L. (2018). The long noncoding RNA SNHG1 promotes nucleus pulposus cell proliferation through regulating miR-326 and CCND1. *Am. J. Physiol. Cell Physiol.* 315, C21–C27.

Tang, L., Ding, J., Zhou, G., and Liu, Z. (2018). LncRNA-p21 promotes chondrocyte apoptosis in osteoarthritis by acting as a sponge for miR-451. *Mol. Med. Rep.* 18, 5295–5301.

Tang, L. P., Ding, J. B., Liu, Z. H., and Zhou, G. J. (2018). LncRNA TUG1 promotes osteoarthritis-induced degradation of chondrocyte extracellular matrix via miR-195/MMP-13 axis. *Eur. Rev. Med. Pharmacol. Sci.* 22, 8574–8581.

Taurog, J. D., Chhabra, A., and Colbert, R. A. (2016). Ankylosing spondylitis and axial spondyloarthritis. *N. Engl. J. Med.* 374, 2563–2574.

Tian, F., Wang, J., Zhang, Z., and Yang, J. (2020). LncRNA SNHG7/miR-34a-5p/SYVN1 axis plays a vital role in proliferation, apoptosis and autophagy in osteoarthritis. *Biol. Res.* 53:9.

van der Heijde, D., Braun, J., Deodhar, A., Baraliakos, X., Landewé, R., Richards, H. B., et al. (2019). Modified stoke ankylosing spondylitis spinal score as an outcome measure to assess the impact of treatment on structural progression in ankylosing spondylitis. *Rheumatology (Oxford, England)* 58, 388–400.

Verduci, L., Strano, S., Yarden, Y., and Blandino, G. (2019). The circRNA-microRNA code: emerging implications for cancer diagnosis and treatment. *Mol. Oncol.* 13, 669–680. doi: 10.1002/1878-0261.12468

Vieira, A. S., Dogini, D. B., and Lopes-Cendes, I. (2018). Role of non-coding RNAs in non-aging-related neurological disorders. *Braz. J. Med. Biol. Res.* 51, e7566.

Vinatier, C., Merceron, C., and Guicheux, J. (2016). Osteoarthritis: from pathogenic mechanisms and recent clinical developments to novel prospective therapeutic options. *Drug Discov. Today* 21, 1932–1937. doi: 10.1016/j.drudis.2016.08.011

Wang, A., Hu, N., Zhang, Y., Chen, Y., Su, C., Lv, Y., et al. (2019). MEG3 promotes proliferation and inhibits apoptosis in osteoarthritis chondrocytes by miR-361-5p/FOXO1 axis. *BMC Med. Genomics* 12:201. doi: 10.1186/s12920-019-0649-6

Wang, G., Bu, X., Zhang, Y., Zhao, X., Kong, Y., Ma, L., et al. (2017). LncRNA-UCA1 enhances MMP-13 expression by inhibiting miR-204-5p in human chondrocytes. *Oncotarget* 8, 91281–91290. doi: 10.18632/oncotarget.20108

Wang, H., He, P., Pan, H., Long, J., Wang, J., Li, Z., et al. (2018a). Circular RNA circ-4099 is induced by TNF-α and regulates ECM synthesis by blocking miR-616-5p inhibition of Sox9 in intervertebral disc degeneration. *Exp. Mol. Med.* 50:27.

Wang, J., Kong, X., Hu, H., and Shi, S. (2020). Knockdown of long non-coding RNA PVT1 induces apoptosis of fibroblast-like synoviocytes through modulating miR-543-dependent SCUBE2 in rheumatoid arthritis. *J. Orthop. Surg. Res.* 15:142.

Wang, J., Yan, S., Yang, J., Lu, H., Xu, D., and Wang, Z. (2019). Non-coding RNAs in rheumatoid arthritis: from bench to bedside. *Front. Immunol.* 10:3129.

Wang, J., and Zhao, Q. (2020). LncRNA LINC-PINT increases SOCS1 expression by sponging miR-155-5p to inhibit the activation of ERK signaling pathway in rheumatoid arthritis synovial fibroblasts induced by TNF-α. *Int. Immunopharmacol.* 84:106497. doi: 10.3389/fimmu.2019.03129

Wang, Q., Wang, W., Zhang, F., Deng, Y., and Long, Z. (2017). NEAT1/miR-181c regulates osteopontin (OPN)-mediated synoviocyte proliferation in osteoarthritis. *J. Cell Biochem.* 118, 3775–3784. doi: 10.1002/jcb.26025

Wang, T., Liu, Y., Wang, Y., Huang, X., Zhao, W., and Zhao, Z. (2019). Long non-coding RNA XIST promotes extracellular matrix degradation by functioning as a competing endogenous RNA of miR-1277-5p in osteoarthritis. *Int. J. Mol. Med.* 44, 630–642.

Wang, X., Peng, L., Gong, X., Zhang, X., Sun, R., and Du, J. (2018b). LncRNA-RMRP promotes nucleus pulposus cell proliferation through regulating miR-206 expression. *J. Cell Mol. Med.* 22, 5468–5476. doi: 10.1111/jcmm.13817

Wang, X., Wang, B., Zou, M., Li, J., Lü, G., Zhang, Q., et al. (2018c). CircSEMA4B targets miR-431 modulating IL-1β-induced degradative changes in nucleus pulposus cells in intervertebral disc degeneration via Wnt pathway. *Biochim. Biophys. Acta Mol. Basis Dis.* 1864, 3754–3768. doi: 10.1016/j.bbadis.2018.08.033

Wang, X., Zou, M., Li, J., Wang, B., Zhang, Q., Liu, F., et al. (2018d). LncRNA H19 targets miR-22 to modulate H(2) O(2) -induced deregulation in nucleus pulposus cell senescence, proliferation, and ECM synthesis through Wnt signaling. *J. Cell Biochem.* 119, 4990–5002. doi: 10.1002/jcb.26738

Wang, Y., Cao, L., Wang, Q., Huang, J., and Xu, S. (2019). LncRNA FOXD2-AS1 induces chondrocyte proliferation through sponging miR-27a-3p in osteoarthritis. *Artif. Cells Nanomed. Biotechnol.* 47, 1241–1247. doi: 10.1080/21691401.2019.1596940

Wang, Z., Chi, X., Liu, L., Wang, Y., Mei, X., Yang, Y., et al. (2018e). Long noncoding RNA maternally expressed gene 3 knockdown alleviates lipopolysaccharide-induced inflammatory injury by up-regulation of miR-203 in ATDC5 cells. *Biomed. Pharmacother.* 100, 240–249. doi: 10.1016/j.biopha.2018.02.018

Wang, Z., Hao, J., and Chen, D. (2019). Long noncoding RNA nuclear enriched abundant transcript 1 (NEAT1) regulates proliferation, apoptosis, and inflammation of chondrocytes via the miR-181a/glycerol-3-phosphate dehydrogenase 1-Like (GPD1L) axis. *Med. Sci. Monit.* 25, 8084–8094. doi: 10.12659/msm.918416

Wen, J., Liu, J., Zhang, P., Jiang, H., Xin, L., Wan, L., et al. (2020). RNA-seq reveals the circular RNA and miRNA expression profile of peripheral blood mononuclear cells in patients with rheumatoid arthritis. *Biosci. Rep.* 40:BSR20193160.

Wu, Y., Zhang, Y., Zhang, Y., and Wang, J. J. (2017). CircRNA hsa_circ_0005105 upregulates NAMPT expression and promotes chondrocyte extracellular matrix degradation by sponging miR-26a. *Cell Biol. Int.* 41, 1283–1289. doi: 10.1002/cbin.10761

Wu, Y. G., Lu, X. X., Shen, B., and Zeng, Y. (2019). The Therapeutic potential and role of miRNA, lncRNA, and circRNA in osteoarthritis. *Curr. Gene Ther.* 19, 255–263. doi: 10.2174/1566523219666190716092203

Xi, Y., Jiang, T., Wang, W., Yu, J., Wang, Y., Wu, X., et al. (2017). Long non-coding HCG18 promotes intervertebral disc degeneration by sponging miR-146a-5p and regulating TRAF6 expression. *Sci. Rep.* 7:13234.

Xiang, Q., Kang, L., Wang, J., Liao, Z., Song, Y., Zhao, K., et al. (2020). CircRNA-CIDN mitigated compression loading-induced damage in human nucleus pulposus cells via miR-34a-5p/SIRT1 axis. *EBioMedicine* 53:102679. doi: 10.1016/j.ebiom.2020.102679

Xiao, L., Ding, B., Xu, S., Gao, J., Yang, B., Wang, J., et al. (2020). circRNA_0058097 promotes tension-induced degeneration of endplate chondrocytes by regulating HDAC4 expression through sponge adsorption of miR-365a-5p. *J. Cell. Biochem.* 121, 418–429. doi: 10.1002/jcb.29202

Xiao, Y., Yan, X., Yang, Y., and Ma, X. L. (2019). Downregulation of long noncoding RNA HOTAIRM1 variant 1 contributes to osteoarthritis via regulating miR-125b/BMPR2 axis and activating JNK/MAPK/ERK pathway. *Biomed. Pharmacother.* 109, 1569–1577. doi: 10.1016/j.biopha.2018.10.181

Xie, L., Huang, W., Fang, Z., Ding, F., Zou, F., Ma, X., et al. (2019). CircERCC2 ameliorated intervertebral disc degeneration by regulating mitophagy and apoptosis through miR-182-5p/SIRT1 axis. *Cell Death Dis.* 10:751.

Xu, J., and Xu, Y. (2017). The lncRNA MEG3 downregulation leads to osteoarthritis progression via miR-16/SMAD7 axis. *Cell Biosci.* 7:69.

Xue, H., Yu, P., Wang, W. Z., Niu, Y. Y., and Li, X. (2020). The reduced lncRNA NKILA inhibited proliferation and promoted apoptosis of chondrocytes via miR-145/SP1/NF-κB signaling in human osteoarthritis. *Eur. Rev. Med. Pharmacol. Sci.* 24, 535–548.

Yan, S., Wang, P., Wang, J., Yang, J., Lu, H., Jin, C., et al. (2019). Long non-coding RNA HIX003209 promotes inflammation by sponging miR-6089 via TLR4/NF-κB signaling pathway in rheumatoid arthritis. *Front. Immunol.* 10:2218. doi: 10.3389/fimmu.2019.02218

Yang, J., Cheng, M., Gu, B., Wang, J., Yan, S., and Xu, D. (2020). CircRNA_09505 aggravates inflammation and joint damage in collagen-induced arthritis mice via miR-6089/AKT1/NF-κB axis. *Cell Death Dis.* 11:833.

Yang, Q., Li, X., Zhou, Y., Fu, W., Wang, J., and Wei, Q. (2019). A LINC00341-mediated regulatory pathway supports chondrocyte survival and may prevent osteoarthritis progression. *J. Cell Biochem.* 120, 10812–10820. doi: 10.1002/jcb.28372

Yang, S., Zhang, F., Ma, J., and Ding, W. (2020). Intervertebral disc ageing and degeneration: The antiapoptotic effect of oestrogen. *Ageing Res. Rev.* 57:100978. doi: 10.1016/j.arr.2019.100978

Yang, Y., Zhong, Z., Zhao, Y., Ren, K., and Li, N. (2019). LincRNA-SLC20A1 (SLC20A1) promotes extracellular matrix degradation in nucleus pulposus cells in human intervertebral disc degeneration by targeting the miR-31-5p/MMP3 axis. *Int. J. Clin. Exp. Pathol.* 12, 3632–3643.

Ye, F., Gao, G., Zou, Y., Zheng, S., Zhang, L., Ou, X., et al. (2019). circFBXW7 inhibits malignant progression by sponging miR-197-3p and encoding a 185-aa protein in triple-negative breast cancer. *Mol. Ther. Nucleic Acids* 18, 88–98. doi: 10.1016/j.omtn.2019.07.023

Ying, H., Wang, Y., Gao, Z., and Zhang, Q. (2019). Long non-coding RNA activated by transforming growth factor beta alleviates lipopolysaccharide-induced inflammatory injury via regulating microRNA-223 in ATDC5 cells. *Int. Immunopharmacol.* 69, 313–320. doi: 10.1016/j.intimp.2019.01.056

Yu, C., Shi, D., Li, Z., Wan, G., and Shi, X. (2019). Long noncoding RNA CHRF exacerbates IL-6-induced inflammatory damages by downregulating microRNA-146a in ATDC5 cells. *J. Cell Physiol.* 234, 21851–21859. doi: 10.1002/jcp.28749

Yu, C. X., and Sun, S. (2018). An emerging role for circular RNAs in osteoarthritis. *Yonsei Med. J.* 59, 349–355. doi: 10.3349/ymj.2018.59.3.349

Yu, Y., Zhang, X., Li, Z., Kong, L., and Huang, Y. (2018). LncRNA HOTAIR suppresses TNF-α induced apoptosis of nucleus pulposus cells by regulating miR-34a/Bcl-2 axis. *Biomed. Pharmacother.* 107, 729–737. doi: 10.1016/j.biopha.2018.08.033

Yuan, W., Che, W., Jiang, Y.-Q., Yuan, F.-L., Wang, H.-R., Zheng, G.-L., et al. (2015). Establishment of intervertebral disc degeneration model induced by ischemic sub-endplate in rat tail. *Spine J.* 15, 1050–1059. doi: 10.1016/j.spinee.2015.01.026

Zhang, G., Wu, Y., Xu, D., and Yan, X. (2016). Long noncoding RNA UFC1 promotes proliferation of chondrocyte in osteoarthritis by acting as a sponge for miR-34a. *DNA Cell Biol.* 35, 691–695. doi: 10.1089/dna.2016.3397

Zhang, H., Li, J., Shao, W., and Shen, N. (2020a). LncRNA CTBP1-AS2 is upregulated in osteoarthritis and increases the methylation of miR-130a gene to inhibit chondrocyte proliferation. *Clin. Rheumatol.* 39, 3473–3478. doi: 10.1007/s10067-020-05113-4

Zhang, L., Wu, H., Zhao, M., Chang, C., and Lu, Q. (2020b). Clinical significance of miRNAs in autoimmunity. *J. Autoimmun.* 109:102438. doi: 10.1016/j.jaut.2020.102438

Zhang, L., Zhang, P., Sun, X., Zhou, L., and Zhao, J. (2018). Long non-coding RNA DANCR regulates proliferation and apoptosis of chondrocytes in osteoarthritis via miR-216a-5p-JAK2-STAT3 axis. *Biosci. Rep.* 38:BSR20181228.

Zhang, P., Sun, J., Liang, C., Gu, B., Xu, Y., Lu, H., et al. (2020c). lncRNA IGHCγ1 Acts as a ceRNA to regulate macrophage inflammation via the miR-6891-3p/TLR4 Axis in osteoarthritis. *Mediators Inflamm.* 2020:9743037.

Zhang, S. B., Lin, S. Y., Liu, M., Liu, C. C., Ding, H. H., Sun, Y., et al. (2019). CircAnks1a in the spinal cord regulates hypersensitivity in a rodent model of neuropathic pain. *Nat. Commun.* 10:4119.

Zhang, W., Zhang, C., Hu, C., Luo, C., Zhong, B., and Yu, X. (2020d). Circular RNA-CDR1as acts as the sponge of microRNA-641 to promote osteoarthritis progression. *J. Inflamm. (Lond)* 17, 8.

Zhang, X., Huang, C. R., Pan, S., Pang, Y., Chen, Y. S., Zha, G. C., et al. (2020e). Long non-coding RNA SNHG15 is a competing endogenous RNA of miR-141-3p that prevents osteoarthritis progression by upregulating BCL2L13 expression. *Int. Immunopharmacol.* 83:106425. doi: 10.1016/j.intimp.2020.106425

Zhang, X., Ji, S., Cai, G., Pan, Z., Han, R., Yuan, Y., et al. (2020f). H19 Increases IL-17A/IL-23 releases via regulating VDR by interacting with miR675-5p/miR22-5p in ankylosing spondylitis. *Mol. Ther. Nucleic Acids* 19, 393–404. doi: 10.1016/j.omtn.2019.11.025

Zhang, X., Liu, X., Ni, X., Feng, P., and Wang, Y. (2019). Long non-coding RNA H19 modulates proliferation and apoptosis in osteoarthritis via regulating miR-106a-5p. *J. Biosci.* 44:128.

Zhang, Y., Ma, L., Wang, C., Wang, L., Guo, Y., and Wang, G. (2020g). Long noncoding RNA LINC00461 induced osteoarthritis progression by inhibiting miR-30a-5p. *Aging (Albany NY)* 12, 4111–4123. doi: 10.18632/aging.102839

Zhang, Y., Wang, F., Chen, G., He, R., and Yang, L. (2019). LncRNA MALAT1 promotes osteoarthritis by modulating miR-150-5p/AKT3 axis. *Cell Biosci.* 9:54.

Zhao, C. Q., Jiang, L. S., and Dai, L. Y. (2006). Programmed cell death in intervertebral disc degeneration. *Apoptosis* 11, 2079–2088. doi: 10.1007/s10495-006-0290-7

Zhao, K., Zhang, Y., Yuan, H., Zhao, M., and Zhao, D. (2019). Long noncoding RNA LINC00958 accelerates the proliferation and matrix degradation of the nucleus pulposus by regulating miR-203/SMAD3. *Aging (Albany NY)* 11, 10814–10825. doi: 10.18632/aging.102436

Zhao, Y., Zhao, J., Guo, X., She, J., and Liu, Y. (2018). Long non-coding RNA PVT1, a molecular sponge for miR-149, contributes aberrant metabolic dysfunction and inflammation in IL-1β-simulated osteoarthritic chondrocytes. *Biosci. Rep.* 38:BSR20180576.

Zheng, H., Wang, T., Li, X., He, W., Gong, Z., Lou, Z., et al. (2020). LncRNA MALAT1 exhibits positive effects on nucleus pulposus cell biology in vivo and in vitro by sponging miR-503. *BMC Mol. Cell Biol.* 21:23.

Zhi, L., Zhao, J., Zhao, H., Qing, Z., Liu, H., and Ma, J. (2020). Downregulation of LncRNA OIP5-AS1 induced by IL-1b aggravates osteoarthritis via regulating miR-29b-3p/PGRN. *Cartilage* 1947603519900801. doi: 10.1177/1947603519900801 [Published online ahead of print]

Zhou, X., Jiang, L., Fan, G., Yang, H., Wu, L., Huang, Y., et al. (2019). Role of the ciRS-7/miR-7 axis in the regulation of proliferation, apoptosis and inflammation of chondrocytes induced by IL-1β. *Int. Immunopharmacol.* 71, 233–240. doi: 10.1016/j.intimp.2019.03.037

Zhou, Y., Li, S., Chen, P., Yang, B., Yang, J., Liu, R., et al. (2019). MicroRNA-27b-3p inhibits apoptosis of chondrocyte in rheumatoid arthritis by targeting HIPK2. *Artif. Cells Nanomed. Biotechnol.* 47, 1766–1771. doi: 10.1080/21691401.2019.1607362

Zhou, Z. B., Du, D., Huang, G. X., Chen, A., and Zhu, L. (2018). Circular RNA Atp9b, a competing endogenous RNA, regulates the progression of osteoarthritis by targeting miR-138-5p. *Gene* 646, 203–209. doi: 10.1016/j.gene.2017.12.064

Zhou, Z. B., Huang, G. X., Fu, Q., Han, B., Lu, J. J., Chen, A. M., et al. (2019). circRNA.33186 contributes to the pathogenesis of osteoarthritis by sponging miR-127-5p. *Mol. Ther.* 27, 531–541. doi: 10.1016/j.ymthe.2019.01.006

Zhu, Y. J., and Jiang, D. M. (2019). LncRNA PART1 modulates chondrocyte proliferation, apoptosis, and extracellular matrix degradation in osteoarthritis via regulating miR-373-3p/SOX4 axis. *Eur. Rev. Med. Pharmacol. Sci.* 23, 8175–8185.

Conflict of Interest: The authors declare that the research was conducted in the absence of any commercial or financial relationships that could be construed as a potential conflict of interest.

Publisher's Note: All claims expressed in this article are solely those of the authors and do not necessarily represent those of their affiliated organizations, or those of the publisher, the editors and the reviewers. Any product that may be evaluated in this article, or claim that may be made by its manufacturer, is not guaranteed or endorsed by the publisher.

frontiers in Cell and Developmental Biology

ORIGINAL RESEARCH
published: 28 October 2021
doi: 10.3389/fcell.2021.644375

Tet1 Regulates Astrocyte Development and Cognition of Mice Through Modulating GluA1

Weize Xu[1,2†], Xicheng Zhang[1,2†], Feng Liang[3†], Yuhang Cao[1,2,4], Ziyi Li[5], Wenzheng Qu[1,2], Jinyu Zhang[1,2,4], Yanhua Bi[1], Chongran Sun[3], Jianmin Zhang[3], Binggui Sun[6], Qiang Shu[1,2] and Xuekun Li[1,2,4*]*

[1] The Children's Hospital, School of Medicine, Zhejiang University, Hangzhou, China, [2] National Clinical Research Center for Child Health, Hangzhou, China, [3] The Second Affiliated Hospital, School of Medicine, Zhejiang University, Hangzhou, China, [4] The Institute of Translational Medicine, School of Medicine, Zhejiang University, Hangzhou, China, [5] Department of Biostatistics, The University of Texas MD Anderson Cancer Center, Houston, TX, United States, [6] Department of Neurobiology and Department of Neurology of the First Affiliated Hospital, Zhejiang University School of Medicine, Hangzhou, China

OPEN ACCESS

Edited by:
Jorg Tost, Commissariat à l'Energie Atomique et aux Energies Alternatives, France

Reviewed by:
Ye Zhang, University of California, Los Angeles, United States
Peng Jin, Emory University, United States

***Correspondence:**
Qiang Shu
shuqiang@zju.edu.cn
Xuekun Li
xuekun_li@zju.edu.cn

[†]These authors have contributed equally to this work

Specialty section:
This article was submitted to Epigenomics and Epigenetics, a section of the journal Frontiers in Cell and Developmental Biology

Received: *21 December 2020*
Accepted: *11 October 2021*
Published: *28 October 2021*

Citation:
Xu W, Zhang X, Liang F, Cao Y, Li Z, Qu W, Zhang J, Bi Y, Sun C, Zhang J, Sun B, Shu Q and Li X (2021) Tet1 Regulates Astrocyte Development and Cognition of Mice Through Modulating GluA1. Front. Cell Dev. Biol. 9:644375. doi: 10.3389/fcell.2021.644375

Tet (Ten eleven translocation) family proteins-mediated 5-hydroxymethylcytosine (5hmC) is highly enriched in the neuronal system, and is involved in diverse biological processes and diseases. However, the function of 5hmC in astrocyte remains completely unknown. In the present study, we show that *Tet1* deficiency alters astrocyte morphology and impairs neuronal function. Specific deletion of *Tet1* in astrocyte impairs learning and memory ability of mice. Using 5hmC high-throughput DNA sequencing and RNA sequencing, we present the distribution of 5hmC among genomic features in astrocyte and show that *Tet1* deficiency induces differentially hydroxymethylated regions (DhMRs) and alters gene expression. Mechanistically, we found that *Tet1* deficiency leads to the abnormal Ca^{2+} signaling by regulating the expression of GluA1, which can be rescued by ectopic GluA1. Collectively, our findings suggest that Tet1 plays important function in astrocyte physiology by regulating Ca^{2+} signaling.

Keywords: astrocyte, Tet1, neuronal development, cognition, GluA1

INTRODUCTION

As the most abundant glial cells in the central nervous system (CNS), astrocytes are involved in regulating the physiology and pathology of the CNS, such as maintaining CNS homeostasis (Allen and Lyons, 2018). Neurogenesis refers to the proliferation of neural stem cells, lineage commitment, morphological development, and synaptic integration of newborn neurons (Song et al., 2002; Sultan et al., 2015; Cope and Gould, 2019). Astrocytes can also regulate synaptic information processing by releasing signaling molecules, such as transmitters, ATP, as well as trophic factors (Harada et al., 2015; Santello et al., 2019). Consequently, the dysfunction of astrocyte can result in behavioral deficits and involves multiple neurodevelopmental and neurodegenerative diseases (Molofsky et al., 2012; Chung et al., 2015; Phatnani and Maniatis, 2015; Sofroniew, 2015; Zuchero and Barres, 2015; Allen and Lyons, 2018; Santello et al., 2019; Valori et al., 2019). Both Rett syndrome and fragile X syndrome are neurodevelopmental disorders caused by mutation of *MeCP2* and *FMR1*, respectively. *MeCP2*- or *FMR1*-deficient astrocytes induce abnormal neuronal development, while the restoration of mutant genes in astrocytes can ameliorate behavioral deficits of mice

(Ballas et al., 2009; Jacobs and Doering, 2010; Lioy et al., 2011). Furthermore, under some pathological conditions, astrocytes can be reactivated (reactive astrogliosis) and is involved in neurodegenerative diseases (Valori et al., 2019).

Tet (Ten-eleven translocation) family proteins including Tet1, Tet2, and Tet3 mediate the 5-hydroxymethylcytosine (5hmC) modification, which serves as a stable epigenetic marker. Emerging evidences have indicated that 5hmC mediated epigenetic modification regulates neuronal activity, neurogenesis, and cognition and is involved in multiple neurological disorders including autism, Rett syndrome, FXTAS, Alzheimer's disease, and Huntington's disease (Mellen et al., 2012; Tan and Shi, 2012; Kaas et al., 2013; Rudenko et al., 2013; Wang et al., 2013; Zhang et al., 2013; Yao et al., 2014; Papale et al., 2015; Shu et al., 2016; Li X. et al., 2017). Tet1, one of the three Tet protein members, is abundant in mouse brain. Constitutive deficiency of *Tet1* leads to deficits of learning and memory by regulating neuronal gene expression (Kaas et al., 2013; Rudenko et al., 2013; Zhang et al., 2013). Given these results are collected with constitutive *Tet1* KO mice, astrocyte Tet1 may contribute to these phenotypes.

Emerging evidence has shown that DNA modification regulates the function of astrocytes (Neal and Richardson, 2018). The expression of astrocytes marker GFAP can be regulated by 5-methylcytosine (5 mC) (Takizawa et al., 2001). Modulating 5-hmC alters the proliferation and lineage commitment of neural stem cells (Zhang et al., 2013; Li X. et al., 2017). In brain cancer glioblastoma, N^6-methyladenine DNA (6 mA) modifications increase remarkably and are involved in cell proliferation of glioblastoma stem cells (Xie et al., 2018). However, the roles of Tet in regulating the function of astrocytes remains completely unknown.

In the present study we found that *Tet1* depletion significantly reduced the global level of 5hmC in astrocytes and that specific depletion of *Tet1* in astrocytes impaired the learning and memory capabilities of mice. *Tet1* deficiency altered the morphology of astrocytes and led to abnormal neuronal development and aberrant Ca^{2+} signaling in astrocytes. *Tet1* deletion induced differentially hydroxymethylated regions (DhMRs) and altered gene expression. Furthermore, *Tet1* deficiency significantly decreased the expression of GluA1 in astrocytes, and ectopic expression of GluA1 partially rescued the deficits of Ca^{2+} signaling in *Tet1* deficient astrocytes. Our results revealed the essential role of astrocyte Tet1 in regulating neuronal development and cognitive function in mice.

RESULTS

Tet1 Deletion Decreases 5hmC Level in Astrocytes and Impairs the Learning and Memory of Mice

To examine the function of Tet1 in astrocytes, we first isolated astrocytes from newborn pups (postnatal day 1, P1) of wild-type (WT) and *Tet1* constitutive knockout (KO) mice. Immunofluorescence staining results showed that the cultured astrocytes were positive for astrocyte markers Aldh1l1 and Glast, but not positive for neuronal cell markers Map2 and Tuj1 (**Supplementary Figures 1A,B**), suggesting a high homogeneity of cultured astrocytes. *Tet1* mRNA was almost non-detectable in *Tet1* KO astrocyte (**Supplementary Figure 1C**). We next performed 5hmC immunofluorescence staining and found that 5hmC was localized in the nuclei of Gfap positive (Gfap +) astrocytes (**Figure 1A**). DNA dot blot with 5hmC specific antibody and quantification results showed a significant decrease of global 5hmC level in KO astrocyte compared to WT astrocyte (**Figures 1B,C**). A representative image of methylene blue staining indicated the equal amount loading of DNA in WT and KO samples (**Supplementary Figure 1D**).

To specifically delete Tet1 in astrocytes, adult (postnatal 8-week-old) *Glast*-CreER^{T2}:*Tet1*$^{loxp/f}$ mice were injected with tamoxifen (i.p.) and sunflower oil, respectively (**Figure 1D**). A Morris water maze test showed that *Tet1* cKO mice spent shorter time in the target quadrant, crossed the platform in less numbers, and had increased escape latency, but showed no difference in swimming speed and distance (**Figures 1E–I** and **Supplementary Figures 1E,F**). We further performed an eight-arm maze test (**Figure 1J**) and found that cKO mice also displayed higher error ratios of working memory and reference memory (**Figures 1K,L** and **Supplementary Figures 1G,H**). Taken together, these data indicate specific deletion of *Tet1* in astrocyte impairs the learning and memory of mice.

Tet1 Deficiency Inhibit Morphological Development of Astrocyte

Next, we performed immunofluorescence staining of astrocyte specific marker Gfap and found that the intensity of Gfap signal was decreased in the hippocampus of cKO mice compared with that of control mice (**Figure 2A**). Quantification results showed that *Tet1* deficient astrocyte displayed smaller size, shorter length of neurites, and fewer intersections compared to control groups (**Figures 2B–G**). Immunostaining of another astrocyte marker s100β also showed the decreased signal intensity in the hippocampus of cKO mice compared with that of control mice (**Supplementary Figures 2A,B**). Collectively, these results suggest that *Tet1* deficiency alters the morphology of astrocytes.

To examine the effects of *Tet1* deficiency in astrocyte on neuronal cells, we adopted a neuron-astrocyte co-culture system (**Supplementary Figure 2C**). We found that hippocampal neurons co-culturing with *Tet1* KO astrocytes exhibited immature morphology compared to control groups (**Figure 3A**). Quantification results indicated that hippocampal neurons co-culturing with KO astrocytes displayed shorter dendrites, fewer intersections, and reduced complexity (**Figures 3B–D**). Of note, the morphology of WT astrocytes became more mature and much larger during the co-culture with neurons, whereas KO astrocytes did not show observable changes (**Supplementary Figures 2D–E**). Furthermore, Golgi staining and quantification results showed that the neurons in the hippocampus of adult cKO mice showed shorter dendrites and fewer spines compared to WT mice (**Figures 3E,F**). Taken together, these results suggest that the deficiency of *Tet1* in astrocyte not only alters the morphology

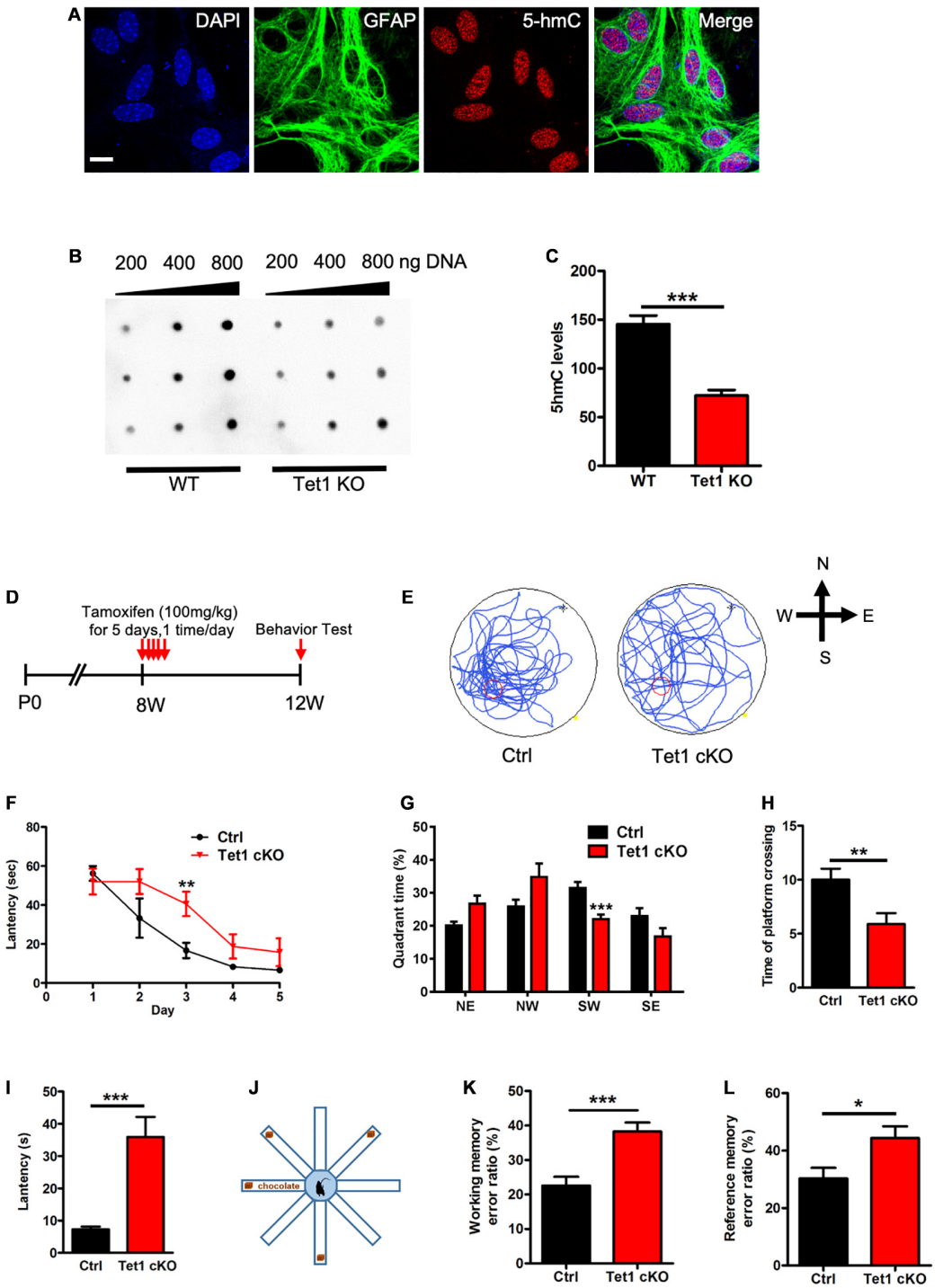

FIGURE 1 | *Tet1* KO reduced the 5hmC level of astrocyte and impaired the learning and memory of mice. **(A)** Representative immunostaining (IF) images of primary astrocyte with nuclei dye DAPI, astrocyte marker Gfap, and 5hmC. Scale bar, 20 μm. **(B,C)** Representative dot blot images with 5hmC-specific antibody **(B)** and quantification showed that *Tet1* KO significantly decreased the level of 5hmC. $n = 3$ for each group. Data were presented as mean ± SEM, unpaired *t*-test; $^{*}P < 0.05$; $^{**}P < 0.01$; $^{***}P < 0.001$. **(D)** Diagram illustrates the scheme of Tamoxifen (TAM) injection to generate *Tet1* cKO mice. Glast-CreER^{T2}:Tet1$^{loxp/loxp}$ male mice received 100 mg/kg TAM, or equal volume of solvent as WT, for five consecutive days at the age of 8-week. 4 weeks after the final TAM injection, mice were used for further experiments. **(E)** The latency of WT and cKO mice during five training days. **(F)** Representative images of the swimming path of WT and cKO mice in Morris water maze (MWM) test. **(G–I)** The percentage of time in the quadrants **(G)**, the number of platform crossings **(H)**, and latency **(I)** of WT and *Tet1* cKO mice in the probe test. Data were presented as mean ± SEM, WT = 9, *Tet1* cKO = 11, unpaired *t*-test; $^{*}P < 0.05$; $^{**}P < 0.01$; $^{***}P < 0.001$. **(J)** The schematic diagram of 8-arm maze test. **(K,L)** Eight-arm maze test showed that cKO mice had higher error ratios for the working memory **(K)** and reference memory **(L)**. Data were presented as mean ± SEM, WT = 9, Tet1 cKO = 11, unpaired *t*-test; $^{*}P < 0.05$; $^{**}P < 0.01$; $^{***}P < 0.001$.

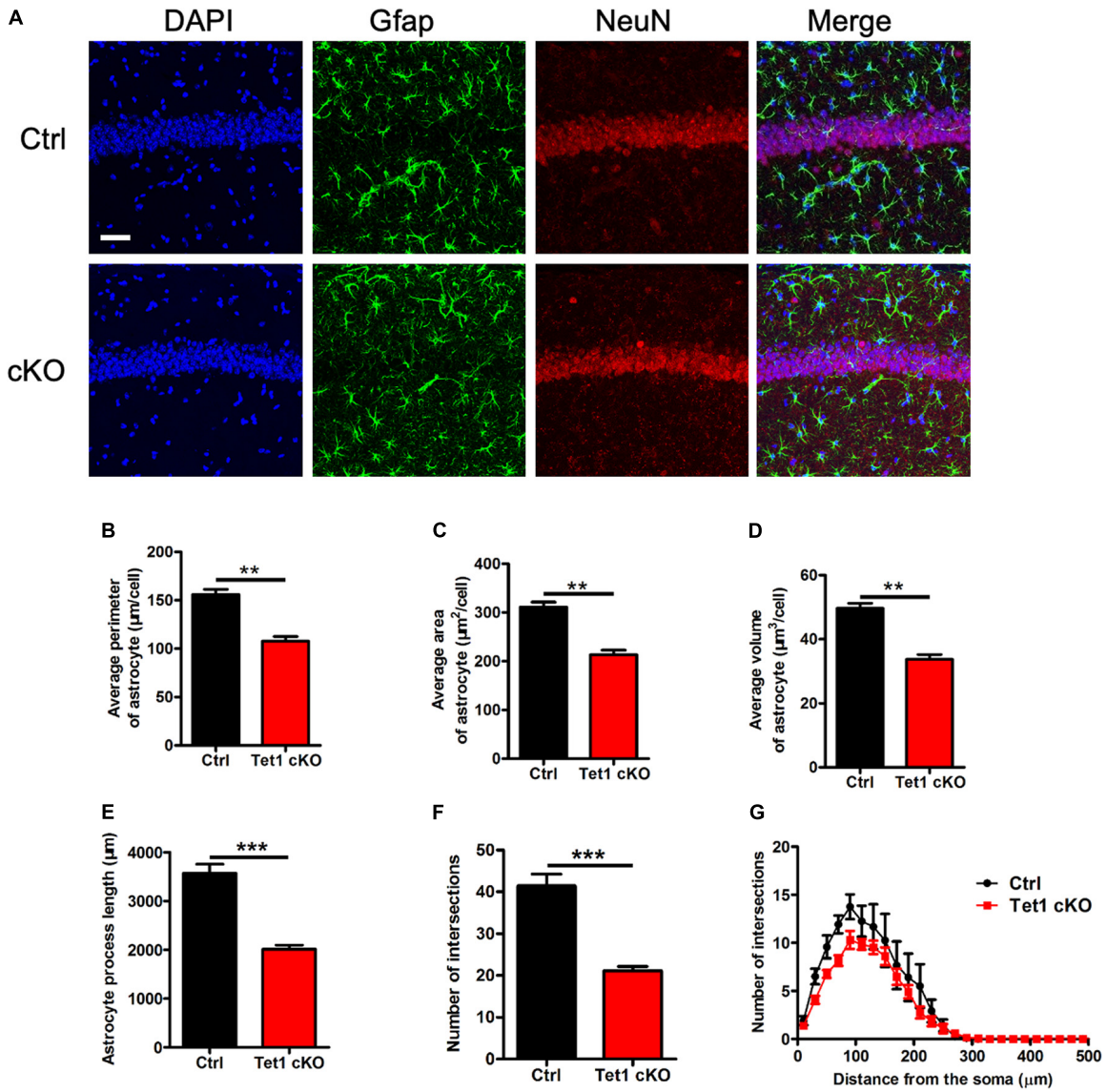

FIGURE 2 | *Tet1* deficiency reduces the complexity of astrocyte morphology. **(A)** Representative immunostaining images of astrocyte marker Gfap and mature neuron marker NeuN with brain sections containing the hippocampus CA1 region of WT and Tet1 cKO mice. Scale bar, 100 μm. **(B–G)** Quantification with Imaris software showed that the perimeter **(B)**, the area **(C)**, the volume **(D)**, the process length **(E)**, the total number of intersections **(F)**, the intersection number at distance from soma **(G)** of astrocyte decreased in Tet1 cKO mice compared to those of Ctrl mice. 5–6 brain sections with the target region were picked up from 3 WT and cKO mice, respectively. Data were presented as mean ± SEM, unpaired *t*-test; $^{*}P < 0.05$; $^{**}P < 0.01$; $^{***}P < 0.001$.

of astrocytes but also inhibits the neuronal development *in vitro* and *in vivo*.

Tet1 Loss Alters Gene Expression and Leads to Dynamic 5hmC Modification in Astrocytes

To reveal the mechanism of astrocyte Tet1 in regulating neuronal development and cognitive function, we next performed RNA-sequencing (RNA-seq) to examine mRNA expression in cultured WT and *Tet1* KO astrocytes. FPKM of astrocyte markers *Gfap*, *Aldh1l1* showed a high level, but the expression markers for neural precursor/stem cell marker *Nestin*, neuronal progenitor cell marker *DCX*, neuronal markers *Map2* and *Tuj1* were almost non-detectable in both WT and KO cells, suggesting a high homogeneity of cultured astrocytes (**Supplementary Figure 3A**). The results of RNA-seq showed that a total of 4,116 genes showed altered expression in KO astrocytes compared to WT cells: 1,943 up-regulated and 2,173 down-regulated ($P < 0.05$, fold change > 1) (**Figure 4A** and **Supplementary Table 1**). Gene Ontology (GO) analysis of the altered genes showed enrichment of genes related to neuronal development, axon development, response to external stimulus, cell activation, and ion transport, etc. (**Figures 4B,C**).

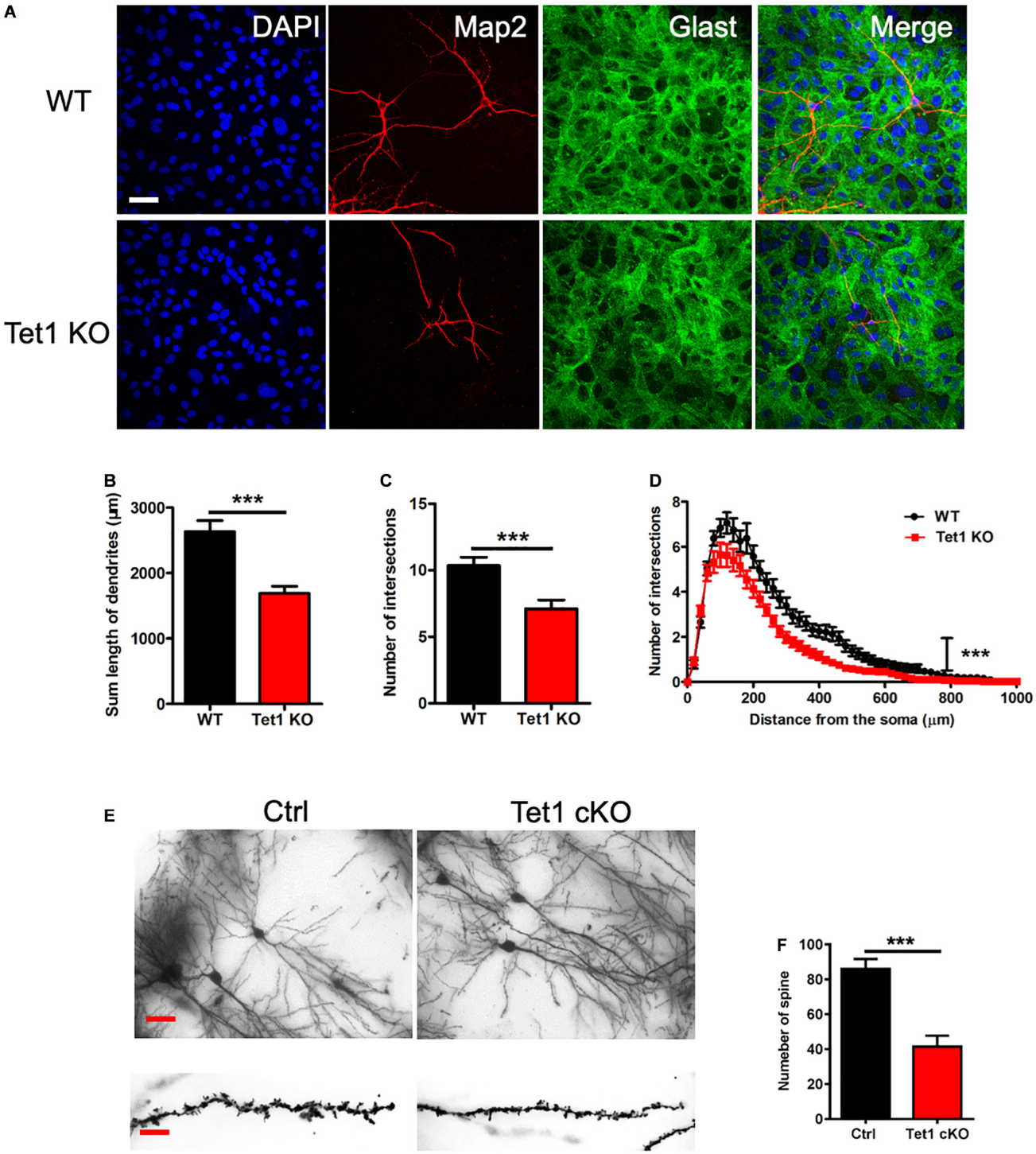

FIGURE 3 | *Tet1* deficiency in astrocyte impairs the morphology of neurons *in vivo* and *in vitro*. **(A)** Representative immunostaining images of astrocyte marker Glast and neuronal cell marker Tuj1. WT hippocampal neurons were co-cultured with WT and KO astrocyte, respectively. Scale bar, 100 μm. **(B–D)** Quantification results showed that neurons co-cultured with KO astrocyte had the decreased dendritic length **(B)** and number of intersections **(C)**. Sholl analysis showed that neurons co-cultured with KO astrocyte also had the reduced intersection number at distance from soma compared to neurons co-cultured with WT astrocyte. 42 neurons co-cultured with WT astrocytes and 36 neurons co-cultured with *Tet1* KO astrocytes were analyzed, respectively. Data were presented as mean ± SEM, unpaired *t*-test; ***$P < 0.001$. **(E)** Representative images of Golgi staining with the brain sections of Ctrl and *Tet1* cKO mice. shows the morphology of neuron of WT and Tet1cKO mice in CA1 region. Scale bars, 200 μm (in the upper panels), and 10 μm (in the lower panels). **(F)** Quantification results showed the decreased spine number of neurons in *Tet1* cKO mice compared to Ctrl mice. 10 neurons from Ctrl mice and 9 neurons from cKO mice were analyzed, respectively. Data were presented as mean ± SEM, unpaired *t*-test; ***$P < 0.001$.

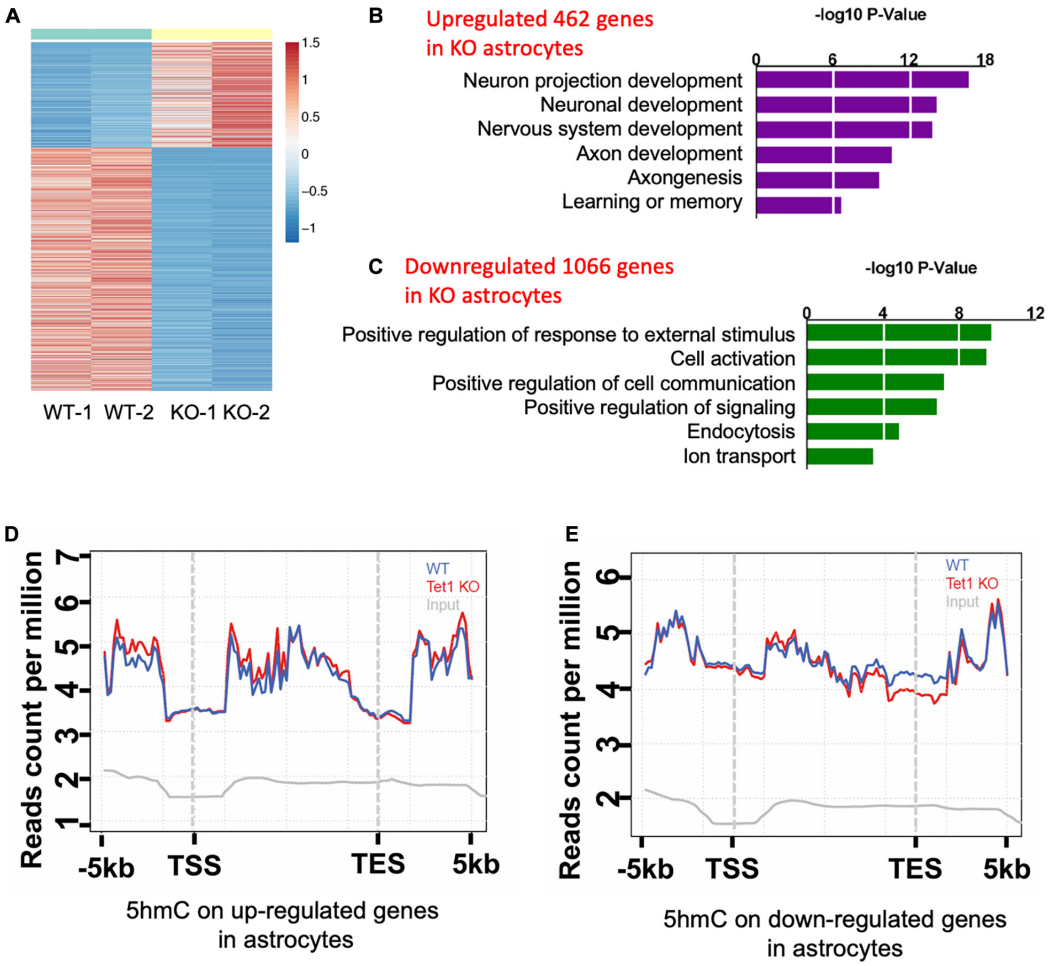

FIGURE 4 | *Tet1* deficiency leads to the altered gene expression and differential hydroxymethylation. **(A)** Heat map drawn from the altered transcriptome of WT and *Tet1* KO astrocytes. Three biological repeats of WT and Tet1 KO cells were adopted for RNA-seq, respectively. The significance of expression was determined by | FC| > 1 and *P*-value < 0.05. **(B,C)** Gene ontology (GO) analysis showed that up-regulated genes enriched for the terms relating with negative regulation of neuronal development and neurogenesis, etc. **(B)**, and down-regulated genes enriched from gliogenesis and cognition, etc. **(D,E)** Averaged 5hmC level over the up-regulated genes **(D)** and down-regulated genes **(E)** of wildtype (WT), Tet1 KO and input astrocyte samples. Tet1 KO astrocyte showed higher 5hmC enrichment on the promoters and gene bodies of up-regulated genes, and lower enrichment on promoters and transcription start sites (TSS) of down-regulated genes.

Next, we performed genome-wide 5hmC profiling of WT and *Tet1* KO astrocytes utilizing an established 5hmC chemical labeling and affinity purification method (Song et al., 2011; Szulwach et al., 2011). We analyzed 5hmC sequencing data with an established pipeline and found that 5hmC was highly enriched in distinct genomic regions, such as intron, exon, promoter, and intergenic regions in WT astrocytes. We also found that *Tet1* KO did not significantly alter the distribution landscape of 5hmC in the genome (**Supplementary Figures 3B,C**). Further, the differential hydroxymethylation regions (DhMRs) induced by *Tet1* KO were enriched in intron, exon, promoter, and intergenic regions (**Supplementary Figures 3D, 4E**), which were associated with 9,547 genes (**Supplementary Table 2**). We further performed a correlation analysis of DhMRs and genes with altered expression indicated by RNA-seq. Our results revealed increased enrichment of 5hmC distribution on up-regulated genes, especially at promoter and gene body regions (**Figure 4D**), and decreased 5hmC distribution on down-regulated genes, especially at promoter, and TSS regions (**Figure 4E**). These results suggest a positive correlation of 5hmC and gene expression in astrocytes.

Tet1 Deficiency Leads to Down-Regulation of *GluA1* and Induces Abnormal Ca^{2+} Signaling

Given *Tet1* deficiency in astrocyte affecting neuronal development and memory, we speculate that *Tet1* deficiency induced the deficits of communication between astrocytes and neurons. RNA-seq data analysis showed that the expression of *GluA1*, the subunit of AMPA receptor, was significantly decreased in *Tet1* KO astrocytes (**Supplementary Figure 4A**), whereas other subunits of AMPA receptor *GluA2-3* were increased (**Supplementary Figures 4B–D**). 5hmC-seq results

and 5hmC-IP followed by qPCR both showed a significant decrease of 5hmC modification on GluA1 (**Figures 5A,B**). Immunofluorescence staining of GluA1 with WT and *Tet1* KO astrocytes showed that the signal intensity of GluA1 was significantly decreased in *Tet1* KO astrocytes compared to WT astrocytes (**Figure 5C**). Consistently, qRT-PCR and western blot assay results showed that the expression of GluA1 was significantly decreased in *Tet1* KO astrocytes (**Figures 5D–F**). Immunofluorescence staining results showed that the signal intensity of GluA1 was significantly decreased in hippocampi region of *Tet1* cKO mice compared to WT mice (**Supplementary Figure 4E**). In addition, qRT-PCR and western blot assays showed that acute knock down of *Tet1* also decreased the expression of *GluA1* (**Supplementary Figures 4F–H**). Taken together, these results suggest that *Tet1* deletion reduced the expression of GluA1 in astrocyte. Considering the important function of GluA1 in Ca^{2+} signaling, we next tested Ca^{2+} signal in WT and KO astrocytes with ATP administration. We found that *Tet1* KO astrocyte almost completely lost response to ATP treatment at concentrations of 100 and 1,000 nM (**Figures 5G,H**).

Finally, we examined whether ectopic GluA1 could rescue the deficits of Ca^{2+} signal in *Tet1* KO astrocytes. Western blot assay results showed a high expression efficiency of lentivirus vector expressing GluA1 in N2a cells (**Supplementary Figures 4I,J**). We then infected the cultured WT and *Tet1* KO astrocyte with lentivirus expressing RFP, and RFP + GluA1, respectively, followed by the treatment with 1,000 nM ATP. We observed that ectopic GluA1 could significantly restored Ca^{2+} signal (**Figure 5I** and **Supplementary Figure 4K**). Taken together, these results suggest that *Tet1*-loss induced the deficits Ca^{2+} signaling can be rescued by ectopic GluA1 in astrocyte.

DISCUSSION

Although previous studies have revealed the function of Tets in neurons, in neural stem cells and in cognitive function, the role of Tet in astrocytes still remains unknown (Kaas et al., 2013; Rudenko et al., 2013; Zhang et al., 2013; Zhu X. et al., 2016; Li X. et al., 2017). In the present study we focused on the physiological function of DNA dioxygenase Tet1 in mouse astrocytes. We found that astrocytes *Tet1* loss significantly decreased the global level of 5-hydroxymethylcytosine (5hmC). Specific ablation of Tet1 in astrocytes impaired learning and memory of adult mice and neuronal development. 5hmC genome sequencing showed that *Tet1* deletion induced differentially hydroxymethylated regions (DhMRs), and RNA-seq results showed that *Tet1* loss altered gene expression. Finally, we revealed that *Tet1* deficiency in astrocytes resulted in the abnormal Ca^{2+} signaling of astrocytes by modulating the expression of GluA1. Taken together, these data suggest that Tet1 is important for the function of astrocytes.

Previous research revealed that modulation of Tet1 and Tet3 affected neuronal activity, gene expression, and consequently regulated memory formation and extinction and the formation cerebellar circuitry (Guo et al., 2011; Kaas et al., 2013; Rudenko et al., 2013; Yu et al., 2015; Zhu X. et al., 2016). Although these studies identified the critical function of Tet1 andTet3 in the neuronal system, the evidence regarding the role of Tet in astrocytes is still lacking. Our results showed that specific ablation of astrocytes Tet1 not only significantly decreased the level of 5hmC and altered the morphology of astrocytes, it also impaired neuronal development and cognitive function of mice. Therefore, on the one hand, our findings, suggest that Tet1 plays important functions in different types of cells including neurons and astrocytes. On the other hand, our study provides a new layer of mechanism for how Tet1 regulates brain function, especially for explaining the *in vivo* data generated with *Tet1* constitutive knockout mice (Rudenko et al., 2013; Zhang et al., 2013).

Tets, including Tet1-, Tet2- and Tet3-mediated 5hmC, are dynamic and also conservative during neuronal development and neurogenesis (Szulwach et al., 2011; Hahn et al., 2013; Li X. et al., 2017). Both tissue/cell and developmental stage affect 5hmC distribution at distinct genomic regions, and they also affect the acquisition and loss of 5hmC (Szulwach et al., 2011). Our results showed that 5hmC is almost equally enriched at promoter and gene bodies regions in astrocytes and is different from those of neurons and neural stem cells, which are highly enriched at gene bodies (Song et al., 2011; Szulwach et al., 2011). Consistently, 5hmC is further enriched at promoter and gene bodies of up-regulated genes, while being less enriched at promoter and TES regions of down-regulated genes, underlining the concept that 5hmC is positively associated with gene expression (Mellen et al., 2012; Hahn et al., 2013; Li X. et al., 2017).

Astrocyte tightly interacts with neuronal cells and are involved in brain development and disorders (Clarke and Barres, 2013; Sloan and Barres, 2014; Phatnani and Maniatis, 2015; Zuchero and Barres, 2015; Allen and Lyons, 2018; Khakh and Deneen, 2019). Astrocyte expresses ionotropic and/or metabotropic receptors, and the binding of glutamate to ionotropic and/or metabotropic receptors activates glutamate signaling. The activation of glutamate receptors induces the generation of intracellular ion signals and/or second messengers including ATP release and calcium signaling in astrocytes (Rose et al., 2017). Astrocyte calcium signaling is not only an essential feature of astrocyte activity, also an important mechanism for neuron-glia interaction at synapses. Aberrant calcium signaling is involved in neurodevelopmental and neurodegenerative diseases (Robel and Sontheimer, 2015; Verkhratsky, 2019). Epigenetic modifications have been shown to regulate gene expression and functioning of astrocytes in both development and diseases (Neal and Richardson, 2018; Puri, 2020). Our study provides evidence that shows that *Tet1* deficiency leads to a significant decrease of GluA1 and impairs astroglial calcium signaling. Our results reveal a new mechanism for how Tet1-mediated 5hmC regulates brain function through affecting astrocyte physiology.

MATERIALS AND METHODS

Animals

Mice were housed in a standard condition of the animal center of Zhejiang University on a 12 h light/dark cycle with free access to food and water. The inducible Tet1 conditional knock out

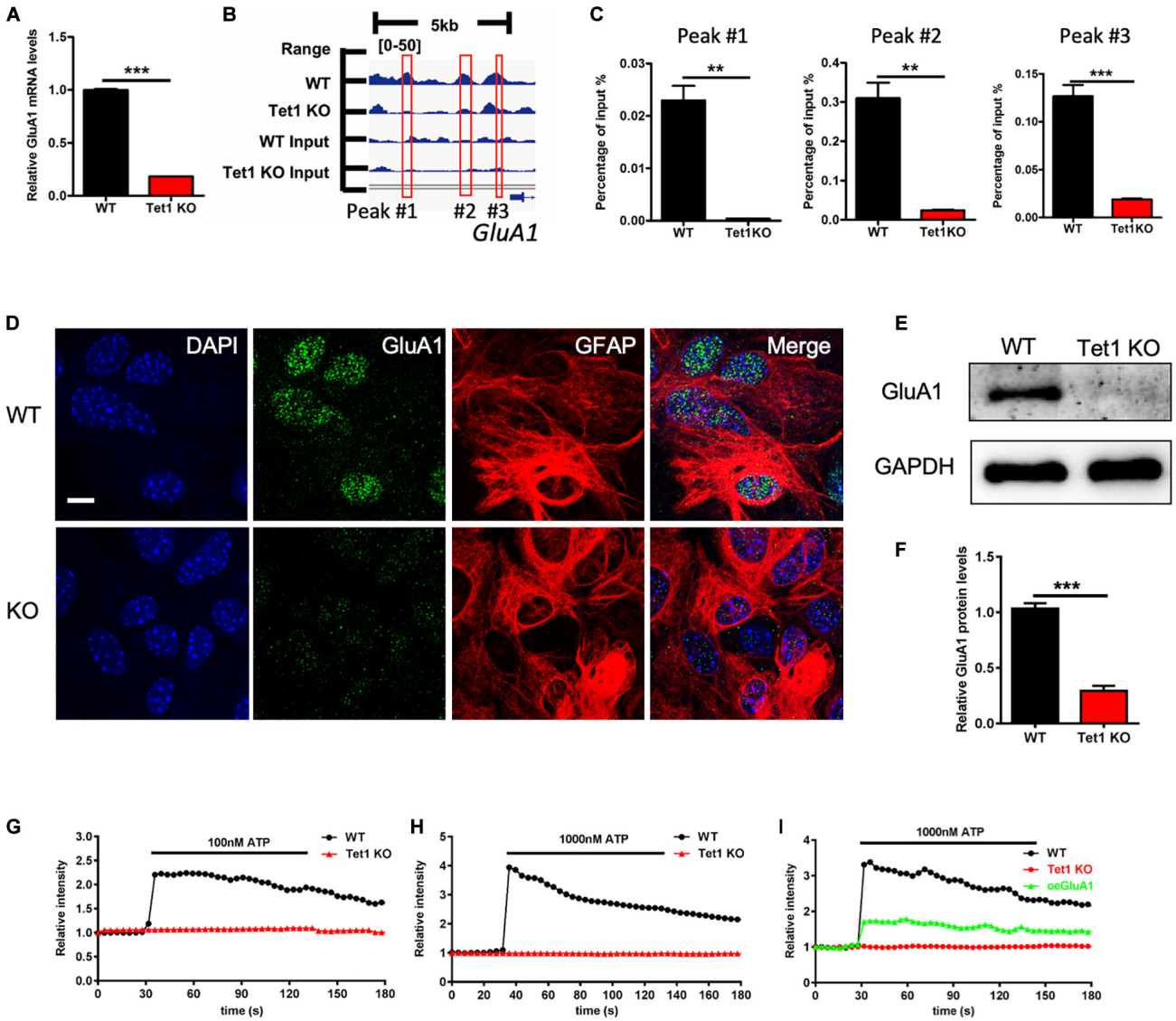

FIGURE 5 | *Tet1* deficiency inhibits the expression of GluA1 and reduces Ca^{2+} signaling. **(A)** 5hmC-seq data analysis identified three loci on GluA1 showing significant 5hmC enrichment for wildtype astrocytes but not for *Tet1* KO astrocytes. **(B)** qPCR results validated the decreased 5hmC enrichment on GluA1. Fold enrichment was calculated as 2-*dCt*, where *dCt* = *Ct* (5-hmC enriched)—*Ct* (input). Data were presented as mean ± SEM, $n = 3$, unpaired *t*-test; $^{**}P < 0.01$; $^{***}P < 0.001$. **(C)** Representative immunostaining images of GluA1 and Gfap with WT and *Tet1* KO astrocytes. Scale bar, 20 μm. **(D–F)** qRT-PCR **(D)** and western blot assay results **(E,F)** showed that *Tet1* KO significantly reduced the level of GluA1. Data were presented as mean ± SEM, $n = 3$, unpaired *t*-test; $^{**}P < 0.01$; $^{***}P < 0.001$. **(G,H)** Representative images show the different Ca^{2+} signal intensity between WT and *Tet1* KO astrocyte evoked by 100 nM ATP **(A)**, 1,000 nM **(B)** ATP, respectively, which indicated by Fluo. 8 am. 8–10 cells were analyzed for each group. **(I)** Ectopic GluA1 restored Ca^{2+} signaling of *Tet1* KO astrocytes. WT astrocyte was infected with lentivirus expressing RFP. KO astrocytes were infected lentivirus expressing RFP, and RFP-GluA1, respectively. 8–10 cells were analyzed for each group.

mice (*Tet1*$^{loxp/loxp}$:*Glast-Cre*^{ERT2}; cKO) by crossing *Tet1*$^{loxp/loxp}$ mice with Glast-Cre^{ERT2} mice (Jackson Laboratory, #012586). *Tet1*$^{loxp/loxp}$ and *Tet1* constitutive knockout (KO) mice were generated as described previously (Zhang et al., 2013). To induce recombination, adult (7–8 weeks old) mice were injected intraperitoneally with sunflower oil only and with Tamoxifen, respectively (100 mg/kg, 1 time/day for five consecutive days). Tamoxifen was prepared in 10% ethanol mixed with sunflower oil (Wako, #196-15265) with occasional vortexing until completely dissolved. All animal experiments were performed according to the protocols approved by the Institutional Animal Care and Use Committee of Zhejiang University.

Behavioral Tests

A Morris water maze test was performed as described previously (Li L. et al., 2017). The test was performed in a round, water-filled tub with 120 cm in diameter. After the mice were trained for 6 days, a probe test was performed. All trials were videotaped

and were analyzed with MazeScan software (Actimetrica, China). The single time-point data were analyzed by Student's *t*-test, and the serial days' data as dependent values were analyzed by two-way ANOVA.

An eight-arm radial maze test was conducted as described previously (Li L. et al., 2017). The apparatus consisted of an octagonal platform at the center and eight identical extending arms equipped with a head-end detector at the end. The movement of the mice was recorded with a video tracking system (Med Associates Inc). The times of the mouse walking through each arm was counted, and data were analyzed by Student's *t*-test.

Isolation and Culture of Astrocytes

Neonatal mice (postnatal day 1–3) were sacrificed, and cortical and hippocampi regions were dissected out with a microscope. The tissues were digested with 0.25% trypsin (Gibco, 25200072) for 25 min at 37°C to dissociate into single cell suspensions. About 1×10^7 cells were plated onto one poly D-lysine coated T25 culture flank with DMEM medium supplemented with 10% FBS, 1% antibiotic-antimycotic, 2 mM L-glutamine, and the medium was replaced every 2 days. After cultured 7–10 days, samples were put on a shaker (240 rpm) for 12 h at 37°C, and the medium was completely replaced with fresh culture medium.

Immunofluorescence Staining

Brain sections were washed with PBS for three times and were blocked with PBS-containing 3% goat serum (Vector Laboratories, #) and 0.1% Triton X-100 for 1 h at room temperature. Sections were incubated with primary antibodies overnight at 4°C and were washed with PBS. The following primary antibodies were used: GFAP (), mouse anti-Neuronal Nuclei (NeuN, Millipore, MAB377), DCX (), and GluA1 (Abcam, ab1232). On the second day, the samples were taken out and washed with PBS for 3 times, 5 min/time, followed by incubation with the secondary antibodies for 1 h at room temperature. Fluorophore-conjugated secondary antibody was used: goat anti-mouse Alexa Fluor 568 (Invitrogen, A11031), goat anti-rat Alexa Fluor 568 (Invitrogen, A11077), goat anti-rabbit Alexa Fluor 488 (Invitrogen, A11008), and goat anti-mouse Alexa Fluor 488 (Invitrogen, A11001). All the sections were observed and images were taken with a confocal microscope (Leica). The images were analyzed with Imarus software.

Golgi Staining

Golgi staining was performed with FD Rapid GolgiStain Kit according to the manufacturer's protocol (FD NeuroTechnologies, #). The morphology of CA1 Neurons of adult control and Tet1 cKO mice were analyzed. The dendritic length, numbers of spines, and sholl analysis were analyzed using Image J software.

Genomic DNA Preparation and Dot Blot

The preparation of Genomic DNA was performed as described previously (Szulwach et al., 2011; Li X. et al., 2017). Briefly, astrocytes were collected, and pellets were lysed with 600 μl DNA lysis buffer (100 mM Tris–HCl, pH 8.0, 5 mM EDTA, 0.2% SDS and 200 mM NaCl) containing Proteinase K and RNase A overnight at 55°C. The second day, equal volumes of phenol:chloroform:isoamyl Alcohol (25:24:1, Sigma, P-3803) were added and completely mixed, followed by centrifugation at 12,000 *g* for 30 min. The supernatant was collected and mixed with 500 μl isopropanol to precipitate DNA. DNA pellets were washed with 70% ethanol and were dissolved with DNase free water. 5-hmC dot blot was performed as described previously (Szulwach et al., 2011; Li X. et al., 2017).

Western Blot

Cell pellets were lysed with RIPA buffer for 30 min on ice. After centrifugation at 12,000 *g* for 30 min at 4°C, the supernatants were collected. The protein concentrations were measured with a biophotometer (Eppendorf). 20 μg total proteins of each sample were applied for SDS-PAGE electrophoresis; then the gel was transferred to PVDF membranes. The following primary antibodies were used: anti-GAPDH (Ambion, AM4300), anti-GluA1 (Abcam, ab1232), anti-Flag (Thermo, MA1-91878), and anti-HA (Diagbio, db5297). The images were measured by Molecular Imager Imaging System (Tanon, China). The intensity of images was analyzed with Adobe Photoshop software.

Total RNA Isolation, Quantitative Real-Time PCR, and RNA-Seq

Total RNA was extracted from cultured astrocytes after using TRIzol reagent following the manufacture's protocol and was purified with chloroform. The concentration of RNA was quantified using a NanoDrop spectrophotometer 2000 (Thermo Fisher Scientific). 0.4 μg of total RNA was used for reverse transcription using a RT reagent kit (Vazyme). Standard real–time qPCR assays were performed using SYBR Green (Vazyme) in triplicate, and the results were analyzed using the $^{\Delta\Delta}$Ct method.

All samples used for the cDNA library was assessed with a NanoDrop spectrophotometer 2000, and the RNA integrity value (RIN) was determined with an Agilent 2100 Bioanalyzer (Agilent Technologies Inc.). The extracted mRNA was fragmented, reverse transcribed into cDNA, and ligated with proprietary adapters to the 3′ and 5′ termini. Subsequently, paired-end sequencing was performed with the Illumina HiSeq sequencing technology (Illumina). Raw sequencing output was filtered, and the retained clean reads were then aligned to the *Mus musculus* reference genome (mm10).

Gene Ontology Analysis

Gene ontology (GO) analysis was performed using the DAVID database (Dennis et al., 2003) as described previously (Chen et al., 2019).

Co-immunoprecipitation

The cultured astrocytes were collected, washed with PBS, and lysed with RIPA buffer on ice for 30 min, followed by treatment of extraction buffer (Thermo Fisher) containing protease inhibitor cocktail (Roche). The samples were sonicated and centrifuged at 12,000 *g* for 10 min at 4°C. The supernatants were collected and

treated with DNase (30 units/ml, Promega) and with RNase A (25 mg/ml) for 20 min at 37°C. The supernatants were incubated with primary antibodies overnight. On the second day, protein A magnetic beads (Sigma) were mixed with samples for 2 h at 4°C. After washing with washing buffer for three times, the beads were re-suspended using 30 μl RIPA buffer and a 10 μl 4X loading buffer. After denaturation, the samples were analyzed using immunoblotting assays, and the second antibodies were used to detect the target proteins.

5-hmC Genome-Wide Sequencing and qPCR

The enrichment of 5-hmC of Genomic DNA was performed as described previously (Szulwach et al., 2011). After purification, biotin-5-N_3-gmC-containing DNA was used for library construction following the Illumina protocol for "preparing samples for ChIP sequencing of DNA." The sequencing data of 5-hmC were analyzed and DhMRs were identified. For the validation of 5hmC enrichment, input or 5-hmC-enriched DNA was used in triplicate 20-μl qPCR reactions. The sequences of used primers were: peak #1: chr11:56821357-56821456,FW-GGTTCTGTGTTGCCGTAAGC,RV-TGGACTGATAGAAGCCAGGGA; peak #2: chr11: 56823323-56823404, FW-TCATTCAATCACGGGCTCTCA, RV-AGGGAGCGAAACTTGTGAGG. Peak #3: chr11:56824653-56824749, FW-TGGGCCAGTGGAGTGTAGAA, RV-ATAGCCCTGGATTCACCAGC.

Calcium Imaging

Fluo8 am (Abcam, ab142773) was used to measure the calcium wave of astrocyte (ref). Briefly, astrocyte was plated on the coverslip at a low confluency. After cultured for 48 h, cells were washed with Hanks' Buffer with 20 mM HEPES and were incubated with 10 μM Fluo8 am for 45 min at room temperature. The calcium signal was evoked by applying ATP, and images were made by confocal microscope (Leica) and were analyzed with a Leica analysis system.

For the rescue of GluA1, WT and Tet1 KO astrocytes were cultured, purified, and plated onto coverslips at a density of 5×10^3/well in 24-well plates. 24 h later, the cells were infected with lentivirus expressing RFP and GluA1, respectively (30 MOI). 2 h later, the medium was replaced with fresh culture medium, and calcium signal was examined 96 h later.

Quantification and Statistical Analysis

All data are expressed as mean ± SE. GraphPad Prism (GraphPad Software Inc.) was used for statistical analysis. Unpaired Student's *t*-test was used to determine the differences between two groups; a two-way ANOVA followed by Tukey's *post hoc* test was used to determine differences between multiple groups. $P < 0.05$ was considered statistically significant.

DATA AVAILABILITY STATEMENT

The datasets presented in this study can be found in online repositories. The names of the repository/repositories and accession number(s) can be found below: NCBI GEO; GSE164025, GSE165370.

ETHICS STATEMENT

The animal study was reviewed and approved by the Institutional Animal Care and Use Committee of Zhejiang University.

AUTHOR CONTRIBUTIONS

XL conceptualized the project and wrote the manuscript. WX, XZ, FL, and YC did astrocytes isolation and culture. YC did immunofluorescence staining, qRT-PCR, western blot and Ca^{2+} signal measurement with the help of JnZ. WQ performed the RNA-seq data analysis. YB and CS maintained the animals and did tamoxifen injection, performed the quantification of immunofluorescence staining and behavioral tests. ZL, YC, and XL analyzed the 5hmC sequencing data. All authors reviewed and approved the final manuscript.

FUNDING

This work was supported by the National Key Research and Development Program of China (2017YFE0196600 to XL) and the National Natural Science Foundation of China (grants 31571518, 31771395 to XL, 81901676 to FL). QS was supported by the Key Research and Development Program of Zhejiang Province (2017C03009). XL was also supported by the Fundamental Research Funds for the Central Universities (2020FZZX003-01-09).

SUPPLEMENTARY MATERIAL

The Supplementary Material for this article can be found online at: https://www.frontiersin.org/articles/10.3389/fcell.2021.644375/full#supplementary-material

Supplementary Figure 1 | (A) Representative immunostaining images of different astrocyte markers including Aldh1l1 and Glast, and neuron markers including Map2 and Tuj1. Scale bar, 50 μm. **(B)** Quantification results showed the homogeneity of the cultured astrocytes. **(C)** qRT-PCR results showed a high knockout efficiency of *Tet1* in astrocytes. Data were presented as mean ± SEM, $n = 3$, unpaired *t*-test; $^*P < 0.05$; $^{**}P < 0.01$; $^{***}P < 0.001$. **(D)** Representative images of methylene blue staining of 5-hmC dot blot. **(E,F)** The average swimming speed **(E)** and swimming distance **(F)** during Morris water maze of Ctrl and *Tet1* cKO mice. Data were presented as mean ± SEM, WT = 9, Tet1 cKO = 11, unpaired *t*-test; $^*P < 0.05$; $^{**}P < 0.01$; $^{***}P < 0.001$. **(G,H)** Eight-arm maze test results showed that cKO mice displayed higher error ratios for both working memory **(G)** and reference memory **(H)** compared to Ctrl mice. Data were presented as mean ± SEM, WT = 9, *Tet1* cKO = 11, unpaired *t*-test; $^*P < 0.05$; $^{**}P < 0.01$; $^{***}P < 0.001$.

Supplementary Figure 2 | (A) Representative immunofluorescence staining images of s100β and NeuN with the brain sections of Ctrl and Tet1 cKO mice. Scale bar, 50 μm. **(B)** Quantification results showed the reduced signal intensity of s100β staining of Tet1 cKO mice compared to that of Ctrl mice. Data were

presented as mean ± SEM, $n = 3$, unpaired t-test; $^{*}P < 0.05$; $^{**}P < 0.01$; $^{***}P < 0.001$. **(C)** Schematic illustration of astrocyte-neuron co-culture system. **(D)** Representative GFAP immunofluorescence staining images of astrocytes before and after co-culture with WT neurons. Scale bar, 30 μm. **(E,F)** The average of area **(E)** and perimeter **(F)** of astrocytes before and after co-culture with neurons. Data were presented as mean ± SEM, $n = 3$, unpaired t-test; $^{*}P < 0.05$; $^{**}P < 0.01$; $^{***}P < 0.001$.

Supplementary Figure 3 | (A) FPKM of astrocyte cell markers *Gfap*, *Aldh1l1*, and *s100β*, neural stem/precursor cell marker *Nestin*, neuronal progenitor cell marker *DCX*, and neuronal cell marker *Map2* and *Tuj1*. **(B,C)** The distribution of 5hmC enrichment in the genome of WT and *Tet1* KO astrocytes. 5hmC is highly enriched at introns, intergenic regions, exons and promoter regions in the genome of both WT and *Tet1* KO astrocytes. **(D,E)** The distribution of differentially 5hmC modified regions (DhMRs) in the genome of WT and *Tet1* KO astrocytes. *Tet1* KO-induced DhMRs are highly enriched at introns, intergenic regions, exons and promoter regions in the genome of both WT and *Tet1* KO astrocytes.

Supplementary Figure 4 | (A) FPKM value of GluA1 of WT and *Tet1* KO astrocytes. **(B–D)** qRT-PCR results showing the expression of *GluA2-4* in WT and *Tet1* KO astrocytes. Data were presented as mean ± SEM, $n = 3$, unpaired t-test; $^{*}P < 0.05$; $^{**}P < 0.01$; $^{***}P < 0.001$. **(E)** Representative images of GluA1 and Gfap immunofluorescence staining with WT and cKO astrocytes. Scale bar, 100 μm. **(F)** qRT-PCR results showed shRNA against *Tet1* significantly decreased the expression of *Tet1* at mRNA level. Data were presented as mean ± SEM, $n = 3$, unpaired t-test; $^{*}P < 0.05$; $^{**}P < 0.01$; $^{***}P < 0.001$. **(G,H)** qRT-PCR results **(G)** and western blot assay **(H)** showed that *Tet1* KD reduced the expression of GluA1 at mRNA and protein levels. Data were presented as mean ± SEM, $n = 3$, unpaired t-test; $^{*}P < 0.05$; $^{**}P < 0.01$; $^{***}P < 0.001$. **(I,J)** Western blot assay **(I)** and quantification results **(J)** validated the expression efficiency of lentivirus-GluA1 plasmid in N2a cells. Data were presented as mean ± SEM, $n = 3$, unpaired t-test; $^{*}P < 0.05$; $^{**}P < 0.01$; $^{***}P < 0.001$. **(K)** Representative images of Ca^{2+} signaling of lentivirus-RFP infected WT astrocytes, lentivirus-RFP infected *Tet1* KO astrocytes, and lentivirus-RFP-GluA1 infected *Tet1* KO astrocytes indicated by fluo-8. Scale bar, 100 μm.

REFERENCES

Allen, N. J., and Lyons, D. A. (2018). Glia as architects of central nervous system formation and function. *Science* 362, 181–185. doi: 10.1126/science.aat0473

Ballas, N., Lioy, D. T., Grunseich, C., and Mandel, G. (2009). Non-cell autonomous influence of MeCP2-deficient glia on neuronal dendritic morphology. *Nat. Neurosci.* 12, 311–317. doi: 10.1038/nn.2275

Chen, J., Zhang, Y. C., Huang, C., Shen, H., Sun, B., Cheng, X., et al. (2019). m(6)A regulates neurogenesis and neuronal development by modulating histone methyltransferase Ezh2. *Genomics Proteomics Bioinformatics* 17, 154–168. doi: 10.1016/j.gpb.2018.12.007

Chung, W. S., Welsh, C. A., Barres, B. A., and Stevens, B. (2015). Do glia drive synaptic and cognitive impairment in disease? *Nat. Neurosci.* 18, 1539–1545. doi: 10.1038/nn.4142

Clarke, L. E., and Barres, B. A. (2013). Emerging roles of astrocytes in neural circuit development. *Nat. Rev. Neurosci.* 14, 311–321. doi: 10.1038/nrn3484

Cope, E. C., and Gould, E. (2019). Adult neurogenesis, glia, and the extracellular matrix. *Cell Stem Cell* 24, 690–705. doi: 10.1016/j.stem.2019.03.023

Dennis, G. Jr., Sherman, B. T., Hosack, D. A., Yang, J., Gao, W., Lane, H. C., et al. (2003). DAVID: database for annotation, visualization, and integrated discovery. *Genome Biol.* 4:3. doi: 10.1186/gb-2003-4-9-r60

Guo, J. U., Su, Y., Zhong, C., Ming, G. L., and Song, H. (2011). Hydroxylation of 5-methylcytosine by TET1 promotes active DNA demethylation in the adult brain. *Cell* 145, 423–434. doi: 10.1016/j.cell.2011.03.022

Hahn, M. A., Qiu, R., Wu, X., Li, A. X., Zhang, H., Wang, J., et al. (2013). Dynamics of 5-hydroxymethylcytosine and chromatin marks in Mammalian neurogenesis. *Cell Rep.* 3, 291–300. doi: 10.1016/j.celrep.2013.01.011

Harada, K., Kamiya, T., and Tsuboi, T. (2015). Gliotransmitter release from astrocytes: functional, developmental, and pathological implications in the brain. *Front. Neurosci.* 9:499. doi: 10.3389/fnins.2015.00499

Jacobs, S., and Doering, L. C. (2010). Astrocytes prevent abnormal neuronal development in the fragile x mouse. *J. Neurosci.* 30, 4508–4514. doi: 10.1523/JNEUROSCI.5027-09.2010

Kaas, G. A., Zhong, C., Eason, D. E., Ross, D. L., Vachhani, R. V., Ming, G. L., et al. (2013). TET1 controls CNS 5-methylcytosine hydroxylation, active DNA demethylation, gene transcription, and memory formation. *Neuron* 79, 1086–1093. doi: 10.1016/j.neuron.2013.08.032

Khakh, B. S., and Deneen, B. (2019). The emerging nature of astrocyte diversity. *Annu. Rev. Neurosci.* 42, 187–207. doi: 10.1146/annurev-neuro-070918-050443

Li, L., Zang, L., Zhang, F., Chen, J., Shen, H., Shu, L., et al. (2017). Fat mass and obesity-associated (FTO) protein regulates adult neurogenesis. *Hum. Mol. Genet.* 26, 2398–2411. doi: 10.1093/hmg/ddx128

Li, X., Yao, B., Chen, L., Kang, Y., Li, Y., Cheng, Y., et al. (2017). Ten-eleven translocation 2 interacts with forkhead box O3 and regulates adult neurogenesis. *Nat. Commun.* 8:15903. doi: 10.1038/ncomms15903

Lioy, D. T., Garg, S. K., Monaghan, C. E., Raber, J., Foust, K. D., Kaspar, B. K., et al. (2011). A role for glia in the progression of Rett's syndrome. *Nature* 475, 497–500. doi: 10.1038/nature10214

Mellen, M., Ayata, P., Dewell, S., Kriaucionis, S., and Heintz, N. (2012). MeCP2 binds to 5hmc enriched within active genes and accessible chromatin in the nervous system. *Cell* 151, 1417–1430. doi: 10.1016/j.cell.2012.11.022

Molofsky, A. V., Krencik, R., Ullian, E. M., Tsai, H. H., Deneen, B., Richardson, W. D., et al. (2012). Astrocytes and disease: a neurodevelopmental perspective. *Genes Dev.* 26, 891–907. doi: 10.1101/gad.188326.112

Neal, M., and Richardson, J. R. (2018). Epigenetic regulation of astrocyte function in neuroinflammation and neurodegeneration. *Biochim. Biophys. Acta Mol. Basis Dis.* 1864, 432–443. doi: 10.1016/j.bbadis.2017.11.004

Papale, L. A., Zhang, Q., Li, S. S., Chen, K. L., Keles, S., and Alisch, R. S. (2015). Genome-wide disruption of 5-hydroxymethylcytosine in a mouse model of autism. *Hum. Mol. Genet.* 24, 7121–7131. doi: 10.1093/hmg/ddv411

Phatnani, H., and Maniatis, T. (2015). Astrocytes in neurodegenerative disease. *Cold Spring Harb. Perspect. Biol.* 7:a020628. doi: 10.1101/cshperspect.a020628

Puri, B. K. (2020). Calcium signaling and gene expression. *Adv. Exp. Med. Biol.* 1131, 537–545. doi: 10.1007/978-3-030-12457-1_22

Robel, S., and Sontheimer, H. (2015). Glia as drivers of abnormal neuronal activity. *Nat. Neurosci.* 19, 28–33. doi: 10.1038/nn.4184

Rose, C. R., Felix, L., Zeug, A., Dietrich, D., Reiner, A., and Henneberger, C. (2017). Astroglial glutamate signaling and uptake in the hippocampus. *Front. Mol. Neurosci.* 10:451. doi: 10.3389/fnmol.2017.00451

Rudenko, A., Dawlaty, M. M., Seo, J., Cheng, A. W., Meng, J., Le, T., et al. (2013). Tet1 is critical for neuronal activity-regulated gene expression and memory extinction. *Neuron* 79, 1109–1122. doi: 10.1016/j.neuron.2013.08.003

Santello, M., Toni, N., and Volterra, A. (2019). Astrocyte function from information processing to cognition and cognitive impairment. *Nat. Neurosci.* 22, 154–166. doi: 10.1038/s41593-018-0325-8

Shu, L. Q., Sun, W. J., Li, L. P., Xu, Z. H., Lin, L., Xie, P., et al. (2016). Genome-wide alteration of 5-hydroxymenthylcytosine in a mouse model of Alzheimer's disease. *BMC Genomics* 17:381. doi: 10.1186/s12864-016-2731-1

Sloan, S. A., and Barres, B. A. (2014). Mechanisms of astrocyte development and their contributions to neurodevelopmental disorders. *Curr. Opin. Neurobiol.* 27, 75–81. doi: 10.1016/j.conb.2014.03.005

Sofroniew, M. V. (2015). Astrocyte barriers to neurotoxic inflammation. *Nat. Rev. Neurosci.* 16, 249–263. doi: 10.1038/nrn3898

Song, C. X., Szulwach, K. E., Fu, Y., Dai, Q., Yi, C., Li, X., et al. (2011). Selective chemical labeling reveals the genome-wide distribution of 5-hydroxymethylcytosine. *Nat. Biotechnol.* 29, 68–72. doi: 10.1038/nbt.1732

Song, H., Stevens, C. F., and Gage, F. H. (2002). Astroglia induce neurogenesis from adult neural stem cells. *Nature* 417, 39–44. doi: 10.1038/417039a

Sultan, S., Li, L., Moss, J., Petrelli, F., Casse, F., Gebara, E., et al. (2015). Synaptic integration of adult-born hippocampal neurons is locally controlled by astrocytes. *Neuron* 88, 957–972. doi: 10.1016/j.neuron.2015.10.037

Szulwach, K. E., Li, X., Li, Y., Song, C. X., Wu, H., Dai, Q., et al. (2011). 5-hmC-mediated epigenetic dynamics during postnatal neurodevelopment and aging. *Nat. Neurosci.* 14, 1607–1616. doi: 10.1038/nn.2959

Takizawa, T., Nakashima, K., Namihira, M., Ochiai, W., Uemura, A., Yanagisawa, M., et al. (2001). DNA methylation is a critical cell-intrinsic determinant of astrocyte differentiation in the fetal brain. *Dev. Cell* 1, 749–758. doi: 10.1016/S1534-5807(01)00101-0

Tan, L., and Shi, Y. G. (2012). Tet family proteins and 5-hydroxymethylcytosine in development and disease. *Development* 139, 1895–1902. doi: 10.1242/dev.070771

Valori, C. F., Guidotti, G., Brambilla, L., and Rossi, D. (2019). Astrocytes: emerging therapeutic targets in neurological disorders. *Trends Mol. Med.* 25, 750–759. doi: 10.1016/j.molmed.2019.04.010

Verkhratsky, A. (2019). Astroglial calcium signaling in aging and Alzheimer's disease. *Cold Spring Harb. Perspect. Biol.* 11:a035188. doi: 10.1101/cshperspect.a035188

Wang, F. L., Yang, Y. R., Lin, X. W., Wang, J. Q., Wu, Y. S., Xie, W. J., et al. (2013). Genome-wide loss of 5-hmC is a novel epigenetic feature of Huntingtons disease. *Hum. Mol. Genet.* 22, 3641–3653. doi: 10.1093/hmg/ddt214

Xie, Q., Wu, T. P., Gimple, R. C., Li, Z., Prager, B. C., Wu, Q., et al. (2018). N(6)-methyladenine DNA modification in glioblastoma. *Cell* 175, 1228–1243.e20. doi: 10.1016/j.cell.2018.10.006

Yao, B., Lin, L., Street, R. C., Zalewski, Z. A., Galloway, J. N., Wu, H., et al. (2014). Genome-wide alteration of 5-hydroxymethylcytosine in a mouse model of fragile X-associated tremor/ataxia syndrome. *Hum. Mol. Genet.* 23, 1095–1107. doi: 10.1093/hmg/ddt504

Yu, H., Su, Y., Shin, J., Zhong, C., Guo, J. U., Weng, Y. L., et al. (2015). Tet3 regulates synaptic transmission and homeostatic plasticity via DNA oxidation and repair. *Nat. Neurosci.* 18, 836–843. doi: 10.1038/nn.4008

Zhang, R. R., Cui, Q. Y., Murai, K., Lim, Y. C., Smith, Z. D., Jin, S., et al. (2013). Tet1 regulates adult hippocampal neurogenesis and cognition. *Cell Stem Cell* 13, 237–245. doi: 10.1016/j.stem.2013.05.006

Zhu, X., Girardo, D., Govek, E. E., John, K., Mellen, M., Tamayo, P., et al. (2016). Role of Tet1/3 genes and chromatin remodeling genes in cerebellar circuit formation. *Neuron* 89, 100–112. doi: 10.1016/j.neuron.2015.11.030

Zuchero, J. B., and Barres, B. A. (2015). Glia in mammalian development and disease. *Development* 142, 3805–3809. doi: 10.1242/dev.129304

Conflict of Interest: The authors declare that the research was conducted in the absence of any commercial or financial relationships that could be construed as a potential conflict of interest.

Publisher's Note: All claims expressed in this article are solely those of the authors and do not necessarily represent those of their affiliated organizations, or those of the publisher, the editors and the reviewers. Any product that may be evaluated in this article, or claim that may be made by its manufacturer, is not guaranteed or endorsed by the publisher.

frontiers in Cell and Developmental Biology

ORIGINAL RESEARCH
published: 08 November 2021
doi: 10.3389/fcell.2021.755409

Identification of ACTA2 as a Key Contributor to Venous Malformation

Song Wang[1], Zifu Zhou[1], Jing Li[1], Yu Wang[1], Hongwen Li[1], Renrong Lv[2], Guangqi Xu[2], Jian Zhang[2], Jianhai Bi[2] and Ran Huo[1,2]**

[1] Department of Burn and Plastic Surgery, Shandong Provincial Hospital, Cheeloo College of Medicine, Shandong University, Jinan, China, [2] Department of Burn and Plastic Surgery, Shandong Provincial Hospital Affiliated to Shandong First Medical University, Jinan, China

Objectives: Proteomics and high connotation functional gene screening (HCS) were used to screen key functional genes that play important roles in the pathogenesis of venous malformation. Furthermore, this study was conducted to analyze and explore their possible functions, establish a gene mutation zebrafish model, and perform a preliminary study to explore their possible pathogenic mechanisms in venous malformation.

Methods: Pathological and normal tissues from patients with disseminated venous malformation were selected for Tandem Mass Tag (TMT) proteomics analysis to identify proteins that were differentially expressed. Based on bioinformatics analysis, 20 proteins with significant differential expression were selected for HCS to find key driver genes and characterize the expression of these genes in patients with venous malformations. *In vitro* experiments were then performed using human microvascular endothelial cells (HMEC-1). A gene mutant zebrafish model was also constructed for *in vivo* experiments to explore gene functions and pathogenic mechanisms.

Results: The TMT results showed a total of 71 proteins that were differentially expressed as required, with five of them upregulated and 66 downregulated. Based on bioinformatics and proteomics results, five highly expressed genes and 15 poorly expressed genes were selected for functional screening by RNAi technology. HCS screening identified ACTA2 as the driver gene. Quantitative polymerase chain reaction (qPCR) and western blot were used to detect the expression of ACTA2 in the pathological tissues of patients with venous malformations and in control tissues, and the experimental results showed a significantly lower expression of ACTA2 in venous malformation tissues ($P < 0.05$). Cell assays on the human microvascular endothelial cells (HMEC-1) model showed that cell proliferation, migration, invasion, and angiogenic ability were all significantly increased in the ACTA2 over-expression group ($P < 0.05$), and that overexpression of ACTA2 could improve the inhibitory effect on vascular endothelial cell proliferation. We constructed an ACTA2-knockdown zebrafish model and found that the knockdown of ACTA2 resulted in defective vascular development, disruption of vascular integrity, and malformation of micro vein

OPEN ACCESS

Edited by:
Zhao-Qian Teng,
Institute of Zoology, Chinese Academy of Sciences (CAS), China

Reviewed by:
Narendra Singh,
Stowers Institute for Medical Research, United States
Apiwat Mutirangura,
Chulalongkorn University, Thailand

***Correspondence:**
Jianhai Bi
bijianhai@126.com
Ran Huo
huoran@medmail.com.cn

Specialty section:
This article was submitted to Epigenomics and Epigenetics, a section of the journal Frontiers in Cell and Developmental Biology

Received: *08 August 2021*
Accepted: *29 September 2021*
Published: *08 November 2021*

Citation:
Wang S, Zhou Z, Li J, Wang Y, Li H, Lv R, Xu G, Zhang J, Bi J and Huo R (2021) Identification of ACTA2 as a Key Contributor to Venous Malformation. Front. Cell Dev. Biol. 9:755409. doi: 10.3389/fcell.2021.755409

development in zebrafish. Further qPCR assays revealed that the knockdown of ACTA2 inhibited the Dll4/notch1 signaling pathway, Ephrin-B2 signaling pathway, and vascular integrity-related molecules and activated the Hedgehog signaling pathway.

Conclusion: This study revealed that ACTA2 deficiency is an important factor in the pathogenesis of venous malformation, resulting in the disruption of vascular integrity and malformed vascular development. ACTA2 can be used as a potential biomarker for the treatment and prognosis of venous malformations.

Keywords: ACTA2, proteomics, zebrafish, vascular development, venous malformation (VM)

INTRODUCTION

Venous malformation (VM) is a common congenital vascular malformations comprising dilated and tortuous veins of variable size with a sparse and disorganized arrangement of vascular smooth muscle cells, which gradually expand and tortuously form clusters with growth and development (Dompmartin et al., 2010; Wassef et al., 2015). It can occur in all parts of the body, with the oral and maxillofacial areas, head and neck, and extremities being the main sites of onset (Judith et al., 2014). The main clinical manifestations are swelling, pain, bleeding, and limited range of motion, which eventually form irreversible dysfunction, leading to severe dysfunction or severe bleeding and becoming life-threatening when the lesions involve vital organs (Dompmartin et al., 2010; Judith et al., 2014; Manoli et al., 2015).

Several pathogenic mutations associated with venous malformation have been recently identified, and attempts have been made to elucidate the pathophysiological pathways involved in their development. Studies have shown that somatic mutations in genes, such as TIE2 (TEK), PIK3CA, and MAP3K3, are associated with VM (Couto et al., 2015; Natynki et al., 2015; Castillo et al., 2016; Seront et al., 2018). Based on the mode of inheritance, VM can be divided into disseminated VM and familial venous malformations (VMCM), of which the familial type is more complex and difficult to treat. Several studies have found that many VMCM patients have specific genetic mutations, namely TIE2-R849W (Calvert et al., 1999; Shu et al., 2012).

In this study, Tandem Mass Tag (TMT) was used to screen proteins that were differentially expressed between patients with disseminated venous malformations and healthy people. The differentially expressed proteins were analyzed by bioinformatics, and their cellular functions and enriched classical molecular pathways were characterized. Twenty differentially expressed proteins were selected for further functional screenings by high-content screening (HCS) at the gene level. The differentially expressed gene ACTA2 was identified and validated in the tissues of patients with venous malformations by RNA and protein expression profiles. Cell assays were performed using human microvascular endothelial cells (HMEC-1) to explore the function of the ACTA2 gene. Finally, we established the ACTA2 zebrafish model to observe how mutations affect the development of the caudal venous plexus and to investigate the related mechanism.

Abbreviations: VM, venous malformations; HCS, high connotation functional gene screening; TMT, Tandem Mass Tag; HMEC, human microvascular endothelial cell; GO, Gene Ontology; GFP, green fluorescent protein; MO, morpholino; CVP, caudal vein plexus; PAV, parachordal vessels; ISV, intersegmental vessel; DLAV, dorsal longitudinal anastomotic vessel.

MATERIALS AND METHODS

Sample Collection

Ten patients with venous malformations from 2019 to 2020 in the Department of Plastic Surgery of Shandong Provincial Hospital were selected, and surgically excised venous malformation tissues were collected (**Table 1**). Ten cases of normal tissues were selected as the control group. The tissue specimens were transferred to liquid nitrogen for preservation. Of these samples, three pairs were used for quantitative proteomics analysis, while all samples were assessed for further validation. Postoperative pathological diagnoses were made by two independent pathologists. The study was approved by the Ethics Committee of Shandong University Provincial Hospital.

Quantitative Proteomics Analysis by Tandem Mass Tag

Protein Extraction, Quantification, and Proteolysis

Each of the control and experimental groups contained three tissue samples that were labeled as A1, A2, and A3 and B1, B2, and B3, respectively. An appropriate amount of SDS Lysis Buffer was added to the samples and transferred to the Lysing Matrix A tube for homogenization with MP homogenizer (24.2, 6.0 M/S, 60 s, twice). After sonication (100 W, 10 s, 10 times), samples were heated in a boiling water bath for 10 min. After centrifugation

TABLE 1 | Clinical characteristics of patients.

ID	Age	Gender	Location	Pathological classification
1	16	Male	Chest	VM
2	9	Female	Leg	VM
3	12	Female	Back	VM
4	12	Male	Leg	VM
5	25	Female	Foot	VM
6	13	Male	Perineum	VM
7	6	Male	Leg	VM
8	10	Female	Face	VM
9	37	Female	Thigh	VM
10	1	Male	Wrist	VM

at 14000 × *g* for 15 min, the supernatant was filtered using a 0.22 μm centrifuge tube, and the filtrate was collected. Protein quantification was performed by the BCA method. The samples were aliquoted and stored at −20°C. Then, 100–200 μg of each sample was retrieved and underwent proteolysis by the filter-aided sample preparation method (Nasevicius and Ekker, 2000), and peptides were quantified by measuring the OD_{280} on the Nanodrop.

Tandem Mass Tag Labeling and High pH RP Peptide Grading

Firstly, 100 μg of the peptide was taken from each sample and labeled by the TMT labeling kit (Thermo, United States) following the manufacturer's instructions. Then, 100 μL of the sample was placed in a centrifuge tube, mixed with TMT solution, vortexed and centrifuged, and left at room temperature for 1 h. The labeled samples were mixed, vortexed and centrifuged, vacuum freeze-dried, and stored at −20°C. The labeled peptides from each group were mixed and graded using the Agilent 1260 Infinity II HPLC system (Agilent, Germany).

Mass Spectrometry Analysis and Identification

Samples were separated using the nanoliter flow rate EASY-nLC System (Thermo, United States). Samples were loaded by autosampler onto an analytical column (Thermo Fisher Scientific Acclaim PepMap RSLC 50 μm × 15 cm, nano viper, P/N164943) for detection and analysis. After separation by chromatography, samples were analyzed by mass spectrometry using a Q Exactive^{TM} plus mass spectrometer (Thermo, United States). The raw data for mass spectrometry analysis were retrieved as raw files, and the software Mascot 2.6 and Proteome Discoverer 2.15 (Thermo, United States) were used for library identification and quantitative analysis.

Bioinformatics Analysis

Gene Ontology (GO) analysis was performed on the collection of differentially expressed proteins, including biological process (BP), molecular function (MF), and cellular component (CC), to explore the function of the target proteins. The kyoto encyclopedia of genes and genomes (KEGG) Orthology (KO) and Links Annotation were used for the pathway enrichment analysis. The target protein sequences were first KO categorized by comparing to the KEGG GENES database, and information on the pathways involved in the target protein sequences was automatically obtained according to the KO categorization.

High-Content Screening Cell Proliferation Assay

The differentially expressed genes were selected based on the results of proteomics and bioinformatics analysis. Multi-target RNAi lentiviral vectors (mix) with a green fluorescent protein (GFP) were prepared for transfection of HMEC-1, and the corresponding control vectors were also prepared. Two-to-three days after the HMEC-1 were transfected with lentiviral vectors, they were inoculated into 96-well plates, and their GFP expression was checked by fluorescence microscopy. When cell fusion reached 70–90%, cells were collected for further experiments. Cell growth was monitored with the Celigo (Nexcelom) high-throughput screening system, which is based on fully automated image acquisition and image data analysis, and light emission was collected from fluorescence-stimulated targets. The targets were the virus-infected GFP-expressing cells, which grew in the 96-well plates. Celigo identified the cells with green fluorescence and took pictures. The images were then analyzed by software to calculate the number of cells in different groups in the plate. After five consecutive days, a cell growth curve was plotted, and statistical analysis was performed on cell proliferation. On day 5, the fold-change values were calculated by comparing the proliferation rate of each group to that of the negative control (NC) group (fold-change of counted cells in the proliferation test NC group/fold-change of counted cells in the experimental group).

Quantitative Real-Time Polymerase Chain Reaction (RT-PCR)

Tissue samples were subjected to total RNA extraction (Trizol kit from Shanghai Pufei). Samples were received according to kit instructions and reverse transcribed to obtain cDNA (Promega M-MLV kit). The reaction system was configured for Real-Time Polymerase Chain Reaction (RT-PCR) in two steps and a melting curve was plotted. Fluorescent amplification was performed using SY and LCPCR amplifiers. Relative quantitative analysis $F = 2^{-\Delta\Delta Ct}$, ΔCt = target gene Ct – internal reference gene Ct; $-\Delta\Delta\Delta Ct$ = mean ΔCt of NC group – ΔCt of each sample; $2^{-\Delta\Delta\Delta Ct}$ reflected the relative expression level of each sample relative to the target gene of samples in the NC group.

Western Blot

Total protein was extracted from the tissues using RIPA lysate (Dingguo Biotech, China). Protein concentration was determined using Bicinchoninic Acid (BCA) Protein Assay Kit (Protein Biotechnology, China). 10% SDS-PAGE electrophoresis was performed. After electrophoresis, proteins were transferred to PVDF (Immobilon-P, Cat. No. IPVH00010) using a transfer electrophoresis device with 150 min of electrotransfer at 4°C and 300 mA constant current. Antibody hybridization: PVDF membranes were closed with a blocking buffer (TBST solution containing 5% skimmed milk) at room temperature for 1 h. The blocking buffer was diluted with primary antibody and then incubated with the closed PVDF membranes at room temperature overnight at 4°C, and the membranes were washed with TBST four times for 8 min each. The PVDF membrane was incubated for 1.5 h at room temperature with the corresponding secondary antibody diluted in the blocking buffer and washed with TBST four times for 8 min each. The protein signal was detected using the ECL kit (Millipore, United States).

Cell Culture and Transfection

The HMEC-1 cell line (CRL-3243) was purchased from the ATCC cell bank. HMEC-1 cell lyophilization tubes were removed from liquid nitrogen and quickly placed in a 37°C water bath and shaken. After complete thawing, the tubes were centrifuged briefly, sterilized with a 75% alcohol wipe, and transferred to a

biosafety cabinet. The supernatant was discarded, and the cells were resuspended and inoculated using a complete medium, gently shaken, and placed in a 5% CO_2 incubator at 37°C. Passaging was performed when the cells reached approximately 80% confluence to maintain good cell growth. HMEC-1 in the logarithmic growth phase was trypsin digested, and 5×10^4 cells/mL cell suspension was made using a complete medium. About 1 mL of cell suspension was inoculated into 12-well culture plates, and the culture was continued to ensure that the spread reached approximately 20% at the time of infection. A 500 uL of infection solution was replaced, and 2.86 uL of virus (7.0E + 8 TU/mL) was added for infection. After 16 h of infection, the fresh culture medium was replaced, and the culture was continued at 37°C. After 72h of infection, the infection efficiency was observed under a fluorescent microscope and photographed. Cells with good growth and successful infection were used for subsequent cytological tests.

Oris™ Cell Migration Assay

The Oris™ stoppers were sterilized in alcohol and placed in a 96-well plate. Then, 3–5 $\times 10^4$ infected cells were seeded into the wells according to the experimental design groups so that the cells could reach 90% confluence the following day. The next day, cells were gently rinsed with PBS 2–3 times, and 1% FBS medium was added to the cell culture. The plate was incubated in a 37°C, 5% CO_2 incubator. Images were captured by Celigo at the appropriate time points three times (generally 0, 8, 16, 24 h, etc.). By adjusting the parameters of the analysis settings, the area of the cells with white or green fluorescence in each scanned well was accurately calculated. Based on the cell area values and time points, differences in the migration ability of tumor cells were determined.

Cell Invasion Assay

The kit (Corning, Cat. No. 354480) was removed, and the chambers were placed in a new 24-well plate with 500 μL of the serum-free medium in each of the upper and lower chambers and placed in an incubator at 37°C for 2 h to allow rehydration of the Matrigel (Corning, Cat. No. 356234) stromal layer. Serum-free HMEC-1 suspension was prepared and counted for 105/well (24-well plate). After rehydration of the Matrigel matrix, all chambers were transferred to new well plates, the medium was removed from the upper chamber, 200 μL of cell suspension was added, and 750 μL of 30% FBS medium was added to the lower chamber. They were incubated for 24 h in a 37°C incubator. The medium was removed, and the non-invasive cells were gently removed from the small chamber with a cotton swab. After staining the transferred cells with 2–3 drops of staining solution (Sigma, Cat. No. 32884) onto the lower surface of the membrane for 3–5 min, the chambers were soaked and rinsed several times and air-dried. Microscopic photographs were taken and counted at 200X for data analysis to compare the difference in the invasion ability of the cells between the experimental and control groups.

Cell Cycle Assay

Cells were grown to 80% confluence in 6 cm diameter dishes. After cells were trypsinized and resuspended into cell suspensions, they were collected in 5 mL centrifuge tubes with three replicate wells per group. After 1300 rpm centrifugation for 5 min, the supernatant was discarded, and cells were washed once with pre-chilled D-Hanks (pH 7.2–7.4) at 4°C. Cells were pelleted by centrifugation at 1300 rpm for 5 min and fixed by pre-chilled 75% ethanol at 4°C for 1 h. After cells were washed again with D-Hanks, they were centrifuged at the same speed for the same period. The cell staining solution was prepared as follows: 40 × PI stock solution:100 × RNase stock:1 × D-Hanks = 25:10:1000. Depending on the number of cells, 0.6–1 mL of cell staining solution was added to resuspend the cells so that the cell passage rate was 300–800 cells/s when tested on the instrument.

Angioplasty Experiments

After HMEC-1 cells were infected, 2×10^5 cells were spread in 6-well plates, walled, washed twice with DPBS (Corning, Cat. No.21-031-CVR), changed to serum-free medium, and cultured for 24 h. The supernatant was collected. Matrigel was removed from −20°C 1 day in advance and left overnight at 4°C. After Matrigel was sufficiently melted, Matrigel was spread in pre-chilled 96-well plates at 70 μL per well and solidified at 37°C for 30 min. HMEC-1 cells were digested, washed 2–3 times with serum-free medium, resuspended to 3×10^4 cells/100 μL with cell culture supernatant, and spread in 96-well plates. After incubation at 37°C for a preset time (2–4 h), the old solution was discarded, and 50 μL of Calcein-AM (Thermo, Cat. No.C3100MP) at a concentration of 0.2 μM was added to each well and incubated at 37°C for 5–10 min. Observation under a fluorescence microscope indicated that the cells had been stained. The plates were placed in a CQ1 instrument and swept to obtain pictures and data.

Zebrafish Care and Maintenance

Adult wild-type AB strain zebrafish were maintained at 28.5°C on a 14 h light/10 h dark cycle. Five to six pairs of zebrafish were set up for nature mating every time. On average, 200–300 embryos were generated. Embryos were maintained at 28.5°C in fish water (0.2% Instant Ocean Salt in deionized water). The embryos were washed and staged. The establishment and characterization of fli1a-EGFP transgenic lines have been described elsewhere. The zebrafish facility at SMOC (Shanghai Model Organisms Center, Inc.) is accredited by the Association for Assessment and Accreditation of Laboratory Animal Care (AAALAC) International.

Zebrafish Microinjections and Angiogenesis Studies

Gene Tools, LLC[1] designed the morpholino (MO). Antisense MO (GeneTools) were microinjected into fertilized one-cell stage embryos according to standard protocols (Nasevicius and Ekker, 2000). The zebrafish ACTA2 gene was targeted by two specific morpholino antisense strategies to prevent either the translation of the zebrafish gene (ATG-MO) or proper splicing of exon2 (E2I2-MO). The sequences of the ACTA2 translation-blocking and splice-blocking morpholinos were 5′-CTTCGT CGTCACACATTTTCAGCTC -3′ (ATG-MO) and 5′- CTTGTGGTACAATAGGTG GTTTACC -3′ (E2I2-MO),

[1]http://www.gene-tools.com/

respectively. The sequence for the standard control morpholino was 5′- CCTCTTACCTCAGTTACAATTTATA -3′ (Gene Tools). The amount of the MOs used for injection was as follows: Control-MO and E2I2-MO, 4ng per embryo; ATG-MO, 4ng per embryo. Primers spanning acta2 exon 1 (forward primer: 5′- CTCCTTGTTTGGGATGTTAGAG -3′) and exon 3 (reverse primer: 5′- CCTCATCACCAACGTAACTATC -3′) were used for RT-PCR analysis for confirmation of the efficacy of the E2I2-MO. The primer ef1α sequences used as the internal control were 5′- GGAAATTCGAGACCAGCAAATAC -3′ (forward) and 5′- GATACCAGCCTCAAACTCACC -3′ (reverse).

To evaluate blood vessels formation in zebrafish, fertilized one-cell fli1a-EGFP transgenic lines embryos were injected with ACTA2-MO and control-MO. At 50-hpf, embryos were dechorionated, anesthetized with 0.016% MS-222 (tricaine methanesulfonate, Sigma-Aldrich, St. Louis, MO, United States). Zebrafish were then oriented on the lateral side (anterior, left; posterior, right; dorsal, top), and mounted with 3% methylcellulose in a depression slide for observation by fluorescence microscopy. The phenotypes of complete intersegmental vessels (ISVs) (i.e., the number of ISVs that connect the DA to the DLAV), CVP (caudal vein plexus) were quantitatively analyzed.

Image Acquisition

Embryos and larvae were analyzed with Nikon SMZ 18 Fluorescence microscope and subsequently photographed with digital cameras. A subset of images was adjusted for levels, brightness, contrast, hue, and saturation with Adobe Photoshop 7.0 software (Adobe, San Jose, CA, United States) to optimally visualize the expression patterns. Quantitative image analyses processed using image-based morphometric analysis (NIS-Elements D4.6, Japan) and ImageJ software (U.S. National Institutes of Health, Bethesda, MD, United States[2]. Ten animals for each treatment were quantified and the total signal per animal was averaged.

Statistical Analysis

All data were presented as the mean ± standard error of mean (SEM). Student's *t*-test (two-tailed) was used for data analysis. Statistical analysis and graphical representation of the data were performed using GraphPad Prism 5.0 (GraphPad Software, San Diego, CA, United States). $P < 0.05$ was considered to be statistically significant.

RESULTS

Quantitative and Statistical Analysis of Proteins Involved in Venous Malformations

A total of 7408 peptides and 801 protein groups were identified in venous malformations and normal tissues. Proteins with expression differences greater than 1.2-fold (upregulated or downregulated) and a *P* value of less than 0.05 were identified as differentially expressed proteins. As a result, 71 differentially expressed proteins were identified, with five of them being upregulated and 66 being downregulated. Quantification results of the proteins were presented in the form of volcano plots, in which red dots indicate the proteins that were significantly upregulated, blue dots indicate that the proteins were significantly down-regulated, and gray dots indicate proteins with no differential expression (**Figure 1A**). Clustering analysis was also performed on these proteins, and the results suggested that there was significant differential expression of proteins in venous malformation tissues compared to normal tissues, where red represents upregulated molecules and blue represents down-regulated molecules (**Figure 1B**).

Bioinformatic Analysis

Gene ontology (GO) analysis was performed on the differentially expressed proteins, including BP, MF, and CC (**Figures 1C,D**). In BP analysis, the differentially expressed proteins primarily focused on the biological regulation, cellular process, and regulation of cytoskeleton organization. In MF analysis, differentially expressed proteins primarily focused on actin filament binding, molecular transducer activity, and binding. In CC analysis, differentially expressed proteins primarily focused on the cytosol, organelles, and cell part.

KEGG Automatic Annotation Server software was used to annotate the KEGG pathways of the target protein collection, and the results showed that the KEGG pathways of differentially expressed proteins primarily included Salmonella infection, the IL-17 signaling pathway, and regulation of the actin cytoskeleton (**Figures 1E,F**).

High-Content Screening Suggested ACTA2 as a Potential Marker for Venous Malformation

Five highly and 15 lowly expressed protein genes were selected based on bioinformatic analysis and proteomics results for the RNAi functional screening test. The upregulated genes were CFHR2, MMP2, COMP, F7, and CD248. The downregulated genes were MAPK1, HSPA8, HSP90AA1, MMP9, ACTA2, YWHAB, HRG, TFPI, TFPI, ACTG1, ACTG1, GSTP1, GAPDH, GAPDH, and S100A9. Based on the HCS platform, *in vitro* knockdown and overexpression of HMEC-1 models were established for the HCS of venous malformations, and 20 selected genes were tested. Lentivirus was used to construct overexpression and knockdown cell models for the corresponding genes. Plasmids were used to construct overexpression cell models for the five upregulated genes. Three RNAi interference sites were designed for 15 downregulated genes, and three plasmids carrying different target sites were packaged into the lentivirus mix. Cells were transfected and cultured in 96-well plates then counted by Incucyte.

The HCS screening results showed that among the 20 genes to be tested, the shACTA2 group with a fold-change > 1.5 was

[2]http://rsbweb.nih.gov/ij/

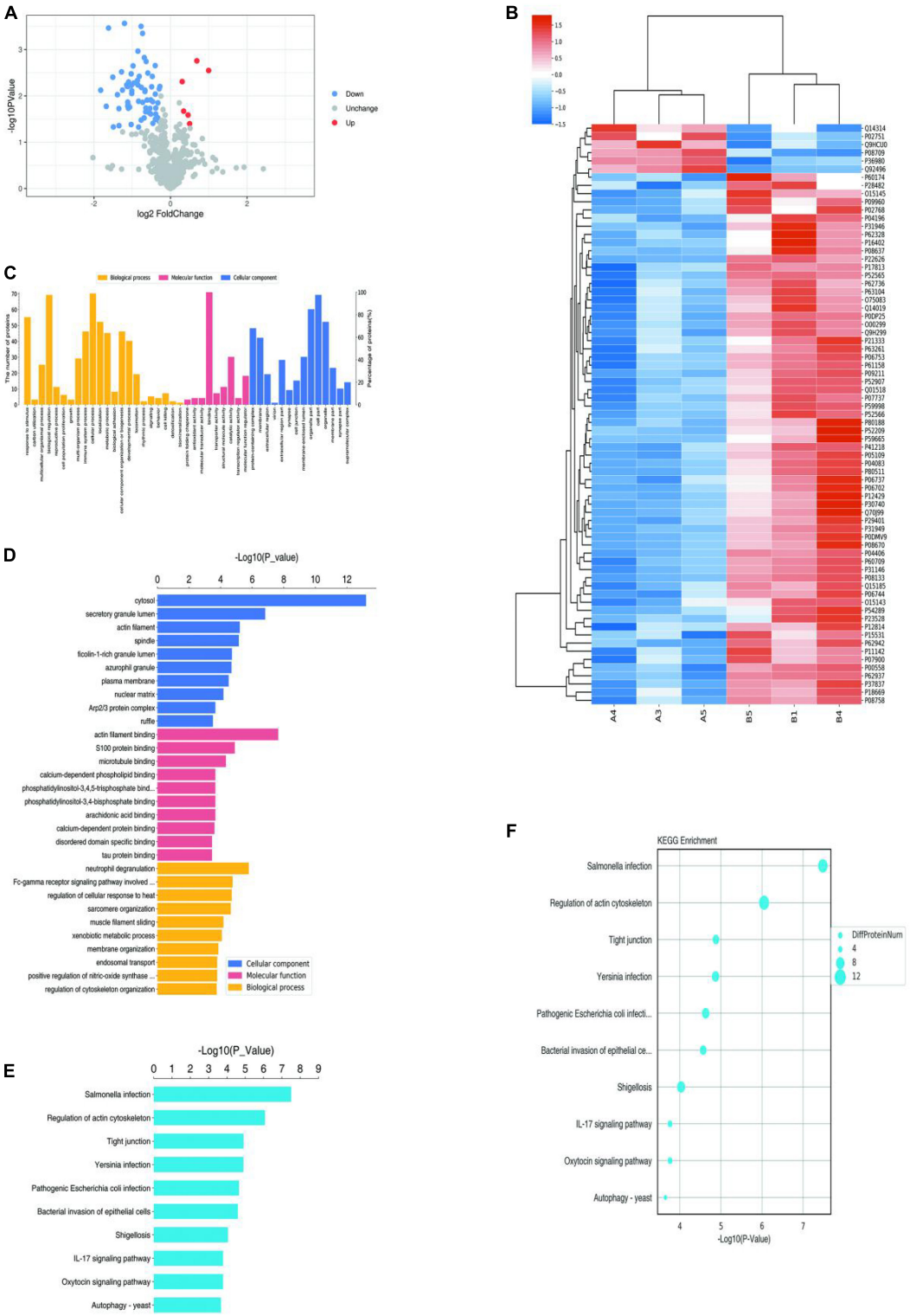

FIGURE 1 | Proteomics and bioinformatics analysis of proteins involved in VM. **(A)** Volcano plots for the differential expression of proteins between VM and the control group (Red—high expression; blue—low expression). **(B)** Heatmap for the differential expression of proteins between VM and control group (Red indicates high expression; blue indicates low expression). **(C)** Gene Ontology (GO) functional annotation analysis of differentially expressed proteins. **(D)** GO functional enrichment analysis of differentially expressed proteins. **(E)** KEGG functional enrichment analysis of differentially expressed proteins. **(F)** KEGG functional enrichment analysis bubble diagram of differentially expressed proteins.

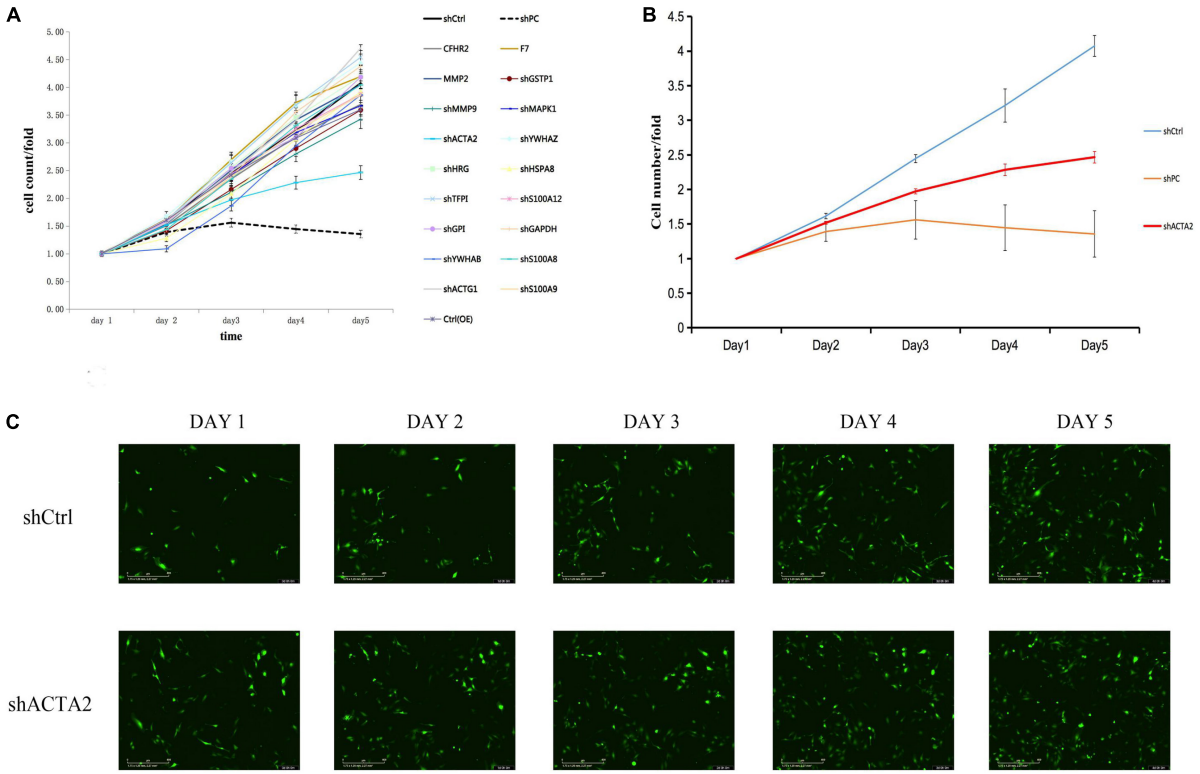

FIGURE 2 | HCS screening identified ACTA2 as a critical gene in promoting VM proliferation. **(A,B)** A total of 20 genes were selected for validation by high-content screening. PC: positive control siRNA targeting b-actin. **(C)** Representative fluorescence images of high-content siRNA screening for ACTA2.

the differentially expressed gene identified in this experiment (proliferation inhibition-positive cell group) (**Figure 2**).

The Actin alpha 2 (ACTA2) gene is widely expressed in most cells, and its mutations have been found to cause a variety of vascular diseases, such as thoracic aortic disease, coronary artery disease, stroke, moyamoya disease, and multisystem smooth muscle dysfunction syndrome.

Lower Expression of ACTA2 in Patients With Venous Malformation

qPCR was used to detect the expression of ACTA2 in pathological tissues of patients with venous malformation and control tissues. The experimental results are shown in **Figures 3A,B**, in which there was a significantly low expression of ACTA2 in venous malformation tissues relative to that in normal tissues ($P < 0.05$). Western blotting results showed that the protein expression of ACTA2 was lower in venous malformation tissues than in control tissues (**Figure 3C**).

Effect of the Overexpression of ACTA2 on the Migration and Invasion Ability of HMEC-1

Considering lower expression of ACTA2 in patients with venous malformation, we performed over-expression of ACTA2 in HMEC1 cells. We constructed LV-ACTA2(27000-1) lentivirus-transfected cells using HMEC1 as the study object, and observed the cells successfully transfected with LV-ACTA2(27000-1) virus overexpressing ACTA2 and negative control virus under a fluorescence microscope after 72 h (**Figure 3D**). RT-PCR assay showed that the expression of TIE2 was significantly higher in the over-expression (OE) group than in the control group (**Figure 3E**), and western blot showed significant overexpression of ACTA2 gene in the OE group (**Figure 3F**). The cells were then used for subsequent functional experiments.

The cell cycle assay revealed that the ACTA2 group had increased cells in the G1/G2 phase ($P < 0.05$), and decreased cells in the S phase ($P < 0.05$), while the NC group was just the opposite (**Figures 4A,B**). The effect of ACTA2 overexpression on vascular endothelial cell migration was detected using Oris^{TM} plate wound-healing, and the results revealed that the migration ability of cells in the overexpression group was higher than that in the control group ($P < 0.05$) (**Figures 4C,D**). As for the invasion ability of cells, the invasion assay results showed that the invasion ability in the overexpression group was significantly higher than that in the control group ($P < 0.05$) (**Figures 4E,F**). Moreover, we used the Cell Counting assay (CCK-8) to analyze the effect of ACTA2 on the proliferation of HMEC-1. Overexpression of ACTA2 significantly increased the proliferative ability of HMEC-1 ($P < 0.05$) (**Figure 4G**). These findings indicate that the overexpression of ACTA2 promotes the proliferation, migration, and invasion ability of human vascular endothelial cells.

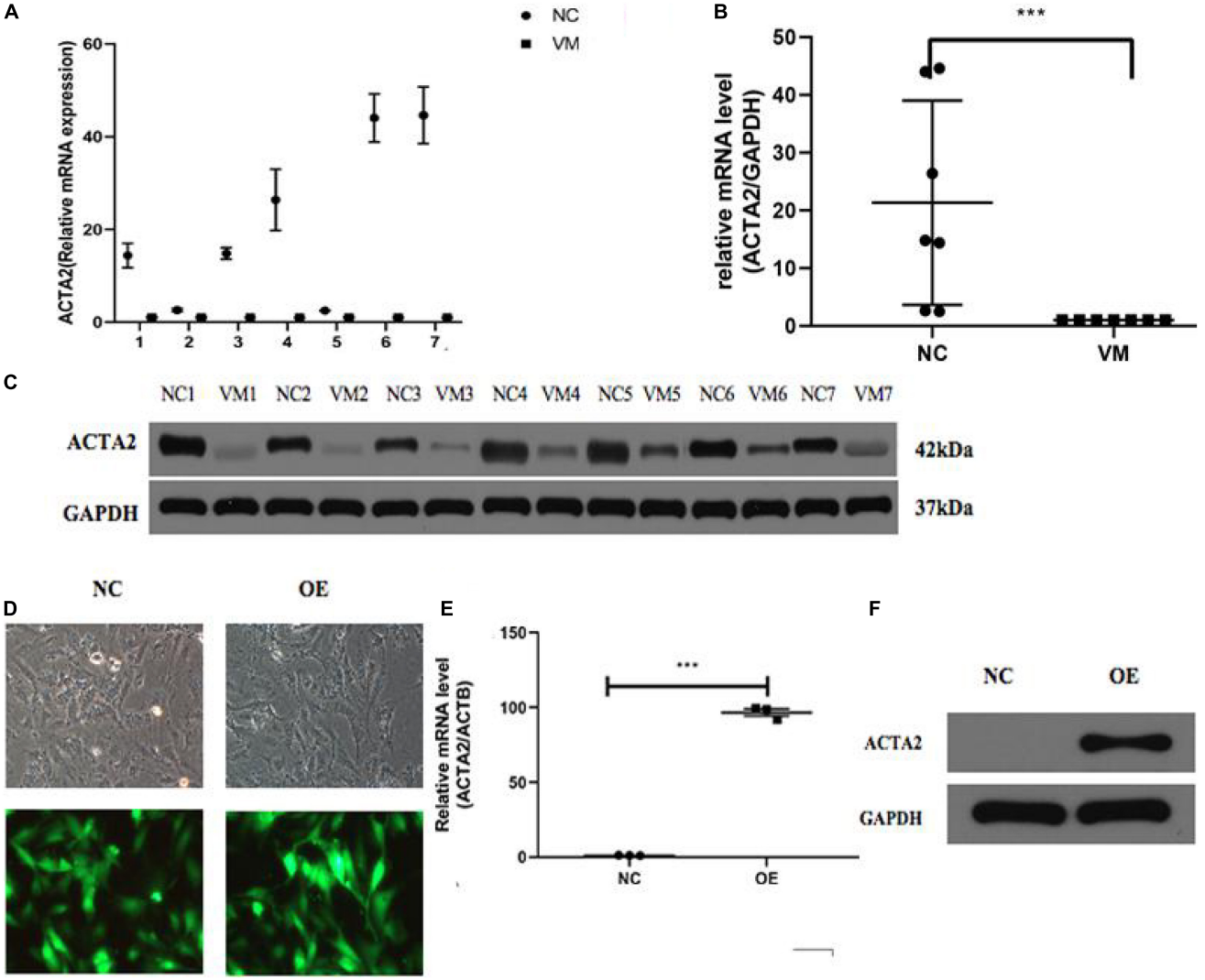

FIGURE 3 | Lower expression of ACTA2 in VM tissues. **(A,B)** The RNA expression level of ACTA2 in 7 pairs of normal and VM tissues. **(C)** Western blotting shows ACTA2 protein expression in 7 pairs of normal and VM tissues. **(D)** Light (up) and fluorescence (down) microscopy images confirming successful transduction of HMEC1 with LV-ACTA2(27000-1) virus and the control group. **(E)** ACTA2 expression levels were assessed by real-time RT-PCR, with GAPDH as an internal control. **(F)** ACTA2 expression levels were assessed by Western blotting. $^{*}P < 0.05$, $^{**}P < 0.01$, $^{***}P < 0.0001$.

Effect of the Overexpression of ACTA2 on Angiogenesis

The *in vitro* angiogenesis assay was used to test whether ACTA2 overexpression leads to the changes relative to the control group. Compared with the normal control group (NC), the angiogenic capacity, including area, length, number of nodes, and number of branches of vessels, were all higher in the overexpression group than in the control group ($P < 0.05$) (**Figure 5**).

Morpholino Knockdown of ACTA2 Causes Vascular Defects, Sprouting Angiogenesis, and Caudal Vein Plexus Formation Defects of Zebrafish

To investigate the vascular formation process affected by ACTA2, a zebrafish model with ACTA2 knockdown was constructed. The zebrafish acta2 gene was targeted by two specific morpholino antisense strategies to prevent either the translation of the zebrafish gene (ATG-MO) or proper splicing of exon2 (E2I2-MO). Primers 1F and 3R interrogate the presence of wild type (non-mutant) transcripts or those in which intron 2 has been inserted and exon 2 has been skipped (**Figure 6A**). And RT-PCR of acta2 transcript from control-MO and E2I2-MO morpholino-injected embryos 2 days after fertilization, demonstrating insertion of intron 2 and skipping of exon 2. Injection of 4 ng of acta2 morpholino alters the splicing between exon 2 and intron 2, as revealed by a shift in PCR bands between control and acta2 morpholino injected embryos (**Figure 6B**). As shown in **Figures 6C,E**, Sanger sequencing of both the wild type band and the intron 2-inserted band and the exon 2-skipped band validating the wild type sequence and the

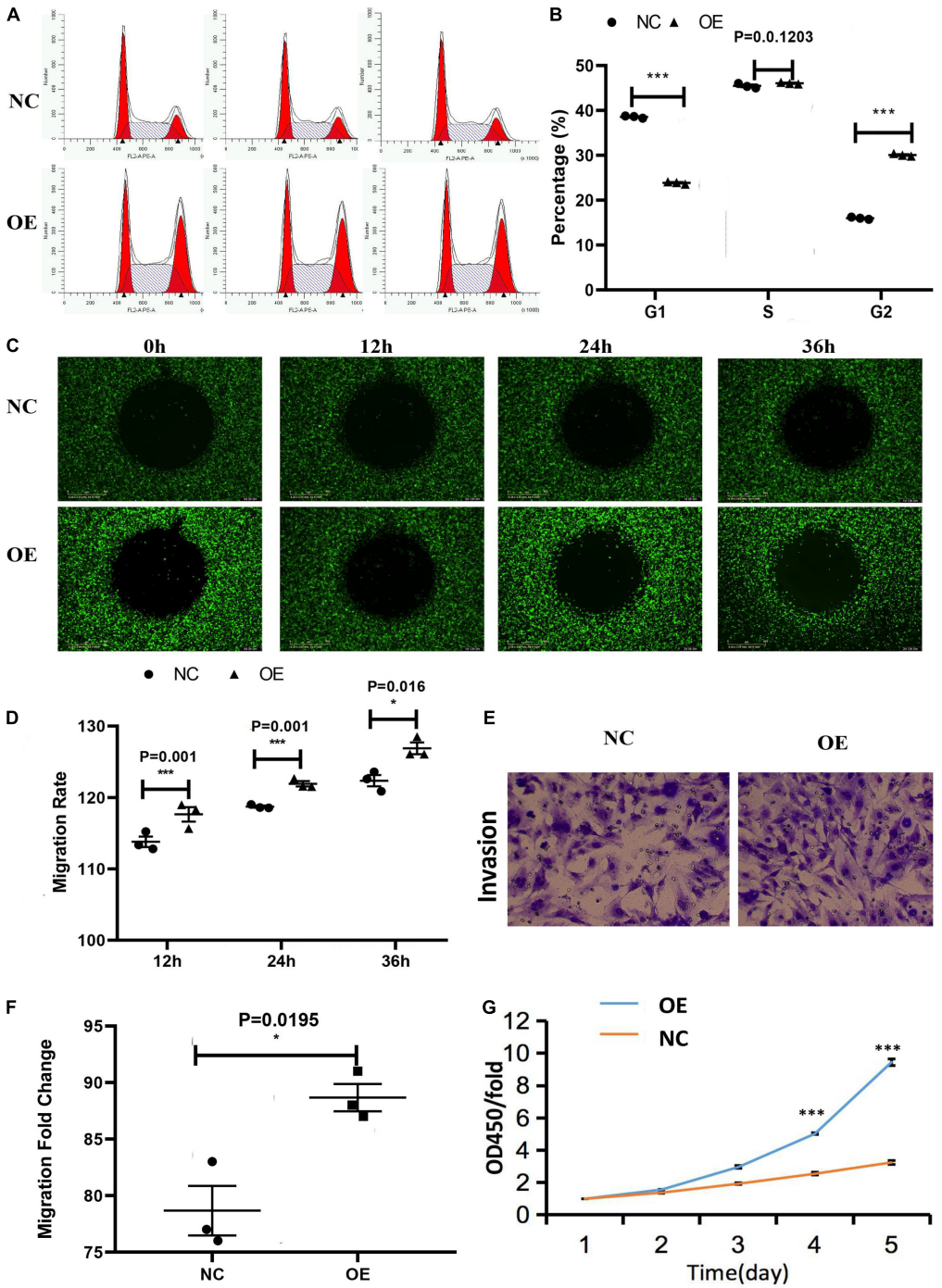

FIGURE 4 | Effect of the overexpression of ACTA2 on the migration and invasion ability of HMEC-1. **(A,B)** Cell cycle distribution was determined by flow cytometry after propidium iodide (PI) staining. **(C,D)** Oris™ plate Wound-healing assay for the migration of HMEC1 after ACTA2 overexpressing. **(E,F)** Invasion assay for the invasion of HMEC1 after ACTA2 overexpressing. **(G)** CCK-8 assay for the proliferation of HMEC1 after ACTA2 overexpressing. $^{*}P < 0.05$, $^{**}P < 0.01$, $^{***}P < 0.0001$.

intron 2-inserted sequence and the exon 2-skipped sequence. Quantitative measurements of acta2 expression levels measured by quantitative qRT-PCR (**Figure 6D**). Samples were collected at 2-dpf after the introduction of 4ng of MO at the one-cell stage ($N = 35$).

Image of trunk regions taken at 50-hpf, with the vascular structures visualized by eGFP fluorescence and labeled ISV (intersegmental vessel) and DLAV (dorsal longitudinal anastomotic vessel) showed regular development in the embryo injected with control MO (**Figures 7A–C**). Compared with

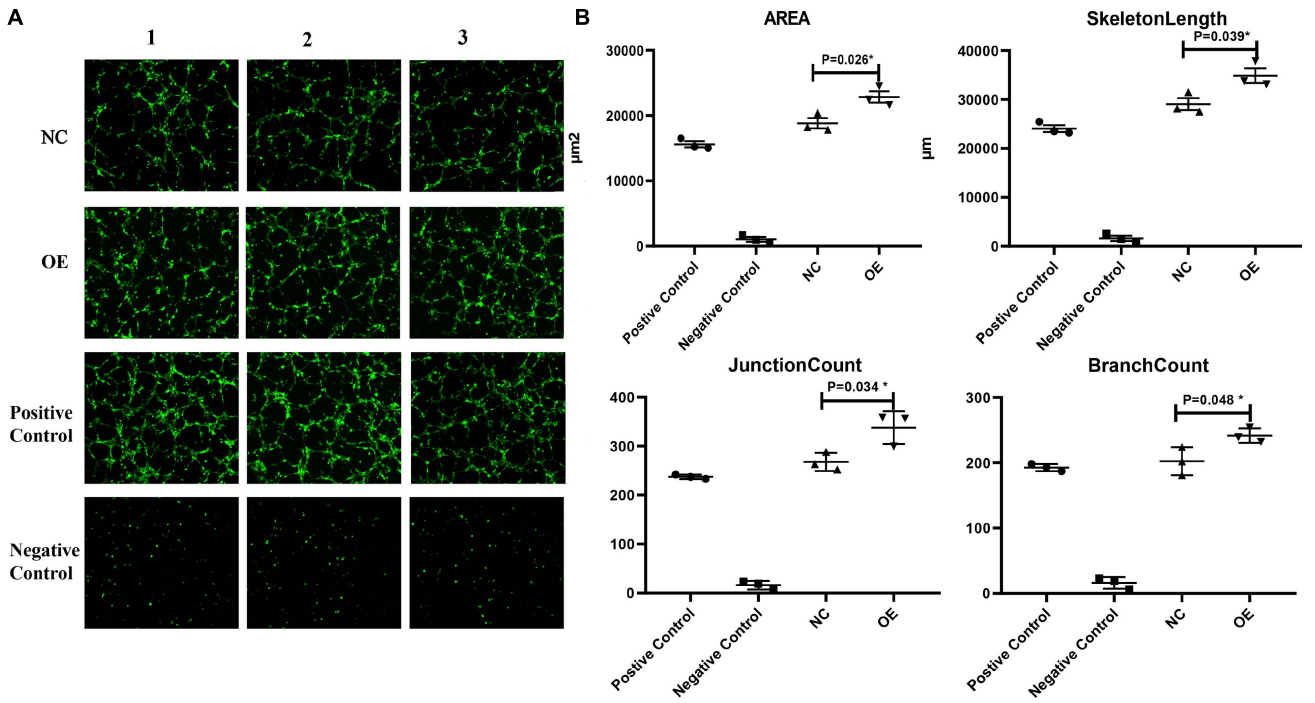

FIGURE 5 | Effect of overexpression of ACTA2 on angiogenesis. **(A)** Representative fluorescence images of angiogenesis in the positive control, negative control, NC, and ACTA2 overexpressing group. **(B)** Quantification of Area, Skeleton Length, Junction Count, Branch Count of positive control, negative control, NC and ACTA2 overexpressing group. *$P < 0.05$, **$P < 0.01$, ***$P < 0.0001$.

control MO, embryos injected with acta2-MO present a lower number of incomplete ISVs and ectopic sprouts (**Figures 7D–I**). In control embryos, the parachordal vessels (PAV) form normally (C, red arrows). While compared with control, MO knockdown acta2 prevents the PAV formation, the precursor to the lymphatic system (**Figures 7F,I**). Quantification of the number of complete ISVs or mean length of ISVs shows a significantly decrease in acta2 morphants (**Figures 7J–L**).

Loss of acta2 impairs the formation of the CVP in zebrafish. In control embryos, caudal vein plexus (CVP) were formed honeycomb-like structures at the tail around 50 h post-fertilization (hpf) (**Figures 8A,B**). In contrast, acta2 knock down resulted in specific defects in CVP formation (**Figures 8C,D**).

According to these results, the direct effect of ACTA2 on early angiogenesis was identified *in vivo*. Morpholino knockdown of acta2 causes vascular defects, sprouting angiogenesis, and CVP (caudal vein plexus) formation defects of zebrafish (**Figure 8E**).

Effect of ACTA2 on the Signaling Pathways in Zebrafish

The knockdown of ACTA2 inhibited the Dll4/notch1signaling pathway, Ephrin-B2 signaling pathway, and vascular integrity-related molecules and activated the Hedgehog (Hh) signaling pathway. The expression of molecules related to each pathway in the control and ACTA2 knockdown groups was detected by qRT-PCR, revealing that dll4, notch1a, notch1b, hey2, efnb2a, ptp-rb, cd146, nuclear receptor subfamily 2 group F member 1a (nr2f1a), and s1pr1, which are associated with the Dll4/notch1signaling pathway, Ephrin-B2 signaling pathway, and vascular endothelial protein tyrosine phosphatase (VE-PTP), were all significantly downregulated (**Figure 9A**). The expression of shha, ptch2, Sufu, Gli1, and Gli2b, which are related to Hh signaling pathway were significantly increased (**Figure 9B**). PCR testing of the knockdown and control groups found that vascular malformation by ACTA2 knockdown may be due to the inhibition of the Dll4/notch1 signaling pathway, Ephrin-B2 signaling pathway, and vascular integrity-related molecules, as well as activation of the Hh signaling pathway.

This implies regulation of ACTA2 knockdown on the vascular malformation, via not only inhibited the Dll4/notch1 signaling pathway, Ephrin-B2 signaling pathway, and vascular integrity-related molecules but also upregulated the Hh signaling pathway. A schematic diagram was proposed to display the visualized relationship between expression levels and roles in the pathway (**Figure 9C**). However, the mechanism of crosstalk between cell signaling pathways *in vivo* is very complex, more work needs to be continued and discussed.

DISCUSSION

Venous malformations are the most common type of vascular malformation in clinical practice, accounting for approximately 66% of congenital vascular malformations, with a prevalence

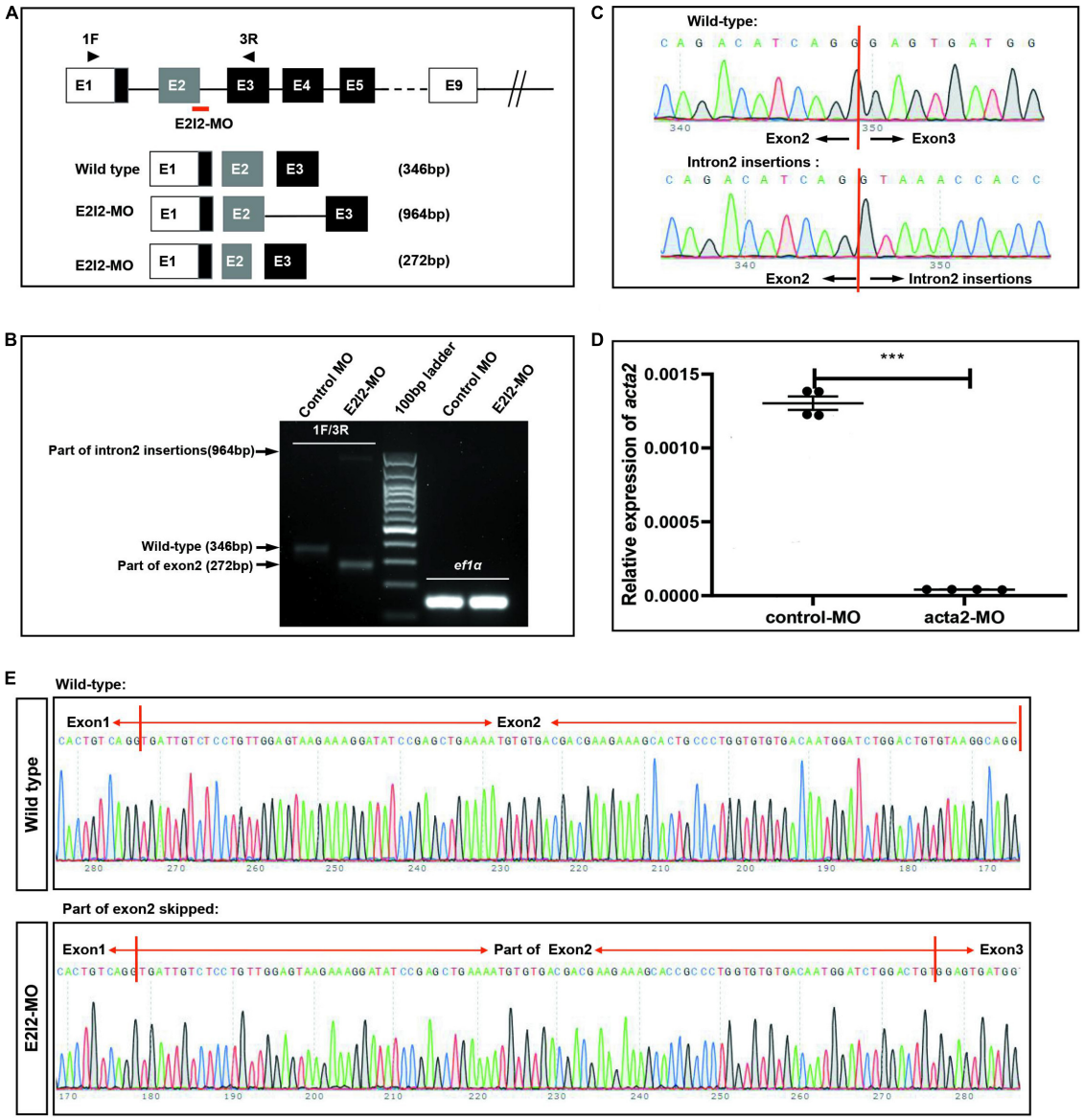

FIGURE 6 | Effectiveness of acta2 knockdown was confirmed by RT-PCR and qRT-PCR. **(A)** The zebrafish acta2 gene was targeted by specific morpholino antisense to prevent proper splicing of exon 2 (E2I2-MO). **(B)** RT-PCR of acta2 transcript from control-MO and E2I2-MO morpholino-injected embryos 2 days after fertilization, demonstrating insertion of intron 2 and skipping of exon 2. **(C,E)** Sanger sequencing of both the wild type band and the intron 2-inserted band and the exon 2-skipped band validating the wild type sequence and the intron 2-inserted sequence **(C)** and the exon 2-skipped sequence **(E)**. **(D)** Quantitative measurements of acta2 expression levels measured by qRT-PCR (***$P < 0.0001$). MO-targeted down-regulation of acta2. dpf, days post-fertilization.

of approximately 1% and an incidence of 1/10,000 to 1/5000 (Dompmartin et al., 2010; Fowell et al., 2017). It may occur anywhere on the body, including the head and neck (40%), extremities (40%), and trunk (20%) (Dompmartin et al., 2010; Cahill and Nijs, 2011; Manoli et al., 2015). It is usually present from birth and progresses with growth and development (Judith et al., 2014; Lee et al., 2015). Its onset is not gendered specific (Carqueja et al., 2018), the exact etiology is unclear, and it was associated with mutated genes, such as TIE2 (TEK), PIK3CA, and MAP3K3 (Couto et al., 2015; Natynki et al., 2015; Castillo et al., 2016; Seront et al., 2018).

In recent years, the development of proteomics has brought about new ideas for the study of many diseases and provided a viable method to identify disease-specific protein markers. The functions of most genes depend on the proteins they encode, so the study of proteins in cells or organisms can help reveal the metabolic processes of cells and the life activities of the organism. Proteomics enables the quantification and analysis of hundreds to thousands of proteins in a single experiment, providing an important method to discover and validate biomarkers and discover new therapeutic targets on a large scale. Currently, mass spectrometry-based methods for proteomics quantification

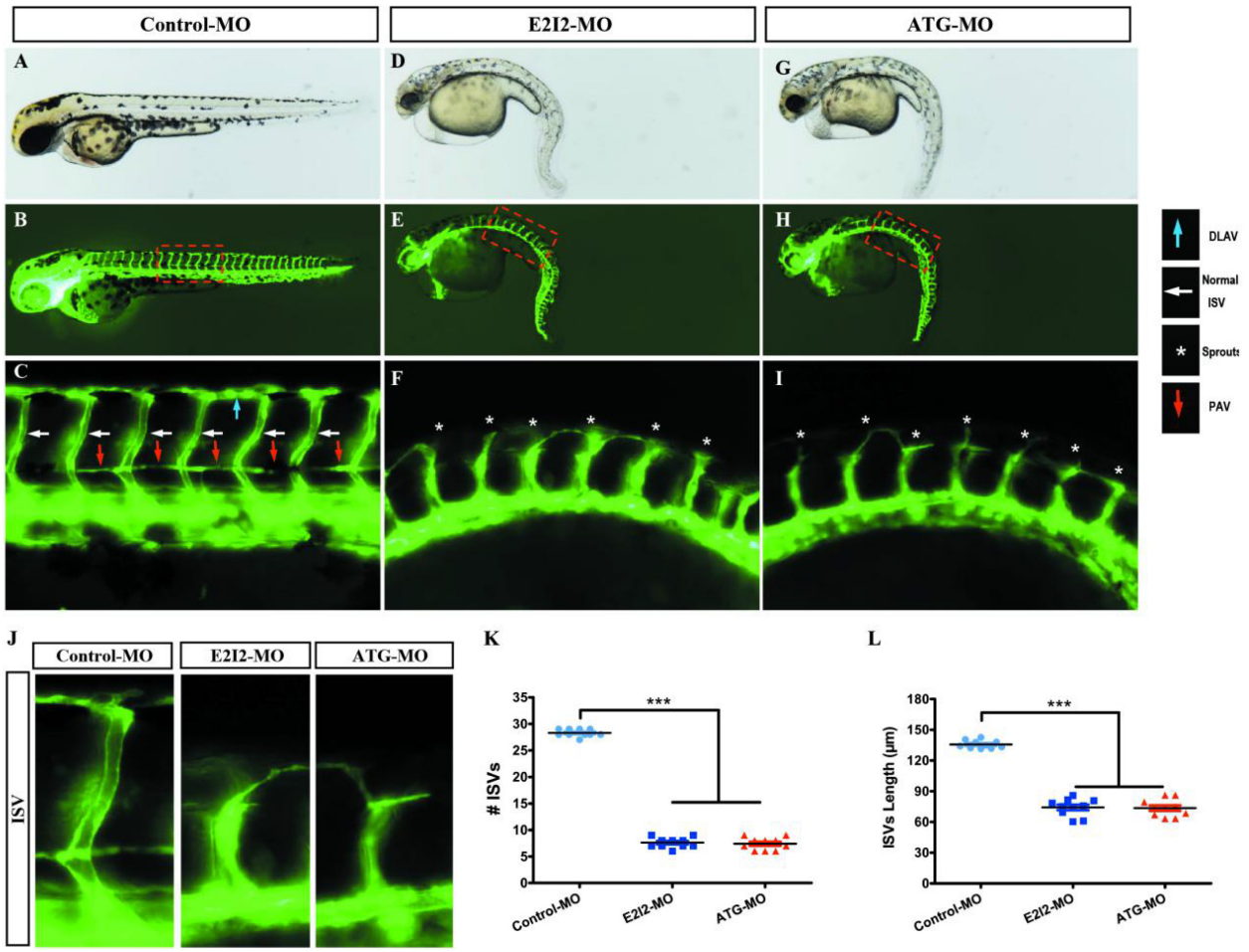

FIGURE 7 | Morpholino knockdown of acta2 causes vascular defects. **(A–I)** Representative bright field and fluorescent images of Tg (fli1a:EGFP)y1 embryos at 50-hpf. **(B,C,E–H)** Image of trunk regions taken at 50-hpf, with the vascular structures visualized by eGFP fluorescence and labeled ISV (intersegmental vessel) and DLAV (dorsal longitudinal anastomotic vessel) showed regular development in the embryo injected with control MO. Compared with control MO, embryos injected with acta2-MO present a lower number of incomplete ISVs and ectopic sprouts (**F,I**, asterisk). In control embryos, the parachordal vessels (PAV) form normally (**C**, red arrows). Compared with control, MO knockdown acta2 prevents the parachordal vessels (PAV) formation, the precursor to the lymphatic system. The boxed regions are shown at higher magnification in the bottom panels. **(J–L)** Quantification of the number of complete ISVs or mean length of ISVs shows a significantly decrease in acta2 morphants. Columns, mean; SEM (n = 10; ANOVA) ***P < 0.0001. hpf, hours post-fertilization.

include TMT, isobaric tags for relative and absolute quantitation, multiple reaction monitoring, and parallel reaction monitoring, among which TMT is the most widely used (Wojdyla et al., 2015). Developed by Thermo Scientific, TMT is a relative and absolute quantitative technology based on *in vitro* isobaric isotope labeling. It has been widely used in proteomics research in recent years. The identification and quantification of proteins by tandem mass spectrometry has the advantages of antibody independence, simultaneous determination of multiple targets in multiple samples, and easy establishment of standard operation protocols (Zhang et al., 2016).

In this study, a total of 7408 peptides and 801 protein groups were identified by TMT technology, and 71 proteins with statistically significant differential expression were further selected, among which five were upregulated and 66 were downregulated. GO functional, KEGG pathway and structural domain annotation of the differentially expressed proteins revealed that their functional differences between the patients with venous malformations and controls primarily included biological regulation, cellular process, actin filament binding, molecular transducer activity, and binding and regulation of the actin cytoskeleton pathway, and the differences in CC were primarily focused on cytosol, organelles, cell part, and so on.

The HCS system generates a large number of images in a short period by fully automated high-speed microscopic imaging. Fully automated image analysis software extracts a large amount of data from these images, and the data management software is responsible for processing and analyzing these images and data to observe differences in cell morphology and biological functions (Anguissola et al., 2014). Celigo is a high-throughput screening system based on automatic image acquisition and

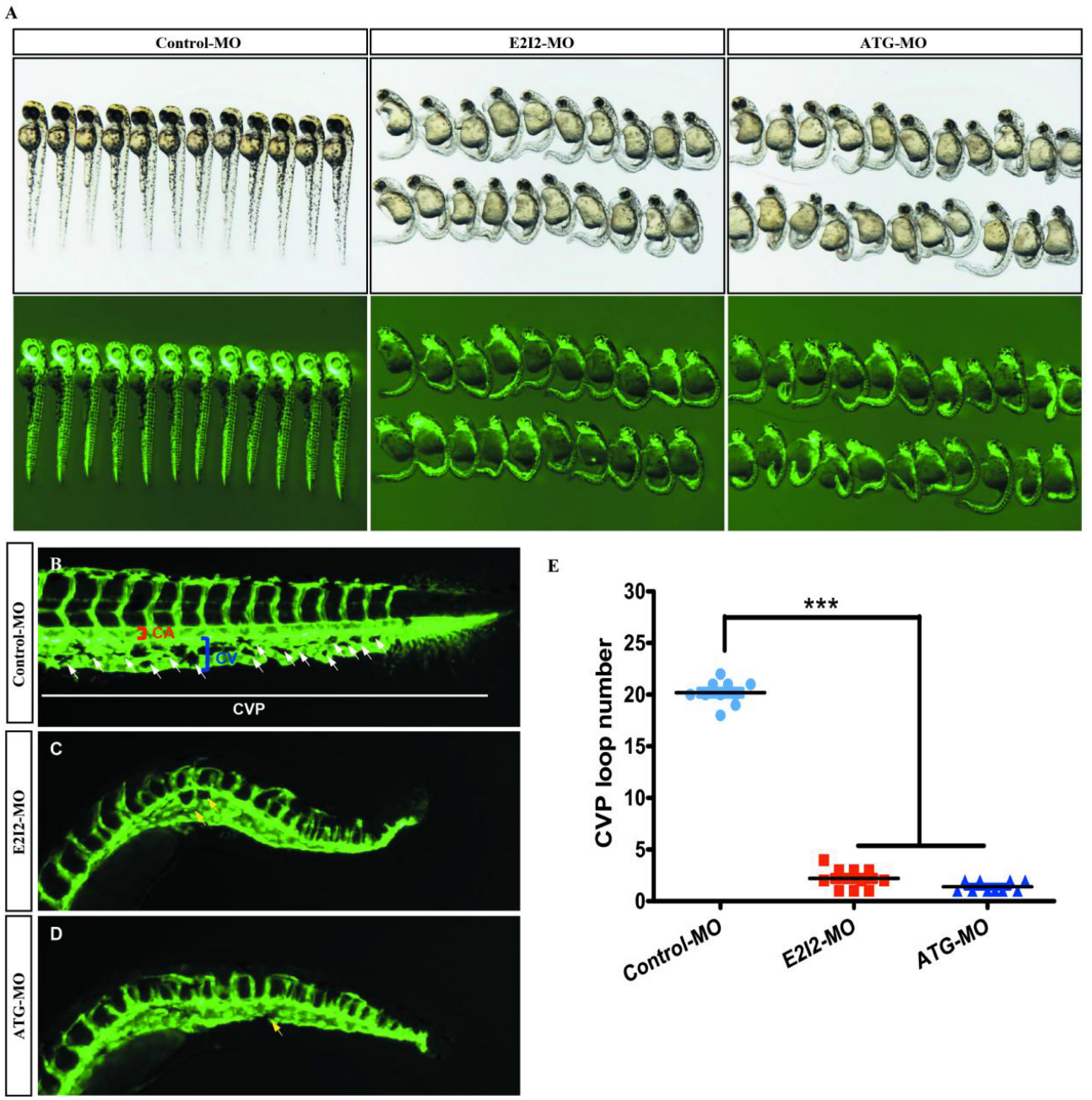

FIGURE 8 | Acta2 knockdown impairs formation of the CVP in zebrafish. **(A)** In control embryos, caudal vein plexus (CVP) were formed honeycomb-like structures at the tail around 50 h post-fertilization (hpf). **(B–D)** Acta2 knockdown resulted in specific defects in CVP formation. **(E)** Quantification of loop number at CVP. Columns, mean; SEM (n = 10; ANOVA) $^{*}P < 0.05$, $^{**}P < 0.01$, $^{***}P < 0.0001$. CVP, caudal vein plexus; CA, caudal artery; CV, caudal vein.

image data analysis. The high throughput of the system is due to automatic target loading, high-speed imaging, and real-time automatic quantitative analysis. The software analyzes the images to determine the corresponding optical information of biological events, including coordinate position, signal intensity, and time information and their combinations and analyzes the biological changes, including cell morphology, cell movement, cell number, cell expression signal strength, cell cycle, apoptosis, and other common biological phenomena. In this study, five highly and 15 lowly expressed proteins were selected based on bioinformatic analysis and proteomics results and were included in HCS for the RNAi functional screening test. This study identified ACTA2 as the most differentially expressed gene associated with vascular endothelial cell proliferation, which was further investigated by tissue expression, cellular function assays, and *in vivo* studies.

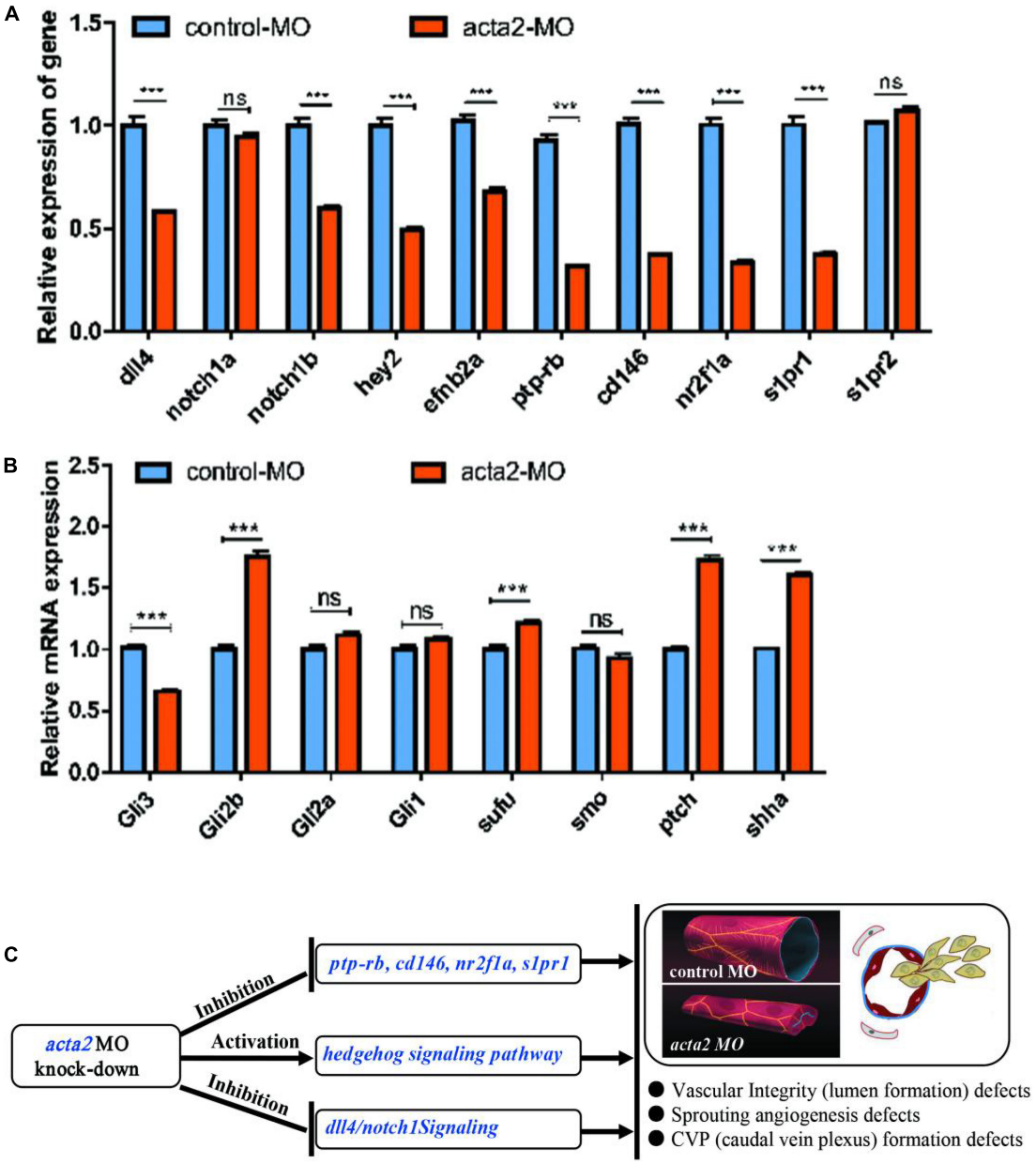

FIGURE 9 | (A) Endogenous dll4, notch1a, notch1b, hey2, efnb2a, ptp-rb, cd146, nr2f1a, s1pr1 and s1pr2 in control and acta2 morphants assessed by qRT-PCR (n = 6–10 individual embryos). *** $P < 0.001$; ns, not significant. **(B)** Endogenous shha, ptch2, smo, Sufu, Gli1, Gli2a, Gli2b, and Gli3 in control and acta2 morphants assessed by qRT-PCR (n = 6–10 individual embryos). **(C)** Schematic model illustrating the MOA (mechanism of action) of acta2 in Zebrafish early development.

The ACTA2 gene is located at chromosome 10q22-q24. Its primary function is to encode actin and it is widely expressed in most cells. It encodes ACTA2, actin with multiple aliases, including alpha-actin, alpha-actin-2, aortic smooth muscle, and alpha-smooth muscle actin. Mutations in this gene have been found to cause a variety of vascular diseases, such as thoracic aortic disease, coronary artery disease, stroke, moyamoya disease, and multisystem smooth muscle dysfunction syndrome (Guo et al., 2009). ACTA2 protein is a ubiquitous cytoskeletal protein that is involved in cell activation, differentiation, and migration. It constitutes a cellular scaffold, maintains cell shape, and mediates intracellular signaling and protein synthesis (Xu et al., 2019). Previous studies have shown that aberrant expression of ACTA2 promotes the invasion and migration of eutopic endometrial stromal cells (Rockey et al., 2013) and leads to significantly enhanced metastasis in lung cancer (Lee et al., 2013). The deletion of ACTA2 leads to reduced cell motility and contraction of myofibroblasts during cranial injury healing (Zhang et al., 2020). In cardiovascular diseases, defects in the function of actin or myosin (ACTA2 or MYH11) result in

diminished actin–myosin interactions and lead to diseases (Fang et al., 2017). In this study, the deletion of ACTA2 resulted in the disruption of HMEC proliferation, leading to a lack of vascular development and causing venous malformations. We found that overexpression of ACTA2 improved proliferation, migration, invasion, and angiogenesis of vascular endothelial cells, and their abnormal proliferation was inhibited.

In the field of vascular development research, as an emerging animal model, zebrafish have unique molecular and histological advantages due to easy manipulation, rapid growth and development, easy observation of blood vessels, and high genetic homology. The expression and distribution of relevant vascular endothelial markers, early vasculogenesis, and maturation can be directly and dynamically observed by transgenic fluorescent labeling techniques (Westerfield, 2007), in which the embryonic caudal vein plexus (CVP) is considered one of the representative models for simulating early vein development. CVP is the basis of the mature caudal vein. At the early stage of development, it is shown as a large aggregation of endothelial cell clusters, followed by an initial sinus lumen morphology 24 h after embryonic fertilization. Endothelial cells proliferate actively outside the CVP and extend to the pseudopodia. At the same time, the cavities of the sinuses are gradually reconstructed, eventually forming a mature caudal vein lumen (Wakayama et al., 2015). The vascular development of this process can be visually recorded based on the fluorescence technique of visualization and the transparent nature of the fish body. In this study, we constructed a zebrafish model with ACTA2 knockdown and observed that ACTA2 knockdown caused defects in vascular integrity, neovascularization, and CVP formation in zebrafish. This indicates that ACTA2 deletion severely affects vascular integrity and causes abnormal vein development.

Notch signaling is an evolutionary conserved, intercellular signaling mechanism that plays myriad roles during vascular development and physiology in vertebrates. Defects in Notch signaling also cause inherited vascular diseases (Gridley, 2010). Delta-like ligand 4 (DLL4) is the only Notch1 ligand specifically present in vascular endothelial cells that regulate vascular sprouting and branching morphology (Hu et al., 2014). Notch1 is the most studied receptor in the Notch signaling pathway, which regulates the biological behavior of cells through interactions between neighboring cells. Aberrant activation of Notch 1 may lead to excessive cell proliferation and invasion (Mckeage et al., 2019). The expression of key molecules, such as DLL4 and Notch1b, was significantly reduced in zebrafish in the ACTA2 knockdown group in this study, suggesting that ACTA2 deletion may lead to the inhibition of the DLL4-Notch1 signaling pathway, resulting in defective vascular development.

Ephrin-B2 is a well-recognized axon guidance factor that affects angiogenesis primarily by regulating endothelial cell function. It plays a crucial role in vascular development and revascularization during embryonic and adult life (Birgit et al., 2010). The Ephrin-B2 signaling pathway can cooperate with VEGF to coregulate vascular growth. Selective inhibition of the Ephrin-B2 signaling pathway can lead to a significant reduction in sprouting angiogenesis (Wang Y. et al., 2010). In this study, the expression of Ephrin-B2 signaling pathway-related molecules was significantly reduced in zebrafish vascular tissues of the ACTA2 knockdown group, indicating that ACTA2 deletion also affects the inhibition of this pathway, causing abnormal angiogenic function.

Vascular integrity is the basis of vascular endothelial cell function and is closely associated with the development of numerous vascular diseases (Dejana et al., 2009). VE-PTP, nr2f1a, and Sphingosine 1-phosphate receptor are closely associated with vascular integrity (Wang C. et al., 2010; Hayashi et al., 2013; Mendelson et al., 2013; Wu et al., 2014). In this study, the expression of molecules related to vascular integrity was significantly reduced in the vascular tissue of zebrafish in the ACTA2 knockdown group, implying that ACTA2 deletion led to the disruption of vascular integrity.

The Hh signaling pathway is essential for embryonic development and plays a key role in human tissue maintenance, renewal, and regeneration. An abnormally activated Hh signaling pathway is associated with the development of several tumors and other diseases (Xin et al., 2018). The expression levels of important transcriptional factors and ligands in this pathway, including shha, ptch2, Sufu, and Gli2b, were significantly increased in the ACTA2 knockdown group of zebrafish, indicating that ACTA2 deletion caused abnormal activation of this pathway and led to abnormal vascular development.

In summary, this study screened differentially expressed proteins in venous malformation and normal human tissues by proteomics and identified the most significantly differentially expressed gene, ACTA2, by HCS. Compared with healthy people, the expression of ACTA2 was significantly reduced in patients with venous malformations. We also established a cell model to overexpress ACTA2 in HMEC-1 and revealed that the abnormalities of cell proliferation, metastasis, invasion, and angiogenesis were reversed by ACTA2 overexpression. We also established a zebrafish animal model and performed *in vivo* experiments, resulting in the finding that knockdown of ACTA2 in zebrafish results in defective vascular development, disrupted vascular integrity, and abnormal development of the caudal vein. PCR testing of the knockdown and control groups found that vascular malformation by ACTA2 knockdown may be due to the inhibition of the Dll4/notch1 signaling pathway, Ephrin-B2 signaling pathway, and vascular integrity-related molecules, as well as activation of the Hh signaling pathway. ACTA2 may be a potential target for the diagnosis and treatment of disseminated venous malformations. However, the mechanism of crosstalk between cell signaling pathways *in vivo* is very complex, more work needs to be continued and discussed.

DATA AVAILABILITY STATEMENT

The datasets presented in this study can be found in online repositories. The data presented in the study are deposited in the ProteomeXchange repository, accession number PXD028848.

ETHICS STATEMENT

The studies involving human participants were reviewed and approved by Shandong Provincial Ethics Committee. Written informed consent to participate in this study was provided by the participants' legal guardian/next of kin. The animal study was reviewed and approved by Shandong Provincial Hospital Ethics Committee. Written informed consent was obtained from the owners for the participation of their animals in this study.

AUTHOR CONTRIBUTIONS

RH and JB conceived and designed the experiments. SW analyzed the experimental results. RL, GX, and JZ collected and analyzed the data. ZZ, JL, YW, and HL performed the experiments. SW wrote the manuscript. All authors have given approval to the final version of the manuscript.

FUNDING

This work was supported by the National Natural Science Foundation of China (Grant Number 81873938).

ACKNOWLEDGMENTS

We would like to thank Tao Wang (Jinan, China), for his technical assistance and contribution to the data processing.

REFERENCES

Anguissola, S., Garry, D., Salvati, A., O'Brien, P. J., and Dawson, K. A. (2014). High content analysis provides mechanistic insights on the pathways of toxicity induced by amine-modified polystyrene nanoparticles. *PLoS One* 9:e108025. doi: 10.1371/journal.pone.0108025

Birgit, M., Bettina, R., Christin, N., and Pietzsch, J. (2010). Eph receptors and ephrin ligands: important players in angiogenesis and tumor angiogenesis. *J. Oncol.* 2010:135285. doi: 10.1155/2010/135285

Cahill, A. M., and Nijs, E. L. (2011). Pediatric vascular malformations: pathophysiology, diagnosis, and the role of interventional radiology. *Cardiovasc. Intervent. Radiol.* 34, 691–704. doi: 10.1007/s00270-011-0123-0

Calvert, J. T., Riney, T. J., Kontos, C. D., Cha, E. H., Prieto, V. G., Shea, C. R., et al. (1999). Allelic and locus heterogeneity in inherited venous malformations. *Hum. Mol. Genet.* 8, 1279–1289. doi: 10.1093/hmg/8.7.1279

Carqueja, I. M., Sousa, J., and Mansilha, A. (2018). Vascular malformations: classification, diagnosis and treatment. *Int. Angiol.* 37, 127–142. doi: 10.23736/S0392-9590.18.03961-5

Castillo, S. D., Tzouanacou, E., Zaw- Thin, M., Berenjeno, I. M., Parker, V. E., Chivite, I., et al. (2016). Somatic activating mutations in PIK3CA cause sporadic venous malformations in mice and humans. *Sci. Transl. Med.* 8:332ra43. doi: 10.1126/scitranslmed.aad9982

Couto, J. A., Vivero, M. P., Kozakewich, H. P., Taghinia, A. H., Mulliken, J. B., Warman, M. L., et al. (2015). A somatic MAP3K3 mutation is associated with verrucous venous malformation. *Am. J. Hum. Genet.* 96, 480–486. doi: 10.1016/j.ajhg.2015.01.007

Dejana, E., Tournier-Lasserve, E., and Weinstein, B. M. (2009). The control of vascular integrity by endothelial cell junctions: molecular basis and pathological implications. *Dev. Cell* 16, 209–221. doi: 10.1016/j.devcel.2009.01.004

Dompmartin, A., Vikkula, M., and Boon, L. M. (2010). Venous malformation: update on aetiopathogenesis, diagnosis and management. *Phlebology* 25:224. doi: 10.1258/phleb.2009.009041

Fang, M., Yu, C., Chen, S., Xiong, W., Li, X., Zeng, R., et al. (2017). Identification of novel clinically relevant variants in 70 Southern Chinese patients with thoracic aortic aneurysm and dissection by next- generation sequencing. *Sci. Rep.* 7:10035. doi: 10.1038/s41598-017-09785-y

Fowell, C., Verea Linares, C., Jones, R., Nishikawa, H., and Monaghan, A. (2017). Venous malformations of the head and neck: current concepts in management. *Br. J. Oral Maxillofac. Surg.* 55, 3–9. doi: 10.1016/j.bjoms.2016.10.023

Gridley, T. (2010). Notch signaling in the vasculature. *Curr. Top. Dev. Biol.* 92, 277–309. doi: 10.1016/S0070-2153(10)92009-7

Guo, D. C., Papke, C. L., Tran-Fadulu, V., Regalado, E. S., Avidan, N., Johnson, R. J., et al. (2009). Mutations in smooth muscle alpha-actin (ACTA2) cause coronary artery disease, stroke, and Moyamoya disease, along with thoracic aortic disease. *Am. J. Hum. Genet.* 84, 617–627. doi: 10.1016/j.ajhg.2009.04.007

Hayashi, M., Majumdar, A., Li, X., Adler, J., Sun, Z., Vertuani, S., et al. (2013). VE-PTP regulates VEGFR2 activity in stalk cells to establish endothelial cell polarity and lumen formation. *Nat. Commun.* 4:1672. doi: 10.1038/ncomms2683

Hu, G. H., Liu, H., Lai, P., Guo, Z. F., Xu, L., Yao, X. D., et al. (2014). Delta-like ligand 4 (Dll4) predicts the prognosis of clear cell renal cell carcinoma, and anti-Dll4 suppresses tumor growth in vivo. *Int. J. Clin. Exp. Pathol.* 7, 2143–2152.

Judith, N., Ulrike, E., Siegmar, R., Matthias, N., and Jürgen, H. (2014). Current concepts in diagnosis and treatment of venous malformations. *J. Craniomaxillofac. Surg.* 42, 1300–1304. doi: 10.1016/j.jcms.2014.03.014

Lee, B. B., Baumgartner, I., Berlien, P., Burrows, P., Gloviczki, P., Huang, Y., et al. (2015). Diagnosis and treatment of venous malformations. Consensus document of the International Union of Phlebology (IUP): updated 2013. *Int. Angiol.* 34, 97–149.

Lee, H. W., Park, Y. M., Lee, S. J., Cho, H. J., Kim, D. H., Lee, J. I., et al. (2013). Alpha-smooth muscle actin (ACTA2) is required for metastatic potential of human lung adenocarcinoma. *Clin. Cancer Res.* 19, 5879–5889. doi: 10.1158/1078-0432.CCR-13-1181

Manoli, T., Micheel, M., Ernemann, U., Schaller, H. E., and Schaller, H. E. (2015). Treatment algorithm and clinical outcome of venous malformations of the limbs. *Dermatol. Surg.* 41:1164. doi: 10.1097/DSS.0000000000000469

Mckeage, M. J., Dusan, K., Ben, M., Hidalgo, M., Millward, M. J., Jameson, M. B., et al. (2019). Phase IB trial of the anti-cancer stem Cell DLL4-binding agent demcizumab with pemetrexed and carboplatin as first-line treatment of metastatic non-squamous NSCLC. *Targ. Oncol.* 13, 89–98. doi: 10.1007/s11523-017-0543-0

Mendelson, K., Zygmunt, T., Torres-Vázquez, J., Evans, T., and Hla, T. (2013). Sphingosine 1-phosphate receptor signaling regulates proper embryonic vascular patterning. *J. Biol. Chem.* 288, 2143–2156. doi: 10.1074/jbc.M112.427344

Nasevicius, A., and Ekker, S. C. (2000). Effective targeted gene 'knockdown' in zebrafish. *Nat. Genet.* 26, 216–220. doi: 10.1038/79951

Natynki, M., Kangas, J., Miinalainen, I., Sormunen, R., Pietilä, R., Soblet, J., et al. (2015). Common and specific effects of TIE2 mutations causing venous malformations. *Hum. Mol. Genet.* 24, 6374–6389. doi: 10.1093/hmg/ddv349

Rockey, D. C., Weymouth, N., and Shi, Z. (2013). Smooth muscle α actin (Acta2) and myofibroblast function during hepatic wound healing. *PLoS One* 8:e77166. doi: 10.1371/journal.pone.0077166

Seront, E., Vikkula, M., and Boon, L. M. (2018). Venous malformations of the head and neck. *Otolaryngol. Clin. North Am.* 51, 173–184. doi: 10.1016/j.otc.2017.09.003

Shu, W., Lin, Y., Hua, R., Luo, Y., He, N., Fang, L., et al. (2012). Cutaneomucosal venous malformations are linked to the TIE2 mutation in a large Chinese family. *Exp. Dermatol.* 21, 456–457. doi: 10.1111/j.1600-0625.2012.01492.x

Wakayama, Y., Fukuhara, S., Ando, K., Matsuda, M., and Mochizuki, N. (2015). Cdc42 mediates Bmpinduced sprouting angiogenesis through Fmnl3 -driven assembly of endothelial filopodia in zebrafish. *Dev. Cell* 32, 109–122. doi: 10.1016/j.devcel.2014.11.024

Wang, C., Tao, W., Wang, Y., Bikow, J., Lu, B., Keating, A., et al. (2010). Rosuvastatin, identified from a zebrafish chemical genetic screen for

antiangiogenic compounds, suppresses the growth of prostate cancer. *Eur. Urol.* 58, 418–426. doi: 10.1016/j.eururo.2010.05.024

Wang, Y., Nakayama, M., Pitulescu, M. E., Schmidt, T. S., Bochenek, M. L., Sakakibara, A., et al. (2010). Ephrin-B2 controls VEGF induced angiogenesis and lymphangiogenesis. *Nature* 465, 483–486. doi: 10.1038/nature09002

Wassef, M., Blei, F., Adams, D., Alomari, A., Baselga, E., Berenstein, A., et al. (2015). Vascular anomalies classification: recommendations from the international society for the study of vascular anomalies. *Pediatrics* 136, e203–e214. doi: 10.1542/peds.2014-3673

Westerfield, M. (2007). *The Zebrafish Book: A Guide for the Laboratory Use of Zebrafish (Brachydanio rerio)*. Eugene, OR: M. Westerfield.

Wojdyla, K., Williamson, J., Roepstorff, P., and Rogowska-Wrzesinska, A. (2015). The SNO/SOH TMT strategy for combinatorial analysis of reversible cysteine oxidations. *J. Proteomics* 113, 415–434. doi: 10.1016/j.jprot.2014.10.015

Wu, B. J., Chiu, C. C., Chen, C. L., Wang, W. D., Wang, J. H., Wen, Z. H., et al. (2014). Nuclear receptor subfamily 2 group F member 1a (nr2f1a) is required for vascular development in zebrafish. *PLoS One* 9:e105939. doi: 10.1371/journal.pone.0105939

Xin, M., Ji, X., De La Cruz, L. K., Thareja, S., and Wang, B. (2018). Strategies to target the Hedgehog signaling pathway for cancer therapy. *Med. Res. Rev.* 38, 870–913. doi: 10.1002/med.21482

Xu, Z., Zhang, L., Yu, Q., Zhang, Y., Yan, L., and Chen, Z. J. (2019). The estrogen-regulated lncRNA H19/miR-216a-5p axis alters stromal cell invasion and migration via ACTA2 in endometriosis. *Mol. Hum. Reprod.* 25, 550–561. doi: 10.1093/molehr/gaz040

Zhang, J., Jiang, X., Zhang, C., Zhong, J., Fang, X., Li, H., et al. (2020). Actin alpha 2 (ACTA2) downregulation inhibits neural stem cell migration through Rho GTPase activation. *Stem Cells Int.* 2020:4764012. doi: 10.1155/2020/4764012

Zhang, Z., Yang, X. Y., Mirokhin, Y. A., Tchekhovskoi, D. V., Ji, W., Markey, S. P., et al. (2016). Interconversion of peptide mass spectral libraries derivatized with iTRAQ or TMT labels. *J. Proteome Res.* 15, 3180–3187. doi: 10.1021/acs.jproteome.6b00406

Conflict of Interest: The authors declare that the research was conducted in the absence of any commercial or financial relationships that could be construed as a potential conflict of interest.

Publisher's Note: All claims expressed in this article are solely those of the authors and do not necessarily represent those of their affiliated organizations, or those of the publisher, the editors and the reviewers. Any product that may be evaluated in this article, or claim that may be made by its manufacturer, is not guaranteed or endorsed by the publisher.

Frontiers in
Cell and Developmental Biology

Explores the fundamental biological processes of life, covering intracellular and extracellular dynamics.

The world's most cited developmental biology journal, advancing our understanding of the fundamental processes of life. It explores a wide spectrum of cell and developmental biology, covering intracellular and extracellular dynamics.

Discover the latest Research Topics

See more →

Frontiers

Avenue du Tribunal-Fédéral 34
1005 Lausanne, Switzerland
frontiersin.org

Contact us

+41 (0)21 510 17 00
frontiersin.org/about/contact